

HAI 2023

TABLE OF CONTENTS

TABLE OF CONTENTS.....	2
Welcome!	13
HAI 2023 TEAM.....	14
HAI2023 SUPPORT (GRANTS/SPONSORSHIP):.....	15
POSTER INDEX (by board number)	16
POSTER INDEX (by presenter’s last name).....	24
HAI 2023 PROGRAM.....	31
HAI 2023 ABSTRACTS	41
Wednesday, January 11, 2023 - 08:30 am - 09:35 am.....	41
Podium Session.....	41
SESSION I: Tracer development and evaluation.....	41
<i>Bennacef, Idriss</i>	42
Advances towards the identification of an α -synuclein Positron Emission Tomography radioligand for the diagnosis of Parkinson’s Disease	42
<i>Capotosti, Francesca</i>	44
Discovery of [18F]ACI-12589, a novel and promising PET-tracer for a-synuclein.....	44
<i>Skaddan, Marc B.</i>	45
Discovery and preclinical evaluation of two novel PET tracers for imaging non-AD tauopathies	45
<i>Tonietto, Matteo</i>	46
In Vivo Head-To-Head Comparison of [18F]GTP1, [18F]PI2620, and [18F]MK6240 in Alzheimer’s Disease... ..	46
<i>Sehlin, Dag</i>	48
DIDACTIC LECTURE: PET imaging beyond amyloid with antibody-based radioligands	48
Wednesday, January 11, 2023 - 10:30 am - 11:15 am.....	49
Poster Session 1A.....	49
<i>Schwarz, Christopher</i>	52
[P1] Effects of de-facing PET and MRI scans on clinical correlations analyses	52
<i>Holy, Emily</i>	55
[P2] Non-invasive quantification and SUVR validation of [18F]-florbetaben with total-body EXPLORER PET ..	55
<i>Gomperts, Stephen</i>	57
[P3] PET imaging probe development for aggregated alpha-synuclein.....	57
<i>Gong, Kuang</i>	58
[P4] Cross-modality transformer for low-dose tau PET imaging	58
<i>Ioannou, Konstantinos</i>	60
[P5] Tau PET positivity reveals Alzheimer’s disease related fast cognitive decline	60
<i>Liu, Feng-Tao</i>	63
[P6] Positive 18F-APN-1607 tau PET imaging findings in patients with Progressive Supranuclear Palsy-like extrapyramidal symptoms caused by TBK1 mutations	63

Liu, Feng-Tao	64
[P7] In vivo visualization of tau deposits in corticobasal syndrome by 18F-Florzolotau PET	64
Chiotis, Konstantinos	65
[P8] Imaging neuroinflammation with astrocyte-PET and bio-fluid biomarkers in patients with cognitive impairment	65
Gatto, Rodolfo	67
[P9] [18] Flortaucipir PET and Diffusion Tensor Tractography Coregistration can Enhance Detection of Brain Changes Associated with Progressive Apraxia of Speech	67
Tunali, Ilke	68
[P10] Towards a simplified flortaucipir-PET read method for assessing tau burden	68
Fu, Jessie Fang-Lu	71
[P12] Digital clock drawing performance is associated with tau deposition measured with PET in preclinical Alzheimer's disease	71
Shekari, Mahnaz	74
[P13] [18F]RO-948 Tau PET Retention and Correlation with Fluid Biomarkers in the Early AD Continuum	74
Langella, Stephanie	77
[P14] Regional tau predicts glucose hypometabolism in autosomal dominant Alzheimer's disease: Findings from the Colombia-Boston (COLBOS) biomarker study	77
Krishnadas, Natasha	79
[P15] Is tau PET a robust biomarker for chronic traumatic encephalopathy?	79
Matsuda, Hiroshi	80
[P16] Centiloid scale measure of amyloid PET by CT of PET/CT equipment	80
Pezzoli, Stefania	81
[P17] Successful cognitive aging is associated with less brain atrophy and lower tau deposition	81
Satoh, Ryota	84
[P18] Subcortical flortaucipir PET and susceptibility analyses to differentiate progressive supranuclear palsy clinical variants and corticobasal syndrome	84
Cogswell, Petrice	86
[P19] Temporal associations of plasma and PET Alzheimer's disease biomarkers using a non-linear mixed effects model	86
McVea, Andrew	88
[P20] Beta-amyloid accumulates at a faster rate in individuals with Down syndrome	88
McVea, Andrew	92
[P21] Magnitude of MK6240 off-target binding correlated with spill-in effects in target regions	92
Chen, Xi	95
[P22] Amyloid and tau pathology associated with different cognitive declines in cognitively normal older people	95
Luckett, Emma	99
[P23] Future amyloid accumulation status affects the preservation of peripheral whole-blood gene co-expression networks at baseline in asymptomatic Alzheimer's disease	99

Stephens, Andrew	101
[P24] Validation of [18f]florbetaben PET quantitation based on the analysis of 15 software pipelines	101
Mejia Perez, Jhony	103
[P25] Preprocessing 10,700 real-world amyloid-PET scans from the IDEAS study: the Good, the Bad and the Ugly	103
Tetzloff, Katerina A.	106
[P26] Longitudinal tau-PET differs between progressive apraxia of speech subtypes	106
Cho, Hanna	108
[P27] Cross-sectional PET Analyses in the Longitudinal Early-onset Alzheimer’s Disease Study (LEADS).....	108
Raman, Fabio	111
[P28] Dynamic amyloid PET: relationships to tau PET and cognition in Alzheimer’s disease	111
Martersteck, Adam	115
[P29] Spatial extent and intensity of Alzheimer-associated tau PET burden is greater in agrammatic than logopenic primary progressive aphasia.....	115
Thomas, Wesley	117
[P30] Comparing PI2620 and Flortaucipir in Progressive Supranuclear Palsy Subjects	117
Feizpour, Azadeh	119
[P31] Assessing a universal neocortical mask for Centiloid quantification.....	119
Oh, Hwamee	122
[P32] Relationships between Neuronal Hyperactivity, Stress Susceptibility, and Alzheimer’s Disease pathology	122
Du, Lianlian	123
[P33] A/T/N, cognitive, health and lifestyle differences across white matter hyperintensities groups in aged 45-85 years adults: Results from the Wisconsin Registry for Alzheimer's Prevention (WRAP).....	123
Spruyt, Laure	127
[P34] Medial temporal 18F-MK6240 levels are associated with global graph characteristics of functional connectivity from high-density EEG in the asymptomatic and prodromal stage of Alzheimer disease.....	127
Endo, Hironobu	129
[P35] Longitudinal PET assessments of tau pathologies in progressive supranuclear palsy with 18F-florzolotau (PM-PBB3/APN-1607).....	129
Klein, Gregory	132
[P36] Head-to-head comparison of tau PET tracers [18F]PI2620 and [18F]RO948 in non-demented individuals with brain amyloid deposition: the TAU-PET FACEHBI cohort.....	132
Wednesday, January 11, 2023 - 11:15 am - 12:35 pm	133
Podium Session	133
SESSION II: Technical advances for clinical applications	133
Becker, J. Alex	134
Minimizing sample sizes for trials using MK-6240 outcomes: impact of processing method and choice of reference and target tissues	134
Franzmeier, Nicolai	138
Inferring full ATN status from tau-PET using deep learning	138

Chaggar, Pavan	141
Longitudinal modelling of tau transport and production dynamics in the human brain	141
Corriveau-Lecavalier, Nick	145
Connectivity- versus gradient-based approaches to predict regional tau-PET across Alzheimer’s disease variants	145
Harrison, Theresa	148
Measuring tau in the basal forebrain: a comparison of MK6240 and flortaucipir	148
Wednesday, January 11, 2023 - 02:00 pm - 02:45 pm	150
KEYNOTE: Synaptic pathology in neurodegeneration	150
Thomas Montine	150
Wednesday, January 11, 2023 - 02:45 pm - 03:50 pm	151
Podium Session	151
SESSION III: Thresholds, visual reads and real world imaging	151
Gogola, Alexandra	152
Biostatistical estimation of tau threshold hallmarks (BETTH) for tau imaging studies	152
Johnson, Sterling	154
Visual read of [18F]florquinitau PET that includes and extends beyond the mesial temporal lobe is associated with amyloid positivity and retrospective cognitive decline in an AD risk-enriched cohort.....	154
Soleimani-Meigooni, David	158
Head-to-head comparison of tau and amyloid PET visual reads for differential diagnosis: An international, multi-center study	158
Zeltzer, Ehud	162
Quantitative analysis of 8,895 real-world amyloid Positron Emission Tomography (PET) scans from the Imaging Dementia–Evidence for Amyloid Scanning (IDEAS) study	162
Wednesday, January 11, 2023 - 05:00 pm - 06:05 pm	165
Podium Session	165
SESSION IV: Non-AD and co-pathologies	165
Gatto, Rodolfo G.	166
Tau Burden Evaluation by [18F] Flortaucipir PET and Quantitative Tau Neuropathology in Alzheimer's Disease And Non-Alzheimer’s Tauopathies	166
Aguero, Cinthya	167
Pathologic Correlations of [18F]-Flortaucipir Imaging in non-Alzheimer Corticobasal Degeneration Syndrome	167
Chen, Yuheng	168
Unveiling the neurobiological basis of F18-flortaucipir in different tauopathies using voxel-to-voxel histology to PET comparisons: the role of p-tau, iron and MAOB	168
Chapleau, Marianne	171
Association of FDG-PET with co-pathologies in autopsy-proven AD.....	171
Thursday, January 12, 2023 - 08:30 am - 09:20 am	174
Podium Session	174

SESSION V: AD neuropathology	174
<i>Salvadó, Gemma</i>	175
Specific associations between plasma biomarkers and post-mortem amyloid plaque and neurofibrillary tau tangle loads	175
<i>Murray, Melissa</i>	179
Intersection of amyloid- β and tau brain pathology influences plasma phosphorylated tau levels.....	179
<i>Moloney, Christina M.</i>	181
Tangle maturity markers associate with tau PET and cognitive measures in hippocampus	181
<i>Betthausen, Tobey</i>	182
Postmortem validation of 18F-MK-6240 PET using autoradiography and in-vitro binding combined with antibody-based assays in frozen brains from two autopsy cases	182
Thursday, January 12, 2023 - 10:00 am - 10:45 am	183
Poster Session 2A	183
<i>Switzer, Aaron R.</i>	186
[P37] Regional [F18]AV1451 uptake in progressive apraxia of speech with and without Alzheimer’s disease, dysexecutive, and logopenic variants of Alzheimer’s disease	186
<i>Galli, Christopher</i>	188
[P38] Estimation of Native Spatial Resolution in Clinical Positron Emission Tomography Imaging Data	188
<i>Finn, Quentin</i>	191
[P39] Neuroinflammation Co-Localizes with Tau in Early-Onset MCI patients.....	191
<i>Engels-Domínguez, Nina</i>	192
[P40] Lower locus coeruleus integrity identifies elevated entorhinal tau in low amyloid individuals and is associated with faster clinical progression.....	192
<i>Winer, Joseph</i>	195
[P41] Substantia nigra 18F-PI-2620 PET signal is associated with motor impairment in Lewy body disease	195
<i>Ourry, Valentin</i>	198
[P42] Sex differences in A β and tau vulnerability in preclinical Alzheimer’s disease	198
<i>Whitlow, Christopher</i>	200
[P43] Alzheimer’s Network for Treatment and Diagnostics (ALZ-NET): Defining the future of Alzheimer's treatment, imaging and care	200
<i>Young, Christina</i>	201
[P44] Acquisition time corrections for SUVR analyses of [18F]-PI-2620	201
<i>Shirzadi, Zahra</i>	204
[P45] Longitudinal accumulation of white matter lesions is associated with amyloidosis and brain atrophy, but not systemic vascular risk	204
<i>Nemes, Sára</i>	207
[P46] Sex-associated differences in cerebrospinal fluid and plasma biomarkers in early-onset Alzheimer’s disease	207
<i>Saad, Ziad S.</i>	209
[P47] Correlations between Janssen Simoa plasma p217+tau and tau PET in participants screened for Janssen’s Autonomy Ph2 anti-tau trial in early Alzheimer’s Disease.....	209

Lui, Kitty	210
[P48] Sleep apnea and poor sleep quality are linked to tau deposition in older women at higher risk for Alzheimer's.....	210
Gebre, Robel	212
[P49] Machine Learning Based Tau Positivity Classification On Tau-PET Scans Considers Biological Variability And Can Aid In Decision Making	212
Johns, Emily	216
[P50] Impact of florbetaben acquisition timing on SUVR and centiloid values	216
Tempest, Paul	218
[P51] Postmortem In Vitro Binding of APN-1607 to PSP and HC Globus Pallidus Homogenates	218
Goodheart, Anna	220
[P52] Histone deacetylase tracer [11C]Martinostat behaves differently in amyloid versus synuclein rich regions in dementia with Lewy bodies	220
Krishnadas, Natasha	222
[P53] A CenTauR scale based on 18F-MK6240.....	222
Krishnadas, Natasha	225
[P54] Tau accumulation across the Alzheimer's disease continuum: an 18F-MK6240 AIBL study	225
Yang, Kao Lee	226
[P55] Multi-modal analysis of myelin and neurofilament light chain in individuals at risk for Alzheimer's disease using MRI, PET, and CSF biomarker assessments.....	226
Moody, Jason	229
[P56] The gut microbiota metabolite trimethylamine n-oxide is associated with white matter degeneration on the Alzheimer's disease continuum	229
Bischof, Gerard	231
[P57] In vivo measures of fibrillar beta-amyloid pathology limits cognitive plasticity in healthy aging: A multi-center intervention study.....	231
Oh, Minyoung	232
[P58] One Year Longitudinal Change of Tau Accumulation on [18F]PI-2620 PET in Alzheimer Spectrum.....	232
Coomans, Emma	233
[P59] The role of vascular pathology in the association between amyloid- β and tau in cognitively unimpaired individuals.....	233
Scott, Catherine J	236
[P60] Dual biomarker amyloid PET for improved subtype and stage inference.....	236
Leuzy, Antoine	238
[P61] Standardization of Tau PET using the CenTauR Scale: Preliminary findings from BioFINDER-2 using [18F]RO948 and [18F]Flortaucipir.....	238
Kostadinova, Ralitsa V	243
[P62] Plasma GFAP and NFL are correlated with measures of global cognition in EOAD and EOnonAD	243
Huang, Kuo-Lun	244
[P63] Comparisons of plasma biomarkers with 18F-Florzolotau PET in AD continuum – a pilot study.....	244

Hammers, Dustin	245
[P64] Validating Tau PET Staging Schemes in Relation to Cognitive Outcomes	245
Mayblyum, Danielle	246
[P65] Shared variance between FDG metabolism and PiB tracer delivery is not predictive of cognitive decline in preclinical AD	246
Phillips, Jeffrey	249
[P66] Amyloid and tau PET are associated with plasma phosphorylated tau 181 and glial fibrillary acidic protein in a sample of heterogeneous dementia syndromes	249
Rahmouni, Nesrine	251
[P67] Combined and independent effects of hyperphosphorylation of tau on microglial activation	251
Hanseeuw, Bernard	254
[P68] Cognitive impairment is more closely associated with the regional extension of F18MK6240 tau-PET signal than with PET signal intensity or CSF tau measures	254
Hojjati, Seyed Hani	257
[P69] Disentangling spatial-temporal remote interaction between tau and Amyloid- β proteins in different stages of tau aggregations	257
Tanner, Jeremy	259
[P70] Predictors of Discordance Between Pre-PET Clinical Diagnosis and Amyloid-PET Results in the Imaging Dementia—Evidence for Amyloid Scanning (IDEAS) Study	259
Cohen, Ann	262
[P71] Mid-life atherosclerotic cardiovascular disease risk score and late-life AT(N) measures	262
Koops, Elouise A.	263
[P72] A clinical diagnosis of Alzheimer’s disease and CSF-based tau positivity are both associated with lower locus coeruleus metabolism	263
Thursday, January 12, 2023 - 10:45 am - 11:50 am	267
Podium Session	267
SESSION VI: Heterogeneity in the AD cascade	267
Zammit, Matt	268
Longitudinal increases in tau emerge alongside early amyloid change in Down syndrome	268
Mundada, Nidhi	271
Cross-sectional and longitudinal associations between amyloid- and tau-PET in early-onset Alzheimer’s Disease: update from the LEADS study	271
Younes, Kyan	274
Amyloid PET Burden Predicts Longitudinal Cognitive Trajectories in a Heterogeneous ADRD Cohort	274
Schultz, Stephanie	276
Variations in gamma-secretase function across PSEN1 pathogenic variants strongly predict the clinical, cognitive, and biomarker progression of autosomal dominant Alzheimer’s disease	276
Thursday, January 12, 2023 - 01:15 pm - 02:35 pm	280
Podium Session	280
SESSION VII: Tau PET and MRI: multimodality insights	280
Ottoy, Julie	281
Mapping tau accumulation to the functional and structural organization of the brain in Alzheimer’s disease	281

<i>Singleton, Ellen</i>	283
Baseline tau PET shows stronger associations with cognitive and behavioral changes over time than cortical thickness.....	283
<i>Bueichekú, Elisenda</i>	286
A Central Role of Locus Coeruleus in the Initial Spatiotemporal Progression of Tau and its Contribution to Cognition	286
<i>Diez, Ibai</i>	289
Tau Propagation in the Brain Olfactory Circuits Contributes to Smell Perception Changes in Aging.....	289
<i>Adams, Jenna</i>	293
Medial temporal lobe subregional microstructure measured with ultra-high resolution diffusion imaging as a biomarker for early tau pathology and memory impairment	293
Thursday, January 12, 2023 - 03:00 pm - 03:45 pm	296
KEYNOTE: On making neuroimaging studies more equitable, inclusive, and relevant	296
<i>Monica Rivera-Mindt</i>	296
Thursday, January 12, 2023 - 04:30 pm - 05:20 pm	297
Podium Session	297
SESSION VIII: Lifestyle and lived experiences	297
<i>Royse, Sarah</i>	298
African American racialization modifies the association between apolipoprotein-E4 and amyloid deposition....	298
<i>Landau, Susan</i>	299
Cardiovascular risk and AD biomarkers in unimpaired older adults: A comparison of U.S. POINTER and ADNI	299
<i>Groechel, Renee</i>	301
Association between mid-life social factors and estimated late life amyloid burden: the Atherosclerosis Risk in Communities (ARIC)-PET study.....	301
Friday, January 13, 2023 - 09:00 am - 10:20 am	303
Podium Session	303
SESSION IX: Longitudinal change in tau and amyloid markers	303
<i>Fonseca, Corrina S.</i>	304
Longitudinal tau accumulation is associated with faster memory decline in typical aging and preclinical Alzheimer's disease	304
<i>Tissot, Cécile</i>	308
The use of plasma markers to predict tau accumulation in a stage-specific manner	308
<i>Betthausen, Tobey</i>	311
Temporal dynamics of plasma pTau217 and amyloid PET in preclinical AD	311
<i>Bilgel, Murat</i>	314
Longitudinal changes in Alzheimer's disease-related plasma biomarkers in relation to changes in PiB PET measures of brain amyloid.....	314
<i>Mohammediyani, BA, Bery</i>	318
Longitudinal bidirectional associations between sleep and Alzheimer's pathology in At-Risk Cognitively Unimpaired Older Adults.....	318
Friday, January 13, 2023 - 10:45 am - 11:30 am	320

POSTER SESSION 3A	320
Gong, Kuang	323
P73 Motion and partial volume corrections in dynamic [18F]-MK6240 PET imaging	323
Fernandez, Jaime	325
P74 Encoding, consolidation and retrieval deficits are differentially shaped by tau and atrophy in the Alzheimer's disease spectrum	325
Abiose, Olamide	328
P75 Comorbid medical conditions, anxiety, and amyloid- β pathology in cognitively unimpaired older adults ..	328
Buckley, Rachel	329
P76 Defining and characterizing neocortical tau resistance in preclinical Alzheimer's disease	329
Luo, Weiquan	332
P77 Development and evaluation of image preprocessing pipelines for the Centiloid method	332
Townsend, Diana	336
P78 Cognitively estimated disease time: Associations with amyloid and tau burden in the Harvard Aging Brain Study	336
Wang, Yi-Ting	338
P79 Synergistic interaction between sex, amyloid and phosphorylated tau predicts the longitudinal progression of tau tangles	338
Blazhenets, Ganna	341
P80 [18F]PI-2620 binding patterns in patients with suspected AD- and FTLD-tauopathies	341
DiFilippo, Alexandra	344
P81 Regional analysis of change in synaptic density over time by cognitive status	344
Kotari, Vikas	347
P82 Regional tau profiles in early tau pathology populations	347
Coath, William	351
P83 [18F]MK-6240 tau-PET in an A β -enriched sample from the 1946 British birth cohort - Insight 46	351
Munro, Catherine	354
P84 Longitudinal trajectories of depressive symptoms and regional amyloid accumulation (PiB PET) in clinically normal older adults	354
Properzi, Michael	356
P85 Improving sub-threshold PiB fidelity using relative radioligand delivery	356
Farrell, Michelle E	360
P86 Improved prediction of preclinical cognitive decline using amyloid PET spatial extent	360
Alosco, Michael	364
P87 18F-MK-6240 Tau PET as a Potential Biomarker for Chronic Traumatic Encephalopathy	364
Johnson, Aubrey S	367
P88 Psychosis and tau burden across the AD continuum	367
Boyle, Rory	369
P89 Classifying cognitive resilience to differing levels of Alzheimer's disease pathology	369
Manchella, Mohit	372

P90	Cerebrospinal fluid neurofilament light predicts increased amyloid, tau, and decreased grey matter density	372
Royse, Sarah		374
P91	Unhealthy white matter connectivity in African American and non-Hispanic white older adults.....	374
Jacobs, Heidi IL		375
P92	Locus coeruleus integrity as neural substrate providing resilience against cognitive decline in the face of Alzheimer's disease pathology	375
Smegal, Lindsay		377
P93	Lower locus coeruleus integrity predicts diminished practice effects in cognitively normal older individuals	377
C. Macedo, Arthur		380
P94	PET-based Braak staging predicts neuropsychiatric burden in the Alzheimer's disease continuum	380
Rahimabadi, Arsalan		382
P95	A computational model to study the combined effect of neuronal connectivity loss and tauopathy progression.....	382
McLachlan, Max		386
P96	Simulated dose reduction in longitudinal [18F]MK-6240 PET	386
Thibault, Emma		389
P97	Regional amyloid change improves prediction of future tau progression over global metrics	389
Cody, Karly		393
P99	Rates of tau PET accumulation along the amyloid timeline in Alzheimer's disease	393
Wang, Xin		396
P100	Body mass index, pathological tau, and cognition in preclinical AD: Could women with high BMI be protected?.....	396
Servaes, Stijn		399
P101	Amyloid drives later tau accumulation for fast progressors in early Braak stages.....	399
Hobbs, Diana		401
P102	Brain-wide and AD-risk genetic expression: A descriptive study.....	401
Ziontz, Jacob		402
P103	Behavioral brain networks underlying the effect of Alzheimer's pathology on cognition	402
Huang, Shao-Yi		406
P104	Exploration of 18F-Florzolotau tau PET distribution patterns using machine learning approach in AD ...	406
Rizvi, Batoool		408
P105	The interplay of vascular disease, peripheral interleukin-6, beta-amyloid, and memory in older adults....	408
Heston, Margo		409
P106	Gut microbiome composition is associated with cortical amyloid burden in a preclinical human cohort ..	409
Lee, Zih-Ning		412
P107	Study on MR-free template-based spatial normalization for Tau PET Image Quantitation using 18F-Florzolotau	412

<i>Vaska, Paul</i>	415
[P108] β -Amyloid in World Trade Center responders: Result indicate age-related toxic encephalopathy mediated by an immunogenic amyloid response.....	415
<i>Lois, Cristina</i>	416
[P109] [18F]MK-6240 PET/MRI Test-Retest performance in cognitively normal elderly subjects	416
Friday, January 13, 2023 - 11:30 am - 01:50 pm.....	419
Podium Session.....	419
SESSION X: Fluid biomarkers in AD	419
<i>Sperling, Reisa</i>	420
Plasma p-tau ₂₁₇ ratios associated with amyloid and tau PET measures in preclinical AD: Findings from the AHEAD 3-45 Study screening data.....	420
<i>Therriault, Joseph</i>	422
Plasma biomarkers as stand-alone tests to rule out Alzheimer's disease	422
<i>Algeciras-Schimmich, Alicia</i>	427
Comparative performance of three plasma A β ₄₂ /A β ₄₀ and two plasma p-tau ₁₈₁ assays versus amyloid-PET imaging status	427
<i>Feizpour, Azadeh</i>	428
Prognostic utility of plasma p ₂₁₇ +tau vs amyloid and tau PET in the Alzheimer continuum	428
<i>Logan, Paige E.</i>	429
Associations of blood biomarkers with early-onset Alzheimer's disease pathology.....	429
<i>Bluma, Marina</i>	431
Associations between amyloid PET, CSF pTau, and plasma biomarkers in memory clinic patients.....	431
Friday, January 13, 2023 - 02:30 pm - 03:15 pm.....	432
KEYNOTE: Biofluids and imaging: two sides of the same coin	432
<i>Thomas Karikari</i>	432
Friday, January 13, 2023 - 04:15 pm - 05:05 pm.....	433
Podium Session.....	433
SESSION XI: Plasma with other modalities	433
<i>Coughlan, Gillian</i>	434
Plasma biomarkers associated with cortical brain structure and multi-domain cognition in Alzheimer's disease and Parkinson's disease	434
<i>Hall, Brandon</i>	436
Relationships of blood insulin with brain structures and plasma A β ₄₂ to A β ₄₀ ratio in a multi-ethnic cohort of older adults.....	436
<i>Kang, Min Su</i>	437
Unique biological pathways associated with plasma ptau species and AD PET: an imaging-transcriptomic study	437

Welcome!

With two editions missed due to the pandemic, I am thrilled that we will reconnect at the 15th edition of the Human Amyloid Imaging Conference hosted in Miami, Florida on January 11-13, 2023.

At this edition, Drs. Bill Klunk (University of Pittsburgh), Chet Mathis (University of Pittsburgh) and Bill Jagust (University of California, Berkeley), my co-conveners of the past 15 years will retire from their organizing "seat" at the organizers' table. With this occasion, I would like to express my profound gratitude for their incredible work and support rendered to HAI in co-organizing this event.

And so, we welcome four new members of the renewed Executive Committee, namely Drs. Teresa Gomez-Isla, Thomas Karikari, Beth Mormino and Julie Price!

At HAI 2023, our lively discussions will continue to spring from brief presentations by active investigators who will report on unpublished, cutting-edge research in human imaging of amyloid-beta, tau and/or other biomarkers that pertain to dementia and Alzheimer's disease related disorders.

We invite you to take part in all podium and poster session across the three days, register to participate in our mentor program, network at the two receptions of Wednesday and Thursday and engage with your fellow researchers.

HAI is most grateful for the generous sponsors of this event, its Executive and Program Committees alongside the Theme Co-chairs, presenters, guest lecturers, audience and all HAI fans around the globe!

Looking forward to a great new edition,



Keith A. Johnson, MD
Massachusetts General Hospital

HAI 2023 TEAM

HAI 2023 Executive Committee

Keith Johnson, MD, *Massachusetts General Hospital*

Maria Carrillo, PhD, *Alzheimer's Association*

Teresa Gomez-Isla, MD, *Massachusetts General Hospital*

Thomas Karikari, PhD, *University of Pittsburgh*

Beth Mormino, PhD, *Stanford University*

Julie Price, PhD, *Massachusetts General Hospital*

HAI 2023 Theme Co-chairs

Suzanne Baker, PhD, *Lawrence Berkeley National Laboratory*

Tobey Betthausen, PhD, *University of Wisconsin*

Anne Cohen, PhD, *University of Pittsburgh*

Brad Christian, PhD, *University of Wisconsin*

Ansel Hillmer, PhD, *Yale University School of Medicine*

Milos Ikonovic, MD, *University of Pittsburgh*

Heidi Jacobs, PhD, *Massachusetts General Hospital*

Thomas Karikari, PhD, *University of Pittsburgh*

Susan Landau, PhD, *University of California, Berkeley*

Laetitia Lemoine, PhD, *Karolinska Institute*

Beth Mormino, PhD, *Stanford University*

Melissa Murray, PhD, *Mayo Clinic*

Julie Price, PhD, *Harvard Medical School*

Gil Rabinovici, MD, *University of California, San Francisco*

Pedro Rosa-Neto, PhD, *McGill University*

Suzanne Schindler, MD, PhD, *Washington University in St Louis*

Henrik Zetterberg, MD, *University of Gothenburg*

HAI 2023 Program Committee

Suzanne Baker, PhD, *Lawrence Berkeley National Laboratory*

Olivier Barret, PhD, *CEA / University Paris-Saclay*

Tobey Betthausen, PhD, *University of Wisconsin*

Brad Christian, PhD, *University of Wisconsin*

Anne Cohen, PhD, *University of Pittsburgh*

Teresa Gomez-Isla, MD, *Massachusetts General Hospital*

Roger Gunn, PhD, *Imperial College*

Ansel Hillmer, PhD, *Yale University*

Kenji Ishii, MD, *Tokyo Metropolitan Inst. of Gerontology*

Milos Ikonovic, MD, *University of Pittsburgh*

Clifford R. Jack, MD, *Mayo Clinic*

Heidi Jacobs, PhD, *Massachusetts General Hospital*

Robert A. Koeppe, PhD, *University of Michigan*

Renaud La Joie, PhD, *University of California, San Francisco*

Susan Landau, PhD, *University of California, Berkeley*

Laetitia Lemoine, PhD, *Karolinska Institute*

Beth Mormino, PhD, *Stanford University*

Melissa Murray, PhD, *Mayo Clinic*

Pedro Rosa-Neto, MD, PhD, *McGill University*

Agneta Nordberg, MD, PhD, *Karolinska Institute*

Rik Ossenkoppele, PhD, *VU University Medical Center*

Julie Ottoy, PhD, *University of Toronto*

Julie Price, PhD, *Harvard Medical School*

Gil Rabinovici, MD, *University of California, San Francisco*

Susan Resnick, PhD, *National Institute on Aging*

Stephen Salloway, MD, *Brown University*

Sandra Sanabria, PhD, *Genentech*

Suzanne Schindler, MD, PhD, *Washington University in St Louis*

Les Shaw, PhD, *Perelman School of Medicine*

Reisa Sperling, MD, *Brigham and Women's Hospital*

Rik Vandenberghe, MD, PhD, *KU Leuven*

Victor Villemagne, MD, *The University of Melbourne*

Sylvia Villeneuve, PhD, *McGill University*

Henrik Zetterberg, MD, *University of Gothenburg*

HAI2023 SUPPORT (GRANTS/SPONSORSHIP):



PLATINUM



GOLD/SCHOLARSHIPS



GOLD



SILVER



BRONZE



POSTER INDEX (by board number)

Board #	Poster Title	Authors	Presenter
01	Effects of de-facing PET and MRI scans on clinical correlations analyses	Schwarz Kremers Weigand Prakaashana Senjem Lowe Gunter Kantarci Vemuri Petersen Knopman Jack	Schwarz, Christopher
02	Non-invasive quantification and SUVR validation of [18F]-florbetaben with total-body EXPLORER PET	Holy Alfaro Fletcher Bhattarai Spencer Cherry DeCarli Fan	Holy, Emily
03	PET imaging probe development for aggregated alpha-synuclein	Gomperts Liu Bai Xu Rose Celikag Ndayisaba Khurana Bartels Wang	Gomperts, Stephen
04	Cross-modality transformer for low-dose tau PET imaging	Jang Lois Becker Thibault Price Johnson El Fakhri Gong	Gong, Kuang
05	Tau PET positivity reveals Alzheimer's disease related fast cognitive decline	Ioannou Bucci Nordberg Chiotis	Ioannou, Konstantinos
06	Positive 18F-APN-1607 tau PET imaging findings in patients with Progressive Supranuclear Palsy-like extrapyramidal symptoms caused by TBK1 mutations	Liu Lu Sun Li Yen Jang Zuo Wang	Liu, Feng-Tao
07	In vivo visualization of tau deposits in corticobasal syndrome by 18F-Florzolotau PET	Liu Lu Li Jiao Chen Yao Liang Ge Li Shen Wu Sun Wu Yen Zuo Wang	Liu, Feng-Tao
08	Imaging neuroinflammation with astrocyte-PET and bio-fluid biomarkers in patients with cognitive impairment	Chiotis Jelic Rodriguez-Vieitez Savitscheva Wall Antoni Nordberg	Chiotis, Konstantinos
09	[18] Flortaucipir PET and Diffusion Tensor Tractography Coregistration can Enhance Detection of Brain Changes Associated with Progressive Apraxia of Speech	Gatto Duffy Utianski Clark Botha Machulda Lowe Josephs Whitwell	Gatto, Rodolfo G.
10	Towards a simplified flortaucipir-PET read method for assessing tau burden	Tunali Iaccarino Ducker Patel DiFabbio Kowaleski Arora Kim Lu Pontecorvo Shcherbinin	Tunali, Ilke
12	Digital clock drawing performance is associated with tau deposition measured with PET in preclinical Alzheimer's disease	Fu Rentz Mayblyum Thibault Buckley Das Papp Sperling Penney Davis Johnson Price	Fu, Jessie Fang-Lu
13	[18F]RO-948 Tau PET Retention and Correlation with Fluid Biomarkers in the Early AD Continuum	Shekari González Escalante Milà-Alomà Falcon Niñerola-Baizán Tonietto Borroni Klein J. Ashton K. Karikari Lantero-Rodriguez Snellman Ortiz Vanmechelen Minguillón Fauria Perissinotti Molinuevo Zetterberg Blennow Grau-Rivera Suárez-Calvet Domingo Gispert	Shekari, Mahnaz
14	Regional tau predicts glucose hypometabolism in autosomal dominant Alzheimer's disease: Findings from the Colombia-Boston (COLBOS) biomarker study	Langella Kaplan Baena Londono Munera Vila-Castelar Alvarez Vidal Properzi Sanchez Sperling Johnson Lopera Hanseeuw Quiroz	Langella, Stephanie
15	Is tau PET a robust biomarker for chronic traumatic encephalopathy?	Krishnadas Doré Lamb Guzman Ponsford Hicks Williams Feizpour Villemagne Rowe	Krishnadas, Natasha

Board #	Poster Title	Authors	Presenter
16	Centiloid scale measure of amyloid PET by CT of PET/CT equipment	Matsuda Hanyu Kaneko	Matsuda, Hiroshi
17	Successful cognitive aging is associated with less brain atrophy and lower tau deposition	Pezzoli Giorgio Harrison Martersteck Jagust	Pezzoli, Stefania
18	Subcortical flortaucipir PET and susceptibility analyses to differentiate progressive supranuclear palsy clinical variants and corticobasal syndrome	Satoh Arani Schwarz Senjem Ali Jack Lowe Josephs Whitwell	Satoh, Ryota
19	Temporal associations of plasma and PET Alzheimer's disease biomarkers using a non-linear mixed effects model	Cogswell Lundt Therneau Graff-Radford Schwarz Senjem Gunter Vemuri Petersen Jack Jr	Cogswell, Petrice
20	Beta-amyloid accumulates at a faster rate in individuals with Down syndrome	McVea DiFilippo McLachlan Murali Zammit Johnson Betthausen Stone Tudorascu Laymon Klunk Cohen Handen Christian	McVea, Andrew
21	Magnitude of MK6240 off-target binding correlated with spill-in effects in target regions	McVea DiFilippo McLachlan Johnson Betthausen Christian	McVea, Andrew
22	Amyloid and tau pathology associated with different cognitive declines in cognitively normal older people	Chen Juarez Baker Harrison Landau Jagust	Chen, Xi
23	Future amyloid accumulation status affects the preservation of peripheral whole-blood gene co-expression networks at baseline in asymptomatic Alzheimer's disease	Luckett Zielonka Schaefferbeke Adamczuk Van Laere Dupont Cleyen Vandenberghe	Luckett, Emma
24	Validation of [18F]florbetaben PET quantitation based on the analysis of 15 software pipelines	Jovalekic Roé-Vellvé Koglin Lagos Quintana Nelson Diemling Lilja Gómez González Doré Bourgeat Whittington Gunn Stephens Bullich	Stephens, Andrew
25	Preprocessing 10,700 real-world amyloid-PET scans from the IDEAS study: the Good, the Bad and the Ugly	Mejia Perez Mundada Blazhenets Soleimani-Meigooni Zeltzer Cho Ranasinghe Windon Yadollahikhales Iaccarino Carrillo Gatsonis March Apgar Siegel Hilner Whitmer Rabinovici La Joie	Mejia Perez, Jhony
26	Longitudinal tau-PET differs between progressive apraxia of speech subtypes	Tetzloff Martin Duffy Clark Utianski Botha Machulda Schwarz Senjem Jack Jr. Lowe Josephs Whitwell	Tetzloff, Katerina A.
27	Cross-sectional PET Analyses in the Longitudinal Early-onset Alzheimer's Disease Study (LEADS)	Cho Mundada Apostolova Carrillo Shankar Amuri Zeltzer Windon Soleimani Meigooni Tanner Lawhn Heath Aisen Eloyan Koeppe Iaccarino Dickerson La Joie Rabinovici	Cho, Hanna
28	Dynamic amyloid PET: relationships to tau PET and cognition in Alzheimer's disease	Raman Charniaux Murchison Fang Tzabari Liu Morris Chen Joseph-Mathurin Ponisio Flores Kennedy Benzinger Roberson McConathy	Raman, Fabio
29	Spatial extent and intensity of Alzheimer-associated tau PET burden is greater in agrammatic than logopenic primary progressive aphasia	Martersteck Sridhar Coventry Weintraub Mesulam Rogalski	Martersteck, Adam
30	Comparing PI2620 and Flortaucipir in Progressive Supranuclear Palsy Subjects	Thomas Blazhenets La Joie Rabinovici Heuer Jagust Boxer Baker	Thomas, Wesley
31	Assessing a universal neocortical mask for Centiloid quantification	Bourgeat Dore Rowe Benzinger Tosun Goyal LaMontagne Jin Weiner Morris Masters Fripp Villemagne	Feizpour, Azadeh

Board #	Poster Title	Authors	Presenter
32	Relationships between Neuronal Hyperactivity, Stress Susceptibility, and Alzheimer's Disease pathology	Sharp Razlighi Oh	Oh, Hwamee
33	A/T/N, cognitive, health and lifestyle differences across white matter hyperintensities groups in aged 45-85 years adults: Results from the Wisconsin Registry for Alzheimer's Prevention (WRAP)	Du Burghy Cody Hermann Jonaitis Betthausen Chin Cadman Rivera-Rivera Peret Johnson Rowley Pompa Lose Christian Janelidze Hansson Johnson Eisenmenger Koscik	Du, Lianlian
34	Medial temporal 18F-MK6240 levels are associated with global graph characteristics of functional connectivity from high-density EEG in the asymptomatic and prodromal stage of Alzheimer disease	Spruyt Reinartz Meade Khachatryan Van Hulle Van Laere Dupont Vandenberghe	Spruyt, Laure
35	Longitudinal PET assessments of tau pathologies in progressive supranuclear palsy with 18F-florzolotau (PM-PBB3/APN-1607)	Endo Takado Tagai Matsuoka Kokubo Hirata Kataoka Oya Matsumoto Kurose Ichihashi Hatano Saiki Hirano Nakano Furukawa Takeda Iose Imai Yagi Nishida Yuasa Ono Seki Takahata Tokuda Shinotoh Shimada Kawamura Zhang Higuchi	Endo, Hironobu
36	Head-to-head comparison of tau PET tracers [18F]PI2620 and [18F]RO948 in non-demented individuals with brain amyloid deposition: the TAU-PET FACEHBI cohort	Klein Marquié Sotolongo-Grau Roé-Vellvé Bullich Tartari Sanabria García-Sánchez Borroni Galli Tonietto Pérez-Martínez Tárraga Ruiz Stephens Boada	Klein, Gregory
37	Regional [F18]AV1451 uptake in progressive apraxia of speech with and without Alzheimer's disease, dysexecutive, and logopenic variants of Alzheimer's disease	Switzer Corriveau-Lecavalier Lowe Jones Ramanan Machulda Graff-Radford Boeve Knopman Jack Petersen Josephs Whitwell Botha	Switzer, Aaron R
38	Estimation of Native Spatial Resolution in Clinical Positron Emission Tomography Imaging Data	Galli Tonietto Klein Holiga Miho Knopf	Galli, Christopher
39	Neuroinflammation Co-Localizes with Tau in Early-Onset MCI patients	Finn Appleton Bradbury Yu Faridar Beers Appel Fujita Masdeu Pascual	Finn, Quentin
40	Lower locus coeruleus integrity identifies elevated entorhinal tau in low amyloid individuals and is associated with faster clinical progression	Engels-Domínguez A. Koops M. Riphagen F. Smegal Bueichekú Becker M. Kwong M. Rentz H. Salat A. Sperling A. Johnson I. L. Jacobs	Engels-Domínguez, Nina
41	Substantia nigra 18F-PI-2620 PET signal is associated with motor impairment in Lewy body disease	Winer Vossler Young Romero Shahid Abdelnour Anders Shen Mormino Poston	Winer, Joseph
42	Sex differences in A β and tau vulnerability in preclinical Alzheimer's disease	Ourry St-Onge Mohammediyan Yakoub Soucy Poirier Breitner Villeneuve	Ourry, Valentin
43	Alzheimer's Network for Treatment and Diagnostics (ALZ-NET): Defining the future of Alzheimer's treatment, imaging and care	Whitlow March Rabinovici Rafii Atri Daffner Edelmayer Gatsonis Lopez Porsteinsson Possin Salloway Sano Snyder Vukmir Wilkins Windon Carrillo	Whitlow, Christopher
44	Acquisition time corrections for SUVR analyses of [18F]-PI-2620	Young Vossler Winer Romero Anders Shen Poston Davidzon Mormino	Young, Christina
45	Longitudinal accumulation of white matter lesions is associated with	Shirzadi Schultz Yau Fitzpatrick Levin Joseph-Mathurin Kantarci Preboske Jack Jr. Farlow	Shirzadi, Zahra

Board #	Poster Title	Authors	Presenter
	amyloidosis and brain atrophy, but not systemic vascular risk	Fagan Hassenstab Jucker Morris Xiong Karch Levey Gordon Schofield Salloway Perrin McDade Levin Cruchaga Allegri Fox Goate Day Koeppe Noble Chui Berman Mori Sanchez-Valle Lee Rosa-Neto Ruthirakuhan Wu Swardfager Benzinger Sohrabi Martins Schultz Bateman Johnson Sperling Greenberg Chhatwal	
46	Sex-associated differences in cerebrospinal fluid and plasma biomarkers in early-onset Alzheimer's disease	Nemes Logan Dage Fagan Hammers Manchella Eloyan Kostadinova Foroud Zetterberg Koeppe Aisen Carrillo Rabinovici Dickerson Apostolova	Nemes, Sára
47	Correlations between Janssen Simoa plasma p217+tau and tau PET in participants screened for Janssen's Autonomy Ph2 anti-tau trial in early Alzheimer's Disease	Saad Triana-Blatzer Moughadam Slemmon Henley Kolb	Saad, Ziad S.
48	Sleep apnea and poor sleep quality are linked to tau deposition in older women at higher risk for Alzheimer's	Lui Shepherd Wang Bernier Bosompra DeYoung Malhotra Sundermann Banks	Lui, Kitty
49	Machine Learning Based Tau Positivity Classification On Tau-PET Scans Considers Biological Variability And Can Aid In Decision Making	Gebre Rial Raghavan Sparrman Wiste Schwarz Lowe Graff-Radford Knopman Petersen Schöll Jack Jr Vemuri	Gebre, Robel
50	Impact of florbetaben acquisition timing on SUVR and centiloid values	Johns Kennedy Young Younes Vossler Poston Davidzon Mormino	Johns, Emily
51	Postmortem In Vitro Binding of APN-1607 to PSP and HC Globus Pallidus Homogenates	Tempest Margolin Paget Campbell Navia	Tempest, Paul
52	Histone deacetylase tracer [11C]Martinostat behaves differently in amyloid versus synuclein rich regions in dementia with Lewy bodies	Goodheart Yoo Striar Quan Wey Wang Gomperts	Goodheart, Anna
53	A CenTauR scale based on 18F-MK6240	Dore Bourgeat Leuzy Huang Krishnadas Feizpour Fripp Villemagne Rowe	Krishnadas, Natasha
54	Tau accumulation across the Alzheimer's disease continuum: an 18F-MK6240 AIBL study	Krishnadas Doré Robertson Ward Fowler Masters Bourgeat Fripp Villemagne Rowe	Krishnadas, Natasha
55	Multi-modal analysis of myelin and neurofilament light chain in individuals at risk for Alzheimer's disease using MRI, PET, and CSF biomarker assessments	Yang Dean III Betthausen Carlsson Johnson Blennow Zetterberg Alexander Bendlin	Yang, Kao Lee
56	The gut microbiota metabolite trimethylamine n-oxide is associated with white matter degeneration on the Alzheimer's disease continuum	Moody Heston Zarbock Blennow Zetterberg Rey Ulland Bendlin	Moody, Jason
57	In vivo measures of fibrillar beta-amyloid pathology limits cognitive plasticity in healthy aging: A multi-center intervention study.	Bischof Fellerhoff Giehl Drzezga	Bischof, Gerard
58	One Year Longitudinal Change of Tau Accumulation on [18F]PI-2620 PET in Alzheimer Spectrum	Oh Oh Lee Oh Seo Roh Lee Kim	Oh, Minyoung

Board #	Poster Title	Authors	Presenter
59	The role of vascular pathology in the association between amyloid- β and tau in cognitively unimpaired individuals	Coomans van Westen Pichet Binette Strandberg Spotorno Palmqvist Stomrud Ossenkoppele Hansson	Coomans, Emma
60	Dual biomarker amyloid PET for improved subtype and stage inference	Scott Coath Dickson McQuaid Cash Schott	Scott, Catherine J
61	Standardization of Tau PET using the CenTauR Scale: Preliminary findings from BioFINDER-2 using [18F]RO948 and [18F]Flortaucipir	Leuzy Doré Klein Collins Henscheid Hostetler Iaccarino Karten Kolb Ossenkoppele Pappas Pontecorvo Saad Mathotaarachchi Sivakuraman Smith Rowe Villemagne Hansson	Leuzy, Antoine
62	Plasma GFAP and NFL are correlated with measures of global cognition in EOAD and EOnonAD	Kostadinova Hammers Logan Manchella Nemes Fagan Foroud Zetterberg Kramer Aisen Carrillo Rabinovici Dickerson Apostolova Dage	Kostadinova, Ralitsa V.
63	Comparisons of plasma biomarkers with 18F-Florzolotau PET in AD continuum – a pilot study	Huang Ing-Tsung Lin Huang	Huang, Kuo-Lun
64	Validating Tau PET Staging Schemes in Relation to Cognitive Outcomes	Hammers Lin Logan Risacher Schwarz Apostolova	Hammers, Dustin
65	Shared variance between FDG metabolism and PiB tracer delivery is not predictive of cognitive decline in preclinical AD	Mayblyum Shirzadi Becker Chhatwal Farrell Jacobs Guehl El Fakhri Sperling Price Johnson Schultz Hanseeuw	Mayblyum, Danielle
66	Amyloid and tau PET are associated with plasma phosphorylated tau 181 and glial fibrillary acidic protein in a sample of heterogeneous dementia syndromes	Cousins Phillips Das Fulop Nasrallah O'Brien McMillan Irwin Massimo Grossman Wolk	Phillips, Jeffrey
67	Combined and independent effects of hyperphosphorylation of tau on microglial activation	Rahmouni Therriault Tissot L. Benedet Ashton Triana-Baltzer Lussier Servaes Macedo Stevenson Stevenson Kunach Fernandez-Arias Wang Gauthier Kolb Karikari Zetterberg Blennow Pascoal Rosa-Neto	Rahmouni, Nesrine
68	Cognitive impairment is more closely associated with the regional extension of F18MK6240 tau-PET signal than with PET signal intensity or CSF tau measures	Hanseeuw Gerard Malotau Colmant Quenon Ivanoiu Lhommel	Hanseeuw, Bernard
69	Disentangling spatial-temporal remote interaction between tau and Amyloid- β proteins in different stages of tau aggregations	Hojjati Feiz Nayak Shteingart Ozoria Fernández Devanand Luchsinger Stern Razlighi	Hojjati, Seyed Hani
70	Predictors of Discordance Between Pre-PET Clinical Diagnosis and Amyloid-PET Results in the Imaging Dementia—Evidence for Amyloid Scanning (IDEAS) Study	Tanner La Joie Hanna Iaccarino Allen Siegel Hillner Whitmer Gatsonis Carrillo Rabinovici	Tanner, Jeremy
71	Mid-life atherosclerotic cardiovascular disease risk score and late-life AT(N) measures	Saeed Chang Royse Lopresti Snitz Villemagne Reis Lopez Cohen	Cohen, Ann
72	A clinical diagnosis of Alzheimer's disease and CSF-based tau positivity are both associated with lower locus coeruleus metabolism	Koops Dutta Becker Van Egroo Riphagen Prokopiou Hanseeuw Sperling El Fakhri Johnson Jacobs	Koops, Elouise A.
73	Motion and partial volume corrections in dynamic [18F]-MK6240 PET imaging	Tiss Gong Lois Becker Thibault Guehl Xia Normandin Ouyang Johnson El Fakhri	Gong, Kuang

Board #	Poster Title	Authors	Presenter
74	Encoding, consolidation and retrieval deficits are differentially shaped by tau and atrophy in the Alzheimer's disease spectrum	Fernandez Therriault Lussier Bezgin Tissot Servaes Wang Matothararchchi Stevenson Rahmouni Kang Pallen Kunach Quispialaya Margherita-Poltronetti Pascoal Rosa-Neto	Fernandez, Jaime
75	Comorbid medical conditions, anxiety, and amyloid- β pathology in cognitively unimpaired older adults	Abiose Young Winer Deters Mormino	Abiose, Olamide
76	Defining and characterizing neocortical tau resistance in preclinical Alzheimer's disease	Buckley Klinger Boyle Coughlan Hanseeuw Yang Amariglio Rentz Townsend Farrell Jacobs Shirzadi Yau Price Chhatwal Schultz Hohman Donohue Properzi Johnson Sperling	Buckley, Rachel
77	Development and evaluation of image preprocessing pipelines for the Centiloid method	Luo Minhas Rubenstein Situ Royle Ances Christian Cohen Handen Klunk Tudorascu Zamon Laymon	Luo, Weiquan
78	Cognitively estimated disease time: Associations with amyloid and tau burden in the Harvard Aging Brain Study	Townsend Properzi Betthausen Klinger Boyle Coughlan Hanseeuw Yang Amariglio Farrell Jacobs Shirzadi Yau Price Chhatwal Rentz Johnson Sperling Schultz Buckley	Townsend, Diana
79	Synergistic interaction between sex, amyloid and phosphorylated tau predicts the longitudinal progression of tau tangles	Wang Therriault Servaes Tissot Fernandez Arias Rahmouni Macedo Stevenson Stevenson Haeger Hosseini Nazneen Rosa-Neto	Wang, Yi-Ting
80	[18F]PI-2620 binding patterns in patients with suspected AD- and FTLD-tauopathies	Blazhenets Soleimani-Meigooni Thomas Brendel Vento VandeVrede Heuer Ljubenkov Rojas Chen Iaccarino Mundada Litvan Grossman Boeve Pantelyat Tartaglia Irwin Dickerson Baker Boxer Rabinovici La Joie	Blazhenets, Ganna
81	Regional analysis of change in synaptic density over time by cognitive status	DiFilippo Mcvea Mclachlan Pasquesi Davenport-Sis Jonaitis Ennis Betthausen Engle Johnson Bendlin Christian	DiFilippo, Alexandra
82	Regional tau profiles in early tau pathology populations	Kotari Morris Svaldi Southekal Lu Pontecorvo Collins Shcherbinin Neuroimaging Initiative	Kotari, Vikas
83	[18F]MK-6240 tau-PET in an A β -enriched sample from the 1946 British birth cohort - Insight 46	Coath Markiewicz Modat Scott Malone Thomas Dickson Schöll Ourselin Richards Fox Cash Schott	Coath, William
84	Longitudinal trajectories of depressive symptoms and regional amyloid accumulation (PiB PET) in clinically normal older adults	Munro Farrell Hanseeuw Buckley Properzi Vannini Amariglio Quiroz Blacker Rentz Sperling Johnson Marshall Gatchel	Munro, Catherine
85	Improving sub-threshold PiB fidelity using relative radioligand delivery	Properzi Shirzadi Buckley Klinger Hanseeuw Amariglio Rentz Farrell Price Chhatwal Marshall Gatchel Johnson Sperling Schultz	Properzi, Michael
86	Improved prediction of preclinical cognitive decline using amyloid PET spatial extent	Farrell Thibault Becker Price Hanseeuw Buckley Papp Jacobs Rentz Sperling Johnson	Farrell, Michelle E.
87	18F-MK-6240 Tau PET as a Potential Biomarker for Chronic Traumatic Encephalopathy	Alosco Mundada La Joie Asken Nowinski Smith Culhane Shankar Amuri Pettway Iaccarino Windon Tripodis Mercier Kowall Stein Grinberg McKee Stern Miller Mez Killiany Rabinovici	Alosco, Michael
88	Psychosis and tau burden across the AD continuum	Johnson* Ziaggi* Huey, MD Kreisl, MD Talmasov, MD Lao, PhD	Johnson, Aubrey S.
89	Classifying cognitive resilience to differing levels of Alzheimer's disease pathology	Boyle Townsend Klinger Coughlan Hanseeuw Yang Amariglio Farrell Jacobs Shirzadi Yau	Boyle, Rory

Board #	Poster Title	Authors	Presenter
		Price Chhatwal Schultz Hohman Donohue Properzi Rentz Johnson Sperling Buckley	
90	Cerebrospinal fluid neurofilament light predicts increased amyloid, tau, and decreased grey matter density	Manchella Logan Dage Hammers Nemes Kostadinova Eloyan Mundada La Joie Iaccarino Fagan Foroud Zetterberg Koeppe Aisen Carrillo Rabinovici Dickerson Apostolova	Manchella, Mohit
91	Unhealthy white matter connectivity in African American and non-Hispanic white older adults	Royse Snitz Hengenius Huppert Roush Cisneros Potopenko Becker Cohen Shaaban	Royse, Sarah
92	Locus coeruleus integrity as neural substrate providing resilience against cognitive decline in the face of Alzheimer's disease pathology	Jacobs Papp Buckley Riphagen Hanseeuw Boyle Donovan Rentz Sperling Johnson	Jacobs, Heidi IL
93	Lower locus coeruleus integrity predicts diminished practice effects in cognitively normal older individuals	Smegal Schneider Jutten Rentz Johnson Sperling Papp Jacobs	Smegal, Lindsay
94	PET-based Braak staging predicts neuropsychiatric burden in the Alzheimer's disease continuum	Macedo Tissot Therriault Servaes Rahmouni Fernandez-Arias Z. Lussier Stevenson Wang Quispialaya Socualaya Nazneen Ali Hosseini Kunach Haeger Stevenson Vitali A. Pascoal Rosa-Neto	C. Macedo, Arthur
95	A computational model to study the combined effect of neuronal connectivity loss and tauopathy progression	Rahimabadi Soucy Benali	Rahimabadi, Arsalan
96	Simulated dose reduction in longitudinal [18F]MK-6240 PET	McLachlan McVea DiFilippo Schöll Betthausen Johnson Christian	McLachlan, Max
97	Regional amyloid change improves prediction of future tau progression over global metrics	Thibault Farrell Properzi Mayblyum Hanseewu Healy Price Becker Sperling Johnson	Thibault, Emma
99	Rates of tau PET accumulation along the amyloid timeline in Alzheimer's disease	Cody Langhough Christian Betthausen Johnson	Cody, Karly
100	Body mass index, pathological tau, and cognition in preclinical AD: Could women with high BMI be protected?	Wang Sundermann Buckley Reas McEvoy Banks	Wang, Xin
101	Amyloid drives later tau accumulation for fast progressors in early Braak stages	Servaes Therriault Tissot Lussier Bezgin Wang Stevenson Rahmouni Stevenson Pallen Kunach Fernandez Arias Cassa Macedo Hosseini Pascoal Gauthier Rosa-Neto	Servaes, Stijn
102	Brain-wide and AD-risk genetic expression: A descriptive study	Hobbs McCullough Millar Gordon	Hobbs, Diana
103	Behavioral brain networks underlying the effect of Alzheimer's pathology on cognition	Ziontz Harrison Jagust	Ziontz, Jacob
104	Exploration of 18F-Florzolotau tau PET distribution patterns using machine learning approach in AD	Huang Lee Lin Huang Hsu Chang Huang Hsiao	Huang, Shao-Yi
105	The interplay of vascular disease, peripheral interleukin-6, beta-amyloid, and memory in older adults	Rizvi Adams Sathishkumar Kim Larson McMillan Brickman Mapstone Thomas Greenia Corrada Kawas Yassa	Rizvi, Batool
106	Gut microbiome composition is associated with cortical amyloid burden in a preclinical human cohort	Heston González Betthausen Johnson Asthana Knight Kaddurah-Daouk Rey Bendlin	Heston, Margo

Board #	Poster Title	Authors	Presenter
107	Study on MR-free template-based spatial normalization for Tau PET Image Quantitation using 18F-Florzolotau	Lee Huang Lin Huang Huang Wu Chang Hsiao	Lee, Zih-Ning
108	β -Amyloid in World Trade Center responders: Result indicate age-related toxic encephalopathy mediated by an immunogenic amyloid response	Clouston Vaska Huang Kritikos Zhou	Clouston, Sean
109	[18F]MK-6240 PET/MRI Test-Retest performance in cognitively normal elderly subjects	Lois Fanglu Fu Salvatore Huell Izquierdo Garcia Garimella Dickerson Johnson Catana Price	Lois, Cristina

POSTER INDEX (by presenter's last name)

Board #	Poster Title	Authors	Presenter
75	Comorbid medical conditions, anxiety, and amyloid- β pathology in cognitively unimpaired older adults	Abiose Young Winer Deters Mormino	Abiose, Olamide
87	18F-MK-6240 Tau PET as a Potential Biomarker for Chronic Traumatic Encephalopathy	Alosco Mundada La Joie Asken Nowinski Smith Culhane Shankar Amuiri Pettway Iaccarino Windon Tripodis Mercier Kowall Stein Grinberg McKee Stern Miller Mez Killiany Rabinovici	Alosco, Michael
57	In vivo measures of fibrillar beta-amyloid pathology limits cognitive plasticity in healthy aging: A multi-center intervention study.	Bischof Fellerhoff Giehl Drzezga	Bischof, Gerard
80	[18F]PI-2620 binding patterns in patients with suspected AD- and FTLT-tauopathies	Blazhenets Soleimani-Meigooni Thomas Brendel Vento VandeVrede Heuer Ljubenkov Rojas Chen Iaccarino Mundada Litvan Grossman Boeve Pantelyat Tartaglia Irwin Dickerson Baker Boxer Rabinovici La Joie	Blazhenets, Ganna
31	Assessing a universal neocortical mask for Centiloid quantification	Bourgeat Dore Rowe Benzinger Tosun Goyal LaMontagne Jin Weiner Morris Masters Fripp Villemagne	Feizpour, Azadeh
89	Classifying cognitive resilience to differing levels of Alzheimer's disease pathology	Boyle Townsend Klinger Coughlan Hanseeuw Yang Amariglio Farrell Jacobs Shirzadi Yau Price Chhatwal Schultz Hohman Donohue Properzi Rentz Johnson Sperling Buckley	Boyle, Rory
76	Defining and characterizing neocortical tau resistance in preclinical Alzheimer's disease	Buckley Klinger Boyle Coughlan Hanseeuw Yang Amariglio Rentz Townsend Farrell Jacobs Shirzadi Yau Price Chhatwal Schultz Hohman Donohue Properzi Johnson Sperling	Buckley, Rachel
22	Amyloid and tau pathology associated with different cognitive declines in cognitively normal older people	Chen Juarez Baker Harrison Landau Jagust	Chen, Xi
08	Imaging neuroinflammation with astrocyte-PET and bio-fluid biomarkers in patients with cognitive impairment	Chiotis Jelic Rodriguez-Vieitez Savitscheva Wall Antoni Nordberg	Chiotis, Konstantinos
27	Cross-sectional PET Analyses in the Longitudinal Early-onset Alzheimer's Disease Study (LEADS)	Cho Mundada Apostolova Carrillo Shankar Amuiri Zeltzer Windon Soleimani Meigooni Tanner Lawhn Heath Aisen Eloyan Koeppe Iaccarino Dickerson La Joie Rabinovici	Cho, Hanna
108	β -Amyloid in World Trade Center responders: Result indicate age-related toxic encephalopathy mediated by an immunogenic amyloid response	Clouston Vaska Huang Kritikos Zhou	Clouston, Sean
83	[18F]MK-6240 tau-PET in an A β -enriched sample from the 1946 British birth cohort - Insight 46	Coath Markiewicz Modat Scott Malone Thomas Dickson Schöll Ourselin Richards Fox Cash Schott	Coath, William
99	Rates of tau PET accumulation along the amyloid timeline in Alzheimer's disease	Cody Langhough Christian Betthausen Johnson	Cody, Karly
19	Temporal associations of plasma and PET Alzheimer's disease biomarkers using a non-linear mixed effects model	Cogswell Lundt Therneau Graff-Radford Schwarz Senjem Gunter Vemuri Petersen Jack Jr	Cogswell, Petrice

Board #	Poster Title	Authors	Presenter
59	The role of vascular pathology in the association between amyloid- β and tau in cognitively unimpaired individuals	Coomans van Westen Pichet Binette Strandberg Spotorno Palmqvist Stomrud Ossenkoppele Hansson	Coomans, Emma
66	Amyloid and tau PET are associated with plasma phosphorylated tau 181 and glial fibrillary acidic protein in a sample of heterogeneous dementia syndromes	Cousins Phillips Das Fulop Nasrallah O'Brien McMillan Irwin Massimo Grossman Wolk	Phillips, Jeffrey
81	Regional analysis of change in synaptic density over time by cognitive status	DiFilippo Mcvea McLachlan Pasquesi Davenport-Sis Jonaitis Ennis Betthausen Engle Johnson Bendlin Christian	DiFilippo, Alexandra
53	A CenTauR scale based on 18F-MK6240	Dore Bourgeat Leuzy Huang Krishnadas Feizpour Fripp Villemagne Rowe	Krishnadas, Natasha
33	A/T/N, cognitive, health and lifestyle differences across white matter hyperintensities groups in aged 45-85 years adults: Results from the Wisconsin Registry for Alzheimer's Prevention (WRAP)	Du Burghy Cody Hermann Jonaitis Betthausen Chin Cadman Rivera-Rivera Peret Johnson Rowley Pompa Lose Christian Janelidze Hansson Johnson Eisenmenger Kosciak	Du, Lianlian
35	Longitudinal PET assessments of tau pathologies in progressive supranuclear palsy with 18F-florzolotau (PM-PBB3/APN-1607)	Endo Takado Tagai Matsuoka Kokubo Hirata Kataoka Oya Matsumoto Kurose Ichihashi Hatano Saiki Hirano Nakano Furukawa Takeda Iose Imai Yagi Nishida Yuasa Ono Seki Takahata Tokuda Shinotoh Shimada Kawamura Zhang Higuchi	Endo, Hironobu
40	Lower locus coeruleus integrity identifies elevated entorhinal tau in low amyloid individuals and is associated with faster clinical progression	Engels-Domínguez A. Koops M. Riphagen F. Smegal Bueichekú Becker M. Kwong M. Rentz H. Salat A. Sperling A. Johnson I. L. Jacobs	Engels-Domínguez, Nina
86	Improved prediction of preclinical cognitive decline using amyloid PET spatial extent	Farrell Thibault Becker Price Hanseeuw Buckley Papp Jacobs Rentz Sperling Johnson	Farrell, Michelle
74	Encoding, consolidation and retrieval deficits are differentially shaped by tau and atrophy in the Alzheimer's disease spectrum	Fernandez Therriault Lussier Bezgin Tissot Servaes Wang Matothaarachchi Stevenson Rahmouni Kang Pallen Kunach Quispialaya Margherita-Poltronetti Pascoal Rosa-Neto	Fernandez, Jaime
39	Neuroinflammation Co-Localizes with Tau in Early-Onset MCI patients	Finn Appleton Bradbury Yu Faridar Beers Appel Fujita Masdeu Pascual	Finn, Quentin
12	Digital clock drawing performance is associated with tau deposition measured with PET in preclinical Alzheimer's disease	Fu Rentz Mayblyum Thibault Buckley Das Papp Sperling Penney Davis Johnson Price	Fu, Jessie Fang-Lu
38	Estimation of Native Spatial Resolution in Clinical Positron Emission Tomography Imaging Data	Galli Tonietto Klein Holiga Miho Knopf	Galli, Christopher
09	[18] Flortaucipir PET and Diffusion Tensor Tractography Coregistration can Enhance Detection of Brain Changes Associated with Progressive Apraxia of Speech	Gatto Duffy Utianski Clark Botha Machulda Lowe Josephs Whitwell	Gatto, Rodolfo
49	Machine Learning Based Tau Positivity Classification On Tau-PET Scans Considers Biological Variability And Can Aid In Decision Making	Gebre Rial Raghavan Sparman Wiste Schwarz Lowe Graff-Radford Knopman Petersen Schöll Jack Jr Vemuri	Gebre, Robel
03	PET imaging probe development for aggregated alpha-synuclein	Gomperts Liu Bai Xu Rose Celikag Ndayisaba Khurana Bartels Wang	Gomperts, Stephen
52	Histone deacetylase tracer [11C]Martinostat behaves differently in	Goodheart Yoo Striar Quan Wey Wang Gomperts	Goodheart, Anna

Board #	Poster Title	Authors	Presenter
	amyloid versus synuclein rich regions in dementia with Lewy bodies		
64	Validating Tau PET Staging Schemes in Relation to Cognitive Outcomes	Hammers Lin Logan Risacher Schwarz Apostolova	Hammers, Dustin
68	Cognitive impairment is more closely associated with the regional extension of F18MK6240 tau-PET signal than with PET signal intensity or CSF tau measures	Hanseeuw Gerard Malotau Colmant Quenon Ivanoiu Lhommel	Hanseeuw, Bernard
106	Gut microbiome composition is associated with cortical amyloid burden in a preclinical human cohort	Heston González Betthausen Johnson Asthana Knight Kaddurah-Daouk Rey Bendlin	Heston, Margo
102	Brain-wide and AD-risk genetic expression: A descriptive study	Hobbs McCullough Millar Gordon	Hobbs, Diana
69	Disentangling spatial-temporal remote interaction between tau and Amyloid- β proteins in different stages of tau aggregations	Hojjati Feiz Nayak Shteingart Ozoria Fernández Devanand Luchsinger Stern Razlighi	Hojjati, Seyed Hani
02	Non-invasive quantification and SUVR validation of [18F]-florbetaben with total-body EXPLORER PET	Holy Alfaro Fletcher Bhattarai Spencer Cherry DeCarli Fan	Holy, Emily
63	Comparisons of plasma biomarkers with 18F-Florzolotau PET in AD continuum – a pilot study	Huang Ing-Tsung Lin Huang	Huang, Kuo-Lun
104	Exploration of 18F-Florzolotau tau PET distribution patterns using machine learning approach in AD	Huang Lee Lin Huang Hsu Chang Huang Hsiao	Huang, Shao-Yi
05	Tau PET positivity reveals Alzheimer's disease related fast cognitive decline	Ioannou Bucci Nordberg Chiotis	Ioannou, Konstantinos
92	Locus coeruleus integrity as neural substrate providing resilience against cognitive decline in the face of Alzheimer's disease pathology	Jacobs Papp Buckley Riphagen Hanseeuw Boyle Donovan Rentz Sperling Johnson	Jacobs, Heidi
04	Cross-modality transformer for low-dose tau PET imaging	Jang Lois Becker Thibault Price Johnson El Fakhri Gong	Gong, Kuang
50	Impact of florbetaben acquisition timing on SUVR and centiloid values	Johns Kennedy Young Younes Vossler Poston Davidzon Mormino	Johns, Emily
88	Psychosis and tau burden across the AD continuum	Johnson* Ziaggi* Huey, MD Kreisl, MD Talmasov, MD Lao, PhD	Johnson, Aubrey
24	Validation of [18f]florbetaben PET quantitation based on the analysis of 15 software pipelines	Jovalekic Roé-Vellvé Koglin Lagos Quintana Nelson Diemling Lilja Gómez González Doré Bourgeat Whittington Gunn Stephens Bullich	Stephens, Andrew
36	Head-to-head comparison of tau PET tracers [18F]PI2620 and [18F]RO948 in non-demented individuals with brain amyloid deposition: the TAU-PET FACEHBI cohort	Klein Marquié Sotolongo-Grau Roé-Vellvé Bullich Tartari Sanabria García-Sánchez Borroni Galli Tonietto Pérez-Martínez Tárraga Ruiz Stephens Boada	Klein, Gregory
72	A clinical diagnosis of Alzheimer's disease and CSF-based tau positivity are both associated with lower locus coeruleus metabolism	Koops Dutta Becker Van Egroo Riphagen Prokopiou Hanseeuw Sperling El Fakhri Johnson Jacobs	Koops, Elouise
62	Plasma GFAP and NFL are correlated with measures of global cognition in EOAD and EOnonAD	Kostadinova Hammers Logan Manchella Nemes Fagan Foroud Zetterberg Kramer Aisen Carrillo Rabinovici Dickerson Apostolova Dage	Kostadinova, Ralitsa

Board #	Poster Title	Authors	Presenter
82	Regional tau profiles in early tau pathology populations	Kotari Morris Svaldi Southehal Lu Pontecorvo Collins Shcherbinin Neuroimaging Initiative	Kotari, Vikas
15	Is tau PET a robust biomarker for chronic traumatic encephalopathy?	Krishnadas Doré Lamb Guzman Ponsford Hicks Williams Feizpour Villemagne Rowe	Krishnadas, Natasha
54	Tau accumulation across the Alzheimer's disease continuum: an 18F-MK6240 AIBL study	Krishnadas Doré Robertson Ward Fowler Masters Bourgeat Fripp Villemagne Rowe	Krishnadas, Natasha
14	Regional tau predicts glucose hypometabolism in autosomal dominant Alzheimer's disease: Findings from the Colombia-Boston (COLBOS) biomarker study	Langella Kaplan Baena Londono Munera Vila-Castelar Alvarez Vidal Properzi Sanchez Sperling Johnson Lopera Hanseeuw Quiroz	Langella, Stephanie
107	Study on MR-free template-based spatial normalization for Tau PET Image Quantitation using 18F-Florzolotau	Lee Huang Lin Huang Huang Wu Chang Hsiao	Lee, Zih-Ning
61	Standardization of Tau PET using the CenTauR Scale: Preliminary findings from BioFINDER-2 using [18F]RO948 and [18F]Flortaucipir	leuzy Doré Klein Collins Henscheid Hostetler Iaacarino Karten Kolb Ossenkoppele Pappas Pontecorvo Saad Mathotaarachchi Sivakuraman Smith Rowe Villemagne Hansson	Leuzy, Antoine
07	In vivo visualization of tau deposits in corticobasal syndrome by 18F-Florzolotau PET	Liu Lu Li Jiao Chen Yao Liang Ge Li Shen Wu Sun Wu Yen Zuo Wang	Liu, Feng-Tao
06	Positive 18F-APN-1607 tau PET imaging findings in patients with Progressive Supranuclear Palsy-like extrapyramidal symptoms caused by TBK1 mutations	Liu Lu Sun Li Yen Jang Zuo Wang	Liu, Feng-Tao
109	[18F]MK-6240 PET/MRI Test-Retest performance in cognitively normal elderly subjects	Lois Fanglu Fu Salvatore Huell Izquierdo Garcia Garimella Dickerson Johnson Catana Price	Lois, Cristina
23	Future amyloid accumulation status affects the preservation of peripheral whole-blood gene co-expression networks at baseline in asymptomatic Alzheimer's disease	Luckett Zielonka Schaeverbeke Adamczuk Van Laere Dupont Cleynen Vandenberghe	Luckett, Emma
48	Sleep apnea and poor sleep quality are linked to tau deposition in older women at higher risk for Alzheimer's	Lui Shepherd Wang Bernier Bosompra DeYoung Malhotra Sundermann Banks	Lui, Kitty
77	Development and evaluation of image preprocessing pipelines for the Centiloid method	Luo Minhas Rubenstein Situ Royse Ances Christian Cohen Handen Klunk Tudorascu Zamon Laymon	Luo, Weiquan
94	PET-based Braak staging predicts neuropsychiatric burden in the Alzheimer's disease continuum	Macedo Tissot Therriault Servaes Rahmouni Fernandez-Arias Z. Lussier Stevenson Wang Quispialaya Socualaya Nazneen Ali Hosseini Kunach Haeger Stevenson Vitali A. Pascoal Rosa-Neto	C. Macedo, Arthur
90	Cerebrospinal fluid neurofilament light predicts increased amyloid, tau, and decreased grey matter density	Manchella Logan Dage Hammers Nemes Kostadinova Eloyan Mundada La Joie Iaccarino Fagan Foroud Zetterberg Koeppe Aisen Carrillo Rabinovici Dickerson Apostolova	Manchella, Mohit
29	Spatial extent and intensity of Alzheimer-associated tau PET burden is greater in agrammatic than logopenic primary progressive aphasia	Martersteck Sridhar Coventry Weintraub Mesulam Rogalski	Martersteck, Adam
16	Centiloid scale measure of amyloid PET by CT of PET/CT equipment	Matsuda Hanyu Kaneko	Matsuda, Hiroshi

Board #	Poster Title	Authors	Presenter
65	Shared variance between FDG metabolism and PiB tracer delivery is not predictive of cognitive decline in preclinical AD	Mayblyum Shirzadi Becker Chhatwal Farrell Jacobs Guehl El Fakhri Sperling Price Johnson Schultz Hanseeuw	Mayblyum, Danielle
96	Simulated dose reduction in longitudinal [18F]MK-6240 PET	McLachlan McVea DiFilippo Schöll Betthausen Johnson Christian	McLachlan, Max
21	Magnitude of MK6240 off-target binding correlated with spill-in effects in target regions	McVea DiFilippo McLachlan Johnson Betthausen Christian	McVea, Andrew
20	Beta-amyloid accumulates at a faster rate in individuals with Down syndrome	McVea DiFilippo McLachlan Murali Zammit Johnson Betthausen Stone Tudorascu Laymon Klunk Cohen Handen Christian	McVea, Andrew
25	Preprocessing 10,700 real-world amyloid-PET scans from the IDEAS study: the Good, the Bad and the Ugly	Mejia Perez Mundada Blazhenets Soleimani-Meigooni Zeltzer Cho Ranasinghe Windon Yadollahikhales Iaccarino Carrillo Gatsonis March Apgar Siegel Hilner Whitmer Rabinovici La Joie	Mejia Perez, Jhony
56	The gut microbiota metabolite trimethylamine n-oxide is associated with white matter degeneration on the Alzheimer's disease continuum	Moody Heston Zarbock Blennow Zetterberg Rey Ulland Bendlin	Moody, Jason
84	Longitudinal trajectories of depressive symptoms and regional amyloid accumulation (PiB PET) in clinically normal older adults	Munro Farrell Hanseeuw Buckley Properzi Vannini Amariglio Quiroz Blacker Rentz Sperling Johnson Marshall Gatchel	Munro, Catherine
46	Sex-associated differences in cerebrospinal fluid and plasma biomarkers in early-onset Alzheimer's disease	Nemes Logan Dage Fagan Hammers Manchella Eloyan Kostadinova Foroud Zetterberg Koeppe Aisen Carrillo Rabinovici Dickerson Apostolova	Nemes, Sára
58	One Year Longitudinal Change of Tau Accumulation on [18F]PI-2620 PET in Alzheimer Spectrum	Oh Oh Lee Oh Seo Roh Lee Kim	Oh, Minyoung
42	Sex differences in A β and tau vulnerability in preclinical Alzheimer's disease	Ourry St-Onge Mohammediyani Yakoub Soucy Poirier Breitner Villeneuve	Ourry, Valentin
17	Successful cognitive aging is associated with less brain atrophy and lower tau deposition	Pezzoli Giorgio Harrison Martersteck Jagust	Pezzoli, Stefania
85	Improving sub-threshold PiB fidelity using relative radioligand delivery	Properzi Shirzadi Buckley Klinger Hanseeuw Amariglio Rentz Farrell Price Chhatwal Marshall Gatchel Johnson Sperling Schultz	Properzi, Michael
95	A computational model to study the combined effect of neuronal connectivity loss and tauopathy progression	Rahimabadi Soucy Benali	Rahimabadi, Arsalan
67	Combined and independent effects of hyperphosphorylation of tau on microglial activation	Rahmouni Therriault Tissot L. Benedet Ashton Triana-Baltzer Lussier Servaes Macedo Stevenson Stevenson Kunach Fernandez-Arias Wang Gauthier Kolb Karikari Zetterberg Blennow Pascoal Rosa-Neto	Rahmouni, Nesrine
28	Dynamic amyloid PET: relationships to tau PET and cognition in Alzheimer's disease	Raman Charniaux Murchison Fang Tzabari Liu Morris Chen Joseph-Mathurin Ponisio Flores Kennedy Benzinger Roberson McConathy	Raman, Fabio
105	The interplay of vascular disease, peripheral interleukin-6, beta-amyloid, and memory in older adults	Rizvi Adams Sathishkumar Kim Larson McMillan Brickman Mapstone Thomas Greenia Corrada Kawas Yassa	Rizvi, Batool

Board #	Poster Title	Authors	Presenter
91	Unhealthy white matter connectivity in African American and non-Hispanic white older adults	Royse Snitz Hengenius Huppert Roush Cisneros Potopenko Becker Cohen Shaaban	Royse, Sarah
47	Correlations between Janssen Simoa plasma p217+tau and tau PET in participants screened for Janssen's Autonomy Ph2 anti-tau trial in early Alzheimer's Disease	Saad Triana-Blatzer Moughadam Slemmon Henley Kolb	Saad, Ziad
71	Mid-life atherosclerotic cardiovascular disease risk score and late-life AT(N) measures	Saeed Chang Royse Lopresti Snitz Villemagne Reis Lopez Cohen	Cohen, Ann
18	Subcortical flortaucipir PET and susceptibility analyses to differentiate progressive supranuclear palsy clinical variants and corticobasal syndrome	Satoh Arani Schwarz Senjem Ali Jack Lowe Josephs Whitwell	Satoh, Ryota
01	Effects of de-facing PET and MRI scans on clinical correlations analyses	Schwarz Kremers Weigand Prakaashana Senjem Lowe Gunter Kantarci Vemuri Petersen Knopman Jack	Schwarz, Christopher
60	Dual biomarker amyloid PET for improved subtype and stage inference	Scott Coath Dickson McQuaid Cash Schott	Scott, Catherine
101	Amyloid drives later tau accumulation for fast progressors in early Braak stages	Servaes Therriault Tissot Lussier Bezgin Wang Stevenson Rahmouni Stevenson Pallen Kunach Fernandez Arias Cassa Macedo Hosseini Pascoal Gauthier Rosa-Neto	Servaes, Stijn
32	Relationships between Neuronal Hyperactivity, Stress Susceptibility, and Alzheimer's Disease pathology	Sharp Razlighi Oh	Oh, Hwamee
13	[18F]RO-948 Tau PET Retention and Correlation with Fluid Biomarkers in the Early AD Continuum	Shekari González Escalante Milà-Alomà Falcon Niñerola-Baizán Tonietto Borroni Klein J. Ashton K. Karikari Lantero-Rodriguez Snellman Ortiz Vanmechelen Minguillón Fauria Perissinotti Molinuevo Zetterberg Blennow Grau-Rivera Suárez-Calvet Domingo Gispert	Shekari, Mahnaz
45	Longitudinal accumulation of white matter lesions is associated with amyloidosis and brain atrophy, but not systemic vascular risk	Shirzadi Schultz Yau Fitzpatrick Levin Joseph-Mathurin Kantarci Preboske Jack Jr. Farlow Fagan Hassenstab Jucker Morris Xiong Karch Levey Gordon Schofield Salloway Perrin McDade Levin Cruchaga Allegri Fox Goate Day Koeppe Noble Chui Berman Mori Sanchez-Valle Lee Rosa-Neto Ruthirakuhan Wu Swardfager Benzinger Sohrabi Martins Schultz Bateman Johnson Sperling Greenberg Chhatwal	Shirzadi, Zahra
93	Lower locus coeruleus integrity predicts diminished practice effects in cognitively normal older individuals	Smegal Schneider Jutten Rentz Johnson Sperling Papp Jacobs	Smegal, Lindsay
34	Medial temporal 18F-MK6240 levels are associated with global graph characteristics of functional connectivity from high-density EEG in the asymptomatic and prodromal stage of Alzheimer disease	Spruyt Reinartz Meade Khachatryan Van Hulle Van Laere Dupont Vandenberghe	Spruyt, Laure
37	Regional [F18]AV1451 uptake in progressive apraxia of speech with and without Alzheimer's disease, dysexecutive,	Switzer Corriveau-Lecavalier Lowe Jones Ramanan Machulda Graff-Radford Boeve	Switzer, Aaron R

Board #	Poster Title	Authors	Presenter
	and logopenic variants of Alzheimer's disease	Knopman Jack Petersen Josephs Whitwell Botha	
70	Predictors of Discordance Between Pre-PET Clinical Diagnosis and Amyloid-PET Results in the Imaging Dementia—Evidence for Amyloid Scanning (IDEAS) Study	Tanner La Joie Hanna Iaccarino Allen Siegel Hillner Whitmer Gatsonis Carrillo Rabinovici	Tanner, Jeremy
51	Postmortem In Vitro Binding of APN-1607 to PSP and HC Globus Pallidus Homogenates	Tempest Margolin Paget Campbell Navia	Tempest, Paul
26	Longitudinal tau-PET differs between progressive apraxia of speech subtypes	Tetzloff Martin Duffy Clark Utianski Botha Machulda Schwarz Senjem Jack Jr. Lowe Josephs Whitwell	Tetzloff, Katerina A.
97	Regional amyloid change improves prediction of future tau progression over global metrics	Thibault Farrell Properzi Mayblyum Hanseewu Healy Price Becker Sperling Johnson	Thibault, Emma
30	Comparing PI2620 and Flortaucipir in Progressive Supranuclear Palsy Subjects	Thomas Blazhenets La Joie Rabinovici Heuer Jagust Boxer Baker	Thomas, Wesley
73	Motion and partial volume corrections in dynamic [18F]-MK6240 PET imaging	Tiss Gong Lois Becker Thibault Guehl Xia Normandin Ouyang Johnson El Fakhri	Gong, Kuang
78	Cognitively estimated disease time: Associations with amyloid and tau burden in the Harvard Aging Brain Study	Townsend Properzi Betthausen Klinger Boyle Coughlan Hanseewu Yang Amariglio Farrell Jacobs Shirzadi Yau Price Chhatwal Rentz Johnson Sperling Schultz Buckley	Townsend, Diana
10	Towards a simplified flortaucipir-PET read method for assessing tau burden	Tunali Iaccarino Ducker Patel DiFabbio Kowaleski Arora Kim Lu Pontecorvo Shcherbinin	Tunali, Ilke
100	Body mass index, pathological tau, and cognition in preclinical AD: Could women with high BMI be protected?	Wang Sundermann Buckley Reas McEvoy Banks	Wang, Xin
79	Synergistic interaction between sex, amyloid and phosphorylated tau predicts the longitudinal progression of tau tangles	Wang Therriault Servaes Tissot Fernandez Arias Rahmouni Macedo Stevenson Stevenson Haeger Hosseini Nazneen Rosa-Neto	Wang, Yi-Ting
43	Alzheimer's Network for Treatment and Diagnostics (ALZ-NET): Defining the future of Alzheimer's treatment, imaging and care	Whitlow March Rabinovici Raffii Atri Daffner Edelmayer Gatsonis Lopez Porsteinsson Possin Salloway Sano Snyder Vukmir Wilkins Windon Carrillo	Whitlow, Christopher
41	Substantia nigra 18F-PI-2620 PET signal is associated with motor impairment in Lewy body disease	Winer Vossler Young Romero Shahid Abdelnour Anders Shen Mormino Poston	Winer, Joseph
55	Multi-modal analysis of myelin and neurofilament light chain in individuals at risk for Alzheimer's disease using MRI, PET, and CSF biomarker assessments	Yang Dean III Betthausen Carlsson Johnson Blennow Zetterberg Alexander Bendlin	Yang, Kao Lee
44	Acquisition time corrections for SUVR analyses of [18F]-PI-2620	Young Vossler Winer Romero Anders Shen Poston Davidzon Mormino	Young, Christina
103	Behavioral brain networks underlying the effect of Alzheimer's pathology on cognition	Ziontz Harrison Jagust	Ziontz, Jacob

HAI 2023 PROGRAM

Wednesday, January 11, 2023

7:30 am	Check-in	
7:30	Breakfast	
8:15	Welcome Notes	
8:25	Announcement	
8:30 – 9:35	SESSION I: TRACER DEVELOPMENT AND EVALUATION	CHAIRS: Julie Price, PhD, Massachusetts General Hospital Chet Mathis, PhD, University of Pittsburgh
8:30	Introduction	Chairs
8:35	Advances towards the identification of an α -synuclein Positron Emission Tomography radioligand for the diagnosis of Parkinson's Disease	Idriss Bennacef , Translational Imaging, MRL, Merck & Co., Inc., West Point, PA, US
8:50	Discovery of [18F]ACI-12589, a novel and promising PET-tracer for a-synuclein	Francesca Capotosti , AC Immune SA, Lausanne, Switzerland
9:05	Discovery and preclinical evaluation of two novel PET tracers for imaging non-AD tauopathies	Marc B. Skaddan , AbbVie Inc., North Chicago, IL, US
9:20	In Vivo Head-To-Head Comparison of [18F]GTP1, [18F]PI2620, and [18F]MK6240 in Alzheimer's Disease	Matteo Tonietto , Research and Early Development (pRED), Hoffmann-La Roche, Basel, Switzerland
9:35	Didactic A	
10:00	Discussion	
10:30 - 11:15	POSTER SESSION 1A	
1	Effects of de-facing PET and MRI scans on clinical correlations analyses	Christopher Schwarz , Mayo Clinic, Rochester, MN, US
2	Non-invasive quantification and SUVR validation of [18F]-florbetaben with total-body EXPLORER PET	Emily Holy , Department of Neurology, UC Davis Health, Davis, CA, US
3	PET imaging probe development for aggregated alpha-synuclein	Stephen Gomperts , Department of Neurology, Massachusetts General Hospital, Boston, MA, US
4	Cross-modality transformer for low-dose tau PET imaging	Se-In Jang , Massachusetts General Hospital, Boston, MA, US
5	Tau PET positivity reveals Alzheimer's disease related fast cognitive decline	Konstantinos Ioannou , Nordberg Translational Molecular Imaging Lab, Division of Clinical Geriatrics, Center for Alzheimer's Research, Department of Neurobiology, Care Sciences and Society, Karolinska Institutet, Stockholm, Sweden
6	Positive 18F-APN-1607 tau PET imaging findings in patients with Progressive Supranuclear Palsy-like extrapyramidal symptoms caused by TBK1 mutations	Feng-Tao Liu , Department of Neurology & National Clinical Research Center for Aging and Medicine, Huashan Hospital, Fudan University, Shanghai, CN
7	In vivo visualization of tau deposits in corticobasal syndrome by 18F-Florzolotau PET	Feng-Tao Liu , Department of Neurology, National Research Center for Aging and Medicine, National Center for Neurological Disorders, and State Key Laboratory of Medical Neurobiology, Huashan Hospital, Fudan University, Shanghai, CN
8	Imaging neuroinflammation with astrocyte-PET and bio-fluid biomarkers in patients with cognitive impairment	Konstantinos Chiotis , Department NVS, Karolinska Institutet, Stockholm, Sweden
9	[18] Flortaucipir PET and Diffusion Tensor Tractography Coregistration can Enhance Detection of Brain Changes Associated with Progressive Apraxia of Speech	Rodolfo G. Gatto , Division of Neurology, Mayo Clinic, Rochester, MN, US

10	Towards a simplified flortaucipir-PET read method for assessing tau burden	Ilke Tunali , Eli Lilly and Company, Indianapolis, IN, US
12	Digital clock drawing performance is associated with tau deposition measured with PET in preclinical Alzheimer's disease	Jessie Fang-Lu Fu , Athinoula A. Martinos Center for Biomedical Imaging, Charlestown, MA, US
13	[18F]RO-948 Tau PET Retention and Correlation with Fluid Biomarkers in the Early AD Continuum	Mahnaz Shekari , Barcelonaβeta Brain Research Center (BBRC), Pasqual Maragall Foundation,, Barcelona, Spain
14	Regional tau predicts glucose hypometabolism in autosomal dominant Alzheimer's disease: Findings from the Colombia-Boston (COLBOS) biomarker study	Stephanie Langella , Massachusetts General Hospital / Harvard Medical School, Boston, MA, US
15	Is tau PET a robust biomarker for chronic traumatic encephalopathy?	Natasha Krishnadas , Florey Institute of Neurosciences & Mental Health, Melbourne, AU
16	Centiloid scale measure of amyloid PET by CT of PET/CT equipment	Hiroshi Matsuda , Fukushima Medical University, Fukushima, Japan
17	Successful cognitive aging is associated with less brain atrophy and lower tau deposition	Stefania Pezzoli , Helen Wills Neuroscience Institute, University of California, Berkeley, CA, US
18	Subcortical flortaucipir PET and susceptibility analyses to differentiate progressive supranuclear palsy clinical variants and corticobasal syndrome	Ryota Satoh , Mayo Clinic, Rochester, MN, US
19	Temporal associations of plasma and PET Alzheimer's disease biomarkers using a non-linear mixed effects model	Petrice Cogswell , Department of Radiology, Mayo Clinic, Rochester, MN, US
20	Beta-amyloid accumulates at a faster rate in individuals with Down syndrome	Andrew McVea , University of Wisconsin - Madison, Madison, WI, US
21	Magnitude of MK6240 off-target binding correlated with spill-in effects in target regions	Andrew McVea , University of Wisconsin - Madison, Madison, WI, US
22	Amyloid and tau pathology associated with different cognitive declines in cognitively normal older people	Xi Chen , University of California, Berkeley, Berkeley, CA, US
23	Future amyloid accumulation status affects the preservation of peripheral whole-blood gene co-expression networks at baseline in asymptomatic Alzheimer's disease	Emma Luckett , Laboratory for Cognitive Neurology, KU Leuven, Leuven, Belgium
24	Validation of [18f]florbetaben PET quantitation based on the analysis of 15 software pipelines	Andrew Stephens , Life Molecular Imaging, Berlin, Germany
25	Preprocessing 10,700 real-world amyloid-PET scans from the IDEAS study: the Good, the Bad and the Ugly	Jhony Mejia Perez , Memory and Aging Center, Department of Neurology, University of California, San Francisco, San Francisco, CA, US
26	Longitudinal tau-PET differs between progressive apraxia of speech subtypes	Katerina A. Tetzloff , Mayo Clinic Department of Neurology, Rochester, MN, US
27	Cross-sectional PET Analyses in the Longitudinal Early-onset Alzheimer's Disease Study (LEADS)	Hanna Cho , Memory and Aging Center, UCSF Weill Institute for Neurosciences, Department of Neurology, University of California, San Francisco, CA, US
28	Dynamic amyloid PET: relationships to tau PET and cognition in Alzheimer's disease	Fabio Raman , The University of Alabama at Birmingham, Department of Radiology, Birmingham, AL, US
29	Spatial extent and intensity of Alzheimer-associated tau PET burden is greater in agrammatic than logopenic primary progressive aphasia	Adam Martersteck , Mesulam Center for Cognitive Neurology and Alzheimer's Disease, Northwestern University, Chicago, IL, US
30	Comparing PI2620 and Flortaucipir in Progressive Supranuclear Palsy Subjects	Wesley Thomas , University of California, Berkeley, Berkeley, CA, US
31	Assessing a universal neocortical mask for Centiloid quantification	Pierrick Bourgeat , Australian eHealth Research Centre, CSIRO Health and Biosecurity, Herston, AU
32	Relationships between Neuronal Hyperactivity, Stress Susceptibility, and Alzheimer's Disease pathology	Hwamee Oh , Carney Institute for Brain Science, Brown University, Providence, RI, US
33	A/T/N, cognitive, health and lifestyle differences across white matter hyperintensities groups in aged 45-85 years adults: Results from the Wisconsin Registry for Alzheimer's Prevention (WRAP)	Lianlian Du , Wisconsin Alzheimer's Institute, University of Wisconsin-Madison School of Medicine and Public Health, Madison, WI, US

34	Medial temporal 18F-MK6240 levels are associated with global graph characteristics of functional connectivity from high-density EEG in the asymptomatic and prodromal stage of Alzheimer disease	Laure Spruyt , Laboratory for Cognitive Neurology, Department of Neurosciences, KU Leuven, Leuven, Belgium
35	Longitudinal PET assessments of tau pathologies in progressive supranuclear palsy with 18F-florzolotau (PM-PBB3/APN-1607)	Hironobu Endo , Department of Functional Brain Imaging, Institute for Quantum Medical Science, Quantum Life and Medical Science Directorate, National Institutes for Quantum Science and Technology, Chiba, Japan
36	Head-to-head comparison of tau PET tracers [18F]PI2620 and [18F]RO948 in non-demented individuals with brain amyloid deposition: the TAU-PET FACEHBI cohort	Gregory Klein , Roche Pharma Research and Early Development, Basel, Switzerland
11:15 am – 12:35 pm	SESSION II: TECHNICAL ADVANCES FOR CLINICAL APPLICATIONS	CHAIRS: Suzanne Baker, PhD , Lawrence Berkeley National Laboratory Bradley Christian, PhD , University of Wisconsin, Madison
11:15	Introduction	Chairs
11:20	Minimizing sample sizes for trials using MK-6240 outcomes: impact of processing method and choice of reference and target tissues	J. Alex Becker , Massachusetts General Hospital, Boston, MA, US
11:35	Inferring full ATN status from tau-PET using deep learning	Nicolai Franzmeier , Institute for AI and Informatics in Medicine, Klinikum rechts der Isar Technical University of Munich, Munich, Germany
11:50	Longitudinal modelling of tau transport and production dynamics in the human brain	Pavan Chaggar , University of Oxford, Oxford, UK
12:05 pm	Connectivity- versus gradient-based approaches to predict regional tau-PET across Alzheimer's disease variants	Nick Corriveau-Lecavalier , Department of Neurology, Mayo Clinic, Rochester, MN, US
12:20	Measuring tau in the basal forebrain: a comparison of MK6240 and flortaucipir	Theresa Harrison , University of California Berkeley, Berkeley, CA, US
12:35	Discussion	
1:00	Lunch break	
2:00	KEYNOTE: SYNAPTIC PATHOLOGY IN NEURODEGENERATION	Thomas Montine, MD , Stanford University
2:30	Keynote Discussion	
2:45 pm – 3:50 pm	SESSION III: THRESHOLDS, VISUAL READS AND REAL WORLD IMAGING	CHAIRS: Pedro Rosa-Neto, MD, PhD , McGill University Ansel Hillmer, PhD , Yale School of Medicine
2:45	Introduction	Chairs
2:50	Biostatistical estimation of tau threshold hallmarks (BETTH) for tau imaging studies	Alexandra Gogola , Department of Radiology, University of Pittsburgh School of Medicine, Pittsburgh, PA, US
3:05	Visual read of [18F]florquinitalu PET that includes and extends beyond the mesial temporal lobe is associated with amyloid positivity and retrospective cognitive decline in an AD risk-enriched cohort	Sterling Johnson , Wisconsin Alzheimer's Disease Research Center, University of Wisconsin School of Medicine and Public Health, Madison, WI, US
3:20	Head-to-head comparison of tau and amyloid PET visual reads for differential diagnosis: An international, multi-center study	David Soleimani-Meigooni , Memory and Aging Center, UCSF Weill Institute for Neurosciences, Department of Neurology, University of California, San Francisco, CA, US
3:35	Quantitative analysis of 8,895 real-world amyloid Positron Emission Tomography (PET) scans from the Imaging Dementia–Evidence for Amyloid Scanning (IDEAS) study	Ehud Zeltzer , University of California, San Francisco, San Francisco, CA, US
3:50	Discussion	

4:15 pm – 05:00 pm	POSTER SESSION 1B	
5:00 pm – 6:05 pm	SESSION IV: NON-AD AND CO-PATOLOGIES	CHAIRS: Milos Ikonomic, MD, University of Pittsburgh Melissa Murray, PhD, Mayo Clinic, Jacksonville
5:00	Introduction	Chairs
5:05	Tau Burden Evaluation by [18F] Flortaucipir PET and Quantitative Tau Neuropathology in Alzheimer's Disease And Non-Alzheimer's Tauopathies	Rodolfo G. Gatto , Division of Neurology, Mayo Clinic, Rochester, MN, US
5:20	Pathologic Correlations of [18F]-Flortaucipir Imaging in non-Alzheimer Corticobasal Degeneration Syndrome	Cinthya Aguero , MassGeneral Institute for Neurodegenerative Disease, Charlestown, MA, US
5:35	Unveiling the neurobiological basis of F18-flortaucipir in different tauopathies using voxel-to-voxel histology to PET comparisons: the role of p-tau, iron and MAOB	Yuheng Chen , Memory and Aging Center, Department of Neurology, University of California, San Francisco, San Francisco, CA, US
5:50	Association of FDG-PET with co-pathologies in autopsy-proven AD	Marianne Chapleau , Memory and Aging Center, Department of Neurology, University of California, San Francisco, San Francisco, CA, US
6:05	Discussion	
6:30 pm – 9:00 pm	Welcome Reception	

Thursday, January 12, 2023

7:30 am	Breakfast	
8:30 – 9:20	SESSION V: AD NEUROPATHOLOGY	CHAIRS: Teresa Gomez-Isla, MD, PhD, Massachusetts General Hospital Laetitia Lemoine, PhD, Karolinska Institutet
8:30	Introduction	Chairs
8:35	Specific associations between plasma biomarkers and post-mortem amyloid plaque and neurofibrillary tau tangle loads	Gemma Salvadó , Clinical Memory Research Unit, Department of Clinical Sciences, Malmö, Lund University, Lund, Sweden
8:50	Intersection of amyloid- β and tau brain pathology influences plasma phosphorylated tau levels	Gemma Salvadó , Clinical Memory Research Unit, Department of Clinical Sciences, Malmö, Lund University, Lund, Sweden
9:05	Tangle maturity markers associate with tau PET and cognitive measures in hippocampus	Christina M. Moloney , Department of Neuroscience, Mayo Clinic, Jacksonville, FL, US
9:20	Postmortem validation of 18F-MK-6240 PET using autoradiography and in-vitro binding combined with antibody-based assays in frozen brains from two autopsy cases	Tobey Betthausen , Wisconsin Alzheimer's Disease Research Center, University of Wisconsin-Madison, Madison, WI, US
9:35	Discussion	
10:00 am – 10:45	POSTER SESSION 2A	
37	Regional [F18]AV1451 uptake in progressive apraxia of speech with and without Alzheimer's disease, dysexecutive, and logopenic variants of Alzheimer's disease	Aaron R Switzer , Department of Neurology, Division of Behavioral Neurology, Mayo Clinic, Rochester, MN, US
38	Estimation of Native Spatial Resolution in Clinical Positron Emission Tomography Imaging Data	Christopher Galli , Roche Pharma Research and Early Development, Therapeutic Modalities, Roche Innovation Center Basel, F.Hoffmann-La Roche Ltd, Grenzacherstrasse 124, 4070 Basel, Switzerland, Basel, Switzerland
39	Neuroinflammation Co-Localizes with Tau in Early-Onset MCI patients	Quentin Finn , Nantz National Alzheimer Center, Houston Methodist Neurological and Research Institute, Houston, TX, US

40	Lower locus coeruleus integrity identifies elevated entorhinal tau in low amyloid individuals and is associated with faster clinical progression	<u>Nina Engels-Domínguez</u> , Gordon Center for Medical Imaging, Department of Radiology, Massachusetts General Hospital/Harvard Medical School, Boston, MA, US
41	Substantia nigra 18F-PI-2620 PET signal is associated with motor impairment in Lewy body disease	<u>Joseph Winer</u> , Department of Neurology and Neurological Sciences, Stanford University, Palo Alto, CA, US
42	Sex differences in A β and tau vulnerability in preclinical Alzheimer's disease	<u>Valentin Ourry</u> , Department of Psychiatry, Faculty of Medicine, McGill University, Montréal, QC, Canada
43	Alzheimer's Network for Treatment and Diagnostics (ALZ-NET): Defining the future of Alzheimer's treatment, imaging and care	<u>Christopher Whitlow</u> , American College of Radiology, Reston, VA, US
44	Acquisition time corrections for SUVR analyses of [18F]-PI-2620	<u>Christina Young</u> , Department of Neurology and Neurological Sciences, Stanford University School of Medicine, Stanford, CA, US
45	Longitudinal accumulation of white matter lesions is associated with amyloidosis and brain atrophy, but not systemic vascular risk	<u>Zahra Shirzadi</u> , Massachusetts General Hospital, Brigham and women's hospital, Harvard Medical School, Boston, MA, US
46	Sex-associated differences in cerebrospinal fluid and plasma biomarkers in early-onset Alzheimer's disease	<u>Sára Nemes</u> , Indiana University School of Medicine, Indiana, IN, US
47	Correlations between Janssen Simoa plasma p217+tau and tau PET in participants screened for Janssen's Autonomy Ph2 anti-tau trial in early Alzheimer's Disease	<u>Ziad S. Saad</u> , Neuroscience Biomarkers and Global Imaging, Janssen R&D, Johnson & Johnson, San Diego, CA, US
48	Sleep apnea and poor sleep quality are linked to tau deposition in older women at higher risk for Alzheimer's	<u>Kitty Lui</u> , San Diego State University/University of California San Diego Joint Doctoral Program in Clinical Psychology, San Diego, CA, US
49	Machine Learning Based Tau Positivity Classification On Tau-PET Scans Considers Biological Variability And Can Aid In Decision Making	<u>Robel Gebre</u> , Department of Radiology, Mayo Clinic, Rochester, MN, US
50	Impact of florbetaben acquisition timing on SUVR and centiloid values	<u>Emily Johns</u> , Stanford University School of Medicine, Stanford, CA, US
51	Postmortem In Vitro Binding of APN-1607 to PSP and HC Globus Pallidus Homogenates	<u>Paul Tempest</u> , Aprinoia Therapeutics, Cambridge, MA, US
52	A CenTauR scale based on 18F-MK6240	<u>Vincent Dore</u> , Health and Biosecurity Flagship, The Australian eHealth Research Centre, CSIRO, Melbourne, AU
53	Histone deacetylase tracer [11C]Martinostat behaves differently in amyloid versus synuclein rich regions in dementia with Lewy bodies	<u>Anna Goodheart</u> , Department of Neurology, Massachusetts General Hospital, Boston, MA, US
54	Tau accumulation across the Alzheimer's disease continuum: an 18F-MK6240 AIBL study	<u>Natasha Krishnadas</u> , Florey Department of Neurosciences & Mental Health, The University of Melbourne, Melbourne, AU
55	Multi-modal analysis of myelin and neurofilament light chain in individuals at risk for Alzheimer's disease using MRI, PET, and CSF biomarker assessments	<u>Kao Lee Yang</u> , Wisconsin Alzheimer's Disease Research Center, University of Wisconsin, Madison, WI, US
56	The gut microbiota metabolite trimethylamine n-oxide is associated with white matter degeneration on the Alzheimer's disease continuum	<u>Jason Moody</u> , Wisconsin Alzheimer's Disease Research Center, University of Wisconsin-Madison, Madison, WI, US
57	In vivo measures of fibrillar beta-amyloid pathology limits cognitive plasticity in healthy aging: A multi-center intervention study.	<u>Gerard Bischof</u> , University of Cologne, University Hospital of Cologne, Department of Nuclear Medicine, Multimodal Neuroimaging Group, Cologne, Germany, Cologne, Germany
58	One Year Longitudinal Change of Tau Accumulation on [18F]PI-2620 PET in Alzheimer Spectrum	<u>Minyoung Oh</u> , Department of Nuclear Medicine, Asan Medical Center, University of Ulsan College of Medicine, Seoul, Korea
59	The role of vascular pathology in the association between amyloid- β and tau in cognitively unimpaired individuals	<u>Emma Coomans</u> , Radiology & Nuclear Medicine, Vrije Universiteit Amsterdam, Amsterdam UMC location VUmc, Amsterdam, The Netherlands
60	Dual biomarker amyloid PET for improved subtype and stage inference	<u>Catherine J Scott</u> , Institute of Nuclear Medicine, University College London Hospitals NHS Foundation Trust, London, UK

61	Standardization of Tau PET using the CenTauR Scale: Preliminary findings from BioFINDER-2 using [18F]RO948 and [18F]Flortaucipir	Antoine leuzy , Clinical Memory Research Unit, Department of Clinical Sciences, Lund University, Malmö, Sweden, Malmö, Sweden
62	Plasma GFAP and NFL are correlated with measures of global cognition in EOAD and EOnonAD	Ralitsa V. Kostadinova , Indiana University School of Medicine, Indianapolis, IN, US
63	Comparisons of plasma biomarkers with 18F-Florzolotau PET in AD continuum – a pilot study	Kuo-Lun Huang , Department of Neurology, Linkou Chang Gung Memorial Hospital, Taoyuan, TW
64	Shared variance between FDG metabolism and PiB tracer delivery is not predictive of cognitive decline in preclinical AD	Danielle Mayblyum , Massachusetts General Hospital, Boston, MA, US
65	Validating Tau PET Staging Schemes in Relation to Cognitive Outcomes	Dustin Hammers , Indiana University School of Medicine, Department of Neurology, Indianapolis, IN, US
66	Amyloid and tau PET are associated with plasma phosphorylated tau 181 and glial fibrillary acidic protein in a sample of heterogeneous dementia syndromes	Jeffrey Phillips , University of Pennsylvania, Philadelphia, PA, US
67	Combined and independent effects of hyperphosphorylation of tau on microglial activation	Nesrine Rahmouni , Translational Neuroimaging Laboratory, McGill Research Centre for Studies in Aging, Montreal, QC, Canada
68	Cognitive impairment is more closely associated with the regional extension of F18MK6240 tau-PET signal than with PET signal intensity or CSF tau measures	Bernard Hanseeuw , Cliniques Universitaires Saint-Luc, Brussels, Belgium
69	Disentangling spatial-temporal remote interaction between tau and Amyloid- β proteins in different stages of tau aggregations	Seved Hani Hojjati , Weill Cornell Medicine, New York, NY, US
70	Predictors of Discordance Between Pre-PET Clinical Diagnosis and Amyloid-PET Results in the Imaging Dementia—Evidence for Amyloid Scanning (IDEAS) Study	Jeremy Tanner , Memory and Aging Center, University of California San Francisco, San Francisco, CA, US
71	Mid-life atherosclerotic cardiovascular disease risk score and late-life AT(N) measures	Ann Cohen , University of Pittsburgh School of Medicine, Pittsburgh, PA, US
72	A clinical diagnosis of Alzheimer’s disease and CSF-based tau positivity are both associated with lower locus coeruleus metabolism	Elouise A. Koops , Gordon Center for Medical Imaging, Department of Radiology, Massachusetts General Hospital, Harvard Medical School, Boston, MA, USA., Boston, MA, US
10:45 – 11:50	SESSION VI: HETEROGENEITY IN THE AD CASCADE	CHAIRS: Heidi Jacobs, PhD , Massachusetts General Hospital Susan Landau, PhD , University of California, Berkeley
10:45	Introduction	Chairs
10:50	Longitudinal increases in tau emerge alongside early amyloid change in Down syndrome	Matt Zammit , University of Wisconsin-Madison, Madison, WI, US
11:05	Cross-sectional and longitudinal associations between amyloid- and tau-PET in early-onset Alzheimer’s Disease: update from the LEADS study	Nidhi Mundada , Memory and Aging Center, Department of Neurology, University of California San Francisco, San Francisco, CA, US
11:20	Amyloid PET Burden Predicts Longitudinal Cognitive Trajectories in a Heterogeneous ADRD Cohort	Kyan Younes , Department of Neurology and Neurological Sciences, Stanford University, Stanford, CA, US
11:35	Variations in gamma-secretase function across PSEN1 pathogenic variants strongly predict the clinical, cognitive, and biomarker progression of autosomal dominant Alzheimer’s disease	Stephanie Schultz , Massachusetts General Hospital, Boston, MA, US
11:50	Discussion	
12:15 pm	Lunch	
1:15 pm – 2:35 pm	SESSION VII: TAU PET AND MRI: MULTIMODALITY INSIGHTS	CHAIRS: Annie Cohen, PhD , University of Pittsburgh Beth Mormino, PhD , Stanford University
1:15	Introduction	Chairs

1:20	Mapping tau accumulation to the functional and structural organization of the brain in Alzheimer's disease	Julie Ottroy , LC Campbell Cognitive Neurology Unit, Hurvitz Brain Sciences Program, Sunnybrook Research Institute, University of Toronto, Toronto, ON, Canada
1:35	Baseline tau PET shows stronger associations with cognitive and behavioral changes over time than cortical thickness	Ellen Singleton , Clinical Memory Research Unit, Department of Clinical Sciences, Lund University, Malmö, Sweden, Lund, Sweden
1:50	A Central Role of Locus Coeruleus in the Initial Spatiotemporal Progression of Tau and its Contribution to Cognition	Elisenda Bueichekú , Gordon Center for Medical Imaging, Department of Radiology, Massachusetts General Hospital, Boston, MA 02114, USA., Boston, MA, US
2:05	Tau Propagation in the Brain Olfactory Circuits Contributes to Smell Perception Changes in Aging	Ibai Diez , Gordon Center for Medical Imaging, Department of Radiology, Massachusetts General Hospital, Harvard Medical School, Boston, MA, US
2:20	Medial temporal lobe subregional microstructure measured with ultra-high resolution diffusion imaging as a biomarker for early tau pathology and memory impairment	Jenna Adams , University of California, Irvine, Irvine, CA, US
2:35	Discussion	
3:00	KEYNOTE: ON MAKING NEUROIMAGING STUDIES MORE EQUITABLE, INCLUSIVE, AND RELEVANT	Monica Rivera-Mindt, PhD , Fordham University
3:30	Keynote Discussion	
3:45	POSTER SESSION 2B	
4:30 pm – 5:20 pm	SESSION VIII: LIFESTYLE AND LIVED EXPERIENCES	CHAIRS: Gil Rabinovici, MD , University of California, San Francisco Tobey Betthausen, PhD , University of Wisconsin-Madison
4:30	Introduction	Chairs
4:35	African American racialization modifies the association between apolipoprotein-E4 and amyloid deposition	Sarah Royse , Department of Epidemiology, University of Pittsburgh, Pittsburgh, PA, US
4:50	Cardiovascular risk and AD biomarkers in unimpaired older adults: A comparison of U.S. POINTER and ADNI	Susan Landau , University of California, Berkeley, Berkeley, CA, US
5:05	Association between mid-life social factors and estimated late life amyloid burden: the Atherosclerosis Risk in Communities (ARIC)-PET study	Renee Groechel , National Institute of Neurological Disorders & Stroke Intramural Research Program, National Institutes of Health, Bethesda, MD, US
5:20	Discussion	
5:45 pm – 8:00 pm	Networking Reception	
Friday, January 13, 2023		
7:30 am	Breakfast	
7:45	Mentor Session	
9:00 – 10:20	SESSION IX: LONGITUDINAL CHANGE IN TAU AND AMYLOID MARKERS	CHAIRS: Keith Johnson, MD , Massachusetts General Hospital William Jagust, MD , University of California, Berkeley
9:00	Introduction	Chairs
9:05	Longitudinal tau accumulation is associated with faster memory decline in typical aging and preclinical Alzheimer's disease	Corrina S. Fonseca , Helen Wills Neuroscience Institute, University of California, Berkeley, Berkeley, CA, US

9:20	The use of plasma markers to predict tau accumulation in a stage-specific manner	Cécile Tissot , McGill University, Montreal, QC, Canada
9:35	Temporal dynamics of plasma pTau217 and amyloid PET in preclinical AD	Tobey Betthausen , Wisconsin Alzheimer's Disease Research Center, University of Wisconsin-Madison, Madison, WI, US
9:50	Longitudinal changes in Alzheimer's disease-related plasma biomarkers in relation to changes in PiB PET measures of brain amyloid	Murat Bilgel , Laboratory of Behavioral Neuroscience, National Institute on Aging, Baltimore, MD, US
10:05	Longitudinal bidirectional associations between sleep and Alzheimer's pathology in At-Risk Cognitively Unimpaired Older Adults	Bery Mohammediyan, BA , Douglas Mental Health University Institute, Montreal, QC, Canada
10:20	Discussion	
10:45 am – 11:30	POSTER SESSION 3A	
73	Motion and partial volume corrections in dynamic [18F]-MK6240 PET imaging	Amal Tiss , Gordon Center for Medical Imaging, Department of Imaging, Massachusetts General Hospital, Boston, MA, US
74	Encoding, consolidation and retrieval deficits are differentially shaped by tau and atrophy in the Alzheimer's disease spectrum	Jaime Fernandez , Translational Neuroimaging Laboratory, Montreal Neurological Institute, McGill University, Montreal, QC, Canada
75	Comorbid medical conditions, anxiety, and amyloid- β pathology in cognitively unimpaired older adults	Olamide Abiose , Stanford University School of Medicine Department of Neurology & Neurological Sciences, Stanford, CA, US
76	Defining and characterizing neocortical tau resistance in preclinical Alzheimer's disease	Rachel Buckley , Massachusetts General Hospital, Department of Neurology, Boston, MA, US
77	Development and evaluation of image preprocessing pipelines for the Centiloid method	Weiquan Luo , Department of Radiology, University of Pittsburgh, Pittsburgh, PA, US
78	Cognitively estimated disease time: Associations with amyloid and tau burden in the Harvard Aging Brain Study	Diana Townsend , Department of Neurology, Massachusetts General Hospital, Boston, MA, US
79	Synergistic interaction between sex, amyloid and phosphorylated tau predicts the longitudinal progression of tau tangles	Yi-Ting Wang , McGill Centre for Studies in Aging, Montreal, QC, Canada
80	[18F]PI-2620 binding patterns in patients with suspected AD- and FTLT-tauopathies	Ganna Blazhenets , Memory and Aging Center, Department of Neurology, University of California, San Francisco, CA, US
81	Regional analysis of change in synaptic density over time by cognitive status	Alexandra DiFilippo , University of Wisconsin-Madison School of Medicine and Public Health, Madison, WI, US
82	Regional tau profiles in early tau pathology populations	Vikas Kotari , Eli Lilly and Company, Indianapolis, IN, US
83	[18F]MK-6240 tau-PET in an A β -enriched sample from the 1946 British birth cohort - Insight 46	William Coath , Dementia Research Centre, UCL Queen Square Institute of Neurology, University College London, London, UK
84	Longitudinal trajectories of depressive symptoms and regional amyloid accumulation (PiB PET) in clinically normal older adults	Catherine Munro , Brigham and Women's Hospital, Boston, MA, US
85	Improving sub-threshold PiB fidelity using relative radioligand delivery	Michael Properzi , Massachusetts General Hospital, Boston, MA, US
86	Improved prediction of preclinical cognitive decline using amyloid PET spatial extent	Michelle E. Farrell , Massachusetts General Hospital, Harvard Medical School, Boston, MA, US
87	18F-MK-6240 Tau PET as a Potential Biomarker for Chronic Traumatic Encephalopathy	Michael Alosco , Boston University Chobanian & Avedisian School of Medicine, Boston, MA, US
88	Psychosis and tau burden across the AD continuum	Aubrey S. Johnson , Columbia University Irving Medical Center, New York, NY, US
89	Classifying cognitive resilience to differing levels of Alzheimer's disease pathology	Rory Boyle , Massachusetts General Hospital, Harvard Medical School, Charlestown, MA, US
90	Cerebrospinal fluid neurofilament light predicts increased amyloid, tau, and decreased grey matter density	Mohit Manchella , Indiana University School of Medicine, Indianapolis, IN, US
91	Unhealthy white matter connectivity in African American and non-Hispanic white older adults	Sarah Royse , Department of Epidemiology, University of Pittsburgh, Pittsburgh, PA, US

92	Locus coeruleus integrity as neural substrate providing resilience against cognitive decline in the face of Alzheimer's disease pathology	Heidi IL Jacobs , Massachusetts General Hospital, Gordon Center for Medical Imaging, Boston, MA, US
93	Lower locus coeruleus integrity predicts diminished practice effects in cognitively normal older individuals	Lindsay Smegal , Gordon Center for Medical Imaging, Department of Radiology, Massachusetts General Hospital/ Harvard Medical School, Boston, MA, US
94	PET-based Braak staging predicts neuropsychiatric burden in the Alzheimer's disease continuum	Arthur C. Macedo , Translational Neuroimaging Laboratory, The McGill University Research Centre for Studies in Aging, Montreal, QC, Canada
95	A computational model to study the combined effect of neuronal connectivity loss and tauopathy progression	Arsalan Rahimabadi , PERFORM Centre, Concordia University, Montreal, QC, Canada
96	Simulated dose reduction in longitudinal [18F]MK-6240 PET	Max McLachlan , Department of Medical Physics, University of Wisconsin – Madison, School of Medicine and Public Health, Madison, WI, US
97	Regional amyloid change improves prediction of future tau progression over global metrics	Emma Thibault , Massachusetts General Hospital, Boston, MA, US
98	Rates of tau PET accumulation along the amyloid timeline in Alzheimer's disease	Karly Cody , Wisconsin Alzheimer's Disease Research Center, University of Wisconsin-Madison, Madison, WI, US
100	Body mass index, pathological tau, and cognition in preclinical AD: Could women with high BMI be protected?	Xin Wang , Department of Neurosciences, University of California, San Diego., La Jolla, CA, US
101	Amyloid drives later tau accumulation for fast progressors in early Braak stages	Stijn Servaes , Translational Neuroimaging Laboratory, McGill Research Centre for Studies in Aging, Montreal, QC, Canada
102	Brain-wide and AD-risk genetic expression: A descriptive study	Diana Hobbs , Washington University in St. Louis, St. Louis, MO, US
103	Behavioral brain networks underlying the effect of Alzheimer's pathology on cognition	Jacob Ziontz , Helen Wills Neuroscience Institute, University of California Berkeley., Berkeley, CA, US
104	Exploration of 18F-Florzolotau tau PET distribution patterns using machine learning approach in AD	Shao-Yi Huang , Medical Imaging & Radiological Sciences and Healthy Aging Research Center, Chang Gung University, Taoyuan, TW
105	The interplay of vascular disease, peripheral interleukin-6, beta-amyloid, and memory in older adults	Batool Rizvi , University of California, Irvine, Irvine, CA, US
106	Gut microbiome composition is associated with cortical amyloid burden in a preclinical human cohort	Margo Heston , Wisconsin Alzheimer's Disease Research Center, Madison, WI, US
107	Study on MR-free template-based spatial normalization for Tau PET Image Quantitation using 18F-Florzolotau	Zih-Ning Lee , Medical Imaging & Radiological Sciences and Healthy Aging Research Center, Chang Gung University, Taoyuan, TW
108	β -Amyloid in World Trade Center responders: Result indicate age-related toxic encephalopathy mediated by an immunogenic amyloid response	Sean Clouston , Stony Brook University, Stony Brook, NY, US
109	[18F]MK-6240 PET/MRI Test-Retest performance in cognitively normal elderly subjects	Cristina Lois , Gordon Center for Medical Imaging, Massachusetts General Hospital, Boston, MA, US
11:30 am – 01:50 pm	SESSION X: FLUID BIOMARKERS IN AD	CHAIRS: Henrik Zetterberg, MD, PhD , University of Gothenburg Donna Wilcox, PhD , University of Kentucky College of Medicine
11:30	Introduction	Chairs
11:35	Plasma p-tau ₂₁₇ ratios associated with amyloid and tau PET measures in preclinical AD: Findings from the AHEAD 3-45 Study screening data	Reisa Sperling , Mass General Brigham, Harvard Medical School, Boston, MA, US
11:50	Plasma biomarkers as stand-alone tests to rule out Alzheimer's disease	Joseph Therriault , McGill University, Montreal, QC, Canada
12:05	Comparative performance of three plasma A β ₄₂ /A β ₄₀ and two plasma p-tau ₁₈₁ assays versus amyloid-PET imaging status	Alicia Algeciras-Schimmich , Mayo Clinic, Rochester, MN, US

12:20	Prognostic utility of plasma p217+tau vs amyloid and tau PET in the Alzheimer continuum	Azadeh Feizpour , Department of Molecular Imaging & Therapy, Austin Health, Melbourne, Victoria, Melbourne, AU
12:35	Associations of blood biomarkers with early-onset Alzheimer's disease pathology	Paige E. Logan , Indiana University School of Medicine, Indianapolis, IN, US
12:50	Associations between amyloid PET, CSF pTau, and plasma biomarkers in memory clinic patients	Marina Bluma , Department of Neurobiology, Care Sciences and Society, Division of Clinical Geriatrics, Center for Alzheimer Research, Karolinska University, Stockholm, Sweden
1:05 pm	Lunch	
2:05 pm	Discussion	
2:30 pm	Keynote: BIOFLUIDS AND IMAGING: TWO SIDES OF THE SAME COIN	Thomas Karikari, PhD, University of Pittsburgh
3:00 pm	Keynote Discussion	
3:15 pm	POSTER SESSION 3B	
04:00 pm	AWARDS CEREMONY	
4:15 pm – 5:05 pm	SESSION XI: PLASMA WITH OTHER MODALITIES	Thomas Karikari Suzanne Schindler
4:15	Introduction	Chairs
4:20	Plasma biomarkers associated with cortical brain structure and multi-domain cognition in Alzheimer's disease and Parkinson's disease	Gillian Coughlan , Massachusetts General Hospital/Harvard Medical School, Boston, MA, US
4:35	Relationships of blood insulin with brain structures and plasma Aβ42 to Aβ40 ratio in a multi-ethnic cohort of older adults	Brandon Hall , Imaging Genetics Center, Mark and Mary Stevens Neuroimaging and Informatics Institute, Keck School of Medicine, University of Southern California, Los Angeles, CA, US
4:50	Unique biological pathways associated with plasma ptau species and AD PET: an imaging-transcriptomic study	Min Su Kang , Artificial Intelligence and Computational Neurosciences lab, Sunnybrook Research Institute, University of Toronto, Toronto, ON, Canada
5:05	Discussion	
5:30	Concluding Remarks	

HAI 2023 ABSTRACTS

Wednesday, January 11, 2023 - 08:30 am - 09:35 am

Podium Session

SESSION I: Tracer development and evaluation

Wednesday, January 11, 2023		
8:30 am - 9:35 am	SESSION I: TRACER DEVELOPMENT AND EVALUATION	CHAIRS: Julie Price, PhD, <i>Massachusetts General Hospital</i> Chet Mathis, PhD, <i>University of Pittsburgh</i>
8:30	Introduction	Chairs
8:35	Advances towards the identification of an α -synuclein Positron Emission Tomography radioligand for the diagnosis of Parkinson's Disease	Idriss Bennacef, PhD, <i>Merck & Co.</i>
8:50	Discovery of [18F]ACI-12589, a novel and promising PET-tracer for a-synuclein	Francesca Capotosti, PhD, <i>AC Immune</i>
9:05	Discovery and preclinical evaluation of two novel PET tracers for imaging non-AD tauopathies	Marc Skaddan, PhD, <i>AbbVie</i>
9:20	In Vivo Head-To-Head Comparison of [18F]GTP1, [18F]PI2620, and [18F]MK6240 in Alzheimer's Disease	Matteo Tonietto, PhD, <i>F. Hoffman-La Roche</i>
9:35	DIDACTIC PRESENTATION: ANTIBODY PET	Dag Sehlin, PhD, Uppsala University
10:00	Discussion	

Advances towards the identification of an α -synuclein Positron Emission Tomography radioligand for the diagnosis of Parkinson's Disease

Idriss Bennacef¹, Zhizhen Zeng¹, Patricia Dockery¹, Kerry Riffel¹, Mona Purcel¹, Kyking Haley¹, Xiangjun Meng¹, Mallory J Stenslik¹, Yuchuan Wang¹, Anthony J Roecker², Robert Drolet³, Tapan Nayak¹, Wenping Li¹, Eric Hostetler¹

¹Translational Imaging, MRL, Merck & Co., Inc., West Point, PA, US

²Discovery Chemistry, MRL, Merck & Co., Inc., West Point, PA, US

³Neuroscience Dept., MRL, Merck & Co., Inc., West Point, PA, US

Background: Deposition of misfolded α -synuclein (α -Syn) aggregates in the human brain is one of the major hallmarks of synucleinopathies. Recently [¹⁸F]ACI-12589 - PET showed elevated tracer uptake in cerebellar white matter in multiple system atrophy patients. However, a target-specific tracer to detect pathological aggregates of α -Syn in PD remains elusive. Here, we present the in-vitro and preclinical in-vivo characterization of compound S.

Method: Competition binding and autoradiographic studies were performed in cortexes of PD patients, healthy control, and Alzheimer's disease brain tissue, as well as the mid-brain region of the aged A30P mouse using [³H]S. [¹¹C]S brain PET experiments were carried out in a healthy non-human primate (NHP) and the 20 mo. A30P mice.

Results: Compound S is a sub-nanomolar affinity ligand to human α -Syn, and the A30P mouse α -Syn. Lower affinity was observed in AD and HC brain tissues (18-27 nM, 16 nM). [³H]S showed displaceable binding in PD brain cortex and A30P mid-brain, and little binding in AD and HC. In the NHP, [¹¹C]S crosses the brain-blood-barrier and the uptake phase is followed by a washout. [¹¹C]S PET studies in A30P mice showed higher uptake in the mid brain and brainstem, with standard uptake value ratios (vs cerebellum) in those regions higher than 2.0.

Binding of [³H]Compound S to Human PD Pooled Brain Homogenate from MJFF (2.2 mg/ml wet weight) (Hot Saturation) SNB0013_2634

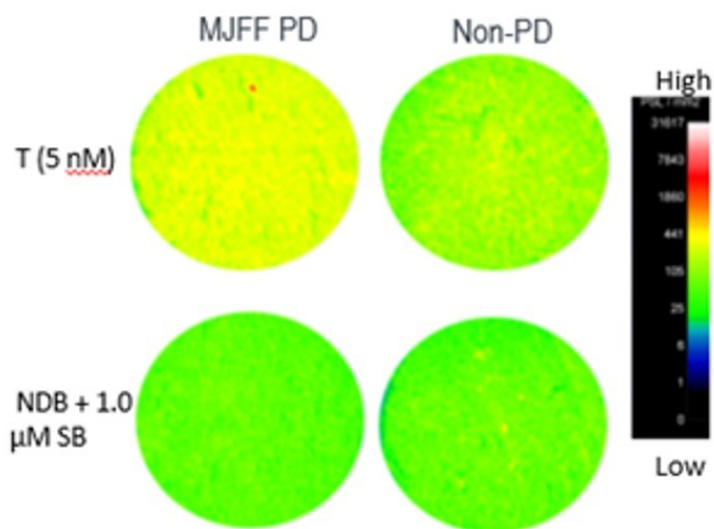
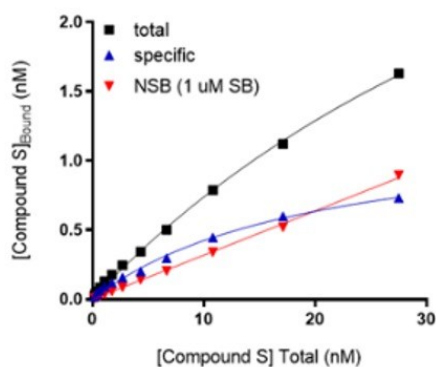


Figure 1. [³H]S competition binding and autoradiographic studies in PD and non-PD tissue, (abbrev. MJFF: Michael J. Fox Foundation, T = total, NDB: Non-displaceable Binding, SB: Self-Block)

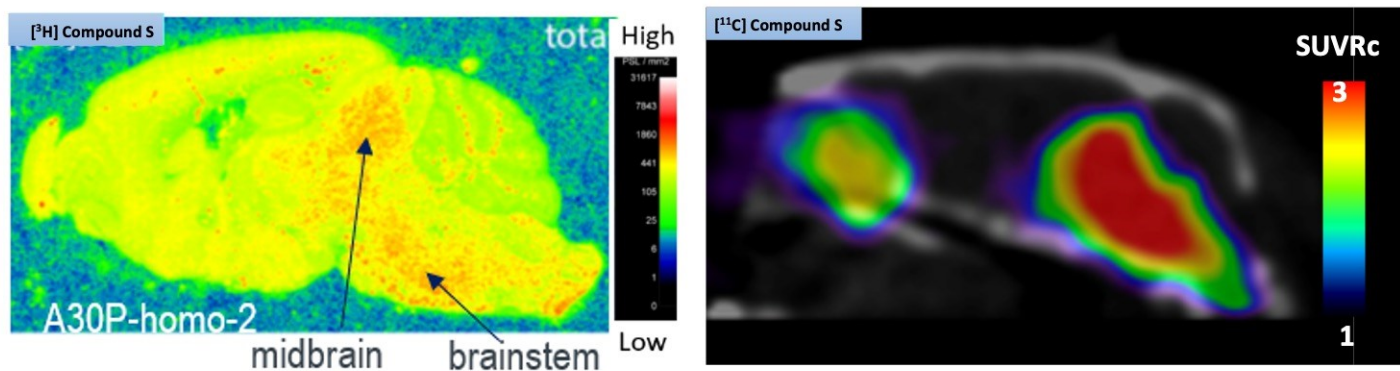


Figure 2. [3H]S autoradiography, and [11C]S brain PET of a 20 month old homozygote A30P mouse.
 Abbrev.: SUVRc: Standard Uptake Value ratio to cerebellum

Conclusion: *Compound S is potent for α -Syn in vitro, and PET imaging in the A30P mice showed an elevated signal in regions known to accumulate α -Syn. This dataset suggests that the Compound S has promise towards imaging α -Syn in PD patients.*

Keywords: alpha-synuclein, protein aggregation/misfolding, A30P, Biomarkers, PET Imaging

Discovery of [18F]ACI-12589, a novel and promising PET-tracer for a-synuclein

Francesca Capotosti¹, Efthymia Vokali¹, Jerome Molette¹, Myriam Ravache¹, Christophe Delgado¹, Jacqueline Kocher¹, Laure Pittet¹, Coralie Vallet¹, Ioannis Dimitrakopoulos¹, Ruth Luthi-Carter¹, Valerie Hliva¹, Ruben Smith^{2,3}, Oskar Hansson^{2,4}, Johannes Streffer^{1,5}, Andrea Pfeifer¹, Marie Kosco-Vilbois¹

¹AC Immune SA, Lausanne, Switzerland

²Clinical Memory Research Unit, Department of Clinical Sciences, Malmö, Sweden

³Department of Neurology, Skåne University Hospital, Lund, Sweden

⁴Memory Clinic, Skåne University Hospital, Lund, Sweden

⁵University of Antwerp, Antwerp, Belgium

Background: Parkinson's disease (PD) and other synucleinopathies such as Multiple System Atrophy (MSA) involve a progressive accumulation of a-synuclein (a-syn) inclusions that correlates with clinical manifestations. The development of a PET agent capable of imaging a-syn inclusions would significantly aid in differential diagnosis, staging and monitoring possible benefits of candidate therapeutic agents targeting a-syn.

Methods: Using our proprietary Morphomer[®] library of conformation-specific ligands, compounds with good affinity and target occupancy were identified. We then iteratively performed medicinal chemistry optimization to improve affinity and selectivity using radiobinding and autoradiography techniques. Optimized compounds were then characterized for off-target binding and pharmacokinetic properties in non-human primates (NHPs). The clinical candidate, [18F]ACI-12589, was subsequently advanced through preclinical assessment prior to evaluation in a clinically diverse set of cases, including healthy controls, patients with synucleinopathies or other neurodegenerative diseases (NDDs).

Results: Promising chemical scaffolds with high-affinity binding to pathological a-syn have been extensively explored. Particularly, ACI-12589 demonstrated good target occupancy on different synucleinopathy samples, including PD and MSA, with a binding pattern aligning closely with the distribution of pathological a-syn. Moreover, ACI-12589 demonstrated selectivity for a-syn versus other potential proteinaceous pathologies including amyloid-beta, Tau and TDP-43 and a clean off-target profile. ACI-12589 also shows binding to a-syn inclusions in tissue from different NDDs when such inclusions were present as co-pathology. Results from ongoing clinical trials confirm favorable pharmacokinetic parameters in patients, including rapid signal equilibration, potentially allowing short scan times. Moreover, in MSA patients, [18F]ACI-12589 uptake occurs in brain areas affected by the disease process based on clinical manifestations.

Conclusions: [18F]ACI-12589 displays preclinical and clinical characteristics deemed necessary to become a reliable PET radiotracer for the imaging of a-syn inclusions with data already demonstrating that the retention distinguishes MSA cases from other NDDs. Investigations are continuing to further understand the utility in other NDDs.

Keywords: a-synuclein, PET, Parkinson's disease, Multiple System Atrophy

Discovery and preclinical evaluation of two novel PET tracers for imaging non-AD tauopathies

Marc B. Skaddan¹, Thomas Erhard², Manolo Mugnaini², Simon Seifarth², Hervé Geneste², Kuo-Hsien Fan¹, David Reuter¹, Yuchuan Zhuang¹, Dan Sunnemark³, Helen Jongsma Wallin³, Dustin W. Wooten¹, Martin J. Voorbach¹, Kyle Wilcox¹, Srirajan Vaidyanathan¹, William Lambert¹, Qi Guo¹, Miroslav Cik², Corinna Klein², Stefan Barghorn², Sjoerd J. Finnema¹, Robert A. Comley¹

¹AbbVie Inc., North Chicago, IL, US

²AbbVie Deutschland GmbH & Co. KG, Neuroscience Research, Ludwigshafen, Germany

³Offspring Biosciences AB, Södertälje, Sweden

Objectives: This work describes the development of ¹⁸F-radiolabeled positron emission tomography (PET) tracers for imaging tau aggregates in progressive supranuclear palsy (PSP) and potentially other tauopathies.

Methods: Structure activity relationships were explored using hits from an AD tau tracer discovery program, focusing on structures which displayed potential binding to PSP tau aggregates. After improving physicochemical properties, off-target selectivity, free fractions, non-specific binding, and pharmacokinetic properties, tau affinity was measured for the most promising compounds using autoradiography (ARG) on PSP tissue. Tau-aggregate binding was confirmed by ARG of ³H-radiolabelled compounds in tau-rich, amyloid-beta negative PSP brain sections. Comprehensive experiments were also conducted to assess potential off-target binding. A small number of candidates were ¹⁸F-radiolabeled and characterized in PET studies in cynomolgus monkeys.

Results: Tracer-1 and Tracer-2 displayed high affinity ($K_D < 20$ nM) and were highly selective for PSP tau, with a binding pattern on PSP tissue matching the distribution of tau aggregates as determined by immunohistochemistry. Both tracers exhibit good binding to AD brain homogenates ($K_i = 18$ -39 nM) and an ARG binding pattern consistent with tau neurofibrillary pathology in AD. In NHP PET studies, both tracers exhibited good brain uptake, a homogeneous distribution, fast washout kinetics, and no specific (off-target) binding.

Conclusions: Tracer-1 and Tracer-2 achieve the pre-clinical performance requirements for brain PET tracers to quantify tau aggregates in PSP. Further evaluation of these tracers in clinical studies is warranted.

Keywords: Tau, positron emission tomography, progressive supranuclear palsy, F-18, non-human primates

In Vivo Head-To-Head Comparison of [18F]GTP1, [18F]PI2620, and [18F]MK6240 in Alzheimer's Disease

Matteo Tonietto¹, Cristian Constantinescu², Sandra Sanabria Bohorquez³, Edmond Teng³, Dan Abramzon³, Cecilia Monteiro³, Roger Gunn⁴, David Russell², Santiago Bullich⁵, Andrew Stephens⁵, Andrew Mueller⁵, Gregory Klein¹

¹Research and Early Development (pRED), Hoffmann-La Roche, Basel, Switzerland

²Invicro LLC, Needham, MA, US

³Research and Early Development (gRED), Genentech, Inc., South San Francisco, CA, US

⁴Invicro LLC, London, UK

⁵Life Molecular Imaging, Berlin, Germany

Introduction: This study compared the *in-vivo* characteristics of [18F]GTP1 and [18F]PI2620, and [18F]GTP1 and [18F]MK6240 tau PET tracers in two cohorts of participants ranging from cognitively unimpaired to moderate AD.

Methods: The characteristics of the two cohorts are presented in Table 1. Images were acquired between 60 and 90min post injection for [18F]GTP1 (injected activity=261±11MBq), between 45 and 75min for [18F]PI2620 (injected activity=189±11MBq), and between 90 and 110min for [18F]MK6240 (injected activity=190±6MBq). SUVR values were calculated using the inferior cerebellar cortex as reference region in two sets of ROIs: one based on Braak stages, the other on brain lobes (medial temporal, lateral temporal, frontal, parietal and occipital regions). Pearson correlation and total least square regression were used to compare SUVR values between tracers. Slope and intercept were expressed with [18F]GTP1 as the independent variable.

Results: In all Braak ROIs except for Braak II (i.e., hippocampus), [18F]GTP1 SUVRs were highly correlated with both [18F]PI2620 SUVRs ($r=[0.86, 0.93]$) and [18F]MK6240 SUVRs ($r=[0.97, 0.99]$). In Braak II, [18F]GTP1 SUVR was poorly correlated with both [18F]PI2620 ($r=0.41$), and [18F]MK6240 ($r=0.44$). Across the Braak ROIs (Braak II excluded), [18F]GTP1 average regression coefficients were slope=1.3±0.1 and intercept=-0.35±0.15 with [18F]PI2620, and slope=2.67±0.21 and intercept=-1.95±0.30 with [18F]MK6240 (Figure 1). Consistent results were found using lobar ROIs (Figure 2).

Conclusion: [18F]GTP1 SUVR values were highly correlated with those of [18F]PI2620 and [18F]MK6240 in all the ROIs considered with exception of Braak II/hippocampus, a result that needs further investigation. [18F]MK6240 had the widest SUVRs range, followed by [18F]PI2620 and [18F]GTP1. However, it remains to be determined if a wider SUVR range translates to higher statistical power. These preliminary results support the development of standardized quantification scales that are tracer independent.

Table 1. Demographic and clinical characteristics of the two cohorts. CU: Cognitively unimpaired; Prod: Prodromal; Mod: moderate; AD: Alzheimer's Disease.

	Cohort [18F]GTP1 - [18F]PI2620				Cohort [18F]GTP1 - [18F]MK6240			
	CU Aβ-	Prod AD	Mild AD	Mod AD	CU Aβ-	Prod AD	Mild AD	Mod AD
N	5 (1F)	10 (6F)	10 (6F)	2 (1F)	5 (4F)	1 (1F)	2 (0F)	3 (1F)
Age	71±1	72±5	70±6	62±1	68±3	73±0	69±6	67±9
MMSE	30	24-30	20-28	16	29-30	29	21-22	15-18
CDR	0	0.5	0.5-1	0.5-1	0	0.5	0.5	0.5-2

Figure 1.

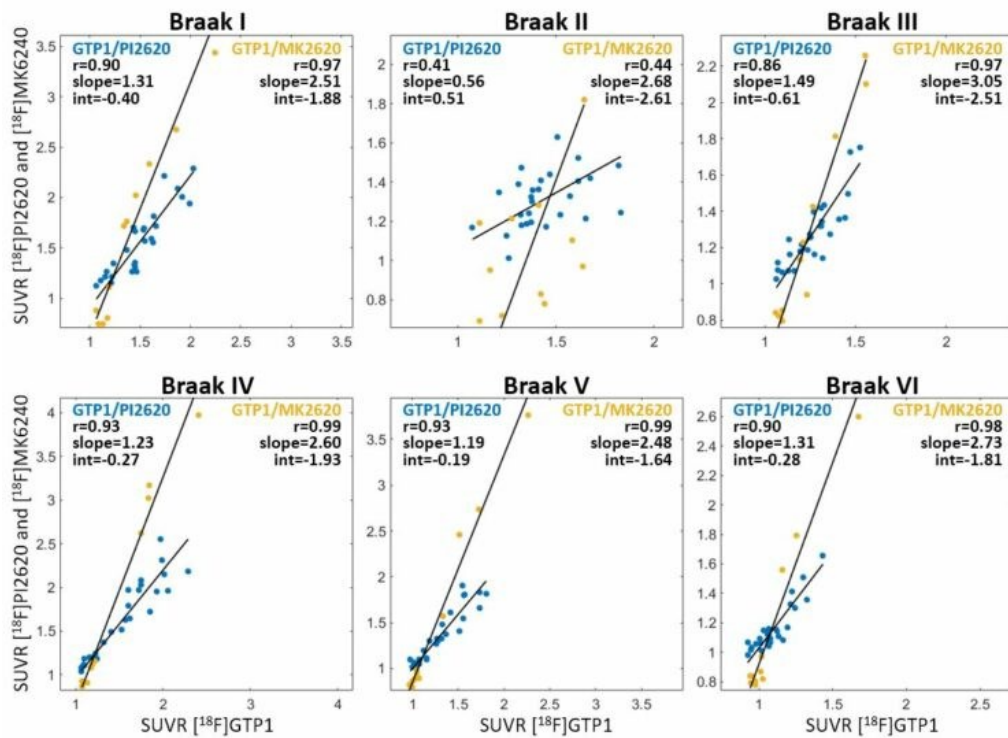
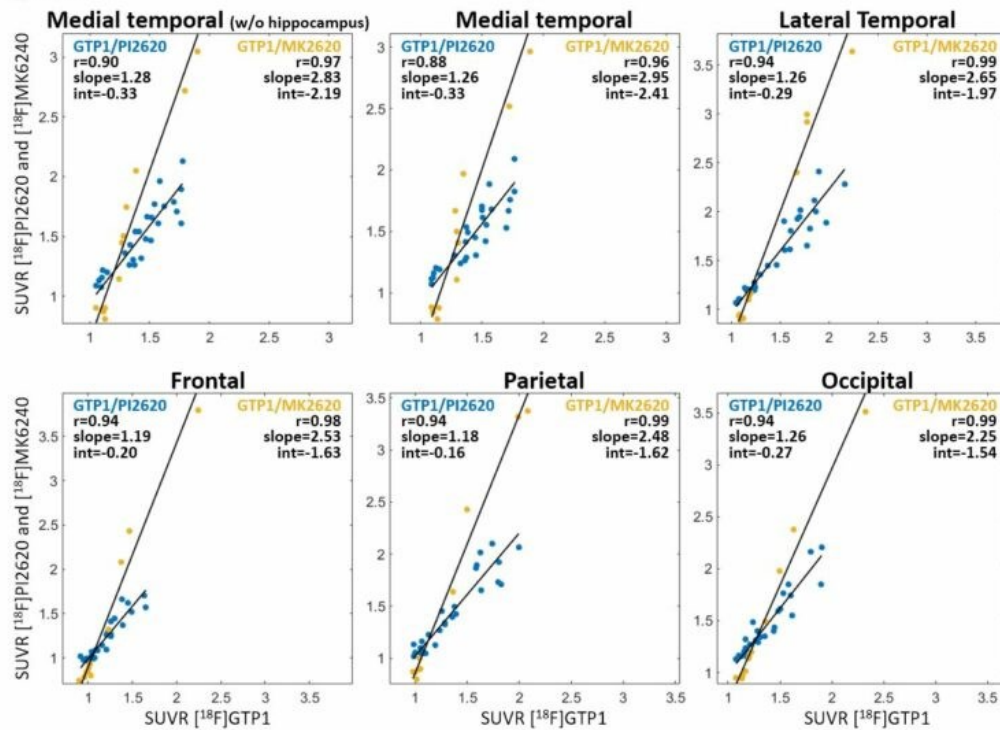


Figure 2.



Keywords: PET, Alzheimer's Disease, imaging, SUVR, GTP1, PI2620, MK6240

DIDACTIC LECTURE: PET imaging beyond amyloid with antibody-based radioligands

Dag Sehlin

Uppsala University

During the past two decades, amyloid PET imaging has been an extremely important tool in Alzheimer's disease (AD) research and drug development. It has increased our understanding of how amyloid plaques deposit in the brain over time and greatly improved patient selection and evaluation of treatment effects in clinical trials. However, current amyloid ligands are based on small molecules with affinity to certain structural elements of the amyloid fibrils that constitute the plaques. As such, they will primarily detect the amyloid core of amyloid- β (A β) deposits, while leaving diffuse and soluble A β aggregates undetected. An alternative to small molecular amyloid ligands could be to use ligands based on antibodies, which can be designed to bind with high affinity to a defined stretch of amino acids or recognize the structure of soluble or diffuse aggregates of a protein such as A β .

Antibodies are large molecules with low and slow brain distribution and have therefore not been used for brain PET. However, they can be designed for more efficient passage across the blood-brain barrier (BBB) into the brain parenchyma, using a 'Molecular Trojan horse' strategy based on receptor mediated transcytosis. This strategy has been used in a number of preclinical studies and in some clinical trials, to shuttle therapeutic antibodies across the BBB for treatment of neurodegenerative diseases. In line with this, we and others are exploring the possibility to use antibody-based radioligands, of different formats and sizes, for PET imaging of aggregated proteins in preclinical models of AD.

This lecture will discuss advantages and challenges of this strategy, with focus on antibody brain uptake, target recognition and detection; ligand pharmacokinetics and how this links to radiolabeling strategies; as well as considerations for translation to clinical use in humans.

Poster Session 1A

Wednesday, January 11, 2023

Board #	POSTER SESSION 1A	
1	Effects of de-facing PET and MRI scans on clinical correlations analyses	Schwarz Kremers Weigand Prakaashana Senjem Lowe Gunter Kantarci Vemuri Petersen Knopman Jack
2	Non-invasive quantification and SUVR validation of [18F]-florbetaben with total-body EXPLORER PET	Holy Alfaro Fletcher Bhattarai Spencer Cherry DeCarli Fan
3	PET imaging probe development for aggregated alpha-synuclein	Gomperts Liu Bai Xu Rose Celikag Ndayisaba Khurana Bartels Wang
4	Cross-modality transformer for low-dose tau PET imaging	Jang Lois Becker Thibault Price Johnson El Fakhri Gong
5	Tau PET positivity reveals Alzheimer's disease related fast cognitive decline	Ioannou Bucci Nordberg Chiotis
6	Positive 18F-APN-1607 tau PET imaging findings in patients with Progressive Supranuclear Palsy-like extrapyramidal symptoms caused by TBK1 mutations	Liu Lu Sun Li Yen Jang Zuo Wang
7	In vivo visualization of tau deposits in corticobasal syndrome by 18F-Florzolotau PET	Liu Lu Li Jiao Chen Yao Liang Ge Li Shen Wu Sun Wu Yen Zuo Wang
8	Imaging neuroinflammation with astrocyte-PET and bio-fluid biomarkers in patients with cognitive impairment	Chiotis Jelic Rodriguez-Vieitez Savitscheva Wall Antoni Nordberg
9	[18] Flortaucipir PET and Diffusion Tensor Tractography Coregistration can Enhance Detection of Brain Changes Associated with Progressive Apraxia of Speech	Gatto Duffy Utianski Clark Botha Machulda Lowe Josephs Whitwell
10	Towards a simplified flortaucipir-PET read method for assessing tau burden	Tunali Iaccarino Ducker Patel DiFabbio Kowaleski Arora Kim Lu Pontecorvo Shcherbinin
12	Digital clock drawing performance is associated with tau deposition measured with PET in preclinical Alzheimer's disease	Fu Rentz Mayblyum Thibault Buckley Das Papp Sperling Penney Davis Johnson Price
13	[18F]RO-948 Tau PET Retention and Correlation with Fluid Biomarkers in the Early AD Continuum	Shekari González Escalante Milà-Alomà Falcon Niñerola-Baizán Tonietto Borroni Klein J. Ashton K. Karikari Lantero-Rodriguez Snellman Ortiz Vanmechelen Minguillón Fauria Perissinotti Molinuevo Zetterberg Blennow Grau-Rivera Suárez-Calvet Domingo Gispert

14	Regional tau predicts glucose hypometabolism in autosomal dominant Alzheimer's disease: Findings from the Colombia-Boston (COLBOS) biomarker study	Langella Kaplan Baena Londono Munera Vila-Castelar Alvarez Vidal Properzi Sanchez Sperling Johnson Lopera Hanseeuw Quiroz
15	Is tau PET a robust biomarker for chronic traumatic encephalopathy?	Krishnadas Doré Lamb Guzman Ponsford Hicks Williams Feizpour Villemagne Rowe
16	Centiloid scale measure of amyloid PET by CT of PET/CT equipment	Matsuda Hanyu Kaneko
17	Successful cognitive aging is associated with less brain atrophy and lower tau deposition	Pezzoli Giorgio Harrison Martersteck Jagust
18	Subcortical flortaucipir PET and susceptibility analyses to differentiate progressive supranuclear palsy clinical variants and corticobasal syndrome	Satoh Arani Schwarz Senjem Ali Jack Lowe Josephs Whitwell
19	Temporal associations of plasma and PET Alzheimer's disease biomarkers using a non-linear mixed effects model	Cogswell Lundt Therneau Graff-Radford Schwarz Senjem Gunter Vemuri Petersen Jack Jr
20	Beta-amyloid accumulates at a faster rate in individuals with Down syndrome	McVea DiFilippo McLachlan Murali Zammit Johnson Betthausen Stone Tudorascu Laymon Klunk Cohen Handen Christian
21	Magnitude of MK6240 off-target binding correlated with spill-in effects in target regions	McVea DiFilippo McLachlan Johnson Betthausen Christian
22	Amyloid and tau pathology associated with different cognitive declines in cognitively normal older people	Chen Juarez Baker Harrison Landau Jagust
23	Future amyloid accumulation status affects the preservation of peripheral whole-blood gene co-expression networks at baseline in asymptomatic Alzheimer's disease	Lockett Zielonka Schaefferbeke Adamczuk Van Laere Dupont Cleynen Vandenberghe
24	Validation of [18f]florbetaben PET quantitation based on the analysis of 15 software pipelines	Jovalekic Roé-Vellvé Koglin Lagos Quintana Nelson Diemling Lilja Gómez González Doré Bourgeat Whittington Gunn Stephens Bullich
25	Preprocessing 10,700 real-world amyloid-PET scans from the IDEAS study: the Good, the Bad and the Ugly	Mejia Perez Mundada Blazhenets Soleimani-Meigooni Zeltzer Cho Ranasinghe Windon Yadollahikhales Iaccarino Carrillo Gatsonis March Apgar Siegel Hilner Whitmer Rabinovici La Joie
26	Longitudinal tau-PET differs between progressive apraxia of speech subtypes	Tetzloff Martin Duffy Clark Utianski Botha Machulda Schwarz Senjem Jack Jr. Lowe Josephs Whitwell
27	Cross-sectional PET Analyses in the Longitudinal Early-onset Alzheimer's Disease Study (LEADS)	Cho Mundada Apostolova Carrillo Shankar Amuri Zeltzer Windon Soleimani Meigooni Tanner Lawhn Heath Aisen Eloyan Koeppe Iaccarino Dickerson La Joie Rabinovici
28	Dynamic amyloid PET: relationships to tau PET and cognition in Alzheimer's disease	Raman Charniaux Murchison Fang Tzabari Liu Morris Chen Joseph-Mathurin Ponisio Flores Kennedy Benzinger Roberson McConathy

29	Spatial extent and intensity of Alzheimer-associated tau PET burden is greater in agrammatic than logopenic primary progressive aphasia	Martersteck Sridhar Coventry Weintraub Mesulam Rogalski
30	Comparing PI2620 and Flortaucipir in Progressive Supranuclear Palsy Subjects	Thomas Blazhenets La Joie Rabinovici Heuer Jagust Boxer Baker
31	Assessing a universal neocortical mask for Centiloid quantification	Bourgeat Dore Rowe Benzinger Tosun Goyal LaMontagne Jin Weiner Morris Masters Fripp Villemagne
32	Relationships between Neuronal Hyperactivity, Stress Susceptibility, and Alzheimer's Disease pathology	Sharp Razlighi Oh
33	A/T/N, cognitive, health and lifestyle differences across white matter hyperintensities groups in aged 45-85 years adults: Results from the Wisconsin Registry for Alzheimer's Prevention (WRAP)	Du Burghy Cody Hermann Jonaitis Betthausen Chin Cadman Rivera-Rivera Peret Johnson Rowley Pompa Lose Christian Janelidze Hansson Johnson Eisenmenger Kosciak
34	Medial temporal 18F-MK6240 levels are associated with global graph characteristics of functional connectivity from high-density EEG in the asymptomatic and prodromal stage of Alzheimer disease	Spruyt Reinartz Meade Khachatryan Van Hulle Van Laere Dupont Vandenberghe
35	Longitudinal PET assessments of tau pathologies in progressive supranuclear palsy with 18F-florzolotau (PM-PBB3/APN-1607)	Endo Takado Tagai Matsuoka Kokubo Hirata Kataoka Oya Matsumoto Kurose Ichihashi Hatano Saiki Hirano Nakano Furukawa Takeda Iose Imai Yagi Nishida Yuasa Ono Seki Takahata Tokuda Shinotoh Shimada Kawamura Zhang Higuchi
36	Head-to-head comparison of tau PET tracers [18F]PI2620 and [18F]RO948 in non-demented individuals with brain amyloid deposition: the TAU-PET FACEHBI cohort	Klein Marquié Sotolongo-Grau Roé-Vellvé Bullich Tartari Sanabria García-Sánchez Borroni Galli Tonietto Pérez-Martínez Tárraga Ruiz Stephens Boada

P1 Effects of de-facing PET and MRI scans on clinical correlations analyses

Christopher Schwarz¹, Walter Kremers¹, Stephen Weigand¹, Carl Prakaashana¹, Matthew Senjem¹, Val Lowe¹, Jeffery Gunter¹, Kejal Kantarci¹, Prashanthi Vemuri¹, Ronald Petersen¹, David Knopman¹, Clifford Jack¹

¹Mayo Clinic, Rochester, MN, US

Background: De-identified brain PET, CT, and MRI scans can potentially be re-identified using face recognition. Direct differences between automated tissue volume and SUVR measurements from original vs. de-faced images are statistically significant but much smaller than scan-rescan differences. However, effects of de-facing on typical analyses correlating imaging biomarkers with clinical variables have not been studied.

Methods: From Mayo Clinic aging studies, we sampled 3 age-and-sex-matched groups (CU, MCI, and clinical AD) each with 61 participants with same-visit MRI, PiB, and Flortaucipir scans (total n=183). We calculated MRI hippocampal volume, PIB global SUVR, and tau temporal meta-ROI SUVR using a) our in-house pipeline with SPM12, MCAL, and ANTs, and b) FreeSurfer 7.3.2 (PETSURFER). For each measurement, we calculated AUC of pair-wise group separation and Spearman's ρ with age and CDR-SOB. We then de-faced all PET and MRI using *mri_reface*, our top-performing automated software that replaces face imagery with an average face, and we replicated all clinical correlations with these de-faced images. We then directly compared the strengths of paired original vs. de-faced analyses.

Results: There was high agreement between clinical correlations using original vs. de-faced images. Only 1/40 paired comparisons was significant (tables 1-2): global PIB SUVR from de-faced images with FreeSurfer more strongly correlated with age (ρ 0.003 vs -0.227, $p=0.046$). Another had $p=0.041$ for a difference in AUCs of +0.008, which we consider not practically meaningful. All others had p -values > 0.05 .

Discussion: De-facing PET and MRI using *mri_reface* did not significantly affect 39/40 correlations between imaging and clinical variables, and the one affected became stronger with re-faced data. Because automated brain segmentations are affected by non-brain image content, including the face, stronger correlations with clinical variables may be explained by de-facing's standardizing these irrelevant sources of variance. Future work will examine voxel-based comparisons and additional de-facing software.

Group-Separation AUC: CU vs AD

Region	Analysis	PVC	Pipeline	auc_original	auc_mri_reface	diff	p.value
Hippocampus	GMVol	None	FreeSurfer	0.837	0.829	-0.008	0.45163
Hippocampus	GMVol	None	Mayo	0.840	0.840	-0.001	0.783
GlobalPiB	PIB	None	FreeSurfer	0.912	0.899	-0.013	0.78417
GlobalPiB	PIB	None	Mayo	1.000	1.000	0.000	1
GlobalPiB	PIB	PVC2	Mayo	0.999	1.000	0.001	0.38449
Tau_Meta	tau	None	FreeSurfer	0.969	0.962	-0.007	1
Tau_Meta	tau	None	Mayo	0.912	0.913	0.001	0.57189
Tau_Meta	tau	PVC2	Mayo	0.928	0.927	-0.001	0.65267

Group-Separation AUC: CU vs MCI

Region	Analysis	PVC	Pipeline	auc_original	auc_mri_reface	diff	p.value
Hippocampus	GMVol	None	FreeSurfer	0.685	0.694	0.009	0.49177
Hippocampus	GMVol	None	Mayo	0.698	0.682	-0.017	0.30834
GlobalPiB	PIB	None	FreeSurfer	0.778	0.729	-0.049	0.65065
GlobalPiB	PIB	None	Mayo	0.999	0.994	-0.005	0.25054
GlobalPiB	PIB	PVC2	Mayo	0.982	0.990	0.008	0.51872
Tau_Meta	tau	None	FreeSurfer	0.844	0.849	0.004	0.67303
Tau_Meta	tau	None	Mayo	0.736	0.744	0.008	0.041896
Tau_Meta	tau	PVC2	Mayo	0.716	0.733	0.018	0.14679

Note: Although row 7 contains a statistically significant p-value < 0.05 , the difference in AUCs of +0.008 is not practically meaningful. We attribute this inconsistent p-value to the nearly perfect correlation between the two methods.

Group-Separation AUC: MCI vs AD

Region	Analysis	PVC	Pipeline	auc_original	auc_mri_reface	diff	p.value
Hippocampus	GMVol	None	FreeSurfer	0.676	0.668	-0.009	0.48139
Hippocampus	GMVol	None	Mayo	0.663	0.678	0.014	0.39132
GlobalPiB	PIB	None	FreeSurfer	0.662	0.626	-0.035	0.56502
GlobalPiB	PIB	None	Mayo	0.633	0.633	0.001	0.70932
GlobalPiB	PIB	PVC2	Mayo	0.662	0.659	-0.003	0.37451
Tau_Meta	tau	None	FreeSurfer	0.749	0.689	-0.059	0.75626
Tau_Meta	tau	None	Mayo	0.777	0.777	-0.001	0.65267
Tau_Meta	tau	PVC2	Mayo	0.796	0.793	-0.003	0.21785

Table 1: Pair-wise clinical group separation AUCs with values computed from original vs. de-faced images. AUC values were computed with `PROC:auc()` in R, and p-values used `PROC:roc.test()` with DeLong's method. PVC refers to partial volume corection, and PVC2 is two-compartment (Meltzer, 1990) PVC. GMVol refers to gray matter volume. PiB refers to Pittsburgh Compound B. AUC refers to the area under the receiver operating characteristic curve.

Spearman correlations for CDR Sum of Boxes

Region	Analysis	PVC	Pipeline	rho_original	rho_mri_reface	diff_mag	p.value
Hippocampus	GMVol	None	FreeSurfer	-0.444	-0.432	0.012	0.44168
Hippocampus	GMVol	None	Mayo	-0.449	-0.469	-0.019	0.31809
GlobalPiB	PIB	None	FreeSurfer	0.502	0.498	0.004	0.66634
GlobalPiB	PIB	None	Mayo	0.695	0.695	-0.000	0.94474
GlobalPiB	PIB	PVC2	Mayo	0.709	0.708	0.001	0.88287
Tau_Meta	tau	None	FreeSurfer	0.591	0.632	-0.041	0.16516
Tau_Meta	tau	None	Mayo	0.589	0.593	-0.004	0.19483
Tau_Meta	tau	PVC2	Mayo	0.615	0.614	0.001	0.87442

Spearman correlations for age

Region	Analysis	PVC	Pipeline	rho_original	rho_mri_reface	diff_mag	p.value
Hippocampus	GMVol	None	FreeSurfer	-0.361	-0.361	-0.001	0.96427
Hippocampus	GMVol	None	Mayo	-0.220	-0.226	-0.006	0.7562
GlobalPiB	PIB	None	FreeSurfer	0.003	-0.227	-0.224	0.04625
GlobalPiB	PIB	None	Mayo	0.036	0.037	-0.001	0.66612
GlobalPiB	PIB	PVC2	Mayo	0.039	0.033	0.005	0.39812
Tau_Meta	tau	None	FreeSurfer	-0.027	-0.171	-0.144	0.11698
Tau_Meta	tau	None	Mayo	-0.145	-0.141	0.004	0.21199
Tau_Meta	tau	PVC2	Mayo	-0.142	-0.145	-0.003	0.65961

Table 2: Spearman correlations of imaging-based measurements with CDR-SOB (Clinical Dementia Rating Sum of Boxes) and with age, using original vs. de-faced images. Spearman's rho values were computed with `cor.test()` in R, and p-values used Choi's Nonparametric Test of Equality of Dependent Spearman Correlations. `diff_mag` gives the difference between the two magnitudes of the rho values.

Keywords: quantification, de-identification, de-facing, amyloid pet, tau pet

P2 Non-invasive quantification and SUVR validation of [18F]-florbetaben with total-body EXPLORER PET

Emily Holy¹, Evelyn Alfaro¹, Evan Fletcher¹, Anjan Bhattarai^{1,2}, Benjamin Spencer³, Simon Cherry³, Charles DeCarli¹, Audrey Fan^{1,2}

¹Department of Neurology, UC Davis Health, Davis, CA, US

²Department of Biomedical Engineering, UC Davis, Davis, CA, US

³Department of Radiology, UC Davis Health, Davis, CA, US

Introduction: The total-body EXPLORER PET scanner supports the acquisition of a full human body in one scan and permits noninvasive Image-Derived Input Functions (IDIFs) as an alternative to arterial blood sampling (Badawi, JNM 2019). Our aim is to quantify amyloid buildup in older individuals with kinetic models that leverage dynamics in aorta IDIFs and the brain utilizing [18F]-Florbetaben EXPLORER PET and validate with standardized uptake value (SUVR).

Methods: Fourteen adults (9 cognitively-normal, 2 Mild Cognitive Impairment, and 3 Alzheimer's disease) aged 66-86 underwent dynamic total-body 18F-florbetaben PET (United Imaging) for 110min. Regions of interests were drawn in the middle descending aorta and eroded to exclude the vessel walls to derive IDIFs. The PET volumes were motion corrected and linearly registered (FSL-FLIRT) to T1W image. The DKT ATLAS was used to segment 10 brain cortical regions that are involved in neurodegeneration for PET SUVR measurements and cerebellar gray reference region. Dynamic time activity curves from the same brain regions were fit to the two-tissue compartment model (2TCM) using population metabolite-corrected IDIFs; and the Multi-linear Reference Tissue Model (MRTM) to calculate distribution volume ratio (DVR) with reference to cerebellar gray (Ichise, JCBFM 2003).

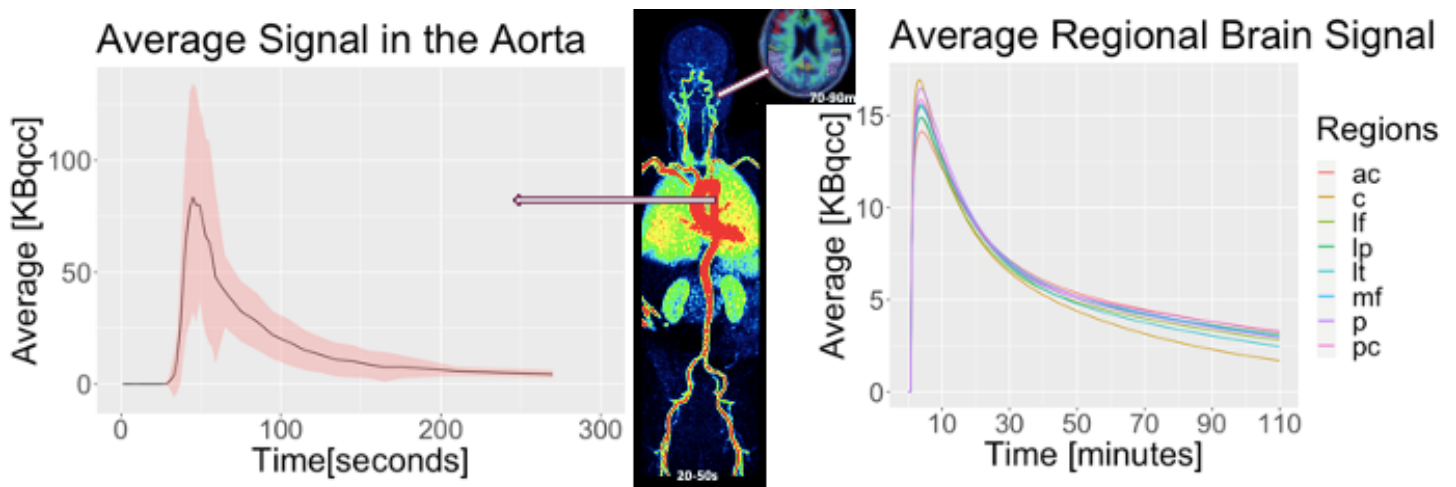


Figure 2. Dynamic PET aorta image-derived input function (left) and brain tissue time-activity curves (right) for a 73 year-old male with Alzheimer's Disease.

Results: Amyloid-positive patients showed the highest SUVR in brain index regions individually. Higher SUVR accumulation was observed in index regions compared to cerebellum at later time points in amyloid-positive cases. SUVR and DVR from kinetic models were strongly correlated; with slight overestimation of SUVR compared to DVR. DVR values from the MRTM were lower than (86.7% of) DVR quantified by 2TCM.

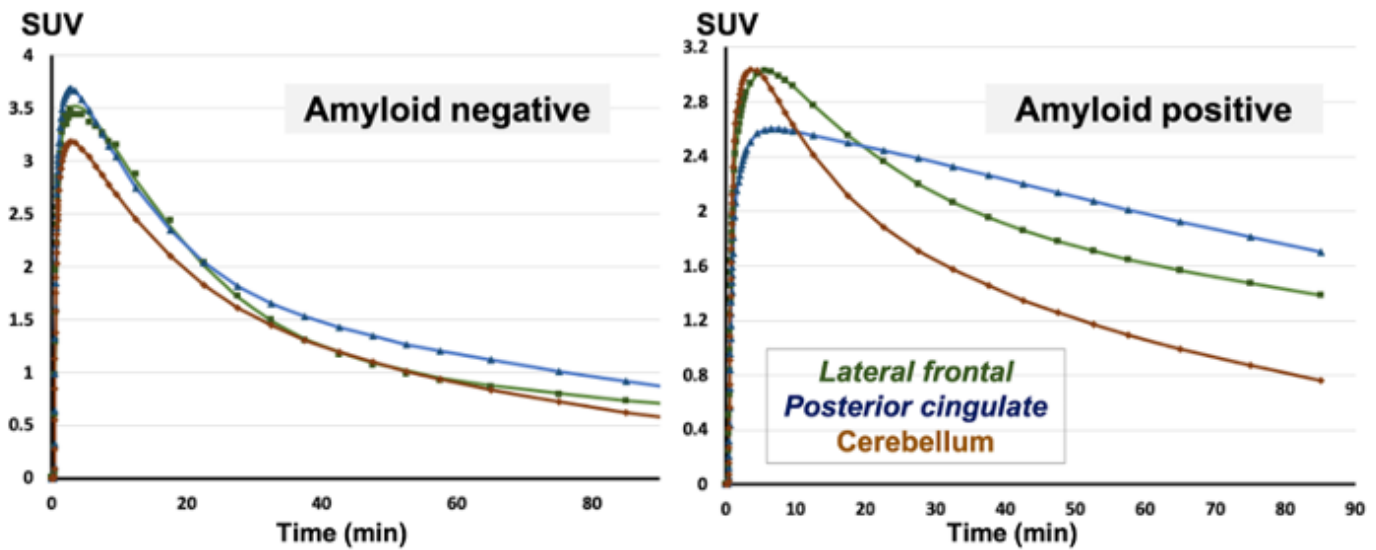


Figure 3. Two-tissue compartment model fits of measured time–activity curves for lateral frontal cortex, posterior cingulate, and cerebellar gray matter in (A) 79-year old male, cognitively normal participant and (B) 81-year old male patient with Alzheimer’s disease. Image-derived input functions from the aorta were corrected for population-estimated metabolic fraction.

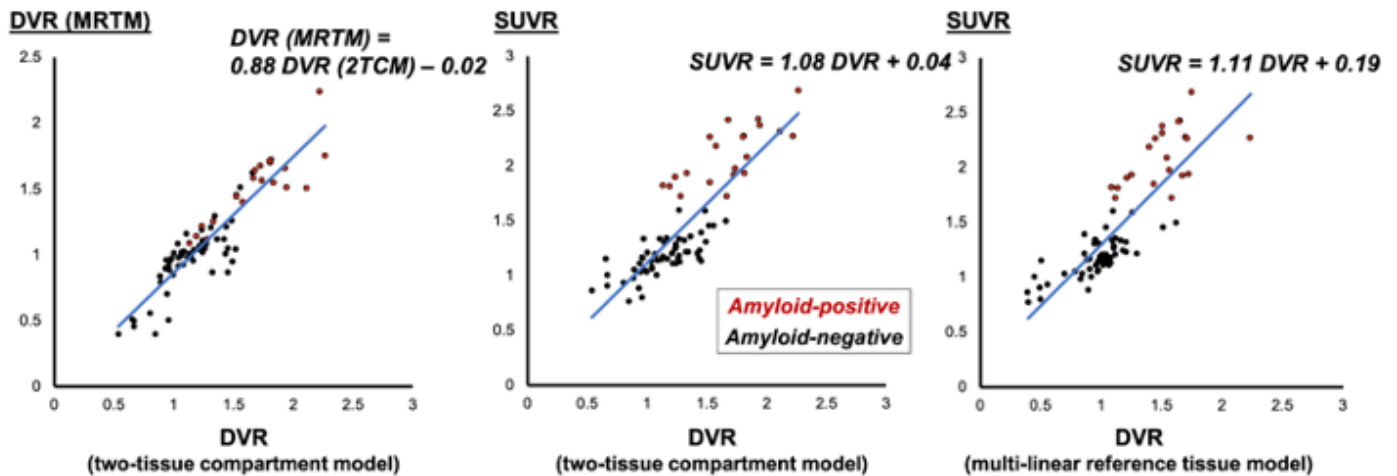


Figure 4. Linear regression analysis of amyloid quantification in brain index regions with correction for subject clustering. (A) DVR computed by multi-tissue reference model [DVR (MRTM)] compared to VR computed by two-tissue compartment model [DVR (2TCM)]. (B) Standardized uptake value ratio (SUVR) and DVR (2TCM). (C) SUVR and DVR (MIRTM).

Conclusions: Absolute quantification of amyloid binding from total-body [18F]-florbetaben PET data is feasible using aorta IDIFs and shows agreement to SUVR in discriminating positive and negative scans.

Total-body EXPLORER PET enables high quality kinetic modeling for accurate measures of amyloid accumulation in clinical research of aging and dementia.

Keywords: [¹⁸F]-florbetaben, Alzheimer disease, β-Amyloid, EXPLORER PET, kinetic modeling, compartment model

P3 PET imaging probe development for aggregated alpha-synuclein

Stephen Gomperts¹, Yan Liu², Ping Bai², Yulong Xu², Kenneth Rose¹, Meral Celikag³, Alain Ndayisaba⁴, Vik Khurana⁴, Tim Bartels³, Changning Wang²

¹Department of Neurology, Massachusetts General Hospital, Boston, MA, US

²Department of Radiology, Massachusetts General Hospital, Boston, MA, US

³UK Dementia Research Institute, UCL, London, UK

⁴Department of Neurology, Brigham and Women's Hospital, Boston, MA, US

Background: Selective PET radioligands are needed to detect aggregated alpha-synuclein, the hallmark pathological feature of Lewy body disease (LBD). Here, we sought to identify and characterize novel PET imaging probes for this purpose.

Methods: To identify lead candidates, we employed the WuXi DEL Technology Service, a hit identification and optimization platform, using an affinity-based selection method against a large (>60 billion) DNA-encoded small molecule library. Samples prepared for screening included alpha-synuclein pre-formed fibrils (PFFs) amplified from Parkinson's brain tissue using protein misfolding cyclic amplification, recombinant PFFs, alpha-synuclein monomer, amyloid-beta fibrils, and tau fibrils. Identified molecules were further characterized.

Results: Molecules from 16 unique scaffolds were identified in the DEL screen. Ten compounds underwent chemical synthesis and secondary screening using bilayer interferometry. One lead compound, SY-08, showed high binding to biotinylated alpha-synuclein PFFs. In human postmortem tissue, K_d was estimated at 0.3-6 nM with B_{max} 697 fmol/mg protein, with >70-fold affinity over AD tissue. Off target binding was low in a 52 target screen. C11-SY08 was studied in the alpha-synucleinA53T transgenic mouse and the AAV-alpha-synucleinA53T rat model, in which an AAV1/2 expression system was used to drive the overexpression and aggregation of alpha-synucleinA53T in the right substantia nigra, with empty AAV1/2 in the left nigra. C11-SY08 showed higher brain uptake in the alpha-synucleinA53T mouse than control mice, and higher uptake in the right than left substantia nigra in the AAV-alpha-synucleinA53T rat model. It is under study in a novel PFF-seeded transgenic iPSC model that forms alpha-synuclein inclusions. PET-MR imaging in the non-human primate showed rapid CNS entry across brain regions and limited brain uptake of radiometabolites.

Conclusions: Several novel scaffolds have been identified that may provide selective binding to alpha-synuclein aggregates. One lead candidate, SY-08, appears to have promising properties for alpha-synuclein PET imaging in Parkinson's and dementia with Lewy bodies.

Keywords: alpha-synuclein, PET, Parkinson, Lewy, preclinical

P4 Cross-modality transformer for low-dose tau PET imaging

Se-In Jang¹, Cristina Lois¹, Alex Becker¹, Emma Thibault¹, Julie C. Price¹, Keith A. Johnson¹, Georges El Fakhri¹, Kuang Gong¹

¹Massachusetts General Hospital, Boston, MA, US

Introduction: Tau PET imaging is an essential imaging modality for tau deposit characterization in aging studies. For longitudinal tau PET studies, radiation exposure is a concern, and low-dose tau PET imaging is desirable. In this work, we focus on developing advanced deep-learning methods to enable low-dose tau PET imaging. Transformer-based network structures which can better exploit long-range spatial information through the self-attention mechanism were utilized. We further designed a cross-modality attention block to combine the low-dose tau PET and MR prior images together to predict the normal-dose tau PET image.

Methods: Our proposed cross-modality transformer block calculated two attention maps using PET and MR images, respectively. Figure 1 shows the proposed cross-modality transformer block. The backbone network used in this work is based on the Restormer structure, and each block in the original transformer block was replaced by the proposed cross-modality transformer block. Simply concatenating PET and MR images together as the Restormer network input was adopted as the reference method. To evaluate the performance of different network structures, one hundred thirty-eight pairs of low-dose and normal-dose 18F-MK-6240 tau PET images acquired from the GE DMI PET/CT scanner were included in this study. Images reconstructed from 0-10 min and 90-110 min post-injection were employed in the evaluation.

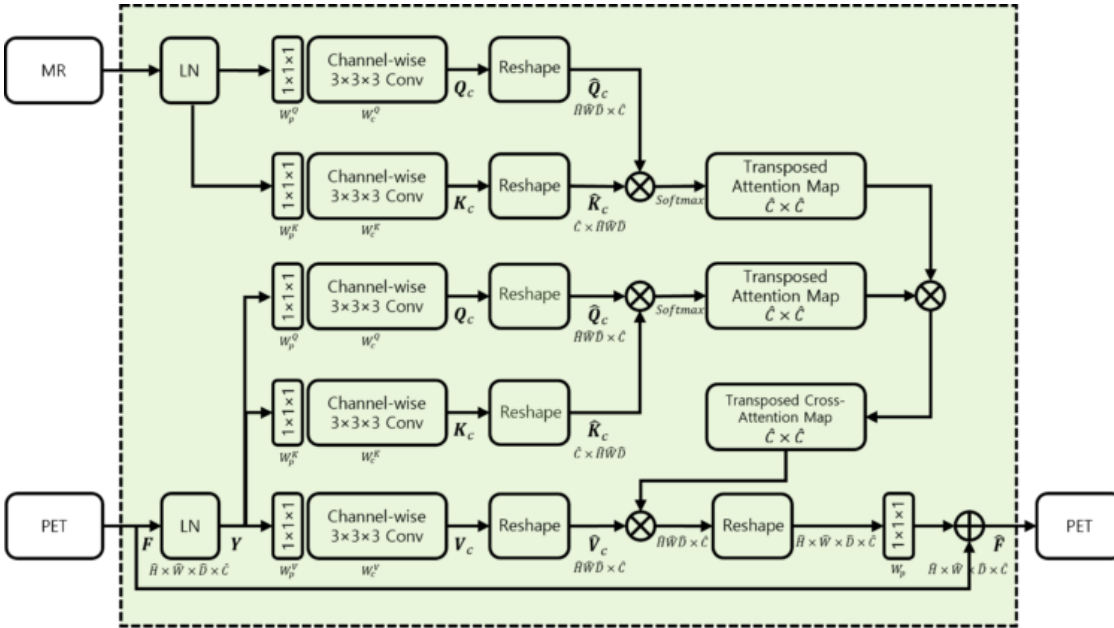
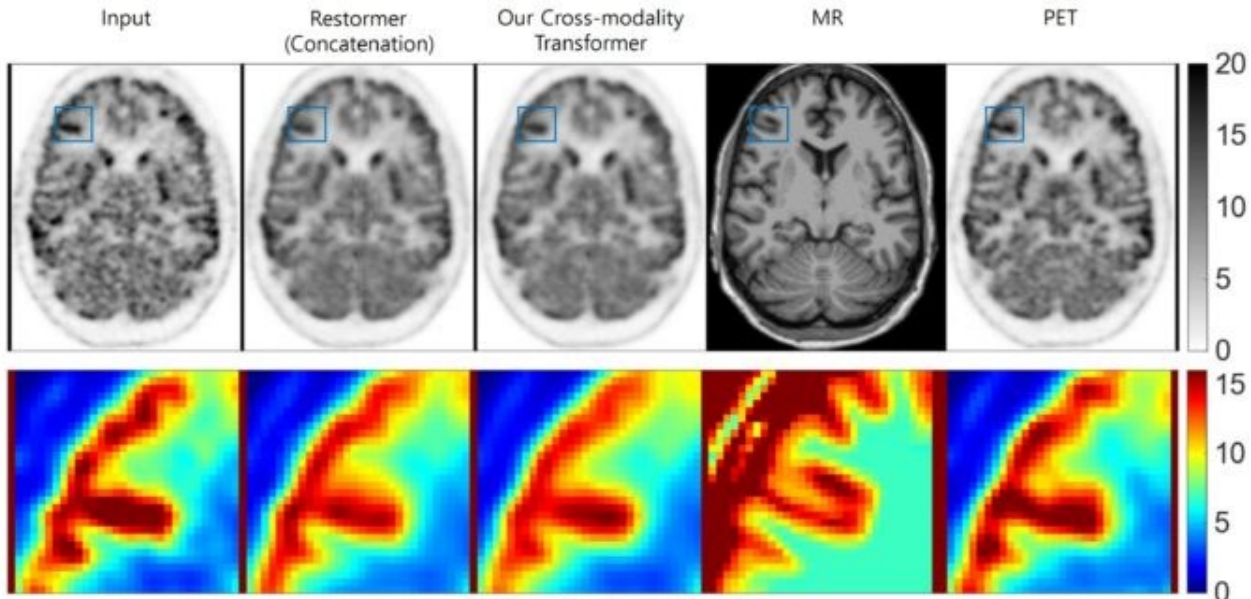
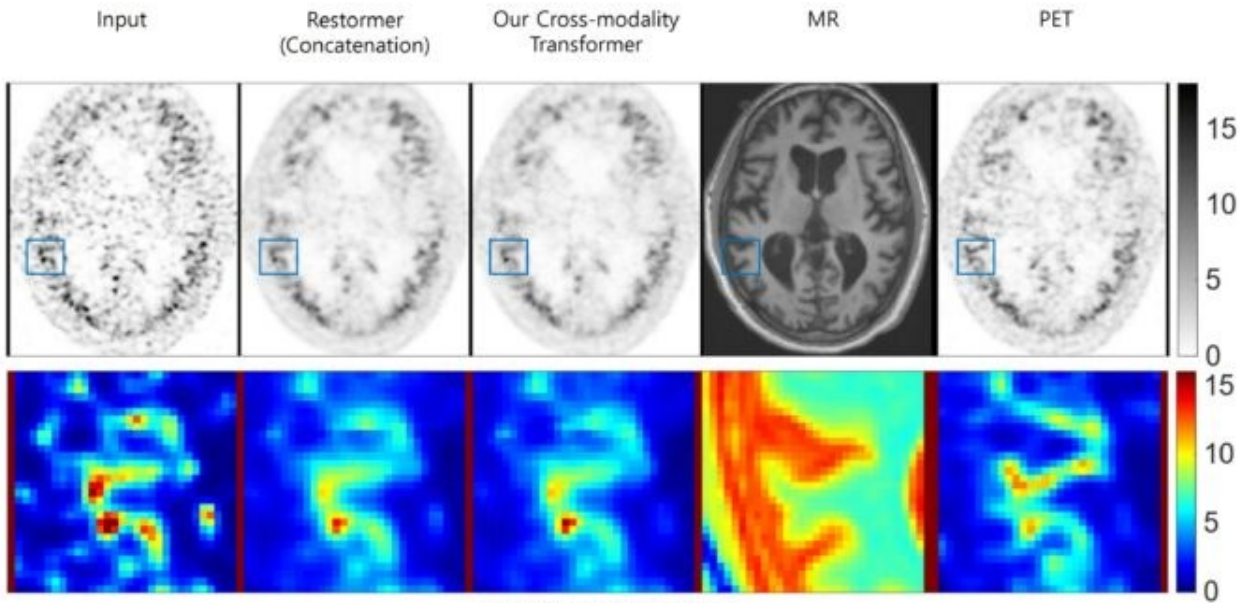


Figure 1. The proposed cross-modality transformer block

Results & Conclusion: Figure 2 shows the denoising performance of different networks on the early- and later-frame datasets. The proposed cross-modality transformer block improved the cortical uptakes in both early- and later-time datasets. Table 1 shows the peak signal-to-noise ratio (PSNR) and structural similarity index (SSIM) values for quantitative comparisons. The proposed network outperformed the Restormer in the early-frame datasets but has inferior performance in the later-time datasets. In our future work, we will further evaluate and improve the cross-modality transformer block to enable low-dose tau imaging.



(a) An early-stage dataset



(b) A later-stage dataset

Figure 2. Qualitative comparison based on one test dataset of (a) early and (b) later-stage datasets. The first row denotes denoised PET images using the input and MR images. The second row is zoomed PET images where the blue box is indicated.

Table 1. Quantitative comparison of PSNR and SSIM based on all the early and later-stage datasets. The network parameters are reported for each method.

		Restormer (Concatenation)		Our Cross-modality Transformer	
		Mean	Std	Mean	Std
Early-stage	PSNR	43.6251	1.8636	43.7741	1.8597
	SSIM	0.8779	0.0151	0.8790	0.0145
Later-stage	PSNR	42.1770	2.8400	42.0309	2.8482
	SSIM	0.7556	0.0265	0.7503	0.0275
Parameters		33,540,105		32,535,077	

P5 Tau PET positivity reveals Alzheimer's disease related fast cognitive decline

Konstantinos Ioannou¹, Marco Bucci^{1,2}, Agneta Nordberg^{1,2}, Konstantinos Chiotis^{1,3}

¹Nordberg Translational Molecular Imaging Lab, Division of Clinical Geriatrics, Center for Alzheimer's Research, Department of Neurobiology, Care Sciences and Society, Karolinska Institutet, Stockholm, Sweden

²Theme Inflammation and Aging, Karolinska University Hospital, Stockholm, Sweden

³Department of Neurology, Karolinska University Hospital, Stockholm, Sweden

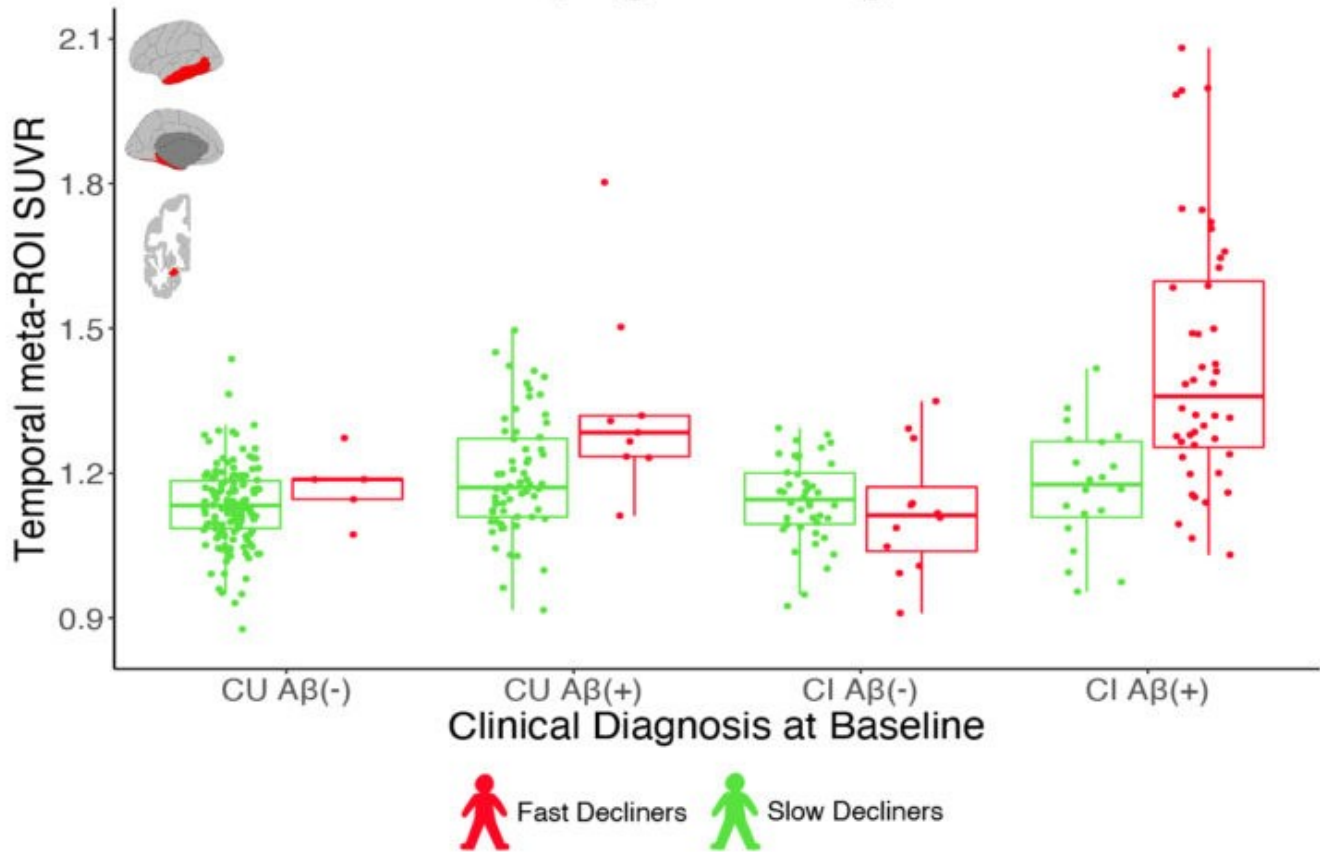
Background: The limited value of β -amyloid ($A\beta$) Positron Emission Tomography (PET) in predicting future cognitive status in Alzheimer's disease (AD) continuum underlines the need for introduction of new biomarkers. We assessed the accuracy of a tau PET biomarker to predict clinically relevant cognitive decline.

Method: A subset of 335 individuals [cognitively unimpaired (n=217), cognitively impaired (n=118)] with baseline $A\beta$ and tau PET scans and a follow-up ≥ 2 years, was selected from the Alzheimer's Disease Neuroimaging Initiative dataset. Based on the Alzheimer's Disease Assessment Scale–Cognitive Subscale and linear mixed-effects models, we defined the annual rate of cognitive decline for all individuals. Gaussian mixture modelling was next used to cluster them into fast (FD) and slow decliners (SD). The accuracy of tau PET to discriminate between these cognitive decline profiles was tested. We investigated the prevalence of non-AD comorbidities in individuals with discordant status between $A\beta$ and tau biomarkers.

Result: $A\beta(+)$ FD showed the highest tau PET uptake independently of baseline cognitive status, compared to the other groups [$A\beta(-)$ FD/SD, $A\beta(+)$ SD]. Baseline tau PET uptake could determine 1. the $A\beta(+)$ FD with an accuracy of 85% (composite temporal region of interest), and 2. was linearly related to the annual rate of cognitive decline in $A\beta(+)$ individuals. The tau positive T(+) individuals constitute a subgroup of those with an $A\beta(+)$ scan, and those have high prevalence of FD. Relative to $A\beta(+)$ T(+)FD (28/41, 68%), $A\beta(+)$ T(-)FD (13/41, 32%) showed higher frequency of cerebrovascular risk factors and comorbid depression.

Conclusion: Tau PET positivity defines AD-driven fast cognitive decline. Fast cognitive decline with isolated $A\beta(+)$ could be associated with other comorbidities. Tau PET imaging combines better diagnostic and prognostic accuracy than $A\beta$ PET does. Introducing tau biomarkers in memory clinics could improve individual prognostic assessment and enrich clinical trials with individuals at risk for AD-driven fast cognitive decline.

Baseline tau load & progress in cognitive decline



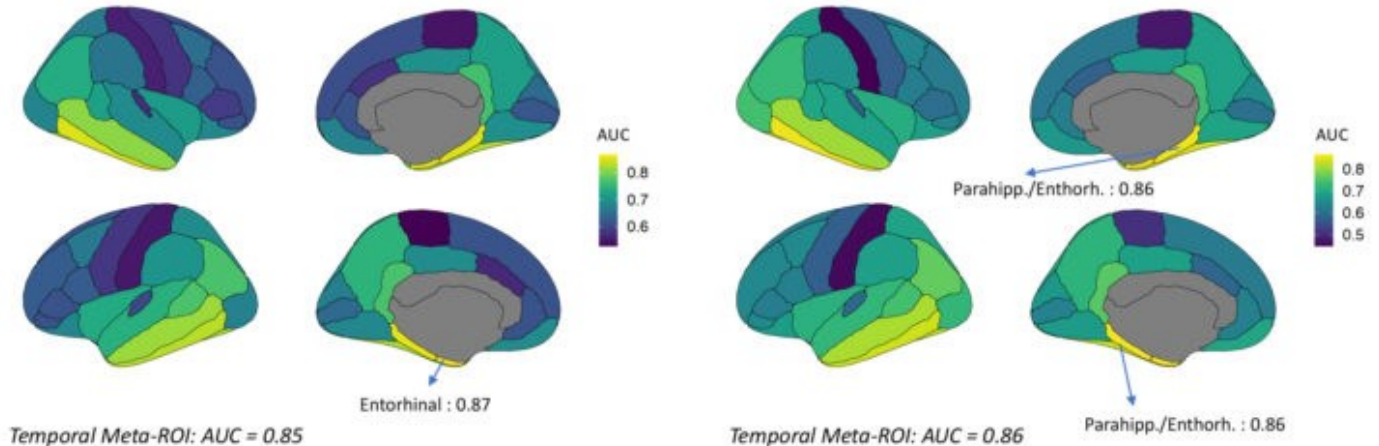
Discrimination of Aβ(+) Fast Decliners using baseline tau PET uptake

Results of ROC analysis

Aβ(+)FD Vs [Aβ(+)SD + Aβ(-)FD/SD]

Discrimination of Aβ(+) Fast Decliners
all groups (CU & CI), 335 individuals

Discrimination of Aβ(+) Fast Decliners
CI group, 118 individuals

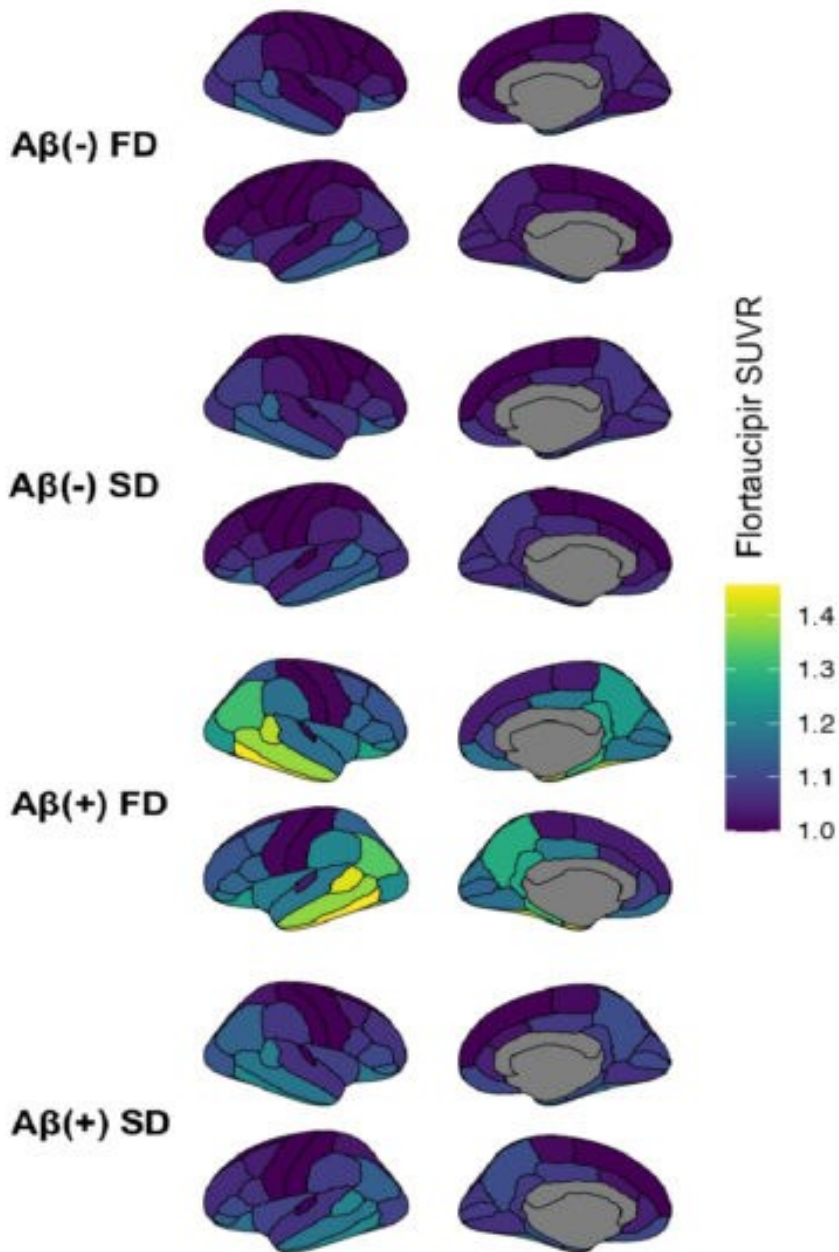


ROC = Receiver Operating Characteristic
AUC = Area Under Curve

FD = Fast Decliners
SD = Slow Decliners

CU = Cognitively Unimpaired
CI = Cognitively Impaired

Average tau PET binding per group



A β PET	Cogn. Decline	CU	CI
A β (-)	Fast (FD)	5	12
	Slow (SD)	139	42
A β (+)	Fast (FD)	9	44
	Slow (SD)	64	20

Keywords: tau, PET, biomarkers, Alzheimer's disease

P6 Positive 18F-APN-1607 tau PET imaging findings in patients with Progressive Supranuclear Palsy-like extrapyramidal symptoms caused by TBK1 mutations

Feng-Tao Liu¹, Jia-Ying Lu², Yi-Min Sun¹, Xin-Yi Li¹, Tzu-Chen Yen³, Ming-Kuei Jang³, Chuan-Tao Zuo², Jian Wang¹

¹Department of Neurology & National Clinical Research Center for Aging and Medicine, Huashan Hospital, Fudan University, Shanghai, CN

²PET Center, Huashan Hospital, Fudan University, Shanghai, CN

³APRINOIA Therapeutics Co., Ltd, Suzhou, CN

Background: Pathogenic mutations in the TANK-binding kinase 1 (*TBK1*) gene have been associated with progressive supranuclear palsy (PSP)-like extrapyramidal symptoms, amyotrophic lateral sclerosis (ALS), as well as cognitive and behavioral alterations. However, the question as to whether *TBK1* mutations may be associated with tau burden remains unanswered.

Methods: To investigate whether patients presenting with PSP-like extrapyramidal symptoms caused by *TBK1* mutations have evidence of tau deposition as reflected by positive ¹⁸F-APN-1607 tau PET imaging findings. Four patients who showed PSP-like extrapyramidal symptoms, ALS, and cognitive/behavioral alterations were consecutively enrolled between August 2019 and August 2020. Patients underwent *TBK1* gene sequencing and ¹⁸F-APN-1607 tau PET imaging. All PET images were interpreted in a blinded fashion with respect to genetic results. Brain structural changes were investigated with MRI, whereas ¹¹C-CFT or ¹⁸F-DTBZ PET imaging was performed to identify dopaminergic degeneration.

Results: Pathogenic *TBK1* mutations were identified in three of the four study patients. The three mutation carriers – but not the case without – showed positive ¹⁸F-APN-1607 binding in PSP-related regions, suggesting the presence of tau pathology. Mesencephalic atrophy (hummingbird sign) was observed in all *TBK1* mutation carriers, and two of them also had evidence of frontotemporal atrophy. Dopaminergic degeneration was evident in all cases, regardless of *TBK1* mutations.

Conclusions: Pathogenic *TBK1* mutations in patients with PSP-like extrapyramidal symptoms are associated with positive ¹⁸F-APN-1607 tau PET imaging findings. Our data should prompt additional investigations on the potential role of tau accumulation in the pathogenesis of disease conditions associated with *TBK1* mutations.

Keywords: progressive supranuclear palsy, amyotrophic lateral sclerosis, *TBK1*, 18F-APN-1607 tau PET imaging

P7 In vivo visualization of tau deposits in corticobasal syndrome by ¹⁸F-Florzolotau PET

Feng-Tao Liu¹, Jia-Ying Lu², Xin-Yi Li¹, Fang-Yang Jiao², Ming-Jia Chen¹, Rui-Xin Yao¹, Xiao-Niu Liang^{1,3}, Jing-Jie Ge², Gen Li¹, Bo Shen¹, Ping Wu², Yi-Min Sun¹, Jian-Jun Wu¹, Tzu-Chen Yen⁴, Chuan-tao Zuo², Jian Wang¹

¹Department of Neurology, National Research Center for Aging and Medicine, National Center for Neurological Disorders, and State Key Laboratory of Medical Neurobiology, Huashan Hospital, Fudan University, Shanghai, CN

²Department of Nuclear Medicine & PET Center, National Center for Neurological Disorders, and National Clinical Research Center for Aging and Medicine, Huashan Hospital, Fudan University, Shanghai, CN

³Institute of Neurology, Fudan University, Shanghai, CN

⁴APRINOLA Therapeutics Co., Ltd, Suzhou, CN

Background: Antemortem determination of the pathology in corticobasal syndrome (CBS) is currently unavailable, inspiring the explorations using various biomarkers, including tau PET imaging.

Objectives: To investigate the utility of ¹⁸F-Florzolotau in detecting the tau pathology *in vivo* in patients with CBS.

Methods: Twenty patients with CBS and 20 healthy controls were consecutively recruited for ¹⁸F-Florzolotau tau PET imaging. Sixteen cases with progressive supranuclear palsy-Richardson syndrome (PSP-RS) and 20 cases with Alzheimer's disease (AD) were retrospectively recruited as controls of tauopathies. The beta-amyloid status was evaluated by CSF β -amyloid (A β) analysis in CBS. The subcortical and cortical ¹⁸F-Florzolotau depositions were quantitatively assessed by standardized uptake value ratio (SUVR). Tau PET positivity was assessed at individual and group levels. The regional bindings were correlated with the clinical severities.

Results: Nineteen cases (95.0 %) were A β (-) CBS, among whom three were tau PET negative. The elevated ¹⁸F-Florzolotau bindings could be found in the regions of cortical (precentral, postcentral and SMA area) and subcortical regions (GP, putamen and STN et al.) compared to HCs. Compared with PSP-RS, more tau depositions could be recognized in the cortical regions at individual level. Compared with AD, more tau depositions could be recognized in the subcortical regions at both individual and group levels. The asymmetric index of cortical and subcortical ¹⁸F-Florzolotau correlated significantly with the asymmetric index of clinical severity. No significant correlations with the original clinical parameters were observed.

Conclusions: ¹⁸F-Florzolotau tau PET was promising in evaluating the 4R tauopathy in CBS, which may potentially be used for monitoring disease severity.

Keywords: 18F-Florzolotau, tau, positron emission tomography, corticobasal syndrome

P8 Imaging neuroinflammation with astrocyte-PET and bio-fluid biomarkers in patients with cognitive impairment

Konstantinos Chiotis^{1,2}, Vesna Jelic³, Elena Rodriguez-Vieitez¹, Irina Savitscheva^{1,4}, Anders Wall⁵, Gunnar Antoni^{5,6}, Agneta Nordberg^{1,3}

¹Department NVS, Karolinska Institutet, Stockholm, Sweden

²Department of Neurology, Karolinska University Hospital, Stockholm, Sweden

³Theme Aging and Inflammation, Karolinska University Hospital, Stockholm, Sweden

⁴Department of Nuclear Medicine, Karolinska University Hospital, Stockholm, Sweden

⁵PET centre, Uppsala University Hospital, Uppsala, Sweden

⁶Department of Medicinal Chemistry, Uppsala University, Uppsala, Sweden

Objectives: Neuroinflammation, which receives ever increasing interest in neurodegenerative diseases, comprises a heterogeneous cascade of events that are thought to be related to the downstream neurodegeneration. The aim of this study was to evaluate the binding of ¹¹C-Deuterium-L-Deprenyl PET (DED) as a measure of reactive astrocytes in patients with different cognitive disorders, and to assess its association with other disease biomarkers.

Methods: Eleven patients with a clinical diagnosis of a semantic variant of primary progressive aphasia (svPPA, n=5) and a behavioral variant of frontotemporal dementia (bvFTD, n=6) were recruited. All patients had a cerebrospinal fluid biomarker profile that was inconsistent with Alzheimer's disease (AD) or a negative amyloid-β PET scan. The imaging protocol included ¹¹C-DED-PET, ¹⁸F-FDG-PET, and a T1 MRI. Groups of healthy controls (HC, n=20) and amyloid-beta positive patients with AD diagnosis (n=20) that underwent similar investigations were used for comparison. Samples of CSF and plasma were analyzed for measuring levels of GFAP, NfL, and tau.

Results: The patients with svPPA and bvFTD showed significantly higher ¹¹C-DED binding in frontotemporal areas, compared to HC. Patients with AD showed significantly higher ¹¹C-DED binding in temporo-occipital areas, compared to HC. The regional distribution of ¹¹C-DED binding in the patients with svPPA and bvFTD was consistent with the expected underlying pattern of neurodegeneration in those disorders, although the load of binding was heterogeneous across patients with the same clinical diagnosis.

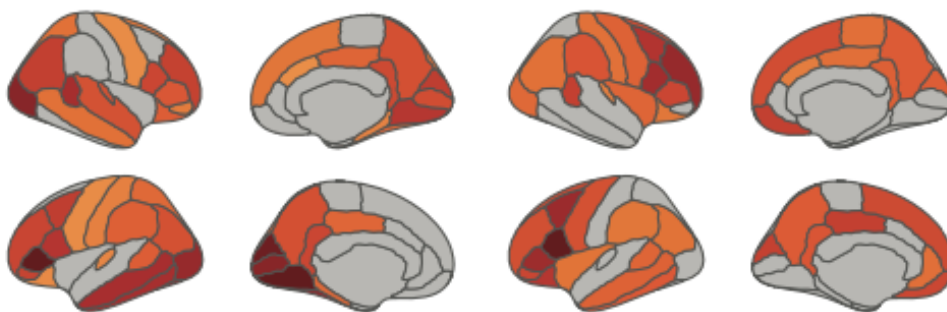
Conclusion: Reactive astrocytes appear to be a common feature of different dementia disorders, although the regional pattern of reactivity differs. Ongoing work evaluates the relationship between patterns of reactive astrocyte activation, cerebral perfusion, glucose metabolism, atrophy, bio-fluid markers, and cognitive performance.

Group comparisons (t-test)

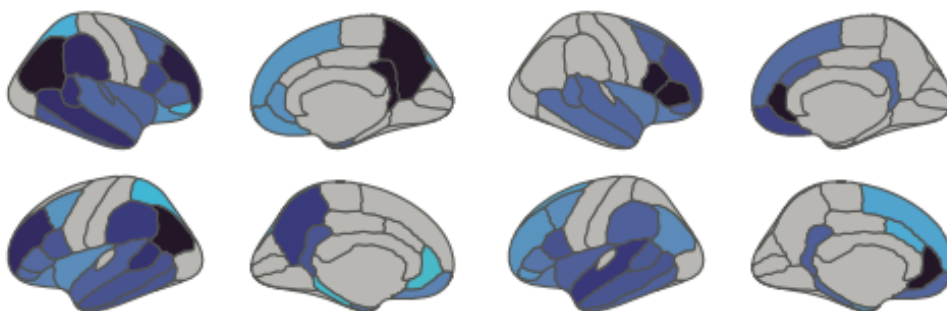
HC vs AD

HC vs FTLD

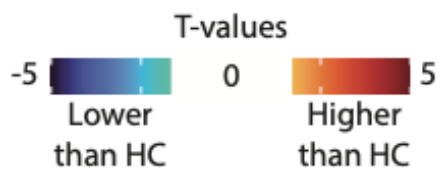
Reactive astrocyte binding
(¹¹C-DED Slope)



Cerebral Perfusion
(¹¹C-DED R1)



*FDR correction ($p < 0.05$)



Keywords: neuroinflammation, frontotemporal dementia, Alzheimer's disease, plasma, CSF

P9 [18] Flortaucipir PET and Diffusion Tensor Tractography Coregistration can Enhance Detection of Brain Changes Associated with Progressive Apraxia of Speech

Rodolfo G. Gatto¹, Joseph R. Duffy¹, Rene L. Utianski¹, Heather M. Clark¹, Hugo Botha¹, Mary M. Machulda³, Val J. Lowe², Keith A. Josephs¹, Jennifer L. Whitwell²

¹Division of Neurology, Mayo Clinic, Rochester, MN, US

²Division of Radiology, Mayo Clinic, Rochester, MN, US

³Division of Psychiatry and Psychology, Mayo Clinic, Rochester, MN, US

Background: Progressive apraxia of speech (PAOS) is a 4R tauopathy characterized by difficulties with motor speech planning. Neurodegeneration in PAOS targets the premotor cortex, including supplementary motor area (SMA) with degeneration of white matter (WM) tracts connecting premotor and motor cortices observed on diffusion tensor imaging (DTI). Previous PAOS studies have shown increased tau-PET uptake in these cortical areas, although uptake is mild and observed in the WM. However, it is unclear whether flortaucipir uptake is elevated across specific WM tracts in PAOS.

Objectives: To assess flortaucipir uptake across speech-related WM tracts in PAOS.

Materials and Methods: Twenty-two patients with PAOS and 22 matched healthy controls were recruited by the Neurodegenerative Research Group (NRG) and underwent MRI and flortaucipir-PET. Flortaucipir PET scans and DTI were coregistered using a rigid body and mutual information cost function in subject space. Alignments between DTI and flortaucipir PET were inspected in all cases. Whole-brain tractography was calculated using deterministic algorithms by a tractography reconstruction tool (DSI-studio). Fractional anisotropy (FA) and flortaucipir standard uptake value ratios (SUVRs) were averaged across the frontal aslant tract, arcuate fasciculi, inferior fronto-occipital fasciculus, inferior and middle longitudinal fasciculi, as well as the SMA commissural fibers.

Results: Reduced FA ($p < 0.0001$) and elevated flortaucipir SUVR ($p = 0.01$) was observed in PAOS cases compared to controls across all combined WM tracts. For flortaucipir SUVR, the greatest differentiation of PAOS from controls was achieved with the left arcuate fasciculus (area under the receiver operator characteristic curve, AUROC=0.75), left frontal aslant tract (AUROC=0.71) and SMA (AUROC=0.83).

Conclusions: Our findings demonstrate that flortaucipir uptake is increased across WM tracts related to speech difficulties in PAOS.

Keywords: Progressive Apraxia of Speech, Flortaucipir PET, Diffusion Tensor Imaging, Tractography, Tau

P10 Towards a simplified flortaucipir-PET read method for assessing tau burden

Ilke Tunali¹, Leonardo Iaccarino¹, Courtney Ducker¹, Sneha Patel¹, Kelly DiFabbio¹, Stacey Kowaleski¹, Anupa Arora¹, Min Jung Kim¹, Ming Lu¹, Michael Pontecorvo¹, Sergey Shcherbinin¹

¹Eli Lilly and Company, Indianapolis, IN, US

Background: Flortaucipir F18 (FTP-PET) is an FDA-approved imaging agent that can estimate the density and distribution of tau neurofibrillary tangle pathology. Accurate quantitation of FTP-PET requires specialized software and sophisticated image processing. In this study, an FTP-PET read method based on identifying the maximum frontal signal was tested as an alternative simplified measure for FTP-PET-based tau accumulation and patient stratification.

Methods: A total of 77 baseline FTP-PET native space images from the confirmatory phase of the 18F-AV-1451-A05 multi-center study (NCT02016560) that are displaying advanced Alzheimer's Disease (AD) tau-patterns (Fleisher et al. *JAMA Neurol*, 2020) were utilized (Table 1). Four imaging experts conducted independent and blinded simplified FTP-PET reads. The maximum frontal uptake value was captured by manually drawing regions-of-interest (ROIs) on visually identified frontal regions with the highest FTP-PET signal. A maximum standardized uptake value ratio (SUVR_{max}) was calculated by scaling identified maximum frontal uptake by the average uptake inside a 2D manually drawn cerebellum ROI. Correlation analyses were conducted between SUVR_{max} and global tau SUVR (i.e., AD-signature weighted neocortical with respect to white matter reference). The classification performance of SUVR_{max} was assessed using Receiver Operating Characteristic (ROC) analysis within tau groups dichotomized via global SUVR cut points (SUVR>1.46, SUVR>1.23, SUVR>1.11). Inter-rater agreement of SUVR_{max} between the readers was determined using an intra-class correlation (ICC) measure.

Results: Frontal SUVR_{max} values were strongly correlated with global tau SUVR (Pearson's $r>0.83$, Fig.1) and, were predictive of all three tau subgroups, with an increasing predictive ability for higher global SUVR cut points (Table 2). Excellent agreement between readers was observed (ICC=0.97).

Conclusion: The proposed simplified FTP-PET read method has the potential to estimate the global tau burden without sophisticated image processing. Further research is required to identify optimal regions and cut points for stratification, and to understand the impact of image acquisition parameters.

Figure 1: Frontal SUVRmax to AD-signature weighted neocortical SUVR correlation graphs. Correlation analyses were conducted only for FTP-PET images showing increased frontal cortex activity compared to the cerebellar mean uptake as assessed by readers. Average uptake inside a 2D manually drawn region around the cerebellum (as mentioned in the Tauvid™ label) was used as a reference to calculate SUVRmax. A subject-specific white matter region (Southehal et al. *J Nucl Med*, 2018) was used as a reference region to calculate the AD-signature weighted neocortical SUVR. Solid lines represent the fitted linear regression line between SUVRmax and AD-signature neocortical SUVR. r : Pearson's r .

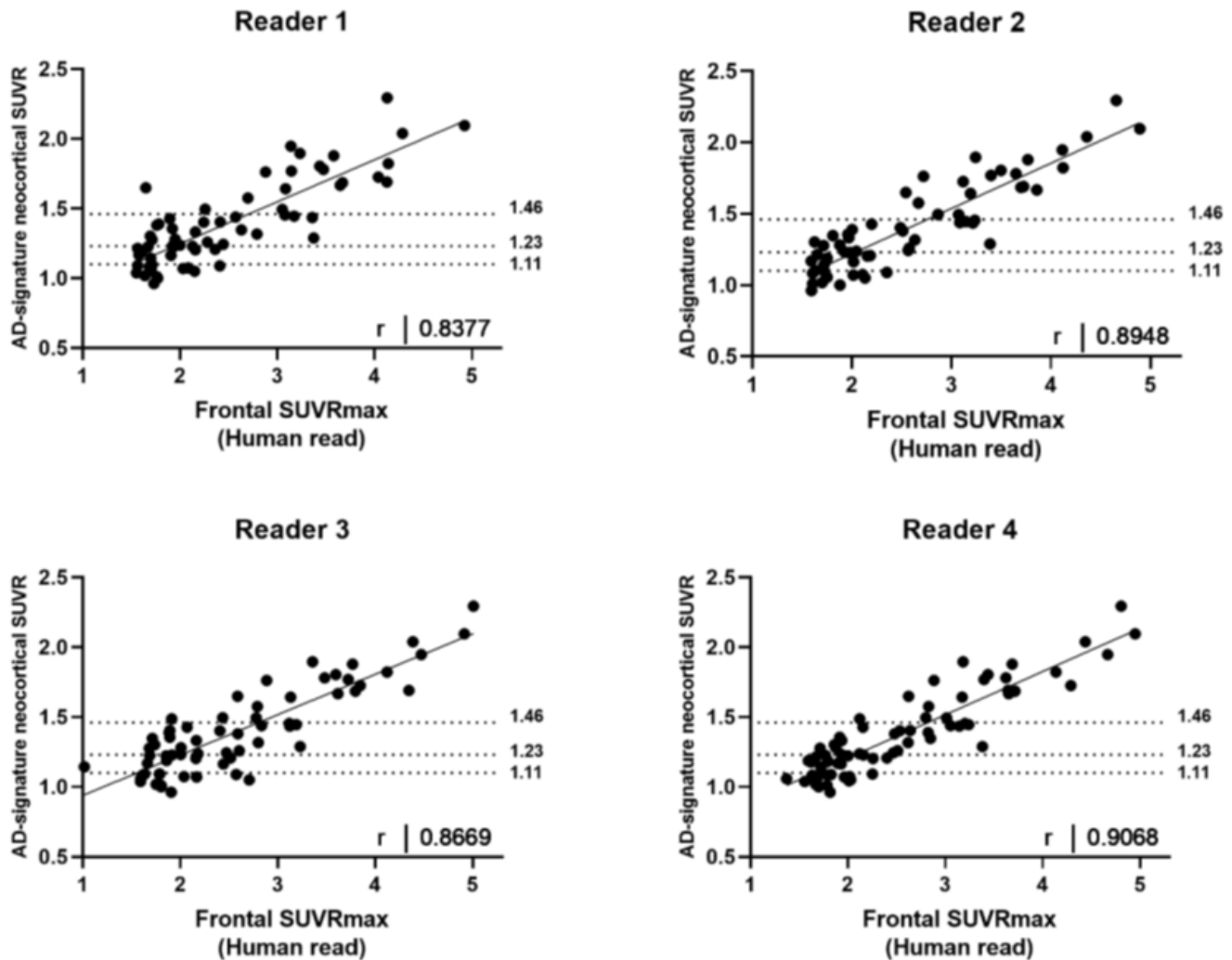


Table 1. Baseline characteristics for subjects displaying advanced-AD tau-patterns that are enrolled in the confirmatory phase of the AV-1451-A05 multi-center study

Total, N (%)	77
MCI	38 (49.4)
AD-dementia	39 (50.6)
Age, median (range)	75.0 (51 – 97)
AD-signature weighted neocortical SUVR¹, median (range)	1.26 (0.96 – 2.29)
Total number of imaging sites	21

Abbreviations: MCI, mild cognitive impairment; AD, Alzheimer’s Disease; SUVR, standardized uptake value ratio.

¹A subject-specific white matter region (Southeast et al. *J Nucl Med*, 2018) was used as a reference region to calculate AD-signature weighted neocortical SUVR.

Table 2. ROC-based analysis for predicting global tau subgroups based on different cut points

	Global tau SUVR cut point ¹		
	1.11	1.23	1.46
Total, N (%)	77	77	77
SUVR > cut point ²	55 (71.4)	42 (54.5)	21 (27.3)
SUVR ≤ cut point ³	22 (28.6)	35 (45.5)	56 (72.7)
Reader 1			
AUC	0.832	0.903	0.893
Youden index-based SUVRmax cut point ⁴	1.78	2.16	2.70
Accuracy	0.779	0.831	0.896
PPA	0.764	0.738	0.857
NPA	0.818	0.943	0.911
Reader 2			
AUC	0.860	0.912	0.927
Youden index-based SUVRmax cut point ⁴	1.75	2.49	2.67
Accuracy	0.818	0.857	0.909
PPA	0.836	0.738	0.905
NPA	0.773	1.000	0.911
Reader 3			
AUC	0.834	0.914	0.946
Youden index-based SUVRmax cut point ⁴	1.85	1.88	2.78
Accuracy	0.805	0.844	0.883
PPA	0.818	0.929	0.857
NPA	0.773	0.743	0.893
Reader 4			
AUC	0.886	0.946	0.953
Youden index-based SUVRmax cut point ⁴	2.12	2.47	2.62
Accuracy	0.779	0.883	0.883
PPA	0.709	0.786	0.952
NPA	0.955	1.000	0.857
Median measures among readers			
AUC	0.847	0.913	0.937
Accuracy	0.792	0.851	0.890
PPA	0.791	0.762	0.881
NPA	0.795	0.971	0.902

Abbreviations: SUVR, standardized uptake value ratio; ROC, receiver operating characteristics; PPA, positive percent agreement; NPA, negative percent agreement.

¹AD-signature weighted neocortical SUVR cut points were based on a previous study (Pontecorvo et al. *Brain*, 2019)

²Number of subjects above the AD-signature weighted neocortical SUVR

³Number of subjects below the AD-signature weighted neocortical SUVR

⁴Youden index-based cut points were SUVRmax values that maximized the Youden index.

Keywords: Alzheimer’s Disease, flortaucipir-PET, FTP-PET visual read

P12 Digital clock drawing performance is associated with tau deposition measured with PET in preclinical Alzheimer's disease

Jessie Fang-Lu Fu^{1,2}, Dorene M. Rentz², Danielle V. Mayblyum², Emma Thibault², Rachel F. Buckley², Sudeshna Das², Kathryn V. Papp², Reisa A. Sperling², Dana Penney³, Randall Davis⁴, Keith A. Johnson², Julie C. Price^{1,2}

¹Athinoula A. Martinos Center for Biomedical Imaging, Charlestown, MA, US

²Massachusetts General Hospital, Harvard Medical School, Boston, MA, US

³Lahey Hospital and Medical Center, Burlington, MA, US

⁴Massachusetts Institute of Technology, Computer Science and Artificial Intelligence Laboratory, Cambridge, MA, US

Background: PET quantifies Alzheimer's disease (AD) tau pathology in preclinical AD. A 2-min digital clock-drawing test (DCTclock) was developed to capture clock-drawing processes (e.g., speed) in addition to the final drawing outcome. A DCTclockcomposite score was developed as the sum of 44 drawing features identified as most clinically relevant for diagnosis between cognitively normal (CN) and AD. The DCTclock composite scores showed stronger correlation with Flortaucipir entorhinal tau burden than paper-and-pencil Preclinical Alzheimer Cognitive Composite scores in CNs; such correlation was driven by drawing features reflecting the Spatial Reasoning subdomain. We aim to identify additional drawing features most correlated with tau burden in preclinical AD.

Methods: A total of 234 CN individuals underwent amyloid- β PET (PiB) and 222 also underwent tau PET imaging (¹⁸F]MK-6240: n=57 or Flortaucipir: n=165, **Table.1**). All underwent DCTclock assessments. Regional FreeSurfer-based PET SUVR were computed (Flortaucipir: 75-105min, [¹⁸F]MK-6240: 90-110min) with cerebellar gray-matter reference and partial volume correction. Partial least squares (PLS) with five-fold cross-validation was performed to identify DCTclock features most correlated with tau PET using age, sex, and years of education as covariates.

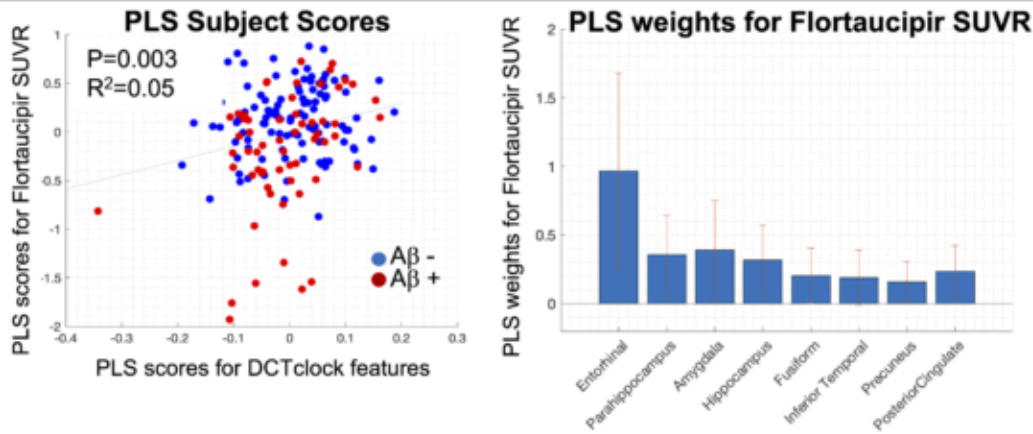
Results: PLS identified significant associations (p=0.003) between higher Flortaucipir uptake (entorhinal) and DCTclock features representing worse Simple Motor, Drawing Efficiency and Spatial Reasoning subdomains (**Table.2, Fig.1A**). Higher [¹⁸F]MK-6240 uptake (entorhinal and parahippocampus) was significantly associated (p=0.003) with similar DCTclock features as Flortaucipir and additional DCTclock features representing worse Information Processing subdomains (**Table.2, Fig.1B**).

Conclusion: Our results suggest that DCTclock performance captures early tau burden in CNs. In addition to DCTclock features previously identified as correlated with Flortaucipir, PLS identified additional features in Simple Motor and Drawing Efficiency subdomains, providing more sensitive measures of tau burden in preclinical AD. Furthermore, compared to Flortaucipir, [¹⁸F]MK-6240 captured additional DCTclock features (e.g., latency), potentially reflecting more subtle cognitive abnormalities than previously identified in preclinical AD.

Table 1. Data characteristics for the cognitively normal (CN) subjects in this study	
	Clinical and Imaging Data
DCTclock baseline	N = 244
Age (yrs)	76±9
Female (n)	138 (57%)
Education (yrs)	16.5±2.8
MMSE	28.9±1.2
PACC5	0.83±7.43
[¹⁸F]MK-6240 (dynamic 0-120 min, GE Discovery MI)	N = 57 Entorhinal SUVR _{90-110min} : 1.11±0.90
[¹⁸F]Flortaucipir (late-frame 75-105 min, Siemens HR+)	N = 165 Entorhinal SUVR _{75-105min} : 1.39±0.30
[¹¹C]Pittsburgh-Compound B (dynamic, 0-60 min, Siemens HR+ or GE Discovery MI)	N = 243 (66 Aβ+) FLR DVR: 1.19±0.22
T1 MRI (Siemens 3T Trim Trio, MPRAGE)	N = 244
DCTclock = digital clock drawing test; CN = cognitively normal; MMSE = Mini-Mental State Examination; PACC = Preclinical Alzheimer Cognitive Composite; SUVR = standardized uptake value ratios; DVR = distribution volume ratios; FLR = frontal, lateral and retrosplenial composite regions;	
* There was no statistically significant difference in age, sex, years of education, MMSE and PACC5 between subjects underwent [¹⁸ F]MK-6240 or Flortaucipir tau PET imaging.	

Table 2. The DCTclock features that correlated with higher tau PET uptake in CN individuals in the partial least squares analysis.			
	Cognitive subdomains	DCTclock versions	DCTclock features
Flortaucipir (p = 0.003)	Simple Motor	Command & Copy	Slower drawing speed
	Drawing Efficiency	Command & Copy	Smaller drawing size
	Drawing Efficiency	Copy	Shorter ink length*
	Drawing Efficiency	Copy	Longer total time
	Spatial Reasoning	Copy	Lower vertical spatial placement [#]
[¹⁸F]MK-6240 (p = 0.003)	Simple Motor	Command & Copy	Slower drawing speed
	Drawing Efficiency	Command & Copy	Smaller drawing size
	Drawing Efficiency	Command & Copy	Longer total time
	Information Processing	Command & Copy	Longer latency [§]
	Spatial Reasoning	Copy	Lower vertical spatial placement [#]
DCTclock = digital clock drawing test; CN = cognitively normal;			
* ink length: total length in millimeters of the ink used in drawing the clock			
[#] vertical spatial placement: measure of the vertical position of the clock on the page, <u>previously identified to be correlated with entorhinal Flortaucipir uptake in Rentz, 2021</u>			
[§] latency: average duration of the delays between each pen stroke and the combined duration of delays that are long compared to the participant's average individual performance			

(A) Associations between DCTclock features and Flortaucipir SUVR_{75-105min}



(B) Associations between DCTclock features and MK6240 SUVR_{90-110min}

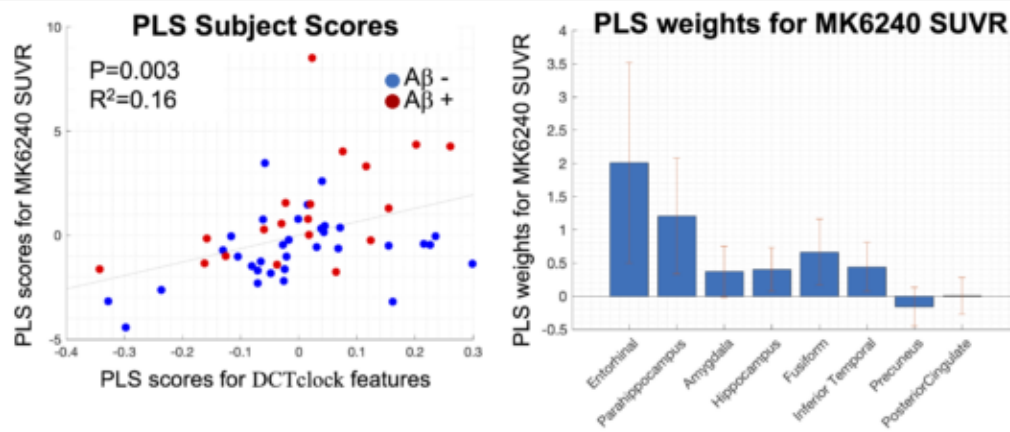


Figure 1. Partial least squares (PLS) results for examining the associations between DCTclock and tau PET using **(A)** Flortaucipir SUVR_{75-105min} and **(B)** MK6240 SUVR_{90-110min}. PLS subject scores (expression of the PLS weights in each subject) showed significant correlations between DCTclock and tau PET uptake in CN individuals. The corresponding PLS weights showed higher tau PET uptake for both Flortaucipir and MK6240 SUVR, with higher tau PET uptake predominantly in the entorhinal cortex for Flortaucipir and in the entorhinal cortex and parahippocampus for MK6240. Error bars for PLS weights were estimated using five-fold cross-validation.

PLS = partial least square; DCTclock = digital clock drawing test; SUVR = standardized uptake value ratios; CN = cognitively normal; Aβ = amyloid-beta status determined by [¹¹C]Pittsburgh-Compound B PET distribution volume ratios.

Keywords: Positron emission tomography, tau, digital clock drawing test, multivariate analysis, Alzheimer's disease

P13 [18F]RO-948 Tau PET Retention and Correlation with Fluid Biomarkers in the Early AD Continuum

Mahnaz Shekari^{1,2,3}, Armand González Escalante^{1,2,3}, Marta Milà-Alomà^{1,2,3,4}, Carles Falcon^{1,2,5}, Aida Niñerola-Baizán^{5,6}, Matteo Tonietto⁷, Edilio Borroni⁷, Gregory Klein⁷, Nicholas J. Ashton^{8,9,10,11}, Thomas K. Karikari^{8,12}, Juan Lantero-Rodriguez⁸, Anniina Snellman^{8,13}, Paula Ortiz^{1,2}, Eugene Vanmechelen¹⁴, Carolina Minguillón^{1,2,4}, Karine Fauria^{1,4}, Andrés Perissinotti^{5,6}, José Luis Molinuevo¹, Henrik Zetterberg^{15,16,17,18}, Kaj Blennow^{15,16}, Oriol Grau-Rivera^{1,2,4,19}, Marc Suárez-Calvet^{1,2,4,19}, Juan Domingo Gispert^{1,2,5}

¹Barcelonaβeta Brain Research Center (BBRC), Pasqual Maragall Foundation, Barcelona, Spain

²IMIM (Hospital del Mar Medical Research Institute), Barcelona, Spain

³Universitat Pompeu Fabra, Barcelona, Spain

⁴Centro de Investigación Biomédica en Red de Fragilidad y Envejecimiento Saludable (CIBERFES), Madrid, Spain

⁵Centro de Investigación Biomédica en Red de Bioingeniería, Biomateriales y Nanomedicina (CIBERBBN), Madrid, Spain

⁶Nuclear Medicine Department, Hospital Clínic, Barcelona, Spain

⁷Pharma Research and Early Development, F Hoffmann-La Roche Ltd., Basel, SZ

⁸Department of Psychiatry and Neurochemistry, Institute of Neuroscience and Physiology, University of Gothenburg, Mölndal, Sweden

⁹Wallenberg Centre for Molecular and Translational Medicine; University of Gothenburg, Gothenburg, Sweden

¹⁰King's College London, Institute of Psychiatry, Psychology & Neuroscience, Maurice Wohl Clinical Neuroscience Institute, London, UK

¹¹NIHR Biomedical Research Centre for Mental Health & Biomedical Research Unit for Dementia at South London & Maudsley NHS Foundation, London, UK

¹²Department of Psychiatry, University of Pittsburgh, PA, USA, Pittsburgh, PA, US

¹³Turku PET Centre, University of Turku, Turku, FI

¹⁴ADx NeuroSciences, Technologiepark 94, Ghent, Belgium

¹⁵Department of Psychiatry and Neurochemistry, Institute of Neuroscience and Physiology, University of Gothenburg, Mölndal, Sweden

¹⁶Clinical Neurochemistry Laboratory, Sahlgrenska University Hospital, Mölndal, Sweden

¹⁷Department of Neurodegenerative Disease, UCL Institute of Neurology, Queen Square, London, UK

¹⁸UK Dementia Research Institute at UCL, London, UK

¹⁹Servei de Neurologia, Hospital del Mar, Barcelona, Spain

Background: Tau positron emission tomography (PET) imaging enables the *in vivo* visualization of tau aggregates occurring during the progression of Alzheimer's disease (AD). Tau PET imaging is a promising biomarker for clinical diagnosis and tracking of disease progression. However, the sensitivity of tau PET in detecting early tau pathology within the early AD continuum and its association with fluid tau biomarkers remains to be established.

Method: cognitively unimpaired individuals from ALFA+ cohort had [¹⁸F]RO-948 and [¹⁸F]flutemetamol PET, T1-weighted magnetic resonance imaging (MRI), cerebrospinal fluid (CSF), and plasma biomarkers available (Table 1). CSF amyloid (A) and tau (T) positivity defined using CSF A β 42/40 ratio and ptau181 measured by exploratory NeuroToolKit and Elecsys® immunoassays, respectively. Centiloid (CL) values were obtained from [¹⁸F]flutemetamol PET scans using a validated pipeline. [¹⁸F]RO-948 uptake was measured in entorhinal (Braak I/II), limbic (Braak III/IV), and neocortical (Braak V/VI) regions and normalized to inferior cerebellum to render SUVR values. Regional positivity thresholds per Braak stage calculated as median plus two robust standard deviations of CSF A-T- group. Associations between [¹⁸F]RO-948 SUVRs and available fluid biomarkers evaluated using Pearson correlations. Receiver Operating Curve (ROC) analysis conducted for fluid biomarkers to discriminate Braak I/II positives from individuals with negative tau PET scans. AUC was calculated using ROC analysis for available biomarkers and positivity threshold was calculated using Youden Index. P-values < 0.05 were considered statistically significant.

Results: In BraakI/II, **nine** cases were considered to be positive, **four** in BraakIII/IV and **one** in BraakV/VI, **eight** of them being A+T+ and **one** was A+T-. Significant correlations with fluid biomarkers observed in all Braak stages(**Figure1**). AUC for differentiating BraakI/II stage was statistically significant for all biomarkers(**Table2**).

Conclusion: A progressively lower number of [¹⁸F]RO-948 PET-positive cases were detected for more advanced Braak stages as expected from neuropathological studies. Using CSF ptau217, ptau 181, and global Centiloid had the highest capacity in predicting elevated level of [¹⁸F]RO-948 tau PET uptake in early stages in cognitively unimpaired individuals.

Biomarker	AUC (p-value)	95%CI
CSF pTau217	0.94 (p<0.001)	0.85-1.00
Centiloid	0.93 (p<0.001)	0.87-1.00
CSF pTau181	0.90 (<0.001)	0.80-0.99
Plasma pTau231	0.88 (p=0.001)	0.61-0.95
CSF pTau231	0.87 (p=0.002)	0.82-1.00
CSF pTau235	0.82 (p=0.006)	0.64-1.00
CSF NFL	0.81 (p=0.008)	0.69-0.99
Plasma ptau181	0.78(p=0.01)	0.61-0.95
Plasma ptau217	0.73(p=0.055)	0.52-0.94

Table 2. Evaluating the sensitivity of imaging, and wet biomarkers to predict tau positivity in early stages using area under the curve (95% confidence interval)

Demographic and biomarkers	Total	A-T-	A+T-	A+T+	A-T+
N	67	14	13	21	9
Age, mean (SD) [58 to 70.46], y	63.19(4.59)	60.55(4.98)	59.43(4.28)	63.48(5.56)	59.88(4.22)
Sex, N (%), F	39 (58.20%)	6(8.95%)	9(13.43%)	14(20.89%)	5(7.46%)
APOE-ε4, N (%), carriers	37(55.22%)	6(8.95%)	9(13.43%)	15(22.38%)	7(10.44%)
CSF Aβ _{42/40} , mean (SD), pg/mL	0.066(0.029)	0.095(0.013)	0.505(0.011)	0.041(0.010)	0.102(0.020)
CSF p-Tau ₁₈₁ , mean (SD), pg/mL	23.240(10.858)	16.690(4.674)	16.599(3.800)	33.117(9.628)	19.976(11.030)
Centiloid	23.601(28.290)	-1.415(8.157)	25.082(20.243)	52.325 (19.066)	2.181(6.544)

Table1. Demographic information of participants. AT group has been defined based on Aβ42/40 ratio and ptau181 in CSF

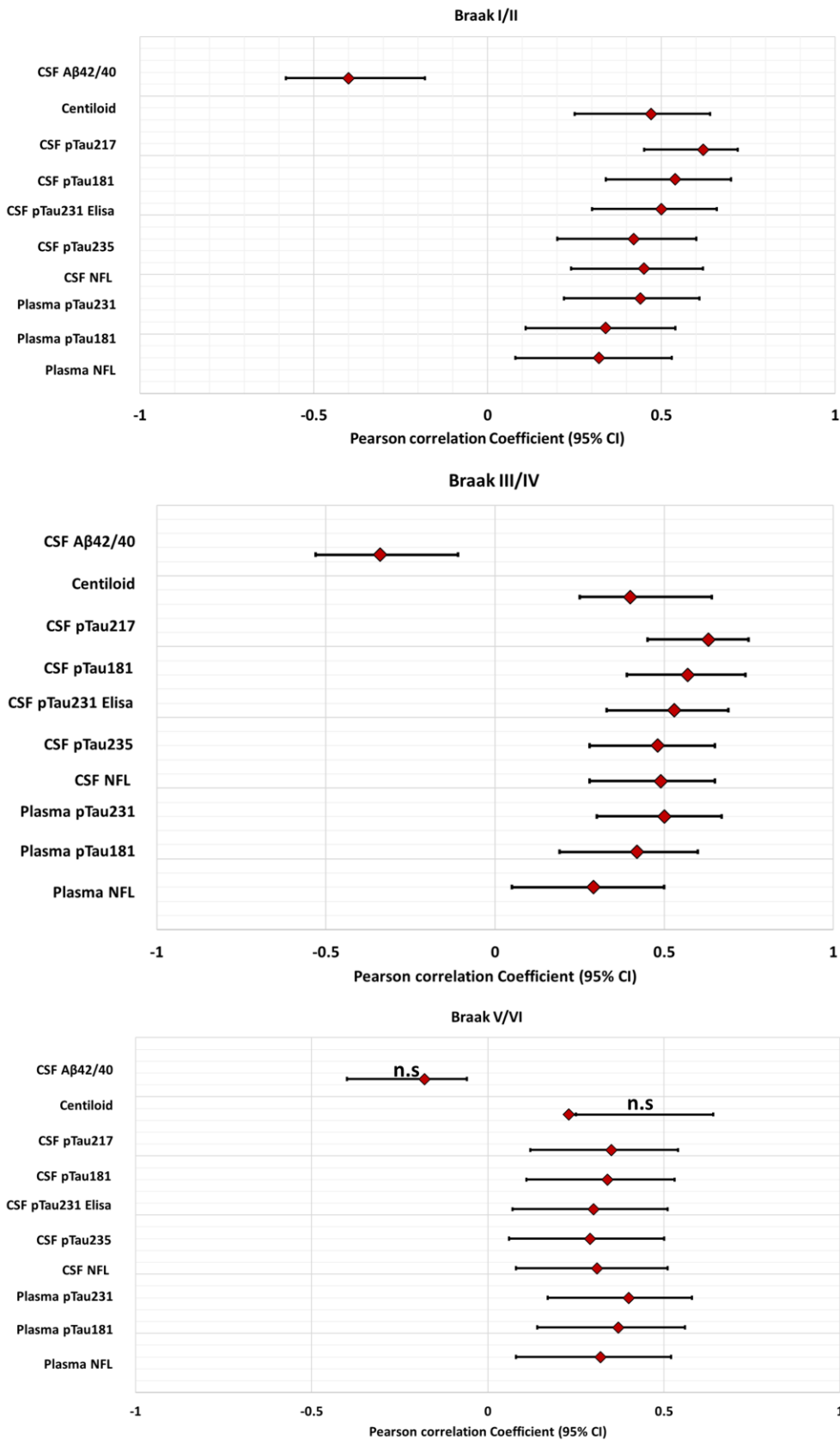


Figure 1. Pearson correlation coefficient and 95% CI between Braak ROIs and fluid biomarkers

Keywords: Tau PET, Braak staging, Alzheimer's disease, blood biomarkers

P14 Regional tau predicts glucose hypometabolism in autosomal dominant Alzheimer's disease: Findings from the Colombia-Boston (COLBOS) biomarker study

Stephanie Langella¹, Elizabeth Kaplan¹, Ana Baena², Natalia Londono², Diana Munera¹, Clara Vila-Castelar¹, Sergio Alvarez³, Monica Vidal³, Michael Properzi¹, Justin Sanchez¹, Reisa Sperling¹, Keith Johnson¹, Francisco Lopera², Bernard Hanseeuw^{1,4}, Yakeel Quiroz^{1,2}

¹Massachusetts General Hospital / Harvard Medical School, Boston, MA, US

²Grupo de Neurociencias de Antioquia, Universidad de Antioquia, Medellin, CO

³Hospital Pablo Tobon Uribe, Medellin, CO

⁴Université Catholique de Louvain, Brussels, Belgium

Background: Hypometabolism is observed in early Alzheimer's disease (AD), though its relation to pathology remains uncertain. We examined the relationships between β -amyloid (A β), tau, and glucose metabolism in presenilin-1 (*PSEN1*) E280A mutation carriers and non-carriers from the Colombia-Boston (COLBOS) Biomarker Study.

Methods: Cross-sectional measures of A β (11C-Pittsburgh compound B), fludeoxyglucose (18F-fludeoxyglucose; FDG), and tau (18F-flortaucipir) positron emission tomography (PET) were assessed from 15 *PSEN1* E280A carriers (9F, mean age=42 years, 8 cognitively unimpaired) and 22 age-matched non-carrier family members (15F, mean age=38 years). FDG-PET was collected on average 1.36 years later than A β - and tau-PET. Entorhinal cortex, precuneus, and inferior temporal cortex were regions of interest (ROIs). Linear regression was used to (1) assess age-related trajectories of each biomarker as function of group, with age centered at 44 years (median age of mild cognitive impairment onset for this kindred); and (2) test whether cortical A β and regional tau predict FDG in carriers.

Results: Carriers had greater cortical A β and tau burden than non-carriers and a positive age-pathology association in all ROIs ($p < .05$). Carriers had lower metabolism in precuneus ($p = .004$) and inferior temporal cortex ($p = .034$). Age-related trajectories of FDG metabolism did not differ by group for any ROI ($p > .05$). Within carriers, higher cortical A β was associated with lower subsequent inferior temporal metabolism ($p = .017$). Precuneus tau was associated with lower metabolism in the inferior temporal cortex ($p = .001$) and precuneus ($p = .020$). Inferior temporal tau was associated with lower inferior temporal ($p = .007$) and entorhinal ($p = .028$) metabolism. Only the relationship between precuneus tau and inferior temporal metabolism survived correction for age and sex ($p = .021$).

Conclusions: These preliminary results provide evidence that tau is more closely associated to glucose metabolism than is A β , and that precuneus tau in particular has an integral role in predicting local and distant regional metabolic changes in autosomal dominant AD.

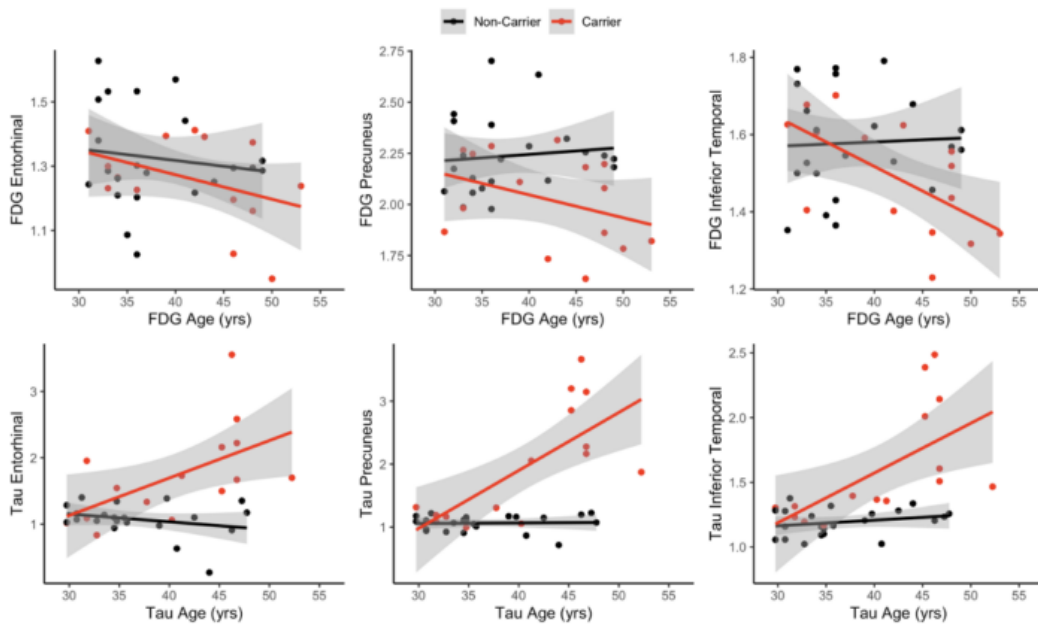


Figure 1. Age-related trajectories of regional FDG- and tau-PET standardized uptake value ratios in *PSEN1* E280A carriers (red) and non-carriers (black) with standard error band.

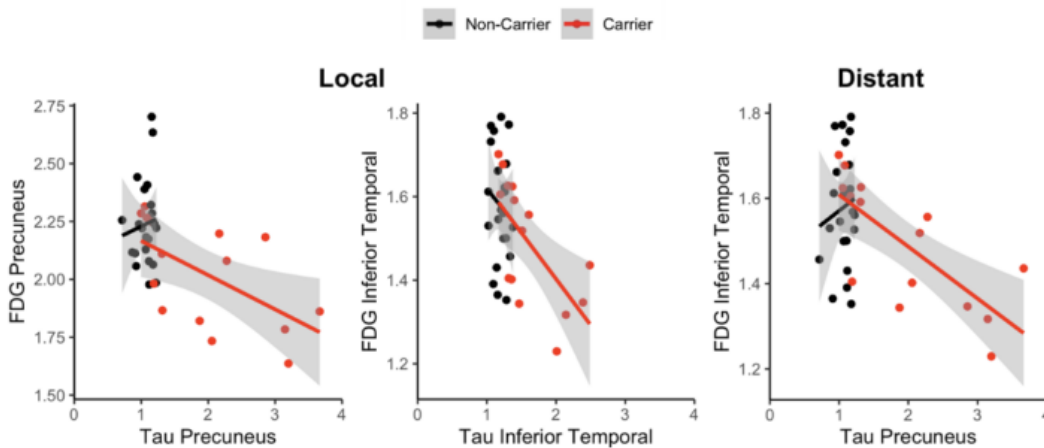


Figure 2. Relationships between regional tau- and FDG-PET standardized uptake value ratios in carriers (red) and non-carriers (black) with standard error band.

Table 1. Linear regression output (standardized β -weights and p -values) of cortical A β and regional tau predicting regional FDG in mutation carriers.

	Predictor							
	Cortical A β		Entorhinal Tau		Precuneus Tau		Inferior Temporal Tau	
	β	p	β	p	β	p	β	p
Entorhinal FDG	-0.13	.170	-0.08	.125	-0.08	.057	-0.18	.028
Precuneus FDG	-0.16	.310	-0.12	.160	-0.15	.020	-0.20	.148
Inferior Temporal FDG	-0.23	.017	-0.10	.060	-0.12	.001	-0.22	.007

Keywords: fludeoxyglucose, tau, positron emission tomography, autosomal dominant Alzheimer's disease, mild cognitive impairment

P15 Is tau PET a robust biomarker for chronic traumatic encephalopathy?

Natasha Krishnadas^{1,2}, Vincent Doré^{2,3}, Fiona Lamb², Rodney Guzman², Jennie L Ponsford⁴, Amelia J Hicks⁴, Rob Williams⁵, Azadeh Feizpour^{1,2}, Victor L Villemagne⁶, Christopher C Rowe^{1,2,7}

¹Florey Institute of Neurosciences & Mental Health, Melbourne, AU

²Department of Molecular Imaging & Therapy, Austin Health, Melbourne, AU

³Health and Biosecurity Flagship, The Australian eHealth Research Centre, Melbourne, AU

⁴Monash-Epworth Rehabilitation Research Centre, Turner Institute for Brain and Mental Health, Monash University, Melbourne, AU

⁵The University of Melbourne, Melbourne, AU

⁶Department of Psychiatry, University of Pittsburgh, Pittsburgh, PA, US

⁷Florey Department of Neurosciences & Mental Health, The University of Melbourne, Melbourne, AU

Objective: To investigate tau ¹⁸F-MK6240 PET, a potential biomarker for chronic traumatic encephalopathy (CTE), in contact sport players with exposure to repetitive head impacts (sRHI).

Background: CTE is a post-mortem diagnosis. We previously reported a frontotemporal predominant ¹⁸F-MK6240 pattern resembling the distribution of CTE in a retired Australian Rules Football player in the context of a moderate amyloid-beta plaque burden.

Methods: sRHI ($n=33$) and age-matched healthy controls (HC) ($n=32$) completed amyloid (¹⁸F-NAV4694) and tau (¹⁸F-MK6240) PET scans. Amyloid PET was quantified in Centiloids. ¹⁸F-MK6240 standardized uptake value ratios (SUVRs) were generated for the dorsolateral prefrontal cortex and composite regions of interest (ROI) (frontal; mesial temporal; temporoparietal).

Results: The primary contact sport for the sRHI was: Australian Rules Football ($n=16$), boxing/ mixed martial arts/ kickboxing ($n=12$), rugby ($n=4$) and soccer ($n=1$), with 39.4% participating at a professional level. sRHI had a mean age of 53.2 (± 9.5) (vs HC 54.2 ± 9.2 , $p=0.61$), and 94% were male (vs HC 78%, $p=0.08$). sRHI did not differ from HC in years of education ($p=0.46$), but had more impaired MMSE (28.1 ± 1.9 vs 29.3 ± 0.8 , $p=0.006$, $d=-0.80$) and Clinical Dementia Rating scores (0.21 ± 0.3 vs 0 ± 0 , $p<0.001$, $d=1.25$). sRHI and HC did not differ in mean Centiloid values (4.5 ± 12.2 vs 3.1 ± 8.4). sRHI and HC did not differ in ¹⁸F-MK6240 SUVR in the regions examined, and no differences were observed between professional and amateur sRHI.

Conclusions: Contact sports players with exposure to repetitive head impacts did not differ from age-matched healthy controls on ¹⁸F-MK6240 SUVR in frontal, mesial temporal, and temporoparietal brain regions. Study limitations include the small sample size, heterogeneity in sports type and highest level of participation, and participants with relatively mild cognitive and functional impairments. Additionally, while ¹⁸F-MK6240 has high affinity for 3R/4R tau in Alzheimer's disease, its affinity in CTE, particularly important at early stages, remains unclear.

Keywords: Tau, PET, chronic traumatic encephalopathy (CTE), biomarker, 18F-MK6240

P16 Centiloid scale measure of amyloid PET by CT of PET/CT equipment

Hiroshi Matsuda^{1,2}, Haruo Hanyu², Chikako Kaneko²

¹*Fukushima Medical University, Fukushima, Japan*

²*Southern Tohoku Research Institute for Neuroscience, Koriyama, Japan*

Background: Centiloid (CL) scaling is a standard quantitative measure for amyloid PET. After amyloid PET images are anatomically standardized with co-registered MRI, the CL scale must be calculated using standard volumes of interest; if MRI is not available, the CL scale may not be accurately calculated. The purpose of this study was to evaluate the measurement accuracy of CT as an alternative to MRI in CL scale calculation in order to clarify the substitutability of CT for PET attenuation correction in PET/CT equipment.

Material and Methods: Amyloid PET images obtained using 11C-PiB from 26 patients with possible or probable Alzheimer's disease were processed to calculate the CL scale using 3D T1-weighted MRI (Optima MR450w, 1.5T, GE healthcare) and CT of digital PET/CT (uMI780, United Imaging Healthcare). CL obtained using MRI and CT for anatomic standardization were defined as CLMRI and CLCT, respectively, and were compared. We used our original software (Amyquant, Matsuda H, et al. Brain Behav 2022;12:e2499) for CL calculation based on the method proposed by the Global Alzheimer's Association Interactive Network. The whole cerebellum was chosen as the reference region for CL calculation.

Results: Bland-Altman plots revealed that CLCT was not significantly different from CLMRI (mean \pm standard deviation, -0.2 ± 1.4 , $p = 0.392$), with 95% limits of agreement ranging from -0.8 to 0.3 . Pearson correlation analysis showed a highly significant positive correlation between CLCT and CLMRI, $r = 0.999$ ($p < 0.001$). The linear regression equation was $CLCT = 0.992 \times CLMRI + 0.01$.

Conclusion: CL measurements with CT of PET/CT can provide nearly identical values to those obtained with MRI; an important advantage of using CT is that PET and CT can be obtained simultaneously. This method can be applied to subjects who cannot undergo MRI.

Keywords: PET MRI CT Amyloid Centiloid

P17 Successful cognitive aging is associated with less brain atrophy and lower tau deposition

Stefania Pezzoli^{1,2}, Joseph Giorgio^{1,3}, Theresa M. Harrison¹, Adam Martersteck¹, William J. Jagust^{1,2}

¹Helen Wills Neuroscience Institute, University of California, Berkeley, CA, US

²Lawrence Berkeley National Laboratory, Berkeley, CA, US

³University of Newcastle, Newcastle, AU

There is no consensus on either the definition of successful agers (SA) or the underlying neural mechanisms. The aim of this study was to compare new and existing definitions, and to understand features associated with SA. We used machine learning algorithms to predict age from neuropsychological tests in 184 cognitively normal adults over the age of 70. Differences between cognitive-predicted age and chronological age (cognitive age gap, CAG) were used as a novel measure of SA (SA-CAG) with a cut-off at the 20th percentile (n=37). SA were similarly defined using episodic memory (SA-EM, n=37) and non-memory cognition (SA-NM, n=37) composite scores, and the California Verbal Learning Test long delay free recall (SA-CVLT, n=31). SA were also combined in one group based on meeting any criterion (SA-ALL, n=74). Each SA group was compared to a group of typical agers (TA, n=110) in cortical thickness, hippocampal volume, APOE genotype, brain β -amyloid (PiB) and tau (FTP). All analyses were adjusted for age, sex, and years of education. Fair to moderate strength of agreement was found between the four definitions (Figure 1). All SA groups showed greater cortical thickness, specifically in the anterior and midcingulate cortices and medial temporal lobes (Figure 2). Compared to TA, greater hippocampal volume was found in SA-ALL, SA-CAG, SA-EM, and SA-CVLT. Lower entorhinal FTP uptake was also found in all SA groups (Figure 3). No between-group differences were detected in the proportion of APOE ϵ 4 carriers and PiB+ participants. Despite imperfect overlap in SA groups, common brain features were found across definitions including greater hippocampal volume and medial prefrontal cortical thickness, and lower entorhinal tau deposition. This suggests that a feature of SA, regardless of its exact definition, is resistance to tau pathology. Greater cortical thickness could reflect either brain reserve or resistance to downstream effects of tau pathology.

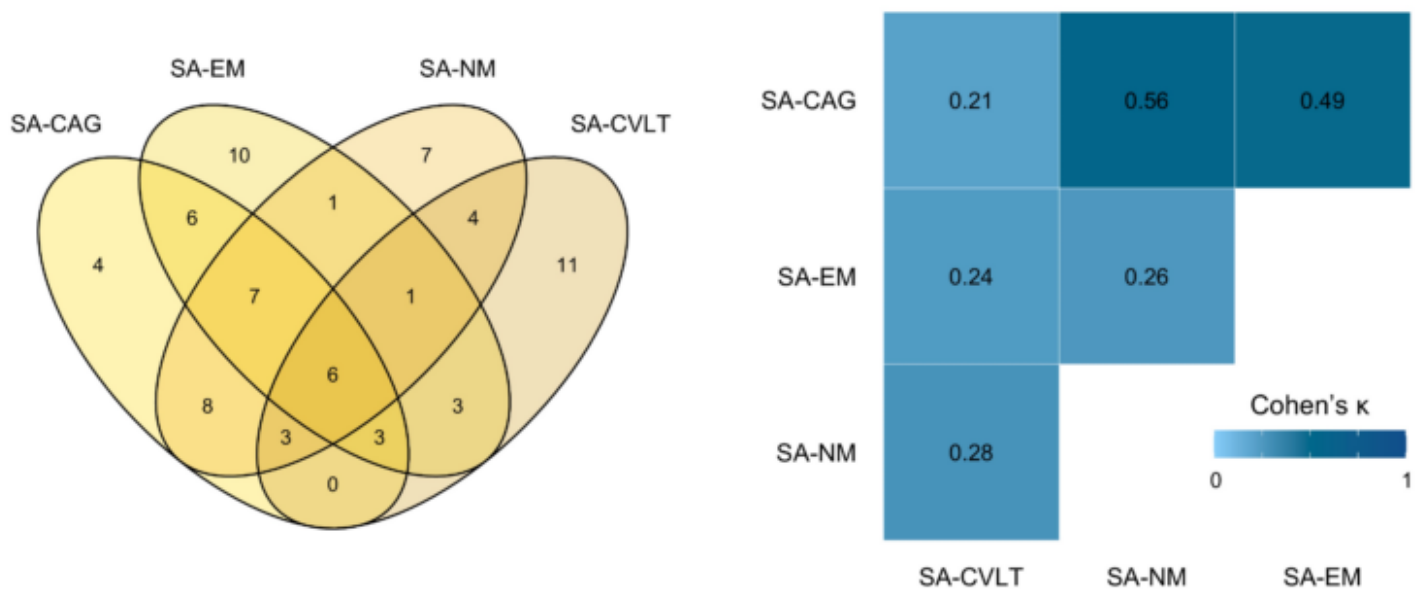


Figure 1 Number of overlapping participants defined as SA by different definitions (left), and Cohen's κ values indicating the strength of agreement between definitions (right).

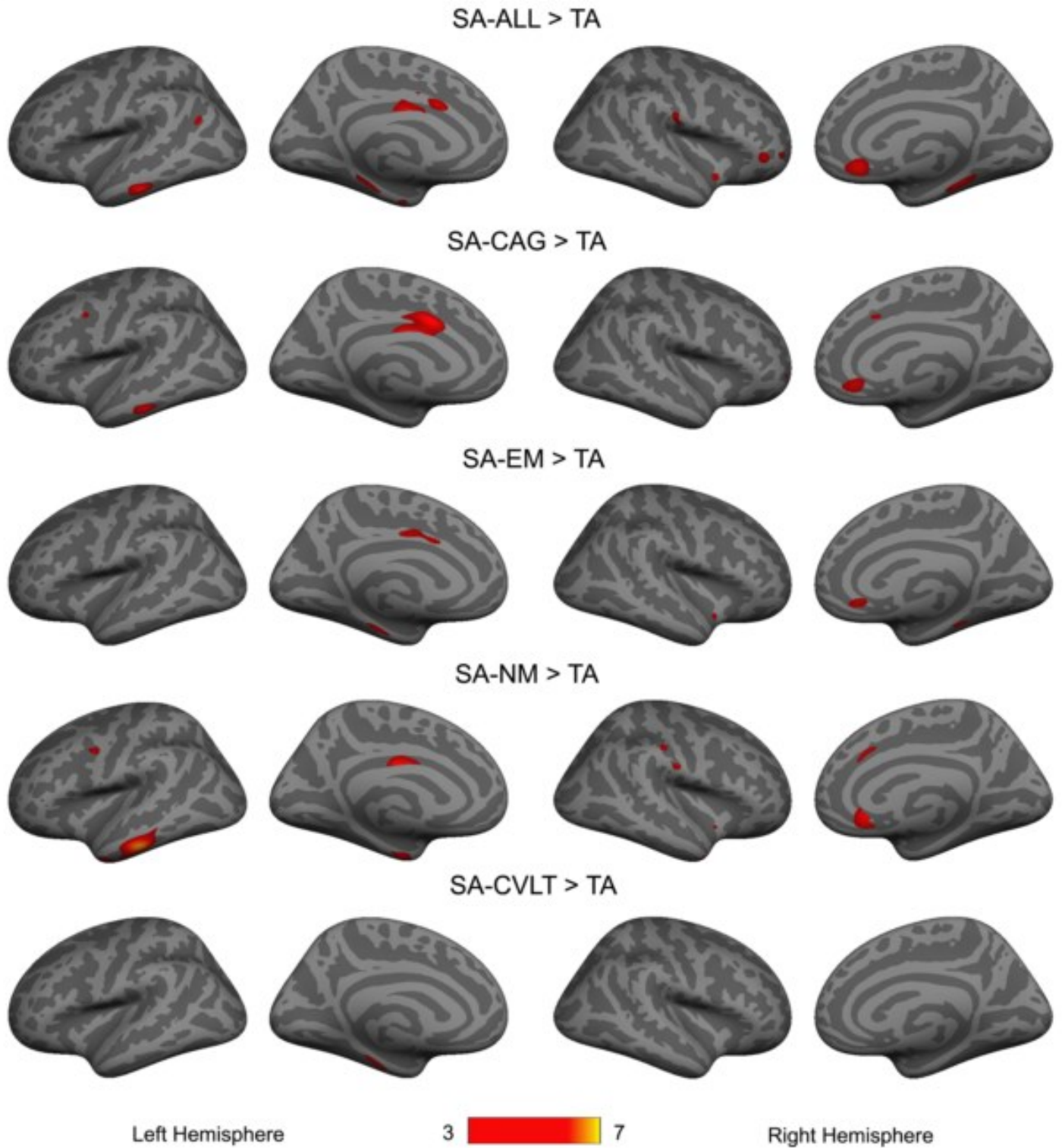


Figure 2 Whole-brain vertex-wise cortical thickness analyses revealing regions of significantly thicker cortex in SA compared to TA accounting for age, sex, and years of education. Significance threshold was set at $p < 0.001$ uncorrected. Color bar indicates logarithmic scale of p-values ($-\log_{10}$). No region was found as significantly thicker in TA compared with SA.

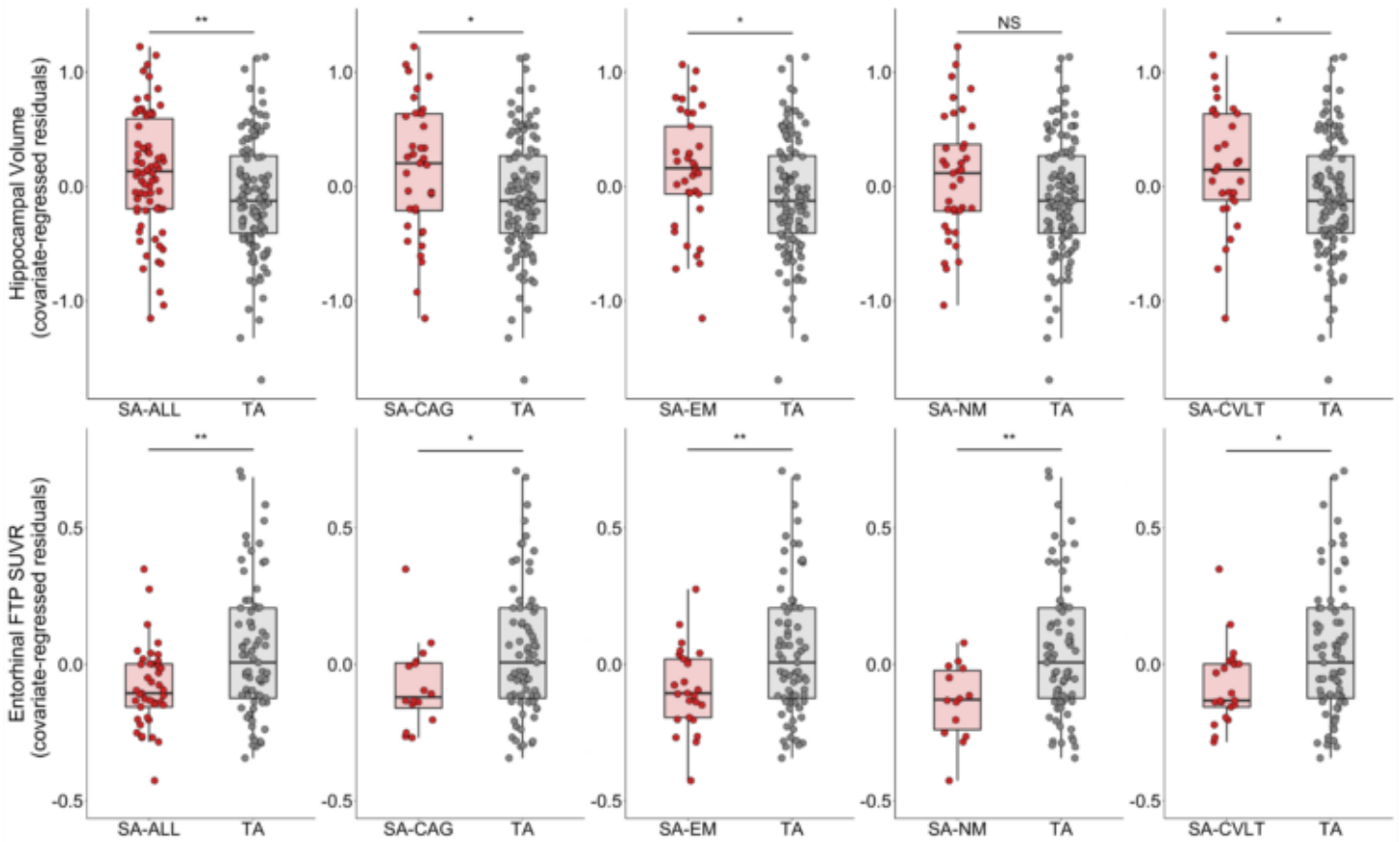


Figure 3 Compared to TA, greater hippocampal volume was found in SA-ALL, $F(1, 179)=8.43$, $p=0.004$), SA-CAG ($F(1, 142)=6.05$, $p=0.02$), SA-EM ($F(1,142)=4.49$, $p=0.04$), and SA-CVLT ($F(1,136)=5.94$, $p=0.02$). In a subsample of participants ($n=114$), lower entorhinal flortaucipir (FTP) uptake, quantified as partial volume corrected standardized uptake value ratios (SUVR), was found in SA-ALL ($F(1, 109)=10.01$, $p=0.002$), SA-CAG ($F(1,84)=4.06$, $p=0.047$), SA-EM ($F(1,93)=7.17$, $p=0.009$), SA-NM ($F(1, 82)=7.69$, $p=0.007$), and SA-CVLT ($F(1,89)=4.46$, $p=0.04$). The analyses were age, sex, and years of education adjusted. * $p<0.05$, ** $p<0.01$, NS: not significant.

Keywords: successful cognitive aging, Alzheimer's disease pathology, PET, tau, cortical thickness

P18 Subcortical flortaucipir PET and susceptibility analyses to differentiate progressive supranuclear palsy clinical variants and corticobasal syndrome

Ryota Satoh¹, Arvin Arani¹, Christopher Schwarz¹, Matthew Senjem¹, Farwa Ali¹, Clifford Jack¹, Val Lowe¹, Keith Josephs¹, Jennifer Whitwell¹

¹Mayo Clinic, Rochester, MN, US

Background: Quantitative susceptibility mapping is a relatively new MRI technique to estimate magnetic susceptibility *in vivo*, and the estimated susceptibility is proportional to iron concentration in some subcortical tissues. Patterns of flortaucipir PET uptake are topographically similar to patterns of elevated susceptibility in progressive supranuclear palsy (PSP); both increased in the basal ganglia and midbrain. However, no studies have directly compared these two modalities in the same PSP cohort. This study aims to compare the patterns of flortaucipir uptake and elevated susceptibility across PSP clinical variants and corticobasal syndrome (CBS).

Methods: Forty-seven patients, 19 with PSP-Richardson’s syndrome (PSP-RS), six PSP-parkinsonism (PSP-P), six PSP-progressive gait freezing (PSP-PGF), five PSP-postural instability (PSP-PI), 11 CBS, and 19 cognitively normal control subjects underwent flortaucipir PET and 3T-MRI scans. Region-of-interest analysis was conducted to obtain flortaucipir standardized uptake value ratios (SUVRs) and susceptibilities in eight subcortical regions (see Table).

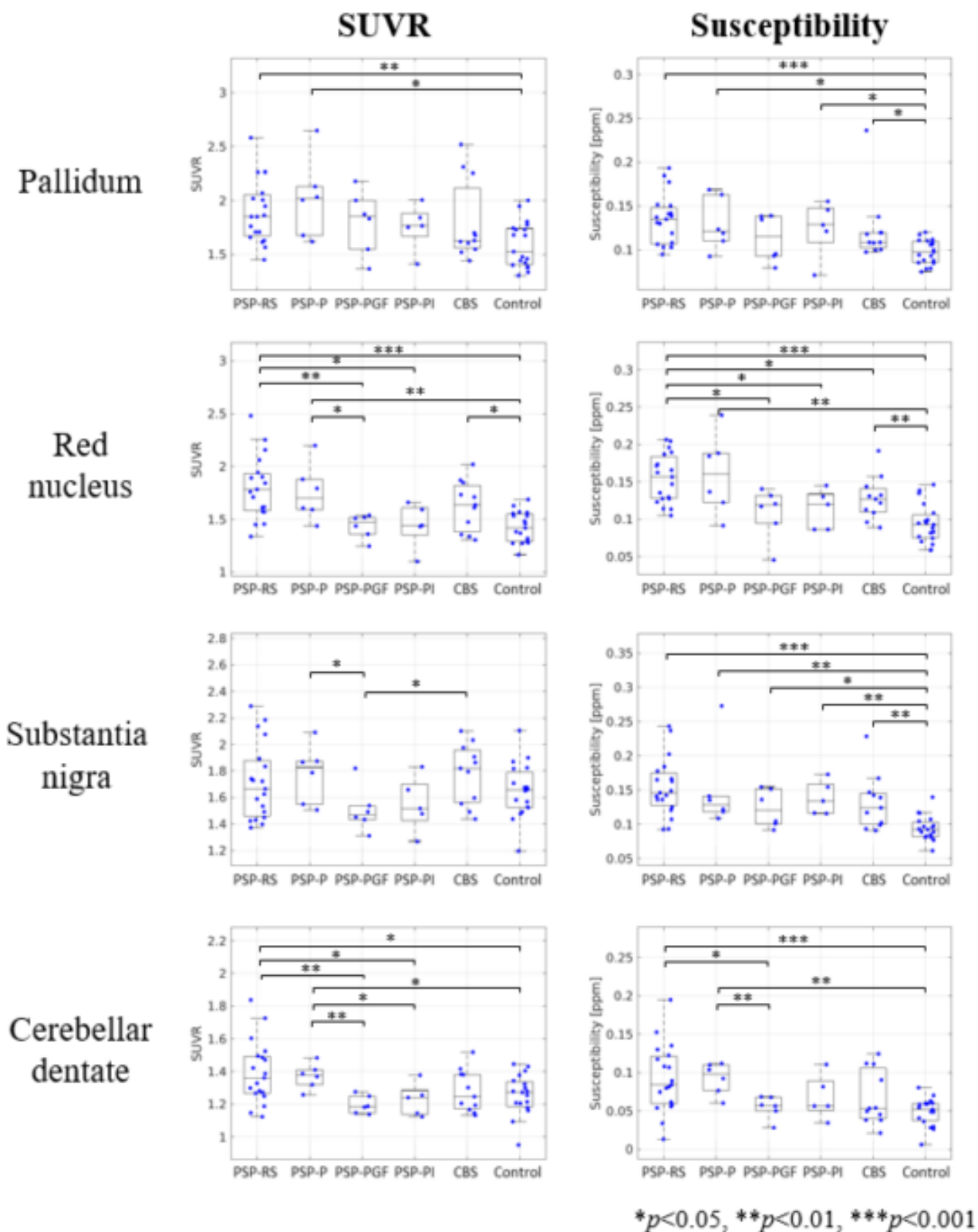
Results: There were significant differences across groups in both flortaucipir SUVR and susceptibility in the pallidum, red nucleus, and cerebellar dentate (Table). In these regions, SUVR and susceptibility were higher in PSP-RS and PSP-P than controls (Figure). They were also higher than those in PSP-PGF and PSP-PI in the red nucleus and cerebellar dentate. The two signals were well correlated in these three regions ($r=0.45-0.59$; $P<0.001$). However, in the substantia nigra, all disease groups showed larger susceptibility than controls, while SUVR did not show any differences between disease and control groups (Figure), and these signals were not well correlated ($r=0.21$; $P=0.10$).

Conclusions: The patterns of flortaucipir uptake and elevated susceptibility were similar in most subcortical regions in PSP and CBS patients, suggesting the possibility that some flortaucipir uptake is related to iron. The relationship between flortaucipir and iron may not have been observed in the substantia nigra due to the involvement of other substances (e.g. neuromelanin).

Table. Outcomes of Kruskal-Wallis test (p-values) to determine if flortaucipir SUVR and susceptibility could originate from the same distribution across all patient cohorts, and the corresponding Pearson’s correlation coefficients (r).

	<i>p</i> (Kruskal-Wallis test)		<i>r</i>
	SUVR	Susceptibility	
Caudate	0.69	0.50	0.36
Putamen	0.64	0.44	0.58
Pallidum	0.02	<0.01	0.55
Thalamus	0.45	0.58	0.11
Substantia nigra	0.14	<0.001	0.21
Red nucleus	<0.001	<0.001	0.59
Subthalamic nucleus	0.02	0.06	0.52
Cerebellar dentate	0.01	<0.01	0.45

Figure. Boxplots of flortaucipir SUVR and susceptibility. The boxes indicate the interquartile ranges, and the whiskers indicate the minimum and maximum values excluding the outliers.



Keywords: flortaucipir, quantitative susceptibility mapping, iron, progressive supranuclear palsy, corticobasal syndrome

P19 Temporal associations of plasma and PET Alzheimer's disease biomarkers using a non-linear mixed effects model

Petrice Cogswell¹, Emily Lundt², Terry Therneau², Jonathan Graff-Radford³, Christopher Schwarz¹, Matthew Senjem^{1,4}, Jeffrey Gunter¹, Prashanthi Vemuri¹, Ronald Petersen^{2,3}, Clifford Jack Jr¹

¹Department of Radiology, Mayo Clinic, Rochester, MN, US

²Department of Quantitative Health Sciences, Mayo Clinic, Rochester, MN, US

³Department of Neurology, Mayo Clinic, Rochester, MN, US

⁴Department of Information Technology, Mayo Clinic, Rochester, MN, US

Objective: The temporal evolution of plasma Alzheimer's disease biomarkers and their relationship to PET biomarker change remains unclear and less extensively studied than cross-sectional associations. One method to assess the longitudinal trajectory of biomarker change is a non-linear mixed effects (NLME) model, which assumes a common pattern of progression for a biomarker that is shifted earlier or later in time for each individual. The aim of this study was to investigate the association of relative timing of progression of plasma p-tau181 vs amyloid and tau PET on an individual level.

Methods: The study included 2169 participants from the Mayo Clinic Study of Aging (MCSA) and Mayo Alzheimer's Disease Research Center (ADRC) with a clinical diagnosis of cognitively unimpaired, mild cognitive impairment, or Alzheimer's Clinical Syndrome with dementia. A non-linear mixed effects model was fit with amyloid (PiB) PET global meta-ROI SUVR, tau PET (flortaucipir) temporal meta-ROI SUVR, and plasma p-tau181 (Simoa, Quanterix HD-X) as the tri-variate endpoints, and sex, APOE genotype status, and years of education as covariates. The model output included a per subject age adjustment (individual adjustment) or time-shift for each biomarker that indicated how much earlier or later the individual was estimated to progress on that biomarker relative to the population mean and the correlation (R) between adjustments for each pair of biomarkers.

Results: There was a strong correlation between earlier onset of amyloid and earlier onset of tau PET (R, 95% credible interval = 0.53(0.47,0.57)) (**Figure 1**). Individual-level adjustments of plasma p-tau181 were more strongly associated with amyloid PET (R=0.44(0.39,0.49)) than tau PET (0.35(0.28, 0.43)). Covariate effects are shown in **Table 1**.

Conclusions: On an individual level, timing of progression of p-tau181 was more strongly associated with amyloid than tau PET progression, supporting that p-tau181 change is more closely related to amyloid than tau accumulation.

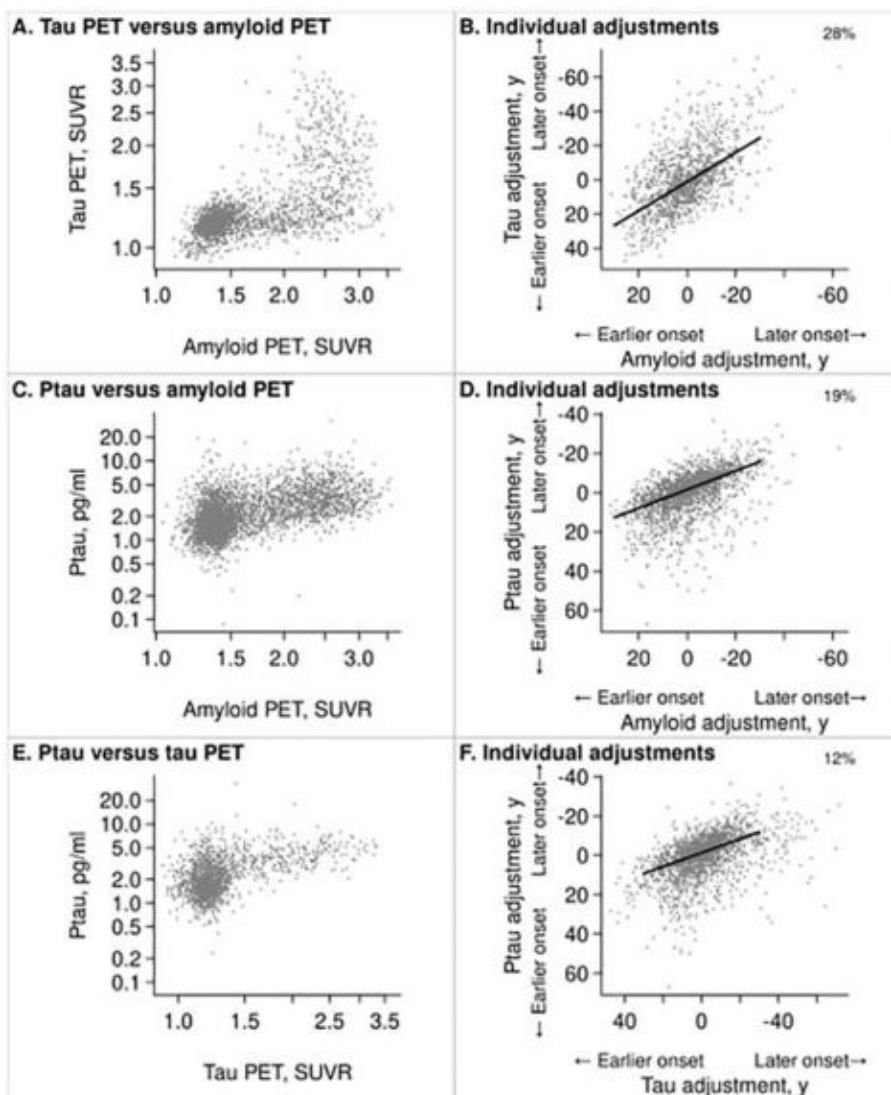


Figure 1: Relationships of raw biomarker values and individual-level adjustments. In the left column (panels A, C, E), scatter plots display each 2-way relationship between the raw outcome measures used in the model; each dot represents one observation, and a participant could have multiple observations. In the right column (panels B, D, F), scatter plots summarize each 2-way relationship between the model output of individual adjustments. The individual adjustments are shown in years and indicate whether a participant's level of disease burden was consistent with earlier onset or later onset relative to their demographic peers; each dot represents one participant, and the number of participants varies across the comparisons based on data availability. The trendline represents the median y-axis variable onset adjustment for a given x-axis variable onset adjustment. The x-axes and y-axes are flipped for the individual adjustments. A higher positive value or earlier onset relative to the population mean is shown to the left of the x-axis and bottom of the y-axis. The percent variation explained (square of the correlation*100) between individual-level adjustments is given in the upper right-hand corner. * SUVR = standardized uptake value

Table 1. Covariate effects. Values shown are mean (95% credible interval). Estimates are in years and represent estimated adjustment or years by which that biomarker's progression is shifted earlier (positive) or later (negative) with vs without that covariate. For example, an estimate of 8.2 (7.1, 9.4) for APOE $\epsilon 4$ genotype on amyloid implies an amyloid accumulation that begins, on average, 8.2 (7.1, 9.4) years earlier in APOE $\epsilon 4$ carriers than non-carriers. APOE carriers had weaker effects on tau PET and p-tau181. The largest covariate effect was referral to the ADRC on tau PET of 24.9 (22.7, 27.2) years earlier, which in part is due to the presence of individuals with early-onset AD in the ADRC.

	Amyloid PET	Tau PET	P-tau181
APOE $\epsilon 4$ carrier	8.2 (7.1, 9.4)	5.9 (3.7, 8.1)	4.2 (2.7, 5.7)
Female sex	2.3 (1.2, 3.5)	2.4 (0.5, 4.4)	-3.0 (-4.4, -1.5)
Education 1-yr	0.2 (-0.0, 0.4)	0.6 (0.2, 1.0)	0.2 (-0.1, 0.4)
Referral to ADRC	17.4 (16.3, 18.5)	24.9 (22.7, 27.2)	16.1 (14.6, 17.5)

Keywords: plasma p-tau, amyloid PET, tau PET, longitudinal modeling, Alzheimer's disease

P20 Beta-amyloid accumulates at a faster rate in individuals with Down syndrome

Andrew McVea¹, Alexandra DiFilippo¹, Max McLachlan¹, Dhanabalan Murali¹, Matthew Zammit¹, Sterling Johnson¹, Tobey Betthausen¹, Charles Stone¹, Dana Tudorascu², Charles Laymon², William Klunk², Ann Cohen², Benjamin Handen², Bradley Christian¹

¹University of Wisconsin - Madison, Madison, WI, US

²University of Pittsburgh, Pittsburgh, PA, US

Background: Down syndrome (DS) is characterized by earlier beta-amyloid (A β) plaque accumulation and increased prevalence of Alzheimer's disease (AD) due to trisomy 21 triplicating the amyloid precursor protein (APP) gene. This study compares accumulation rates of A β between DS and non-DS populations measured with longitudinal [C-11]PiB at the same imaging site with identical scanning procedures to minimize experimental variation.

Methods: Individuals with four or more [C-11]PiB scans spanning 8+ yrs on the UW-Madison ECAT HR+ scanner, including at least one A β + scan (SUVR>1.40) and one A β - scan, were selected for this study. 11 DS participants in the ABC-DS study and 9 non-DS participants from the PREDICT study fit these criteria. Scans were acquired up to 70min post-injection. Reconstructed PET images were aligned and spatially normalized into template space and converted into 50-70min SUVR images using a cerebellar grey matter reference region. Using global SUVR as the metric of A β deposition, the data were fit against age with a logistic growth curve () to determine the rate of A β accumulation as subjects transition to A β +. The model fixed $NS=1.12$, the average baseline SUVR of all A β - subject scans ($n=491$), and $K=1.28$, the highest specific binding in any participant.

Results: Plotting [C-11]PiB SUVR against age provides visual comparisons of cohorts (Fig 1) and transforming the x-axis to amyloid chronicity ($t=0$ at Ab^+) illustrates differences in accumulation rates between groups (Fig 2). The average rate of amyloid accumulation (DSUVR/yr) when becoming A β + in the DS cohort is 0.077(0.028) versus 0.042(0.009) for non-DS ($p=0.002$).

Conclusions: A β accumulation is faster in our DS cohort than in non-DS which is consistent with the additional APP gene copy in DS. We observed an increase of 86% in accumulation rate between these groups. However, the variability in DS accumulation rates requires further investigation towards understanding genetic and lifestyle factors.

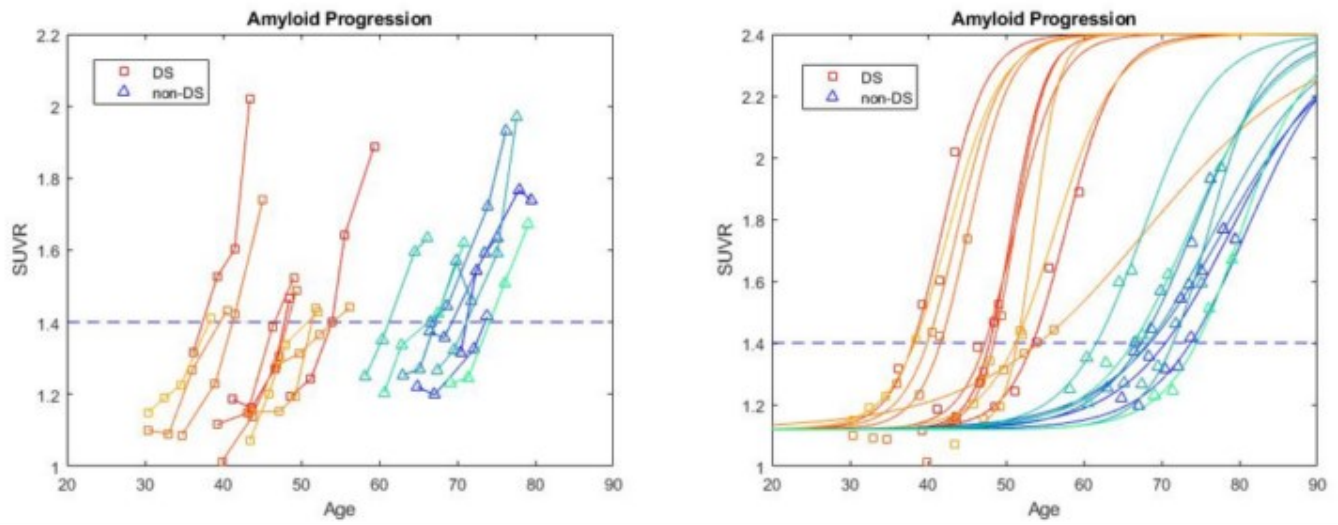


Fig. 1: Plots showing the age at appointment and global PiB SUVR for participants included in our analysis (left) and their curve fits (right). Global SUVR was calculated using the average signal in the frontal, parietal, superior temporal, medial temporal, inferior temporal, occipital lobes and cingulate gyri as defined by the AAL atlas. There is no overlap in age of A β + between the DS and non-DS cohorts.

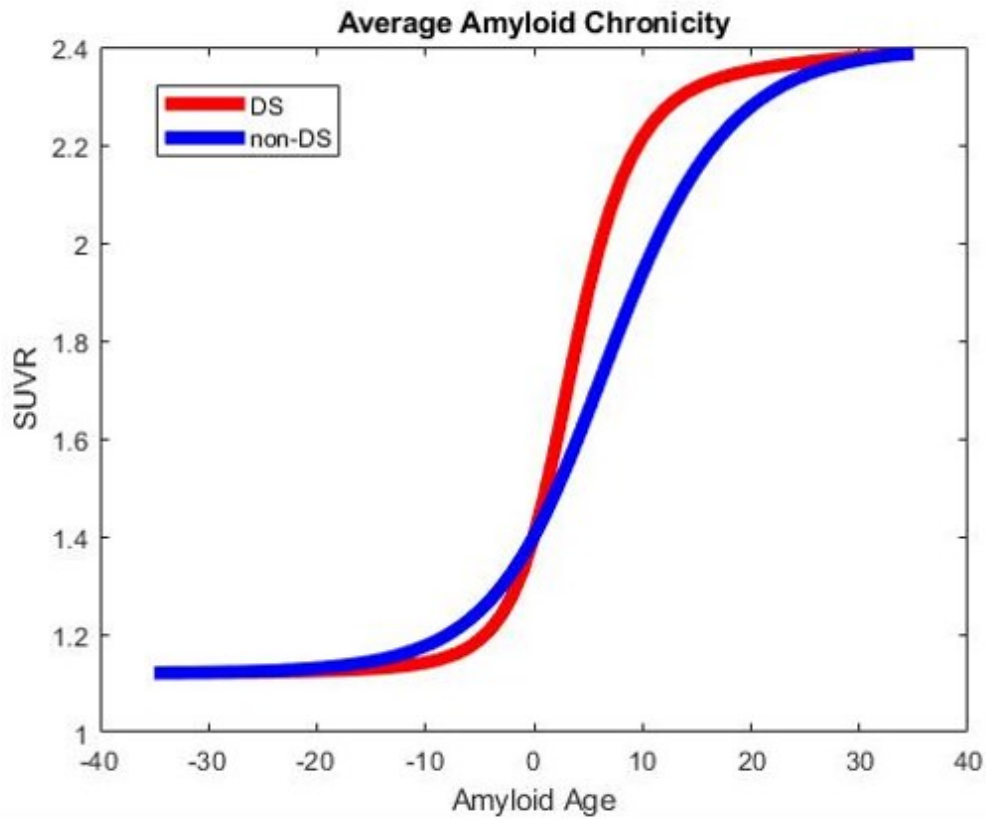


Fig. 2: Amyloid chronicity plots showing the increase in global SUVR as a function of time in years relative to becoming $A\beta+$. Of the two cohorts, the DS group on average has a steeper slope throughout and at $t=0$ a higher amyloid accumulation rate they become $A\beta+$.

Amyloid Accumulation

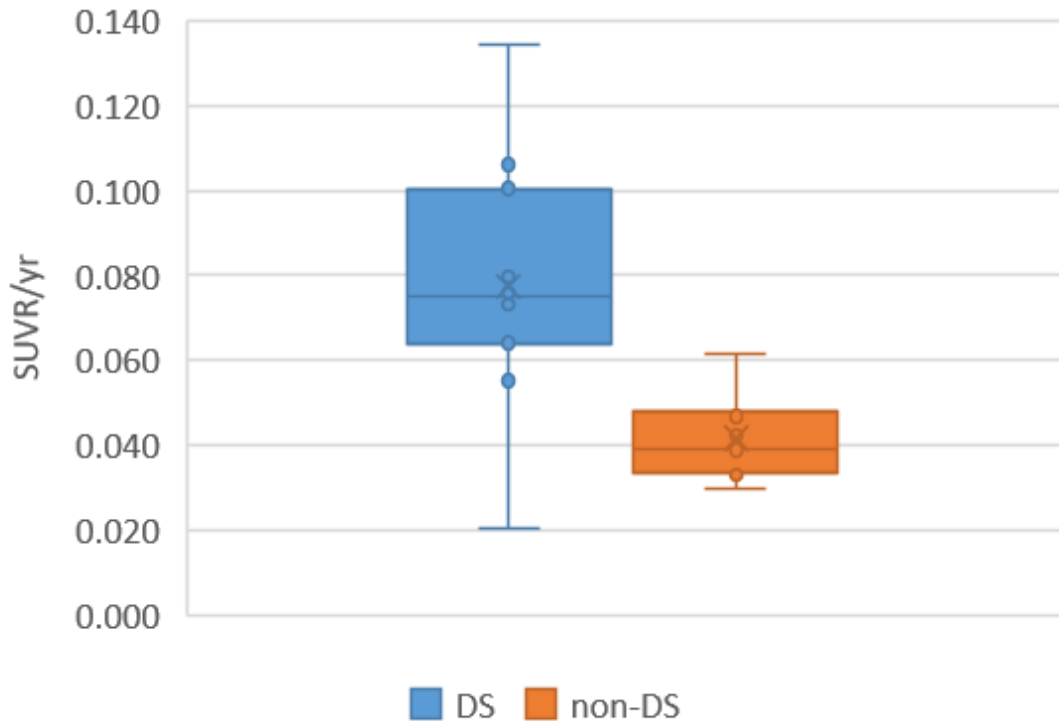


Fig. 3: Box plot showing the distribution of between A β accumulation rates as participants become A β +. There is a clear separation between the two cohorts, however, there is a high variance in the DS accumulation rates, including one participant with very slow but steady amyloid accumulation over the course of our observation that will be of interest for further studies.

Keywords: Down syndrome, [C-11]PiB, Amyloid accumulation, Sporadic Alzheimer's disease, Global SUVR

P21 Magnitude of MK6240 off-target binding correlated with spill-in effects in target regions

Andrew McVea¹, Alexandra DiFilippo¹, Max McLachlan¹, Sterling Johnson¹, Tobey Betthausen¹, Bradley Christian¹

¹University of Wisconsin - Madison, Madison, WI, US

Background: Alzheimer's disease (AD) is a neurodegenerative disorder characterized by accumulation of tau tangles starting in the entorhinal cortex (ERC). [F-18]MK6240 binds to tau with high affinity and can be used to evaluate early-stage tau progression. However, off-target (OT) MK6240 binding in the sinus and meninges can increase signal in the ERC and cerebellum, influencing MK6240's ability to identify tau binding in the ERC. Our study evaluates how off-target binding distributions impact quantification of regions used in early AD research.

Method: PET-SORTEO (Reilhac, 2004) is a Monte-Carlo based simulation software that generates PET data from an input emission brain map (Fig. 1) with associated time activity curves (TAC). We simulated MK6240 scans using cranial TACs equal to the average taken from 338 MK6240 scans at our site. Six different OT profiles were simulated, four based on representative participant scans, one with no OT signal and one of the average OT binding across all scans. Ten simulations for each cohort were generated (70-90min, i.d.= 370MBq) and analysed using SUV to evaluate spill-in effects to the cerebellum and ERC.

Results: Plotting cerebellar SUV against meningeal SUV (Fig. 3) we see a strong linear relationship ($R^2=0.99$). An increase of 282% in meningeal SUV results in a cerebellar SUV increase of 24%. The correlation between sinus SUV and ERC SUV is less strong ($R^2=0.84$), but has a greater influence compared to the meninges. A 354% increase in sinus SUVR corresponds to a 57% higher ERC SUV.

Conclusions: Spill-in from the meninges into the cerebellum reference region and the sinus into the ERC act in different directions on the SUVR metric of MK6240 uptake. The relationship between magnitude of OT binding and spill-in effects is highly linear, and correction factors taking into account OT patterning can improve MK6240 quantification of early AD.

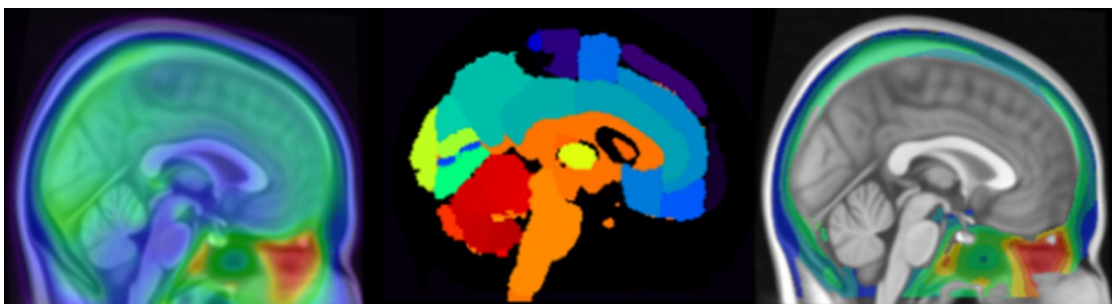


Fig. 1: Average image of 338 MK6240 PET images from our site at the University of Wisconsin – Madison (left) used to generate TACs used as an input to SORTEO. Cortical ROI in the emission map (center) are identical between simulation cohorts and correspond to these average TACs. Additional regions for OT binding in the meninges and sinus are also included in the individual emission maps (right).

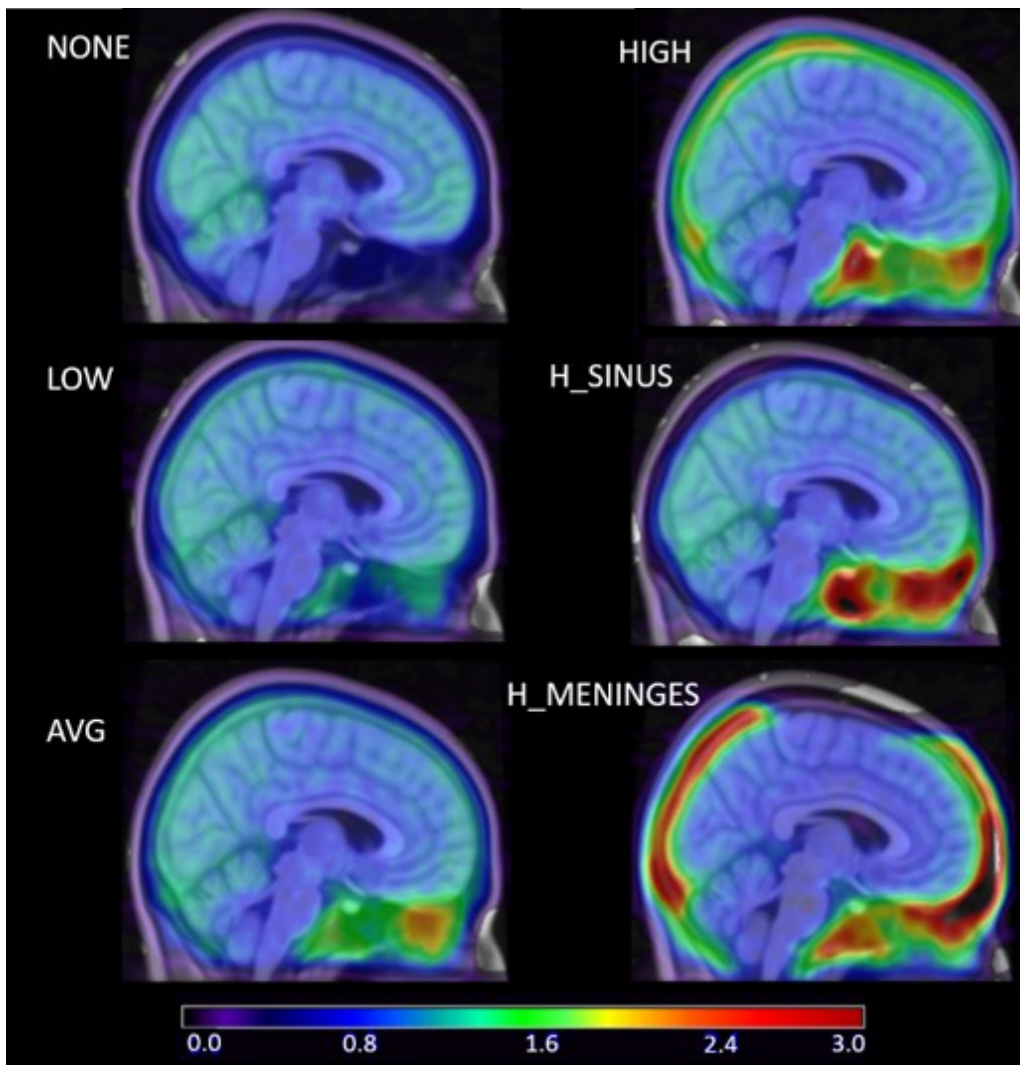


Fig. 2: Average of 10 realizations of simulations from the six cohorts ordered by increasing sinus SUV. The H_SINUS simulations are unique in that they have a high sinus SUV (16.77), but low meningeal SUV (6.67) compared to the averages of 12.68 and 8.30 respectively.

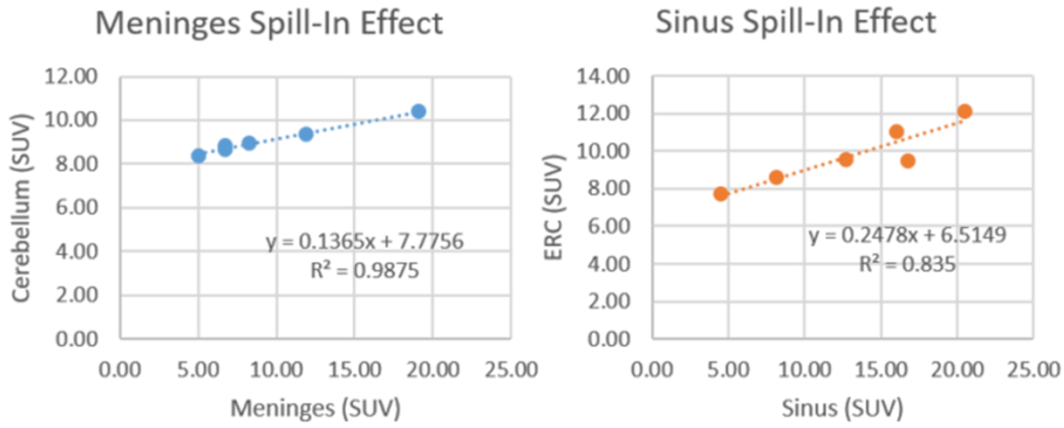


Fig. 3: Scatter plots showing the relationship between the OT SUV measures in the meninges and sinus and their corresponding increase in cerebellar and ERC signal respectively.

Keywords: Simulation, Tau, [F-18]MK6240, Early AD, Off-target binding

P22 Amyloid and tau pathology associated with different cognitive declines in cognitively normal older people

Xi Chen^{1,2}, Alexis Juarez¹, Suzanne Baker², Theresa Harrison¹, Susan Landau^{1,2}, William Jagust^{1,2}

¹University of California, Berkeley, Berkeley, CA, US

²Lawrence Berkeley National Laboratory, Berkeley, CA, US

Background: The early accumulation of amyloid and tau in cognitively normal people is predictive of future cognitive decline. It has been difficult, however, to disentangle the effects of amyloid and tau on cognition. The present study aims to examine whether there are specific pathology-cognitive associations. We specifically focused on longitudinal change in executive function and memory, and developed two domain-specific residual scores that reflect performance variability in one domain while controlling for the other. We tested whether faster decline in one cognitive domain, beyond its expected level based on the other, could reflect the emergence of amyloid or tau pathology.

Methods: A total of 78 cognitively normal older adults from the Berkeley Aging Cohort Study underwent longitudinal 11C-Pittsburgh compound-B (PiB) PET, 18F-flortaucipir (FTP) PET, and cognitive assessments of executive function and memory. We used linear mixed-effects models to estimate the longitudinal change in amyloid, temporal tau, executive function (Fig.1A), and memory (Fig.1B). Two cognitive decline residual scores (executive function controlling for memory, Fig.1C, E; memory controlling for executive function, Fig.1D, F) were computed to represent domain-specific individual variability.

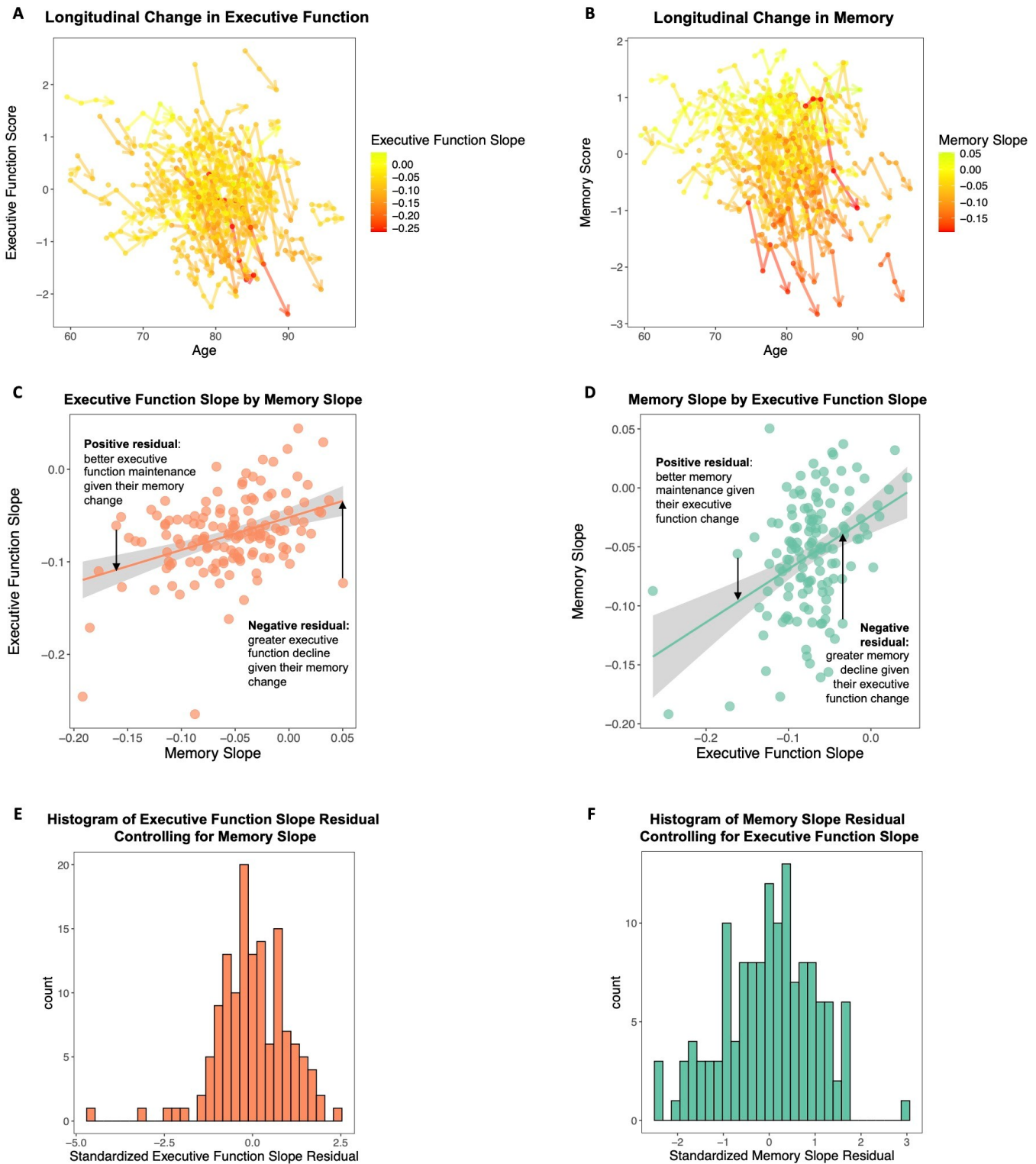


Figure 1. Cognitively normal older people showed longitudinal decline in executive function (A) and memory (B). Intra-individual variability in domain-specific declines was assessed by regressing memory change from executive function change (C) and regressing executive function change from memory change (D). The resulted slope residuals (E, F) represent individual variability in longitudinal change in one domain, given the performance change in the other domain.

Results: Amyloid accumulation across wide-spread regions was associated with faster executive function decline, but not memory, particularly in frontal and parietal regions, after controlling for meta-temporal tau change (Fig.2A). On the other hand, temporal tau accumulation was consistently related to faster memory declines, but not executive function, after controlling for global amyloid change (Fig.2B). LASSO regression (Fig.3) revealed similar patterns: faster executive

function decline was exclusively related to amyloid accumulation, while faster memory decline was only related to tau accumulation.

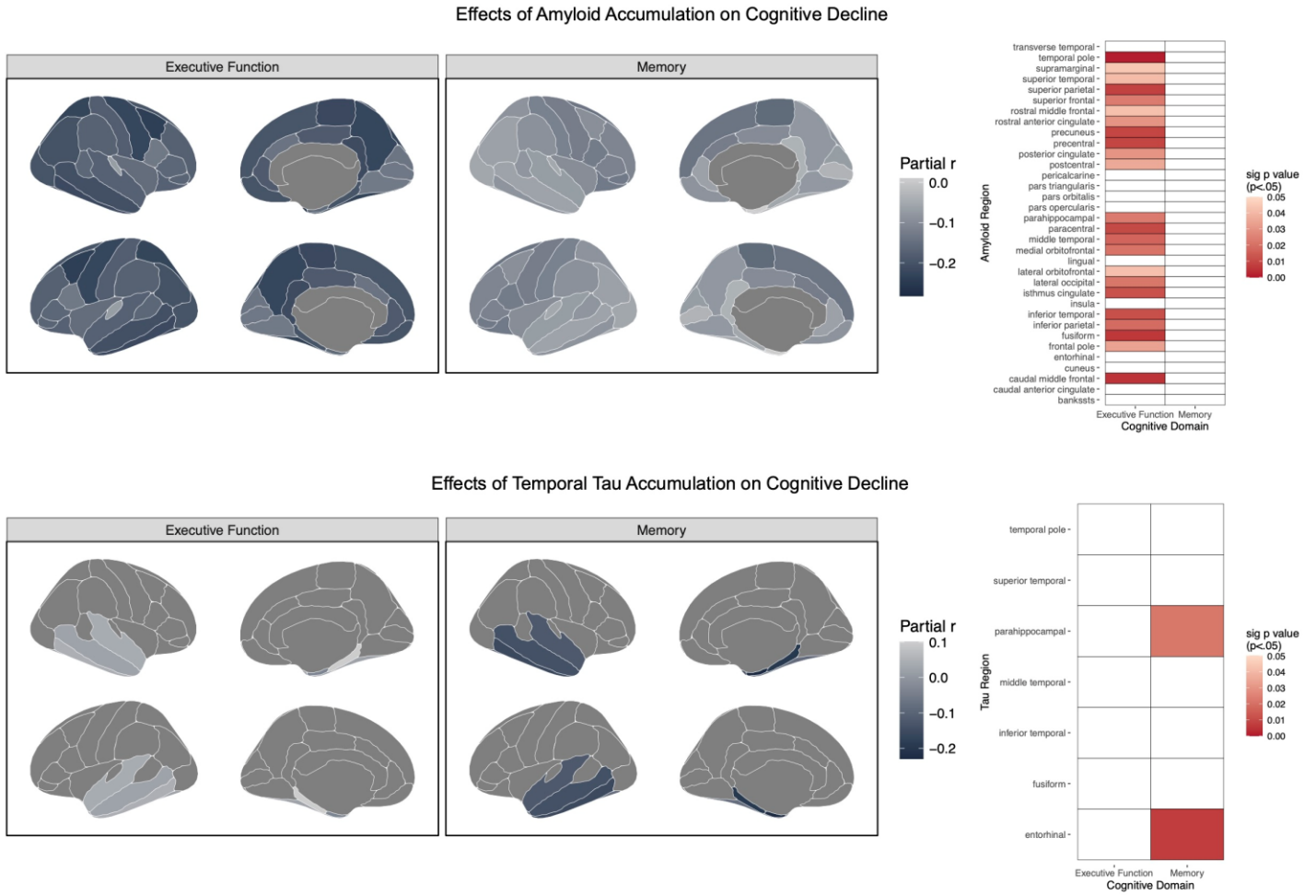


Figure 2. Executive function decline was related to amyloid accumulation, but not tau. Memory decline was related to tau accumulation, but not amyloid.

Lasso Regression Beta

	Executive Function	Memory
bankssts	.	.
caudal anterior cingulate	.	.
caudal middle frontal	-3.145528	.
cuneus	.	.
entorhinal	.	.
fusiform	.	.
inferior parietal	.	.
inferior temporal	.	.
isthmus cingulate	.	.
lateral occipital	.	.
lateral orbitofrontal	.	.
lingual	.	.
medial orbitofrontal	.	.
middle temporal	.	.
parahippocampal	.	.
paracentral	.	.
pars opercularis	.	.
pars orbitalis	.	.
pars triangularis	.	.
pericalcarine	.	.
postcentral	.	.
posterior cingulate	.	.
precentral	.	.
precuneus	.	.
rostral anterior cingulate	.	.
rostral middle frontal	.	.
superior frontal	.	.
superior parietal	.	.
superior temporal	.	.
supramarginal	.	.
frontal pole	.	.
temporal pole	-19.5684551	.
transverse temporal	.	.
insula	.	.
entorhinal	.	-17.5163335
fusiform	.	.
inferior temporal	.	.
middle temporal	.	.
parahippocampal	.	.
superior temporal	.	.
temporal pole	.	.

Figure 3. When including all biomarkers in a Lasso regression, executive function decline was only predicted by amyloid accumulation, while memory decline was only predicted by tau accumulation.

Conclusion: We found evidence supporting specific associations between accumulating pathology and domain-specific cognitive decline in early AD. Executive function decline greater than expected reflects the early emergence of amyloid pathology, whereas faster memory decline strongly suggests tau propagation in the temporal regions.

P23 Future amyloid accumulation status affects the preservation of peripheral whole-blood gene co-expression networks at baseline in asymptomatic Alzheimer's disease

Emma Luckett^{1,2,3}, Magdalena Zielonka³, Jolien Schaefferbeke^{1,2}, Katarzyna Adamczuk⁴, Koen Van Laere^{5,6}, Patrick Dupont^{1,2}, Isabelle Cleynen³, Rik Vandenberghe^{1,2,7}

¹Laboratory for Cognitive Neurology, KU Leuven, Leuven, Belgium

²Alzheimer Research Centre KU Leuven, Leuven Brain Institute, Leuven, Belgium

³Laboratory for Complex Genetics, KU Leuven, Leuven, Belgium

⁴Clario, Princeton, NJ, US

⁵Division of Nuclear Medicine, UZ Leuven, Leuven, Belgium

⁶Department of Nuclear Medicine and Molecular Imaging, Department of Imaging and Pathology, KU Leuven, Leuven, Belgium

⁷Neurology Department, University Hospitals Leuven, Leuven, Belgium

Objectives: Gene expression is dysregulated in Alzheimer's disease (AD) patients, both in postmortem brain and peripheral blood. We investigated peripheral blood gene co-expression networks to determine to what extent they are preserved between groups of interest in asymptomatic AD.

Methods: Sixty-six cognitively healthy F-PACK participants (68 (56-80) years) received amyloid-PET and structural MRI at baseline and follow-up (interval 4.8 (3.4-8.6) years), and RNA was extracted and sequenced from whole-blood taken at baseline. There were 40 accumulators, and 26 non-accumulators, based on rate of change ($[(\text{follow-up} - \text{baseline amyloid load}) / \text{time interval (years)}]$). Gene co-expression modules were constructed based on 9,095 genes passing QC for non-accumulators and accumulators separately using WGCNA. We then tested for preservation of non-accumulator-specific modules in accumulators, and vice versa, using the *modulePreservation* function. We also assessed preservation of APOE4 carrier-specific modules in non-APOE4 carriers and vice versa. Modules with a composite *Zsummary* score < 2 were considered as non-preserved; > 2 and < 10 as moderately preserved; > 10 as well preserved. Modules were annotated using KEGG and Gene Ontology (GO).

Results: Eighteen non-accumulator modules were constructed. The darkturquoise and darkgreen modules were only moderately preserved (*Zsummary*=7.5 and 9.7, respectively, Fig.1A) in accumulators, the rest were all well preserved. The darkturquoise module was enriched for AD (KEGG), and oxidative phosphorylation (GO); the darkgreen module for citrate cycle (KEGG), and negative regulation of dephosphorylation (GO). Nineteen accumulator modules were constructed. One module was only moderately preserved in non-accumulators (*Zsummary*=5.6, Fig.1B), the rest were all well preserved. This was enriched for chromatin remodelling and histone modification (GO). There were 21 modules constructed in APOE4 carriers and 27 in APOE4 non-carriers, however, all modules were well preserved in the other group (Fig.1C-D).

Conclusions: This work highlights that specific gene networks at baseline, enriched for pathways known to be associated with AD, are partially disrupted in peripheral whole-blood in future amyloid accumulators.

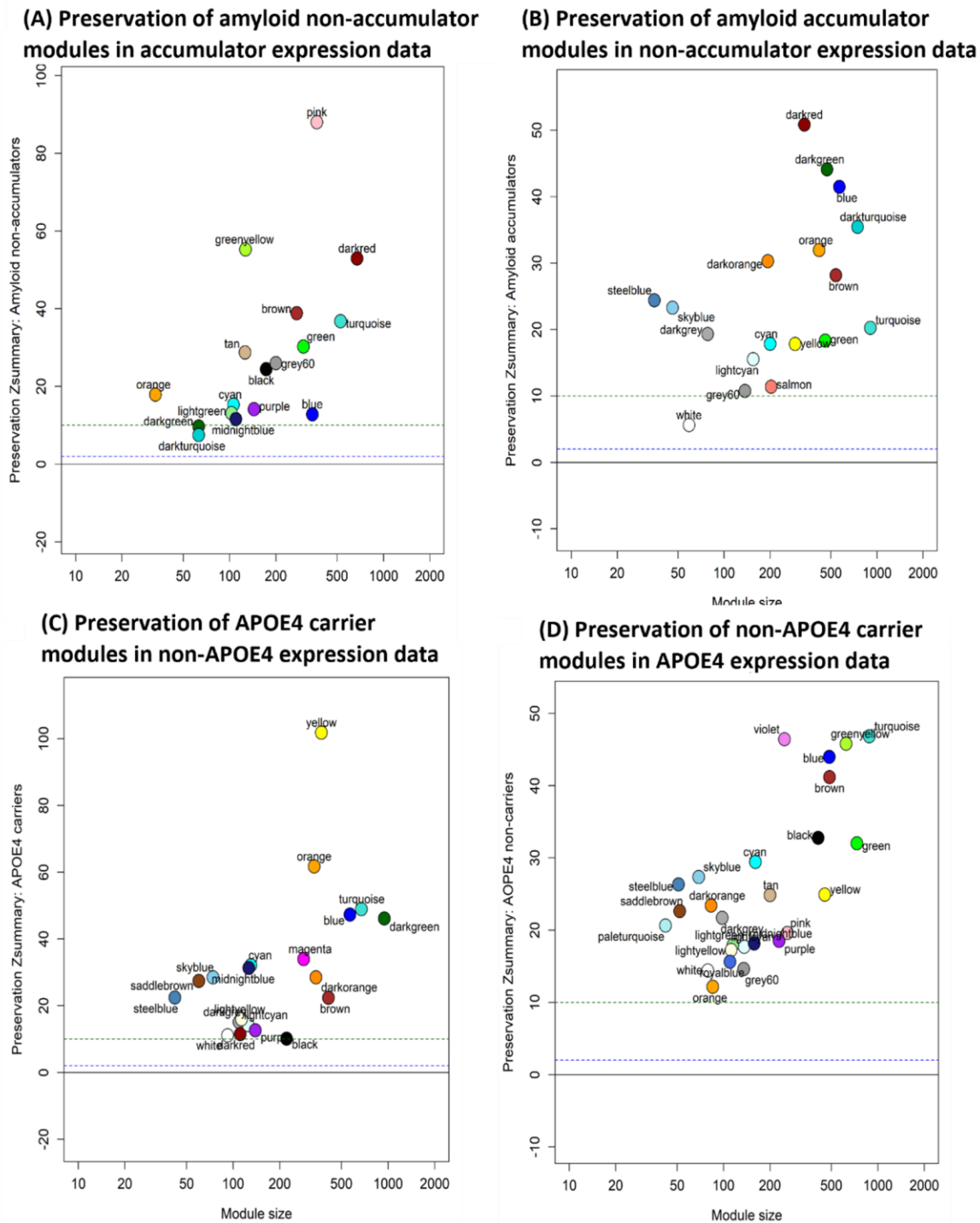


Figure 1: Preservation of gene co-expression network modules of (A) amyloid non-accumulator modules in accumulator expression data, (B) amyloid accumulator modules in non-accumulator expression data, (C) APOE4 carrier modules in non-APOE4 carrier expression data, (D) non-APOE4 carrier modules in APOE4 carrier expression data. Modules with a composite $Z_{summary}$ score < 2 (below the blue line) were considered as non-preserved; > 2 and < 10 as moderately preserved; > 10 as well preserved (above the green line).

Keywords: Alzheimer's disease, RNA sequencing, network preservation analysis, amyloid change, APOE4

P24 Validation of [18f]florbetaben PET quantitation based on the analysis of 15 software pipelines

Aleksandar Jovalekic¹, Núria Roé-Vellvé¹, Norman Koglin¹, Mariana Lagos Quintana¹, Aaron Nelson², Markus Diemling³, Johan Lilja³, Juan Pablo Gómez González⁴, Vincent Doré⁵, Pierrick Bourgeat⁵, Alex Whittington⁶, Roger Gunn⁶, Andrew Stephens¹, Santiago Bullich¹

¹Life Molecular Imaging, Berlin, Germany

²MIM Software, Cleveland, OH, US

³Hermes Medical Solutions, Stockholm, Sweden

⁴QuBiotech, A Coruna, Spain

⁵CSIRO, Brisbane, AU

⁶Invicro, London, UK

Objectives: Amyloid positron emission tomography (PET) with [18F]florbetaben is an established tool for detecting A β deposition in the brain in vivo based on visual assessment of PET scans. Quantitative measures are, however, commonly used in the research context and allow continuous measurement of amyloid burden. The aim of this study was to demonstrate the robustness and added value of florbetaben PET quantification using 15 different analytical pipelines.

Methods: This is a retrospective analysis of florbetaben PET images, consisting of 589 subjects. Florbetaben PET scans were quantified with 15 analytical pipelines using nine software packages (MiMneuro, Hermes BRASS, Neurocloud, Neurology Toolkit, statistical parametric mapping (SPM8), PMOD Neuro, CapAIBL, non-negative matrix factorization (NMF), Amyloid^{IQ}) that used several metrics to estimate A β load (SUVR, Centiloid, amyloid load and amyloid index). Six analytical pipelines reported Centiloid (MiMneuro, standard Centiloid pipeline, Neurology Toolkit, SPM8 (PET-only), CapAIBL, NMF). All results were quality controlled.

Results: The mean sensitivity, specificity and accuracy was 96.1 \pm 1.6%, 96.9 \pm 1.0% and 96.4 \pm 1.1%, respectively, for all quantitative methods tested when compared to histopathology. The mean percentage of agreement between binary quantitative assessment across all 15 pipelines and visual majority assessment was 92.4 \pm 1.5%. Concordance rate between quantitative assessment and VA was highest for cases with substantial presence or absence of amyloid (i.e. Centiloid levels <20 or >35) and lowest for cases with intermediate amyloid accumulation (i.e. Centiloid levels between 20-35, see Figure 1).

Assessments of reliability, correlation analyses and comparisons across software packages showed excellent performance and consistent results.

Conclusion: Software quantification methods, such as Centiloid analysis, can complement visual assessment of florbetaben PET images. Based on this study, quantification of [18F]florbetaben PET as an adjunct to visual assessment

was recently approved by the European Medicines Agency (EMA) in the EU for Neuraceq®.

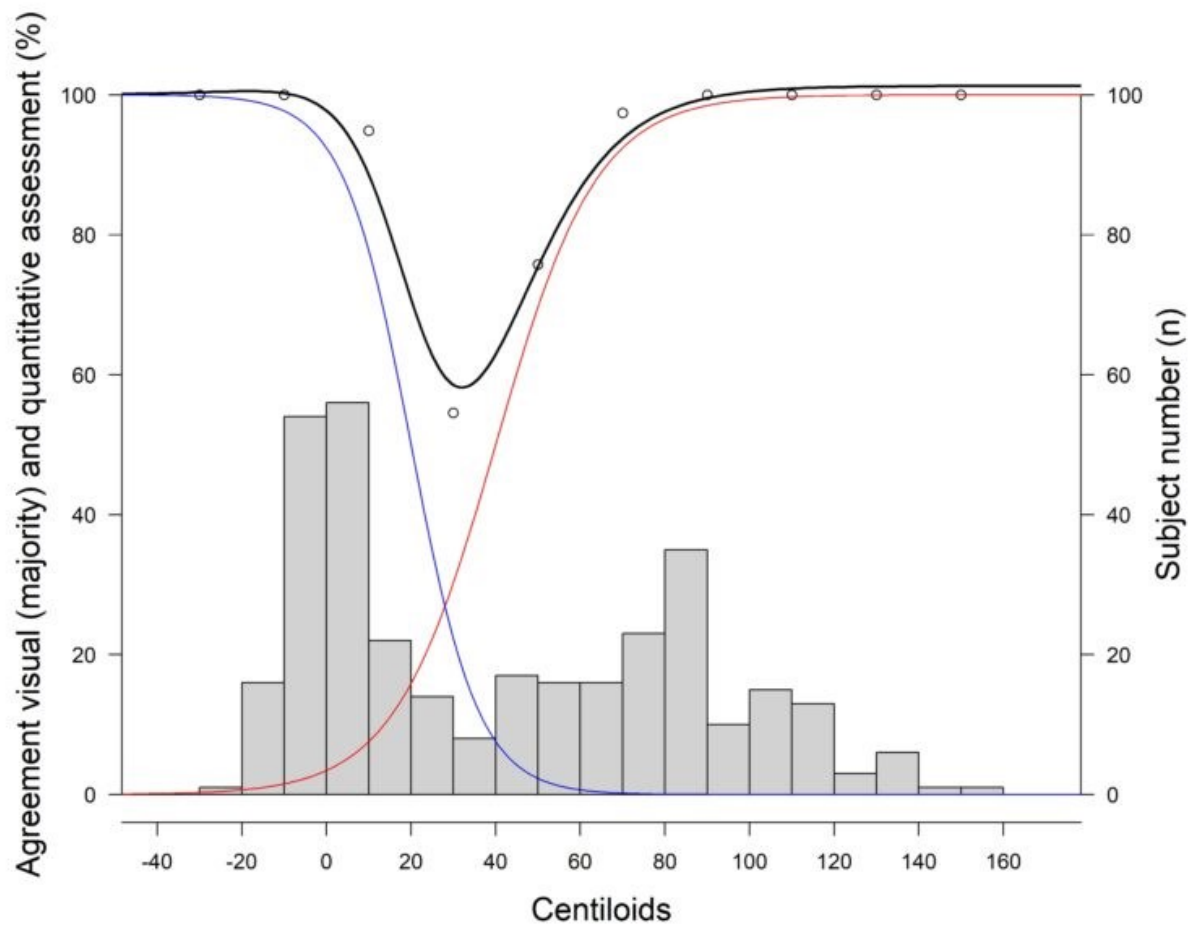


Figure 1: Illustration for uncertainty of visual reads around the Grey Zone.

Keywords: florbetaben, amyloid, quantitation, centiloid

P25 Preprocessing 10,700 real-world amyloid-PET scans from the IDEAS study: the Good, the Bad and the Ugly

Jhony Mejia Perez¹, Nidhi Mundada¹, Ganna Blazhenets¹, David Soleimani-Meigooni¹, Ehud Zeltzer¹, Hanna Cho¹, Kamalini Ranasinghe¹, Charles Windon¹, Golnaz Yadollahikhales¹, Leonardo Iaccarino^{1,2}, Maria Carrillo³, Constantine Gatsonis^{4,5}, Andrew March⁶, Charles Apgar⁷, Barry Siegel⁸, Bruce Hilner⁹, Rachel Whitmer^{10,11}, Gil D Rabinovici^{1,12}, Renaud La Joie¹

¹Memory and Aging Center, Department of Neurology, University of California, San Francisco, San Francisco, CA, US

²Eli Lilly and Company, Indianapolis, IN, US

³Alzheimer's Association, Chicago, IL, US

⁴Center for Statistical Sciences, Brown University School of Public Health, Providence, RI, US

⁵Department of Epidemiology, Brown University School of Public Health, Providence, RI, US

⁶Center for Research and Innovation, American College of Radiology, Philadelphia, Pennsylvania, Philadelphia, PA, US

⁷Center for Research and Innovation, American College of Radiology, Reston, Virginia, Reston, VA, US

⁸Edward Mallinckrodt Institute of Radiology, Washington University School of Medicine, St Louis, MO, US

⁹Department of Medicine, Virginia Commonwealth University, Richmond, VA, US

¹⁰Division of Research, Kaiser Permanente, Oakland, CA, US

¹¹Department of Public Health Sciences, University of California, Davis, Davis, CA, US

¹²Department of Radiology & Biomedical Imaging, University of California, San Francisco, San Francisco, CA, US

Objective. To preprocess and quantify PET scans from Imaging Dementia - Evidence for Amyloid Scanning (IDEAS), a large-scale real-world study of amyloid-PET in patients with cognitive impairment. Major challenges lie in scans being acquired on various PET/PET-CT/PET-MR scanners without standardization of acquisition protocols or reconstruction parameters, and without MRI to preprocess data.

Methods. PET scans were performed in 18,295 patients using 18F-Florbetapir, 18F-Florbetaben or 18F-Flutemetamol. 14,931 scans were shared by local centers and analyzed at UCSF. After excluding duplicated and incomplete files, we processed 10,700 scans using a PET-only pipeline (10.1016/j.neuroimage.2021.118775) which performs warping to standard space, smoothing to a common resolution, and extraction of cortical and cerebellar counts to calculate SUVR values. Ten raters performed Quality Control (QC) using a custom-built program that displayed standardized 2D images of warped scans with and without outlined regions of interest (**Fig 1**). Each image was independently classified by two raters as Pass, Needs Consensus, or Fail.

Results. 8,895/10,700 scans (83.1%) were passed by both raters and ready to be quantified (**Fig 2A**), although high variability in the quality of scans was observed (**Fig 2B, C**). In contrast, 825 (7.8%) were failed by at least one rater (**Fig 3A**). These scans were reviewed in a consensus meeting to determine the source of artifacts and suggest troubleshooting options. Most failures were due to warping errors (26.7%) or major anatomical lesions (27.4%), truncated field of view (13.0%) or other acquisition problems (13.1%) (**Fig 3B, C**). Efforts are ongoing to adapt the pipeline and analyses to quantify these scans.

Conclusion. Although the quality of IDEAS PET scans was more heterogeneous than typical research cohorts, most could be used for quantification. Data processing and final QC will be completed in December 2022 and data will be released through the Global Alzheimer's Association Interactive Network in early 2023.

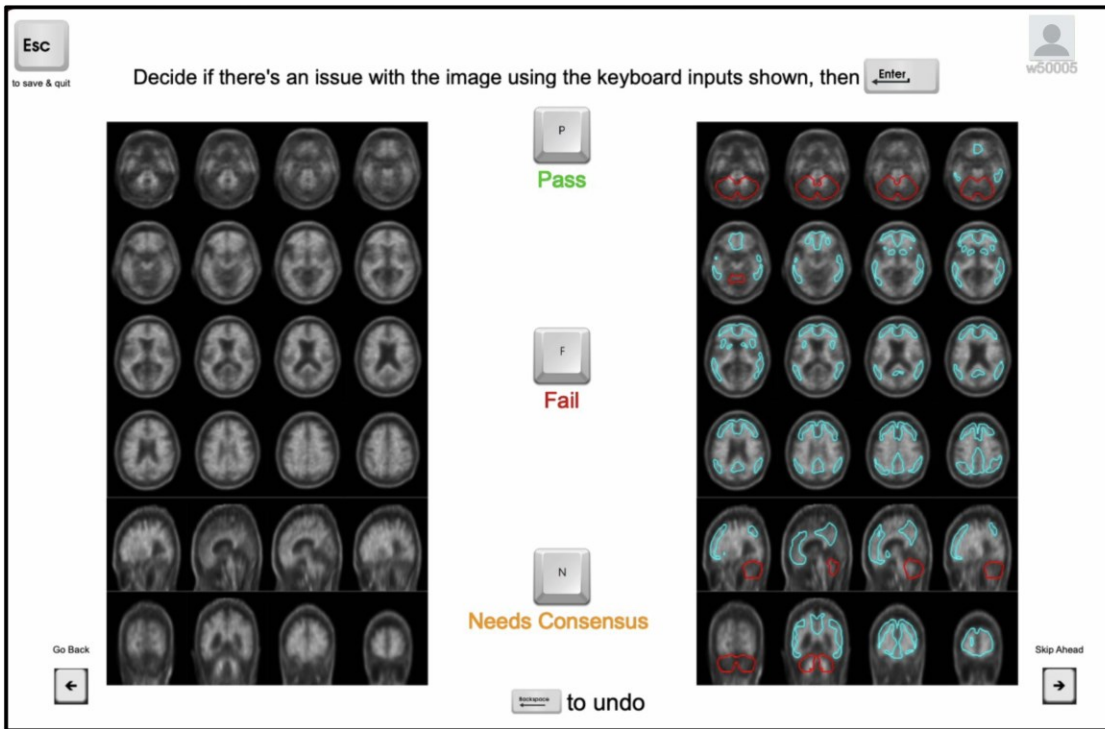


Figure 1. Matlab Graphical Interface for performing Quality Control (QC) of warped unsmoothed PET scans. Raters assessed the scan suitability for SUVR quantification as good (Pass), bad (Fail), or if they were unsure (Consensus). The criteria for each category was reported on a succinct guideline with graphical examples. Each of the 10 raters signed up for rating batches of 100 scans.

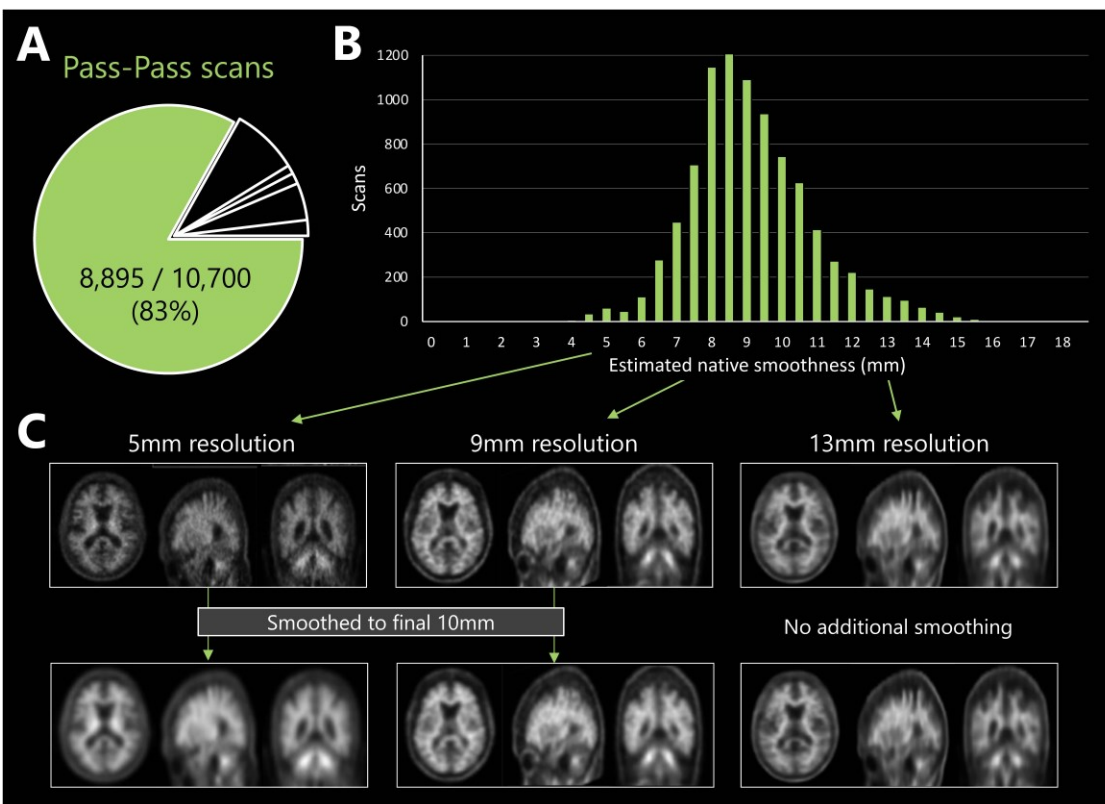


Figure 2. Illustration of the heterogeneity of IDEAS PET scans, for scans passed by both reviewers.
A) Distribution of scans based on their assessment by 2 independent raters.
B) Histogram with the estimated spatial resolution based on AFNI's $3dFWHMx$ function used in our PET-only pipeline.
C) Specific cases illustrating each tercile of the estimated resolution distribution. Scans with an estimated FWHM < 10mm are smoothed to reach a final 10 mm resolution. No additional smoothing is applied to scans with lower resolution (FWHM > 10mm).

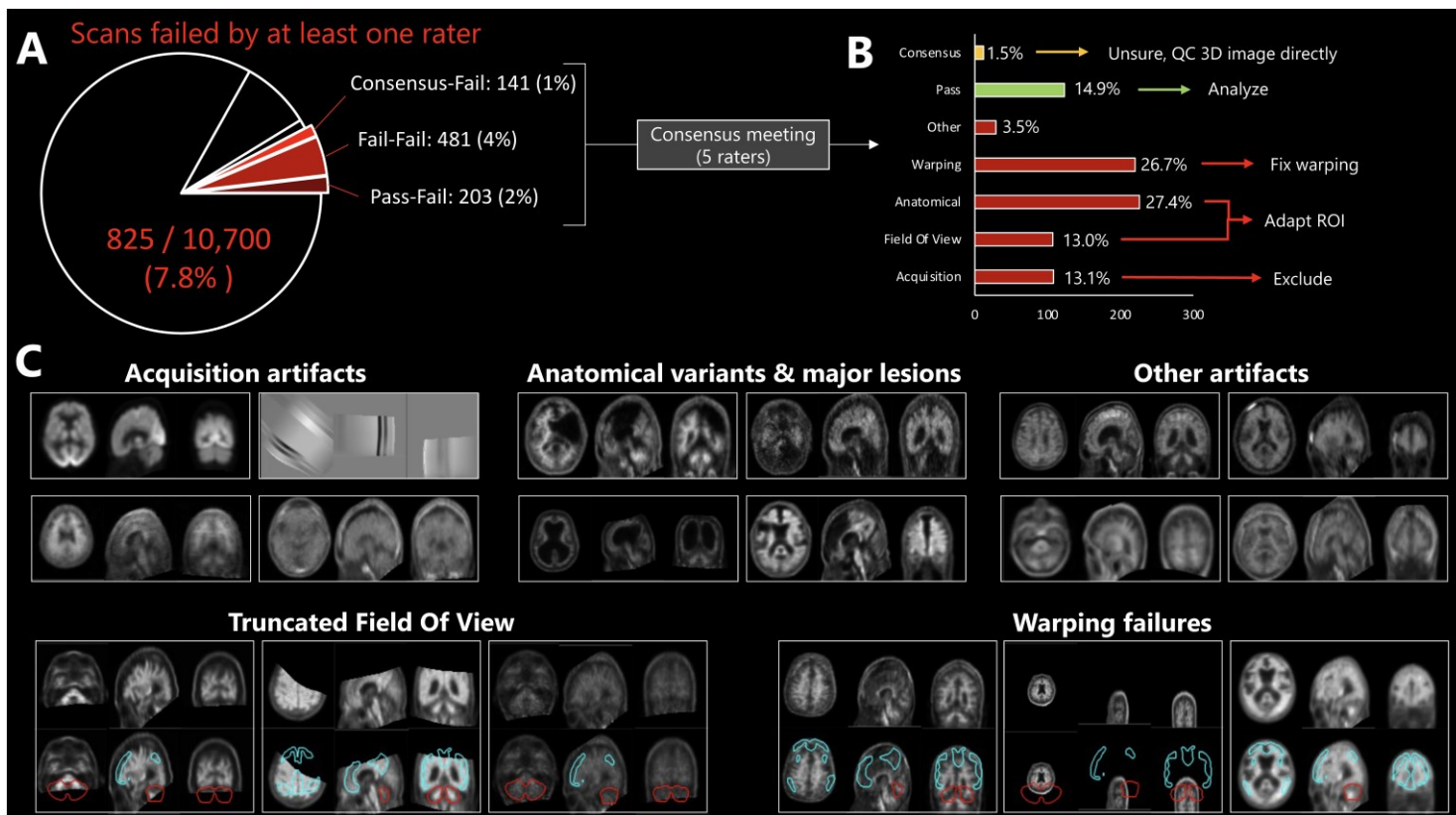


Figure 3. Illustration of the heterogeneity of IDEAS PET scans, for scans failed by at least one reviewer.

A) Distribution of scans based on their assessment by 2 independent raters. Detailed breakdown for each possible combination of fail responses is shown.

B) Those scans were reviewed in a consensus meeting with 5 raters to identify source of artifact and propose options to re-process the image (e.g. re-warping the image after manual recentering) or analyze it differently (e.g. adapt Regions of Interest in case of major anatomical lesion). Part of the scans that were failed in the original QC step could still be analyzed pending small adjustments, while others were excluded from quantification (e.g. in case of major technical artifact).

C) Examples of common sources of artifacts that might impact SUVR quantification. These examples were all failed by at least one rater.

Keywords: Clinical PET, Quality Control, Real-world data, Standardization, IDEAS

P26 Longitudinal tau-PET differs between progressive apraxia of speech subtypes

Katerina A. Tetzloff¹, Peter R. Martin², Joseph R. Duffy¹, Heather M. Clark¹, Rene L. Utianski¹, Hugo Botha¹, Mary M. Machulda³, Christopher G. Schwarz⁴, Matthew L. Senjem⁴, Clifford R. Jack Jr.⁴, Val J. Lowe⁴, Keith A. Josephs¹, Jennifer L. Whitwell⁴

¹Mayo Clinic Department of Neurology, Rochester, MN, US

²Mayo Clinic Department of Health Science Research (Biostatistics), Rochester, MN, US

³Mayo Clinic Department of Psychology and Psychiatry, Rochester, MN, US

⁴Mayo Clinic Department of Radiology, Rochester, MN, US

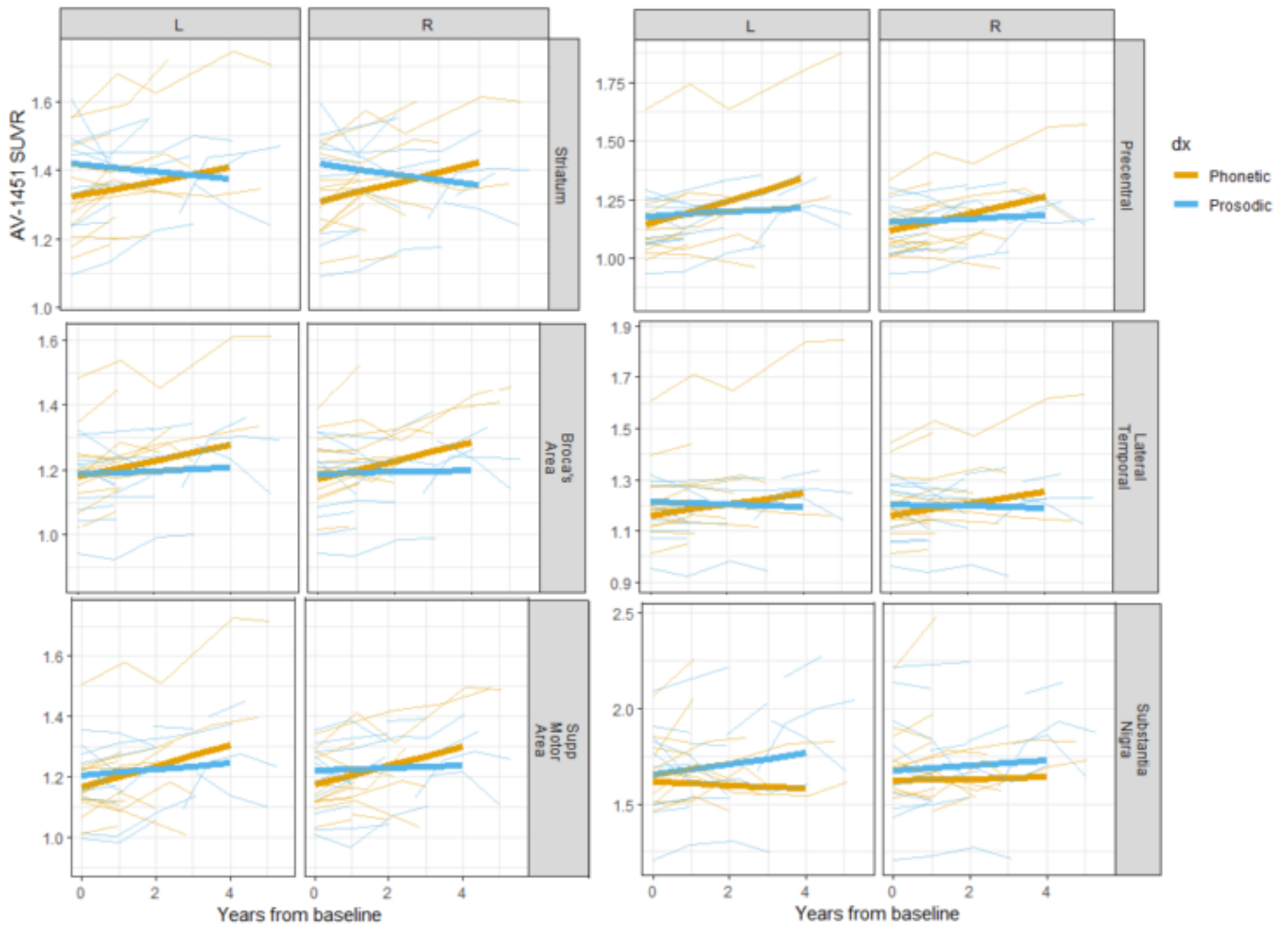
Introduction: Progressive apraxia of speech (PAOS) is a neurodegenerative syndrome that presents with motor-speech difficulties, resulting from a 4R tauopathy. Two PAOS subtypes have been recognized: phonetic PAOS (Ph-PAOS) predominated by distorted sound substitutions, and prosodic PAOS (Pr-PAOS) predominated by slow, segmented speech. Tau PET studies using flortaucipir have shown uptake in premotor/motor cortices and subcortical structures in PAOS, although it is unclear if patterns or spread of tau differ between subtypes. We aimed to model the regional spread of flortaucipir PET in the PAOS subtypes.

Methods: Ninety-one PAOS patients (51 Ph-PAOS, 40 Pr-PAOS) were recruited by the Neurodegenerative Research Group and underwent [¹⁸F]flortaucipir PET. Fifty-four patients (27 Ph-PAOS, 27 Pr-PAOS) returned for annual follow-up visits, with up to seven longitudinal visits. Regional flortaucipir standardized uptake value ratios (SUVRs) were calculated, and Bayesian hierarchical models were used to model longitudinal change in regional SUVRs with groups compared at baseline, 4-years from baseline, and in terms of rates of change.

Results: At baseline, Pr-PAOS showed greater flortaucipir uptake in the cerebellar dentate, midbrain, striatum, and thalamus than Ph-PAOS. Differences in cerebellar dentate and midbrain persisted over time, although the striatum and thalamus did not differ 4-years from baseline. Ph-PAOS did not show greater flortaucipir uptake than Pr-PAOS in any region at baseline. However, Ph-PAOS showed greater uptake 4-years from baseline and faster rates of accumulation in the striatum, Broca's area, supplementary motor cortex, and precentral and temporal cortex than Pr-PAOS. Conversely, Pr-PAOS showed greater uptake 4-years from baseline and faster rates of accumulation in the substantia nigra versus Ph-PAOS (Figure).

Conclusions: Regional tau deposition can distinguish PAOS subtypes throughout the disease: Ph-PAOS is associated with faster rates of tau accumulation in corticostriatal region, while prosodic Pr-PAOS, with greater uptake in brainstem and cerebellar structures. These results have implications for clinical diagnosis.

Longitudinal tau uptake in PAOS



Keywords: tau-PET, apraxia of speech, progressive apraxia of speech, longitudinal, neurodegeneration

P27 Cross-sectional PET Analyses in the Longitudinal Early-onset Alzheimer's Disease Study (LEADS)

Hanna Cho^{1,2}, Nidhi S Mundada¹, Liana Apostolova^{3,4,5}, Maria C. Carrillo⁶, Ranjani Shankar¹, Alinda Amuiri¹, Ehud Zeltzer¹, Charles Windon¹, David Soleimani Meigooni¹, Jeremy Tanner¹, Courtney Lawhn Heath¹², Paul Aisen⁷, Ani Eloyan⁸, Robert Koeppe⁹, Leonarado Iaccarino^{1,10}, Bradford C. Dickerson¹¹, Renaud La Joie¹, Gil D. Rabinovici¹

¹Memory and Aging Center, UCSF Weill Institute for Neurosciences, Department of Neurology, University of California, San Francisco, CA, US

²Department of Neurology, Gangnam Severance Hospital, Yonsei University College of Medicine, Seoul, Korea

³Department of Neurology, Indiana University School of Medicine, Indianapolis, IN, US

⁴Department of Radiology and Imaging Sciences, Center for Neuroimaging, Indiana University School of Medicine, Indianapolis, IN, US

⁵Department of Medical and Molecular Genetics, Indiana University School of Medicine, Indianapolis, IN, US

⁶Medical & Scientific Relations Division, Alzheimer's Association, Chicago, IL, US

⁷Alzheimer's Therapeutic Research Institute, University of Southern California, San Diego, CA, US

⁸Department of Biostatistics, Center for Statistical Sciences, Brown University, Providence, RI, US

⁹Division of Nuclear Medicine, Department of Radiology, University of Michigan, Ann Arbor, MI, US

¹⁰Eli Lilly and Company, Indianapolis, IN, US

¹¹Department of Neurology, Massachusetts General Hospital and Harvard Medical School, Boston, MA, US

¹²Department of Radiology, University of California San Francisco, San Francisco, CA, US

Objective: To report baseline amyloid and tau PET findings from the Longitudinal Early-onset Alzheimer's Disease Study (LEADS), a prospective longitudinal multi-site observational study of sporadic early-onset Alzheimer disease (EOAD, age<65).

Methods: A total of 408 participants were enrolled at 19 sites in the U.S. from May 2018 to May 2022 (Table). Baseline florbetaben (FBB)-A β and flortaucipir (FTP)-tau PET scans were completed in 321 cognitively impaired (CI) and 87 cognitively normal (CN) subjects. Image acquisition, quality control and processing were performed following ADNI protocols. Amyloid PET scans in CI were clinically interpreted by trained raters based on merging visual read and a quantitative threshold (SUVR \geq 1.18), with a second visual read breaking the tie in discordant cases.

Results: 243/321 (75.7%) of the CI group were amyloid PET positive and assigned to an EOAD group, 78/321 (24.3%) were designated EOnonAD based on negative amyloid PET. Compared to CN and EOnonAD, EOAD had higher FBB-PET Centiloids, and higher FTP-PET in temporal and all Braak ROIs, with 95.1% of EOAD classified as "tau-positive" based on meta-Temporal ROI SUVR \geq 1.27 (Figure 1). EOnonAD showed FTP retention in known off-target regions and more variably in regions showing neurodegeneration. Three EOnonAD participants had an advanced AD FTP-PET pattern, suggesting their amyloid PET may represent false negative results. FBB and FTP associations with age, sex, MMSE and APOE genotype are shown in Figure 2. APOE ϵ 4 genotype was associated with lower global FBB and higher FTP entorhinal/whole cortex ratio in a dose-dependent manner.

Conclusions: ~25% of patients meeting clinical criteria for EOAD have negative amyloid PET, likely representing misdiagnosis. At study entry, patients with EOAD already have advanced tau PET binding. Within EOAD, younger age and female sex are associated with higher FTP-PET, while APOE genotype modifies the burden and distribution of amyloid and tau PET signal.

Table. Demographic, clinical, and PET imaging characteristics of the study participants

	EOAD	EOnonAD	CN
<i>N</i>	243	78	87
Demographics			
Age, y	59.2 ± 4.1 ^a	58.7 ± 5.9	56.9 ± 5.9
Sex, female (%)	131 (54%) ^b	27 (35%) ^a	54 (62%)
Education, y	15.4 ± 2.4 ^a	15.5 ± 2.5 ^a	16.7 ± 2.1
ApoE ε4 genotype, 0/1/2	97/85/32 ^b	42/28/2	49/28/8
Ethnicity, Hispanic (%)	8 (3%)	3 (4%)	7 (8%)
Race, White/ Black/ Asian/ More than one/ Unknown	226/8/4/4/1 ^a	68/4/1/3/2	63/15/5/3/1
Clinical characteristics			
CDR total, 0/0.5/1	3/144/78 ^{ab}	3/54/14 ^a	86/1/0
CDR sum of boxes	3.7 ± 1.8 ^{ab}	3.0 ± 2.1 ^a	0.0 ± 0.1
MMSE	21.6 ± 5.1 ^{ab}	25.5 ± 4.2 ^a	29.2 ± 0.9
MOCA	16.1 ± 6.0 ^{ab}	21.6 ± 4.7 ^a	27.0 ± 2.5
Clinical severity, MCI/Dementia, MCI (%)	64 (27%) ^b	42 (54%)	n.a.
PET imaging			
Amyloid-PET (Florbetaben)			
Clinical read positivity, n (%)	243 (100%) ^b	2 (3%)	n.a.
Centiloid	96.1 ± 26.3 ^{ab}	5.9 ± 10.2	9.8 ± 13.6
Centiloid > 25, n (%)	243 (100%) ^{ab}	3 (4%)	7 (8%)
Tau-PET (Flortaucipir)			
Temp-meta-ROI SUVR	2.11 ± 0.45 ^{ab}	1.21 ± 0.28	1.16 ± 0.14
Temp-meta-ROI SUVR > 1.27, n (%)	231 (95%) ^{ab}	6 (8%)	2 (2%)
Braak I ROI SUVR	1.71 ± 0.27 ^{ab}	1.18 ± 0.21	1.13 ± 0.12
Braak III-IV ROI SUVR	1.88 ± 0.38 ^{ab}	1.17 ± 0.23	1.13 ± 0.11
Braak V-VI ROI SUVR	1.84 ± 0.44 ^{ab}	1.09 ± 0.19	1.07 ± 0.07

Data is shown as mean ± SD for continuous variables or n (%) for categorical variables

^a*P* < 0.05 between EOAD and CN or EOnonAD and CN

^b*P* < 0.05 between EOAD and EOnonAD

Abbreviations: CDR, clinical dementia rating; CN, cognitively normal; EOAD, early-onset Alzheimer disease; EOnonAD, early-onset non-Alzheimer disease; MCI, mild cognitive impairment; MOCA, Montreal cognitive assessment; MMSE, mini-mental state examination; ROI, region of interest; Temp-meta-ROI, temporal-meta-ROI; SUVR, standardized uptake value ratio

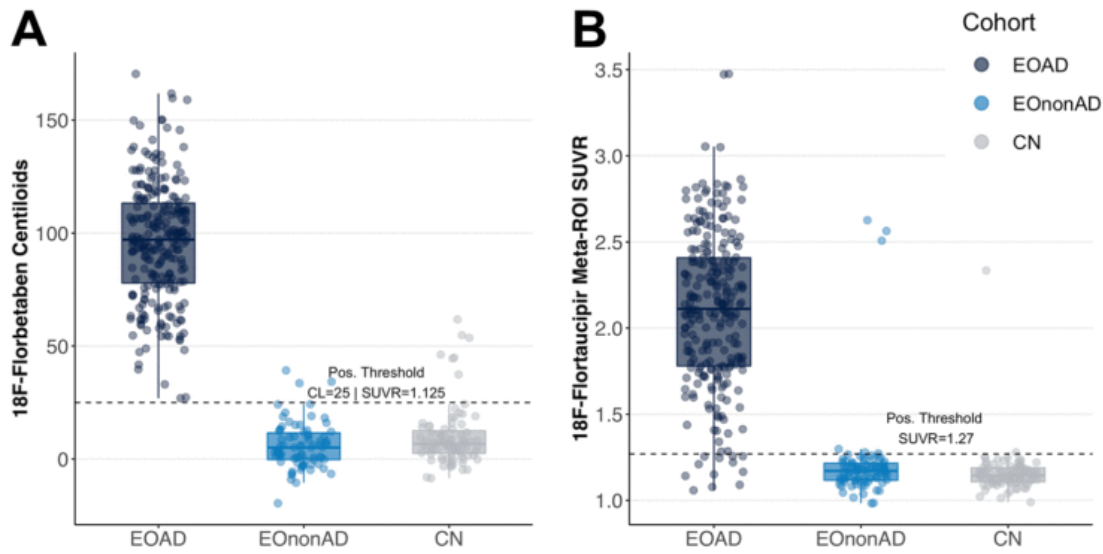


Figure 1

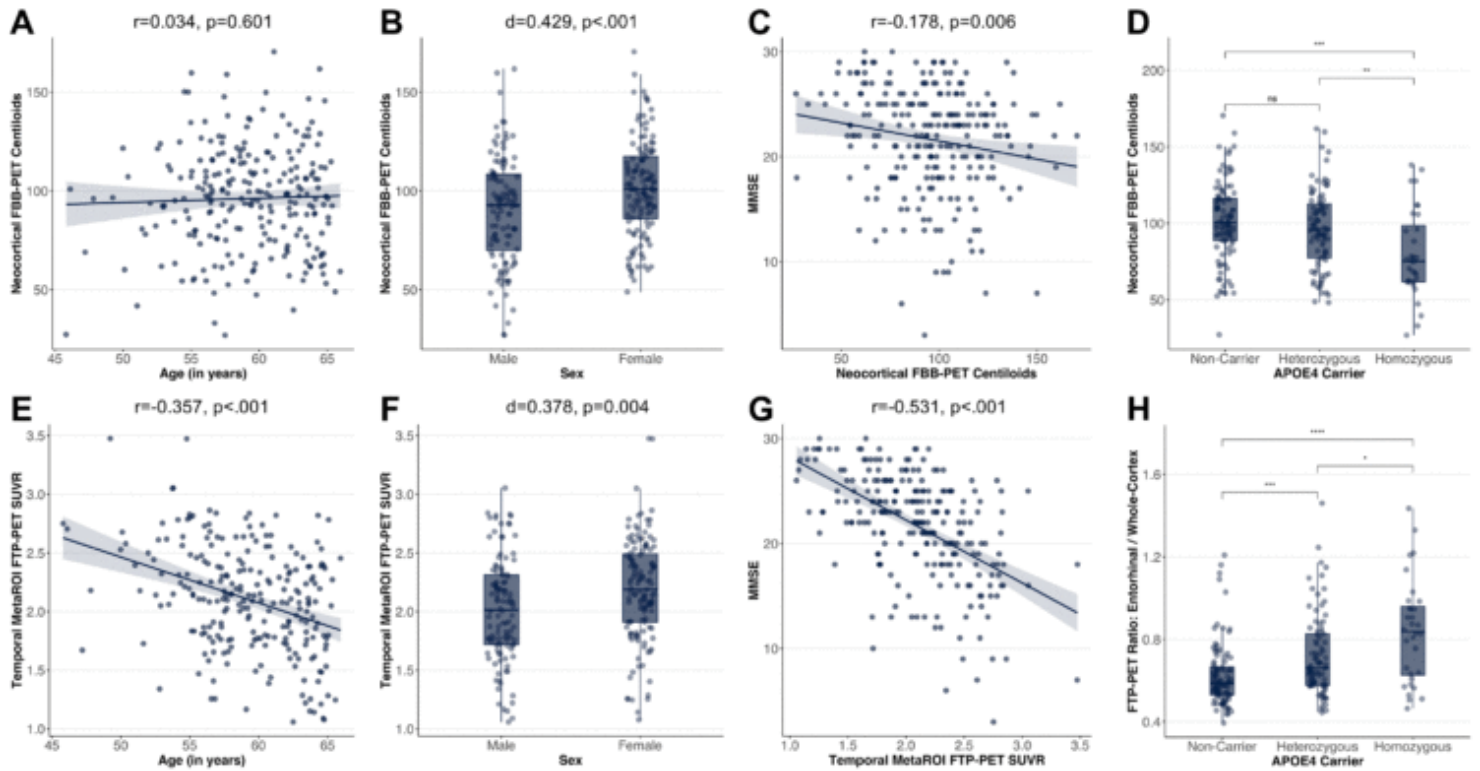


Figure 2

Keywords: Alzheimer's disease, early-onset, EOAD, LEADS, amyloid PET, tau PET

P28 Dynamic amyloid PET: relationships to tau PET and cognition in Alzheimer's disease

Fabio Raman¹, Kayla Charniaux², Charles Murchison², Yu-Hua Dean Fang¹, Jordan Tzabari¹, Evan Liu², John Morris⁴, Charlie Chen⁵, Nelly Joseph-Mathurin⁵, Maria Ponisio⁵, Shaney Flores⁵, Richard Kennedy², Tammie Benzinger⁵, Erik Roberson³, Jonathan McConathy¹

¹The University of Alabama at Birmingham, Department of Radiology, Birmingham, AL, US

²The University of Alabama at Birmingham, Department of Medicine, Birmingham, AL, US

³The University of Alabama at Birmingham, Department of Neurology, Birmingham, AL, US

⁴Washington University in St. Louis School of Medicine, Department of Neurology, St. Louis, MO, US

⁵Washington University in St. Louis School of Medicine, Mallinckrodt Institute of Radiology, St. Louis, MO, US

Background: Neuroimaging biomarkers, such as amyloid and tau acquired through PET and hippocampal volume acquired through MR have been associated with cognition in subjects being evaluated for Alzheimer's disease. Information related to flow can be acquired by early frames of amyloid PET (efAP) or R1 assessment. We hypothesized that hippocampal R1 and efAP are similarly associated with tau PET and both can predict future cognitive trajectory beyond hippocampal volume alone.

Method: 257 participants with dynamic [¹⁸F]florbetapir amyloid PET/MR with at least 18 months of neuropsychological follow-up were selected from a retrospective cohort. Parameters for R1 quantification were optimized for stratification of tau PET positivity on [¹⁸F]florbetapir tau PET in a subset of 63 amyloid-positive participants. Regression models were used to assess the longitudinal relationships between cognition and hippocampal efAP, R1, and volume.

Result: Hippocampal R1 and efAP were both significantly associated with tau PET ($r_{R1} = -0.63$, $r_{efAP} = -0.60$, $p_{R1/efAP} < 0.0001$) with strong predictive ability for tau PET positivity ($AUC_{R1} = 0.926$, $AUC_{efAP} = 0.913$, Figure 1). Both R1 and efAP provided significant additive value above hippocampal volume in predicting attention and executive function aggregate Z-score (standardized effect size $[\beta]_{R1} = 4.079$, $\beta_{efAP} = 4.007$) but not memory ($\beta_{R1} = 0.064$, $\beta_{efAP} = -0.891$) or language ($\beta_{R1} = -0.679$, $\beta_{efAP} = -0.844$, Table 1). Additionally, R1 but not efAP, also better predicted the trajectory of semantic fluency ($\beta_{animals/vegetables/MINT, R1} = 2.040/2.045/2.106$, $\beta_{animals/vegetables/MINT, efAP} = 0.078/-0.055/1.160$), a component of language z-score, better than hippocampal volume alone (Table 2).

Conclusion: Both hippocampal R1 and efAP, biomarkers acquired during the dynamic phase of amyloid PET, can be used to predict tau PET positivity and provide additional information beyond hippocampal volume in predicting attention and executive function. Compared to efAP, R1 is less sensitive to bolus injection scheme with significant association with semantic fluency and verbal learning and memory but requires more sophisticated methods for calculation.

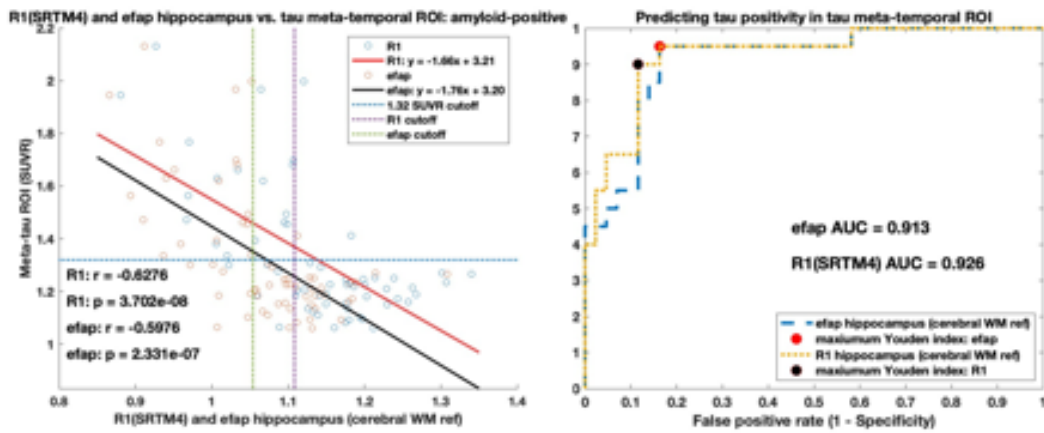


Figure 1. R1 parallels efAP and predicts tau PET pathology. Comparison of hippocampal efAP and R1 and tau PET temporal meta-ROI for tau PET across amyloid-positive participants. A) R1 ($r = -0.63$, $p < 0.0001$) and efAP ($r = -0.60$, $P < 0.0001$). Tau PET SUVR cutoff of 1.32 was used to stratify tau positivity. Cutoffs for predictor variables, 1.1083 (R1) and 1.0539 (efAP), were derived from receiver operating characteristics (ROC) curve. Linear regression shows parallel relationships for R1 ($m = -1.66$) and efAP ($m = -1.76$) with tau PET. B) ROC curve shown with area under the curve (AUC) of 0.926 (R1) and 0.913 (efAP). Sensitivity and specificity shown at point of maximum Youden index that was used to derive cutoffs for efAP and R1.

Neuropsych measure	β_{efap}	β_{R1}	β_{volume}
Digit Symbol	3.558	3.941	2.915
Trails Making A	-4.061	-3.116	-2.421
Trails Making B	-3.737	-3.218	-2.783
Attention and Executive Function Z-score	4.355	4.330	2.354
MINT Naming Total	1.690	2.400	1.716
Animals	0.264	2.208	1.473
Vegetables	0.516	2.441	2.519
F Verbal Fluency	0.163	-0.131	0.553
L Verbal Fluency	-0.190	0.050	1.200
F+L word Verbal Fluency	-0.027	-0.267	0.847
Language Z-score	-1.025	-0.798	-0.728
Craft Story 21 (Immediate verbatim)	-0.664	-0.372	-1.438
Craft Story 21 (Immediate paraphrase)	-1.228	-1.702	-2.621
Craft Story 21 (Delayed verbatim)	-0.371	-0.559	-1.579
Craft Story 21 (Delayed paraphrase)	0.738	-0.178	-1.088
Benson Recall	1.957	1.678	1.768
Logical Memory Immediate	0.670	0.845	1.826
Logical Memory Delayed	-0.361	0.516	0.888
Selective Reminding Test	-1.091	-2.618	-2.556
Associative Learning	-0.128	-1.985	-0.571
Memory Z-score	-0.438	0.393	2.238

Table 1. Attention and executive function show strongest relationship across all imaging biomarkers but neuropsych measures for language and memory show unique relationships with each biomarker. Standardized effect size (β) reported from linear regression after correcting for demographic regressors (sex, ApoE4, age, and education). Italics signifies that the standardized effect size of the given imaging variable was a significant contributor to the variance of the model.

Neuropsych measure	β_{efap}	β_{R1}	$\beta_{\text{efap (Adj)}}$	$\beta_{\text{R1 (Adj)}}$
Digit Symbol	2.932	4.019	3.004	3.493
Trails Making A	-3.681	-3.307	-3.605	-2.850
Trails Making B	-3.351	-3.428	-3.331	-2.920
Attention and Executive Function Z-score	4.058	4.557	4.007	4.079
MINT Naming Total	1.257	2.960	1.160	2.106
Animals	0.634	2.859	0.078	2.040
Vegetables	-0.064	2.115	-0.055	2.045
F Verbal Fluency	0.134	0.407	-0.085	-0.223
L Verbal Fluency	-0.443	0.050	-0.504	-0.145
F+L word Verbal Fluency	-0.162	0.034	-0.306	-0.408
Language Z-score	-0.933	-0.638	-0.844	-0.679
Craft Story 21 (Immediate verbatim)	-0.469	-0.499	-0.358	-0.146
Craft Story 21 (Immediate paraphrase)	-0.880	-2.122	-0.629	-1.320
Craft Story 21 (Delayed verbatim)	-0.024	-0.452	-0.027	-0.187
Craft Story 21 (Delayed paraphrase)	0.988	-0.191	1.035	-0.005
Benson Recall	1.701	1.921	1.543	1.531
Logical Memory Immediate	0.132	0.457	0.043	0.470
Logical Memory Delayed	-0.681	0.517	-0.700	0.332
Selective Reminding Test	-0.798	-2.825	-0.714	-2.362
Associative Learning	-0.244	-2.526	-0.026	-1.907
Memory Z-score	-0.370	0.977	-0.891	0.064

Table 2. Both PET biomarkers provide significant additive utility beyond hippocampal volumes for neuropsych measures of attention and executive function. However, only R1, not efAP, showed significant utility beyond volumes for semantic fluency measures (MINT, Animals, and Vegetables). Standardized effect size (β) beyond hippocampal volume reported from linear regression both unadjusted and adjusted (adj) for demographic regressors (sex, ApoE4, age, and education). Italics signifies that the standardized effect size of the given imaging variable was a significant contributor to the variance of the model beyond hippocampal volume.

Keywords: cognition, [18F]florbetapir-PET, [18F]flortaucipir-PET, early frame amyloid PET, R1

P29 Spatial extent and intensity of Alzheimer-associated tau PET burden is greater in agrammatic than logopenic primary progressive aphasia

Adam Martersteck^{1,2}, Jaiashre Sridhar¹, Christina Coventry¹, Sandra Weintraub^{1,3}, M.-Marsel Mesulam^{1,4}, Emily Rogalski^{1,3}

¹Mesulam Center for Cognitive Neurology and Alzheimer's Disease, Northwestern University, Chicago, IL, US

²Department of Radiology, Northwestern University, Chicago, IL, US

³Department of Psychiatry and Behavioral Sciences, Northwestern University, Chicago, IL, US

⁴Department of Neurology, Northwestern University, Chicago, IL, US

Background: Primary progressive aphasia (PPA) is a clinical dementia syndrome characterized by selective vulnerability of the language network, with salient deficits in language domains. The most common neuropathologies reported for PPA are one of the forms of frontotemporal lobar degeneration (FTLD; ~60%) or Alzheimer disease neuropathologic change (ADNC; ~40%). PPA can be subdivided into clinical subtypes based on specific language deficits. PPA subtypes have differing probabilistic relationships with underlying neuropathology. Semantic and agrammatic (PPA-G) subtypes have the strongest association with FTLD while the logopenic subtype (PPA-L) is most associated with ADNC.

Objective: Examine the flortaucipir PET differences between PPA-L and PPA-G with evidence of ADNC.

Methods: 21 PPA participants were identified based on (1) an agrammatic or logopenic subtype, (2) ¹⁸F-flortaucipir PET and structural MRI, and (3) CSF or amyloid PET indicating ADNC and/or autopsy-confirmed ADNC. FreeSurfer segmentations and surfaces provided MRI-guided PET analysis, referenced by hotspot-removed inferior cerebellar gray, analyzed with and without Müller-Gärtner partial volume correction (PVC). Vertex-wise general linear models tested tau PET uptake on subtype covarying for age and meta-region of interest (meta-ROI) tau. All analyses were corrected for multiple comparisons at Benjamini-Hochberg false discovery rate $q=0.05$.

Results: 4 PPA-G participants (average age=67.9±2.7; average meta-ROI-SUVR=2.06±0.42) and 17 PPA-L participants (average age=68.8±7.6; average meta-ROI-SUVR=2.14±0.43) were included (**Figure 1**). There were significant differences in flortaucipir uptake between the groups, with greater uptake in left and right motor cortex, paracentral lobule, and V2 of the occipital lobe in PPA-G participants compared to PPA-L (**Figure 2**). Analyzing the data without PVC and using models without covariates did not alter the results.

Conclusions: This study adds further evidence ADNC can result in a PPA-G phenotype. Further, PPA-G may present with an extended spatial distribution and intensity of Alzheimer type tau, which may inform prognosis, emergence of additional symptoms, and disease progression.

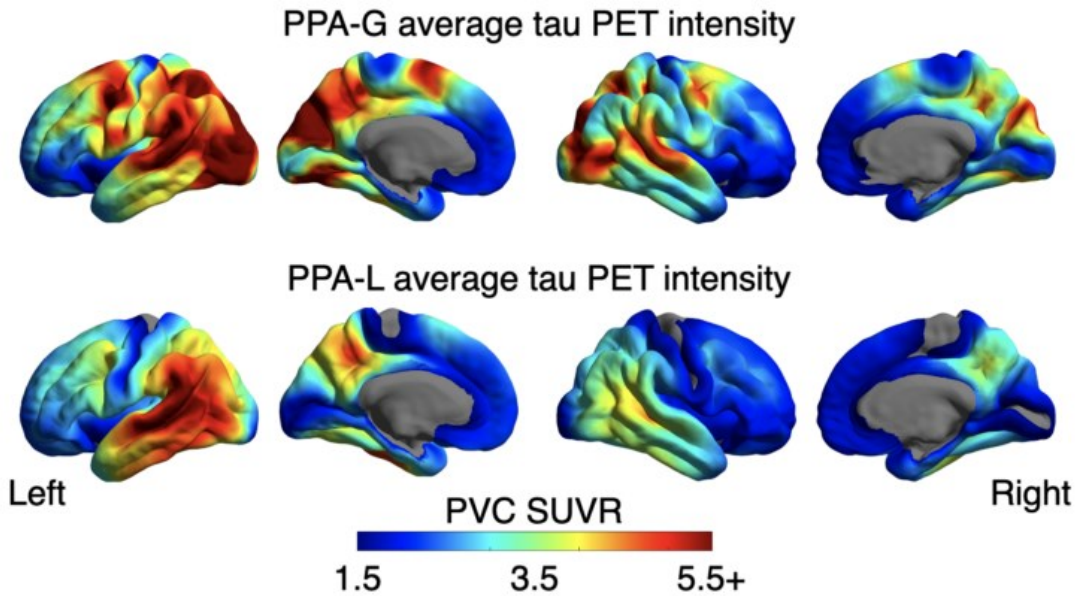


Figure 1. Average tau PET signal across the cortex in primary progressive aphasia (PPA) agrammatic (PPA-G) and logopenic (PPA-L) subtypes. Correcting for partial volume correction (PVC) and referenced by the hot-spot removed inferior cerebellar gray to calculate the standard uptake value ratio (SUVR).

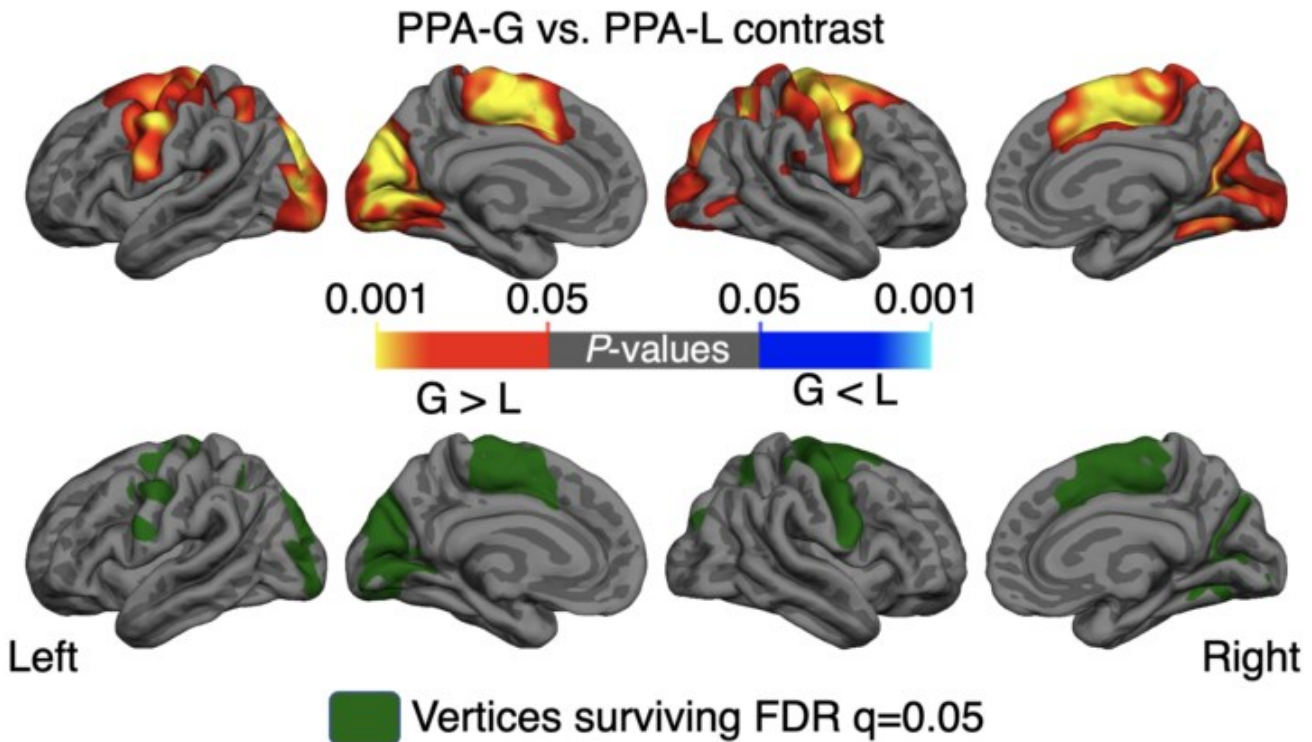


Figure 2. Significant vertices for the contrast comparing primary progressive aphasia (PPA) agrammatic (PPA-G) and logopenic (PPA-L) subtypes, covarying for age and average meta-ROI uptake. In the upper panel, warmer colors indicate increased PET uptake in the PPA-G group. In the lower panel, green color vertices survive the false discovery rate (FDR) correction for multiple comparisons.

P30 Comparing PI2620 and Flortaucipir in Progressive Supranuclear Palsy Subjects

Wesley Thomas^{1,3}, Ganna Blazhenets², Renaud La Joie², Gil Rabinovici², Hilary Heuer², William Jagust^{1,3}, Adam Boxer², Suzanne L Baker^{1,3}

¹University of California, Berkeley, Berkeley, CA, US

²University of California, San Francisco, San Francisco, CA, US

³Lawrence Berkeley National Laboratory, Berkeley, CA, US

Background: Progressive Supranuclear Palsy Richardson’s Syndrome (PSP-RS) is a primary 4R tauopathy. Current tau tracers have higher affinity for 3R/4R tau, but exhibit some sensitivity to 4R tau. Using FTP or PI2620, studies have shown increased tracer binding relative to healthy controls (HC) in the pallidum, dentate nucleus, thalamus, putamen, and midbrain. Only one found tau signal correlated with disease severity.

Objective: Examine performance of FTP in one cohort and PI2620 in another by comparing tracer retention in patients with PSP-RS compared to controls.

Methods: Subjects were age-matched, PSP patients were more male and had lower MMSE/MoCA’s than HC and FTP scanned PSP patients had less years of education than controls (table 1). PI2620 scans were acquired 30-60min post-injection, FTP scans were acquired 80-100min post-injection, reference region was inferior cerebellar gray. Only amyloid negative subjects were included. Tau PET scans were warped to MNI space, mean SUVRs of dorsal midbrain, pallidum, putamen, subthalamic nucleus, substantia nigra, and dentate nucleus were calculated. PSP-RS>HC comparisons were made. PSP-RS SUVRs were Z-scored relative to HCs within tracer and compared between tracers. The correlation of PSP-RS and the severity score was calculated.

Results: When comparing PSP-RS>HCs, all ROIs were significantly different ($p<0.05$) except substantia nigra in FTP and dentate nucleus in PI2620 (Figure 1). PI2620 showed a trend of higher average Z-scores than FTP, but only significantly in the substantia nigra (Figure 2). Severity score only correlated with PSP-RS PI2620 in the putamen, but was no longer significant after controlling for age.

Conclusions: PI2620 and FTP tracer retention differs between PSP-RS and HCs on the group level. Given that PSP severity doesn’t correlate with tau when measured with either tracer, either the amount of tau doesn’t impact severity or more likely that the tracer insensitivity and small sample make small correlations difficult to detect.

	FTP		PI2620	
	HC	PSP-RS	HC	PSP-RS
n	589	29	15	11
age	69.1(12.2)	68.4(6.2)	70.3(10.0)	69.3(7.2)
sex,female (%F)	311 (53)	10(34)*	10(68)	3(33) *
education	16.8(2.3) ¹	14.7(2.7)*	15.5(4.0) ¹	17.2(2.3) ¹
MMSE/MoCA	28.7(1.7) ²	21.4(3.0) ¹ *	28.6(1.3) ²	23.2(2.8) ² *
PSP Rating Scale		31.9 (11.5) ²		32.7 (9.1) ³
	1. one missing	1. six missing	1. five missing	1. one missing
	2. two missing	2. one missing	2. one missing	2. six missing
* Indicates statistical difference from controls				3. two missing

Figure 1

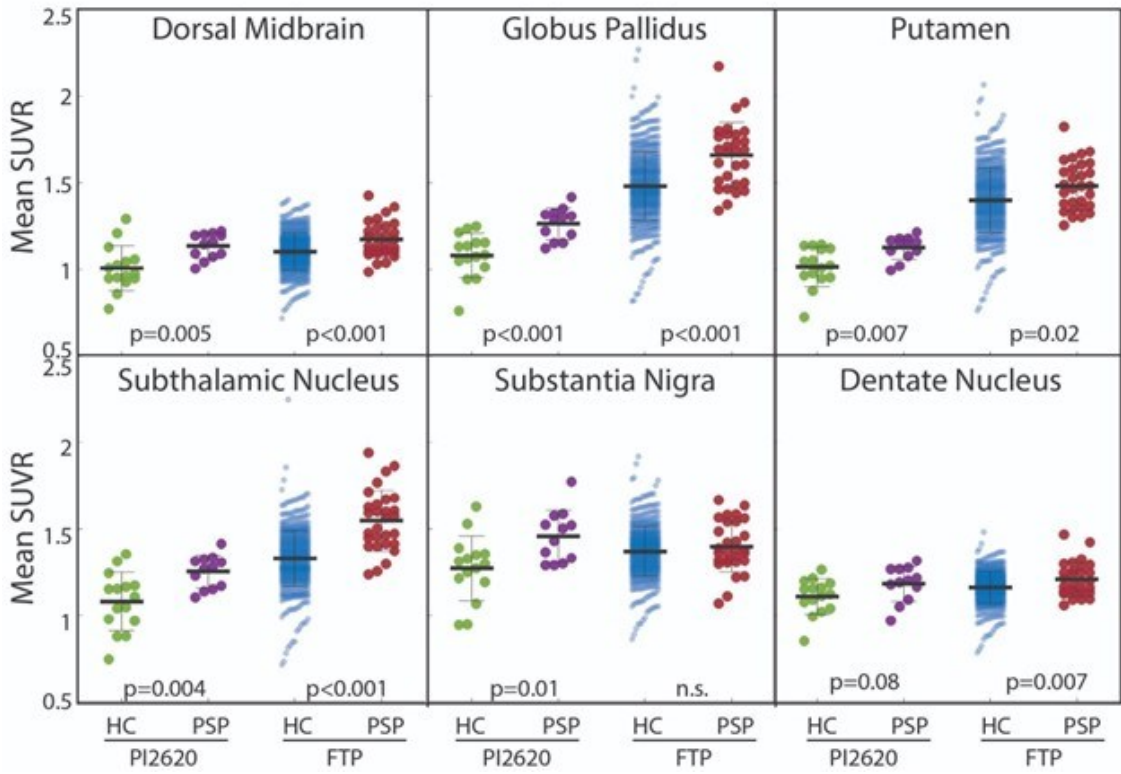
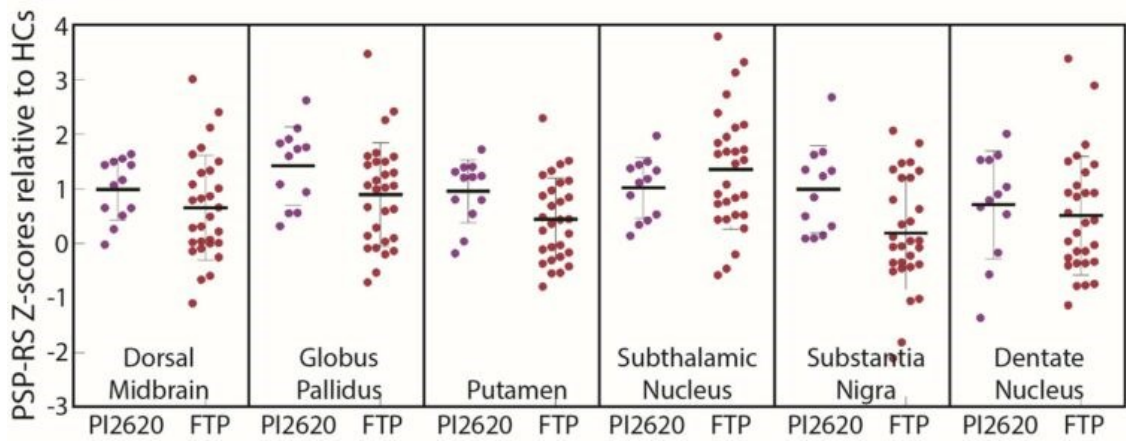


Figure 2



Keywords: flortaucipir, PI2620, PSP

P31 Assessing a universal neocortical mask for Centiloid quantification

Pierrick Bourgeat¹, Vincent Dore^{1,2}, Christopher Rowe^{2,6}, Tammie Benzinger³, Duygu Tosun^{4,7}, Manu Goyal⁵, Pamela LaMontagne⁵, Liang Jin⁶, Michael Weiner^{4,7}, John Morris⁸, Colin Masters⁶, Jurgen Fripp¹, Victor Villemagne^{2,9}

¹Australian eHealth Research Centre, CSIRO Health and Biosecurity, Herston, AU

²Department of Molecular Imaging & Therapy, Austin Health, Melbourne, AU

³Knight Alzheimer Disease Research Center, St Louis, MO, US

⁴San Francisco Veterans Affairs Medical Center, San Francisco, CA, US

⁵Mallinckrodt Institute of Radiology, Washington University School of Medicine, St Louis, MO, US

⁶The Florey Institute of Neuroscience and Mental Health, University of Melbourne, Parkville, AU

⁷Department of Radiology and Biomedical Imaging, University of California, San Francisco, CA, US

⁸Washington University in St. Louis, St. Louis, MO, US

⁹Department of Psychiatry, The University of Pittsburgh, Pittsburgh, PA, US

Background: The Centiloid (CL) project was developed to harmonise the quantification of A β -PET scans to a unified scale. The CL neocortical mask was defined using ¹¹C-PiB, overlooking potential differences in regional distribution among A β tracers. We created a universal mask using an independent dataset of 5 A β tracers, and investigated its impact on inter-tracer agreement, tracer variability and group separation.

Method: Using data from the ADOPIC study (AIBL+ADNI+OASIS), age-matched pairs of mild Alzheimer's disease (AD) (MMSE=20-24;CL>25) and healthy controls (MMSE \geq 28;CDR=0;CL<15) were selected: ¹⁸F-Florbetapir (N=147 pairs), ¹⁸F-Florbetaben (N=22), ¹⁸F-Flutemetamol (N=10), ¹⁸F-NAV (N=42), ¹¹C-PiB (N=63). The images were spatially normalised using the SPM CL pipeline and transformed into SUVR (whole cerebellum). For each tracer, the mean AD-HC difference image was computed and mirrored. The threshold for each difference image was optimised to maximise the overlap with the standard CL mask. The universal mask was defined as the intersection of all 5 masks. It was evaluated on the GAAIN head-to-head calibration datasets in terms of inter-tracer agreement and variance in the young controls (YC) and on the ADOPIC dataset with the effect-size (d) between baseline HC/AD and HC/MCI.

Results: The overlap between each tracer specific mask was high (mean Dice=0.82). The universal mask was 26% smaller than the standard one, but the overlap was high (Dice=0.74). The universal mask led to a small reduction in the variance of the YC in most tracers (-2.8%) and a small increase in the R² between each of the ¹¹C-PiB/¹⁸F-tracer pairs (+0.25%). In ADOPIC, it led to a higher effect-size between HC/AD (1.895 vs 1.956) and HC/MCI (0.599 vs 0.601).

Conclusions: The universal CL mask led to an increase in inter-tracer agreement and group separation. Those increases were however relatively small indicating that the existing standard CL mask is suitable for the quantification of all A β tracers.

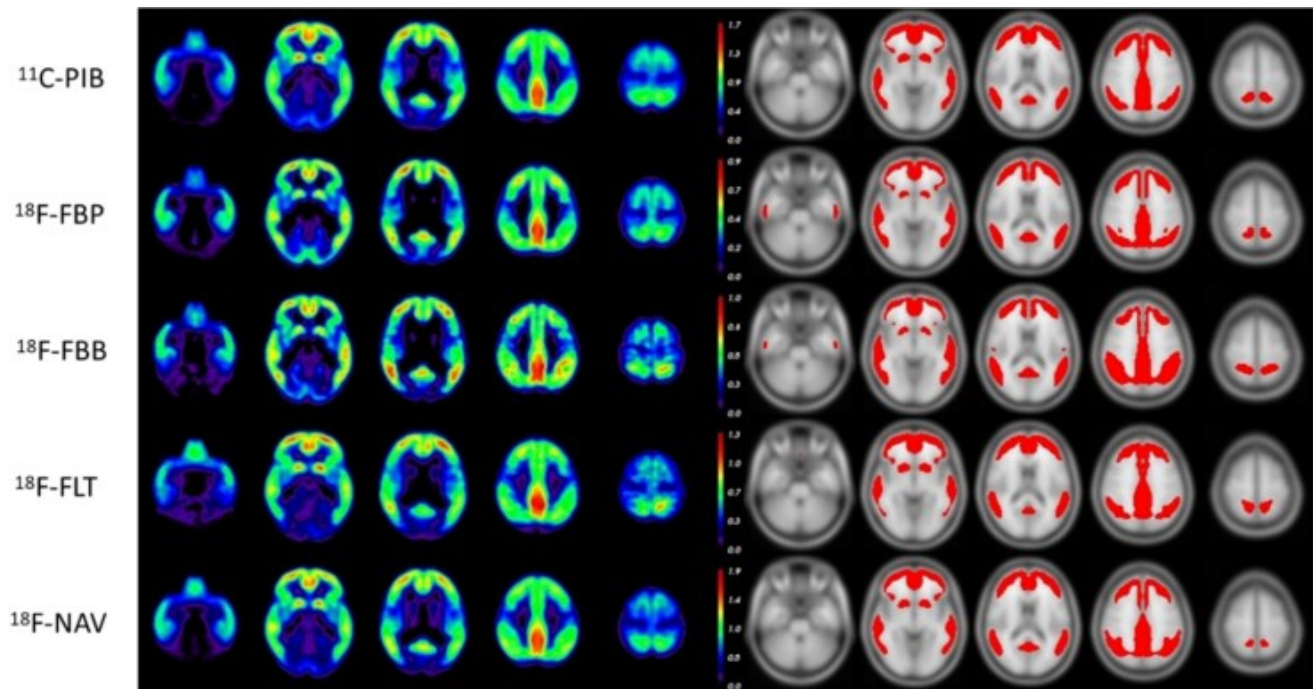


Figure 1. Difference images (AD-HC) for all 5 tracers (with colour-scale maximum set at twice the optimal threshold value) and their corresponding masks

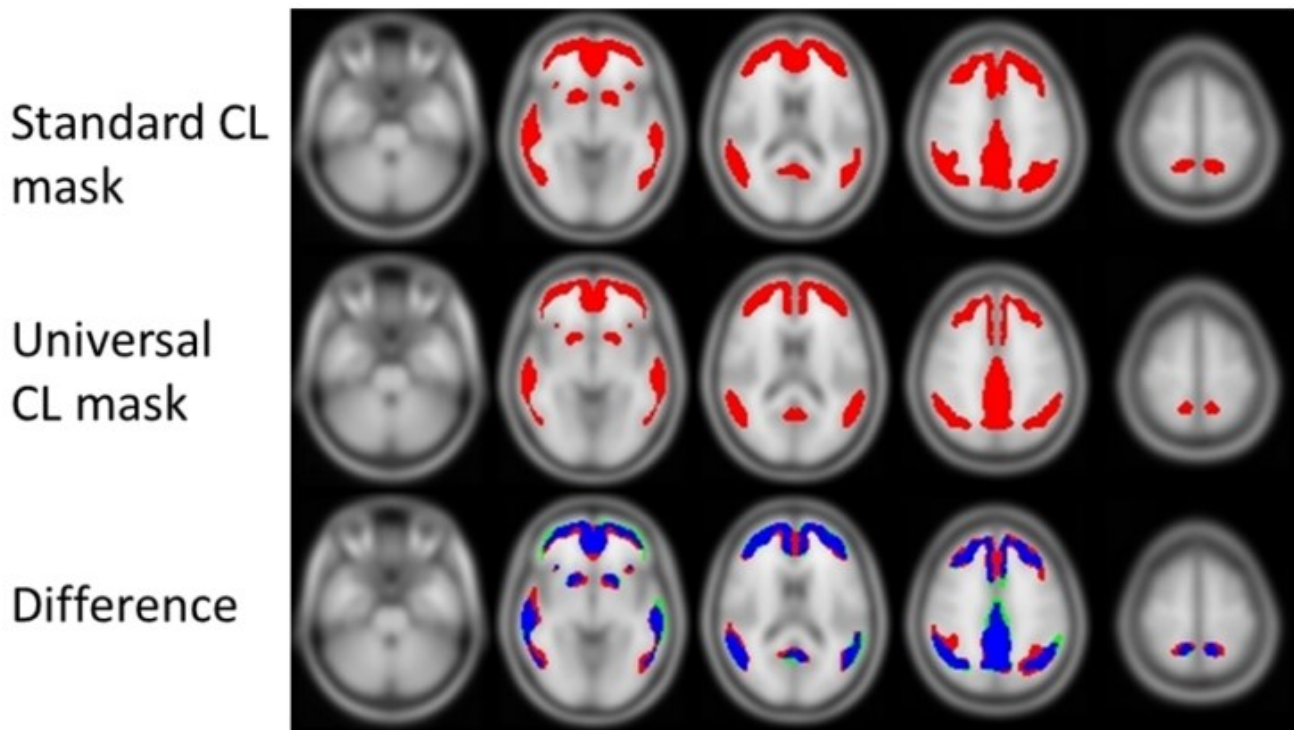


Figure 2. Standard and universal CL masks along with their difference (Blue: Common to both masks, Red: Only in Standard mask, Green: Only in Universal mask)

<i>Measure</i>	<i>Target</i>	<i>Centiloid mask</i>	
		<i>Standard</i>	<i>Universal</i>
Variance in Young controls	¹¹ C-PiB	0.00227	0.00218
	¹⁸ F-Florbetapir	0.00269	0.00253
	¹⁸ F-Florbetaben	0.00195	0.00182
	¹⁸ F-Flutemetamol	0.00369	0.00371
	¹⁸ F-NAV	0.00218	0.00225
Agreement between ¹¹ C-PiB and ¹⁸ F-tracer pairs	¹⁸ F-Florbetapir	0.898	0.902
	¹⁸ F-Florbetaben	0.956	0.959
	¹⁸ F-Flutemetamol	0.965	0.967
	¹⁸ F-NAV	0.987	0.987
Baseline CL Effect Size	HC Vs MCI	0.599	0.601
	HC Vs AD	1.895	1.956

Table 1. Comparison of the universal and standard centiloid masks on tracer variability in YC, inter-tracer agreement, and group separation. For each test, the best results are shown in bold.

Keywords: Centiloid

P32 Relationships between Neuronal Hyperactivity, Stress Susceptibility, and Alzheimer's Disease pathology

Elizabeth Sharp^{1,4}, Ray Razlighi², Hwamee Oh^{1,3,4}

¹*Department of Psychiatry and Human Behavior, Brown University, Providence, RI, US*

²*Quantitative Neuroimaging Laboratory, Brain Health Imaging Institute, Department of Radiology, Weill Cornell Medicine, New York, NY, US*

³*Carney Institute for Brain Science, Brown University, Providence, RI, US*

⁴*Memory and Aging Program, Butler Hospital, Providence, RI, US*

Background: Recent studies in both animal and human literature have suggested a relationship between stress responses and an increased susceptibility to extracellular beta-amyloid (A β) plaque aggregation as well as clinical symptoms of Alzheimer's disease (AD). Despite this evidence, a neuro-mechanistic pathway that underlies the relationship between the psychological stress response and brain neuropathologies associated with AD remains poorly understood. In this study, we tested the hypothesis that increased stress responses are associated with neuronal hyperactivity and increased brain A β deposition along the spectrum of AD.

Methods: We included 166 study subjects (mean age = 74.21; 90 Females) spanning diagnostic spectrums along cognitively normal (CN) individuals and AD patients from the Alzheimer's Disease Neuroimaging Initiative (ADNI) II dataset. Neuronal activity was quantified by applying the amplitude of low frequency fluctuations method to time series of fMRI blood oxygenation-level-dependent signals obtained during resting-state fMRI (rsfMRI) scan. Amyloid pathology was quantified by AV45-SUV_R measures. Mini-Mental State Exam (MMSE) and the Neuropsychiatric Inventory Questionnaire (NPI-Q) scores were used as cognitive and stress susceptibility measures.

Results: Behavioral measures of stress were significantly associated with brain A β indices across the entire cohort, spanning from CN older adults to AD patients. Relationships between the neural activity, stress responses, and A β deposition, however, differ by diagnostic groups. As stress indicators increased, CN subjects exhibited increased activity in brain regions collectively known as the default mode network (DMN), while AD participants exhibited decreased activity. Moreover, as brain A β load increased, CN participants experienced DMN hyperactivity, while AD participants experienced hypoactivity.

Conclusion: These results indicate a potential link between heightened stress responses and increased susceptibility to the development of AD pathologies through neuronal hyperactivity, especially in the early stages of AD. The study also validates a potential use of rsfMRI to quantify neuronal hyperactivity in a non-invasive manner.

Keywords: Neuronal hyperactivity, beta-amyloid deposition, fMRI, Neuropsychiatric symptoms

P33 A/T/N, cognitive, health and lifestyle differences across white matter hyperintensities groups in aged 45-85 years adults: Results from the Wisconsin Registry for Alzheimer's Prevention (WRAP)

Lianlian Du^{1,3}, Cory Burghy¹, Karly Cody^{1,2,4}, Bruce Hermann^{1,5}, Erin Jonaitis^{1,2,4}, Tobey Betthausen^{1,2,4}, Nathaniel Chin^{2,5}, Robert Cadman^{2,4}, Leonardo Rivera-Rivera^{2,4,6}, Anthony Peret⁷, Kevin Johnson^{6,7}, Howard Rowley^{2,7}, Christian Pompa², Sarah Lose², Bradley Christian⁶, Shorena Janelidze⁸, Oskar Hansson⁸, Sterling Johnson^{1,2,4,9}, Laura Eisenmenger⁷, Rebecca Kosciak^{1,2,4}

¹Wisconsin Alzheimer's Institute, University of Wisconsin-Madison School of Medicine and Public Health, Madison, WI, US

²Wisconsin Alzheimer's Disease Research Center, Madison, WI, US

³Department of Biostatistics and Medical Informatics, University of Wisconsin-Madison School of Medicine and Public Health, Madison, WI, US

⁴Department of Medicine, University of Wisconsin-Madison School of Medicine and Public Health, Madison, WI, US

⁵Department of Neurology, University of Wisconsin-Madison School of Medicine and Public Health, Madison, WI, US

⁶Department of Medical Physics, University of Wisconsin-Madison School of Medicine and Public Health, Madison, WI, US

⁷Department of Radiology, University of Wisconsin School of Medicine and Public Health, Madison, WI, US

⁸Clinical Memory Research Unit, Lund University, Sölvegatan 18, Lund, Sweden

⁹Madison VA GRECC, William S. Middleton Memorial Hospital, Madison, WI, US

Background: Previous studies have suggested that white matter hyperintensities (WMH), a common neuroimaging feature of chronic cerebral small-vessel disease, may play a role in the evolution of Alzheimer's disease (AD). Here we identified MRI WMH groups using Gaussian Mixture Modeling (GMM) and examined how demographic, health, cognitive, and AD-related measures varied across these groups.

Methods: Data from late middle-aged, baseline dementia-free participants were drawn from the Wisconsin Registry for Alzheimer's Prevention. TIV-normalized WMH volumes were segmented from T2-FLAIR images using the SPM Lesion Segmentation Tool. GMM was applied to last available WMH volumes to identify WMHV subgroups. AD biomarker measures included PET amyloid using Pittsburgh compound B (DVR derived from a 0-70 min dynamic scan) and tau using florquinitalu (MK6240 SUVR from 70-90 min post-injection scanning window), plasma P-tau217 pg/ml, and MRI TIV-normalized hippocampal volume (HV) and global brain atrophy (GBA). Biomarkers were also categorized as abnormal/normal using data-driven cut-offs. We compared demographic, baseline and last visit health characteristics, cognitive performance, and last available biomarker measures across WMHV groups. Significant omnibus tests ($p < .05$) were followed with pairwise comparisons.

Results: Mean(sd) last MRI age was 67.1(8.4) years. GMM identified a no-elevation WMHV group ($n(\%)=195(39.6\%)$) and low (182(37.0%)), medium (94(19.1%)), and high (21(4.3%)) elevation groups (Figure 1: WMHV spaghetti plot). The groups differed in numbers of prescriptions and comorbidities, executive function and 3-test preclinical Alzheimer's cognitive composite (PACC3) performance, and HV and GBA, but did not differ on other measures examined. Post-hoc comparisons indicated the no-elevation group was younger, had fewer prescriptions and comorbidities, better cognitive performance, and less neurodegeneration than one or more WMHV groups (see Figures 2&3).

Conclusions: WMHV elevation groups showed associations with age, cognitive performance, and neurodegeneration biomarkers, but not amyloid and tau. Future analyses will investigate whether WMHV and amyloid have synergistic effects on pre-clinical cognitive decline.

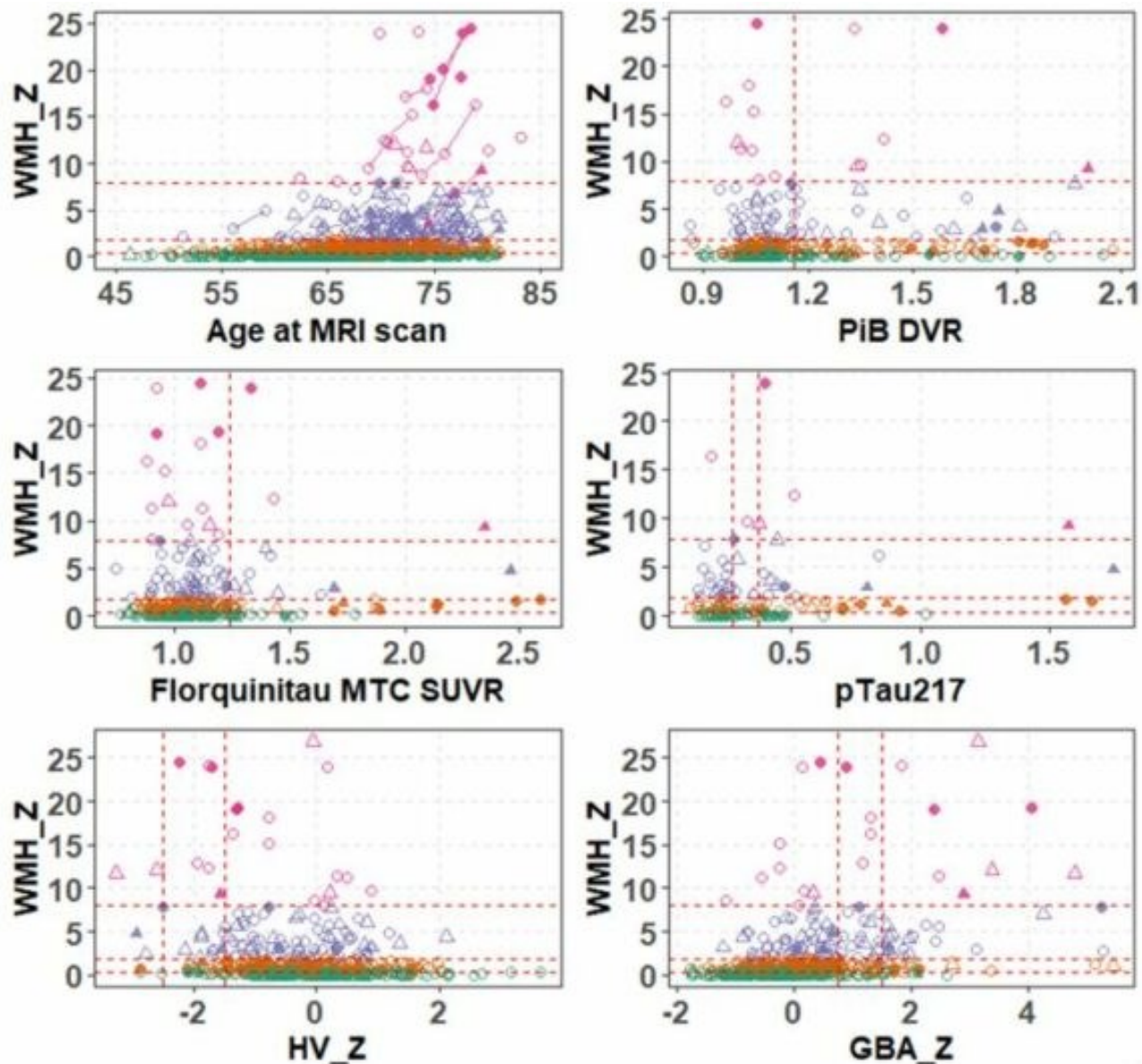


Fig. 1. The spaghetti plot of WMH lesion volume by WMH elevation group (top left panel) and the scatter plot of WMH lesion volume vs A/T/N biomarkers. All participants were non-demented at baseline. The WMH raw volume was normalized to total intracranial volume and expressed as percent TICV occupied by WMH lesions ($WMH_Z = WMH/TICV * mean(TICV)$). GMM using last MRI scan identified a no-elevation WMH group ($n(\%)=195(39.6\%)$) and low (182(37.0%)), medium (94(19.1%)), and high (21(4.3%)) elevation groups (horizontal dotted lines in each plot). Top left: Spaghetti plots of WMH_Z vs age. The HV_Z and GBA_Z value were normalized by total intracranial volume ($TICV(L) = GM + WM + CSF$ volumes from SPM segmentation) using a regression-based approach in amyloid negative and cognitive normal subset. Two cutpoints were defined for HV and GBA, one is based on distribution (1.5 SD worse than expected), and the other is from GMM model (-2.51 for HV and 0.745 for GBA). The dots are raw values from the last measurement. The horizontal lines are the thresholds for WMHV groups. The vertical lines stand the cutpoint for each A/T/N biomarkers. Proportion biomarker positive on HV and GBA was significantly higher in those with more WMHV.

Abbreviations: CU-S = Cognitive unimpaired Stable, CU-D = Cognitive unimpaired Decline, MCI = Mild cognitive impairment. DVR = distribution volume ratio. PiB = Pittsburgh compound B. MTC = Meta-temporal composite (mid-to-late tau stage composite, based on Mayo meta-temporal composite) (Jack, Wiste, et al. 2018), HV = Hippocampus Volume. GBA = Global brain atrophy. WMH = White matter hyperintensities, TICV: Total intracranial volume.

	No WMH Elevation N=195(19.6%)	WMH level		
		Low 182(37.0%)	Medium 94(19.1%)	High 21(4.3%)
Demographic Variables				
Female (n(%))	140 (71.8)	124 (68.1)	73 (77.7)	15 (71.4)
White/Caucasian (n(%))	176 (90.3)	167 (92.3)	83 (88.3)	20 (95.2)
APOE e4 carriers (n(%))	78 (43.1)	67 (39.2)	36 (40.0)	7 (35.0)
Family History (n(%))	147 (76.2)	139 (77.2)	67 (71.3)	14 (66.7)
education (mean (SD))	15.96 (2.10)	16.09 (2.32)	16.00 (2.41)	15.24 (2.57)
WRAT3 Reading (mean (SD))	105.27 (9.33)	105.93 (9.65)	107.82 (8.34)	106.52 (9.14)
WMH baseline Age (mean (SD))	63.63 (7.0)	67.55 (6.4)*	70.75 (5.2)*+	73.31 (4.6)*+
Health Variables				
Baseline BMI (mean (SD))	28.28 (6.36)	28.18 (5.91)	29.81 (6.21)	29.74 (7.11)
Last BMI (mean (SD))	28.98 (6.60)	28.52 (5.89)	29.93 (6.22)	29.25 (7.00)
Baseline WHR (mean (SD))	0.85 (0.10)	0.86 (0.10)	0.86 (0.09)	0.85 (0.09)
Last WHR (mean (SD))	0.86 (0.10)	0.88 (0.09)	0.87 (0.09)	0.86 (0.08)
Baseline HOMA-IR (mean (SD))	2.11 (1.70)	2.34 (1.99)	2.47 (1.88)	2.75 (2.28)
Last HOMA-IR (mean (SD))	2.55 (2.26)	2.39 (1.67)	2.30 (1.38)	2.54 (1.93)
Baseline SRH Fair (n(%))	13 (7.0)	10 (5.8)	9 (10.1)	1 (4.8)
Baseline SRH Good (n(%))	66 (35.5)	51 (29.7)	30 (33.7)	6 (28.6)
Baseline SRH Very Good (n(%))	68 (36.6)	82 (47.7)	40 (44.9)	10 (47.6)
Baseline SRH Excellent (n(%))	39 (21.0)	29 (16.9)	10 (11.2)	4 (19.0)
Last SRH Fair (n(%))	11 (5.9)	6 (3.5)	7 (7.7)	2 (9.5)
Last SRH Good (n(%))	73 (39.5)	57 (32.9)	33 (36.3)	7 (33.3)
Last SRH Very Good (n(%))	73 (39.5)	92 (53.2)	43 (47.3)	9 (42.9)
Baseline SRH Excellent (n(%))	26 (14.1)	18 (10.4)	8 (8.8)	3 (14.3)
Baseline Number of prescription (mean (SD))	2.46 (2.78)	2.74 (2.98)	2.91 (2.88)	3.29 (3.44)
Last Number of prescription (mean (SD))	2.95 (2.86)	3.37 (3.03)	4.29 (3.49)*+	4.00 (3.07)
Baseline Comorbidity (mean (SD))	2.60 (2.22)	3.55 (2.27)*	3.11 (2.16)	3.50 (2.67)
Last Comorbidity (mean (SD))	3.40 (2.66)	4.53 (2.60)*	3.85 (2.60)	4.39 (3.09)
Baseline Depression scores (mean (SD))	6.71 (7.03)	6.99 (6.67)	6.22 (7.47)	7.05 (8.80)
Last Depression scores (mean (SD))	5.30 (6.28)	6.66 (7.41)	5.96 (7.08)	8.52 (9.00)
Baseline LIBRA Index (median [Q1-Q3])	1.10 [0.0, 2.7]	1.10 [0.0, 2.6]	1.60 [0.0, 3.2]	1.10 [0.4, 2.9]
Last LIBRA Index (median [Q1-Q3])	1.40 [0.0, 2.7]	0.60 [-1.0, 2.2]	1.10 [-1.0, 2.5]	0.60 [0.0, 2.9]
Baseline EF Z score (mean (SD))	0.28 (0.9)	0.03 (1.0)*	-0.06 (0.9)*	-0.81 (1.0)*+‡
Last EF Z score (mean (SD))	0.12 (0.9)	-0.27 (1.1)*	-0.49 (1.1)*	-1.25 (1.3)*+‡
Baseline PACC3 Z score (mean (SD))	0.28 (1.0)	-0.07 (1.1)*	-0.11 (1.0)*	-0.34 (1.2)*
Last PACC3 Z score (mean (SD))	0.29 (1.0)	-0.20 (1.1)*	-0.43 (1.2)*	-0.83 (1.2)*+
Baseline CU-S (n(%))	161 (86.6)	141 (81.0)	76 (83.5)	15 (71.4)
Baseline CU-D (n(%))	23 (12.4)	27 (15.5)	14 (15.4)	6 (28.6)
Baseline MCI (n(%))	2 (1.1)	6 (3.4)	1 (1.1)	0 (0.0)
last CU-S (n(%))	170 (91.4)	143 (82.2)*	68 (74.7)*	14 (66.7)*+
last CU-D (n(%))	13 (7.0)	23 (13.2)*	19 (20.9)*	6 (28.6)*+
last MCI (n(%))	3 (1.6)	8 (4.6)*	4 (4.4)*	1 (4.8)*+
Biomarker Variables				
A+ (n(%))	33 (25.2)	36 (28.8)	22 (33.8)	6 (40.0)
Amyloid onset age (A+) (median [Q1-Q3])	64.1 [51.2, 68.1]	57.8 [51.8, 66.8]	63.6 [58.6, 69.9]	64.5 [60.3, 66.8]
T+ (n(%))	14 (11.3)	15 (13.3)	9 (14.1)	3 (17.6)
pTau217_T+ (n(%))	13 (23.6)	21 (42.9)	10 (29.4)	4 (66.7)
abnormal HV (n(%))	10 (5.2)	13 (7.3)*	12 (13.2)*	8 (38.1)*+‡
abnormal GBA (n(%))	6 (3.1)	14 (7.8)*	19 (20.9)*+	8 (38.1)*+

Fig. 2. How did the WMH groups differ? Visual Summary of Results. The significant omnibus tests of WMH group differences were noted in Bold. Chi² square or Fisher's exact for categorical; analysis of variance (ANOVA) for continuous where M (SD) reported; Kruskal-Wallis for continuous where median [Q1-Q3] reported and Likert-scale items. Significant omnibus tests (p<.05) were followed with pairwise comparisons. These values are nominal p-values only. Post hoc pairwise group differences at unadjusted P < 0.05 noted in red symbol. *stands significant difference compared no elevation group, + means significant difference compared to low group, ‡ means significant difference compared to medium group. A(+) threshold (global PiB DVR = 1.16). T(+) threshold (PET MK-6240 Meta-temporal composite SUVR >1.24). P-Tau217_T+ threshold (P-tau217 > 0.37). %abnormal HV and %abnormal GBA are using 1.5 SD on Z scores. **Abbreviations:** BMI = Body mass index. WHR = Waist-to-hip Ratio. SRH = Self-rated health. LIBRA index = Lifestyle for Brain Health index. PACC3 = Preclinical Alzheimer's Cognitive Composite (comprised of averaged z-scores for 3 tests: Auditory Verbal Learning Test (AVLT) Total Learning, Logical Memory Delayed Recall, and Digit Symbol Substitution). EF = Executive Function (comprised of averaged z-scores for 3 tests: Stroop Color- Word, Trail Making Test Part B and Digit Symbol Substitution). CU-S = Cognitive unimpaired Stable, CU-D = Cognitive unimpaired Decline, MCI = Mild cognitive impairment. HV = Hippocampus Volume. GBA = Global Brain Atrophy. Estimates Amyloid onset age in the A+ subset, the details were described in Kosik, Betthausen et al., 2020, and Betthausen et al., 2022.

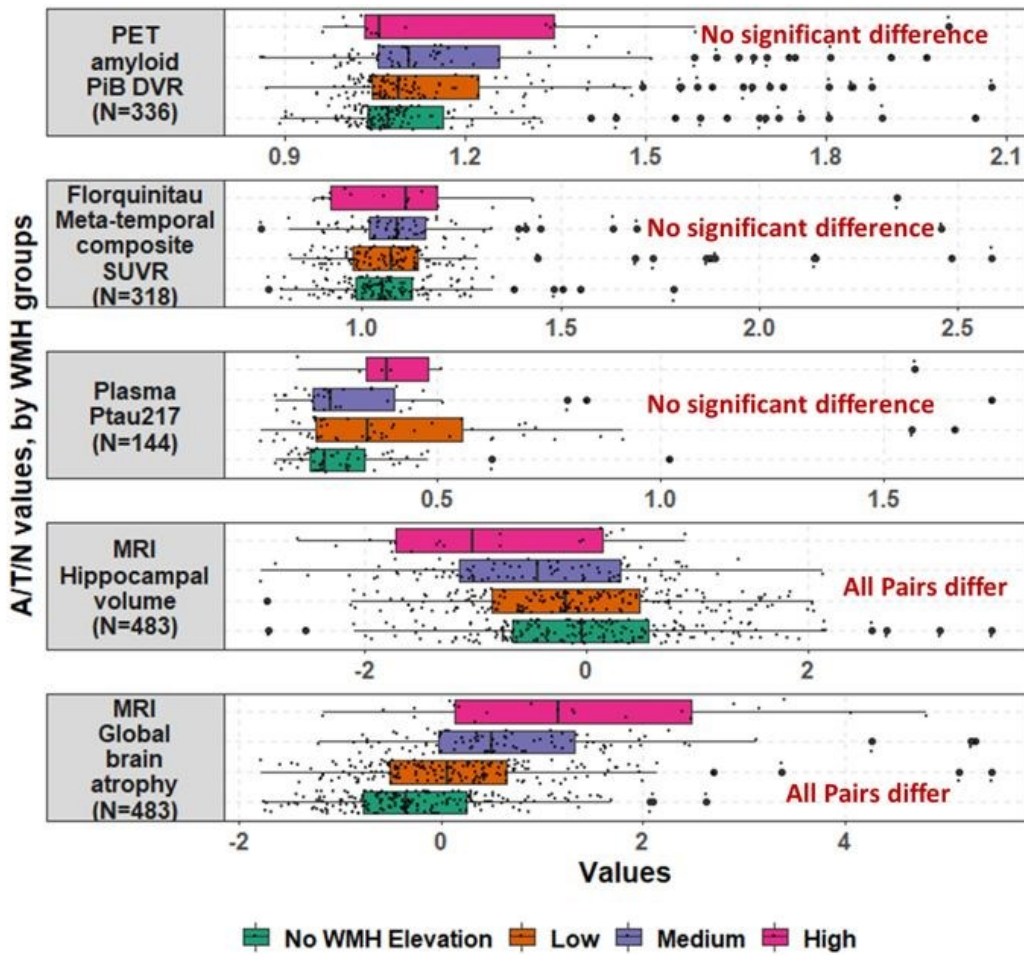


Fig. 3. Comparison most recent of PET amyloid measures, MK-6240, MRI outcomes and pTau217 across WMH lesion volume groups. Statistical tests: analysis of variance (ANOVA) for total hippocampus volume and global brain atrophy z score; Kruskal - Wallis for other continuous variables. Post hoc significant pairwise group differences using unadjusted method $P < 0.05$ are shown in the figure. The black dots stand for the raw values. One individual with Plasma pTau217 = 6.55 was excluded in Figure.

Keywords: white matter hyperintensities, Alzheimer's disease, A/T/N, Gaussian Mixture Modeling, cognition

P34 Medial temporal 18F-MK6240 levels are associated with global graph characteristics of functional connectivity from high-density EEG in the asymptomatic and prodromal stage of Alzheimer disease

Laure Spruyt^{1,2}, Mariska Reinartz^{1,2}, Gabriela Meade^{1,3}, Elvira Khachatryan⁴, Marc Van Hulle⁵, Koen Van Laere⁶, Patrick Dupont^{1,2}, Rik Vandenberghe^{1,2,7}

¹Laboratory for Cognitive Neurology, Department of Neurosciences, KU Leuven, Leuven, Belgium

²Alzheimer Research Centre KU Leuven, Leuven Brain Institute, Leuven, Belgium

³Department of Neurology, Mayo Clinic, 200 First Street SW, Rochester, MN, US

⁴Department of Neurology, Ghent University Hospital, Gent, Belgium

⁵Laboratory for Neuro- and Psychophysiology, KU Leuven, Leuven, Belgium

⁶Department of Nuclear Medicine & Molecular Imaging, University Hospitals Leuven, Leuven, Belgium

⁷Neurology Department, University Hospitals Leuven, Leuven, Belgium

Background: Functional connectivity is considered as the communication between spatially separated brain regions over time. We examined the effect of early spread of tau aggregates on global graph measures of brain connectivity from high-density EEG.

Methods: 25 cognitive normal (CN) individuals (age 68.7 ± 6.8 years, 9 male) and six patients in the prodromal stage of biomarker-proven Alzheimer disease (AD) (age 71.5 ± 7.2 years, 4 male) underwent cognitive testing, a 100 minute dynamic 18F-MK6240 PET scan and 128-channel resting-state EEG, measured in the eyes open and eyes closed condition, and analyzed in sensor space. The weighted Phase Lag Index was calculated and two global graph measures, characteristic path length and global clustering coefficient, were determined in four frequency bands and for each resting-state condition. Using a spearman correlation analysis with FDR correction, we examined how these global graph characteristics related to tau load in an a priori defined early-metaVOI comprising entorhinal and perirhinal cortex, hippocampus, parahippocampus and fusiform cortex. Furthermore, we examined the correlation with each of the constituent regions of the early-metaVOI and with a metaVOI that comprised inferior temporal cortex in addition.

Results: The DVR of 19 CN amyloid-negative subjects was 0.97 ± 0.07 , of the six CN amyloid-positive subjects was 1.11 ± 0.25 and of the six patients with prodromal AD 1.33 ± 0.36 . There was a significant correlation ($r = -0.38$; $p_{\text{corrected}} = 0.048$) between tau in the early-metaVOI and the global clustering coefficient in the alpha frequency band with eyes closed. The correlation between the global clustering coefficient and tau load in the entorhinal cortex ($r = -0.39$; $p_{\text{corrected}} = 0.04$), fusiform cortex ($r = -0.40$; $p_{\text{corrected}} = 0.03$) and with the larger metaVOI ($r = -0.39$; $p_{\text{corrected}} = 0.04$) was also significant.

Eyes closed condition in alpha frequency band

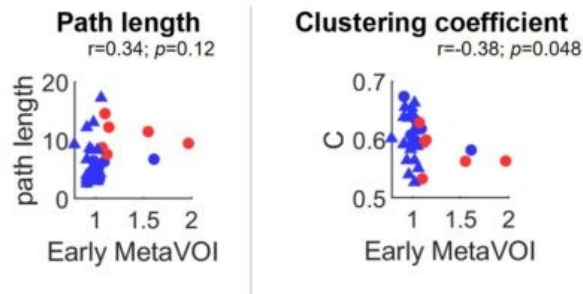


Figure 1: Tau load of early-metaVOI correlated with graph measures in the alpha frequency band during the eyes closed condition. The 19 blue triangles illustrate amyloid-negative cognitive normal subjects and the 6 blue dots represent the amyloid-positive cognitive normal subjects. The 6 red dots illustrate patients in the prodromal stage of biomarker-proven AD. C: clustering coefficient.

Conclusion: The global clustering coefficient was reduced with higher tau load in early affected regions, for the alpha frequency band with eyes closed. This suggests loss of coupling strength when tau pathology is present.

Keywords: Nuclear imaging, high-density EEG, Graph analysis, tau protein, Alzheimer's disease

P35 Longitudinal PET assessments of tau pathologies in progressive supranuclear palsy with 18F-florzolotau (PM-PBB3/APN-1607)

Hironobu Endo¹, Yuhei Takado¹, Kenji Tagai¹, Kiwamu Matsuoka¹, Naomi Kokubo¹, Kosei Hirata¹, Yuko Kataoka¹, Masaki Oya¹, Hideki Matsumoto^{1,2}, Shin Kurose¹, Masanori Ichihashi¹, Taku Hatano³, Shinji Saiki³, Shigeki Hirano⁴, Yoshikazu Nakano⁵, Shogo Furukawa⁶, Takahiro Takeda⁷, Sagiri Iose⁷, Hisamasa Imai⁸, Yohsuke Yagi⁹, Yoichiro Nishida⁹, Tatsuhiko Yuasa¹⁰, Maiko Ono¹, Chie Seki¹, Keisuke Takahata¹, Takahiko Tokuda¹, Hitoshi Shinotoh¹¹, Hitoshi Shimada¹², Kazunori Kawamura¹³, Ming-Rong Zhang¹³, Makoto Higuchi¹

¹Department of Functional Brain Imaging, Institute for Quantum Medical Science, Quantum Life and Medical Science Directorate, National Institutes for Quantum Science and Technology, Chiba, Japan

²Department of Oral and Maxillofacial Radiology, Tokyo Dental College, Tokyo, Japan

³Department of Neurology, Juntendo University Hospital, Tokyo, Japan

⁴Department of Neurology, Chiba University Hospital, Chiba, Japan

⁵Department of Neurology, Saiseikai Narashino Hospital, Chiba, Japan

⁶Department of Neurology, Japanese Red Cross Narita Hospital, Chiba, Japan

⁷Department of Neurology, National Hospital Organization Chiba-Higashi-Hospital, Chiba, Japan

⁸Department of Neurology, Tokyo Rinkai Hospital, Tokyo, Japan

⁹Department of Neurology, Tokyo Medical and Dental University Hospital, Tokyo, Japan

¹⁰Department of Neurology, Kamagaya General Hospital, Chiba, Japan

¹¹Neurology Clinic Chiba, Chiba, Japan

¹²Department of Functional Neurology & Neurosurgery, Center for Integrated Human Brain Science, Brain Research Institute, Niigata University, Niigata, Japan

¹³Department of Advanced Nuclear Medicine Sciences, Institute for Quantum Medical Science, Quantum Life and Medical Science Directorate, National Institutes for Quantum Science and Technology, Chiba, Japan

Objectives: 18F-florzolotau PET has been shown to capture four-repeat tau aggregates in progressive supranuclear palsy (PSP) with high contrast (Tagai et al., 2021), but its performance in time-course assays remains unknown. Here, we report a 1-year longitudinal investigation of tau PET data in PSP patients and healthy controls (HCs).

Methods:

Participants

Fifteen patients with probable PSP Richardson syndrome (PSP-RS), one with probable PSP-parkinsonism, and three HCs were recruited. One PSP-RS patient was A β -positive according to visual inspection of 11C-PiB-PET images, while the others were A β -negative.

Image analysis

Standardized uptake value ratio (SUVR) images were generated from PET images at 90–110 min after 18F-florzolotau injection. Reference voxels were extracted from the gray matter based on a frequency histogram of radioprobe retentions (Tagai et al., 2022). PSP-tau scores were also calculated using a machine learning-based analysis of multi-regional SUVRs with age-sex corrections (Endo et al., 2022).

Results

PSP-tau scores were significantly increased from 0.75 ± 0.57 to 0.86 ± 0.67 during the observation in PSP cases, while their change from -0.13 ± 0.23 to -0.20 ± 0.11 in HCs was insignificant (**Fig1**).

Changes in SUVRs from 1.59 ± 0.30 to 1.64 ± 0.33 in the globus pallidus and 1.52 ± 0.31 to 1.54 ± 0.32 in the midbrain of PSP cases were unremarkable (**Fig2**).

There was a significant correlation between chronological changes in PSP rating scale scores and PSP tau scores (Fig3).

Conclusion

Retentions of 18F-florzolotau in putatively tau-enriched regions of PSP patients showed only modest and insignificant increases over time, in line with a recent report showing the lack of progressive increases in 18F-MK6240 retentions among AD cases (Vaz et al., 2022). By contrast, PSP-tau scores increased over time in association with clinical disease advancement, supporting the potential utility of this AI-generated index for pursuing the evolution of tau pathologies.

Fig1: Annual change in PSP-tau scores

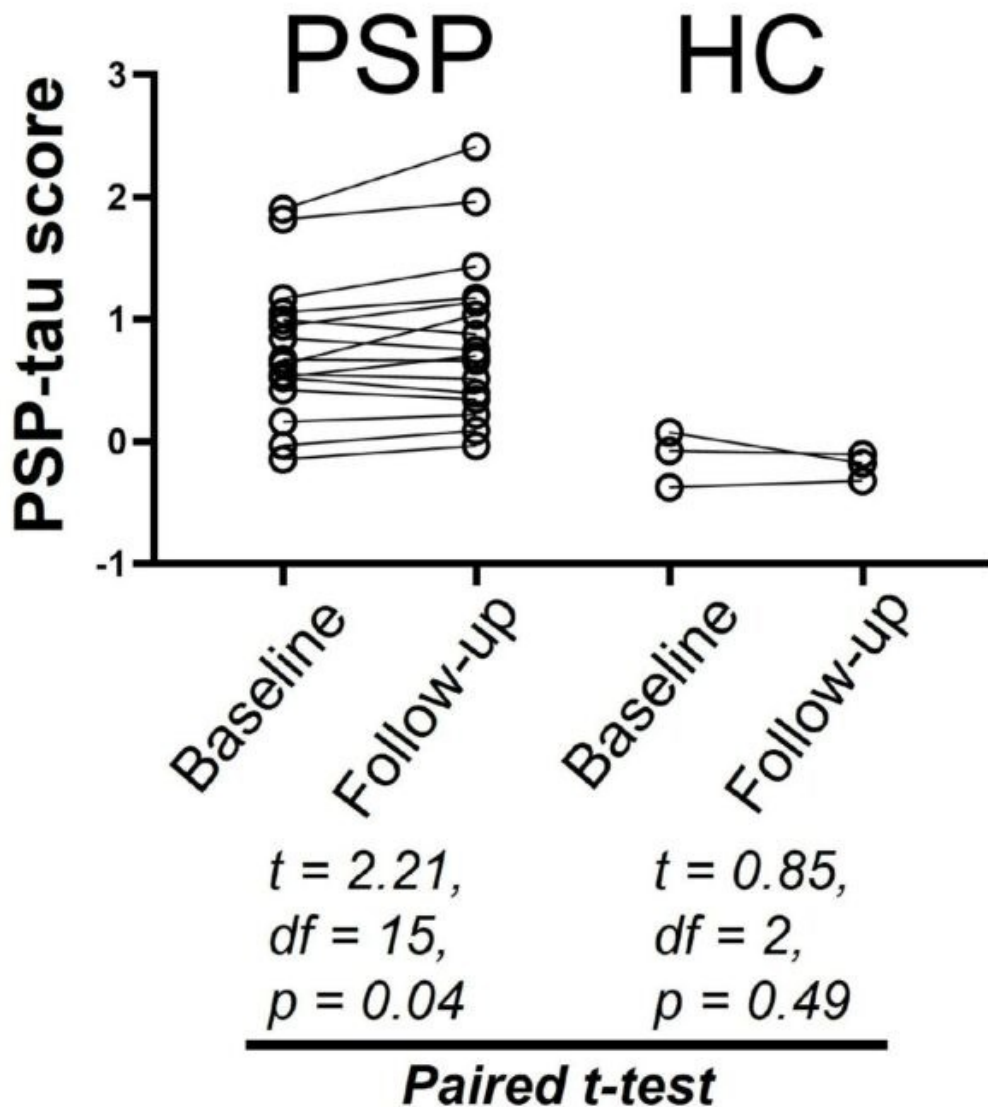


Fig2 : SUVRs annual changes in the globus pallidus and the midbrain

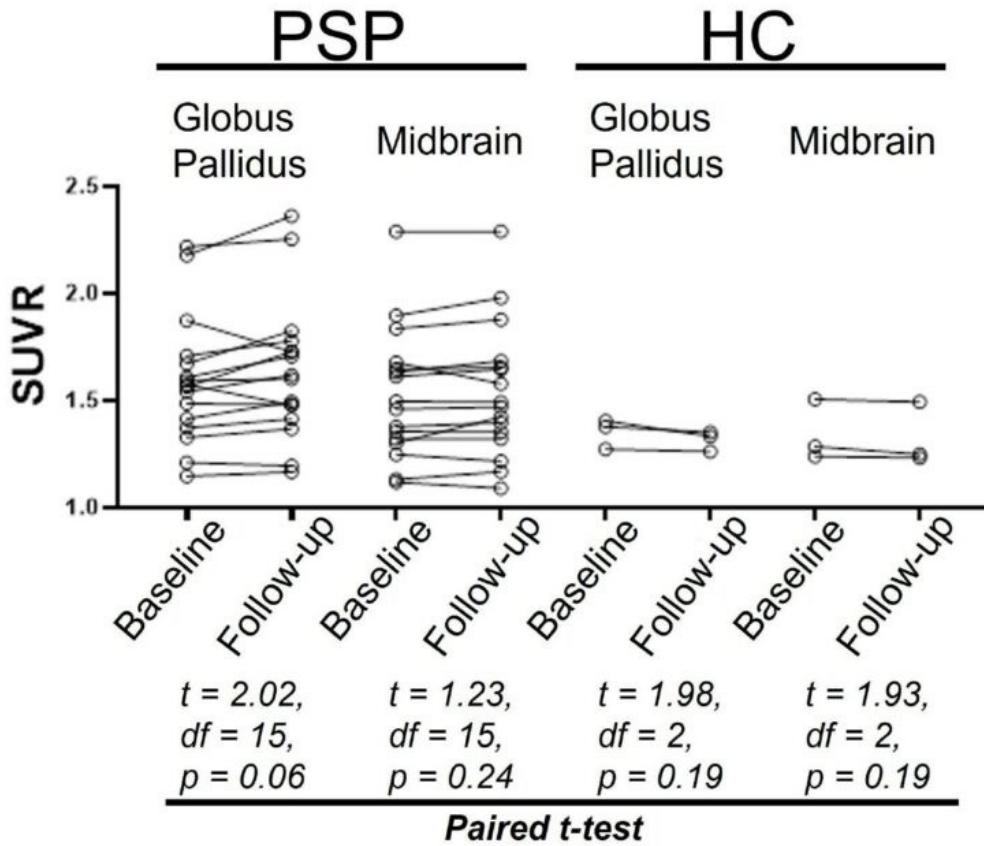
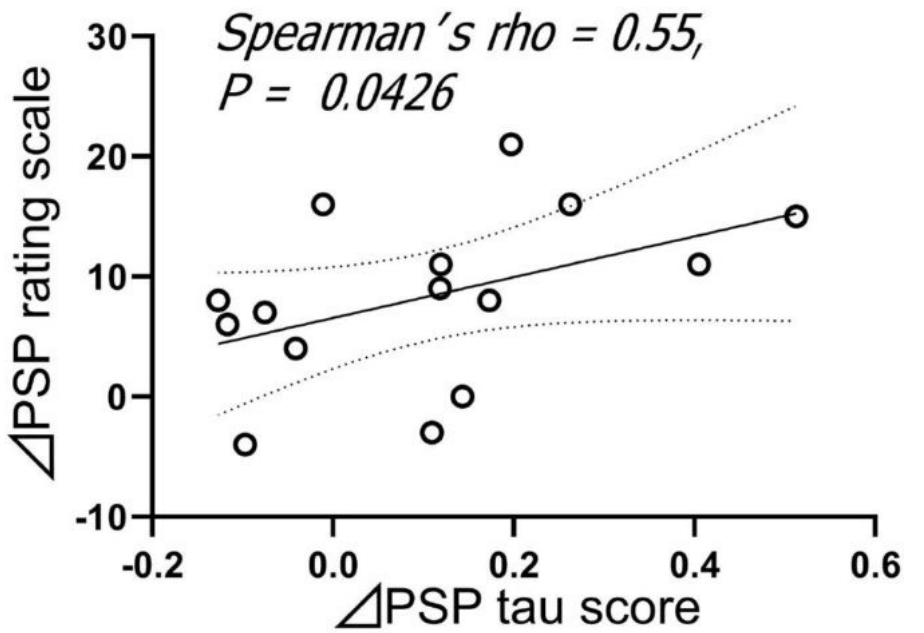


Fig3 : Chronological changes in PSP rating scale scores and PSP-tau scores



One case PSP rating scale data not available.

P36 Head-to-head comparison of tau PET tracers [¹⁸F]PI2620 and [¹⁸F]RO948 in non-demented individuals with brain amyloid deposition: the TAU-PET FACEHBI cohort

Gregory Klein¹, Marta Marquié^{2,3}, Oscar Sotolongo-Grau², Núria Roé-Vellvé⁴, Santiago Bullich⁴, Juan Pablo Tartari², Angela Sanabria^{2,3}, Ainhoa García-Sánchez², Edilio Borroni¹, Christopher Galli¹, Matteo Tonietto¹, Esther Pérez-Martínez⁴, Lluís Tàrraga^{2,3}, Agustín Ruiz^{2,3}, Andrew W. Stephens⁴, Mercè Boada^{2,3}

¹Roche Pharma Research and Early Development, Basel, Switzerland

²Ace Alzheimer Center Barcelona – Universitat Internacional de Catalunya, Barcelona, Spain

³Centro de Investigación Biomédica en Red de Enfermedades Neurodegenerativas (CIBERNED), Instituto de Salud Carlos III, Barcelona, Spain

⁴Life Molecular Imaging GmbH, Berlin, Germany

Introduction and aims: Second generation tau radiotracers for positron emission tomography (PET) show high affinity to paired helical filaments tau deposits characteristic of Alzheimer's disease (AD) and low off-target binding. Differences in chemical structure though may lead to variations in their regional *in vivo* uptake. We aimed to compare the *in vivo* uptake of [¹⁸F]PI2620 and [¹⁸F]RO948 in early stages of the AD continuum.

Methods: Data from the TAU-PET FACEHBI study, a clinical trial (EUDRA-CT 2021-000473-83) performed at Ace Alzheimer Center Barcelona, were analyzed. Participants underwent neurology evaluation and cognitive testing and were not demented. All participants were scanned with [¹⁸F]PI2620 and [¹⁸F]RO948 within 3 months. They also underwent Florbetaben-PET max. 13 months before the tau-PET scans. Florbetaben centiloid values ranged from 17-159. Tau-PET images were quantified using FreeSurfer and standardized uptake value ratios (SUVR) in brain regions from the Braak staging.

Results: The cohort consisted of 17 individuals with subjective cognitive decline (n=13) and mild cognitive impairment (n=4). Mean age of the sample was 73.65±6.33, 52.9% were male, mean education was 15.81±4.83 years and 65% were APOE ε4 carriers. *In vivo* tau uptake was not significant when Florbetaben CL was < 50. SUVR measurements for [¹⁸F]PI2620 and [¹⁸F]RO948 showed high correlation in all Braak staging regions (R² range [0.65, 0.79], **Figure 1**). Visual reading showed that both tau tracers presented a distinct off-target signal pattern but had similar tau pathology distribution (**Figure 2**).

Conclusions: In a cohort of individuals in early stages of the AD continuum (SCD and MCI with brain amyloid deposition), both tau-PET tracers [¹⁸F]PI2620 and [¹⁸F]RO948 showed similar *in vivo* tau uptake in all brain regions from the Braak staging. These preliminary results support the development of standardized quantification scales that are tracer independent.

Keywords: Tau, RO948, PI2620

Wednesday, January 11, 2023 - 11:15 am - 12:35 pm

Podium Session

SESSION II: Technical advances for clinical applications

Wednesday, January 11, 2023		
11:15 am – 12:35 pm	SESSION II: TECHNICAL ADVANCES FOR CLINICAL APPLICATIONS	CHAIRS: Suzanne Baker, PhD, <i>Lawrence Berkeley National Laboratory</i> Bradley Christian, PhD, <i>University of Wisconsin, Madison</i>
11:15	Introduction	Chairs
11:20	Minimizing sample sizes for trials using MK-6240 outcomes: impact of processing method and choice of reference and target tissues	J. Alex Becker, PhD, <i>Massachusetts General Hospital</i>
11:35	Inferring full ATN status from tau-PET using deep learning	Nicolai Franzmeier, PhD, <i>LMU Munich</i>
11:50	Longitudinal modelling of tau transport and production dynamics in the human brain	Pavan Chaggar, PhD, <i>University of Oxford</i>
12:05	Connectivity- versus gradient-based approaches to predict regional tau-PET across Alzheimer's disease variants	Nick Corriveau-Lecavalier, PhD, <i>Mayo Clinic, Rochester</i>
12:20	Measuring tau in the basal forebrain: a comparison of MK6240 and flortaucipir	Theresa Harrison, PhD, <i>University of California, Berkeley</i>
12:35	Discussion	

Minimizing sample sizes for trials using MK-6240 outcomes: impact of processing method and choice of reference and target tissues

J. Alex Becker¹, Kuang Gong¹, Amal Tiss¹, Cristina Lois¹, Emma Thibault¹, Jessie Fanglu Fu¹, Justin Sanchez³, Brian Healy², Marc Normandin¹, Julie Price¹, Georges El Fakhri¹, Keith Johnson¹

¹Massachusetts General Hospital, Boston, MA, US

²Harvard T.H. Chan School of Public Health, Boston, MA, US

³Washington University School of Medicine, St. Louis, MO, US

Introduction: Processing method and choice of target and reference tissues impact parameter-estimates and variances when modeling PET data for clinical trial design. We investigated effects of these choices on estimated sample-sizes required to detect tau change-rate differences using PiB and longitudinal MK-6240 data in a cohort of amyloid+ subjects.

Methods: PiB and MK-6240 PET acquired on a GE-MI tomograph for N=30 ab+ (PiB FLR>1.14 DVR) subjects were processed using two processing pipelines: OSEM-reconstruction and neighboring-frame motion-correction (MC) with/without GTM-PVC (“GE-OSEM”), and MR-guided OSEM reconstruction (ref. 1; see Figure 1 caption) and data-driven MC (“Kernel”)(2). MK-6240 PET (0-8 min) was registered to Freesurfer-processed T1-MR and quantified by SUVR (90-110min) in Desikan atlas regions and aggregates. Five reference tissues were considered: cerebellar-cortex, cerebellar-cortex with 3mm erosion, cerebellar-white-matter, cerebral-white-matter, and 4mm eroded cerebral-white-matter. PiB was quantified by Logan DVR (40-60 min, cerebellar-cortex reference). Longitudinal mixed-effects models (random intercept and slope) were fit to log-transformed tau-SUVR data. Tau change-rates and variance-components were used to estimate sample sizes by analytic formulae (3,4). Sample sizes and their bootstrapped confidence intervals were derived for each target region assuming treatment- and placebo-group change-rates in the target differed by a fraction of that target’s mean change-rate, for a hypothetical trial with 3 PET time-points: baseline, 1 and 2yrs.

Results: The amygdala quantified using cerebellar-white-matter reference and kernel processing yielded the smallest estimated sample size and variance to detect a 30% treatment-effect: 50 subjects/arm (95% CI: 23,102), closely followed by RCPCAM and cerebellar-cortex reference (Table 2). Eroded references, cerebral-white-matter reference and GE-OSEM-processed GTM-PV-corrected data performed less-well; e.g., size/arm 162 (95% CI: 67,485) for kernel-processed amygdala with 4mm-eroded white-matter-reference.

Conclusions: Optimizing processing and analysis of PET data can reduce sample sizes, thereby reducing subject burden, trial cost and duration.

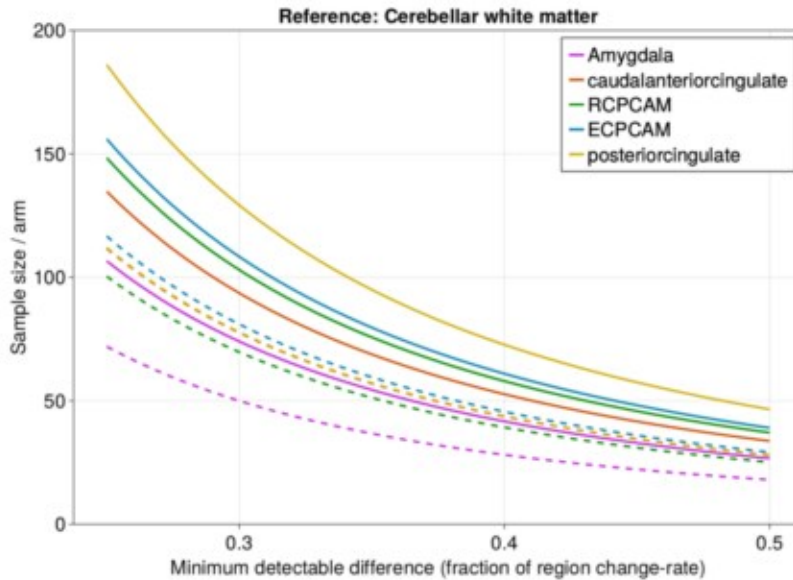
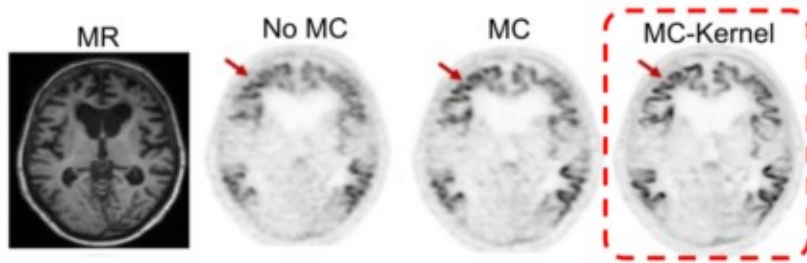


Figure 1. (A) Example of PET processing via the “kernel” pipeline. The structural MR (left) is used during OSEM reconstruction to enhance PET resolution. “No MC” illustrates an uncorrected “raw” PET slice, “MC” the same slice corrected by dynamic motion correction, and “MC-Kernel” shows reconstruction by the kernel method (1,2). Specific tau binding in cortical ribbon is visually isolated with MC-Kernel correction (red arrow). (B) Estimated sample size curves derived from a pilot cohort of N=30 ab+ subjects with MK-6240 parameterized by SUVR with cerebellar white matter reference. Solid and dashed curves show estimated sample size per arm (y-axis) as a function of fraction of the target tissue’s change-rate (x-axis) for GE-OSEM and kernel processing, respectively. Target tissues are arranged in the legend by increasing sample size by GE-OSEM processing, with amygdala found to have the smallest sample size for both processing pipelines. ECPCAM and RCPCAM are aggregates of entorhinal cortex + parahippocampal cortex + amygdala, and rhinal cortex + parahippocampal cortex + amygdala, respectively. Sample sizes were estimated assuming 0.80 power, significance $\alpha < 0.05$, and for a trial with PET samples at baseline, 1 and 2 years. For numerical values see Table 2.

- 1) Gong, K et al. “Correction of partial volume effects for tau PET imaging using the kernel method”, Human Amyloid Imaging, 2020.
- 2) Tiss, A et al. “Impact of motion correction on longitudinal [18F]-MK6240 tau PET imaging” SNMMI Annual Meeting 2022.
- 3) Diggle, P “Analysis of Longitudinal Data” Oxford Univ. Press 2013
- 4) Zhao, Y and Edland, SD “Power formulas for mixed effects models with random slope and intercept comparing rate of change across groups” Int. J. Biostat. 2022; 18(1): 173–182.

N = 30	Mean (SD) [min-max]
Age	72.4 (9.3) [52-87]
Sex: F	15 (50%)
Education (yr)	17 (3) [11-20]
MMSE	26.7 (4.1) [13-30]
a β (centiloids)	53.4 (34.5) [7-124]
a β FLR (DVR,CG)	1.56 (0.31) [1.14-2.20]
IT BL tau (SUVR,CG)	1.66 (1.21) [0.84-6.05]
Time-points (N)	2.4 (1.1) [1-4]
Follow-up (yr)	1.48 (1.18) [0.00-3.03]
APOE e4+	11 (41%)

Table 1: Subject demographics and other statistics. *IT BL: inferior-temporal MK6240 tau measure at baseline; CG: cerebellar grey reference tissue. FLR is an aggregate cortical region prone to amyloid accumulation.

	Frac	Cerebellum white matter		Cerebellum cortex	
		Sample size (95% CI) GE-OSEM	Sample size (95% CI) Kernel	Sample size (95% CI) GE-OSEM	Sample size (95% CI) Kernel
amygdala	30%	74 (31,169)	50 (23,102)	120 (50,307)	68 (34,142)
RCPCAM	30%	103 (43,262)	69 (31,159)	133 (54,400)	77 (34,173)
ECPCAM	30%	108 (43,285)	81 (39,179)	141 (56,481)	99 (43,236)
entorhinal	30%	152 (61,506)	170 (69,555)	241 (75,1254)	268 (90,1528)
rhinal	30%	146 (56,454)	119 (46,353)	219 (69,1282)	147 (54,526)
parahippocampal	30%	163 (62,642)	91 (44,215)	161 (65,525)	93 (44,214)
inferiortemporal	30%	303 (78,2460)	202 (64,1190)	248 (72,1398)	179 (59,705)
amygdala	40%	42 (17,96)	28 (13,58)	68 (28,174)	38 (19,80)
RCPCAM	40%	58 (24,148)	39 (17,90)	75 (31,227)	44 (19,98)
ECPCAM	40%	61 (25,161)	46 (22,101)	80 (32,273)	56 (24,134)
entorhinal	40%	86 (34,287)	96 (39,315)	137 (43,711)	152 (51,867)
rhinal	40%	83 (32,257)	68 (26,200)	124 (39,727)	83 (31,298)
parahippocampal	40%	93 (35,364)	52 (25,122)	91 (37,298)	53 (25,121)
inferiortemporal	40%	172 (44,1395)	115 (36,675)	141 (41,793)	102 (34,400)

Table 2: Sample size estimates and 95% confidence intervals determined by 3000 bootstrap resamples for MK-6240 tau PET data (SUVR 90-110 min) in target tissues (rows), to detect a minimum change-rate difference expressed as a fraction (column 2) of the mean change-rate in that tissue. Results are shown for both GE-OSEM and kernel processing methods and for two reference tissues: cerebellar white matter (columns 3 and 4) and cerebellar cortex (columns 5 and 6).

Keywords: PET processing, MK-6240, sample size, tau, power

Inferring full ATN status from tau-PET using deep learning

Nicolai Franzmeier^{2,4,7}, Paul Hager¹, Davina Biel², Anna Dewenter², Anna Steward², Sebastian Römer^{2,3}, Anna Rubinski², Martin Dichgans^{2,4,5}, Daniel Rückert¹, Michael Ewers^{2,5}, Matthias Brendel^{4,6}

¹*Institute for AI and Informatics in Medicine, Klinikum rechts der Isar Technical University of Munich, Munich, Germany*

²*Institute for Stroke and Dementia Research (ISD), University Hospital, LMU Munich, Munich, Germany*

³*Department of Neurology, University Hospital, LMU Munich, Munich, Germany*

⁴*Munich Cluster for Systems Neurology (SyNergy), Munich, Germany*

⁵*German Center for Neurodegenerative Diseases (DZNE), Munich, Germany*

⁶*Department of Nuclear Medicine, University Hospital, LMU Munich, Munich, Germany*

⁷*University of Gothenburg, The Sahlgrenska Academy, Institute of Neuroscience and Physiology, Department of Psychiatry and Neurochemistry, Gothenburg, Sweden*

Alzheimer's disease (AD) is biologically defined by the presence of beta-amyloid (A) and tau (T) followed by neurodegeneration (N) and cognitive decline. This biological framework of AD has been summarized in the ATN framework, which allows an unbiased, biological classification system for AD, to aid in research, clinical decision making and stratifying patients for clinical trials. However, full ATN classification requires multiple, cost intensive and often invasive biomarker assessments, including PET, lumbar puncture and MRI. Tau deposition as assessed via tau-PET typically follows amyloid deposition and precedes neurodegeneration and cognitive decline and is increasingly used as an essential imaging modality for research and in diagnostic settings. Since tau pathology mediates the link between amyloid deposition and neurodegeneration, we tested whether full ATN classification can be inferred from a single tau-PET scan. Therefore, we applied neural network-based deep learning to regional tau-PET from N=907 individuals of the Alzheimer's disease neuroimaging initiative cohort. The sample spanned the clinical spectrum from cognitively normal, mild cognitively impaired to dementia patients from which a dedicated test set of N=212 were held out for model evaluation. In the held-out test set, we find strong predictive accuracy of the trained deep learning model to predict continuous amyloid-PET ($r=0.80$, $p<0.001$) and MRI-based grey matter density data ($r=0.76$, $p<0.001$), consistently across diagnostic groups (Fig.1) and brain regions (Fig.2). Further, we achieve AUCs of 0.89 and 0.82 for predicting global amyloid-PET positivity and neurodegeneration status (i.e. based on hippocampal atrophy) respectively, purely based on tau-PET. Full tau-PET-based ATN classification accuracy is 0.71. These findings suggest that tau-PET can be used for inferring a proxy of full ATN status from a single image, as well as inferring regional amyloid deposition and neurodegeneration patterns, which can be critical for participant screening and selection in clinical trials.

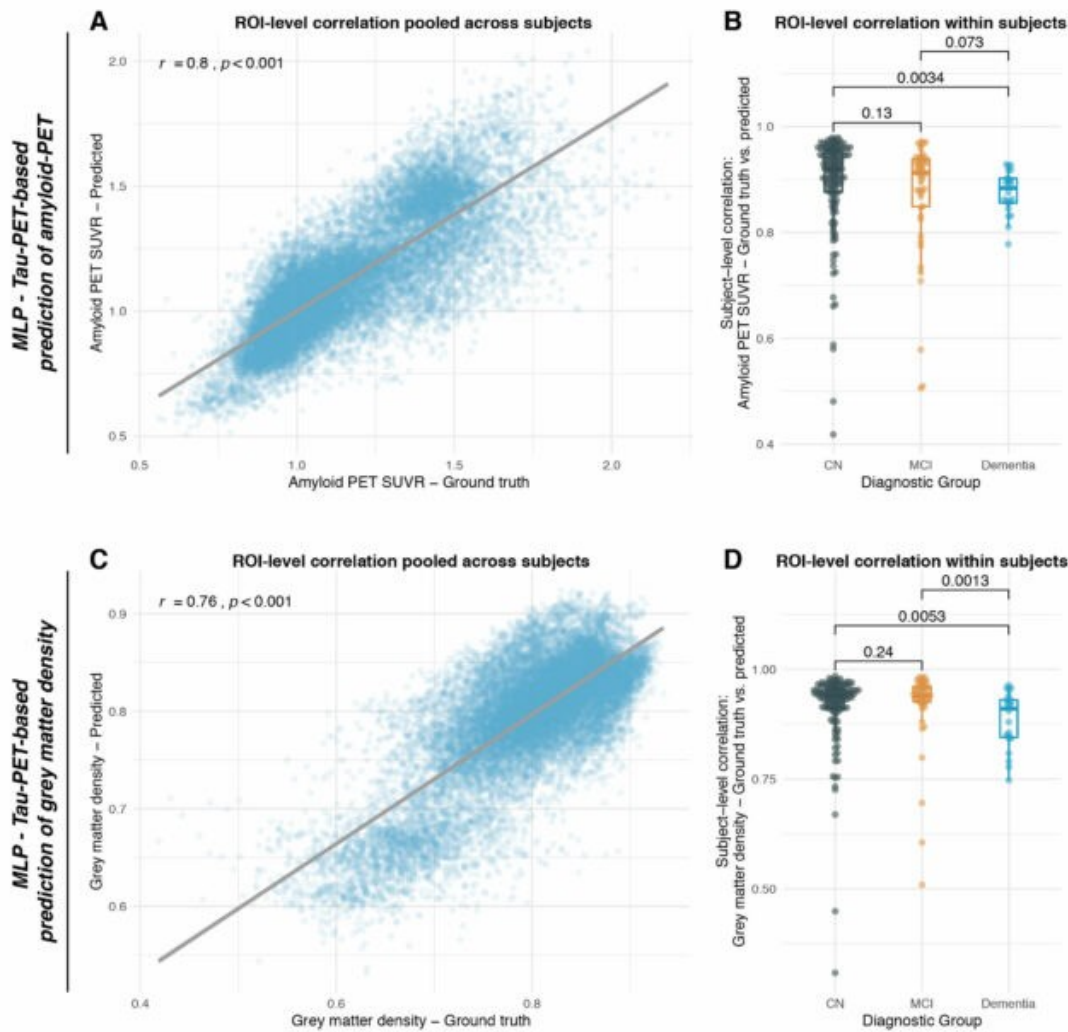


Figure 1: Tau-PET based prediction of regional amyloid-PET uptake and MRI-based neurodegeneration. Scatterplots illustrate the association between ground-truth regional amyloid-PET SUVRs and those inferred by the tau-PET-based MLP model (A), when assessed across all ROIs pooled across subjects. Assessing within-subject correlations for predicted regional ground-truth vs. predicted amyloid-PET SUVRs showed high accuracy across diagnostic groups (B). Equivalent plots are shown for the tau-PET-based prediction of MRI-based grey matter density as a proxy of neurodegeneration pooled across subjects (C) as well as subject-level correlations split by diagnostic groups (D).

Tau-PET-based prediction accuracy - ROI-level

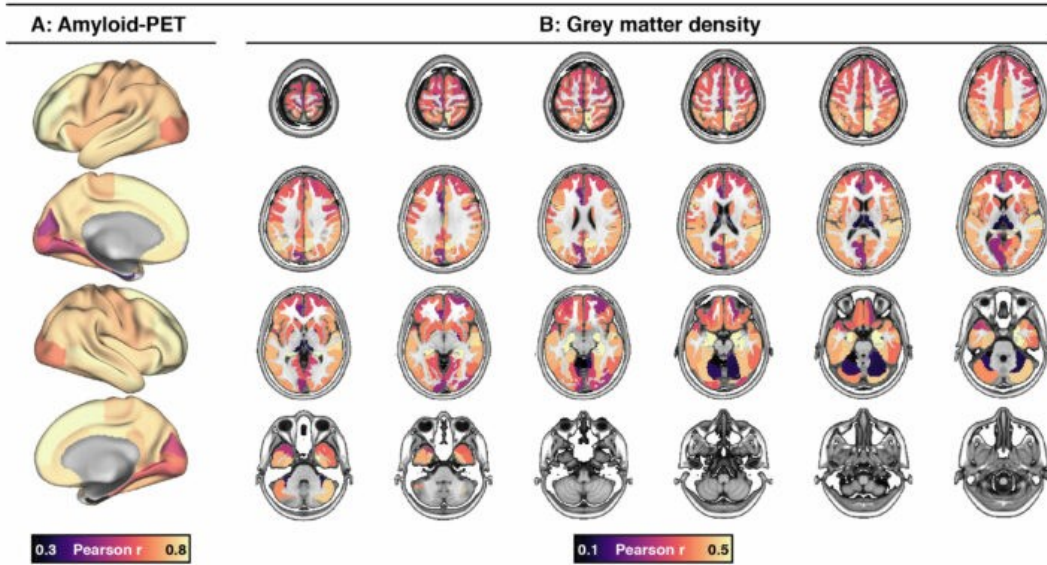


Figure 2: Surface renderings, illustrating the regional prediction accuracy for the MLP models to predict brain-wide amyloid-PET SUVRs (A) as well as MRI-based grey matter density as a proxy of neurodegeneration (B). Note that highest prediction accuracy for predicting grey matter density was found for the hippocampus, which was subsequently used for assessing neurodegeneration status (i.e. N).

Keywords: Tau-PET, ATN staging, deep learning, amyloid, neurodegeneration

Longitudinal modelling of tau transport and production dynamics in the human brain

Pavan Chaggar¹, Jacob Vogel², Saad Jbabdi¹, Alexa Pichet Binette², Olof Strandberg², Erik Stomrud², Gregory Klein⁴, Stefano Magon⁴, Oskar Hansson^{2,3}, Alain Goriely¹

¹University of Oxford, Oxford, UK

²Lund University, Lund, Sweden

³Skåne University Hospital, Sweden, UK

⁴F. Hoffmann-La Roche Ltd, Basel, Switzerland

Introduction: Tau spreads through the brain during Alzheimer's disease (AD), though it is unclear whether this process is dominated by increased production or transport (or both) of tau. This question can be resolved by finding parsimonious models of tau spread and interrogating their parameters. We derive a physics-informed, connectome-based generative model of tau spread to predict longitudinal tau-PET spread in the human brain

Methods: 96 subjects with at least three tau-PET scans from ADNI were divided into three groups, amyloid negative (A-), amyloid positive tau negative (A+T-) and amyloid positive tau positive (A+T+). Mean AV1451 signal was summarised over the cortical regions of the Desikan-Killiany atlas. We use a dynamical system with only two free parameters to describe tau proteinopathy as a combination of transport through the structural (white matter) connectome and regional growth by a prion-like process (Figure 1). We augment the model with regionally specific baseline values and carrying capacities derived from mixture modelling. We use hierarchical Bayesian inference to calibrate the model to each of the subject groups. The analysis was validated on 135 subjects with at least 3 tau-PET scans from the BioFINDER-2 cohort.

Results: over time (Figure 2). Our results show that AD is primarily driven by growth of toxic tau, with fast accumulation and slow transport. A+T- subjects display faster transport through the brain network, whereas that A+T+ shows higher growth, indicating greater movement of tau during early AD before an acceleration of growth when participants harbor high levels of both amyloid and tau proteins. Our Bayesian approach allows for predictions of future tau-PET levels that account for uncertainty (Figure 3).

Conclusions: A regionally specific dynamical model of tau proteinopathy accurately describes longitudinal tau-PET data. Our model suggests transport vs production dynamics change across the AD timeline.

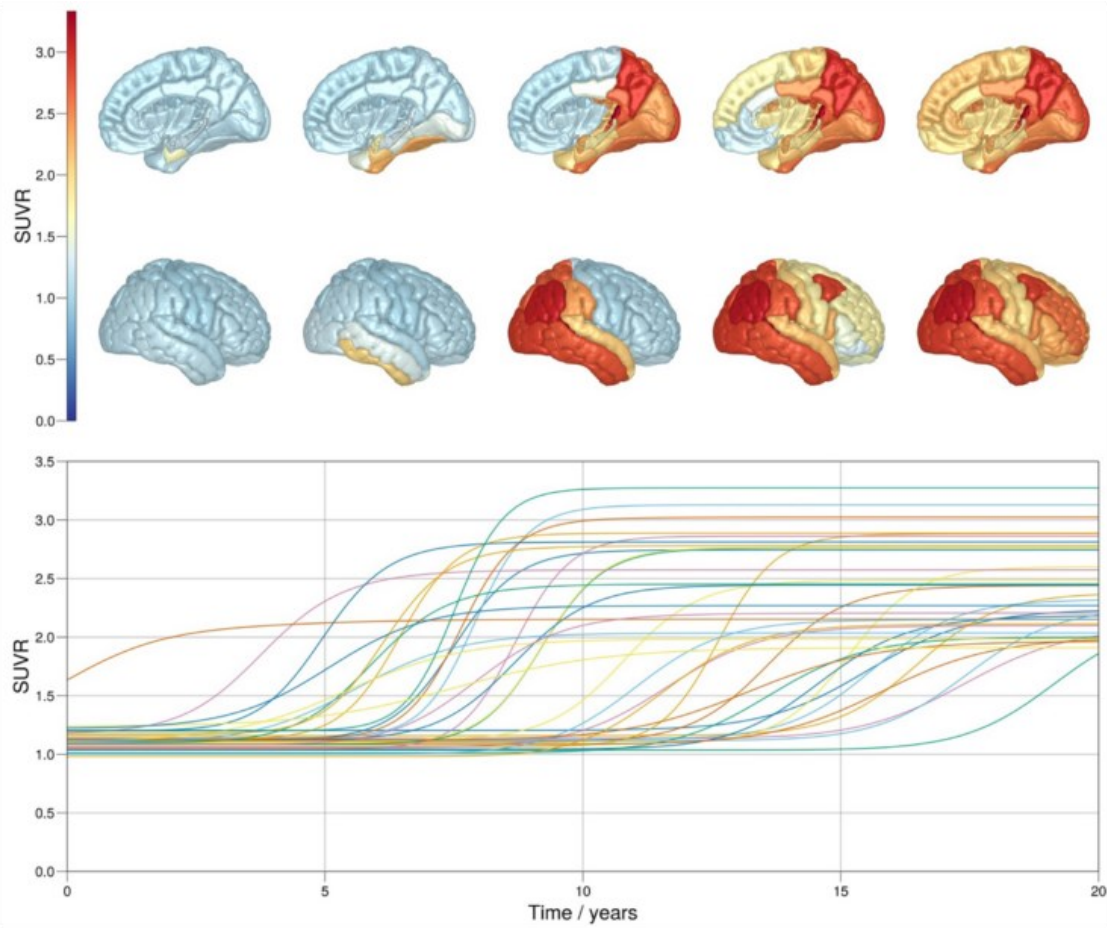


Figure 1. **Physics based model of tau PET** in a growth dominated region with synthetic global parameters (diffusion coefficient = 0.05, growth = 1.0) and an initial seeding of 50% in the entorhinal cortex. (Top) Visualisation of protein spread and growth on the right hemisphere at $t = [0.0, 5.0, 10.0, 15.0, 20.0]$. (Bottom) Time series for regions in the right hemisphere, showing regionally heterogeneous baseline values and varying capacities. Each line represents a brain region.

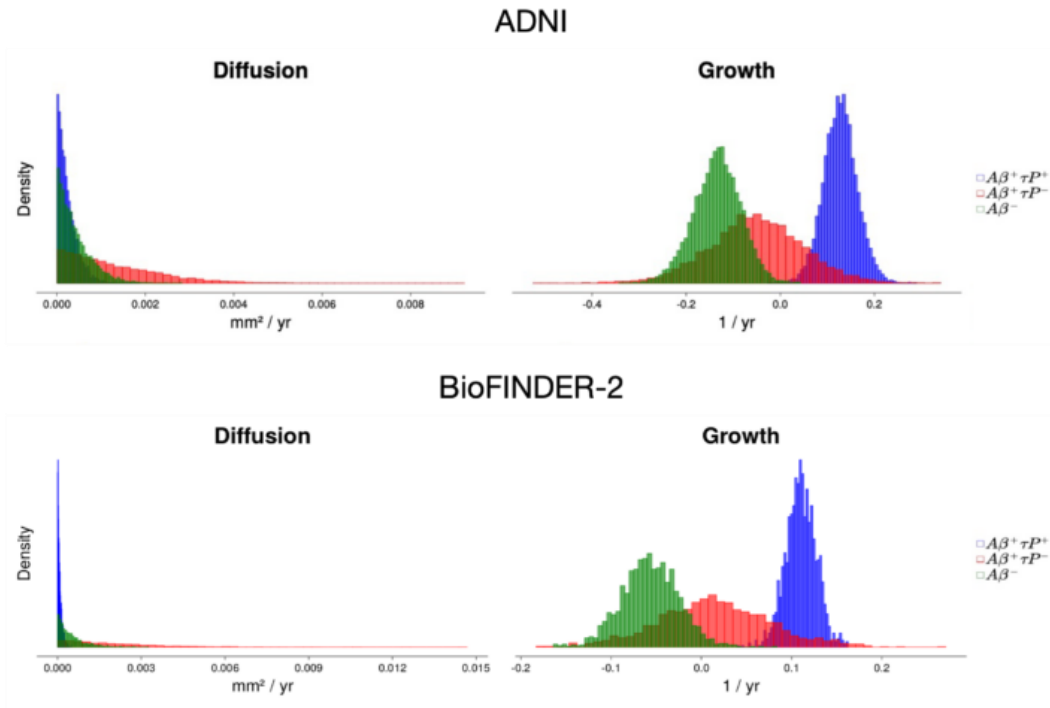


Figure 2. Posterior distributions for model parameters using ADNI data (top) and BioFINDER 2 data (bottom). (Left) Diffusion coefficient. Both A- and A+T+ are heavily skewed toward zero, whereas the A+T- have a wider tail, indicating a higher level of transport through the structural connectome. (Right) Growth coefficient. As tau accumulates, there is an acceleration in disease progression, with A+T+ progressing the fastest, followed by A+T- and A-. Subjects are classified as A- if they have subthreshold amyloid PET or CSF biomarkers; subjects are classified as T- if they have subthreshold tau-PET in both the medial temporal lobe (entorhinal cortices and amygdalae) or lateral temporal lobe (inferior temporal and middle temporal) and T+ if they are suprathreshold in either of these regions

ADNI

BioFINDER-2

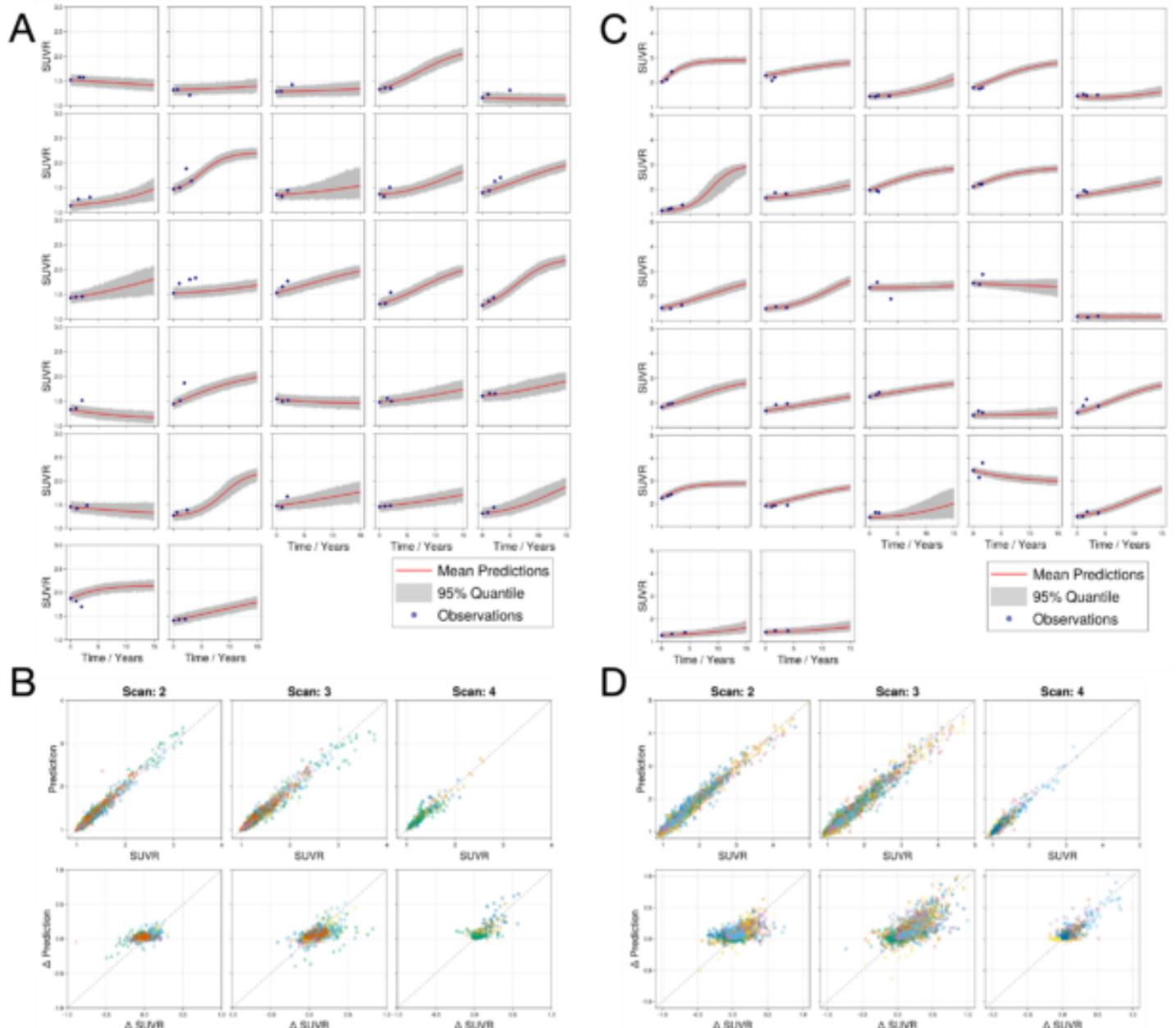


Figure 3. Posterior predictive simulations for the A+T+ group in ADNI and BioFINDER-2. (A-B) show posterior predictions for the ADNI A+T+ cohort. (C-D) show posterior predictions for 27 subjects in the BioFINDER-2 A+T+ cohort. (A, C) Simulated trajectories using samples from the posterior distributions of the model and noise parameters for ADNI (A) and BioFINDER-2. Most data points are described by the dynamics and noise model, as captured by the 95% quantiles. Data points that are not captured are likely due to either (1) constraints of a uniform growth rate across regions or (2) lack of coupling with important factors such as amyloid (regional acceleration) or atrophy (regional decline in SUVR). (B, D) Top row show predicted SUVR vs observed SVR, bottom show predictive change in SUVR vs observed change in SUVR.

Keywords: tau-PET, longitudinal, modelling

Connectivity- versus gradient-based approaches to predict regional tau-PET across Alzheimer's disease variants

Nick Corriveau-Lecavalier¹, Hugo Botha¹, Julia Schumacher^{2,3,4}, Ellen Dicks¹, Leland Barnard¹, Jeyeon Lee², Irene Sintini², Jeffrey Gunter², Michael Kamykowski⁵, Jonathan Graff-Radford¹, Bradley Boeve¹, Val Lowe², Kejal Kantarci², David Knopman¹, Jennifer Whitwell², Keith Josephs¹, Ronald Petersen¹, Clifford Jack², David Jones^{1,2}

¹Department of Neurology, Mayo Clinic, Rochester, MN, US

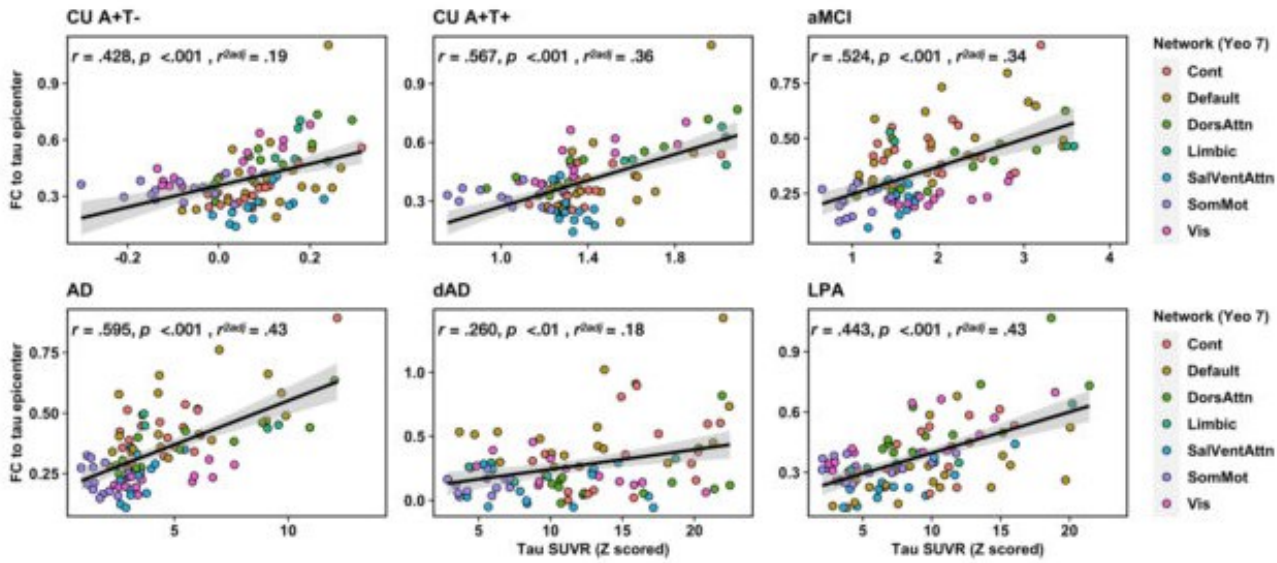
²Department of Radiology, Mayo Clinic, Rochester, MN, US

³German Center for Neurodegenerative Diseases (DZNA) Rostock-Greifswald, Rostock, Germany

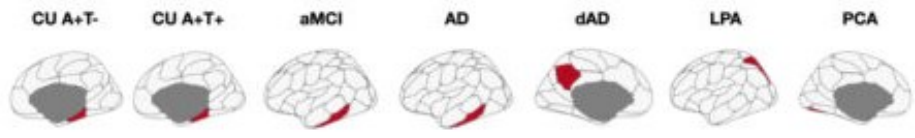
⁴Department of Neurology, University Medical Center Rostock, Rostock, Germany

⁵Department of Information Technology, Mayo Clinic, Rochester, MN, US

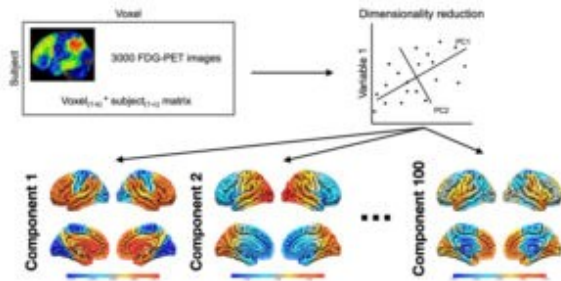
Predictive models of tau have largely relied on the functional connectome to estimate its spatial patterns in Alzheimer's disease (AD). Gradients of macro-scale organization represent a promising avenue as they encapsulate many biological properties relevant to cognition and degeneration. We compared connectivity (from task-free fMRI)- and gradient-based (from FDG-PET) approaches to predict regional tau-PET in individuals spanning the phenotypic spectrum of AD. This included 430 cognitively unimpaired (CU) individuals (214 A+T-, 216 A+T+) and 62 mild cognitive impairment (aMCI), 64 AD, 21 dysexecutive AD (dAD), 41 logopenic aphasia (LPA) and 49 posterior cortical atrophy (PCA) patients (all A+T+) from the ADRC/MCSA/NRG cohorts (Mayo Cohort). The connectivity approach consisted in assessing the relationship between a region's tau level and its functional connectivity to the region of highest tau (epicenter). This yielded adjusted R^2 values ranging from 0.19-0.45 across groups (Fig.1). The gradient-based approach consisted in 1) performing a principal component analysis on 3000 FDG-PET images that did not overlap with the Mayo cohort, 2) projecting FDG-PET images of the Mayo cohort onto the low-dimensional space generated in (1) and extracting corresponding weights across the first 100 components, 3) using these weights as predictors of regional tau-PET in a linear model, and 4) using this model to predict tau in the ADNI cohort ($n = 86$) (Fig.2). The model yielded averaged adjusted R^2 and predicted R^2 values of 0.71 and 0.63, respectively, in the Mayo cohort. Out-of-sample median R^2 in the ADNI cohort was 0.41 (range 0.10-0.60) when excluding primary sensorimotor cortices (Fig.3). An unbiased gradient-based approach based on an imaging modality widely used in clinical settings outperformed a connectome-based one to predict regional tau-PET across the AD phenotypic spectrum. Patterns of tau accumulation may better relate to the large-scale physiology of the brain underlying specific mental functions rather than focal toxicity.



Epicenters (regions with highest tau)



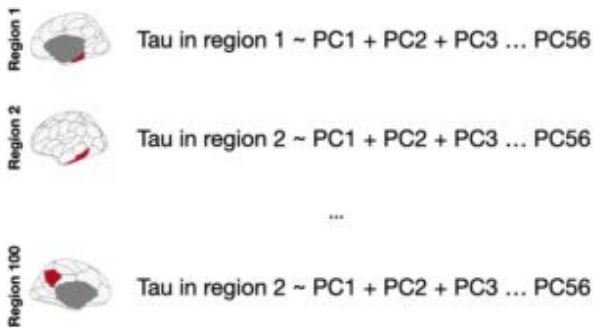
1) Principal component analysis on FDG-PET images from 3000 unique patients from Mayo Clinic



2) Projection of the Mayo cohort and extraction of component weights

	PC1	PC2	PC3	...	PC100
CU A+T-, n = 143	-0.15	-0.26	0.53	...	0.67
CU A+T+, n = 152	-0.98	0.47	-0.32	...	-0.89
aMCI, n = 43					
AD, n = 51					
dAD, n = 18					
LPA, n = 26					
PCA, n = 24	0.10	-0.56	-0.54	...	0.78

3) Regression models between regional tau and component weights and finding optimal parameters based on R^{2pred}



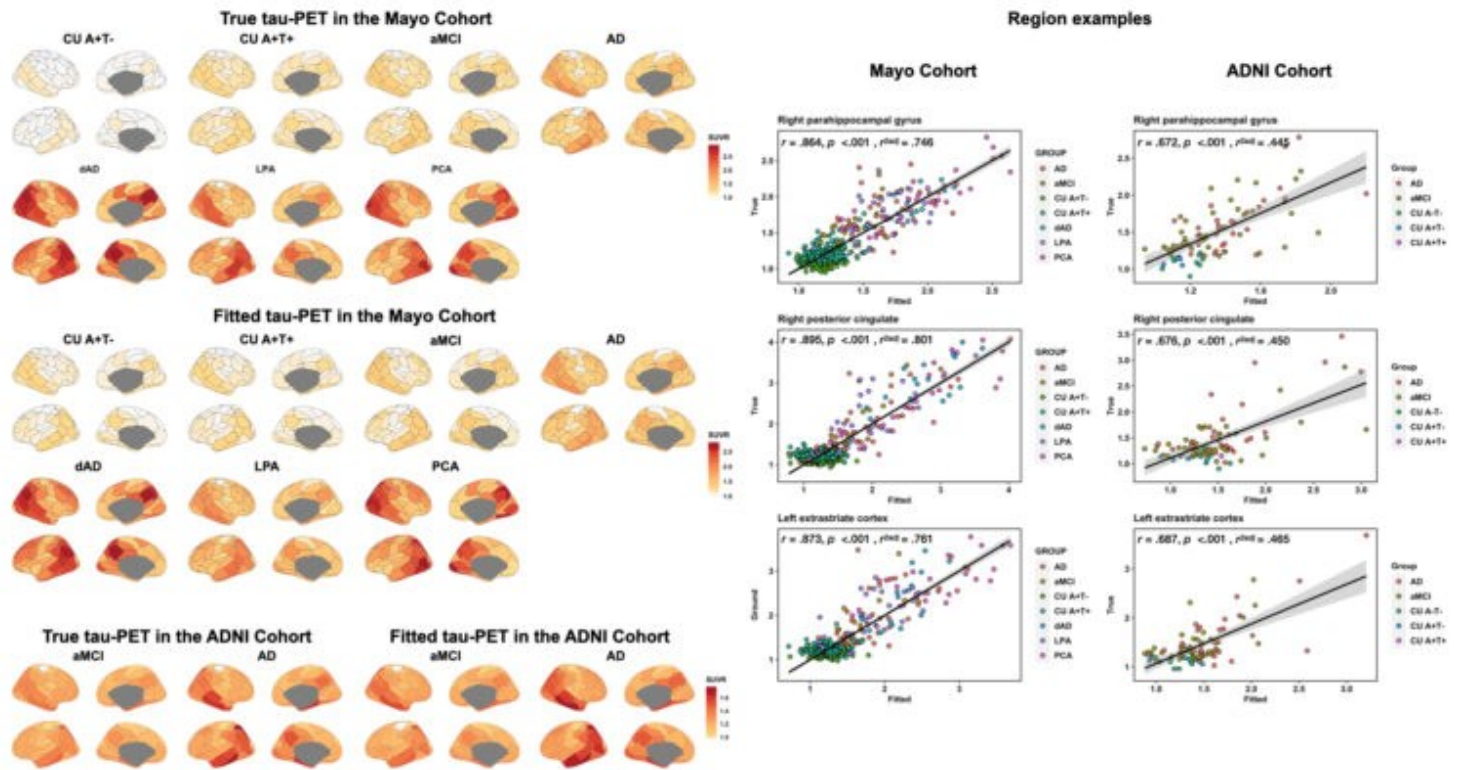
4) Out-of-sample predictions in the ADNI cohort

	PC1	PC2	PC3	...	PC56
CU A-T-, n = 7	-0.86	-0.66	0.09	...	0.45
CU A+T-, n = 5					
CU A+T+, n = 1	-0.78	0.47	0.98	...	-0.89
aMCI, n = 44					
AD, n = 29	0.12	-0.76	-0.43	...	0.78

Predicted tau in region 1 = PC1*BetaPC1 + PC2*BetaPC2 + PC3*BetaPC3 ... PC56*BetaPC56

...

Predicted tau in region 100 = PC1*BetaPC1 + PC2*BetaPC2 + PC3*BetaPC3 ... PC56*BetaPC56



Keywords: Tau-PET, FDG, Gradients, Epicenters, Alzheimer's disease

Measuring tau in the basal forebrain: a comparison of MK6240 and flortaucipir

Theresa Harrison¹, Tyler Ward¹, Suzanne Baker², William Jagust^{1,2}, Susan Landau¹

¹University of California Berkeley, Berkeley, CA, US

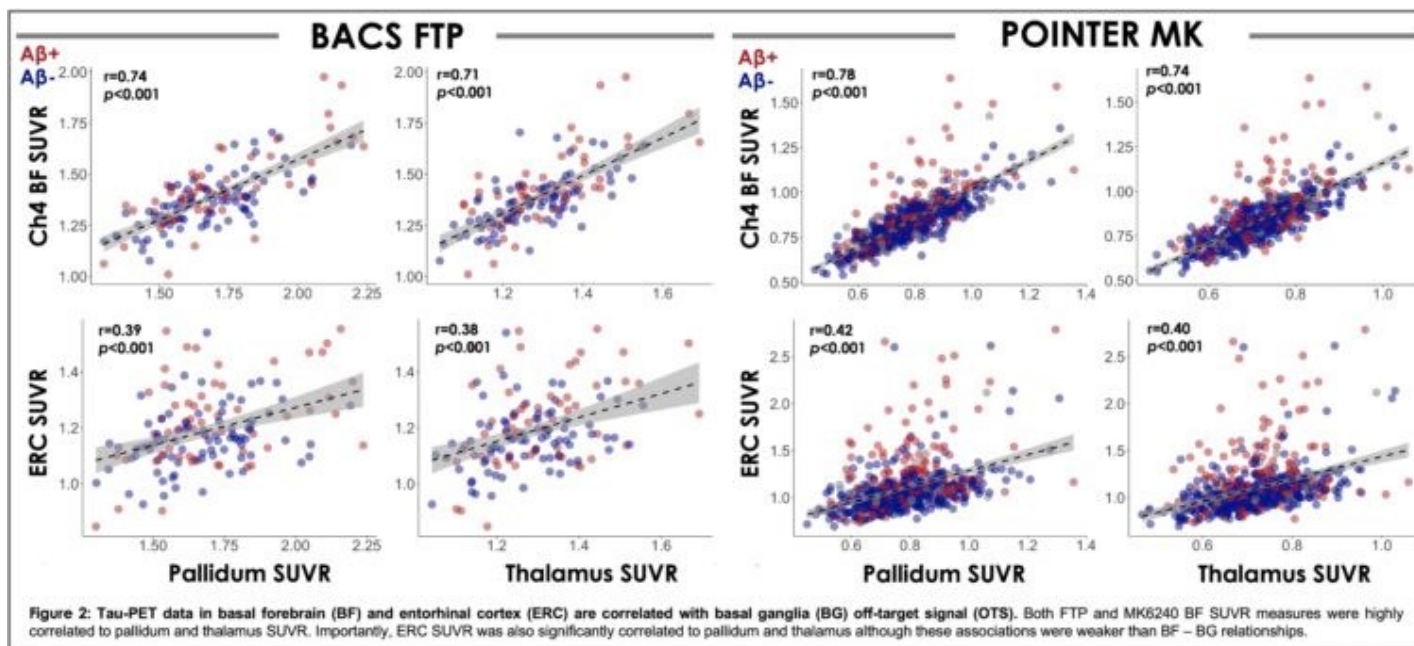
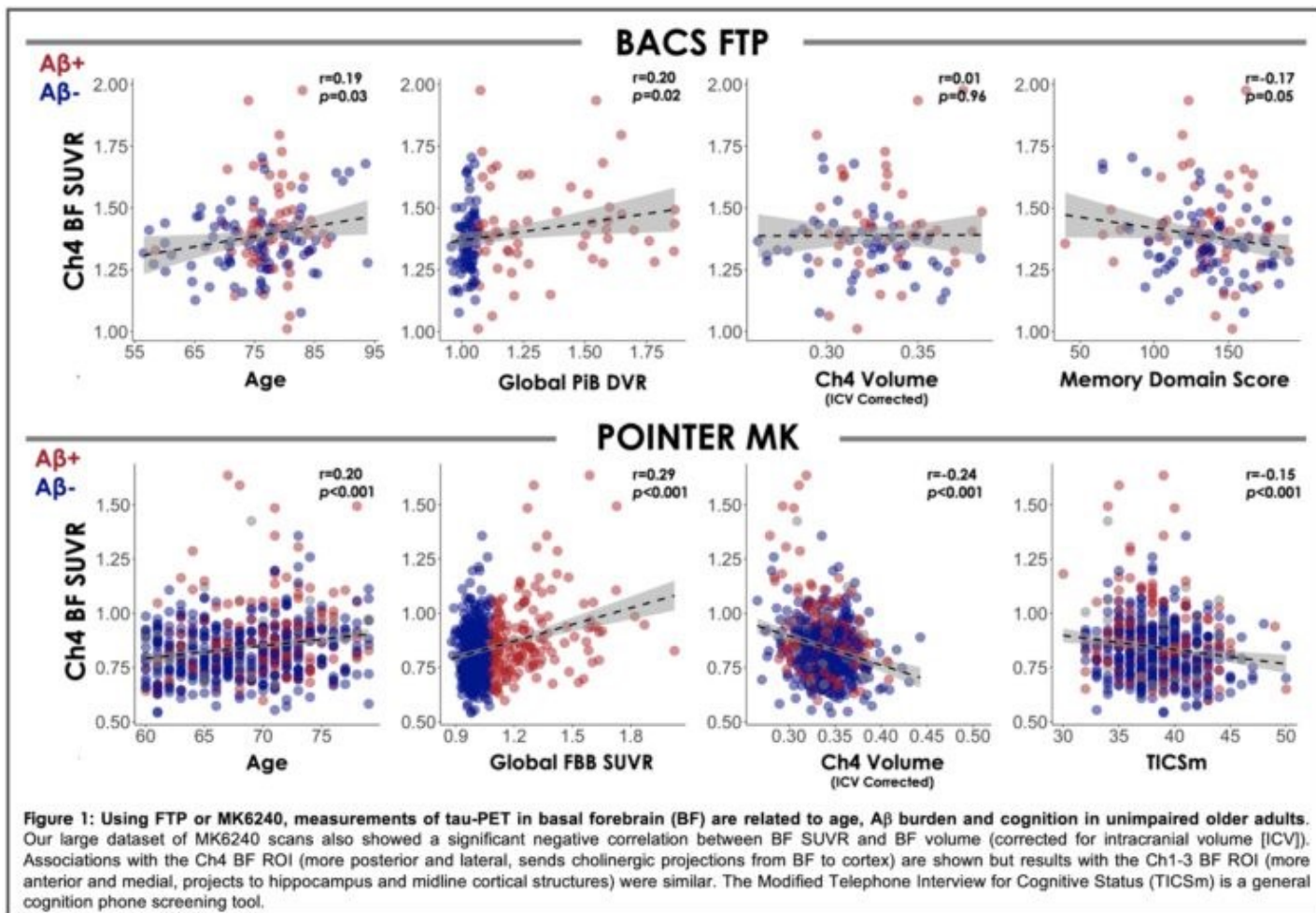
²Lawrence Berkeley National Laboratory, Berkeley, CA, US

Background: Tau pathology is present in the basal forebrain (BF) early in the course of Alzheimer's disease. Tau-PET tracers have varying patterns of off-target signal (OTS), including age associated OTS in the basal ganglia (BG), which may result in partial volume effects (PVE) that interfere with quantification of tau in BF.

Methods: Using two separate cohorts of cognitively unimpaired older adults, we compared measurements of tau in BF with FTP and MK6240. 141 FTP scans (76.2±7.1 years, 57% F) from the Berkeley Aging Cohort Study (BACS) and 582 MK6240 scans (68.5±5.0 years, 64% F) from the POINTER Imaging study were processed identically to obtain inferior cerebellar gray normalized FreeSurfer regions and template space BF. Linear regression was used to examine tau-PET ROIs in the BF (Ch1-3, Ch4), BG (pallidum, thalamus) and temporal lobe (entorhinal cortex [ERC], temporal metaROI) and their relationships to age, sex, BF volume, beta amyloid (A β) burden and cognition.

Results: FTP and MK6240 BF SUVR positively correlated with age, A β , and negatively correlated with cognition (Fig. 1). BF SUVR was higher in males versus females and negatively correlated with BF volume in POINTER. With both tracers, OTS BG ROIs were significantly correlated with BF ROIs, but also with ERC (Fig. 2) and MetaROI, even after adjusting for age. BG ROIs were related to age (pallidum only) and sex (M>F) but were not associated with A β or cognition (age and sex adjusted).

Conclusions: Despite relatively higher OTS in BG with FTP versus MK6240 and the proximity of BG to BF, measurement of BF tau with either tracer yielded expected associations with age, A β and cognition. Evidence of more problematic BF PVE or OTS with FTP versus MK6240 was subtle. These findings provide support for novel studies of *in vivo* aggregation of tau in BF, an early tau-accumulating region.



Keywords: off-target signal, partial volume effects, cognitively normal older adults, preclinical AD, typical aging

Wednesday, January 11, 2023 - 02:00 pm - 02:45 pm

KEYNOTE: Synaptic pathology in neurodegeneration

Thomas Montine

Stanford University

The anatomical basis for cognitive decline in both Alzheimer's disease (AD) and Lewy body dementia (LBD) is synaptic injury. Yet virtually all of our data on human synapses is from ultrastructural evaluation or bulk preparations, neglecting the vast molecular diversity of synapses.

We have invented mass synaptometry by time of flight mass spectrometry (SynTOF) for the multiplex molecular characterization of tens of millions of single-synapse events from synaptosome preparations. Buttressed by non-human primate quality controls and close alignment with ultrastructural estimates, SynTOF unveiled key differences in presynaptic molecular composition between late-onset AD and aged PS/APP mice; reinforced the relevance of synaptic pathologic tau species in AD; and highlighted presynaptic roles for CD47, DJ1, and ApoE in AD.

SynTOF provides an unparalleled opportunity for multiplex molecular analysis of millions of single-synapse events.

Wednesday, January 11, 2023 - 02:45 pm - 03:50 pm

Podium Session

SESSION III: Thresholds, visual reads and real world imaging

Wednesday, January 11, 2023		
2:45 pm – 3:50 pm	SESSION III: THRESHOLDS, VISUAL READS AND REAL WORLD IMAGING	CHAIRS: Pedro Rosa-Neto, MD, PhD, McGill University Ansel Hillmer, PhD, Yale School of Medicine
2:45	Introduction	Chairs
2:50	Biostatistical estimation of tau threshold hallmarks (BETTH) for tau imaging studies	Alexandra Gogola, PhD, <i>University of Pittsburgh School of Medicine</i>
3:05	Visual read of [18F]florquinitau PET that includes and extends beyond the mesial temporal lobe is associated with amyloid positivity and retrospective cognitive decline in an AD risk-enriched cohort	Sterling Johnson, PhD, <i>University of Wisconsin School of Medicine and Public Health</i>
3:20	Head-to-head comparison of tau and amyloid PET visual reads for differential diagnosis: An international, multi-center study	David Soleimani-Meigooni, PhD, <i>University of California, San Francisco</i>
3:35	Quantitative analysis of 8,895 real-world amyloid Positron Emission Tomography (PET) scans from the Imaging Dementia–Evidence for Amyloid Scanning (IDEAS) study	Ehud Zeltzer, MD, <i>University of California, San Francisco</i>
3:50	Discussion	

Biostatistical estimation of tau threshold hallmarks (BETTH) for tau imaging studies

Alexandra Gogola¹, Brian Lopresti¹, Dana Tudorascu², Beth Snitz³, Davneet Minhas¹, Vincent Doré^{4,5}, Milos Ikonomic^{3,6}, C. Elizabeth Shaaban⁷, Cristy Matan¹, Pierrick Bourgeat⁵, N Scott Mason¹, Christopher Rowe⁴, Howard Aizenstein², Chester Mathis¹, William Klunk², Oscar Lopez³, Ann Cohen², Victor Villemagne^{2,4}

¹Department of Radiology, University of Pittsburgh School of Medicine, Pittsburgh, PA, US

²Department of Psychiatry, University of Pittsburgh School of Medicine, Pittsburgh, PA, US

³Department of Neurology, University of Pittsburgh School of Medicine, Pittsburgh, PA, US

⁴Department of Molecular Imaging & Therapy, Austin Health, Melbourne, AU

⁵Commonwealth Scientific and Industrial Research Organisation, Health & Biosecurity, Melbourne, AU

⁶Geriatric Research Education and Clinical Center, Veterans Affairs Pittsburgh Healthcare System, Pittsburgh, PA, US

⁷Department of Epidemiology, University of Pittsburgh School of Public Health, Pittsburgh, PA, US

Background: A sensitive methodology for determining tau PET thresholds is needed to confidently detect early tau deposition. We compared several threshold-determining methods and six composite-regions in participants who underwent either ¹⁸F-flortaucipir (FTP) or ¹⁸F-MK-6240 (MK) PET scans.

Methods: 453 FTP and 251 MK scans were processed and sampled to obtain regional SUVR values. To better facilitate threshold determination, two subgroups were established based on participant diagnosis, age, amyloid status, and neurodegeneration status: older adult cognitively unimpaired (CU) (age 55 years, A-N-) and cognitively impaired (MCI/AD, A+N+). This yielded 93 CU (73.14.1 years) and 33 CI (80.17.7 years) FTP scans and 32 CU (73.14.9 years) and 68 CI (71.37.8 years) MK scans. These groups were then randomly split into training (70%) and testing (30%) datasets. We tested 12 thresholding methods in the Amygdala, Inferior Temporal, Lateral Occipital, LateralTemporal, MesialTemporal, and MetaTemporal composite-regions. Composite regions were assessed using effect size. The combinations for method and composite-region were assessed using sensitivity, specificity, positive predictive value (PPV), and negative predictive value (NPV).

Results: The Amygdala, MesialTemporal, and MetaTemporal composite-regions showed the largest effect sizes for both FTP (1.29, 1.08, and 1.02) and MK (2.85, 2.48, and 2.20), with the MK effect sizes consistently more than twice that of the FTP. MK outperformed FTP for a majority for the comparisons we performed (12 thresholding methods x three composite-regions x four assessment metrics) (Table 1), most notably in its sensitivity for detecting tau in CI.

Conclusions: Accounting for both effect sizes and potential influence of primary age-related tauopathy, we believe the MetaTemporal region is optimal for determining tau thresholds and found that the non-parametric double receiver operating characteristic (ROC) curve for determining tau thresholds maximizes sensitivity. MK better and more consistently differentiates CU from CI. Future work will test the methods' performance for other tau tracers.

Table 1. Performance of derived thresholds in differentiating between CU and CI as determined by the 12 methods tested and the three composite-regions with the largest effect sizes (*d*).

		FTP				MK			
		Sens.	Spec.	PPV	NPV	Sens.	Spec.	PPV	NPV
Amygdala	90%ile	0.64	0.88	0.78	0.78	1.00	0.88	0.95	1.00
	95%ile	0.55	0.94	0.86	0.76	1.00	0.88	0.95	1.00
	CenTauRz 1.5	0.55	0.97	0.92	0.76	1.00	0.88	0.95	1.00
	CenTauRz 2	0.41	1.00	1.00	0.72	1.00	0.94	0.97	1.00
	Double ROC (np)	0.77	0.73	0.65	0.83	1.00	1.00	1.00	1.00
	Double ROC (p)	0.77	0.73	0.65	0.83	1.00	0.88	0.95	1.00
	GMM	0.36	1.00	1.00	0.70	0.72	1.00	1.00	0.62
	Hierarchical Clustering	0.27	1.00	1.00	0.67	0.28	1.00	1.00	0.38
	IO	0.36	1.00	1.00	0.70	0.97	1.00	1.00	0.94
	K-means Clustering	0.41	1.00	1.00	0.72	0.58	1.00	1.00	0.52
	ROC	0.95	0.52	0.57	0.94	1.00	0.94	0.97	1.00
	Youden Index	0.95	0.55	0.58	0.95	1.00	1.00	1.00	1.00
MesialTemporal	90%ile	0.50	0.91	0.79	0.73	1.00	0.75	0.90	1.00
	95%ile	0.45	0.97	0.91	0.73	1.00	0.81	0.92	1.00
	CenTauRz 1.5	0.45	1.00	1.00	0.73	1.00	0.81	0.92	1.00
	CenTauRz 2	0.45	1.00	1.00	0.73	1.00	0.94	0.97	1.00
	Double ROC (np)	0.77	0.73	0.65	0.83	0.94	1.00	1.00	0.89
	Double ROC (p)	0.68	0.85	0.75	0.80	1.00	0.88	0.95	1.00
	GMM	0.45	1.00	1.00	0.73	0.78	1.00	1.00	0.67
	Hierarchical Clustering	0.45	1.00	1.00	0.73	0.64	1.00	1.00	0.55
	IO	0.45	1.00	1.00	0.73	1.00	0.94	0.97	1.00
	K-means Clustering	0.32	1.00	1.00	0.69	0.56	1.00	1.00	0.50
	ROC	0.86	0.70	0.66	0.88	0.94	1.00	1.00	0.89
	Youden Index	0.77	0.73	0.65	0.83	0.94	1.00	1.00	0.89
MetaTemporal	90%ile	0.55	0.88	0.75	0.74	1.00	0.75	0.90	1.00
	95%ile	0.45	0.94	0.83	0.72	1.00	0.88	0.95	1.00
	CenTauRz 1.5	0.45	0.97	0.91	0.73	1.00	0.81	0.92	1.00
	CenTauRz 2	0.45	1.00	1.00	0.73	1.00	0.94	0.97	1.00
	Double ROC (np)	0.73	0.76	0.67	0.81	1.00	0.94	0.97	1.00
	Double ROC (p)	0.68	0.88	0.79	0.81	1.00	0.75	0.90	1.00
	GMM	0.45	1.00	1.00	0.73	0.56	1.00	1.00	0.50
	Hierarchical Clustering	0.45	1.00	1.00	0.73	0.17	1.00	1.00	0.35
	IO	0.45	1.00	1.00	0.73	1.00	0.75	0.90	1.00
	K-means Clustering	0.27	1.00	1.00	0.67	0.50	1.00	1.00	0.47
	ROC	0.68	0.88	0.79	0.81	1.00	0.94	0.97	1.00
	Youden Index	0.55	0.88	0.75	0.74	0.94	1.00	1.00	0.89

Abbreviations: Sensitivity (Sens.), Specificity (Spec.), 90th-percentile (90%ile), 95th-percentile (95%ile), non-parametric (np), parametric (p), Gaussian mixture model (GMM), and iterative outlier (IO).

Color coding: Highest (green), second highest (blue), and lowest (red) sensitivity, specificity, PPV, and NPV in each composite-region and tracer pairs.

Visual read of [18F]florquinitau PET that includes and extends beyond the mesial temporal lobe is associated with amyloid positivity and retrospective cognitive decline in an AD risk-enriched cohort

Sterling Johnson^{1,2,3}, Karly Cody^{1,2}, Nathaniel Chin¹, Rebecca Langhough^{1,2}, Erin Jonaitis^{1,2}, Barbara Bendlin¹, Ozioma Okonkwo¹, Lindsay Clark^{1,2}, Matthew Zammit^{4,5}, Jon Engle⁴, Todd Barnhart⁴, Sanjay Asthana^{1,2,3}, Bradley Christian^{4,5}, Tobey Betthausen^{1,4}, Laura Eisenmenger^{1,6}

¹Wisconsin Alzheimer's Disease Research Center, University of Wisconsin School of Medicine and Public Health, Madison, WI, US

²Wisconsin Alzheimer's Institute, University of Wisconsin School of Medicine and Public Health, Madison, WI, US

³Geriatric Research Education and Clinical Center, Wm. S. Middleton Memorial VA Hospital, Madison, WI, US

⁴Department of Medical Physics, University of Wisconsin School of Medicine and Public Health, Madison, WI, US

⁵Waisman Center, University of Wisconsin-Madison, Madison, WI, US

⁶Department of Radiology, University of Wisconsin School of Medicine and Public Health, Madison, WI, US

Background: This study examined the utility of a pattern of [F-18]florquinitau (FQT or MK-6240) PET involving the mesial temporal lobe *and* neocortex in comparison to a pattern confined to the MTL only, ascertained from a qualitative visual read. We assessed frequency of amyloid positivity and relationships with cognitive decline across FQT patterns of uptake.

Methods: FQT PET (SUVR 70-90 minutes; inferior cerebellar GM reference region), [C-11]PiB (DVR 0-70 minute dynamic scan), and MRI were acquired on n=459 participants from the Wisconsin Registry for Alzheimer's Prevention or the Wisconsin Alzheimer's Disease Research Center. Participants were cognitively unimpaired at baseline cognitive assessment (Table 1). FQT visual reads were performed on the SUVR image (ACTC colormap; 0-2.5 scale), according to three uptake categories: T-(no uptake), MTL only, and MTL& neocortex. Linear mixed effects (LME) models (covarying for education, sex, cohort, and practice effects) were used to assess differences in retrospective cognitive trajectories across amyloid and FQT visual biomarker groups (eg. A-/T-, A+/T-, A+/MTL only T+, A+/MTL& neocortex T+).

Results: 93% of the MTL& neocortex group and 42% of the MTL-only group were A+. The LME (Figure 1) demonstrated a significant interaction between age (~9 years of follow up) and biomarker grouping. Both T+ groups exhibited significantly faster cognitive decline relative to T- groups, and by age 70, *post hoc* comparisons indicated the A+/MTL& neocortex T+ declined faster than the A+/MTL only T+ group. Moreover, 31% of the MTL& neocortex and 0% of MTL-only groups were cognitively impaired at most recent cognitive assessment.

Conclusions: Visual assessment of tau signal in the MTL *and* neocortex largely occurred in the presence of amyloid proteinopathy. While both T+ patterns were associated with retrospective cognitive decline, the MTL& neocortical pattern exhibited more pronounced decline and was more likely to transition to impairment.

Table 1. Participant Characteristics

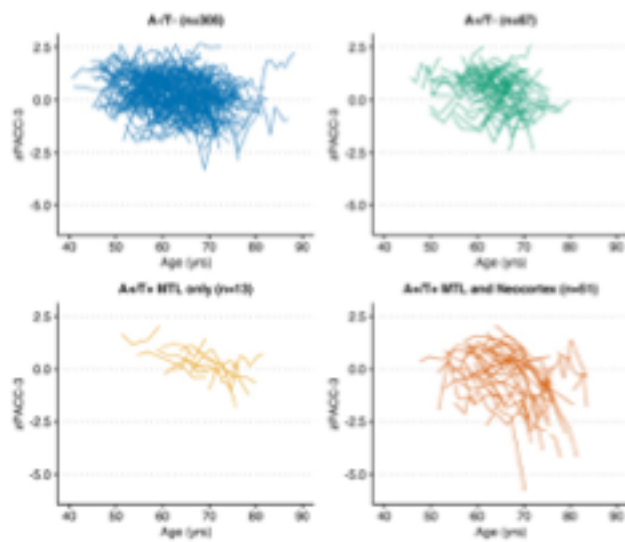
Characteristic	N	Visual Rating Tau Groups				p-value ²
		Overall, N = 459 ¹	T-, N = 373 ¹	T+ MTL only, N = 31 ¹	T+ MTL & Neo, N = 55 ¹	
Cohort	459					0.6
ADRC		111 (24%)	93 (25%)	8 (26%)	10 (18%)	
WRAP		348 (76%)	280 (75%)	23 (74%)	45 (82%)	
Age at first PACC-3 (years)	459	59.16 (7.00)	58.28 (6.74)	64.20 (6.70)	62.33 (6.90)	<0.001
Age at most recent PACC-3 (years)	459	67.56 (7.19)	66.56 (7.05)	72.94 (6.07)	71.32 (6.15)	<0.001
Age at most recent tau PET (years)	459	68.44 (7.23)	67.36 (7.07)	73.77 (5.52)	72.71 (6.25)	<0.001
PACC-3 follow-up (years)	443	8.71 (3.02)	8.64 (3.03)	8.74 (3.45)	9.16 (2.76)	0.5
Sex	459					0.057
Female		313 (68%)	245 (66%)	24 (77%)	44 (80%)	
Male		146 (32%)	128 (34%)	7 (23%)	11 (20%)	
APOE4 carriage	434	176 (41%)	125 (36%)	12 (40%)	39 (74%)	<0.001
Education	459					0.3
BA		82 (18%)	71 (19%)	5 (16%)	6 (11%)	
No BA		377 (82%)	302 (81%)	26 (84%)	49 (89%)	
Baseline zPACC-3	459	0.18 (0.88)	0.22 (0.83)	0.18 (0.94)	-0.05 (1.10)	0.4
Most recent zPACC-3	459	0.16 (1.15)	0.36 (0.94)	-0.10 (1.19)	-1.07 (1.55)	<0.001
zPACC-3 change/year	443	0.01 (0.15)	0.03 (0.14)	-0.04 (0.15)	-0.13 (0.17)	<0.001
Clinical diagnosis at most recent PACC-3	459					<0.001
CU		441 (96%)	371 (99%)	31 (100%)	39 (71%)	
MCI		14 (3.1%)	1 (0.3%)	0 (0%)	13 (24%)	
DEM		3 (0.7%)	0 (0%)	0 (0%)	3 (5.5%)	
IO		1 (0.2%)	1 (0.3%)	0 (0%)	0 (0%)	

¹ n (%); Mean (SD)
² Fisher's exact test; Kruskal-Wallis rank sum test

Table 1. Imaging Characteristics at most recent tau PET

Characteristic	N	Visual Rating Tau Groups				p-value ²
		Overall, N = 459 ¹	T-, N = 373 ¹	T+ MTL only, N = 31 ¹	T+ MTL & Neo, N = 55 ¹	
Age at tau PET (years)	459	68.44 (7.23)	67.36 (7.07)	73.77 (5.52)	72.71 (6.25)	<0.001
Time btwn tau PET & most recent PACC3 (years)	459	-0.87 (1.51)	-0.80 (1.47)	-0.83 (1.42)	-1.40 (1.73)	0.080
Global PiB DVR at tau PET	459	1.17 (0.23)	1.11 (0.15)	1.20 (0.20)	1.59 (0.26)	<0.001
PiB Pos at tau PET	459	131 (29%)	67 (18%)	13 (42%)	51 (93%)	<0.001

Observed PACC-3 performance over time



Modelled PACC-3 performance over time

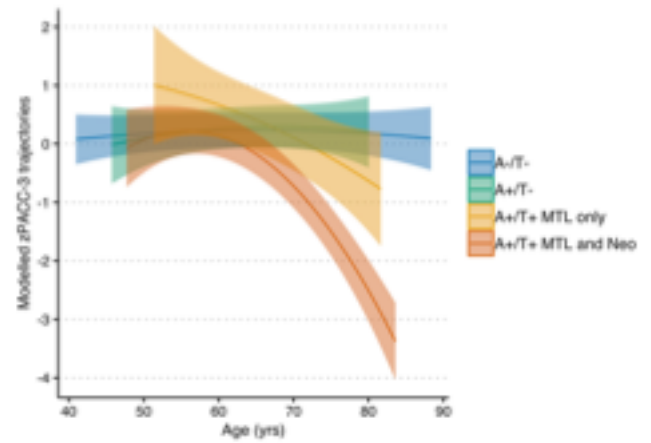


Figure 1. An LME model covarying age, sex, education, cohort, practice effects, and time between last cognitive and last tau visit was used to characterize the difference in rates of PACC3 decline between visual tau groups in N=437 participants with ~9 years of cognitive follow-up. The plot on the right shows the group-level modelled PACC-3 simple slopes and confidence intervals over the range of the ages present in each group, with individual observed cognitive performance displayed as points in the background. Results of the LME model indicated significant linear and quadratic group by age interactions. Tukey-adjusted pairwise comparisons indicated that each of the visually T+ groups declined significantly faster on average compared to T- groups during the period of observation.

Primary model statistics			
PACC-3 ~ Covariates + Age + Age ² + Group + Age×Group + Age ² ×Group + random intercept + random slope			
Variable	β	95% CI	p
Covariates			
Intercept	-0.03	-0.41 – 0.34	0.861
Gender [Male]	-0.51	-0.67 – -0.36	<.0001
Edu [BA]	0.48	0.14 – 0.82	.013
Cohort [WRAP]	0.25	-0.06 – 0.56	.111
Practice	0.06	0.01 – 0.11	.024
Time interval	-0.02	-0.07 – 0.03	.681
Predictors of interest			
Age	0.00	-0.01 – 0.01	.0004
Age ²	-0.00	-0.00 – 0.00	<.0001
Group			
Group 2	0.06	-0.15 – 0.27	
Group 3	0.17	-0.27 – 0.62	.0007
Group 4	-0.41	-0.66 – -0.17	
Age × Group			
Age × Group 2	0.00	-0.02 – 0.02	
Age × Group 3	-0.06	-0.10 – -0.02	<.0001
Age × Group 4	-0.09	-0.11 – -0.07	
Age² × Group			
Age ² × Group 2	-0.00	-0.00 - 0.00	
Age ² × Group 3	-0.00	-0.00 - 0.00	<.0001
Age ² × Group 4	-0.00	-0.01 - -0.00	

Keywords: [F-18]MK-6240; florquinitau; cognitive decline

Head-to-head comparison of tau and amyloid PET visual reads for differential diagnosis: An international, multi-center study

David Soleimani-Meigooni¹, Ruben Smith², Karine Provost³, Orit Lesman-Segev⁴, Isabel Elaine Allen⁵, Miranda Chen¹, Hanna Cho^{1,6}, Lauren Edwards⁷, Leonardo Iaccarino⁸, Shorena Janelidze², Renaud La Joie¹, Rik Ossenkoppele^{2,9}, Erik Stomrud², Olof Strandberg², Amelia Strom¹⁰, Adam Boxer¹, Jeffrey Dage¹¹, Maria Luisa Gorno-Tempini¹, Joel Kramer¹, Bruce Miller¹, Julio Rojas-Martinez¹, Howard Rosen¹, Chul Lyoo⁶, Oskar Hansson², Gil Rabinovici^{1,12}

¹Memory and Aging Center, UCSF Weill Institute for Neurosciences, Department of Neurology, University of California, San Francisco, CA, US

²Clinical Memory Research Unit, Lund University, Lund, Sweden

³Department of Nuclear Medicine, Centre Hospitalier de l'Université de Montréal, Montréal, QC, Canada

⁴Department of Diagnostic Imaging, Sheba Medical Center, Tel Hashomer, Ramat Gan, IL

⁵Department of Epidemiology and Biostatistics, University of California, San Francisco, CA, US

⁶Department of Neurology, Gangnam Severance Hospital, Yonsei University College of Medicine, Seoul, Korea

⁷Clinical Psychology, San Diego State University & University of California, San Diego, CA, US

⁸Eli Lilly and Company, Indianapolis, IN, US

⁹Alzheimer Center Amsterdam, Department of Neurology, Amsterdam Neuroscience, Amsterdam UMC, Amsterdam, The Netherlands

¹⁰Health Sciences and Technology, Harvard & Massachusetts Institute of Technology, Cambridge, MA, US

¹¹Stark Neuroscience Research Institute, Indiana University School of Medicine, Indianapolis, IN, US

¹²Department of Radiology and Biomedical Imaging, University of California, San Francisco, CA, US

Introduction: We aimed to compare diagnostic accuracy of A β - and FTP-PET visual reads (latter with inclusion and exclusion of isolated medial temporal lobe tracer retention in positive FTP Alzheimer's disease [AD] pattern) for distinguishing patients with CSF or plasma biomarker-confirmed AD dementia and mild cognitive impairment (MCI) from other neurodegenerative diseases and cognitively normal (CN) controls.

Methods: We included 298 participants with FTP- and A β -PET (¹¹C]PIB or [¹⁸F]Flutemetamol) at UCSF and Lund University (Table 1). Each patient had CSF (A β ₄₂/A β ₄₀, threshold<0.054 UCSF or <0.10 Lund) or plasma (P-Tau217, threshold>0.19 pg/mL) biomarkers as the reference standard. Three visual raters interpreted A β -PET using tracer-specific criteria and FTP-PET using a method developed by Sonni *et al.* (2021, Figure 1). The majority interpretation of each scan as amyloid positive/negative and tau positive with mild temporal binding/positive with AD-like binding/negative (negative scan or non-AD like binding) was used in the primary analysis. Diagnostic performance of A β - and FTP-PET visual reads (including or excluding mild temporal binding) were calculated.

Results: In comparison to A β -PET visual reads: 1. FTP-PET visual reads that exclude mild temporal binding have similar specificity (89.2% vs. 86.0% for A β -PET, N.S.) and sensitivity (91.7% vs. 95.2%, N.S.). 2. FTP-PET visual reads that include mild temporal binding have similar specificity (76.3% vs. 86.0% for A β -PET, N.S.) and sensitivity (97.2% vs. 95.2%, N.S.). Comparing the two FTP-PET visual read methods, exclusion of mild temporal binding increases specificity (89.2% vs. 76.3%, $P<0.001$), whereas inclusion of this binding increases sensitivity (97.2% vs. 91.7%, $P<0.001$) (Table 2A). Additional diagnostic performance analyses are shown in Table 2.

Conclusions: A β - and FTP-PET have similar sensitivity. A β - and FTP-PET have similar specificity when medial and inferior temporal lobe FTP binding are included in criteria for positive FTP AD pattern; however, specificity of FTP-PET increases when these temporal regions are excluded.

Table 1: Participant characteristics by clinical diagnosis

	Mean (SD)			
	Cognitively Normal (n=64)	Mild Cognitive Impairment (n=60)	Alzheimer's Disease Dementia (n=108)	Non-Alzheimer Diseases* (n=66)
Age, yrs.	74.3 (6.8) ^a	66.7 (11.2)	67.0 (8.8)	66.0 (9.4)
Age range, yrs.	32-88	32-88	48-84	37-87
Sex, male	48.4%	61.7%	50.0%	59.1%
Duration of education, yrs.	12.4 (3.9) ^a	15.0 (4.2)	14.9 (3.9)	16.4 (4.8) ^b
MMSE score	29.0 (1.1) ^a	26.5 (2.8)	21.1 (5.6) ^a	25.0 (4.8)
CDR scale				
Global	0 (0.1) ^a	0.5 (0.4) ^a	0.9 (0.5) ^a	0.7 (0.5) ^a
Sum of boxes	0.1 (0.3) ^a	1.9 (1.0) ^a	5.4 (2.9) ^a	3.9 (2.8) ^a
β -Amyloid positivity	44 (68.8%)	42 (70.0%)	103 (95.4%) ^a	16 (24.2%) ^a
APOE ϵ 4 positivity, No./total No.	27/59 (45.8%)	23/44 (52.3%)	55/89 (61.8%) ^c	14/43 (32.6%)
Time between PET and diagnosis, mean days (SD)	239 (169) ^a	51 (58)	54 (62)	48 (61)
No. of patients by biomarker [†]				
CSF A β ₄₂ /A β ₄₀ , Lund	62 (100%)	27 (100%)	44 (100%)	21 (100%)
CSF A β ₄₂ /A β ₄₀ , UCSF	0 (0%)	13 (39.4%) ^d	40 (62.5%)	36 (80.0%)
Plasma P-Tau217, UCSF	2 (100%)	32 (97%) ^d	49 (77%)	24 (53.3%)
Patients with both CSF and plasma biomarkers, UCSF	0 (0%)	12 (36.3%)	25 (39.1%)	15 (33.3%)
No. of patients by center				
UCSF	2 (3.1%) ^a	33 (55.0%)	64 (59.3%)	45 (68.1%)
Lund	62 (96.9%) ^a	27 (45.0%)	44 (40.7%)	21 (31.9%)

Differences in baseline characteristics between groups were assessed using ANOVA with *post hoc* Bonferroni tests for continuous variables and χ^2 test for dichotomous/categorical variables. ^a*P* < 0.01 vs. all other diagnoses. ^b*P* < 0.05 vs. all other diagnoses. ^c*P* < 0.05 vs. non-Alzheimer disease group. ^d*P* < 0.01 vs. non-Alzheimer disease group. *This category includes patients with behavioral variant frontotemporal dementia (N = 16), nonfluent/agrammatic variant of primary progressive aphasia (N = 12), semantic variant of primary progressive aphasia (N = 6), progressive supranuclear palsy (N = 15), corticobasal syndrome (N = 10), dementia with Lewy bodies (N = 3), Parkinson's disease dementia (N = 1), vascular dementia (N = 2), and traumatic brain injury (N = 1). [†]Some UCSF patients had both CSF A β ₄₂/A β ₄₀ and plasma P-Tau217 biomarkers. In these patients, CSF A β ₄₂/A β ₄₀ was used to classify Alzheimer's disease biomarker status as positive or negative.

Figure 1: [¹⁸F]Flortaucipir PET visual read algorithm

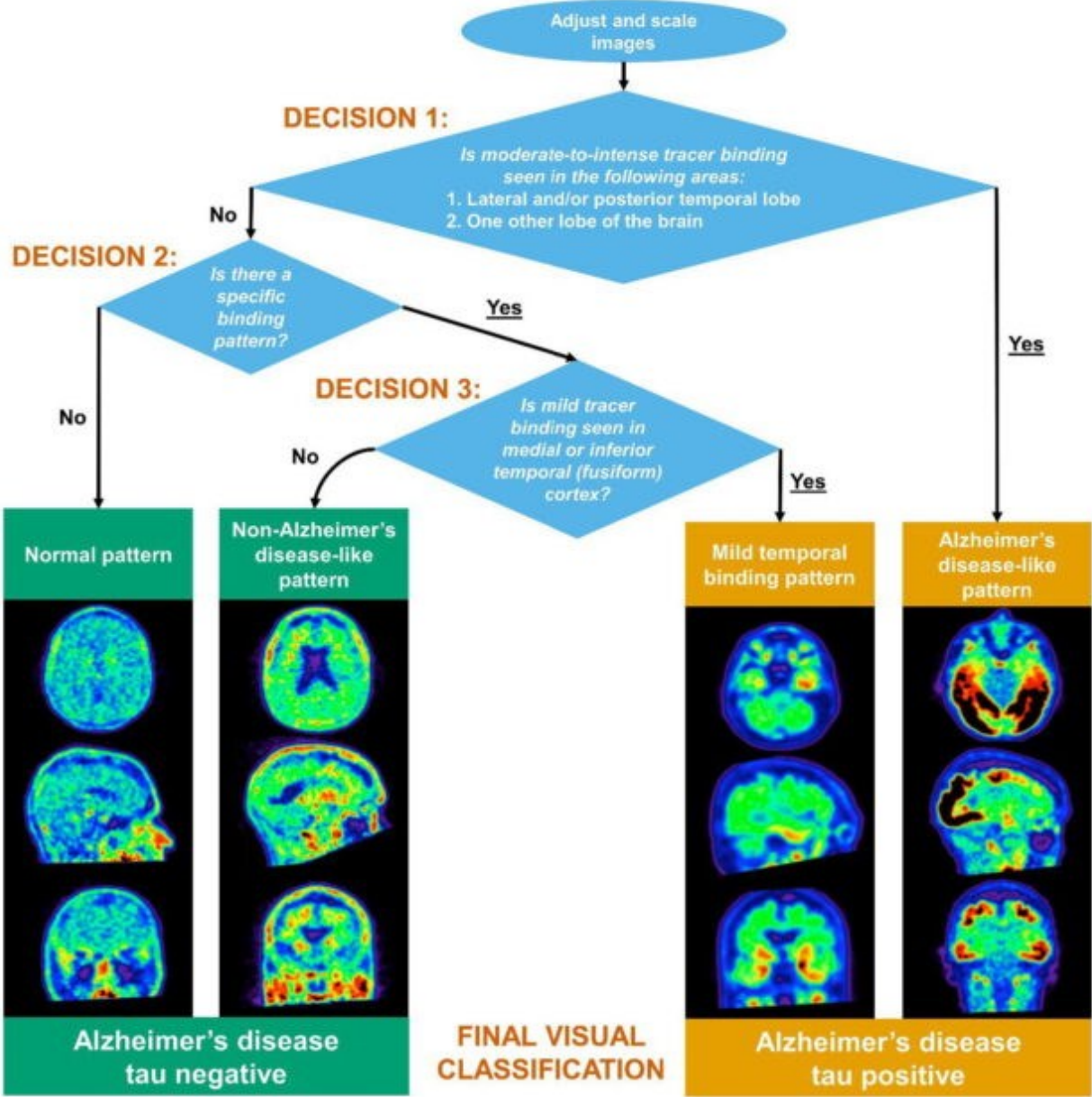


Table 2: Diagnostic performance of amyloid and [¹⁸F]Flortaucipir PET consensus visual reads

A. Distinguishing patients with CSF or plasma biomarker-confirmed Alzheimer's disease dementia and mild cognitive impairment from CSF or plasma biomarker negative patients with other diagnoses and cognitively normal controls.

	AUC (95% CI)	Sensitivity % (95% CI)	Specificity % (95% CI)	Positive Likelihood Ratio (95% CI)	Negative Likelihood Ratio (95% CI)
Amyloid PET	0.91 (0.87-0.95)	95.2 (90.3-98.0)	86.0 (77.3-92.3)	6.81 (4.11-11.30)	0.06 (0.03-0.12)
[¹⁸ F]Flortaucipir PET (including mild temporal binding pattern in positive scan criteria)	0.87 (0.82-0.91)	97.2 ^a (93.1-99.2)	76.3 (66.4-84.5)	4.11 (2.85-5.93)	0.04 (0.01-0.10)
[¹⁸ F]Flortaucipir PET (excluding mild temporal binding pattern from positive scan criteria)	0.91 (0.87-0.94)	91.7 (86.0-95.7)	89.2 ^a (81.1-94.7)	8.53 (4.74-15.4)	0.09 (0.05-0.16)

B. Distinguishing patients with CSF or plasma biomarker-confirmed Alzheimer's disease dementia and mild cognitive impairment from patients with other diagnoses and cognitively normal controls

	AUC (95% CI)	Sensitivity % (95% CI)	Specificity % (95% CI)	Positive Likelihood Ratio (95% CI)	Negative Likelihood Ratio (95% CI)
Amyloid PET	0.85 (0.81-0.88)	95.1 (90.2-98.0)	73.9 (66.1-80.6)	3.64 (2.78-4.76)	0.07 (0.03-0.14)
[¹⁸ F]Flortaucipir PET (including mild temporal binding pattern in positive scan criteria)	0.84 (0.80-0.88)	97.2 ^a (93.1-99.2)	70.6 (62.7-77.7)	3.31 (2.58-4.23)	0.04 (0.01-0.10)
[¹⁸ F]Flortaucipir PET (excluding mild temporal binding pattern from positive scan criteria)	0.89 (0.85-0.92)	91.7 (86.0-95.7)	85.6 ^{a,b} (79.0-90.8)	6.38 (4.32-9.42)	0.10 (0.06-0.17)

C. Distinguishing patients with CSF or plasma biomarker-confirmed Alzheimer's disease dementia from CSF or plasma biomarker negative patients and controls.

	AUC (95% CI)	Sensitivity % (95% CI)	Specificity % (95% CI)	Positive Likelihood Ratio (95% CI)	Negative Likelihood Ratio (95% CI)
Amyloid PET	0.91 (0.87-0.95)	96.1 (90.4-98.9)	86.0 (77.3-92.3)	6.88 (4.15-11.4)	0.05 (0.02-0.12)
[¹⁸ F]Flortaucipir PET (including mild temporal binding pattern in positive scan criteria)	0.87 (0.83-0.92)	98.1 (93.2-99.8)	76.3 (66.4-84.5)	4.15 (2.87-5.98)	0.03 (0.01-0.10)
[¹⁸ F]Flortaucipir PET (excluding mild temporal binding pattern from positive scan criteria)	0.93 (89.6-96.7)	97.1 (91.7-99.4)	89.2 ^a (81.1-94.7)	9.03 (5.02-16.20)	0.03 (0.01-0.10)

D. Distinguishing patients with CSF or plasma biomarker-confirmed mild cognitive impairment due to Alzheimer's disease from CSF or plasma biomarker negative patients and controls.

	AUC (95% CI)	Sensitivity % (95% CI)	Specificity % (95% CI)	Positive Likelihood Ratio (95% CI)	Negative Likelihood Ratio (95% CI)
Amyloid PET	0.89 (0.84-0.95)	92.9 (80.5-98.5)	86.0 (77.3-92.3)	6.64 (3.98-11.10)	0.08 (0.03-0.25)
[¹⁸ F]Flortaucipir PET (including mild temporal binding pattern in positive scan criteria)	0.86 (0.80-0.92)	95.2 ^a (83.8-99.4)	76.3 (66.4-84.5)	4.03 (2.78-5.84)	0.06 (0.02-0.24)
[¹⁸ F]Flortaucipir PET (excluding mild temporal binding pattern from positive scan criteria)	0.84 (0.77-0.91)	78.6 (63.2-89.7)	89.2 ^a (81.1-94.7)	7.31 (3.98-13.40)	0.24 (0.13-0.43)

Differences in sensitivity and specificity between PET methods was assessed by the global Wald test (H_0 : sensitivity of method 1 = sensitivity of method 2 and specificity of method 1 = specificity of method 2), and if H_0 was rejected, McNemar's test was applied to determine if there were significant differences between the individual sensitivities and specificities of the two methods. ^a $P < 0.001$ vs. other [¹⁸F]Flortaucipir PET visual read method. ^b $P < 0.001$ vs. amyloid PET. AUC = Area Under Receiver Operating Characteristic Curve; CI = Confidence Interval

Quantitative analysis of 8,895 real-world amyloid Positron Emission Tomography (PET) scans from the Imaging Dementia–Evidence for Amyloid Scanning (IDEAS) study

Ehud Zeltzer¹, Nidhi Mundada¹, Ganna Blazhenets¹, Jhony Mejia Perez¹, David Soleimani-Meigooni¹, Hanna Cho¹, Kamalini Ranasinghe¹, Charles Windon¹, Golnaz Yadollahikhales¹, Charles Apgar², Constantine Gatsonis³, Maria Carrillo⁴, Lucy Hanna³, Bruce Hillner⁵, Robert Koeppel⁶, Andrew March², Barry Siegel⁷, Karen Smith¹, Rachel Whitmer⁹, Leonardo Iaccarino¹, Renaud La Joie¹, Gil Rabinovici¹

¹University of California, San Francisco, San Francisco, CA, US

²American College of Radiology, Reston, VA, US

³Brown University, Providence, RI, US

⁴Alzheimer's Association, Chicago, IL, US

⁵Virginia Commonwealth University, Richmond, VA, US

⁶University of Michigan, Ann Arbor, MI, US

⁷Washington University in St Louis, St. Louis, MO, US

⁸University of California, Berkeley, Berkeley, CA, US

⁹Kaiser Permanente, Oakland, CA, US

Background: Amyloid PET had been validated in research settings, using highly selected samples, harmonized acquisition protocols, co-registration with MRI, and central interpretation by highly experienced experts. We assessed the validity of real-world clinically acquired MRI-free amyloid PET scans.

Method: IDEAS acquired 18,295 PET scans of Medicare beneficiaries with MCI or dementia at 343 PET facilities using ¹⁸F-florbetapir, ¹⁸F-florbetaben, or ¹⁸F-flutemetamol. Scans were visually interpreted by local physicians at each site as negative or positive for cortical tracer retention. Scans were processed using a specifically designed PET-only pipeline (Iaccarino, 2022) that quantifies cortical uptake in Centiloids. As of October 2022, 8,895 scans were successfully processed (see Mejia-Perez et al, submitted to HAI for more information) and included in the current analysis (Table 1 for demographics). A neuropathology-based threshold of 24.4 Centiloids (La Joie, 2019) was used to define positivity independent of visual reads.

Results: In the whole group, Centiloids exhibited a bimodal distribution (figure 1a). The mean (\pm SD) Centiloids of visually negative scans was 3 ± 26 , very close to the expected 0, while visually positive scans had a mean Centiloids of 72 ± 40 (figure 1b). High concordance was found between local visual reads and Centiloids-based positivity (86.7% agreement; Cohen's $\kappa=.720$, 95%CI [.704, .736], $p<.001$; figure 1c). Discordant cases had values around the positivity threshold (figure 1d) and were more likely to use ¹⁸F-florbetapir ($p<.001$ Bonferroni) and to belong to male patients ($p=.004$). Centiloid values correlated with both the level of confidence in the diagnosis of AD indicated by clinicians before PET ($r=0.128$, $p<.001$, figure 2a) and with MMSE ($r=-0.202$, $p<.001$, figure 2b).

Conclusions: Quantitative analysis of a large heterogeneous dataset of real-world amyloid PET scans shows high concordance with visual reads and expected relationships with clinical and neuropsychological measures. The findings support the feasibility of quantification and the validity of clinical amyloid PET.

All (n=8,895)	
Age (mean ± SD)	76 ± 6
MMSE* (mean ± SD)	24.5 ± 4.9
MoCA[#] (mean ± SD)	21.0 ± 5.2
Female	51.1%
Dementia / MCI	36.4% / 63.6%
¹⁸F-florbetaben	29.1%
¹⁸F-florbetapir	64.8%
¹⁸F-flutemetamol	6.1%
Visually Positive^{&}	62.1%
Quantitatively Positive (Centiloids > 24.4)	60.2%

Table 1: Patients and Scans characteristics.

MMSE = Mini-Mental State Examination; MoCA = Montreal Cognitive Assessment; MCI = Mild Cognitive Impairment; *n=6,973; #n=2,353; &n=8,887.

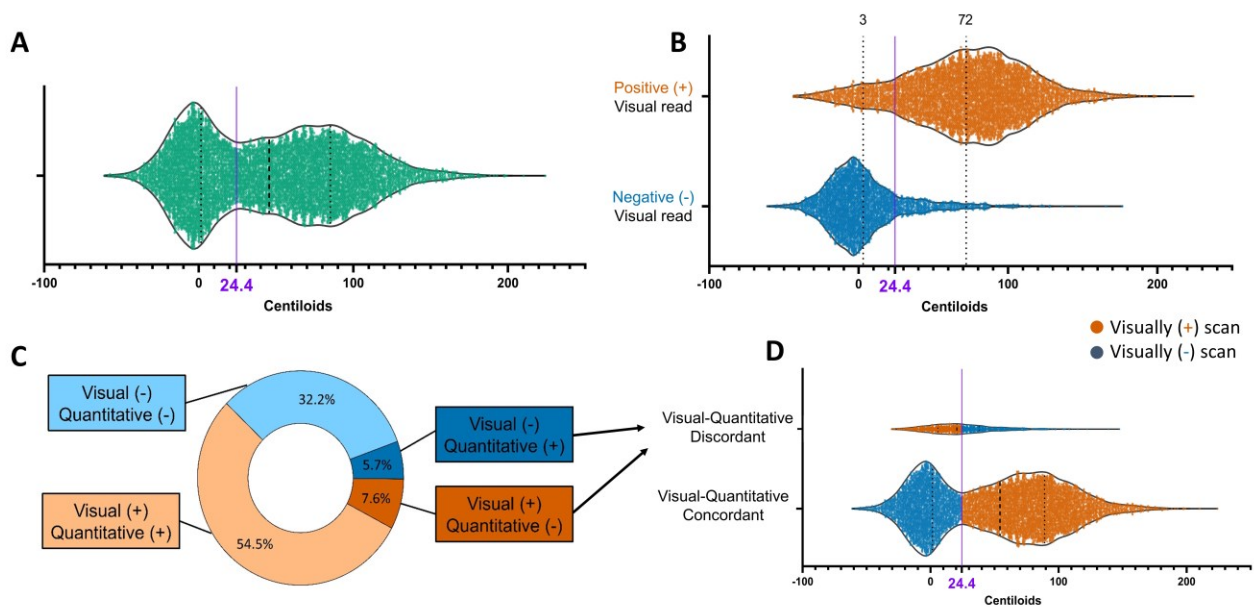


Figure 1: Image quantification (Centiloids) versus visual reads.

A) Bimodal distribution of Centiloids in the whole cohort; the predetermined threshold of 24.4 Centiloids is indicated in purple. **B)** Centiloids distribution in scans read as negative (mean = 3) versus positive (mean = 72). **C)** Breakdown of scans by their visual read (positive versus negative) and by their quantification (positive versus negative based on the 24.4-Centiloids threshold). **D)** Distribution of Centiloids in cases where quantification and visual read were concordant or discordant. The concordant scans exhibit a bimodal distribution away from the 24.4-Centiloids positivity threshold, whereas the discordant cases have Centiloid values around it. Visually positive scans are marked in orange and negative in blue.

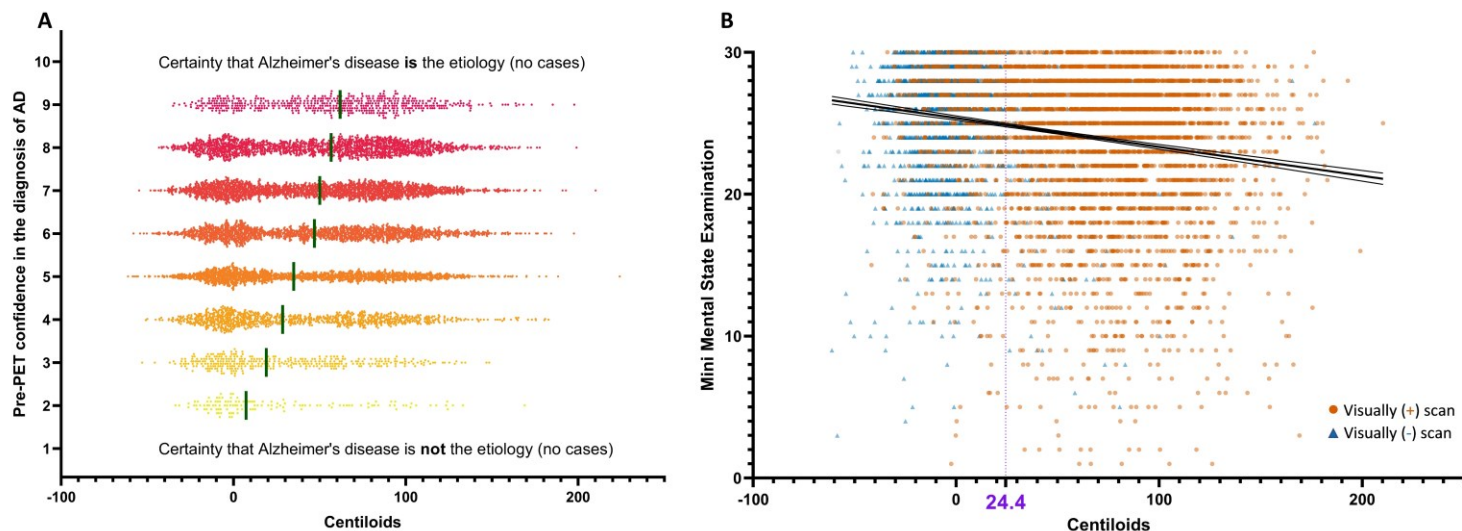


Figure 2: Correlations between Centiloids and clinical variables.

A) Pre-PET confidence that Alzheimer's disease (AD) neuropathology contributes to cognitive decline correlated with the subsequently obtained Centiloid values ($r = 0.128$, $p < .001$, $n = 8,894$). Green lines indicate median Centiloids. The level of confidence was indicated by clinicians, before the performance of PET, on a 1-10 Likert scale, with 1 indicating that AD is certainly not the etiology and 10 that it certainly is. Because inclusion criteria required that etiology would be uncertain and that AD would be a consideration, no patients received confidence levels of 1 or 10. **B)** Mini Mental State Examination scores correlated with Centiloid values ($r = -0.202$, $p < .001$, $n = 6,973$). Visually positive scans are marked in orange dots and negative scans in blue triangles. The purple line indicates the 24.4 Centiloids positivity threshold. For 7 scans visual reads were not available (grey dots).

Keywords: Amyloid Positron Emission Tomography, Alzheimer's disease

Wednesday, January 11, 2023 - 05:00 pm - 06:05 pm

Podium Session

SESSION IV: Non-AD and co-pathologies

CHAIRS: *Milos Ikonovic, Melissa Murray*

Wednesday, January 11, 2023		
5:00 pm – 6:05 pm	SESSION IV: NON-AD AND CO-PATHOLOGIES	Milos Ikonovic, MD, <i>University of Pittsburgh</i> Melissa Murray, PhD, <i>Mayo Clinic, Jacksonville</i>
5:00	Introduction	Chairs
5:05	Tau Burden Evaluation by [18F] Flortaucipir PET and Quantitative Tau Neuropathology in Alzheimer's Disease And Non-Alzheimer's Tauopathies	Rodolfo Gatto, PhD, <i>Mayo Clinic, Rochester</i>
5:20	Pathologic Correlations of [18F]-Flortaucipir Imaging in non-Alzheimer Corticobasal Degeneration Syndrome	Cinthyia Agüero, MD, <i>MassGeneral Institute for Neurodegenerative Disease</i>
5:35	Unveiling the neurobiological basis of F18-flortaucipir in different tauopathies using voxel-to-voxel histology to PET comparisons: the role of p-tau, iron and MAOB	Yuheng Chen, PhD, <i>University of California, San Francisco</i>
5:50	Association of FDG-PET with co-pathologies in autopsy-proven AD	Marianne Chapleau, PhD, <i>University of California, San Francisco</i>
6:05	Discussion	

Tau Burden Evaluation by [18F] Flortaucipir PET and Quantitative Tau Neuropathology in Alzheimer's Disease And Non-Alzheimer's Tauopathies

Rodolfo G. Gatto¹, Jennifer L. Whitwell², Val J. Lowe², R. Ross Reichard³, Keith A. Josephs¹

¹Division of Neurology, Mayo Clinic, Rochester, MN, US

²Division of Radiology, Mayo Clinic, Rochester, NM, US

³Division of Anatomic Pathology, Mayo clinic, Rochester, MN, US

Background: Over the last decade, there has been a rapid development of neuroimaging techniques to measure underlying tau proteins in the brain using positron emission tomography (PET). One of the most widely used ligands to measure in vivo tau is [18F] flortaucipir (FTP). However, limited information exists on the relationship between antemortem FTP uptake and the postmortem burden of tau in different tauopathies.

Objectives: The purpose of this study is to determine how well antemortem FTP uptake matches the burden of postmortem tau in Alzheimer's Disease (AD) versus non-AD tauopathies.

Material and methods: We compared regional ante-mortem FTP uptake with postmortem tau burden measured using a phospho-tau marker (AT8) in four autopsied cases with none, low, intermediate, and high likelihood AD and in five non-AD tauopathies, including progressive supranuclear palsy (n=3), Pick's disease (PiD) (n=1), and Globular Glial tauopathy (GGT) (n=1). Quantitative FTP uptake was determined using standardized uptake value ratios (SUVR) from nine established regions of interest (ROIs) and was compared with quantitative measures of AT8 immunohistochemically labeled tau using digital pathology in these same regions.

Results: The median age at death of the AD cases was 79 years (range: 78-80) and 82 years (range: 68- 87) in the non-AD tauopathies. Quantitative neuropathological burden of tau showed a good correlation with antemortem FTP uptake in AD ($r= 0.70$, $p < 0.001$) but poor correlation in the non-AD tauopathies ($r=0.07$, $p=0.62$). However, in some ROIs in the AD cases, we found disparities between FTP SUVRs and quantitative tau burden in brain regions, such as the hippocampus, particularly in cases with no or low FTP content, and in the context of age-related 4R tauopathies.

Conclusion: Our findings support the notion that FTP uptake better corresponds to tau burden in AD cases than in non-AD tauopathies, although regional disparities do exist in AD.

Keywords: Non-Alzheimer Tauopathies, Alzheimer's Disease, Flortaucipir PET, Neuropathology, Tau Burden

Pathologic Correlations of [18F]-Flortaucipir Imaging in non-Alzheimer Corticobasal Degeneration Syndrome

Cinthya Aguero^{1,2}, Margaret Scapellato^{1,2}, Maeva Dhaynaut^{3,4}, Sunny Kumar^{1,2}, Justin Sanchez^{3,4}, Anna Goodheart^{1,2}, Stephen Gomperts^{1,2}, Angelica Gaona^{1,2,5}, Theresa Connors^{1,2,5}, Alexandra Melloni^{1,2,5}, Romain Perbet^{1,2}, Georges El Fakhri^{3,4}, Matthew P Frosch^{1,2,5}, Marc D. Normandin^{3,4}, Teresa Gomez-Isla^{1,2}

¹MassGeneral Institute for Neurodegenerative Disease, Charlestown, MA, US

²Department of Neurology, Massachusetts General Hospital, Boston, MA, US

³Department of Radiology, Massachusetts General Hospital, Boston, MA, US

⁴Gordon Center for Medical Imaging, Division of Nuclear Medicine and Molecular Imaging, Massachusetts General Hospital, Boston, MA, US

⁵C.S. Kubik Laboratory for Neuropathology, Massachusetts General Hospital, Boston, MA, US

Background: Corticobasal syndrome (CBS) is a disorder of movement, cognition, and behavior associated with a heterogeneous spectrum of underlying pathologies, including corticobasal degeneration (CBD), Alzheimer's disease (AD), and progressive supranuclear palsy (PSP), among others. Recent studies have suggested that subjects with non-AD CBS exhibit greater regional [18F]-Flortaucipir PET retention and associated regional atrophy in areas commonly associated with corticobasal degeneration than healthy control subjects.

Objective: To examine the correlation of in vivo [18F]-Flortaucipir retention and postmortem regional tau lesion burden in four non-AD CBS cases that came to autopsy.

Methods: Four subjects with CBS underwent structural MRI, tau-PET with [18F]-Flortaucipir (3.1±1.2yr prior to death), amyloid-PET with [11C]-Pittsburgh compound B, detailed clinical examinations and neuropsychological testing, and came to autopsy. [18F]-Flortaucipir autoradiography (with and without ethanol washing steps) and postmortem quantitative tau measures were performed. Flortaucipir standard uptake value ratios (SUVRs) were compared to AT8 phosphorylated tau (pTau) burden in brain samples containing 19-20 matching regions of interest (ROIs).

Results: The four subjects exhibited greater [18F]-Flortaucipir PET in vivo retention in subcortical than in cortical regions. All were amyloid negative. Neuropathological examination confirmed a CBD diagnosis in two subjects, PSP in one and thalamic gliosis in one. Quantification of tau burden in immunostained sections revealed robust loads of tau lesions in the CBD and PSP cases. No tau pathology was detected in the subject with thalamic gliosis. No significant correlation was detected between [18F]-Flortaucipir in vivo retention and postmortem tau burden in matching ROIs in any of the cases. Autoradiography failed to show detectable [18F]-Flortaucipir binding in the regions containing tau lesions.

Conclusion: [18F]-Flortaucipir PET may help to distinguish CBS due to AD from non-AD CBS but has limited utility for the reliable detection and quantification of pathological tau burdens in non-AD CBS cases.

Keywords: Tau-PET, CBS, Autoradiography, Flortaucipir

Unveiling the neurobiological basis of F18-flortaucipir in different tauopathies using voxel-to-voxel histology to PET comparisons: the role of p-tau, iron and MAOB

Yuheng Chen¹, Renaud La Joie¹, Duygu Tosun^{7,8}, Daniela Ushizima^{2,3,5}, Helmut Heinsen⁶, Gil Rabinovici¹, Lea T. Grinberg^{1,4,5}

¹Memory and Aging Center, Department of Neurology, University of California, San Francisco, San Francisco, CA, US

²Berkeley Institute for Data Science, University of California, Berkeley, Berkeley, CA, US

³Lawrence Berkeley National Laboratory, Berkeley, CA, US

⁴LIM-22, Department of Pathology, University of Sao Paulo, Sao Paulo, BR

⁵Bakar Institute for Computational Health Sciences, University of California San Francisco, San Francisco, CA, US

⁶Julius-Maximilians University Würzburg, Würzburg, Germany

⁷Department of Radiology, University of California San Francisco, San Francisco, CA, US

⁸Veterans Affairs San Francisco, San Francisco, CA, US

Introduction/Objectives: We aimed to identify the contributions of p-tau (Ser 202,CP-13), iron, and MAOB to flortaucipir signal in different tauopathies by performing voxel-to-voxel correlations between histological and PET uptake values.

Methods: Full coronal slides of ~1cm thickness from four tauopathy cases (AD, progressive supranuclear palsy, corticobasal degeneration, and (FTLD due to MAPT mutation P305S) and one FTLD-TDP type-A case were processed following a computational histopathology pipeline (Ushizima, Chen, et al. 2021), allowing for whole 3D reconstruction of the histological deposits/markers maps at microscopical level, aligned to their corresponding neuroimaging maps (Fig. 1). Serial 120um thick histological slides underwent immunohistochemistry to p-tau (Ser 202, CP-13) and MAOB and Perls' staining for detecting iron. Density of pathological changes per voxel ($1.22 \times 1.22 \times 120 \mu\text{m}^3$) was measured using convolution neuron network algorithms. Flortaucipir images were thresholded at 1.2 SUVR. Bivariate and multiple linear regressions were used to compare area of high flortaucipir signal to histological counterparts.

Results: The time gap between PET and autopsy was 0.75 to 4.16 years. Figure 2 depicts voxel-to-voxel correlations. Association between p-tau and flortaucipir was highest in AD (Table 1). Multiple regression shows coefficient between iron and flortaucipir to be twice higher than coefficient between p-tau and flortaucipir in non-AD cases. MAOB showed a very poor correlation with flortaucipir, except in cases with tau pathology (and accompanying MAOB increase) in white matter.

Figure 1: Data segmentation/registration pipeline from microscopic histology to MRI/PET scan space. Fig 1A to D represents the Iron staining pipeline (Perl's staining), and Fig 1E to H represents the p-Tau staining pipeline (CP13 anti-tau antibody). Fig. 1A and E show microscopic scanned digital images with pathological marker staining (Iron and p-Tau). Images are processed through computational histopathology pipeline (Ushizima, Chen et al 2021) for deep-learning biomarker segmentation, the resulting quantitative heatmaps are then registered to the postmortem tissue image, show in Fig. 1B and F. In Fig. 1C and G, histological heatmap are further registered to MRI, and thus co-registered with the PET scan data (flortaucipir PET) in Fig. 1D and H

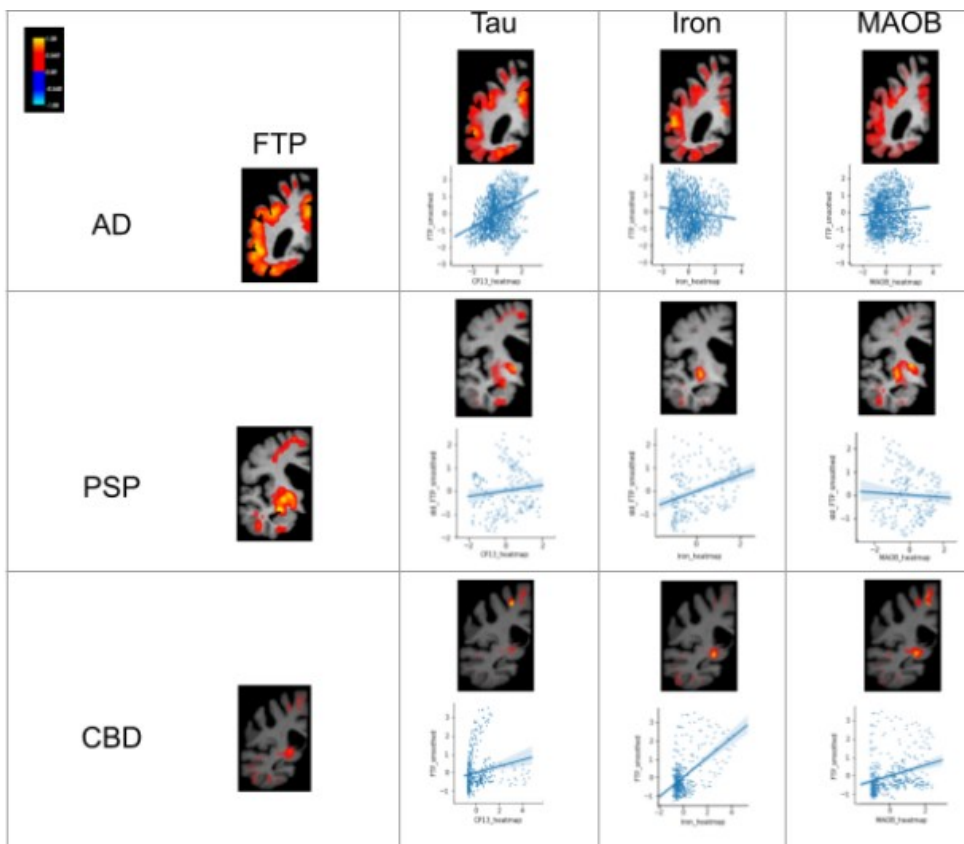
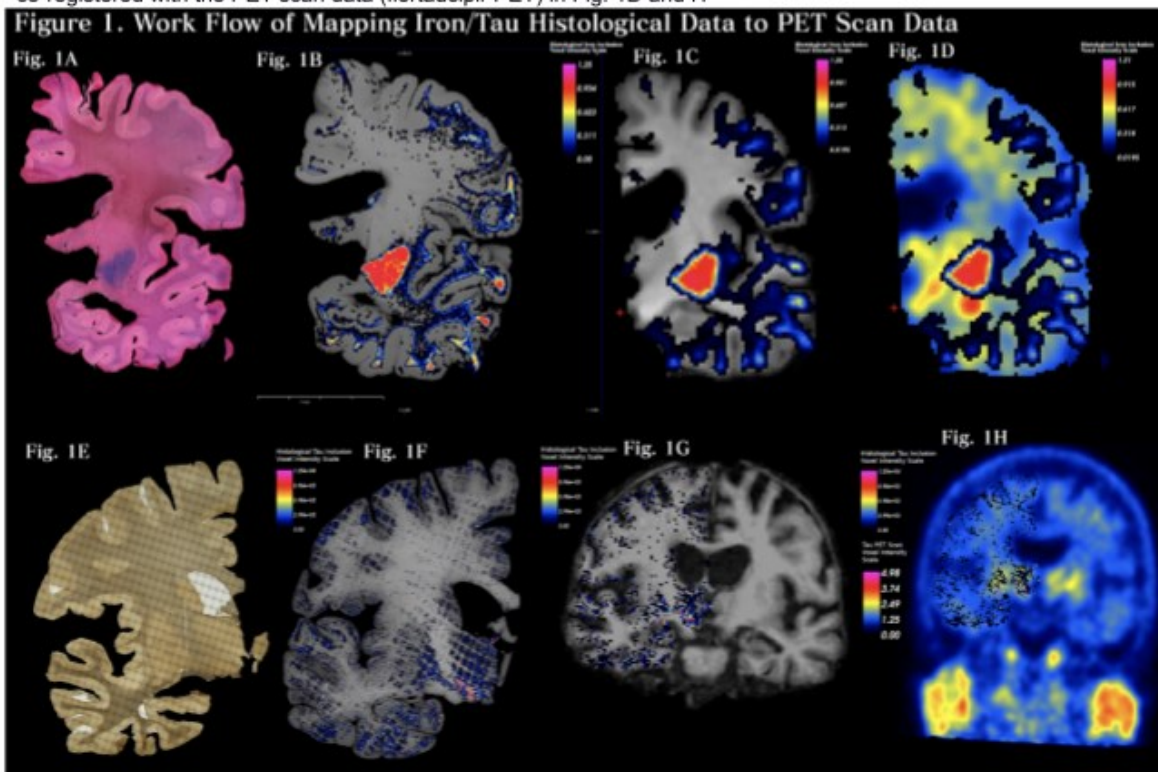


Figure 2. Bivariate linear regressions of coregistered, masked flortaucipir (FTP)-PET data to the corresponding histological staining data: p-tau (Ser 202, CP-13), MAOB (HPA002328, Atlas antibody) and Perls' staining for detecting iron. Heatmap shows the intensity for each voxel from low (red) to high (yellow), pathology density. Each row shows data that are collected from different tauopathies: AD (Alzheimer's disease), PSP (progressive supranuclear palsy) and CBD (corticobasal degeneration). Each scatterplot with regression line represent the linear regression for different pairs of data: FTP vs p-tau, FTP vs Iron, and FTP vs MAOB for each tauopathy. Each dot represents a voxel.

Table 1. Bivariate and multiple linear regression results comparing Flortaucipir signal intensity of various neuropathological measures. Tissue was masked to only include areas with Flortaucipir signal
AD: Alzheimer's disease. CBD: corticobasal degeneration; FTLD: frontotemporal lobar degeneration; FTP: Flortaucipir; nan: no available number; PSP: progressive supranuclear palsy

		case 1		case 2	case 3	case 4	case 5
		AD	AD	PSP	CBD	FTLD w/ MAPT mutation P305S	FTLD-TDP-43 type A
Level of coronal slide		amygdala	splenium of corpus callosum	amygdala	lateral geniculate body	supraoptic area	amygdala
ADNC ABC score		A3B3C3		A1B1C1	A0B1C0	A0B0C0	A1B1C0
p-tau vs. FTP	R ²	0.115	0.029	0.092	0.03	0.059	0.001
	coefficient	0.3392	0.171	0.1507	0.1731	-0.2423	0
	p-value	<0.0001	<0.0001	<0.0001	<0.0001	<0.0001	nan
Iron vs. FTP	R ²	0.01	0.084	0.117	0.283	0.045	0.112
	coefficient	-0.1007	0.2891	0.3424	0.5321	0.2122	0.334
	p-value	<0.0001	<0.0001	<0.0001	<0.0001	<0.0001	<0.0001
MAOB vs FTP	R ²	0.007	0.014	0.052	0.083	0.063	0.185
	coefficient	0.0842	-0.1169	-0.0645	0.2877	0.2513	-0.4296
	p-value	0.001	0.005	0.001	0.001	<0.0001	<0.0001
Multiple regression	R ²	0.123	0.227	0.133	0.348	0.175	0.271
	p-tau coefficient	0.3284	0.419	0.184	0.3083	-0.3069	0
	Iron coefficient	-0.0633	0.4791	0.2814	0.5694	0.1977	0.2966
	MAOB coefficient	0.0598	-0.1423	-0.0558	-0.1957	0.2324	-0.4013
	p-value (p-tau)	<0.0001	<0.0001	<0.0001	<0.0001	<0.0001	nan
	p-value (iron)	<0.0001	<0.0001	<0.0001	<0.0001	<0.0001	<0.0001
	p-value (MAOB)	0.013	<0.0001	<0.0001	<0.0001	<0.0001	<0.0001

Conclusion: Confirming previous studies, the correlation of p-tau and flortaucipir was higher in AD than in other tauopathies. Our results suggest that iron deposition contributes to flortaucipir uptake independent of p-tau, whereas MAOB contribution is almost null in gray matter. The time gap between PET and autopsy and low resolution of PET compared to histology may explain the weak associations, but other unexplored contributors cannot be discarded.

Keywords: histology, PET, Tau, Iron, Machine Learning

Association of FDG-PET with co-pathologies in autopsy-proven AD

Marianne Chapleau¹, Nidhi Mundada¹, Salvatore Spina¹, William Seeley^{1,3}, Lea T. Grinberg^{1,3}, Renaud La Joie¹, Gil D. Rabinovici^{1,2}

¹Memory and Aging Center, Department of Neurology, University of California, San Francisco, San Francisco, CA, US

²Department of Radiology & Biomedical Imaging, University of California, San Francisco, San Francisco, CA, US

³Department of Pathology, University of California, San Francisco, San Francisco, CA, US

Background: The presence of multiple pathologies is the rule and not the exception in Alzheimer's disease (AD). The goal of this study was to assess whether 18F fluorodeoxyglucose (FDG) PET can provide information about the presence of non-AD pathologies in patients with autopsy-proven AD.

Method: Our cohort included 55 patients with antemortem FDG-PET and autopsy-proven intermediate/high ADNC from the UCSF Neurodegenerative Diseases Brain Bank. All patients underwent FDG-PET (~5–10 mCi dose, acquired at 30–60 minutes post-injection) on one of two PET scanners (Siemens ECAT or Biograph). Standardized uptake value ratio (SUVR) images were computed using the pons as reference region. W-maps (adjusted Z-score maps) were created, comparing each patient to a group of 187 controls (age range: 20–96, 40% males), adjusted for age, sex, and scanner type. Voxel-wise correlations were computed to verify the unique contribution of each neuropathology to cerebral hypometabolism, while controlling for age, sex, time between FDG-PET scan and death, scanner type, Braak staging, and the presence of all other co-pathologies.

Results: The sample consisted of 55% males, mean age was 63.8 ± 10.5 , mean time between FDG and death was 6.2 ± 2.8 , and mean MMSE was 21.1 ± 7.1 at the time of PET (Table 1). Group averaged W-map showed the typical temporoparietal AD pattern; hypometabolism in these regions was associated with higher Thal phase and Braak stage (Figure 1). Argyrophilic thorny astrocyte clusters (ATAC) and cerebral amyloid angiopathy (CAA) were associated with hypometabolism in the left antero-medial temporal lobe, while limbic-predominant age-related TDP43 encephalopathy neuropathologic change (LATE-NC) was associated with bilateral hypometabolism in the same regions (Figure 2).

Conclusion: Antero-medial temporal hypometabolism is a crucial marker of AD pathology, but our findings further show that it is also indicative of the presence of other common co-pathologies in AD patients.

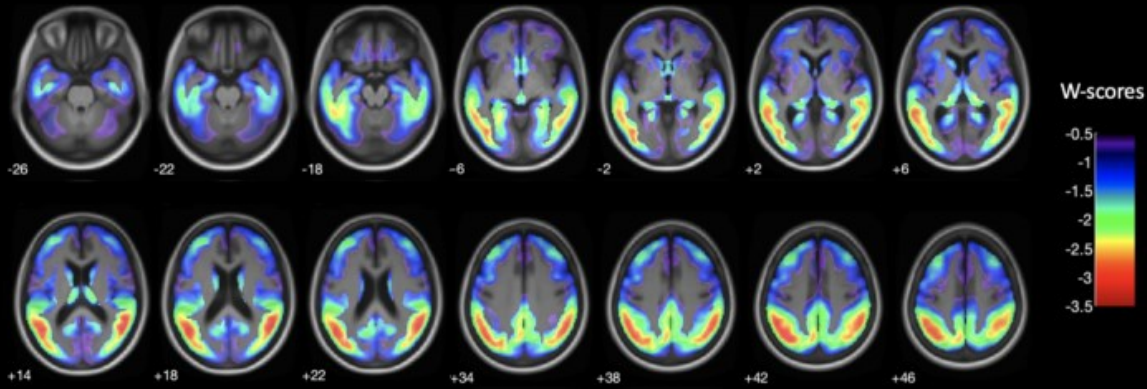
Table 1. Demographics and clinical information of the AD cohort (n=55)

DEMOGRAPHICS	Age at PET	63.8 ± 10.5
	Age at death	70.0 ± 10.3
	Male, %	55%
	Education	17 ± 1.5
CLINICAL INFORMATION	MMSE at PET	21.1 ± 7.1
	Global CDR at PET	0.8 ± 0.4
	Clinical diagnosis at PET	AD (52%) bvAD (2%) bvFTD (4%) limbic-predominant process (2%) lvPPA (13%) MCI (4%) PD dementia (2%) PCA (21%) progressive aphasia (2%)
PATHOLOGICAL INFORMATION	Amyloid	100% Thal phase 2 (n=1), 3 (n=2), 4 (n=3), 5 (n=50)
	Tau	100% Braak stage IV (n=3), V (n=5), VI (n=48)
	CERAD score	2 (n=1), 3 (n=55)
	Arteriolosclerosis	100%
	CAA	84% None (n=9), mild (n=36), moderate (n=9), severe (n=1), NA (n=1)
	AGD	66% None (n=19), limbic (n=36), diffuse (n=1)
	LBD	46% None (n=30), limbic-transitional (n=6), diffuse neocortical (n=5), amygdala-predominant (n=12), non-conforming (n=3)
	VBI	46%
	ARTAG	40%
	ATAC	21%
	LATE-NC	16% None (n=47), hippocampus (n=9)
	HS	7%

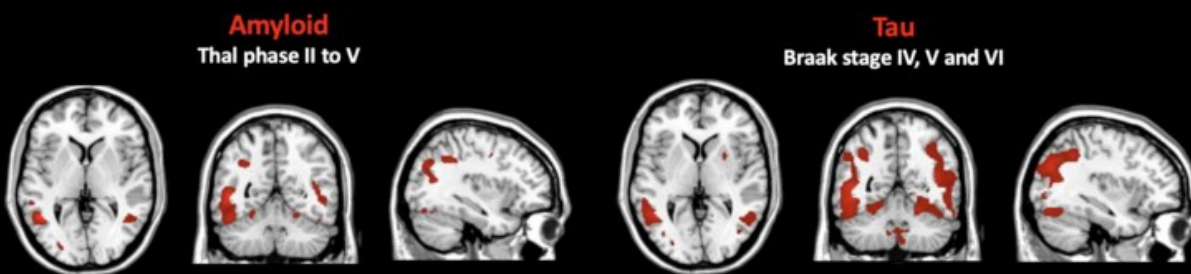
Legend. Values are expressed as % or mean ± standard deviation. MMSE=Mini-Mental State Examination; CDR=Clinical Dementia Rating; AD: Alzheimer's disease; bvAD: behavioral variant Alzheimer's disease; lvPPA: logopenic variant primary progressive aphasia; MCI: mild cognitive impairment; PD: Parkinson's disease dementia; PCA: posterior cortical atrophy. Pathological information. The first rows represent % of presence, and the second rows represent the specific breakdown in participants. CERAD score: Consortium to Establish a Registry for Alzheimer's Disease; CAA: cerebral amyloid angiopathy; AGD: argyrophilic grain disease; LBD: Lewy body disease; VBI: vascular brain injury; ARTAG: aging-related tau astroglipathy; ATAC: argyrophilic thorny astrocyte clusters; LATE-NC: limbic-predominant age-related TDP43 encephalopathy neuropathologic change; HS: hippocampal sclerosis.

Figure 1. Hypometabolism pattern in pathology-proven AD patients

A. Mean hypometabolism pattern



B. More hypometabolism with increasing staging of x

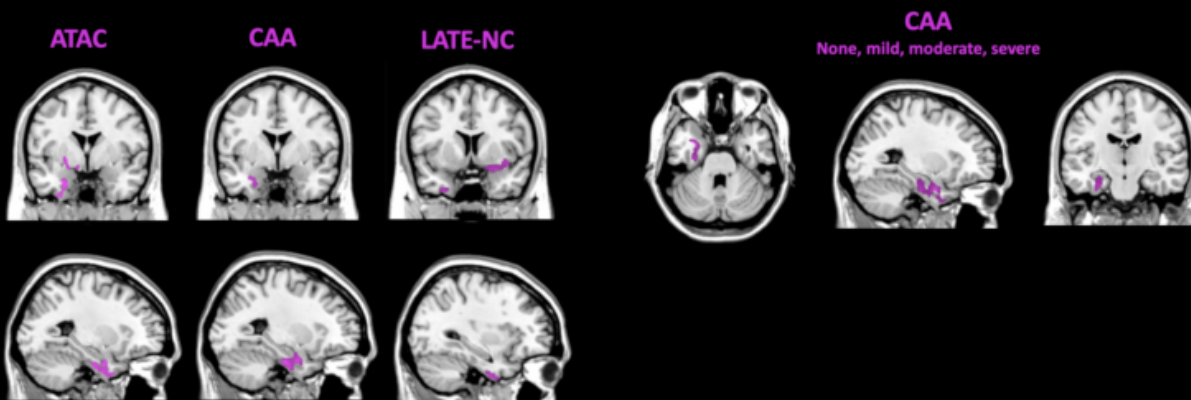


Legend. Panel A shows the mean hypometabolism pattern in our cohort of 55 AD patients after adjusting for age, sex, and scanner type. Panel B shows the linear relationship between amyloid and tau and the hypometabolism pattern, after adjusting for age, sex, time between FDG-PET scan and death, scanner type, and all other co-pathologies. The results are displayed at uncorrected $p < 0.001$. AD: Alzheimer's disease.

Figure 2. Contribution of co-pathologies to the pattern of hypometabolism

A. Unique contribution of x to the pattern of hypometabolism

B. More hypometabolism with increasing staging of x



Legend. The results are showing the linear relationship between each co-pathology and FDG-PET hypometabolism, after adjusting for age, sex, time between FDG-PET scan and death, scanner type, Braak staging, and the presence of all other copathologies. The results are displayed at uncorrected $p < 0.001$. The following pathologies did not yield significant results and were not included in the figure: AGD, ARTAG, HS, LBD (including staging), and VBI. CAA: cerebral amyloid angiopathy; AGD: argyrophilic grain disease; LBD: Lewy body disease; VBI: vascular brain injury; ARTAG: aging-related tau astrogliaopathy; ATAC: argyrophilic thorny astrocyte clusters; LATE-NC: limbic-predominant age-related TDP43 encephalopathy neuropathologic change; HS: hippocampal sclerosis. Staging of CAA: none (n=9), mild (n=36), moderate (n=9) and severe (n=1).

Keywords: Alzheimer's disease; co-pathologies; FDG-PET

Thursday, January 12, 2023 - 08:30 am - 09:20 am

Podium Session

SESSION V: AD neuropathology

Thursday, January 12, 2023		
8:30 am – 9:20 am	SESSION V: AD NEUROPATHOLOGY	CHAIRS: Teresa Gomez-Isla, MD, PhD, <i>Massachusetts General Hospital</i> Laetitia Lemoine, PhD, <i>Karolinska Institutet</i>
8:30	Introduction	Chairs
8:35	Specific associations between plasma biomarkers and post-mortem amyloid plaque and neurofibrillary tau tangle loads	Gemma Salvado, PhD, <i>Lund University</i>
8:50	Intersection of amyloid- β and tau brain pathology influences plasma phosphorylated tau levels	Melissa Murray, PhD, <i>Mayo Clinic, Jacksonville</i>
9:05	Tangle maturity markers associate with tau PET and cognitive measures in hippocampus	Christina Moloney, PhD, <i>Mayo Clinic, Jacksonville</i>
9:20	Postmortem validation of 18F-MK-6240 PET using autoradiography and in-vitro binding combined with antibody-based assays in frozen brains from two autopsy cases	Tobey Betthausen, PhD, <i>University of Wisconsin-Madison</i>
9:35	Discussion	

Specific associations between plasma biomarkers and post-mortem amyloid plaque and neurofibrillary tau tangle loads

Gemma Salvadó¹, Rik Ossenkoppele^{1,2,3}, Nicholas J. Ashton^{4,5,6}, Thomas G. Beach⁷, Geidy E. Serrano⁷, Gwendlyn Kollmorgen⁸, Alexander Jethwa⁸, Margherita Carboni⁹, Henrik Zetterberg^{4,10,11,12,13}, Niklas Mattsson-Carlgrén^{1,14,15}, Shorena Janelidze¹, Kaj Blennow^{4,10}, Oskar Hansson^{1,16}

¹Clinical Memory Research Unit, Department of Clinical Sciences, Malmö, Lund University, Lund, Sweden

²Alzheimer Center Amsterdam, Neurology, Vrije Universiteit Amsterdam, Amsterdam UMC location VUmc, Amsterdam, The Netherlands

³Amsterdam Neuroscience, Neurodegeneration, Amsterdam, The Netherlands

⁴Department of Psychiatry and Neurochemistry, Institute of Neuroscience and Physiology, The Sahlgrenska Academy, University of Gothenburg, Gothenburg, Sweden

⁵Institute of Psychiatry, Psychology and Neuroscience, Maurice Wohl Institute Clinical Neuroscience Institute, King's College London, London, UK

⁶NIHR Biomedical Research Centre for Mental Health and Biomedical Research Unit for Dementia at South London and Maudsley, NHS Foundation, London, UK

⁷Banner Sun Health Research Institute, Sun city, AR, US

⁸Roche Diagnostics GmbH, Penzberg, Germany

⁹Roche Diagnostics International Ltd, Rotkreuz, Switzerland

¹⁰Clinical Neurochemistry Laboratory, Sahlgrenska University Hospital, Mölndal, Sweden

¹¹Department of Neurodegenerative Disease, UCL Institute of Neurology, Queen Square, London, UK

¹²UK Dementia Research Institute at UCL, London, UK

¹³Hong Kong Center for Neurodegenerative Diseases, Hong Kong, CN

¹⁴Department of Neurology, Skåne University Hospital, Lund, Sweden

¹⁵Wallenberg Center for Molecular Medicine, Lund University, Lund, Sweden

¹⁶Memory Clinic, Skåne University Hospital, Malmö, Sweden

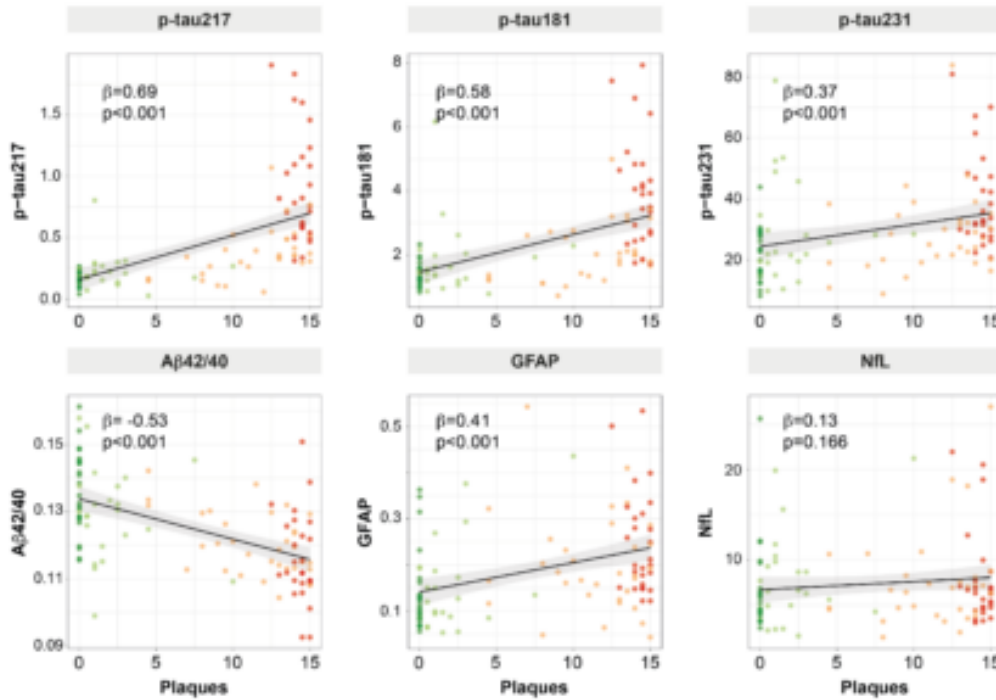
Introduction: Our objective was to investigate and compare specific associations between multiple plasma biomarkers (p-tau217 and p-tau181 (Lilly), p-tau231 (Gothenburg University) and A β 42/40, GFAP and NfL (Roche Diagnostics)) and neuropathological measures of amyloid and tau.

Methods: We included 105 participants from the Arizona Study of Aging and Neurodegenerative Disorders (AZSAND) with post-mortem neuropathological exam and antemortem collected plasma samples, 48 of whom had longitudinal p-tau217 and p-tau181. To assess specific associations between plasma biomarkers and each of the two pathologies, we used linear regression models, with both amyloid and tau measures as independent variables. Contribution of amyloid and tau on biomarker levels were assessed using partial R². Optimal combination of biomarkers for predicting presence (intermediate/high) of Alzheimer's disease neuropathologic change (ADNC) was selected based on the Akaike criterion (AIC). Longitudinal rates of change of p-tau217 and p-tau181 were compared on those with presence/absence of ADNC at death using linear mixed models. All models were adjusted for age, sex and time between blood sampling and death.

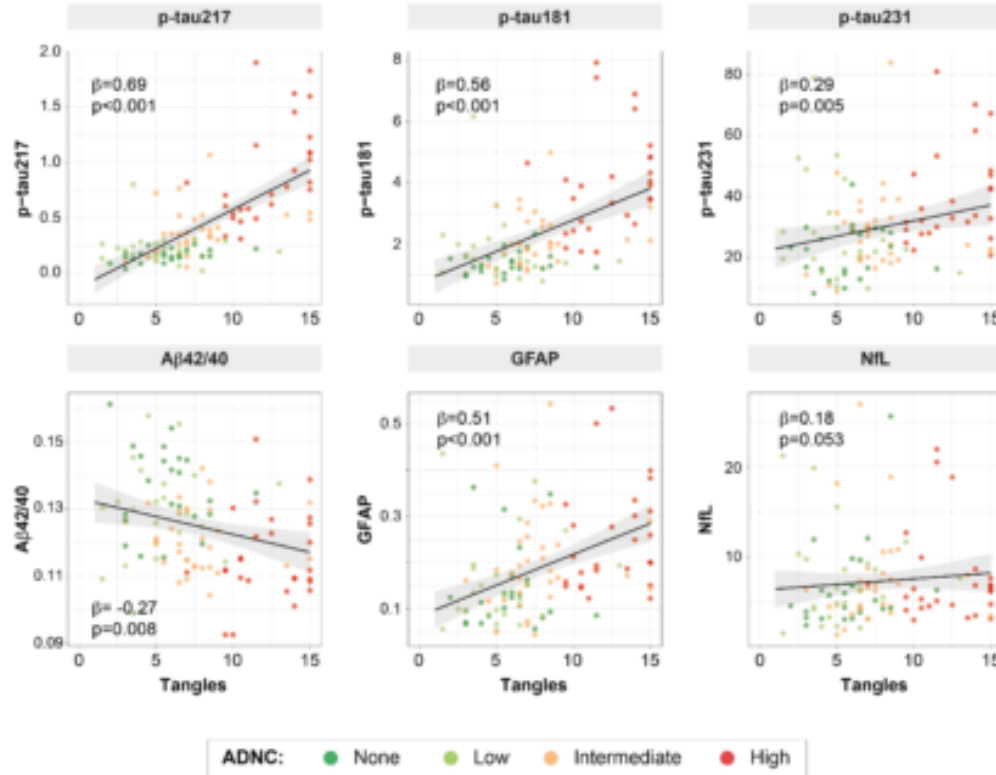
Results: All biomarkers except NfL were associated with plaques ($|b| \geq 0.37$, $p < 0.001$) and tangles ($|b| \geq 0.27$, $p < 0.008$, Figure 1) when assessed in independent models. When both measures were included in the same model, A β 42/40 and p-tau231 were specifically associated with plaques (bA β 42/40=-0.59, bp-tau231=0.32, $p \leq 0.007$), GFAP with tangles (bGFAP=0.39 $p < 0.001$) and p-tau181 and p-tau217 were associated with both pathologies (plaques: bp-tau217=0.46, bp-tau181=0.41, $p < 0.001$; tangles: bp-tau217=0.40; bp-tau181=0.30, $p \leq 0.004$). Plaques had a higher contribution (p-tau217=40.4%, p-tau181=35.7% total variance) than tangles (p-tau217=30.7%, p-tau181=17.1%) on these two biomarkers levels (Figure 2). Combining p-tau217 and A β 42/40 was optimal for detecting ADNC presence (AUC[95%CI]=0.90[0.84-0.96], Figure 3). P-tau217 longitudinal changes were significantly higher on those participants with presence of ADNC at death (b[95%CI]=0.13[0.02,0.24], $p=0.018$).

Conclusions: In our models, plasma p-tau217 was the most accurate for assessing tau tangles and amyloid plaques.

A) Plaques



B) Tangles



ADNC: ● None ● Low ● Intermediate ● High

Figure 1 Associations between plasma biomarkers and amyloid plaque or neurofibrillary tau tangle loads
 Black lines represent the association between plasma biomarkers and amyloid plaque (top) and tau tangle (bottom) loads after adjusting for covariates (age, sex, and time between blood sampling and death), but dots represent raw data. Datapoints are coloured based on the ADNC classification. Standardized betas and p-values of the association between plasma biomarkers and load of amyloid plaques or tau tangles are shown in the plot. Abbreviations: A β , amyloid- β ; ADNC, Alzheimer's disease neuropathologic change; GFAP, glial fibrillary acidic protein; NFL, neurofilament light; p-tau, phosphorylated tau.

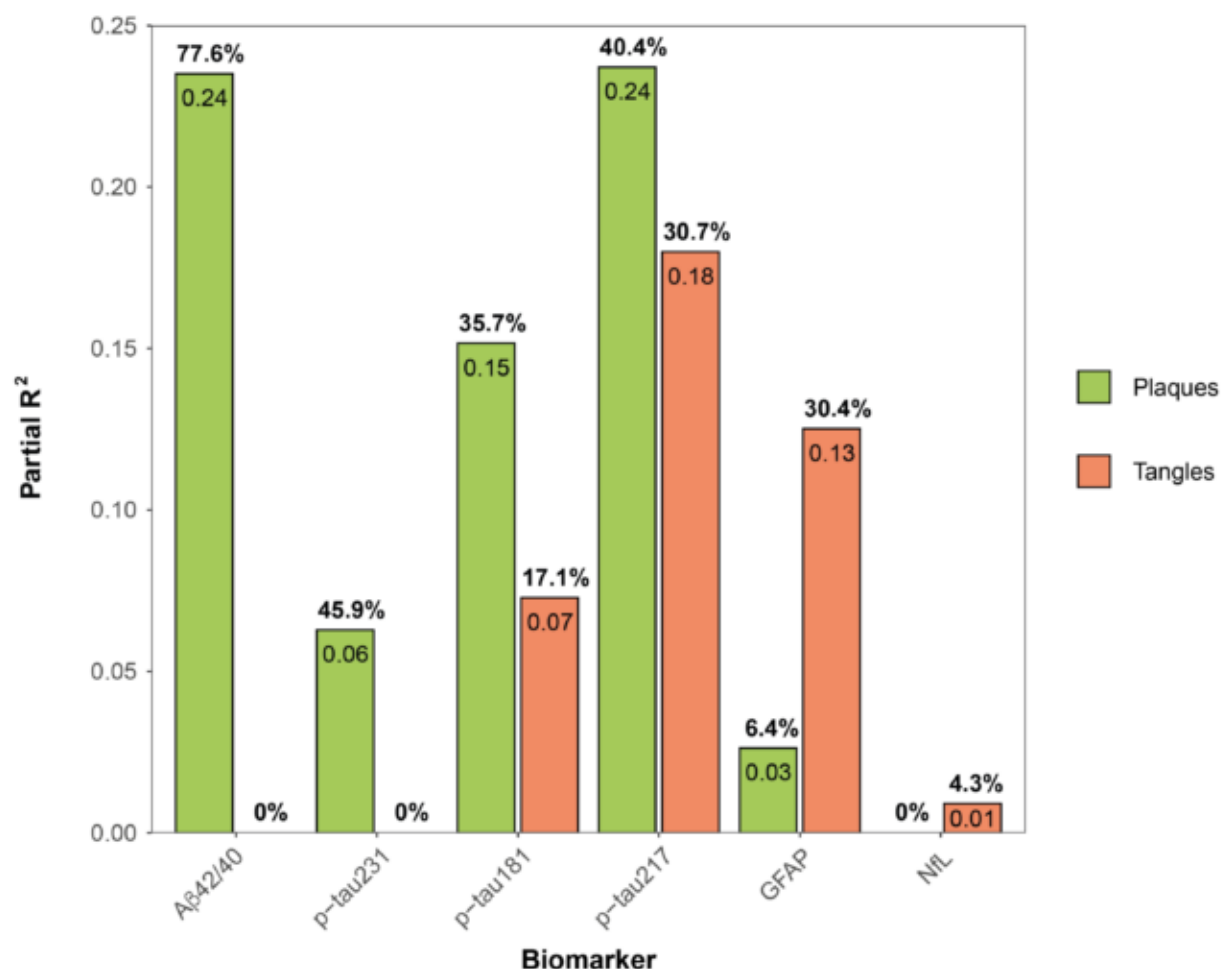


Figure 2 Contribution of amyloid plaque load and tau tangle load on plasma levels

Bars represent the partial R² of amyloid plaque load (green) and tau tangle load (orange) on plasma levels. Linear regression models were used for these analyses with each biomarker as an outcome, in independent models, and both amyloid load and tau load as independent variables in a multivariable model. Age, sex, and time between blood sampling and death were included as covariates. Numbers inside the bars represent partial R² and numbers above the bars represent the percent partial R² over the total R² of each model (%partial R² = 100*partial R²/total R²).

Abbreviations: Aβ, amyloid-β; GFAP, glial fibrillary acidic protein; NfL, neurofilament light; p-tau, phosphorylated tau.

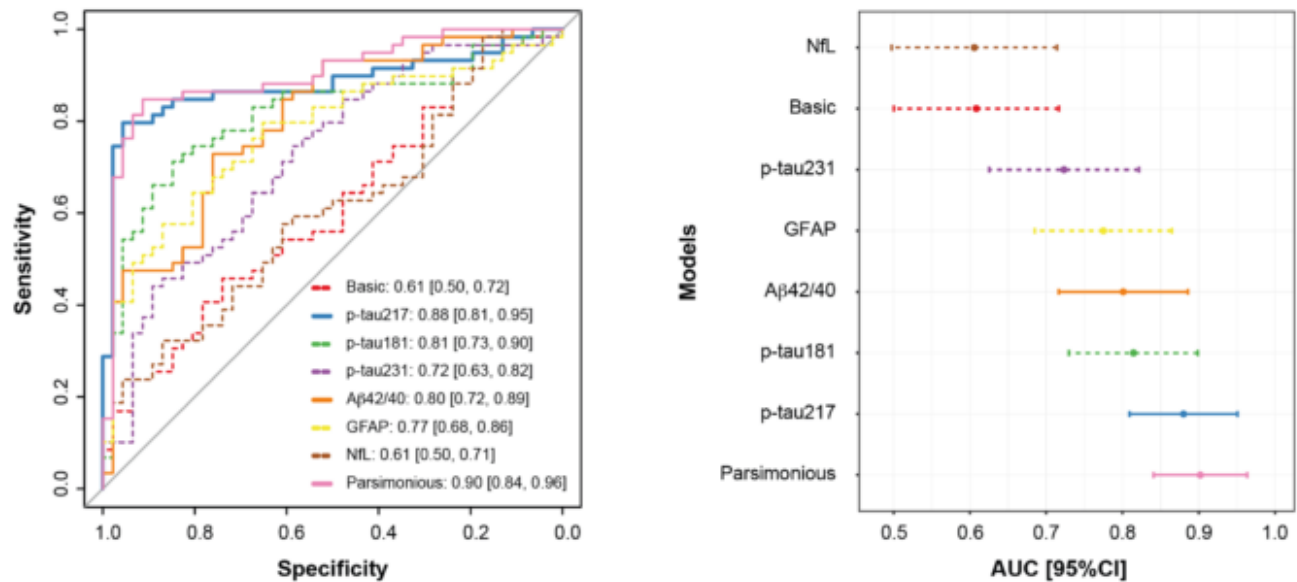


Figure 3 Plasma biomarkers for predicting presence of ADNC

ROC curves for all individual plasma biomarkers are shown in the left column and the correspondent AUC and 95%CI are shown in the right column, adjusting in all cases for age, sex and time between blood sampling and death. The parsimonious model for ADNC included p-tau217 and Aβ42/40 as predictors and age, sex and time between blood sampling and death as covariates. The basic model includes only covariates. ADNC was dichotomized as negative (none/low) or positive (intermediate/high). The individual biomarker with best performance is shown as a solid bold line. Dashed lines represent individual biomarkers with significant ($p < 0.05$) lower AUC than the best individual biomarker (p-tau217). Other models with solid lines represent AUC equivalent to that of the best individual biomarker.

Abbreviations: Aβ, amyloid-β; ADNC, Alzheimer's disease neuropathologic change; AUC, area under the curve, CI, confidence interval; GFAP, glial fibrillary acidic protein; NfL, neurofilament light; p-tau, phosphorylated tau; ROC, receiver operating characteristic.

Keywords: Plasma, neuropathology, head-to-head, p-tau species, longitudinal

Intersection of amyloid- β and tau brain pathology influences plasma phosphorylated tau levels

Melissa E. Murray¹, Christina M. Moloney¹, Naomi Kouri¹, Jeremy A. Syrjanen², Billie J. Matchett¹, Darren M. Rothberg¹, Jessica F. Tranovich¹, Tiffany N. Hicks Sirmans¹, Heather J. Wiste², Baayla D. C. Boon¹, Aivi T. Nguyen³, R. Ross Reichard³, Dennis W. Dickson¹, Val J. Lowe⁴, Jeffrey L. Dage⁶, Ronald C. Petersen⁵, Clifford R. Jack Jr.⁴, David S. Knopman⁵, Prashanthi Vemuri⁴, Jonathan Graff-Radford⁵, Michelle M. Mielke^{2,7}

¹Department of Neuroscience, Mayo Clinic, Jacksonville, FL, US

²Department of Quantitative Health Sciences, Mayo Clinic, Rochester, MN, US

³Department of Laboratory Medicine and Pathology, Mayo Clinic, Rochester, MN, US

⁴Department of Radiology, Mayo Clinic, Rochester, MN, US

⁵Department of Neurology, Mayo Clinic, Rochester, MN, US

⁶Department of Neurology, Indiana University, Indianapolis, IN, US

⁷Wake Forest University School of Medicine, Winston-Salem, NC, US

Advances in ultrasensitive detection of phosphorylated tau (p-tau) in plasma has enabled the measure of Alzheimer's disease (AD) biomarker changes using blood tests. Examination of postmortem brains of participants with antemortem plasma p-tau levels remains critical to understanding comorbid and AD-specific contribution to these changes. We analyzed 35 population-based Mayo Clinic study participants with plasma p-tau at threonine181 and threonine217 (p-tau181, p-tau217) available ≤ 3 years of death. Autopsied participants included cognitively unimpaired, mild cognitive impairment, AD dementia, and non-AD neurodegenerative disorders. Global neuropathologic scales of tau, amyloid- β , TDP-43, and cerebrovascular disease were examined. Regional digital pathology measures of tau (phosphorylated threonine181 and 217 [pT181, pT217]) and amyloid- β (6F/3D) were quantified in hippocampus and parietal cortex. Neurotransmitter hubs reported to influence development of tangles (nucleus basalis of Meynert) and amyloid- β plaques (locus coeruleus) were evaluated. The strongest regional associations were with parietal cortex for tau burden (p-tau181 $R=0.55$, $p=0.003$; p-tau217 $R=0.66$, $p<0.001$) and amyloid- β burden (p-tau181 $R=0.59$, $p<0.001$; p-tau217 $R=0.71$, $p<0.001$). Linear regression analysis of global neuropathologic scales explained 31% of variability in plasma p-tau181 and 59% in plasma p-tau217 (**Figure**). Neither TDP-43 nor cerebrovascular disease global scales independently contributed to variability. Global scales of tau pathology (β -coefficient=0.060, $p=0.016$) and amyloid- β pathology (β -coefficient=0.080, $p<0.001$) independently predicted plasma p-tau217 when modeled together with co-pathologies, but only amyloid- β (β -coefficient=0.33, $p=0.021$) predicted plasma p-tau181. While nucleus basalis of Meynert neuron count was not associated with plasma levels, lower locus coeruleus neuron count associated with higher plasma p-tau181 ($R=-0.50$, $p=0.007$) and plasma p-tau217 ($R=-0.55$, $p=0.002$). Cognitive scores ($R^2=0.31-0.34$) were predicted by the global tau scale, but not by global amyloid- β scale or plasma p-tau when modeled simultaneously. Higher soluble plasma p-tau levels may result from an intersection between insoluble deposits of amyloid- β and tau accumulation in brain, and may be associated with locus coeruleus degeneration.

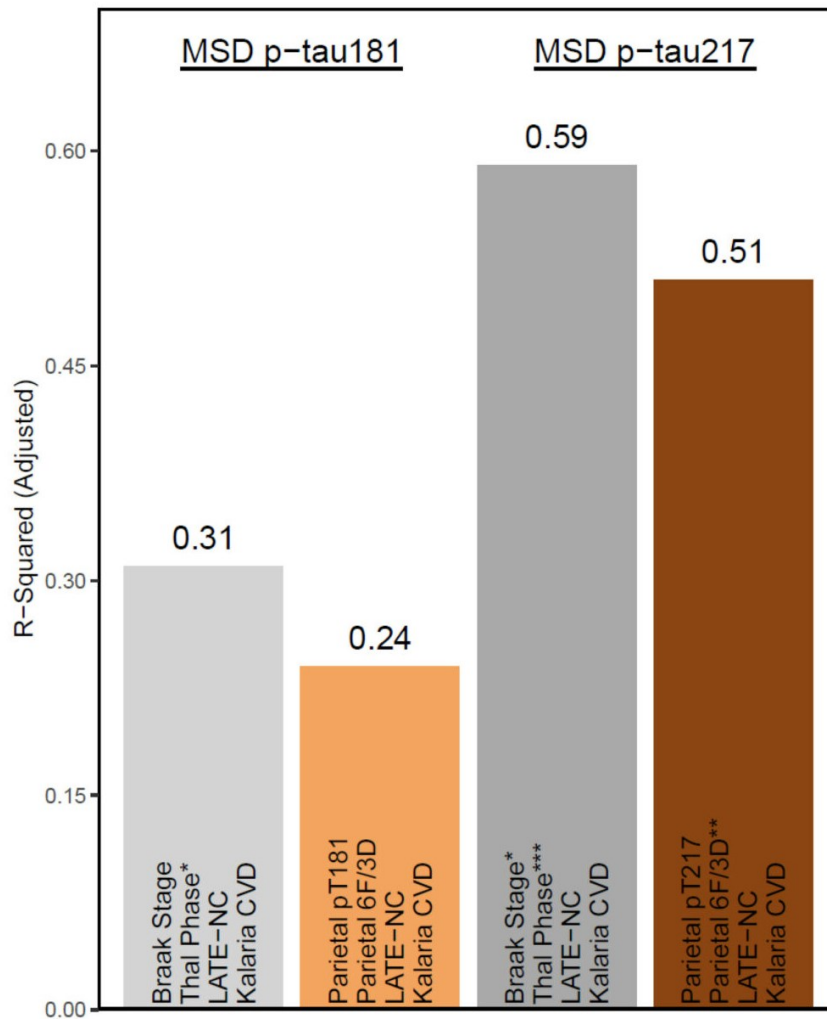


Figure. Multivariable linear regression modeling of neuropathologic variables as predictors of plasma p-tau levels.

Global scales of tau and amyloid- β (Braak and Thal, gray bars) and the strongest regional measure of tau and amyloid- β (parietal cortex, brown bars) were investigated as predictors of variability observed in plasma p-tau181 (left) and p-tau217 levels (right). To account for common co-pathologies, LATE-NC and Kalaria cerebrovascular disease were added to each model. Overall, the global scales performed better than the regional cortical measures with amyloid- β observed as strongest contributor to plasma p-tau variability. Time from plasma draw to death was not used to adjust, as it was not observed to associate with plasma p-tau levels. All variables in the model are shown. Significance denoted as * $p < 0.05$, ** $p < 0.01$, *** $p < 0.001$. Acronyms: 6F/3D=amyloid- β antibody. CVD=cerebrovascular disease. LATE-NC=limbic predominant age-related TDP-43 encephalopathy neuropathologic change. MSD=meso scale discovery. p-tau=phosphorylated tau for plasma levels. pT=phosphorylated threonine for immunohistochemical measures of tau.

Keywords: Alzheimer's Disease, Neuropathology, Blood Biomarker, Phosphorylated Tau, Neurofibrillary Tangles

Tangle maturity markers associate with tau PET and cognitive measures in hippocampus

Christina M. Moloney¹, Matthew H. Rutledge², Zhongwei Peng³, Ashley C. Wood¹, Darren M. Rothberg¹, Larissa E. Kries¹, Jessica F. Tranovich¹, Ekaterina I. Hofrenning⁴, Mary M. Machulda⁵, Ronald C. Petersen⁶, Clifford R. Jack Jr⁷, Dennis W. Dickson¹, Aivi T. Nguyen⁸, R. Ross Reichard⁸, Rickey E. Carter³, Prashanthi Vemuri⁷, Val J. Lowe⁷, Melissa E. Murray¹

¹Department of Neuroscience, Mayo Clinic, Jacksonville, FL, US

²Department of Neurology AI, Mayo Clinic, Rochester, MN, US

³Department of Quantitative Health Sciences, Mayo Clinic, Jacksonville, FL, US

⁴Department of Quantitative Health Sciences, Mayo Clinic, Rochester, MN, US

⁵Department of Psychology, Mayo Clinic, Rochester, MN, US

⁶Department of Neurology, Mayo Clinic, Rochester, MN, US

⁷Department of Radiology, Mayo Clinic, Rochester, MN, US

⁸Department of Laboratory Medicine and Pathology, Mayo Clinic, Rochester, MN, US

Background: The hippocampus is often considered a problematic area to obtain quantitative tau PET data. Although signal may be compromised, we hypothesized that tau PET measures would be strongly correlated with middle and advanced tangle maturity markers (Moloney Alzheimer’s & Dementia 2021).

Methods: Posterior hippocampus from n=30 cases were cut at 5 μm thick sections. Sections were stained with markers for early (AT8), middle (PHF-1), or advanced (2E9) tangles (Figure). To contextualize hippocampal analyses, parahippocampus and fusiform were additionally investigated for comparisons using digital pathology and tau PET standard uptake value ratio (SUVr). SUVr was obtained by normalizing to cerebellar crus. Memory was tested by Auditory-Verbal Learning Test (AVLT). Cognitive measures were obtained by Mini-Mental State Exam (MMSE) and Clinical Dementia Rating (CDR).

Results: Tau PET SUVr was correlated with AT8, PHF-1, and 2E9 burden in the hippocampus, parahippocampus, and fusiform (Table). The correlation between tau PET SUVr and tau burden strengthened from early to middle and advanced tangle markers. In the hippocampus, AVLT delayed recall and MMSE negatively correlated with AT8 and PHF-1 burden, with the strength weakening through the tangle maturity levels. In the parahippocampus, burden for all three markers correlated with AVLT delayed recall and MMSE with the correlation weakening in advanced tangles. In the fusiform, MMSE correlated with tau burden from all three markers, and weakened through the tangle maturity. Additionally, AVLT delayed recall was correlated to 2E9 burden and CDR was positively correlated to AT8 burden.

Table. Spearman correlations

Antemortem measure	Hippocampus						Parahippocampus						Fusiform					
	AT8 burden		PHF-1 burden		2E9 burden		AT8 burden		PHF-1 burden		2E9 burden		AT8 burden		PHF-1 burden		2E9 burden	
	R	p value	R	p value	R	p value	R	p value	R	p value	R	p value	R	p value	R	p value	R	p value
Tau-PET measures																		
Hippocampus SUVr (n=27)	0.61	p<0.001	0.69	p<0.001	0.71	p<0.001	0.6	p=0.001	0.66	p<0.001	0.72	p<0.001	0.57	p=0.002	0.62	p<0.001	0.71	p<0.001
Parahippocampus SUVr (n=27)	0.7	p<0.001	0.78	p<0.001	0.71	p<0.001	0.7	p<0.001	0.75	p<0.001	0.76	p<0.001	0.66	p<0.001	0.73	p<0.001	0.75	p<0.001
Fusiform SUVr (n=27)	0.73	p<0.001	0.78	p<0.001	0.7	p<0.001	0.71	p<0.001	0.76	p<0.001	0.75	p<0.001	0.67	p<0.001	0.74	p<0.001	0.75	p<0.001
Cognitive Measures																		
AVLT delayed recall (n=11)	-0.67	p=0.024	-0.61	p=0.045	-0.58	p=0.059	-0.7	p=0.017	-0.69	p=0.020	-0.67	p=0.024	-0.56	p=0.076	-0.58	p=0.059	-0.64	p=0.034
MMSE (n=18)	-0.56	p=0.004	-0.49	p=0.015	-0.4	p=0.051	-0.5	p=0.014	-0.5	p=0.013	-0.47	p=0.020	-0.53	p=0.008	-0.47	p=0.022	-0.41	p=0.044
CDR (n=19)	0.42	p=0.075	0.38	p=0.108	0.24	p=0.328	0.44	p=0.061	0.43	p=0.068	0.25	p=0.307	0.51	p=0.027	0.44	p=0.061	0.27	p=0.255

Data are presented as correlation coefficient (R) and significance (p-value). Nonparametric Spearman correlation was used to quantify the association between two continuous variables. All the tests were two-sided and p-values < 0.05 were considered statistically significant. Acronyms: SUVr, standard uptake value ratio; AVLT, Auditory-Verbal Learning Test; MMSE, Mini-Mental State Exam; CDR, Clinical Dementia Rating

Conclusion: Tau PET SUVr correlated strongly with advanced tangle markers compared to early tangle markers, whereas cognitive measures were more strongly correlated with early tangle markers. These results suggest that antemortem measures may be differentially associated with tangle maturity levels, even in regions like the hippocampus where quantification may be difficult to interpret.

Keywords: Neuropathology, neurofibrillary tangle maturity, tau PET, hippocampus, tau

Postmortem validation of ¹⁸F-MK-6240 PET using autoradiography and in-vitro binding combined with antibody-based assays in frozen brains from two autopsy cases

Tobey Betthauser^{1,2,3}, Eric Abrahamson^{4,6}, Maddy Barger^{1,2}, Brooke Schroeder^{1,2}, Bradley Christian^{1,3}, Victor Villemagne⁵, Sanjay Asthana^{1,2}, Sterling Johnson^{1,2,7}, M Shahriar Salamat^{1,8}, Milos Ikonovic^{4,5,6}

¹Wisconsin Alzheimer's Disease Research Center, University of Wisconsin-Madison, Madison, WI, US

²Department of Medicine, School of Medicine and Public Health, University of Wisconsin-Madison, Madison, WI, US

³Department of Medical Physics, School of Medicine and Public Health, University of Wisconsin-Madison, Madison, WI, US

⁴Departments of Neurology, University of Pittsburgh, Pittsburgh, PA, US

⁵Department of Psychiatry, University of Pittsburgh, Pittsburgh, PA, US

⁶Geriatric Research Education and Clinical Center, VA Pittsburgh HS, Pittsburgh, PA, US

⁷Wisconsin Alzheimer's Institute, Madison, WI, US

⁸Department of Pathology, School of Medicine and Public Health, University of Wisconsin-Madison, Madison, WI, US

Objective: The goal of this study was to investigate antemortem-postmortem correlates for the tau tracer ¹⁸F-MK-6240 in two autopsy brains.

Methods: Two Alzheimer's disease (AD) dementia cases (one early onset) from the Wisconsin ADRC underwent antemortem ¹⁸F-MK-6240 and ¹¹C-PiB PET imaging, MRI, and neuropsychological assessment prior to death. Right brain hemispheres were cut into ~1 cm coronal slabs and frozen. PET images were aligned to tissue slabs (SPM12), and 10 cortical and subcortical ROIs were hand-drawn and used to extract MK-6240 SUVRs and dissect matching tissue ROIs. Each ROI tissue sample was divided, and one portion sectioned for ³H-MK-6240 autoradiography (ARG) and tau and A β immunohistochemistry (IHC) while the other portion was homogenized for ³H-MK-6240 and ³H-PiB in-vitro binding assays and ELISA assays for total tau, p-tau (pS199, pS396, and pT231), and A β 1-42 and A β 1-40.

Results: Case-1 had a low density of tangles, neuritic plaques, and neuropil threads, and infrequent A β plaques, whereas Case-2 had a high degree of AD pathology. Imaging-postmortem correlations were weak/absent in Case-1 and significant in Case-2. Across all ROIs from two cases, ¹⁸F-MK-6240 SUVRs correlated directly with ³H-MK-6240 binding and p-tau ELISAs, and inversely with total-tau ELISA, while there were no significant correlations with ³H-PiB binding and A β ELISAs. ¹⁸F-MK-6240 SUVRs also correlated with ³H-MK-6240 ARG. There was a close correspondence of ³H-MK-6240 ARG signal with tau IHC, most prominently in entorhinal cortex (ERC) layer II tangles, dystrophic neurites surrounding cortical neuritic plaques, and neuropil threads.

Conclusions: Mature ERC tangles and tau positive cortical neuritic plaques appear to be primary pathological substrates for ¹⁸F-MK-6240 binding, while neuropil threads contribute less signal. Correlations of ¹⁸F-MK-6240 with p-tau, but not A β , demonstrate selectivity of this ligand for tau pathology in AD.

Keywords: neuropathology, tau, PET, MK-6240, validation

Poster Session 2A

Thursday, January 12, 2023		
Board #	POSTER 2A	
37	Regional [F18]AV1451 uptake in progressive apraxia of speech with and without Alzheimer's disease, dysexecutive, and logopenic variants of Alzheimer's disease	Switzer Corriveau-Lecavalier Lowe Jones Ramanan Machulda Graff-Radford Boeve Knopman Jack Petersen Josephs Whitwell Botha
38	Estimation of Native Spatial Resolution in Clinical Positron Emission Tomography Imaging Data	Galli Tonietto Klein Holiga Miho Knopf
39	Neuroinflammation Co-Localizes with Tau in Early-Onset MCI patients	Finn Appleton Bradbury Yu Faridar Beers Appel Fujita Masdeu Pascual
40	Lower locus coeruleus integrity identifies elevated entorhinal tau in low amyloid individuals and is associated with faster clinical progression	Engels-Domínguez A. Koops M. Riphagen F. Smegal Bueichekú Becker M. Kwong M. Rentz H. Salat A. Sperling A. Johnson I. L. Jacobs
41	Substantia nigra 18F-PI-2620 PET signal is associated with motor impairment in Lewy body disease	Winer Vossler Young Romero Shahid Abdelnour Anders Shen Mormino Poston
42	Sex differences in A β and tau vulnerability in preclinical Alzheimer's disease	Ourry St-Onge Mohammediyan Yakoub Soucy Poirier Breitner Villeneuve
43	Alzheimer's Network for Treatment and Diagnostics (ALZ-NET): Defining the future of Alzheimer's treatment, imaging and care	Whitlow March Rabinovici Rafii Atri Daffner Edelmayer Gatsonis Lopez Porsteinsson Possin Salloway Sano Snyder Vukmir Wilkins Windon Carrillo
44	Acquisition time corrections for SUVR analyses of [18F]-PI-2620	Young Vossler Winer Romero Anders Shen Poston Davidzon Mormino
45	Longitudinal accumulation of white matter lesions is associated with amyloidosis and brain atrophy, but not systemic vascular risk	Shirzadi Schultz Yau Fitzpatrick Levin Joseph-Mathurin Kantarci Preboske Jack Jr. Farlow Fagan Hassenstab Jucker Morris Xiong Karch Levey Gordon Schofield Salloway Perrin McDade Levin Cruchaga Allegri Fox Goate Day Koeppe Noble Chui Berman Mori Sanchez-Valle Lee Rosa-Neto Ruthirakuhan Wu Swardfager Benzinger Sohrabi Martins Schultz Bateman Johnson Sperling Greenberg Chhatwal
46	Sex-associated differences in cerebrospinal fluid and plasma biomarkers in early-onset Alzheimer's disease	Nemes Logan Dage Fagan Hammers Manchella Eloyan Kostadinova Foroud Zetterberg Koeppe Aisen Carrillo Rabinovici Dickerson Apostolova
47	Correlations between Janssen Simoa plasma p217+tau and tau PET in participants	Saad Triana-Blatzer Moughadam Slemmon Henley Kolb

	screened for Janssen's Autonomy Ph2 anti-tau trial in early Alzheimer's Disease	
48	Sleep apnea and poor sleep quality are linked to tau deposition in older women at higher risk for Alzheimer's	Lui Shepherd Wang Bernier Bosompra DeYoung Malhotra Sundermann Banks
49	Machine Learning Based Tau Positivity Classification On Tau-PET Scans Considers Biological Variability And Can Aid In Decision Making	Gebre Rial Raghavan Sparrman Wiste Schwarz Lowe Graff-Radford Knopman Petersen Schöll Jack Jr Vemuri
50	Impact of florbetaben acquisition timing on SUVR and centiloid values	Johns Kennedy Young Younes Vossler Poston Davidzon Mormino
51	Postmortem In Vitro Binding of APN-1607 to PSP and HC Globus Pallidus Homogenates	Tempest Margolin Paget Campbell Navia
52	Histone deacetylase tracer [11C]Martinostat behaves differently in amyloid versus synuclein rich regions in dementia with Lewy bodies	Goodheart Yoo Striar Quan Wey Wang Gomperts
53	A CenTauR scale based on 18F-MK6240	Dore Bourgeat Leuzy Huang Krishnadas Feizpour Fripp Villemagne Rowe
54	Tau accumulation across the Alzheimer's disease continuum: an 18F-MK6240 AIBL study	Krishnadas Doré Robertson Ward Fowler Masters Bourgeat Fripp Villemagne Rowe
55	Multi-modal analysis of myelin and neurofilament light chain in individuals at risk for Alzheimer's disease using MRI, PET, and CSF biomarker assessments	Yang Dean III Betthausen Carlsson Johnson Blennow Zetterberg Alexander Bendlin
56	The gut microbiota metabolite trimethylamine n-oxide is associated with white matter degeneration on the Alzheimer's disease continuum	Moody Heston Zarbock Blennow Zetterberg Rey Ulland Bendlin
57	In vivo measures of fibrillar beta-amyloid pathology limits cognitive plasticity in healthy aging: A multi-center intervention study.	Bischof Fellerhoff Giehl Drzezga
58	One Year Longitudinal Change of Tau Accumulation on [18F]PI-2620 PET in Alzheimer Spectrum	Oh Oh Lee Oh Seo Roh Lee Kim
59	The role of vascular pathology in the association between amyloid- β and tau in cognitively unimpaired individuals	Coomans van Westen Pichet Binette Strandberg Spotorno Palmqvist Stomrud Ossenkoppele Hansson
60	Dual biomarker amyloid PET for improved subtype and stage inference	Scott Coath Dickson McQuaid Cash Schott
61	Standardization of Tau PET using the CenTauR Scale: Preliminary findings from BioFINDER-2 using [18F]RO948 and [18F]Flortaucipir	Leuzy Doré Klein Baker Carrillo Charil Collins Collins Haeberlein Henscheid Hostetler Higuchi Muthinson Iaacarino Irizarry Jagust Johnson Karten Kolb Lopresti Ossenkoppele Pascoal Pappas Pontecorvo Rabinovici Raket Bohorquez Saad Stephens Mathotaarachchi Mintun

		Sivakuraman Smith Rowe Villemagne Hansson
62	Plasma GFAP and NFL are correlated with measures of global cognition in EOAD and EOnonAD	Kostadinova Hammers Logan Manchella Nemes Fagan Foroud Zetterberg Kramer Aisen Carrillo Rabinovici Dickerson Apostolova Dage
63	Comparisons of plasma biomarkers with 18F-Florzolotau PET in AD continuum – a pilot study	Huang Ing-Tsung Lin Huang
64	Validating Tau PET Staging Schemes in Relation to Cognitive Outcomes	Hammers Lin Logan Risacher Schwarz Apostolova
65	Shared variance between FDG metabolism and PiB tracer delivery is not predictive of cognitive decline in preclinical AD	Mayblyum Shirzadi Becker Chhatwal Farrell Jacobs Guehl El Fakhri Sperling Price Johnson Schultz Hanseeuw
66	Amyloid and tau PET are associated with plasma phosphorylated tau 181 and glial fibrillary acidic protein in a sample of heterogeneous dementia syndromes	Cousins Phillips Das Fulop Nasrallah O'Brien McMillan Irwin Massimo Grossman Wolk
67	Combined and independent effects of hyperphosphorylation of tau on microglial activation	Rahmouni Therriault Tissot L. Benedet Ashton Triana-Baltzer Lussier Servaes Macedo Stevenson Stevenson Kunach Fernandez-Arias Wang Gauthier Kolb Karikari Zetterberg Blennow Pascoal Rosa-Neto
68	Cognitive impairment is more closely associated with the regional extension of F18MK6240 tau-PET signal than with PET signal intensity or CSF tau measures	Hanseeuw Gerard Malotau Colmant Quenon Ivanoiu Lhommel
69	Disentangling spatial-temporal remote interaction between tau and Amyloid- β proteins in different stages of tau aggregations	Hojjati Feiz Nayak Shteingart Ozoria Fernández Devanand Luchsinger Stern Razlighi
70	Predictors of Discordance Between Pre-PET Clinical Diagnosis and Amyloid-PET Results in the Imaging Dementia—Evidence for Amyloid Scanning (IDEAS) Study	Tanner La Joie Hanna Iaccarino Allen Siegel Hillner Whitmer Gatsonis Carrillo Rabinovici
71	Mid-life atherosclerotic cardiovascular disease risk score and late-life AT(N) measures	Saeed Chang Royse Lopresti Snitz Villemagne Reis Lopez Cohen
72	A clinical diagnosis of Alzheimer's disease and CSF-based tau positivity are both associated with lower locus coeruleus metabolism	Koops Dutta Becker Van Egroo Riphagen Prokopiou Hanseeuw Sperling El Fakhri Johnson Jacobs

P37 Regional [F18]AV1451 uptake in progressive apraxia of speech with and without Alzheimer's disease, dysexecutive, and logopenic variants of Alzheimer's disease

Aaron R Switzer¹, Nick Corriveau-Lecavalier², Val J Lowe³, David Jones¹, Vijay K Ramanan¹, Mary M Machulda², Jonathan Graff-Radford¹, Bradley Boeve¹, David Knopman¹, Clifford R Jack⁴, Ronald Petersen¹, Keith A Josephs¹, Jennifer Whitwell⁴, Hugo Botha¹

¹Department of Neurology, Division of Behavioral Neurology, Mayo Clinic, Rochester, MN, US

²Department of Psychiatry and Psychology (Neuropsychology), Mayo Clinic, Rochester, MN, US

³Department of Radiology, Division of Nuclear Medicine, Mayo Clinic, Rochester, MN, US

⁴Department of Radiology, Division of Neuroradiology, Mayo Clinic, Rochester, MN, US

Progressive apraxia of speech (PAOS) is typically associated with 4R tau and shows minimal flortaucipir ([F18]AV1451; FTP) uptake. Here we describe amyloid-positive PAOS with considerable FTP uptake, suggesting the presence of underlying Alzheimer's disease (AD) pathology, and compare these patients to amyloid negative PAOS and atypical AD variants.

Twenty-seven patients were selected from the Neurodegenerative Research Group and Alzheimer's Disease Research Center cohorts, of which 5 had PAOS as the dominant neurological deficit with AD biomarker positivity (PAOS-AD), 8 had PAOS without AD biomarker positivity (PAOS), 7 with logopenic progressive aphasia and AD biomarker positivity (LPA), and 7 with left-predominant dysexecutive AD (dAD). We also included a group of age- and sex-matched healthy controls for comparison purposes. Standard uptake value ratio (SUVr) values in the left precentral, supplementary motor, middle frontal, and superior frontal cortices were compared across groups.

FTP uptake was higher in PAOS-AD, LPA, and dAD compared to PAOS and controls in the left precentral and supplementary motor cortices. FTP uptake was highest in dAD followed by LPA and PAOS-AD compared to PAOS and controls in the left middle frontal and superior frontal cortices (Figure 1). Voxel-wise comparisons between each patient group and controls for FTP- and FDG-PET highlighted these patterns (Figure 2).

Significant tau deposition in regions associated with motor speech production may not be sufficient to produce clinically meaningful apraxia of speech. Despite high levels of tau in these regions, dAD and LPA do not exhibit apraxia of speech. This suggests that PAOS, regardless of AD pathology status, may be the result of degeneration in the broader speech planning network.

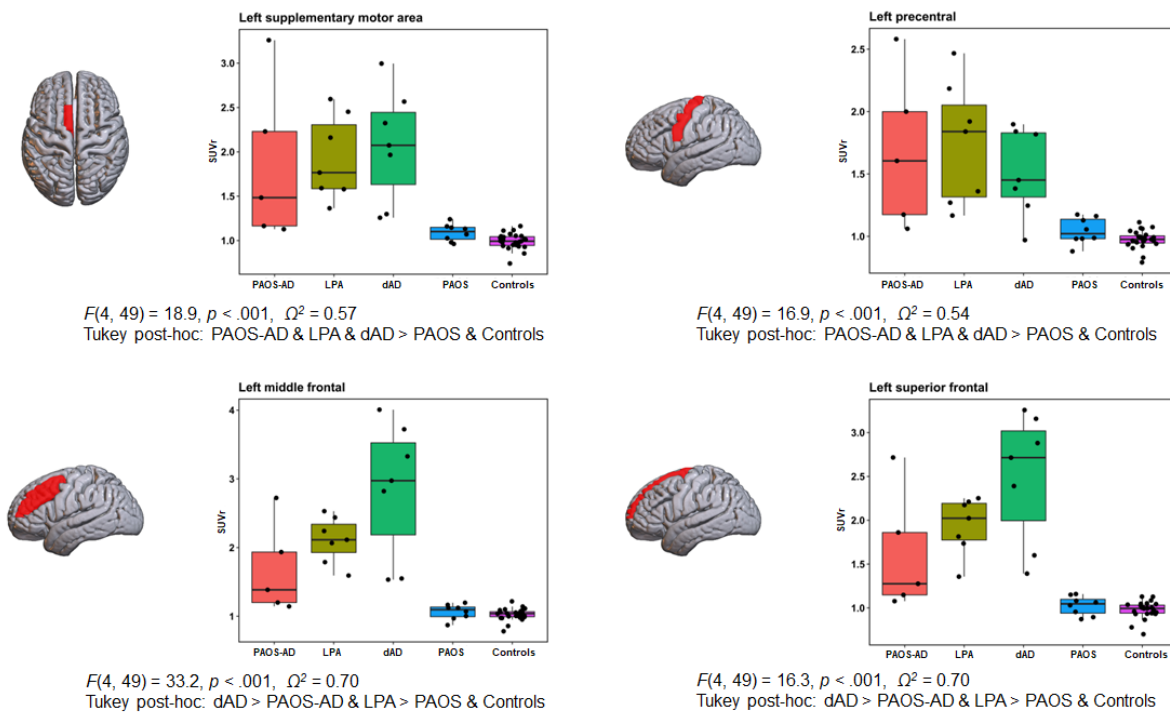


Figure 1. Box and whisker plots of flortaucipir uptake across all groups in the left supplementary motor, precentral, middle frontal, and superior frontal cortices. SUVR = standard uptake value ratio; PAOS-AD = apraxia of speech with Alzheimer’s biomarker positivity; LPA = logopenic progressive aphasia with Alzheimer’s biomarker positivity; dAD = dysexecutive Alzheimer’s disease; PAOS = progressive apraxia of speech

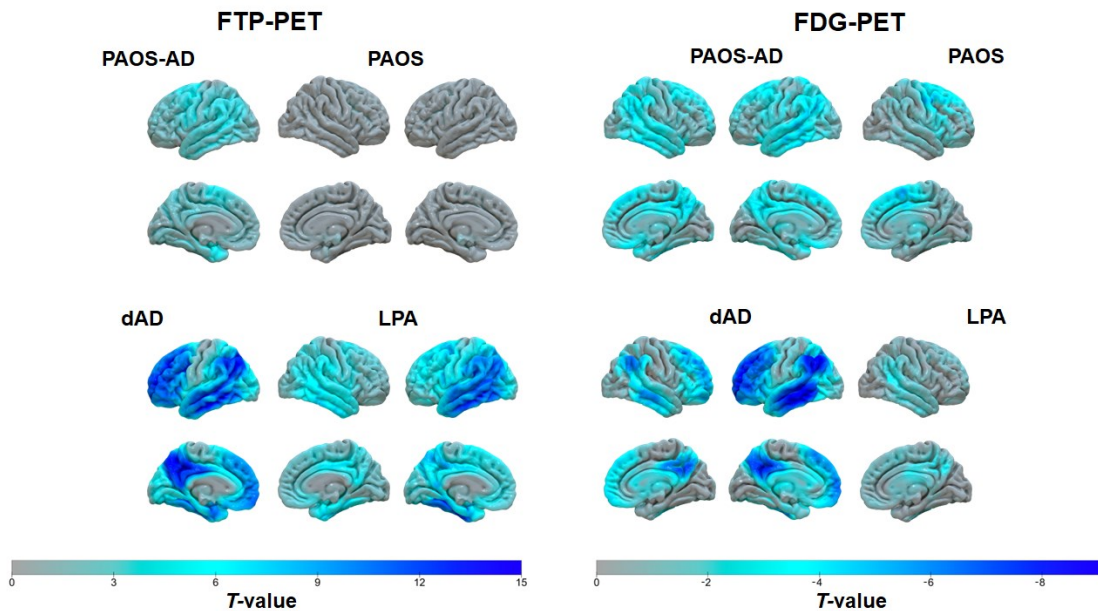


Figure 2. Regional flortaucipir (left panel) or FDG (right panel) uptake between each group and their age- and sex-matched controls. Higher T-values represent higher or lower flortaucipir or FDG uptake, respectively, compared to controls. FTP = Flortaucipir; FDG = Fluorodeoxyglucose; PAOS-AD = apraxia of speech with Alzheimer’s biomarker positivity; LPA = logopenic progressive aphasia with Alzheimer’s biomarker positivity; dAD = dysexecutive Alzheimer’s disease; PAOS = progressive apraxia of speech

P38 Estimation of Native Spatial Resolution in Clinical Positron Emission Tomography Imaging Data

Christopher Galli^{1,2}, Matteo Tonietto¹, Gregory Klein¹, Stefan Holiga¹, Enkelejda Miho^{2,3,4}, Antje Knopf^{2,5}

¹Roche Pharma Research and Early Development, Therapeutic Modalities, Roche Innovation Center Basel, F.Hoffmann-La Roche Ltd, Grenzacherstrasse 124, 4070 Basel, Switzerland, Basel, Switzerland

²Institute of Medical Engineering and Medical Informatics, School of Life Sciences, FHNW University of Applied Sciences and Arts Northwestern Switzerland, 4132 Muttenz, Switzerland, Muttenz, Switzerland

³aiNET GmbH, 4002 Basel, Switzerland, Basel, Switzerland

⁴Swiss Institute of Bioinformatics, 1015 Lausanne, Switzerland, Lausanne, Switzerland

⁵Center for Proton Therapy, Paul Scherrer Institute; Villigen, Switzerland, Villigen, Switzerland

Introduction: Estimation of native spatial resolution of PET scanners is important for harmonization procedure in multicenter studies. Spatial resolution is generally estimated from 3D Hoffman phantom, which however may not always be available. Here, we propose a method to determine the spatial resolution directly from clinical [18F]FDG PET images, independent of phantom measurements.

Methods: In this study, we implemented the logarithmic intensity plot (Mizutani et al., 2016) on the ADNI data set to estimate the FWHM among 34 different PET scanners and reconstruction methods. It can be shown that the FWHM is quadratically related to the slope of the logarithmic power spectrum plotted versus the squared spatial frequency from the PET images (Figure 1).

We used a leave-one-out approach to evaluate the performance of this method: for each scanner model, we estimated the linear regression coefficients to convert the log-power derived slopes to the Hoffman-derived FWHMs from the PET images obtained from the other scanner models, and used them to estimate the FWHM of the scanner under analysis.

Results: Logarithmic power derived FWHMs showed a Pearson correlation of $r=0.94$ with the Hoffman-derived FWHMs (Figure 2), and a mean absolute difference of 0.21mm. The highest difference (0.92mm) was observed for a PET scanner with 4.5mm in-plane resolution PET (Figure 3).

Conclusions: The proposed method was able to determine accurately the native spatial resolution of PET images without the need for a Hoffman phantom. The relatively poorer performance of the method for the scanner with a native in-plane resolution of 4.5mm is probably due to the fact that only one scanner model had such a high resolution.

Reference:

[R. Mizutani et al., "A method for estimating spatial resolution of real image in the Fourier domain," *J. Microsc.*, doi: 10.1111/jmi.12315.](https://doi.org/10.1111/jmi.12315)

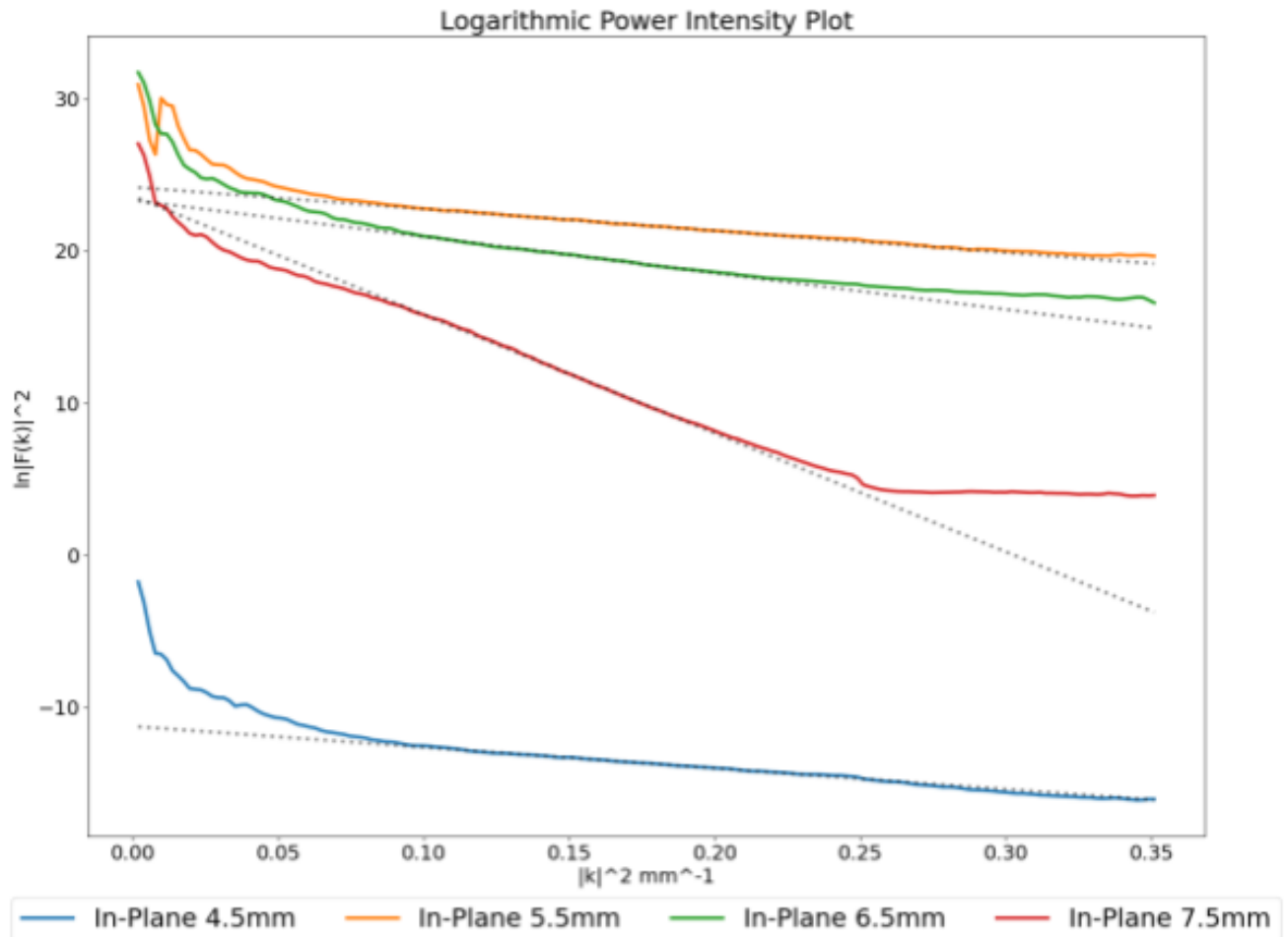
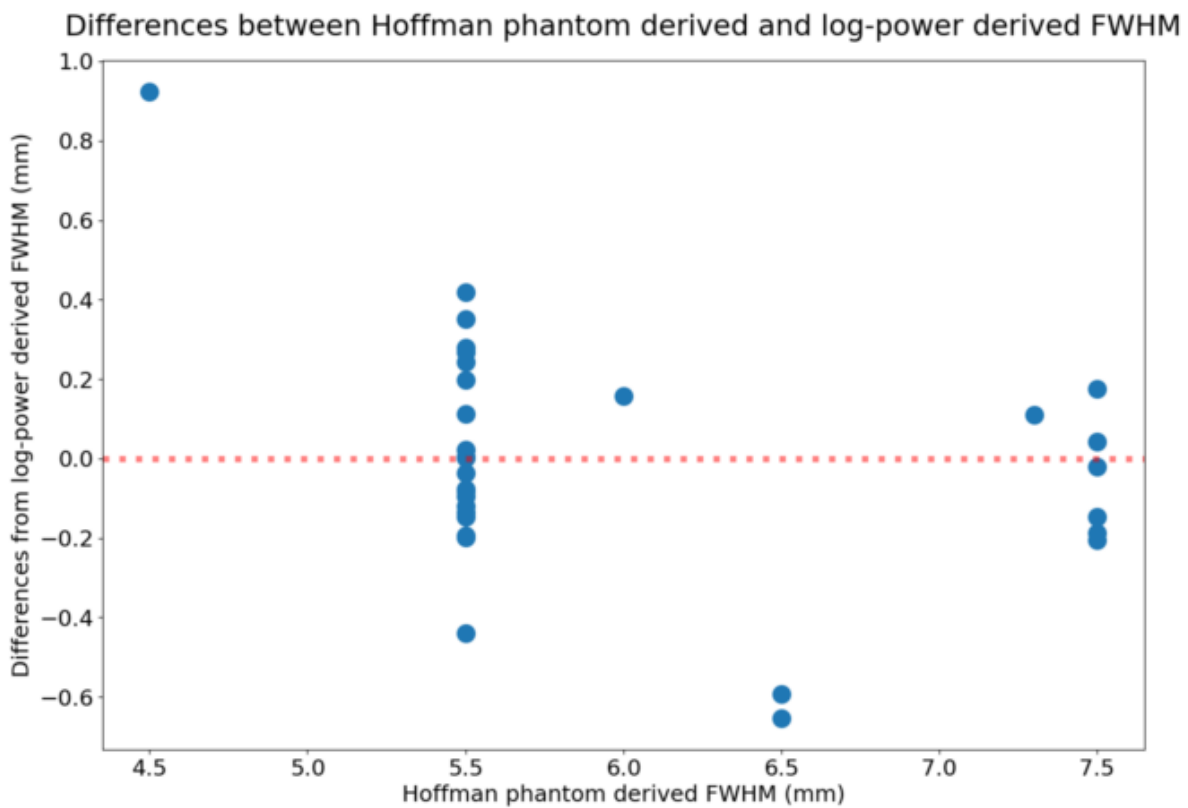
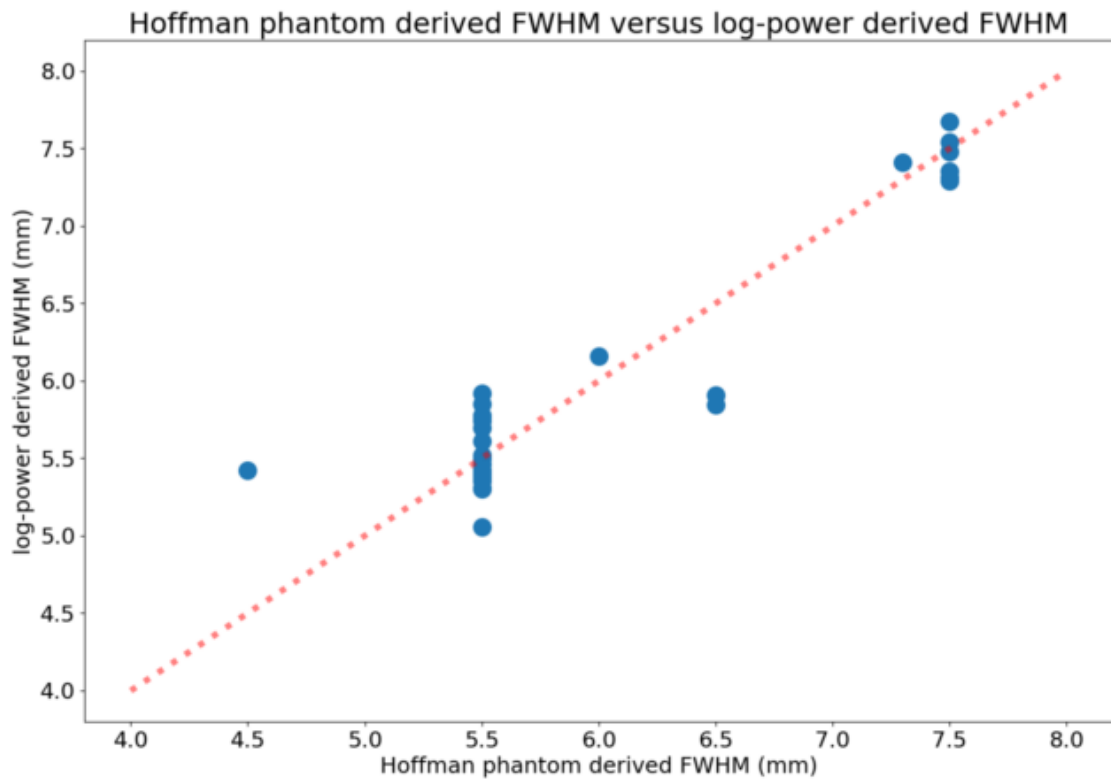


Figure 1. Solid lines represent the logarithmic power spectral distribution along the squared spatial frequency obtained from four $[^{18}\text{F}]\text{FDG}$ PET images coming from different PET scanner models. Dotted lines represent the fit of the linear portion of the plot. The square root of the slope of the linear fit is proportional to the scanner in-plane FWHM.



Keywords: spatial resolution, fwhm, logarithmic intensity plot, 3D Hoffman phantom

P39 Neuroinflammation Co-Localizes with Tau in Early-Onset MCI patients

Quentin Finn¹, Johanna Appleton¹, Kathleen Bradbury¹, Meixiang Yu^{2,3}, Alireza Faridar^{1,2}, David Beers^{1,2}, Stanley Appel^{1,2}, Masahiro Fujita^{1,2}, Joseph Masdeu^{1,2}, Belen Pascual^{1,2}

¹Nantz National Alzheimer Center, Houston Methodist Neurological and Research Institute, Houston, TX, US

²Weill Cornell Medicine, New York City, NY, US

³Cyclotron and Radiopharmaceutical Core, Houston Methodist Research Institute, Houston, TX, US

Background: Neuroinflammation, a potential diagnostic biomarker and therapeutic target in patients with Alzheimer's disease (AD), needs characterization at various stages of AD. TSPO PET is used to image brain inflammation, but some tracers have low affinity for TSPO and "second-generation" tracers, with higher affinity, cannot image subjects with a low-binder TSPO rs6971 genotype. We overcame this problem by using ¹¹C-ER176, a high-affinity tracer allowing for imaging of all participants and which has a favorable metabolite profile (Fujita, 2017). We used ¹¹C-ER176 to study neuroinflammation in participants with early-onset mild cognitive impairment (EOMCI).

Methods: EOMCI patients (N=16, mean age 60±4, 5 women) and healthy controls, HC (N=15, mean age 65±7, 8 women) underwent ¹¹C-ER176 PET. TSPO affinity was similar (EOMCI/HC: 3/3 low, 11/7 mixed, 7/5 high). A full-factorial analysis was performed on region-wise V_T values (Hammer's atlas). Thirteen EOMCI patients underwent β amyloid (¹¹C-PIB, ¹⁸F-florbetaben or ¹⁸F-florbetapir) and tau (¹⁸F-flortaucipir) PET. Standard uptake value ratios (SUVRs) were calculated for β amyloid and tau tracers with cerebellum as reference. Images were corrected for partial volume. Intra-subject regional correlations among the three imaging targets were determined and averaged across subjects.

Results: Neuroinflammation was bilaterally increased in precuneus, inferior parietal lobule, temporal lobe and middle frontal gyrus. Localization of amyloid and tau in the brain correlated ($r=0.56\pm 0.23$). However, neuroinflammation and tau co-localized more tightly ($r=0.615\pm 0.28$) and more so than neuroinflammation and β amyloid ($r=0.455\pm 0.16$).

Conclusion: In EOMCI, ¹¹C-ER176 PET enabled the identification of neuroinflammation in regions known to be involved in AD. Importantly, subjects with any TSPO genotype could be studied. As expected, the localization of amyloid and tau in the brain was correlated, but the co-localization of neuroinflammation with tau was higher. This finding highlights the importance of neuroinflammation as a biomarker in the AD process and as a potential therapeutic target.

Keywords: Neuroinflammation, Alzheimer's Disease, TSPO PET, Tau PET, Amyloid PET

P40 Lower locus coeruleus integrity identifies elevated entorhinal tau in low amyloid individuals and is associated with faster clinical progression

Nina Engels-Domínguez^{1,2}, Elouise A. Kooops¹, Joost M. Riphagen¹, Lindsay F. Smegal¹, Elisenda Bueichekú¹, J. Alex Becker¹, Kenneth M. Kwong⁵, Dorene M. Rentz^{3,4}, David H. Salat^{5,6}, Reisa A. Sperling^{3,4}, Keith A. Johnson^{1,3,4}, Heidi I. L. Jacobs^{1,2}

¹Gordon Center for Medical Imaging, Department of Radiology, Massachusetts General Hospital/Harvard Medical School, Boston, MA, US

²Faculty of Health, Medicine and Life Sciences, School for Mental Health and Neuroscience, Alzheimer Centre Limburg, Maastricht University, Maastricht, The Netherlands

³Center for Alzheimer Research and Treatment, Department of Neurology, Brigham and Women's Hospital/Harvard Medical School, Boston, MA, US

⁴Department of Neurology, Massachusetts General Hospital/Harvard Medical School, Boston, MA, US

⁵Athinoula A. Martinos Center for Biomedical Imaging, Department of Radiology, Massachusetts General Hospital/Harvard Medical School, Boston, MA, US

⁶Neuroimaging Research for Veterans Center, VA Boston Healthcare System, Boston, MA, US

The locus coeruleus (LC) is among the first sites accumulating tau, with the entorhinal cortex (EC) succeeding. MRI-derived LC integrity is negatively related to EC tau, even in asymptomatic individuals. Tau tracks closely with cognition and is present in the EC before PET detects fibrillar amyloid, making it an early target candidate for prevention interventions. This work investigates whether LC integrity has predictive value for differentiating between amyloid-negative individuals with low or elevated EC tau, and clinical progression.

Data consisted of 213 participants (age=38.75-94.25 years; female=~58%; n=23 cognitively impaired; group of interest=CDR=0/PiB- (n=124); Table 1), undergoing baseline 3T-MRI, PiB-PET (cut-off=1.324 DVR) and FTP-PET (cut-off=1.414 SUVr), and longitudinal neuropsychological testing (average follow-up=1.9 years). LC intensity was derived by normalizing the LC to the reference and averaging 5-voxel-clusters with the highest intensities. Logistic regression (age-, sex-adjusted) and ROC analyses evaluated associations between biomarkers (LC intensity, hippocampal volume, PiB) and EC-FTP. Sensitivity analyses were run on asymptomatic subsamples with differing PiB ranges. Cox proportional hazard models (age-, sex-, education-adjusted) related LC integrity with clinical progression (CDR-SB>0).

LC intensity was negatively associated with EC-FTP ($p<0.001$), but not with hippocampal volume ($p=0.41$) or PiB ($p=0.06$). LC intensity predicted elevated EC-FTP better than hippocampal volume or PiB (AUC=85%, 76%, 77%, respectively; Figure 1). Results were similar with restricted and slightly elevated PiB subsamples. LC intensity showed 77% sensitivity and 85% specificity, and was, when low, associated with a two-fold increase in clinical progression (Hazard ratio=2.12, $p=0.037$; Figure 2).

This work demonstrates that lower LC integrity identifies, more accurately than hippocampal volume or beta-amyloid-PET, elevated EC tau in amyloid-negative individuals. Additionally, lower LC integrity is associated with a two-fold increased clinical progression risk. This suggests that LC integrity has promise as screening tool to detect early AD-related tau deposition and future clinical progression in asymptomatic, amyloid-negative individuals.

Characteristics of participants for the entire sample and the early prediction sample

	Entire sample N=213	CDR=0 & PiB - N=124
Age in years	71.84 (11.52) Range: 38.75 – 94.25	71.11 (9.31) Range: 50.25 – 89.50
Sex, n females (%)	124 (58.22 %)	74 (59.68 %)
Education in years	16.28 (2.96) #	16.17 (3.01)
MMSE score	28.73 (1.58) #	29.01 (1.27)
CDR=0, n (%)	171 (88.14 %) #	124 (100 %)
CDR>0, n (%)	23 (11.86 %)	0 (0 %)
Neocortical PiB, DVR, PVC	1.39 (0.42)	1.19 (0.06)
PiB+, n (%)	60 (28.17 %)	0 (0 %)
Entorhinal tau, SUVR, PVC *	1.35 (0.35)	1.27 (0.26)
LC intensity	1.33 (0.05)	1.34 (0.05)
Hipp volume (mm ³)	7298.59 (880.93)	7498.40 (827.24)

Table 1. Characteristics of participants for the entire sample and the early prediction sample. Data is represented in mean and standard deviation (sd), unless otherwise specified. #: Information is missing for n=17 (years of education), n=13 (MMSE) and n=19 (CDR). *: To dichotomize EC tau, GMM was applied to the entire sample, which resulted in an EC FTP cut-off value of 1.414 SUVR. Abbreviations: MMSE = Mini Mental State Examination, CDR = Clinical Dementia Rating, DVR = Distribution Volume Ratio, PVC = partial volume corrected, PiB = Pittsburgh Compound B, SUVR = standardized uptake value ratio, LC = locus coeruleus, Hipp = hippocampus, GMM = Gaussian Mixture Modelling, FTP = flortaucipir.

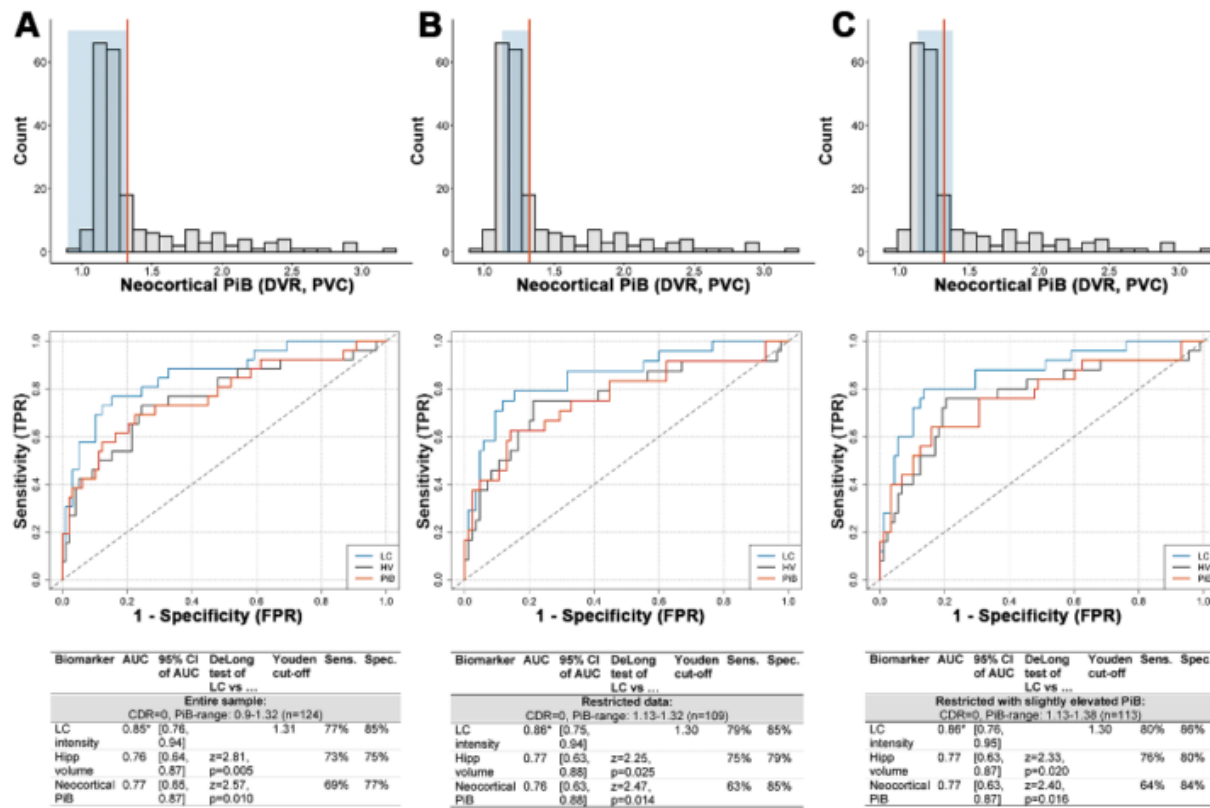


Figure 1. Predictive ability of LC intensity, hippocampal volume, and neocortical PiB for elevated EC tau in three subsets of asymptomatic individuals. A-C) Histograms of the entire dataset (n=213) with the portion of the selected sub-dataset highlighted in blue and the PiB+ threshold indicated in orange. Below each histogram are corresponding Receiver Operating Curves discriminating low from elevated EC-FTP based on the biomarkers for A) all CDR=0, PiB- individuals (n=124), B) the restricted group (n=109): CDR=0, PiB-range: 1.13-1.32 DVR, and C) the slightly elevated PiB group (n=113): CDR=0, PiB-range: 1.13-1.38 DVR. Blue = LC intensity; grey = hippocampal volume (HV), orange = PiB. Below each ROC are the corresponding statistics. Youden cut-off values represent LC intensity values obtained from corresponding biomarker models (LC intensity, hippocampal volume, neocortical PiB). Abbreviations: DVR = Distribution Volume Ratio, PVC = partial volume corrected, LC = locus coeruleus, HV = hippocampal volume, PiB = Pittsburgh Compound B, TPR = True positive rate, FPR = False positive rate, AUC = Area under the curve, CI = confidence interval, Sens. = Sensitivity, Spec. = Specificity, CDR = Clinical Dementia Rating, Hipp = hippocampus, a.u. = arbitrary unit, EC = entorhinal cortex, FTP = Flortaucipir. *: significant models.

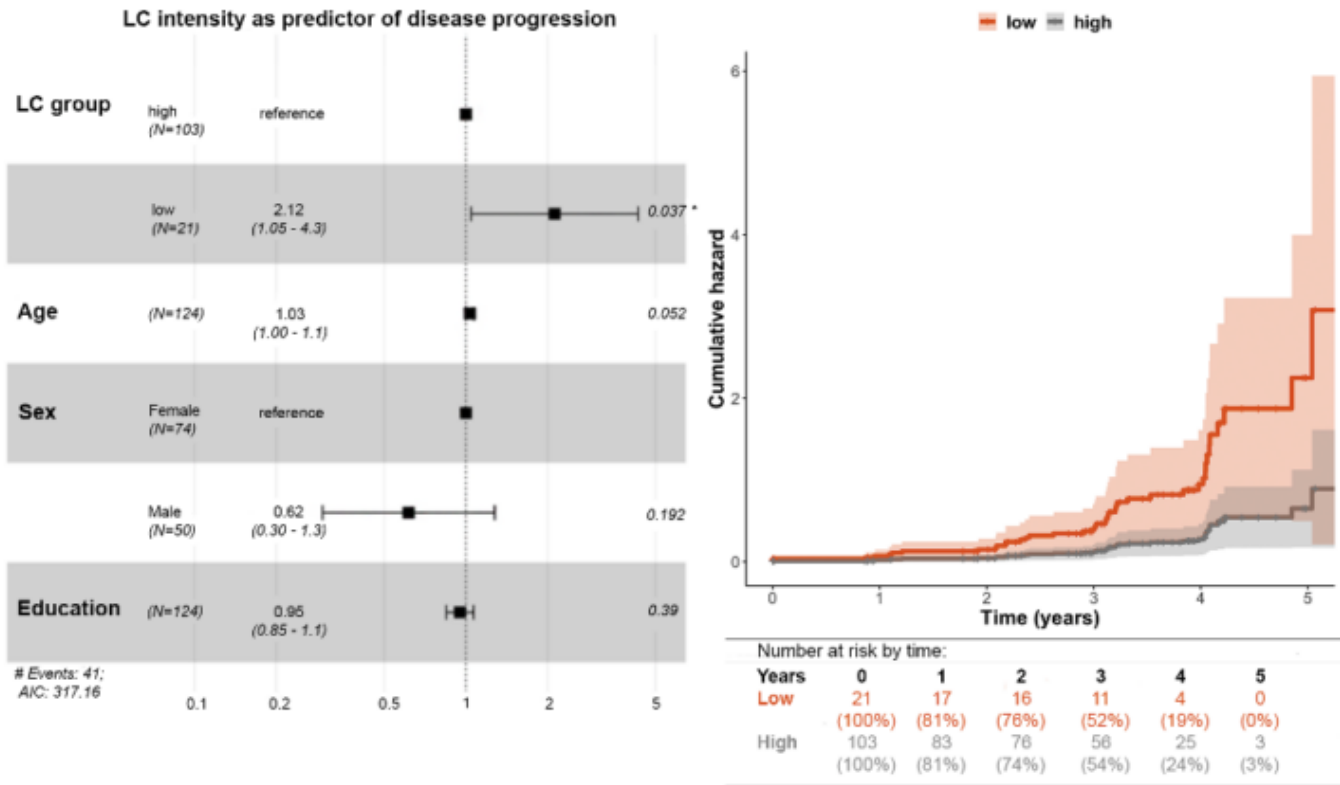


Figure 2. Disease progression as a function of LC intensity level. Left: forest plot showing the effect sizes for the cox proportional regression. From left to right: variable name, sample size, hazard ratio, and its 95% confidence interval, p-values. LC intensity dichotomization cut-off value is based on the Youden cut-off value obtained from the corresponding ROC biomarker model. Right: Cumulative hazard function for LC group (low: orange, high: grey) along with the number at risk by time in absolute values and percentages.

Keywords: Locus coeruleus, Entorhinal tau, Clinical progression, Biomarkers

P41 Substantia nigra ^{18}F -PI-2620 PET signal is associated with motor impairment in Lewy body disease

Joseph Winer¹, Hillary Vossler¹, Christina Young¹, America Romero¹, Marian Shahid¹, Carla Abdelnour¹, David Anders², Bin Shen², Elizabeth Mormino¹, Kathleen Poston¹

¹Department of Neurology and Neurological Sciences, Stanford University, Palo Alto, CA, US

²Department of Radiology, Stanford University, Palo Alto, CA, US

Background: Several tau PET ligands are known to bind to neuromelanin within substantia nigra (SN). Previous studies have shown that ^{18}F -flortaucipir uptake is reduced in the SN of patients with Parkinson's disease relative to healthy individuals. It is unknown to what extent next generation tau PET ligands may be sensitive to Lewy body disease-related changes in SN.

Methods: A total of 116 participants from the Stanford Alzheimer's Disease Center (ADRC) and the Stanford Aging and Memory Study (SAMS) were recruited for PET scanning with ^{18}F -PI-2620. We compared ^{18}F -PI-2620 uptake within SN across patients from the Parkinson's disease spectrum (PD, n=20), dementia with Lewy bodies spectrum (DLB, n=5), and Alzheimer's disease spectrum (AD, n=25), as well as cognitively normal older adults (healthy controls, HC, n=66). ^{18}F -PI-2620 SUVRs (inferior cerebellar gray reference) were normalized to template space and an anatomical mask was used to extract mean SUVR within bilateral SN for each image. MDS-UPDRS-III motor exam scores, collected in an off-medication state for all patients, were used as a measure of motor impairment.

Results: SN SUVR was significantly lower in the PD group compared to the HC and AD group (**Figure 1**). SN SUVR was correlated with older age in the full cohort (**Figure 2**), and marginally correlated with age within the HC group alone. In patients with Lewy body disease (PD & DLB), MDS-UPDRS-III scores were negatively associated with SN SUVR, such that less ^{18}F -PI-2620 binding within SN predicted greater motor impairment (**Figure 3**).

Conclusions: These findings suggest that neuromelanin-related ^{18}F -PI-2620 signal within SN carries information about disease severity in Lewy body diseases. Tau PET may therefore serve as a tool in studying Lewy body disease beyond measuring cortical tau deposition.

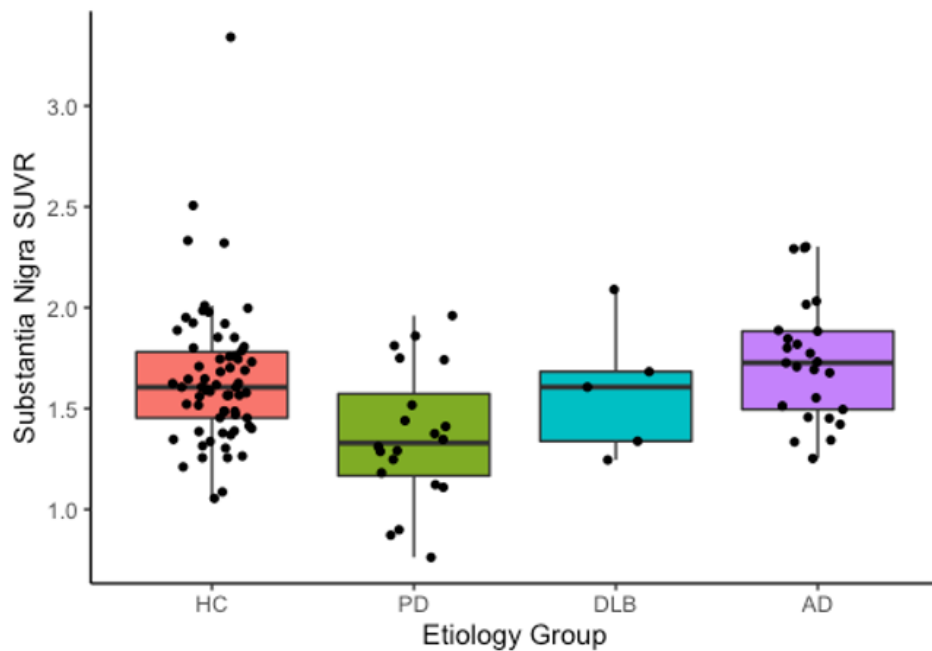


Figure 1 - Mean ^{18}F -PI-2620 SUVR within substantia nigra is lower in Parkinson's disease compared to Alzheimer's disease and healthy controls.

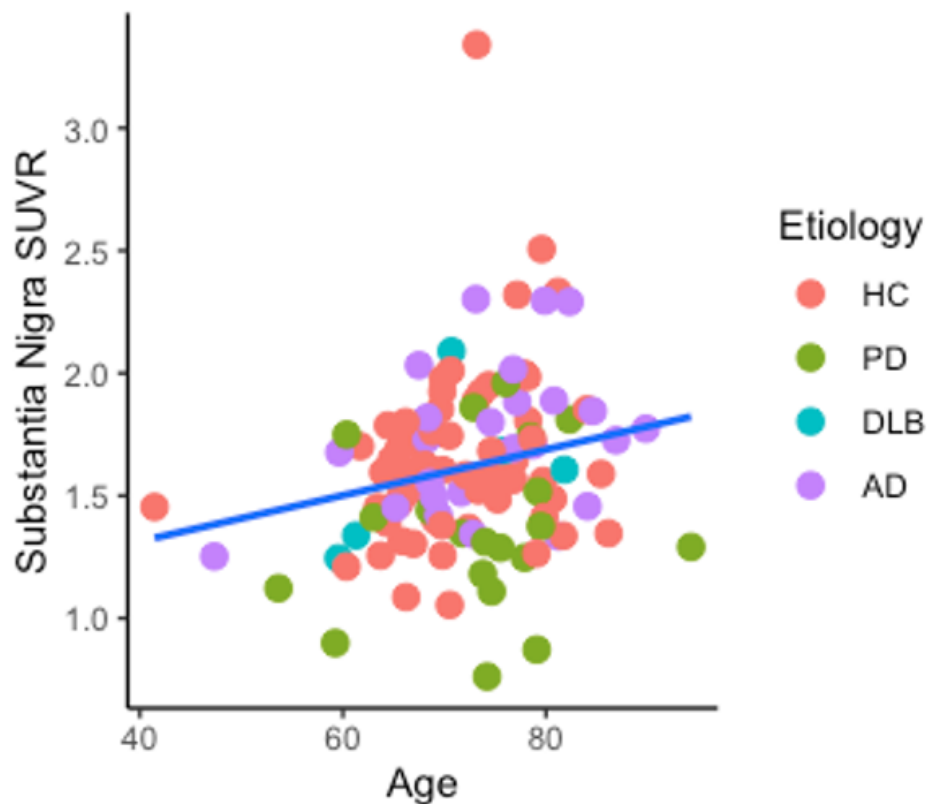


Figure 2 - Mean ^{18}F -PI-2620 SUVR within substantia nigra is associated with age.

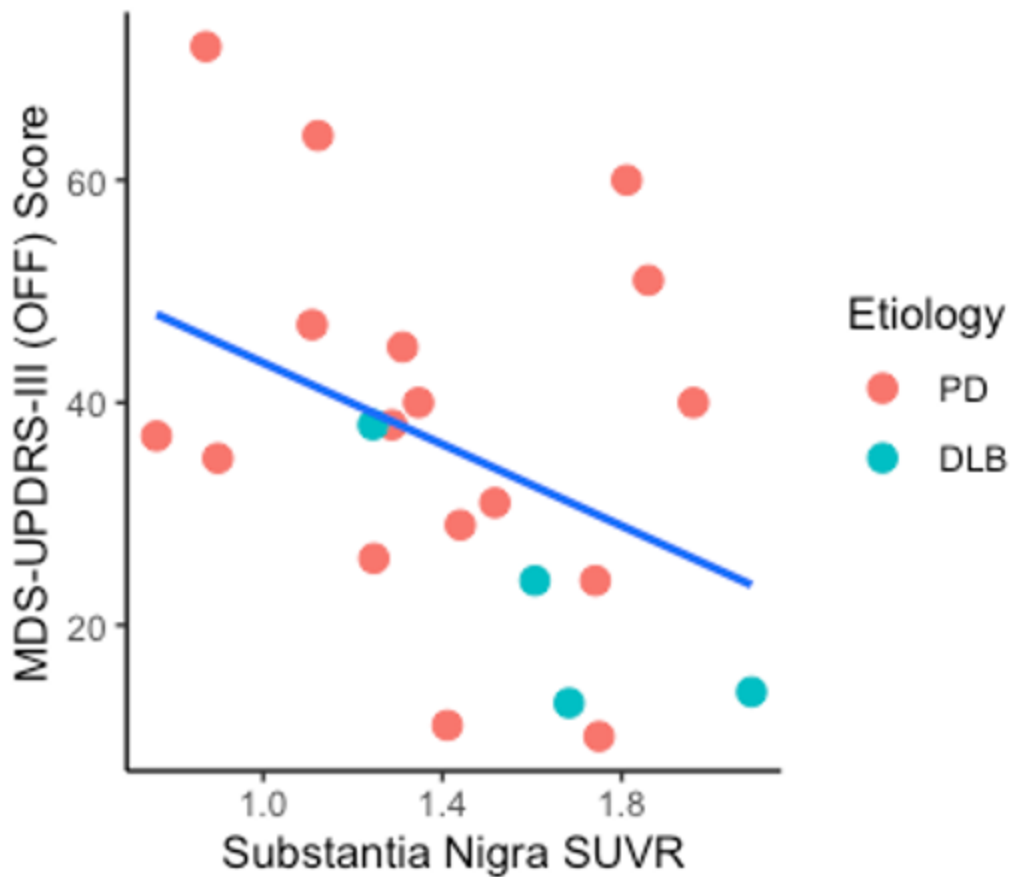


Figure 3 - Mean ^{18}F -PI-2620 SUVR within substantia nigra is associated with motor impairment severity in patients with Lewy body disease.

Keywords: tau PET; Lewy body disease; Parkinson's disease

P42 Sex differences in A β and tau vulnerability in preclinical Alzheimer's disease

Valentin Ourry^{1,2}, Frédéric St-Onge^{2,3}, Bery Mohammadiyan^{1,2}, Yara Yakoub^{2,3}, Jean-Paul Soucy⁴, Judes Poirier^{1,2}, John C.S Breitner^{1,2}, Sylvia Villeneuve^{1,2,4}

¹Department of Psychiatry, Faculty of Medicine, McGill University, Montréal, QC, Canada

²Douglas Mental Health University Institute, Montréal, QC, Canada

³Integrated Program in Neuroscience, Faculty of Medicine, McGill University, Montréal, QC, Canada

⁴McConnell Brain Imaging Center, Montreal Neurological Institute, McGill University, Montréal, QC, Canada

Introduction: Women are considered at higher risk of Alzheimer's disease (AD) than men. Our main objectives were to 1) assess if women accumulate amyloid-beta (A β) and/or tau faster than men and 2) assess if sex influences the rate of A β driving tau, such that less A β would be needed in women to show the same rate of tau burden and/or accumulation than in men.

Methods: Eighty-one older adults (age: 67.2 ± 4.6 years, women: 72.8%) from PREVENT-AD cohort, cognitively unimpaired at baseline (MMSE: 28.9 ± 1.3), underwent two [¹⁸F]-NAV4694 and [¹⁸F]-AV1451 positron emission tomography (PET) scans 4.3 ± 0.5 years apart. We extracted and averaged the standard uptake value ratio (SUVR) in the lateral and medial prefrontal, parietal, lateral temporal, and cingulate cortical regions for A β and in the entorhinal, amygdala, parahippocampal, fusiform, inferior, and middle temporal regions (temporal meta-ROI) for tau.

Results: Sex differences on A β and tau burden or annual change did not reached significance (*figure 1*, $p=0.13$ and 0.1 respectively), but no men had tau values higher than SUVR 1.3 while women SUVR's reached 1.7. We found an interaction between sex and A β on tau at baseline ($p<0.001$), but not with tau annual change, such that women had higher levels of tau than men for the same levels of A β burden (*figure 2*).

Conclusion: Women may be more vulnerable to A β effect on tau than men in the preclinical stage of AD. It is also possible that less tau pathology is needed in men to develop cognitive impairments which would explain why no men exhibited high tau values. Identifying individuals who are more vulnerable to AD pathology, by disentangling sex-specific effects, would help to design personalized interventions for AD.

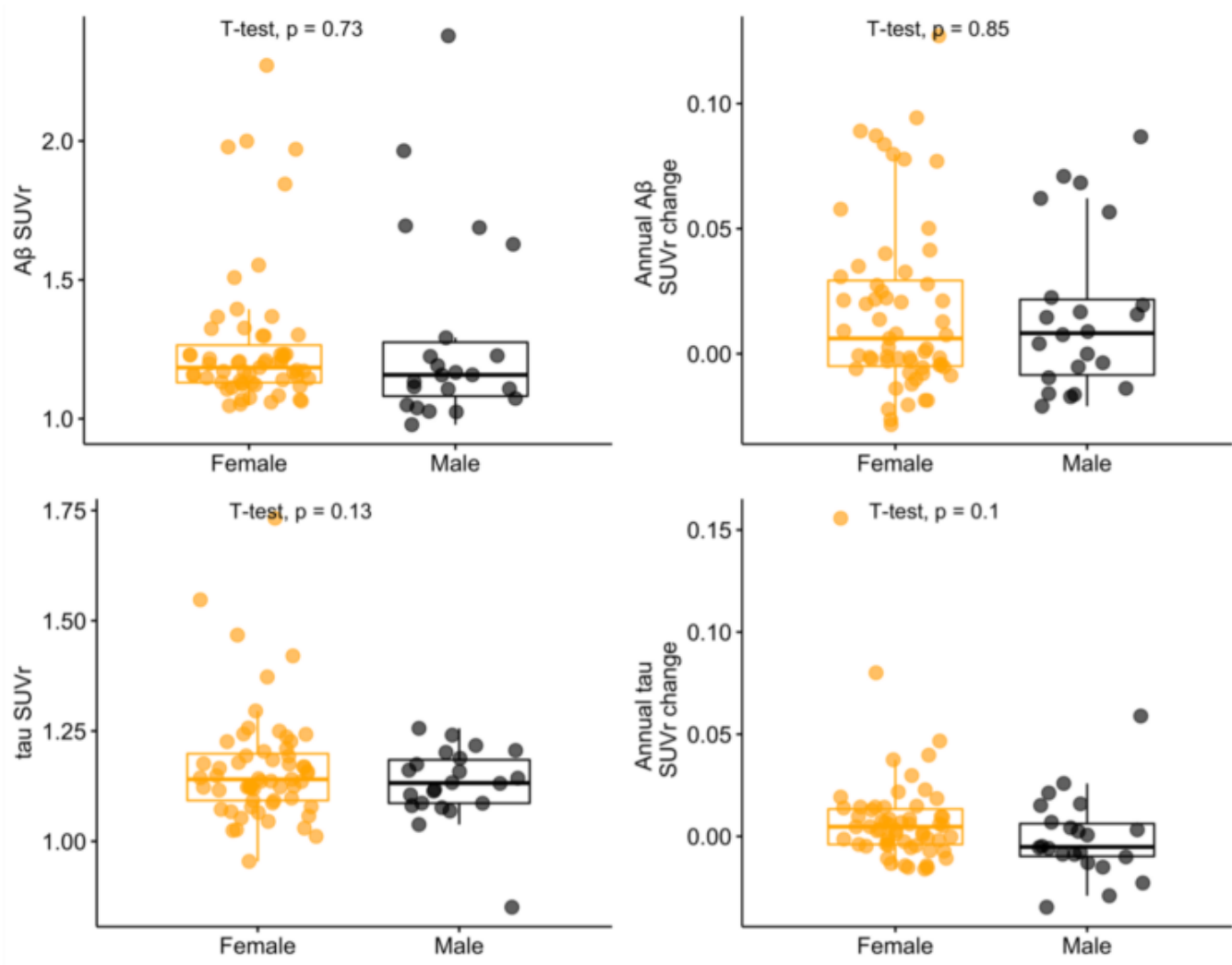


Figure 1: Between-sex differences

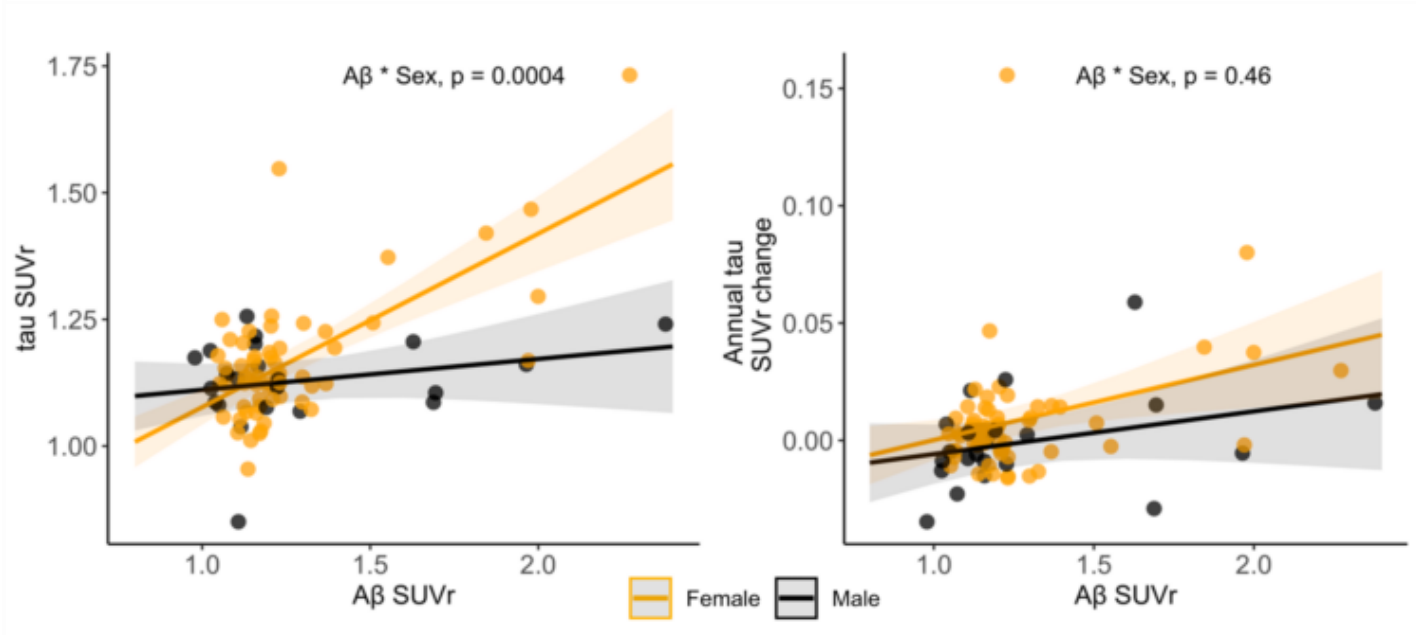


Figure 2: Sex interaction

Keywords: Alzheimer's disease, PET, sex, amyloid, tau

P43 Alzheimer's Network for Treatment and Diagnostics (ALZ-NET): Defining the future of Alzheimer's treatment, imaging and care

Christopher Whitlow², Andrew March¹, Gil Rabinovici³, Michael Rafii⁵, Alireza Atri⁶, Kirk Daffner⁷, Rebecca Edelmayer⁴, Constantine Gatsonis⁸, Oscar Lopez⁹, Anton Porsteinsson¹⁰, Katherine Possin³, Stephen Salloway¹¹, Mary Sano¹², Heather Snyder⁴, Rade Vukmir⁴, Consuelo Wilkins¹³, Charles Windon³, Maria Carrillo⁴

¹American College of Radiology, Reston, VA, US

²Wake Forest School of Medicine, Winston-Salem, NC, US

³University of California, San Francisco, Memory and Aging Center, San Francisco, CA, US

⁴Alzheimer's Association, Chicago, IL, US

⁵University of Southern California, Keck School of Medicine, Los Angeles, CA, US

⁶Banner Sun Health Research Institute, Sun City, AZ, US

⁷Harvard Medical School, Boston, MA, US

⁸Brown University School of Public Health, Providence, RI, US

⁹University of Pittsburgh School of Medicine, Pittsburgh, PA, US

¹⁰University of Rochester School of Medicine, Rochester, NY, US

¹¹Butler Hospital / Warren Alpert Medical School of Brown University, Providence, RI, US

¹²Mount Sinai School of Medicine, New York, NY, US

¹³Vanderbilt University Medical Center, Nashville, TN, US

Background: More than 140 Alzheimer's disease (AD) therapies are being tested in clinical trials, with many currently under regulatory review. In response, the Alzheimer's Association recently convened a group of clinical research and imaging experts to launch the Alzheimer's Network for Treatment and Diagnostics (ALZ-NET) in August 2022; a provider-enrolled network that collects real-world clinical and imaging data from patients treated with novel FDA-approved AD therapies.

Methods: ALZ-NET collects longitudinal data to track health outcomes associated with therapeutic use in patients from diverse backgrounds and communities. Patients treated with a novel FDA-approved AD therapy are eligible to enroll. Demographic, clinical, neurologic, genetic and biomarker data are collected at baseline and every 6-12 months. Using established infrastructure provided by American College of Radiology (ACR), a central repository collects all neuroimaging (PET and MRI) conducted as part of clinical care. Adverse events, outcomes, and resource utilization are tracked.

Results: ALZ-NET will utilize the network of over 1,000 dementia healthcare providers and imaging facilities across the U.S. created through the IDEAS and New IDEAS studies. Trajectories for change in cognitive function and behavior will be evaluated longitudinally, assessing predictors of therapeutic response. Sites will have access to recommend training, acquisition protocols, and scanner information, as well as required standardized imaging sequences, reporting guidelines and templates. Cumulative data will be used for general hypothesis testing, artificial intelligence clinical decision making, developing processing pipelines, establishing best practices and education, and guiding legislative and payment policy decisions. Anonymized raw and processed imaging data sets will be made available to the research community.

Conclusions: It is important to track clinical response and safety outcomes in the real-world clinical practice setting for novel therapies approved for use. ALZ-NET will be a resource for evidence gathering, information sharing, and education across clinical and research communities, encouraging innovative, inclusive research.

Keywords: Real-world data, Image repository, Alzheimer's disease, Amyloid Positron Emission Tomography, Imaging network

P44 Acquisition time corrections for SUVR analyses of [18F]-PI-2620

Christina Young¹, Hillary Vossler¹, Joseph Winer¹, America Romero¹, David Anders², Bin Shen², Kathleen Poston¹, Guido Davidzon², Elizabeth Mormino¹

¹Department of Neurology and Neurological Sciences, Stanford University School of Medicine, Stanford, CA, US

²Department of Radiology, Stanford University School of Medicine, Stanford, CA, US

Background: [18F]-PI-2620 is a next-generation tau PET tracer whose timing acquisition recommendation changed from 60-90 min to 45-75 min.

Objectives: To determine whether acquisition time and reference region impacts [18F]-PI-2620 signal across the Alzheimer's disease spectrum.

Methods: 85 participants from the Stanford Alzheimer's Disease Research Center (ADRC) and Stanford Aging and Memory Study (SAMS) were scanned with [18F]-PI-2620 (**Table 1**). 20 participants had both 60-90 min and 45-75 min data, and 70 additional participants had data from one timing window only. For participants with 60-90 min data, voxelwise adjustments using the slope of mean intensities across all possible frames were made to interpolate 45-75 min SUVRs at each voxel (Pontecorvo et al., 2019). For participants with both timing windows, real and imputed 45-75 min SUVRs were compared. Inferior cerebellum (IC) and white matter (WM) reference regions were examined. Real and imputed 45-75 min SUVRs were merged to compare SUVRs across cognitive status and amyloid groups.

Results: There was regional variation in the strength of associations between SUVRs derived from 45-75 min and 60-90 min data (**Figure 1**; IC reference region correlations = 0.869–1.000; WM reference region correlations = 0.899–0.998). Acquisition time had greater impact in those with higher tau SUVRs, especially when a WM reference region was used. After voxelwise adjustments, real and imputed 45-75 min SUVRs were highly correlated (**Figure 1**; IC reference region correlations = 0.948–1.000; WM reference region correlations = 0.963–1.000). Real and imputed 45-75 min SUVRs showed the expected stepwise increase in tau burden in those along the Alzheimer's disease spectrum (**Figure 2**).

Conclusion: Voxelwise adjustments can be used to harmonize [18F]-PI-2620 data that were collected using different acquisition time windows. The impact of acquisition time is greatest in those with higher tau burden and when using a WM reference region.

Table 1. Participant demographics.

Diagnosis	Age, mean (SD)	Sex, M/F	Amyloid Status, negative/positive/unknown
Participants with 45-75 min and 60-90 min data used to validate voxelwise timing adjustments			
Clinically Unimpaired (n=12)	69.1 (4.7)	7/5	8/4/0
Dementia (n=4)	69.8 (12.8)	1/3	0/3/1
Non-Alzheimer's Disease Mild Cognitive Impairment and Dementia (n=4)	76.1 (3.2)	4/0	1/0/3
Participants with 45-75 min or imputed 45-75 min data used to compare diagnostic groups			
Clinically Unimpaired (n=62)	71.3 (7.4)	26/36	40/22/0
Mild Cognitive Impairment (n=12)	71.8 (12.1)	7/5	2/10/0
Dementia (n=11)	71.1 (8.6)	4/7	0/11/0

Figure 1. Pearson correlations and Bland-Altman plots for SUVRs derived from (left) 45-75 min and 60-90 min data and (right) real and imputed 45-75 min data.

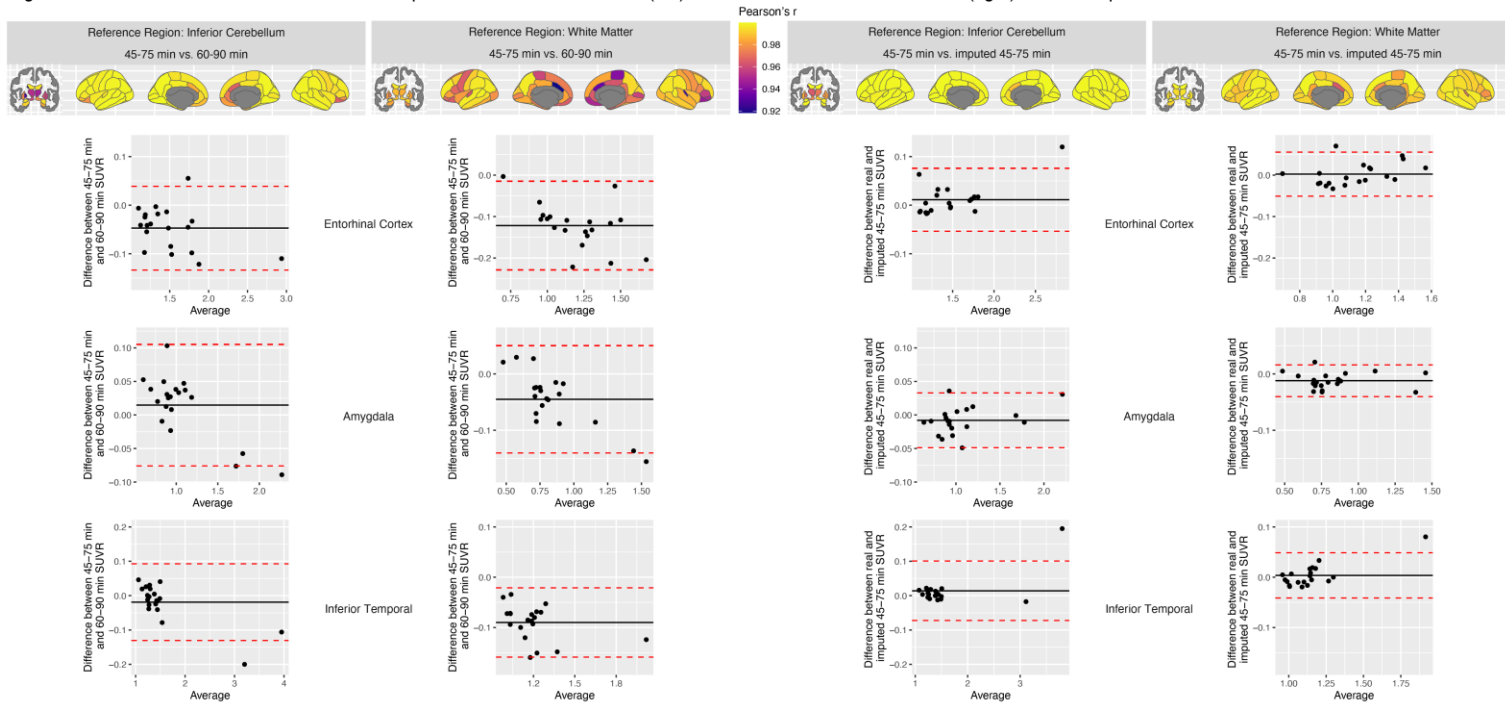
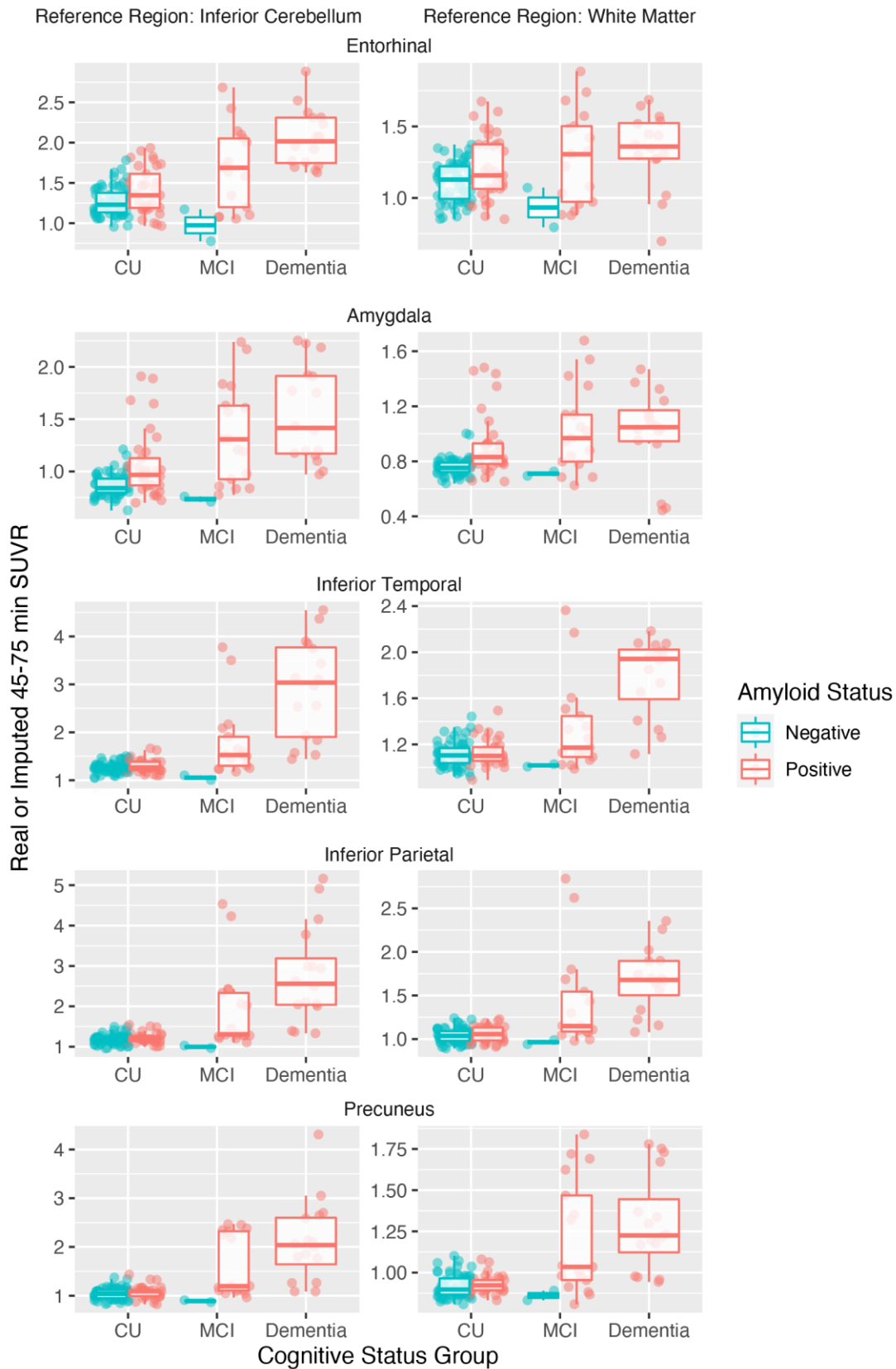


Figure 2. [18F]-PI-2620 SUVRs for inferior cerebellum and white matter reference regions across medial temporal lobe (entorhinal, amygdala) and early neocortical (inferior temporal, inferior parietal, precuneus) regions for each diagnostic group.



Keywords: acquisition time, reference region, [18F]-PI-2620, tau, PET

P45 Longitudinal accumulation of white matter lesions is associated with amyloidosis and brain atrophy, but not systemic vascular risk

Zahra Shirzadi¹, Stephanie A. Schultz¹, Wai-Ying W. Yau¹, Colleen D Fitzpatrick¹, Raina Levin¹, Nelly Joseph-Mathurin², Kejal Kantarci³, Gregory M. Preboske³, Clifford R. Jack Jr.³, Martin R. Farlow⁴, Anne M. Fagan², Jason Hassenstab², Mathias Jucker⁵, John C Morris², Chengjie Xiong², Celeste M. Karch², Allan I. Levey⁶, Brian A. Gordon², Peter R. Schofield⁷, Stephen P. Salloway⁸, Richard J. Perrin², Eric McDade², Johannes Levin⁹, Carlos Cruchaga², Ricardo Francisco Allegri¹⁰, Nick C Fox¹¹, Alison Goate², Gregory Day¹², Robert Koeppe¹³, James Noble¹⁴, Helena C Chui¹⁵, Sarah Berman¹⁶, Hiroshi Mori¹⁷, Raquel Sanchez-Valle¹⁸, Jae-Hong Lee¹⁹, Pedro Rosa-Neto²⁰, Myuri Ruthirakuhan²¹, Che-Yuan Wu²¹, Walter Swardfager²¹, Tammie L.S. Benzinger², Hamid R Sohrabi²², Ralph N Martins²³, Aaron P. Schultz¹, Randall J. Bateman², Keith A. Johnson¹, Reisa Sperling¹, Steven M Greenberg¹, Jasmeer P. Chhatwal¹

¹Massachusetts General Hospital, Brigham and women's hospital, Harvard Medical School, Boston, MA, US

²Washington University in St. Louis School of Medicine, St. Louis, MO, US

³Mayo Clinic, Radiology, Rochester, MN, US

⁴Indiana Alzheimer's Disease Research Center, Indianapolis, IN, US

⁵German Center for Neurodegenerative Diseases (DZNE), Tuebingen, Germany

⁶Emory University School of Medicine, Atlanta, GA, US

⁷Neuroscience Research Australia, Sydney, AU

⁸Alpert Medical School of Brown University, Providence, RI, US

⁹German Center for Neurodegenerative Diseases e.V. (DZNE), Munich, Germany

¹⁰INEBA, Buenos Aires, AR

¹¹UK Dementia Research Institute, UCL, London, UK

¹²Mayo Clinic, Jacksonville, FL, US

¹³University of Michigan, Ann Arbor, MI, US

¹⁴Columbia University, New York, NY, US

¹⁵University of Southern California, Los Angeles, CA, US

¹⁶University of Pittsburgh, Pittsburgh, PA, US

¹⁷Osaka Metropolitan University Medical School, Nagaoka Sutoku University, Osaka, Japan

¹⁸Neurological Tissue Bank Hospital Clinic, IDIBAPS, Barcelona, Spain

¹⁹Asan Medical Center, University of Ulsan College of Medicine, Seoul, Korea

²⁰Montreal Neurological Institute, McGill University, Montreal, QC, Canada

²¹Sunnybrook research institute, University of Toronto, Toronto, ON, Canada

²²Department of Biomedical Sciences, Macquarie University, Sydney, AU

²³Edith Cowan University, Perth, AU

Background: Damage to cortical white matter and the accumulation of white matter lesions (WML) are thought to contribute to late-onset (LOAD) and autosomal dominant Alzheimer's disease (ADAD). Though WML are often attributed to small vessel ischemic changes secondary to elevated systemic vascular risk, recent work demonstrates that increased WML is seen even in young people with low-vascular risk who carry pathogenic variants of ADAD. We hypothesized that increased WML is more closely related to the AD-intrinsic processes of neurodegeneration, parenchymal, and vessel amyloidosis as opposed to systemic vascular risk factors.

Methods: Using MRI data from ADAD (N=221, Dominantly Inherited Alzheimer's Network) and LOAD (N=678, Alzheimer's Disease Neuroimaging Initiative), we assessed the independent contributions of neurodegeneration, parenchymal, and vessel amyloidosis to WML accumulation.

Results: We observed that longitudinal increases in WML (1) were greater in individuals with evidence of vessel

amyloidosis (as evidenced by cortical microbleeds; CMBs) compared to those without (ADAD: $t=2.7$, $p=0.007$; LOAD: $t=2.0$, $p=0.05$); (2) were highly associated with longitudinal decreases in gray matter volume (ADAD: $t=-4.6$, $p<0.001$; LOAD: $t=-11.0$, $p<0.001$); (3) were related to parenchymal amyloid burden as measured by amyloid PET (ADAD: $t=3.9$, $p<0.001$; LOAD: $t=4.0$, $p<0.001$); (4) and had no clear relationships with systemic vascular risk factors (Table 1) in both ADAD (Figure 1) and LOAD (Figure 2) after accounting for age, gray matter volume, CMB, and amyloid burden. Lastly, we observed that greater WML volume in older adults without CMBs at baseline was predictive of the development of CMBs during longitudinal follow-up (Cox HR=1.58, $p=0.007$).

Conclusion: These results suggest WML in AD are associated with neurodegeneration, parenchymal, and vessel amyloidosis and may not reflect the additive effects of elevated systemic vascular risk. These findings also suggest that optimized WML measures may be useful as biomarkers of vessel amyloidosis prior to the emergence of CMBs.

Table 1: Participants' demographics and study information for DIAN and ADNI. The mean (Standard deviation) or percentage is reported.

	DIAN (N=221)	ADNI (N=678)
Age (years)	38.3 (11.0)	72.8 (7.2)
Estimated year-to-symptom onset (years)	-8.3 (11.4)	NA
APOE e4 (yes)	29%	48%
Sex (Female)	55%	47%
Education (years)	14 (3)	16 (3)
Cerebral microbleeds (yes)	7.4%	10%
Clinical dementia rating (0/0.5/1+)	58% /11% /31%	28% /16% /56%
Follow-up time	3.6 (2.2)	3.7 (2.8)
Hypertension (yes)	5.4%	48%
Hypercholesterolemia (yes)	11%	49%
Diabetes (yes)	1.2%	8.2%

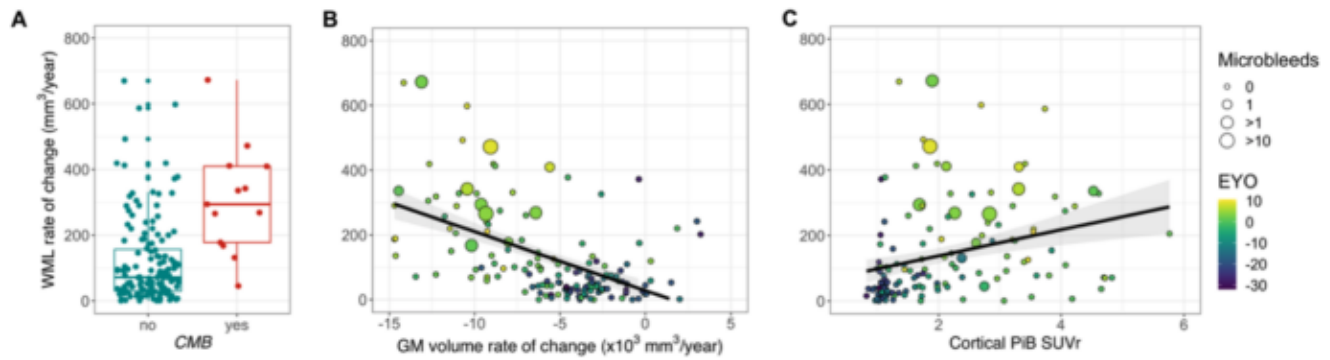


Figure 1: Longitudinal accumulation of white matter lesions (WML) is associated with the presence of cerebral microbleeds, changes in gray matter volume, and amyloid PET signal in ADAD. Using cross-sectional and longitudinal MRI and PET data from ADAD mutation carriers participating in the Dominantly Inherited Alzheimer’s Network Observational Study (DIAN), we calculated the WML rate of change and observed that it is elevated in ADAD carriers with CMBs compared to those without CMBs (A), it is related to gray matter volume loss (B), and it is related to amyloid PET SUVR (C11-PiB; C). Models were adjusted for age and estimated years to symptom onset (EYO).

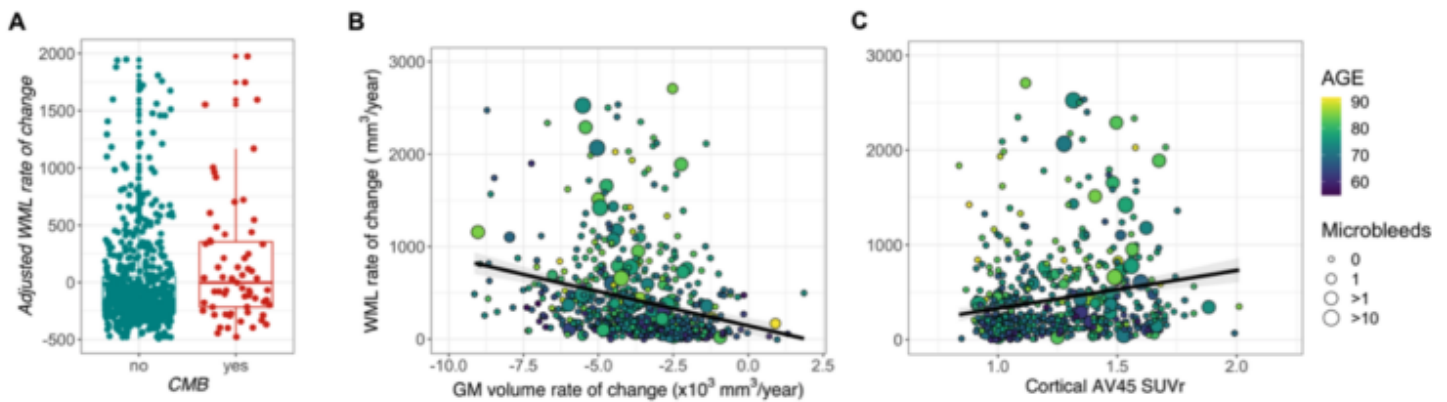


Figure 2: Longitudinal accumulation of white matter lesions (WML) is associated with the presence of cerebral microbleeds, changes in gray matter volume, and amyloid PET signal in older adults with and without symptomatic LOAD. Using cross-sectional and longitudinal MRI and PET data from older adults participating in the Alzheimer’s Disease Neuroimaging Initiative (ADNI), we calculated the WML rate of change and observed that it is elevated in older adults with CMBs compared to those without CMBs (A), it is related to gray matter volume loss (B), and it is related to amyloid PET SUVR (18F-AV45; C). Models were adjusted for age.

Keywords: White matter lesions, vessel amyloidosis, gray matter atrophy, amyloid burden

P46 Sex-associated differences in cerebrospinal fluid and plasma biomarkers in early-onset Alzheimer's disease

Sára Nemes¹, Paige E. Logan¹, Jeffrey L. Dage¹, Anne M. Fagan², Dustin B. Hammers¹, Mohit K. Manchella^{1,10}, Ani Eloyan³, Ralitsa V. Kostadinova¹, Tatiana M. Foroud¹, Henrik Zetterberg⁴, Robert A. Koeppe⁵, Paul S. Aisen⁶, Maria C. Carrillo⁷, Gil D. Rabinovici⁸, Bradford C. Dickerson⁹, Liana G. Apostolova¹

¹Indiana University School of Medicine, Indiana, IN, US

²Washington University School of Medicine, St. Louis, MO, US

³Brown University, Providence, RI, US

⁴UCL Queen Square Institute of Neurology, London, UK

⁵University of Michigan School of Medicine, Ann Arbor, MI, US

⁶Keck School of Medicine of USC, Los Angeles, CA, US

⁷Alzheimer's Association, Chicago, IL, US

⁸UCSF School of Medicine, San Diego, CA, US

⁹Harvard Medical School, Boston, MA, US

¹⁰University of Southern Indiana, Evansville, IN, US

Background: Female sex has been associated with greater pathology burden in Early-Onset Alzheimer's Disease (EOAD) in the Longitudinal EOAD Study (LEADS). Females presented with greater atrophy, amyloid, and tau on neuroimaging biomarkers. *APOE-ε4* non-carrier-status was found to be a further predictor of EOAD pathology burden. Analysis was expanded by examining the impact of sex and *APOE-ε4* carrier-status on plasma and cerebrospinal fluid (CSF) biomarkers of AD including neurofilament light chain (NfL), plasma glial fibrillary acidic protein (GFAP), neurogranin, tTau, pTau and visinin-like protein-1 (VILIP1). Plasma NfL is a marker of axonal damage and neurodegeneration and GFAP of astrocytosis. CSF neurogranin marks synaptic dysfunction correlating with degree of amyloid and tau pathology. tTau and pTau are associated with tau pathology and may predict AD pathology before tau PET abnormality. VILIP1 is associated with neuronal synaptic structure, indicating neuronal damage.

Method: We included 201 EOAD LEADS participants with available plasma biomarker data and 100 with CSF (all cohorts in **Table 1**). Sex, age, education, *APOE-ε4* carrier-status, and MMSE were assessed as demographic variables. Participants were split by sex and *APOE-ε4* carrier-status. Demographics and biomarker differences were analyzed using ANOVA.

Results: Compared to males, EOAD females showed greater levels of plasma NfL ($p=0.029$), and GFAP ($p=0.000031$). In CSF, EOAD females showed higher levels of neurogranin ($p=0.008$), tTau ($p=0.007$), pTau181 ($p=0.009$), VILIP1 ($p=0.015$).

No significant sex-differences were found between plasma A β 42/40 ratio, CSF NfL, YKL40, and synaptosomal-associated protein-25 (SNAP25).

APOE-ε4 carrier-status was not associated with differences in plasma or CSF biomarkers in either sex.

Conclusion: Understanding of sex-based differences in CSF and plasma is imperative as highly selective and specific fluid biomarkers emerge. In EOAD, female sex is associated with higher levels in certain AD-associated biomarkers, supporting previous neuroimaging biomarker analyses showing greater pathology burden in females.

CSF	EOAD			EOnonAD			CN		
	Males	Females	p-value	Males	Females	p-value	Males	Females	p-value
N	47	53		22	13		18	20	
Age, years, mean (SD)	58.53 (4.01)	58.81 (3.57)	p = 0.7126	57.86 (5.76)	58.08 (2.45)	p = 0.6471	56.55 (5.87)	55.85 (4.81)	p = 0.6888
Education, years, mean (SD)	15.04 (2.24)	15.81 (2.51)	p = 0.1106	15.5 (2.03)	15.46 (2.13)	p = 0.9562	17.06 (1.81)	16.7 (2.32)	p = 0.5860
MMSE, mean (SD)	22.04 (4.18)	22.13 (5.23)	p = 0.9251	26.05 (4.73)	24.17 (1.83)	p = 0.1784	28.94 (1.10)	29.05 (.52)	p = 0.6910
Aβ 42/40 ratio, mean (SD)	0.04 (0.01)	0.04 (0.01)	p = 0.2510	1.52 (0.01)	0.76 (0.01)	p = 0.5111	0.08 (0.01)	0.08 (0.01)	p = 0.8072
pTau181	4.51 (0.45)	4.74 (0.40)	p = 0.0094	3.58 (0.43)	3.54 (0.45)	p = 0.7714	1.44 (0.17)	1.51 (0.18)	p = 0.2259
tTau	6.37 (0.45)	6.60 (0.38)	p = 0.0077	5.75 (0.41)	5.78 (0.44)	p = 0.8037	2.38 (0.13)	2.42 (0.18)	p = 0.4846
Neurofilament light chain, mean (SD)	6.85 (0.31)	6.83 (0.35)	p = 0.7710	6.54 (0.77)	6.66 (0.86)	p = 0.6711	2.65 (0.15)	2.65 (0.16)	p = 0.9086
Neurogranin, mean (SD)	7.78 (0.73)	8.15 (0.62)	p = 0.0084	7.40 (0.67)	7.57 (0.73)	p = 0.4850	3.02 (0.41)	3.22 (0.28)	p = 0.0847
Visinin-like protein-1, mean (SD)	5.33 (0.42)	5.54 (0.35)	p = 0.0154	5.22 (0.41)	5.25 (0.38)	p = 0.8524	2.22 (0.17)	2.27 (0.17)	p = 0.3832
YKL40	5.48 (0.32)	5.54 (0.29)	p = 0.3479	5.28 (2.30)	5.30 (2.30)	p = 0.8882	5.17 (0.54)	5.22 (0.28)	p = 0.7204
Synaptosomal-associated protein 25, mean (SD)	2.82 (0.51)	2.95 (0.42)	p = 0.2089	2.56 (0.45)	2.53 (0.63)	p = 0.9100	1.08 (0.15)	1.20 (0.13)	p = 0.0307
APOE-ε4+ (%)	53%	54.71%		39%	46%		33%	65%	
% White	95.74%	92.45%		81.82%	84.62%		83.33%	70%	
PLASMA	EOAD			EOnonAD			CN		
	Males	Females	p-value	Males	Females	p-value	Males	Females	p-value
N	92	109		39	25		33	53	
Age, years, mean (SD)	58.89 (3.74)	58.67 (4.05)	p = 0.0287	57.97 (5.18)	56.64 (6.51)	p = 0.3686	56.33 (6.18)	55.96 (5.73)	p = 0.7782
Education, years, mean (SD)	15.06 (2.19)	15.72 (2.54)	p = 0.0696	15.79 (2.79)	14.96 (2.13)	p = 0.2095	17.06 (2.15)	16.42 (2.12)	p = 0.1793
MMSE (SD)	22.04 (5.33)	21.63 (4.85)	p = 0.5689	26.38 (2.89)	25.08 (5.12)	p = 0.1989	29.21 (.82)	29.21 (.90)	p = 1.0000
Aβ 42/40 ratio, mean (SD)	0.06 (0.01)	0.05 (0.01)	p = 0.3208	0.06 (0.01)	0.07 (0.01)	p = 0.1703	0.07 (0.01)	0.07 (0.01)	p = 0.9268
Plasma glial fibrillary acidic protein, mean (SD)	5.08 (0.51)	5.36 (0.44)	p < 0.0001	4.47 (0.52)	4.81 (0.52)	p = 0.0161	4.36 (0.48)	4.37 (0.38)	p = 0.9588
Neurofilament light chain, mean (SD)	2.90 (0.44)	3.03 (0.40)	p = 0.0297	2.60 (0.82)	2.74 (0.58)	p = 0.4739	2.45 (0.45)	2.35 (0.52)	p = 0.3649
APOE-ε4+ (%)	58.69%	52.29%		41%	48%		33%	45.28%	
% White	95.65%	92.66%		92.31%	92.00%		75.76%	71.70%	

Table 1. Demographic and biomarker comparison between males and females in the Early-Onset Alzheimer's Disease (EOAD), Early-Onset non Alzheimer's Disease (EOnonAD), and Cognitively Normal (CN) cohorts

Keywords: Sex-Differences, Biomarkers, Early-Onset Alzheimer's Disease, APOE4

P47 Correlations between Janssen Simoa plasma p217+tau and tau PET in participants screened for Janssen's Autonomy Ph2 anti-tau trial in early Alzheimer's Disease

Ziad S. Saad¹, Gallen Triana-Blatzer¹, Setareh Moughadam¹, Randy Slemmon¹, David Henley², Hartmuth C. Kolb¹

¹Neuroscience Biomarkers and Global Imaging, Janssen R&D, Johnson & Johnson, San Diego, CA, US

²Clinical Development, Janssen R&D, Johnson & Johnson, Titusville, NJ, US

Tau PET is the gold standard for in-vivo quantification of tau Neuro Fibrillary Tangles (NFT), which along with amyloid plaques and neurodegeneration, constitute the pathological hallmarks of Alzheimer's Disease (AD). The Autonomy trial (JNJ63733657ALZ2002), enrolls participants presenting with mild cognitive impairment (MCI) or mild AD dementia who are tau PET positive using the Janssen plasma p217+tau assay as a pre-screen to reduce patient burden and improve screening efficiency. Using screening data available to date, we report on the correlations observed between plasma p217+tau and ¹⁸F-MK-6240 Tau PET uptake across brain regions.

Simoa-based plasma p217+tau testing was conducted at Quanterix (Billerica, MA) in weekly batches.^[1] Participants with levels exceeding 0.1 pg/ml were then scanned to confirm the presence of NFT on tau PET. NFT levels were quantified using ¹⁸F-MK-6240 SUVR in Braak Regions Of Interest (ROI)^[2] (reference region: cerebellar gray). The results reported herein are from the first set of 355 participants for which the Tau PET analysis was completed.

Spearman rank correlations (ρ) between plasma p217+tau concentration and MK6240 SUVR were significant ($p < 10^{-15}$) across all 6 Braak ROIs. Correlations across Braak ROIs were moderate between 0.41 and 0.61, with the highest correlation in Braak4 and lowest in Braak2 ($\rho_{\text{Braak1}}=0.42$, $\rho_{\text{Braak2}}=0.41$, $\rho_{\text{Braak3}}=0.59$, $\rho_{\text{Braak4}}=0.61$, $\rho_{\text{Braak5}}=0.59$, $\rho_{\text{Braak6}}=0.53$). These correlations are consistent with those observed in cognitively impaired individuals in Doré et al. 2022^[3].

Significant correlations were found between Janssen's plasma p217+tau and Tau PET in a clinical trial setting using screening data from the Autonomy trial. Correlations were consistent with those from an independent observational study, further supporting the robustness of the assay and the utility of plasma p217+tau as a pre-screen in AD trials.

[1] Triana-Baltzer et al. *Alzheimers Dement* (Amst). 2021; [2] Schöll et al. *Neuron* 2016; [3] Doré et al. *Alzheimer's Dement*. 2022

Keywords: Blood, Fluid, Biomarkers, Enrichment

P48 Sleep apnea and poor sleep quality are linked to tau deposition in older women at higher risk for Alzheimer's

Kitty Lui¹, Alyx Shepherd², Xin Wang², Rachel Bernier², Naa-Oye Bosompra³, Pamela DeYoung³, Atul Malhotra³, Erin Sundermann⁴, Sarah Banks^{2,4}

¹San Diego State University/University of California San Diego Joint Doctoral Program in Clinical Psychology, San Diego, CA, US

²Department of Neurosciences, University of California San Diego, La Jolla, CA, US

³Department of Medicine, Pulmonary, Critical Care and Sleep Division, University of California San Diego, La Jolla, CA, US

⁴Department of Psychiatry, University of California San Diego, La Jolla, CA, US

Background: Obstructive sleep apnea (OSA) is linked to Alzheimer's Disease (AD) pathology. Older women are more vulnerable to AD, have increased OSA risk (but are often underdiagnosed), and report worse sleep quality than men. Here, in the Women: Inflammation Tau Study (WITS), we examined OSA prevalence in older women at higher-risk for AD, and in those with OSA, whether OSA features and subjective sleep quality were related to pathological tau.

Methods: WITS recruits women with elevated genetic risk for AD and mild cognitive impairment indicated by the Montreal Cognitive Assessment (range:13-20). Participants completed at-home sleep tests to derive measures of apneas, hypopneas, and oxygen saturations (OSat). The Pittsburgh Sleep Quality Index (PSQI) assessed subjective sleep quality. They also underwent 18F-MK6240 positron emission tomography (PET) to determine tau deposition. Standardized uptake value ratios (SUVRs) in two regions of interest (ROIs) (meta-temporal ROI and Braak III/IV stage region) were calculated. Partial correlations assessed the associations between sleep and tau while controlling for either age or body mass index (BMI).

Results: Here, we report on the initial 17 women (aged 71.8±3.3 years). None had prior diagnoses of OSA. 13 (76.5%) met OSA diagnosis (with an apnea-hypopnea index (AHI)≥5/h; 6 mild, 6 moderate). In women with OSA, lower mean OSat, greater proportion of time in bed (TIB) with OSat<88%, and worse subjective sleep quality were associated with more pathological tau in meta-temporal ROIs and Braak III/IV (Figure 1; all p's<0.05).

Conclusion: Undiagnosed OSA was highly prevalent in this sample of older women. Further, OSA-related intermittent hypoxemia and poor self-reported sleep quality were linked to temporal tau, thus suggesting that OSA may promote tau accumulation and contribute to older women's vulnerability to AD. Future studies will be necessary to evaluate the effectiveness of OSA treatment and other sleep interventions on reducing risk of AD.

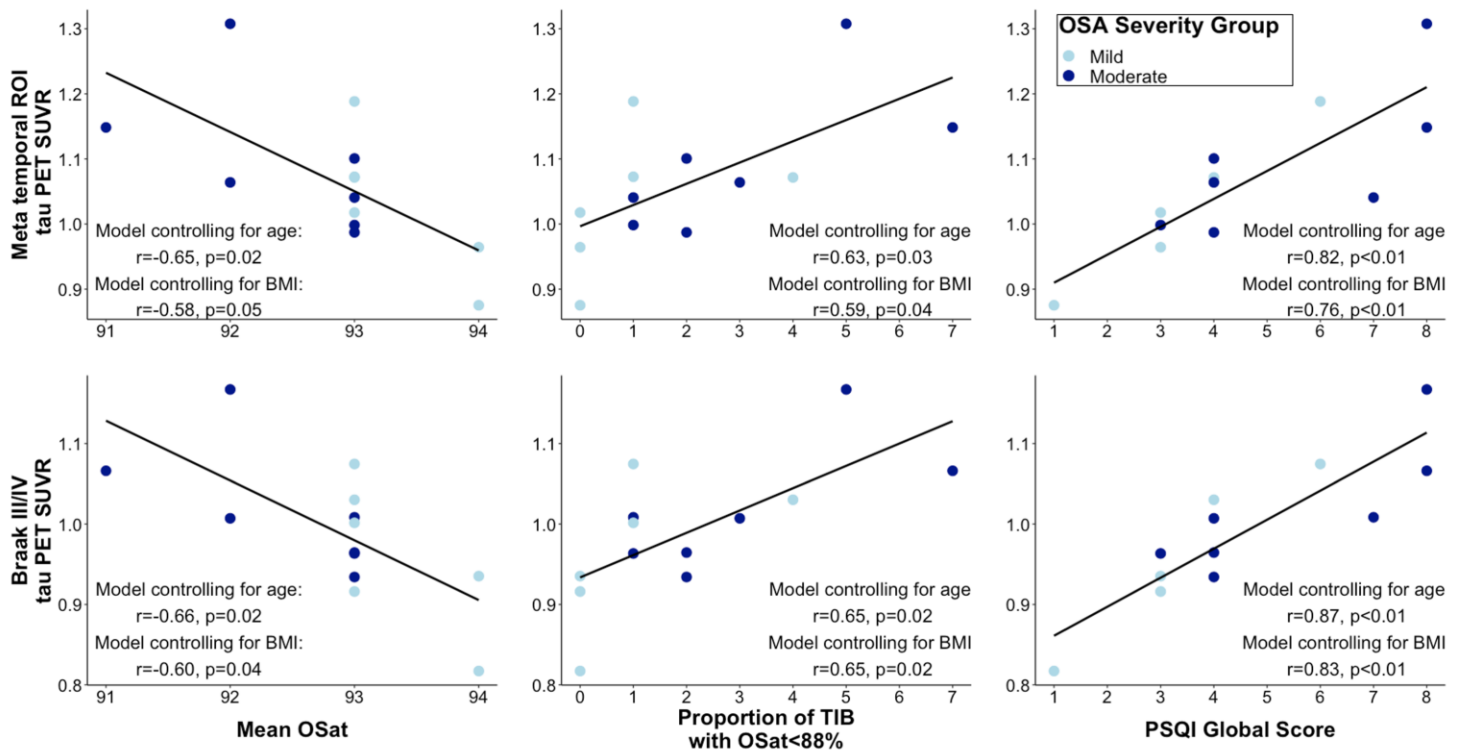


Figure 1. Lower mean OSat, higher proportion of TIB with OSat<88%, and worse subjective sleep quality were associated with greater tau deposition in meta-temporal ROI and regions in Braak III/IV. Results are shown for models that controlled for age or BMI. Mild OSA is an AHI≥5/h and AHI<15 denoted in light blue. Moderate OSA is an AHI≥15/h and AHI<30 denoted in dark blue.

Keywords: sleep, tau, Alzheimer's

P49 Machine Learning Based Tau Positivity Classification On Tau-PET Scans Considers Biological Variability And Can Aid In Decision Making

Robel K. Gebre¹, Alexis Moscoso Rial^{2,3}, Sheelakumari Raghavan¹, Kohl L Johnson Sparrman¹, Heather J Wiste⁴, Christopher G. Schwarz¹, Val J. Lowe¹, Jonathan Graff-Radford⁵, David S. Knopman⁵, Ronald C. Petersen⁵, Michael Schöll^{2,3,6}, Clifford R. Jack Jr¹, Prashanthi Vemuri¹

¹Department of Radiology, Mayo Clinic, Rochester, MN, US

²Department of Psychiatry and Neurochemistry, Institute of Neuroscience and Physiology, The Sahlgrenska Academy, University of Gothenburg, Gothenburg, Sweden

³Wallenberg Centre for Molecular and Translational Medicine, University of Gothenburg, Gothenburg, Sweden

⁴Department of Qualitative Health Sciences, Mayo Clinic, Rochester, MN, US

⁵Department of Neurology, Mayo Clinic, Rochester, MN, US

⁶Dementia Research Centre, Queen Square Institute of Neurology, University College London, London, UK

INTRODUCTION: Research determination of tau PET positivity is often done using a temporal lobe Tau-PET SUVR in a meta-region of interest (meta-ROI) which does not consider spatial heterogeneity across participants. Leveraging clinically approved visual assessments, our goals were to i) develop a machine learning method for predicting Tau-PET positivity using visual assessments by three trained raters; ii) assess model performance when the raters disagreed; iii) compare model performance to meta-ROI-based tau positivity.

Methods: We trained a binary classifier of machine learning models which were ensembled for maximum accuracy. Inputs were tau SUVRs from 84 ROIs obtained from Tau-PET scans (n=1316, Mayo ADRC and MCSA, 73% cognitively unimpaired) which were visually assessed by three raters with 94% agreement and 6% (n=81) disagreement where at least one rated differently. We partitioned the agreement data into 70% training (negative=696/positive=168) and 30% testing (299/72). The disagreement cases were majority voted to assess the model performance. The meta-ROIs were also compared against ratings in the agreement test sets. SHAP AI explainer was used to assess the contribution of regional SUVRs in the model tau positive predictions.

Results: The model accuracy and AUC on the test dataset was 89% and 0.99, respectively, outperforming the meta-ROI (AUC=0.95) (Fig.1). The top predictors are shown in Fig.2. When the raters disagreed (AUC≤0.69), the method concurred with the majority vote (AUC=0.71). There was variability in predicting tau positivity (Fig.3). In 15% of participants (11/72 positives), the contribution of inferior temporal SUVR was zero (no contribution to model prediction) for determining tau positivity.

Conclusions: We developed a machine learning model to identify tau positivity from clinically approved visual criteria. The method concurred with the majority visual reader vote demonstrating its usefulness in making ambiguous/difficult decisions. This promising automated method considers spatial variability across participants unlike fixed predetermined ROI methods currently utilized.

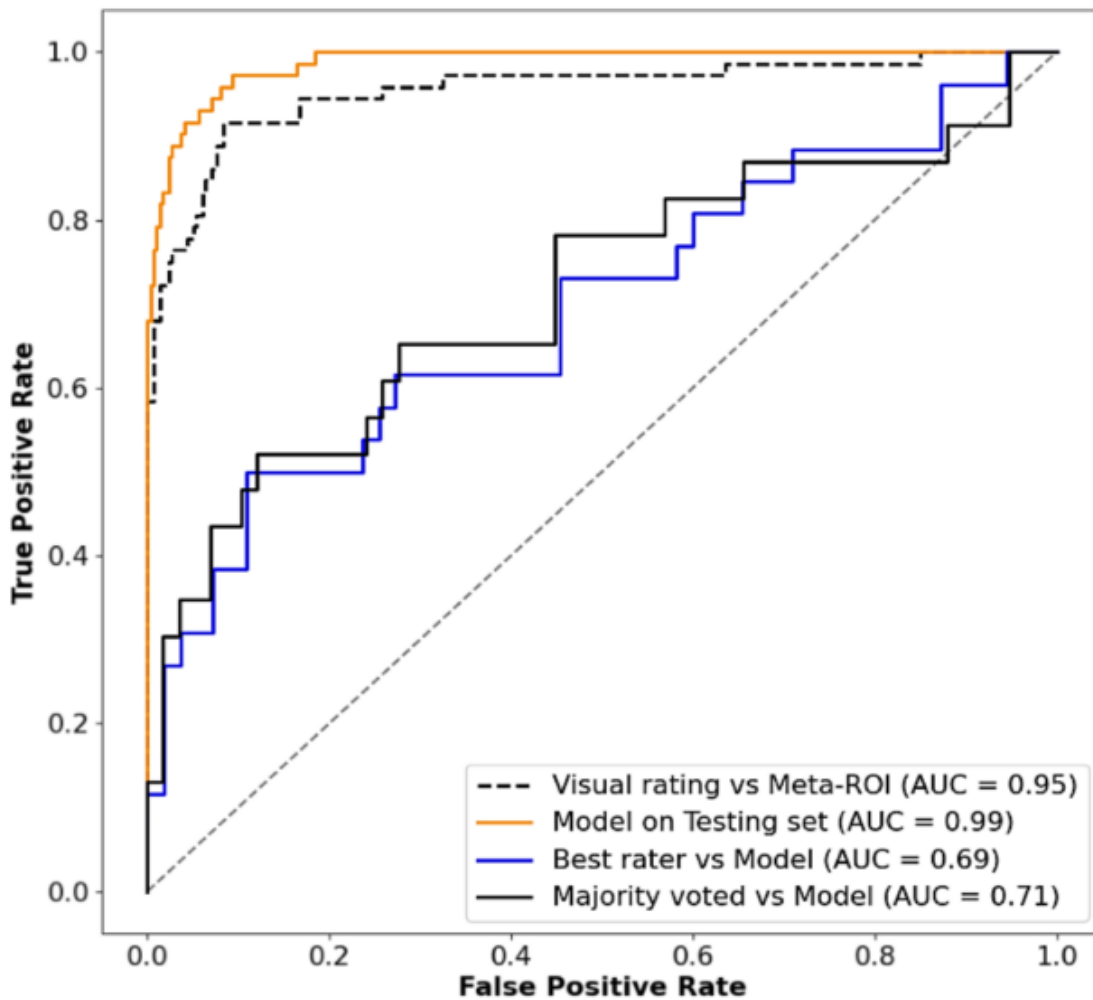


Figure 1. Receiver operating characteristics curves for the model on the testing set, and the majority vote of the human raters against the model predictions and visual ratings against the meta-ROIs. The model outperformed the meta-ROI-based assessment.

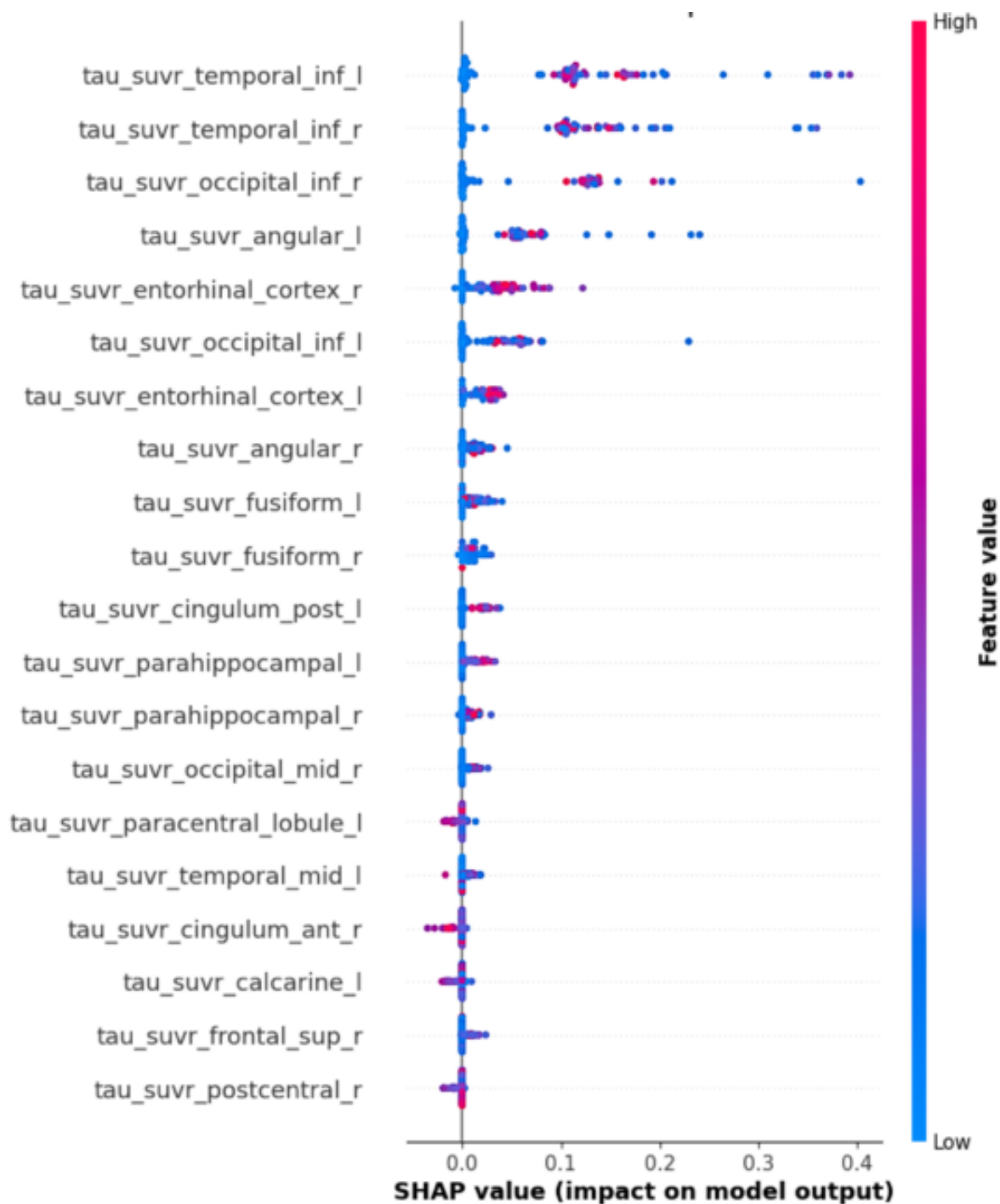


Figure 2. SHAP (SHapely Additive exPlanations) feature importance summary plot of the top regional SUVR measures that had a greater impact for predicting tau positivity. The x-axis shows the model contributions (SHAPs) and values greater than 0 show a positive impact. The color bar shows the individual feature values where the low values (blue) represent smaller SUVRs, and the reds show the higher SUVRs.

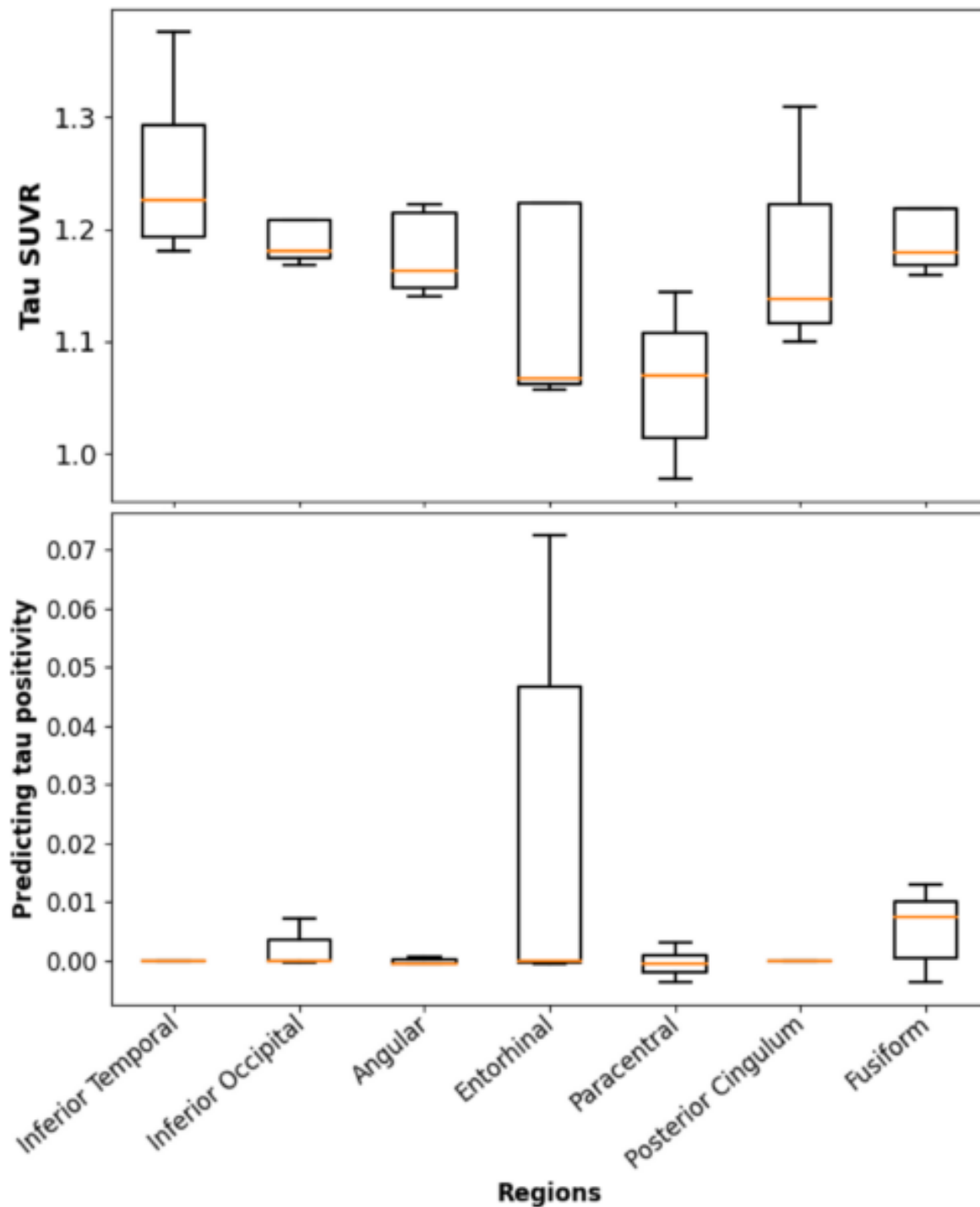


Figure 3. Demonstrating biological variability captured by the machine learning model. The SHAP values are shown in the bottom plot when the contribution of the inferior temporal region to making tau positivity predictions is zero compared to the other regions in the test set. (n=72). The top plot shows the corresponding actual tau SUVR measures.

Keywords: Tau-PET, Machine learning, Tau positivity, Visual rating

P50 Impact of florbetaben acquisition timing on SUVR and centiloid values

Emily Johns¹, Gabriel Kennedy¹, Christina B. Young¹, Kyan Younes¹, Hillary A. Vossler¹, Kathleen L. Poston¹, Guido A. Davidzon¹, Elizabeth C. Mormino¹

¹Stanford University School of Medicine, Stanford, CA, US

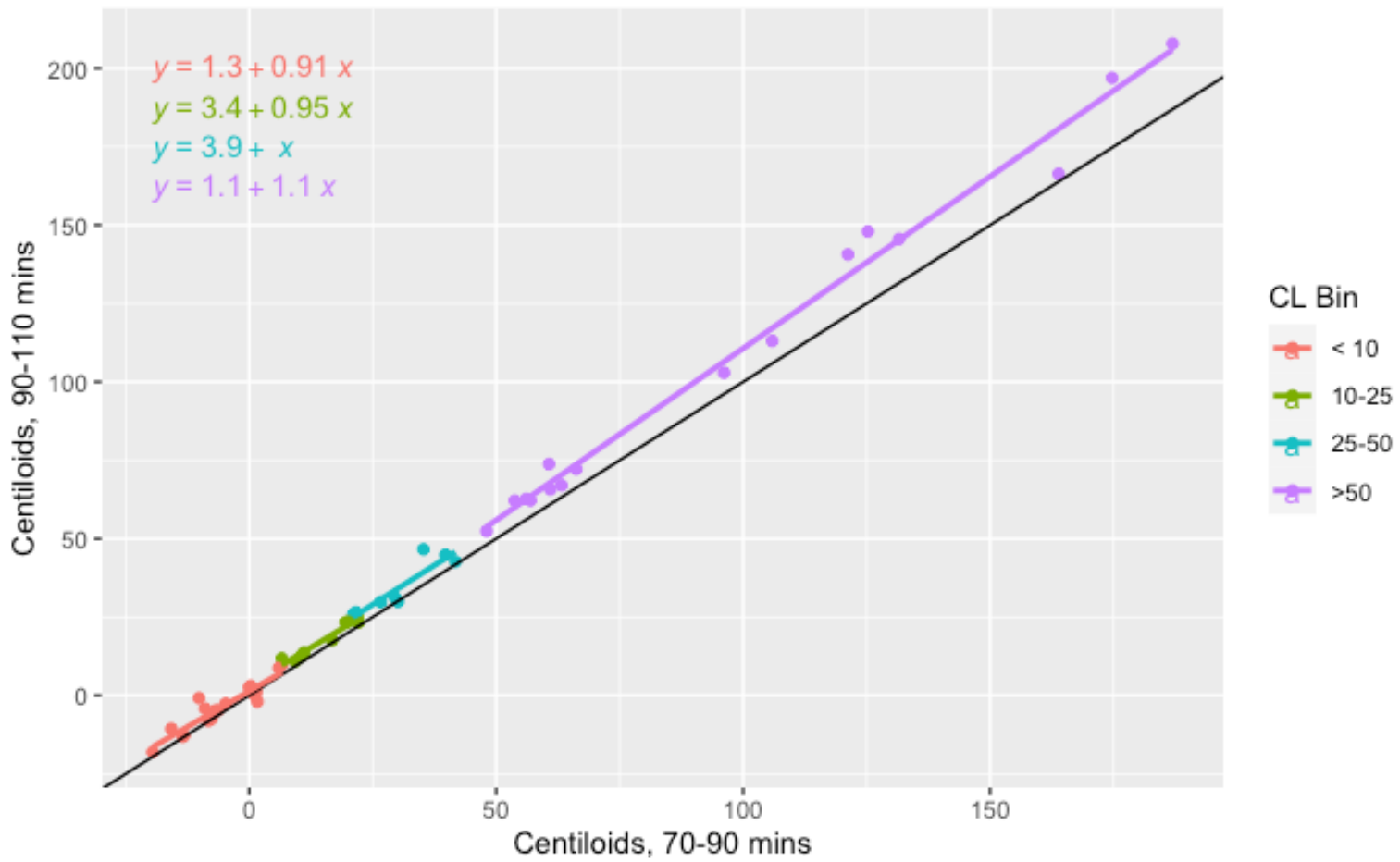
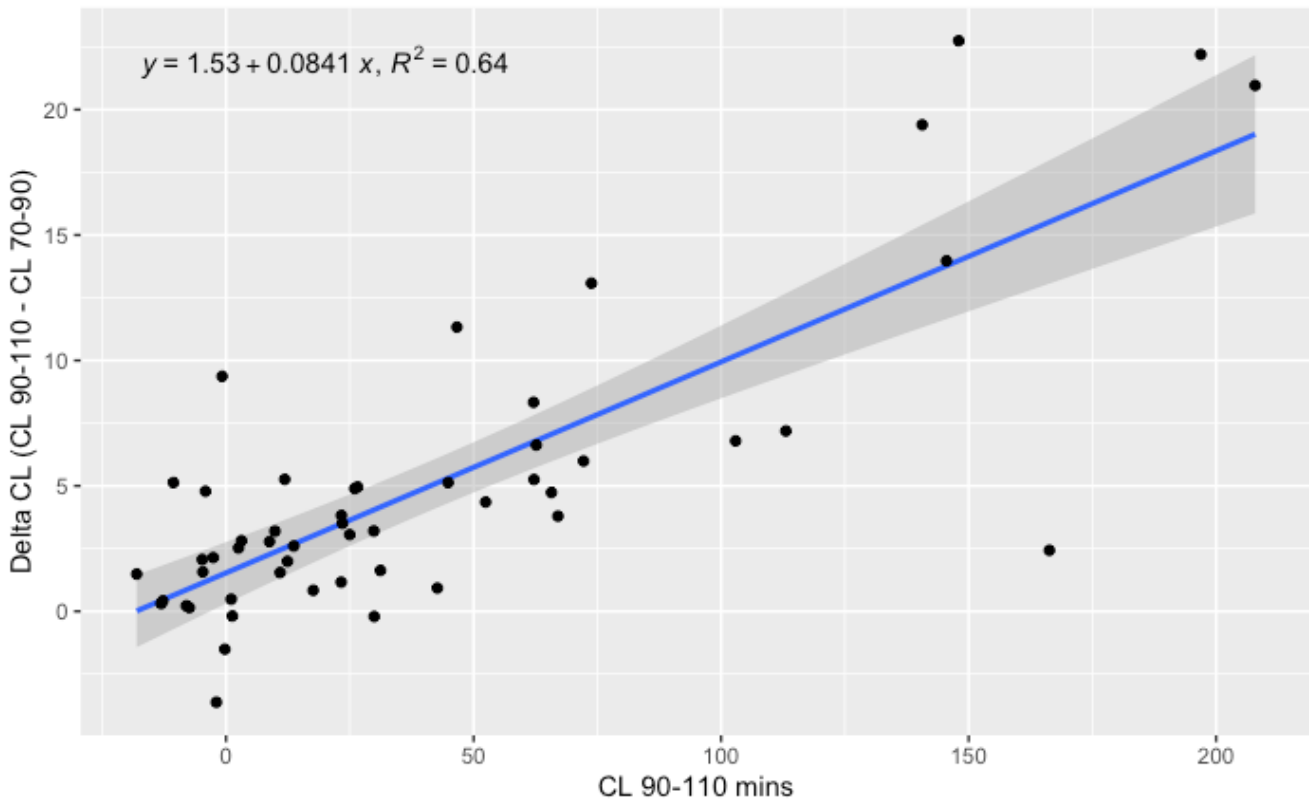
Background: Integration of amyloid PET data collected across different timepoints, scanners, and sites provides opportunities to address scientific questions that depend on large datasets. However, inconsistent acquisition protocols may confound the ability to combine across-cohort data.

Objectives: We sought to understand the impact of acquisition start time of florbetaben (FBB) amyloid PET on centiloid levels (CL) as a function of acquisition time.

Methods: We analyzed 52 FBB amyloid PET scans from the Stanford Alzheimer's Disease Research Center (ADRC) with 5-minute frame data spanning 70-110 minutes post-injection. Frame data was motion correction and summed into both 70-90 and 90-110-minute files. Summed files were processed through an MRI-Free pipeline involving spatial normalization to an FBB-Template (Landau, 2021). A global cortical target region and a whole cerebellum reference region from the GAAIN atlas were first used to create Standardized Uptake Volume ratios (SUVRs) and then converted to CLs (Klunk, 2014). SUVRs and CLs computed across the two acquisition windows were compared. Follow-up analyses using the 90-110 min data examined effects as a function of CL bins: <10(N=19), 10-25(N=9), 25-50(N=8), and >50(N=16).

Results: As expected, CLs were systematically lower during the earlier acquisition window. Comparison between 90-110 min CLs and change in CL between the two acquisitions revealed a linear positive relationship, such that higher CL values were associated with a greater difference between acquisition (Fig. 1). Additionally, comparison of 70-90 min and 90-110 min data across CL bins revealed mean increases of 1.80 CL for the CL<10 group (range=-3.62,9.36), 2.64 CL for the 10-25 group (range=0.83,5.26), 3.98 CL for the 25-50 group (range=-0.21,11.33), and 10.49 for the >50 group (range=2.43,22.75) (Fig. 2).

Conclusion: Adjustments are needed when combining varying acquisition timing protocols. The impact of acquisition is greater in subjects with higher CL values than those with lower CL values.



Keywords: florbetaben, acquisition, centiloid

P51 Postmortem In Vitro Binding of APN-1607 to PSP and HC Globus Pallidus Homogenates

Paul Tempest¹, Richard Margolin², Steve Paget³, Andrew Campbell⁴, Bradford Navia⁵

¹Aprinoia Therapeutics, Cambridge, MA, US

²Aprinoia Therapeutics, Cambridge, MA, US

³Aprinoia Therapeutics, Cambridge, MA, US

⁴Aprinoia Therapeutics, Cambridge, MA, US

⁵Aprinoia Therapeutics, Cambridge, MA, US

There are no approved in vivo imaging agents to detect tau protein aggregates in the PSP brain. APN-1607 shows high affinity to 3R and 4R tau aggregates in diverse tauopathies, including AD, PSP, CBD, and Pick's disease (Tagai 2021, Li 2021, Zhou 2022). Reproducible uptake has been reported in the expected brain regions of PSP patients and correlated with the cellular distribution of tau by immunohistochemistry (Li 2021, Tagai 2021). To support the development of APN-1607 as a novel PET agent for PSP, we used [³H]APN-1607 in saturation binding experiments to characterize tau aggregates from two PSP donors (19077A001 and HEIA001) and a healthy control donor (18085A003). Clinical and molecular pathology of the donors are described in Table 1. The healthy control tissue lacked pathological tau, amyloid-beta (A β), and alpha-synuclein (α -syn) aggregates. PSP donor 19077A001 tissue was positive for tau without evidence for A β and α -syn aggregates. PSP donor HEIA001 had both pathological tau and A β aggregates. Saturation binding experiments were carried out with varying concentrations of APN-1607 in crude globus pallidus homogenates to determine the K_d and B_{max}, using non-linear regression analysis (Figure 1). No saturable binding for the healthy control was observed. Excellent separation in B_{max} between PSP donors and the healthy control was observed (Figure 1). The K_d's of PSP donors (4 nM to 7 nM) were consistent with that reported by Tagai et al. The B_{max}'s were within range albeit lower than that reported by Tagai et al. (119 nM to 191 nM versus 688 nM). This B_{max} difference could be attributed to the different ROIs used, globus pallidus vs motor cortex. These results expand on those reported by Tagai et al and provide further support for the development of APN-1607 as diagnostic agent for PSP.

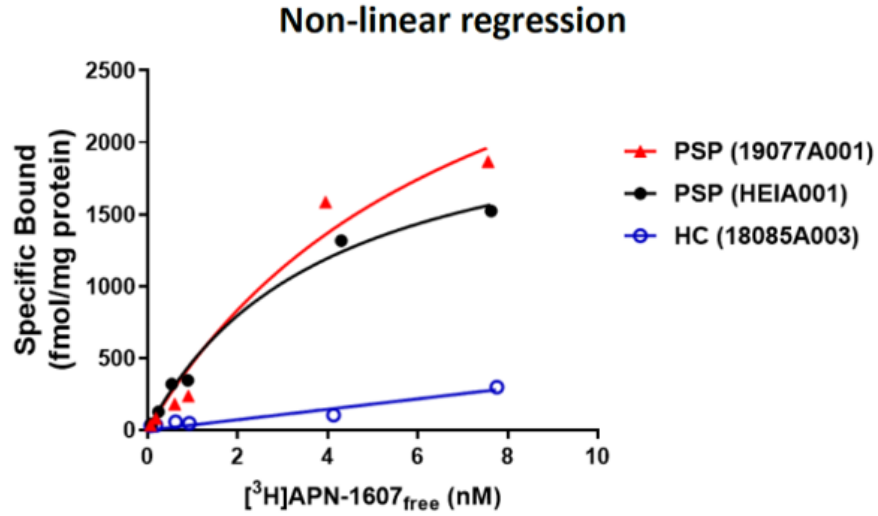
Table 1 Characteristics of Human Globus Pallidus Tissue

Condition	Donor	Vendor	Tissue	Fraction	Gender	Age (years)	PMI (hours)	IHC		
								Tau (p202,pT205) (ch40E8)	A β (3-8 aa) (6E10)	α -syn (pS129) (EP1536Y)
HC	18085A003	Tissue Solutions	Globus pallidus	Crude	F	85	10	(-)	(weak +)	(-)
PSP	19077A001	Tissue Solutions	Globus pallidus	Crude	F	77	6	(+)	(-)	(-)
	HEIA001	Tissue Solutions	Globus pallidus	Crude	F	76	3	(+)	(+)	(-)

Abbreviations: α -syn, α -synuclein; F, female; HC, healthy control; IHC, immunohistochemistry; PMI, postmortem interval; PSP, progressive supranuclear palsy.

Figure 1

APN-1607 Binding to PSP and HC Globus Pallidus: Non-linear Regression Analysis



Abbreviations: [³H]APN-1607, APN-1607; B_{MAX}, concentration of binding components; K_D, dissociation constant; PSP, progressive supranuclear palsy.

Keywords: PET, Tau, PSP, APN-1607

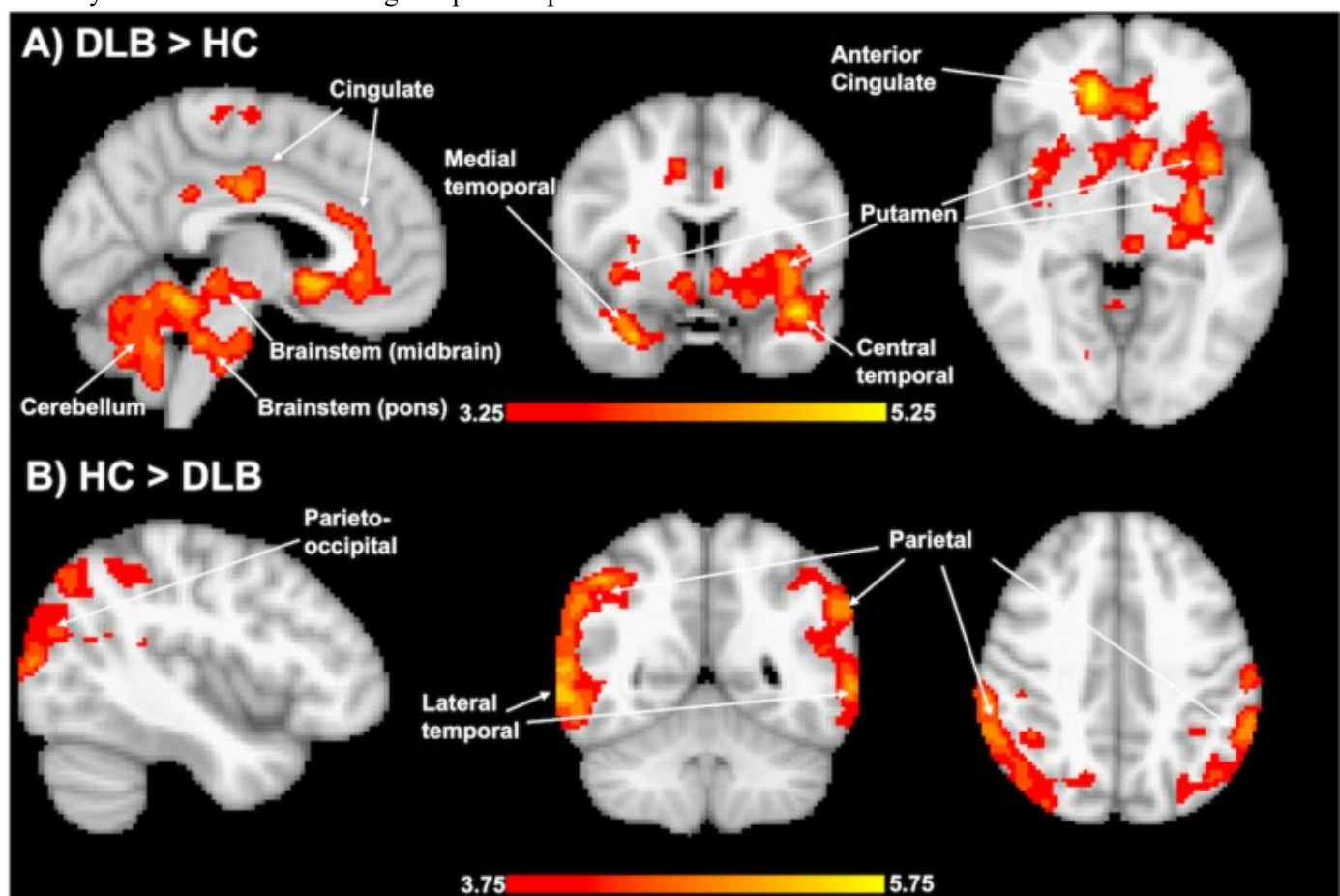
P52 Histone deacetylase tracer [11C]Martinostat behaves differently in amyloid versus synuclein rich regions in dementia with Lewy bodies

Anna Goodheart¹, Chi-Hyeon Yoo², Robin Striar², Moqing Quan¹, Hsiao-Ying Wey², Changning Wang², Stephen Gomperts¹

¹Department of Neurology, Massachusetts General Hospital, Boston, MA, US

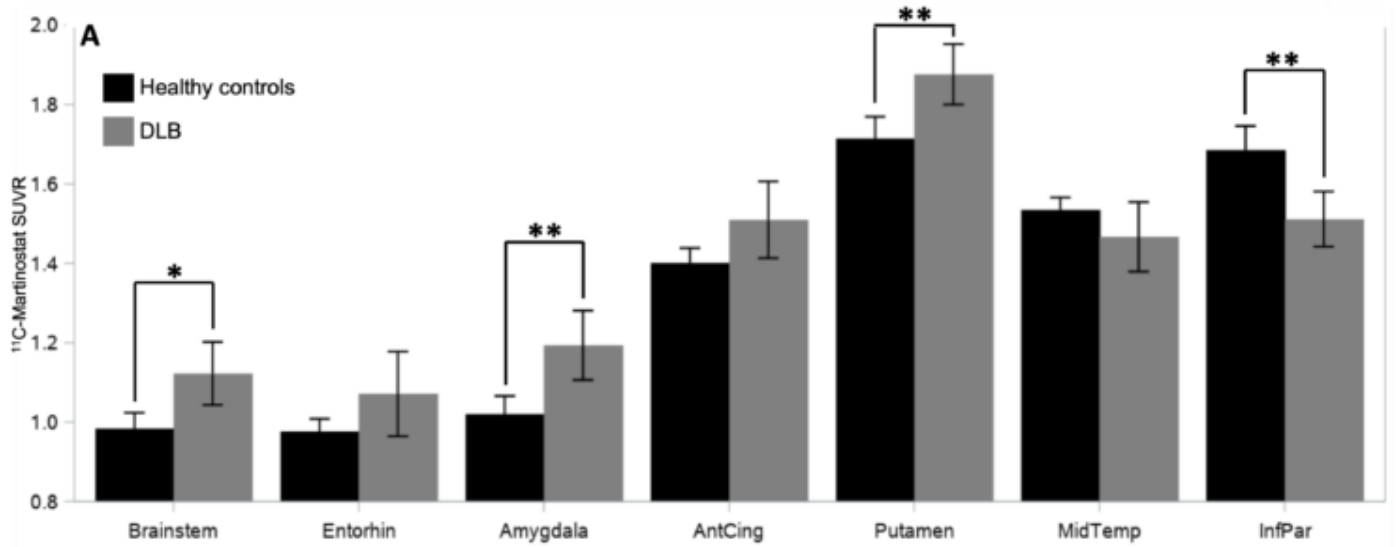
²Department of Radiology, Massachusetts General Hospital, Boston, MA, US

[11C]Martinostat is a novel PET tracer that binds to class I histone deacetylases (HDACs). Here we used [11C]Martinostat to quantify and map HDAC expression in dementia with Lewy bodies (DLB), a neurodegenerative alpha-synucleinopathy that also commonly has beta-amyloid co-pathology. HDACs are powerful epigenetic regulators that are implicated in the pathogenesis of neurodegenerative disease and have been of interest as potential drug targets in Alzheimer's disease, Parkinson's disease, and others. [11C]Martinostat PET from seven DLB and 17 healthy control (HC) subjects were compared using both a whole brain voxel-wise analysis and a targeted region of interest analysis. [11C]Martinostat uptake was elevated in regions classically implicated in DLB-related alpha-synuclein neuropathology, as well as in motor circuitry that interfaces with those regions. [11C]Martinostat uptake was decreased in DLB in cortical regions, notably the parietal and temporal lobes, areas in which beta-amyloid and tau co-pathology can be seen in DLB and regions in which [11C]Martinostat uptake was previously found to be reduced in Alzheimer's disease. These findings imply that class I HDACs may behave differently in the context of alpha-synuclein or beta-amyloid/tau accumulation, even in the same degenerating brain. This implication indicates that the question of the potential role of HDACs as drug targets in neurodegenerative disease is complex. Additional larger studies are needed to determine if [11C]Martinostat PET may be a useful tool to distinguish proteinopathies antemortem.



Voxel-wise analysis. A) Areas of increased uptake in DLB compared to healthy controls. B) Areas of decreased uptake in

DLB compared to healthy controls. PET is partial volume corrected.



ROI analysis. ROIs chosen based on known areas of DLB pathology as well as two representative areas of beta-amyloid localization

Keywords: DLB, amyloid, synuclein, HDAC, PET

P53 A CenTauR scale based on 18F-MK6240

Vincent Dore^{1,2}, Pierrick Bourgeat³, Antoine Leuzy⁴, Kun Huang², Natasha Krishnadas^{2,5}, Azadeh Feizpour^{2,5}, Jurgen Fripp³, Victor Villemagne^{2,6}, Christopher Rowe^{2,5,7}

¹Health and Biosecurity Flagship, The Australian eHealth Research Centre, CSIRO, Melbourne, AU

²Department of Molecular Imaging & Therapy, Austin Health, Melbourne, AU

³Health and Biosecurity Flagship, The Australian eHealth Research Centre, CSIRO, Brisbane, AU

⁴Clinical Memory Research Unit, Department of Clinical Sciences, Lund University, Malmo, Sweden

⁵Florey Department of Neurosciences & Mental Health, The University of Melbourne, Melbourne, AU

⁶Department of Psychiatry, University of Pittsburgh, Pittsburgh, PE, US

⁷Florey Institute of Neurosciences & Mental Health, Melbourne, AU

Background: A standardized scale for the quantification of tau PET imaging would allow comparison and combination of data across tracers and sites resulting in large meta-analysis and the application of universal cut-offs. The proposed approach called CenTauR (CTR) was evaluated on ¹⁸F-MK6240 using both global and regional anchoring.

Methods: 375 ¹⁸F-MK6240 PET & T1w scan pairs (HC Aβ⁻=179/MCI Aβ⁺=98/AD Aβ⁺=98) from AIBL&ADNeT were SUVR normalised using SPM8 and the cerebellar cortex. PET scans were then quantified in 4 composite ROIs [Mesial-Temporal (Me), Meta-Temporal (MT), Temporo-Parietal (TP) and Frontal (FT)] from a previously defined “universal” cortical mask. To anchor the 0 and 100 CTR, we only included HC and AD individuals younger than 75y, with MMSE ≥20, we also excluded HC participants with a quantification higher than the 75%tile in the Me and AD patients with a quantification lower than the 25%tile in the MT, resulting in 77 HC Aβ⁻ and 29 AD Aβ⁺. We investigated two CTR scaling approaches using either a single transform based on the TP anchors to transform SUVR into CTR for all composites or using region-based equations scaled with regional anchors.

Results:

Group demographics and ROI statistics are reported in Table 1.

Using a single transformation resulted in the following equation:

$$\text{CTR} = 100 \times (\text{SUVR} - 0.97) / 2.26$$

Region-based equations can be extrapolated from Table 1. Figures 1 and 2 show that regional CTR overstretches quantification in FT compared to single equation-derived CTR. Thresholds set at 2 std above the HC were 2.38, 9.43, 7.66, 1.82, and 6.16 CTR for Me, MT, TP, FT and Global respectively, and were 7.05, 7.48, 7.66, 10.20, 7.68 CTR when using regional equation-derived CTR.

Conclusion: The region-based approach provided slightly more consistent CTR distributions in the HC across the ROIs however, this approach tends to over-stretch the CTR values in the frontal region.

Table 1: Demographics, reported as mean (standard deviation)

	HC Aβ ⁻	AD Aβ ⁺
Age	70.4 (3.1)	65.0 (6.1)
MMSE	29.0 (1.1)	24.0 (1.9)
Mesial Temporal SUVR	0.88 (0.07)	2.98 (0.66)
Meta Temporal SUVR	1.02 (0.09)	3.23 (0.89)
Temporo-Parietal SUVR	0.97 (0.09)	3.23 (1.03)
Frontal SUVR	0.84 (0.08)	2.49 (1.07)
Universal cortical SUVR	0.94 (0.08)	3.09 (0.95)

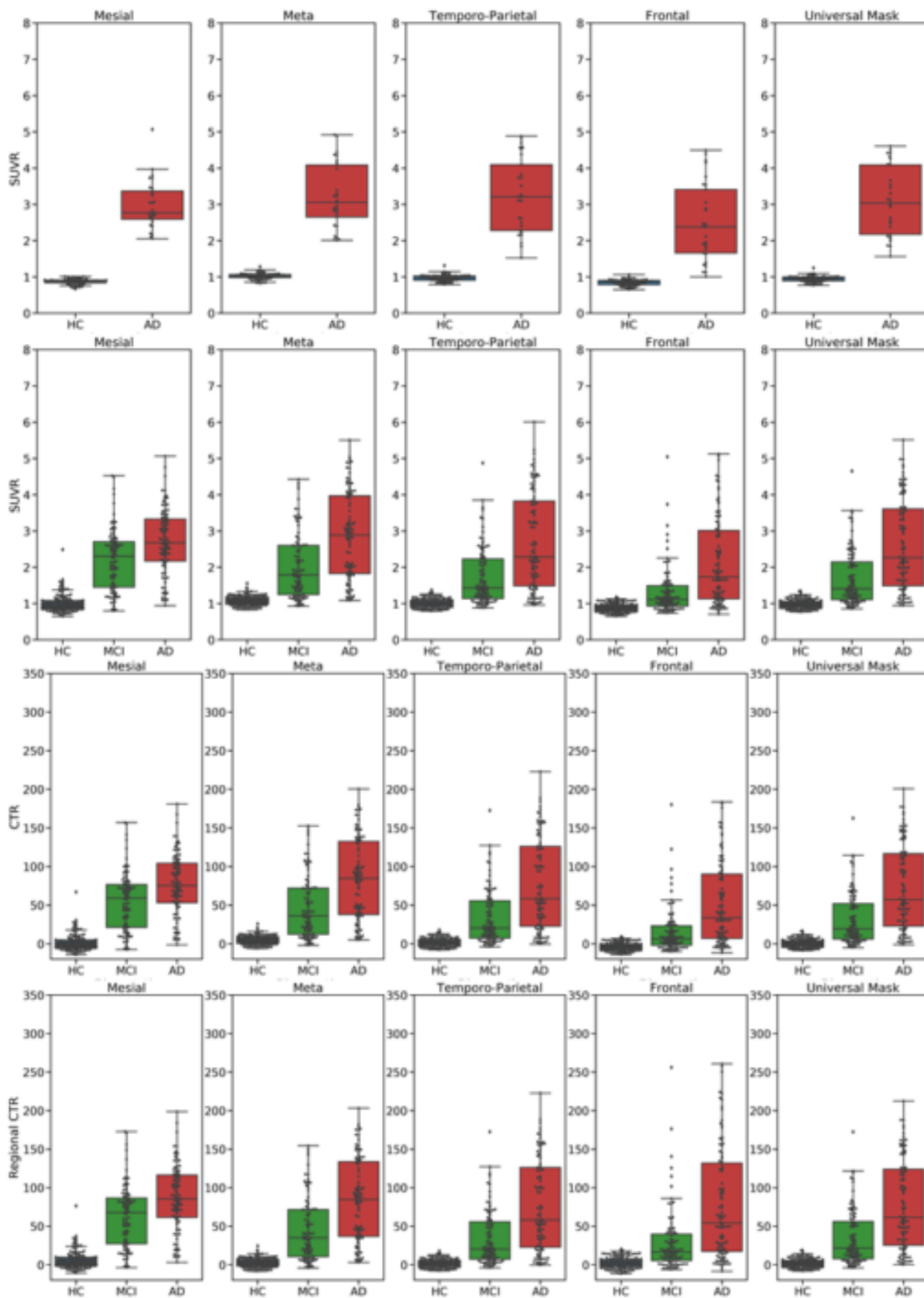


Figure 1: Top row Boxplot of the SUVR values versus clinical diagnosis in anchoring populations. Bottom rows: SUVR, CTR and Regional CTR in the full cohort

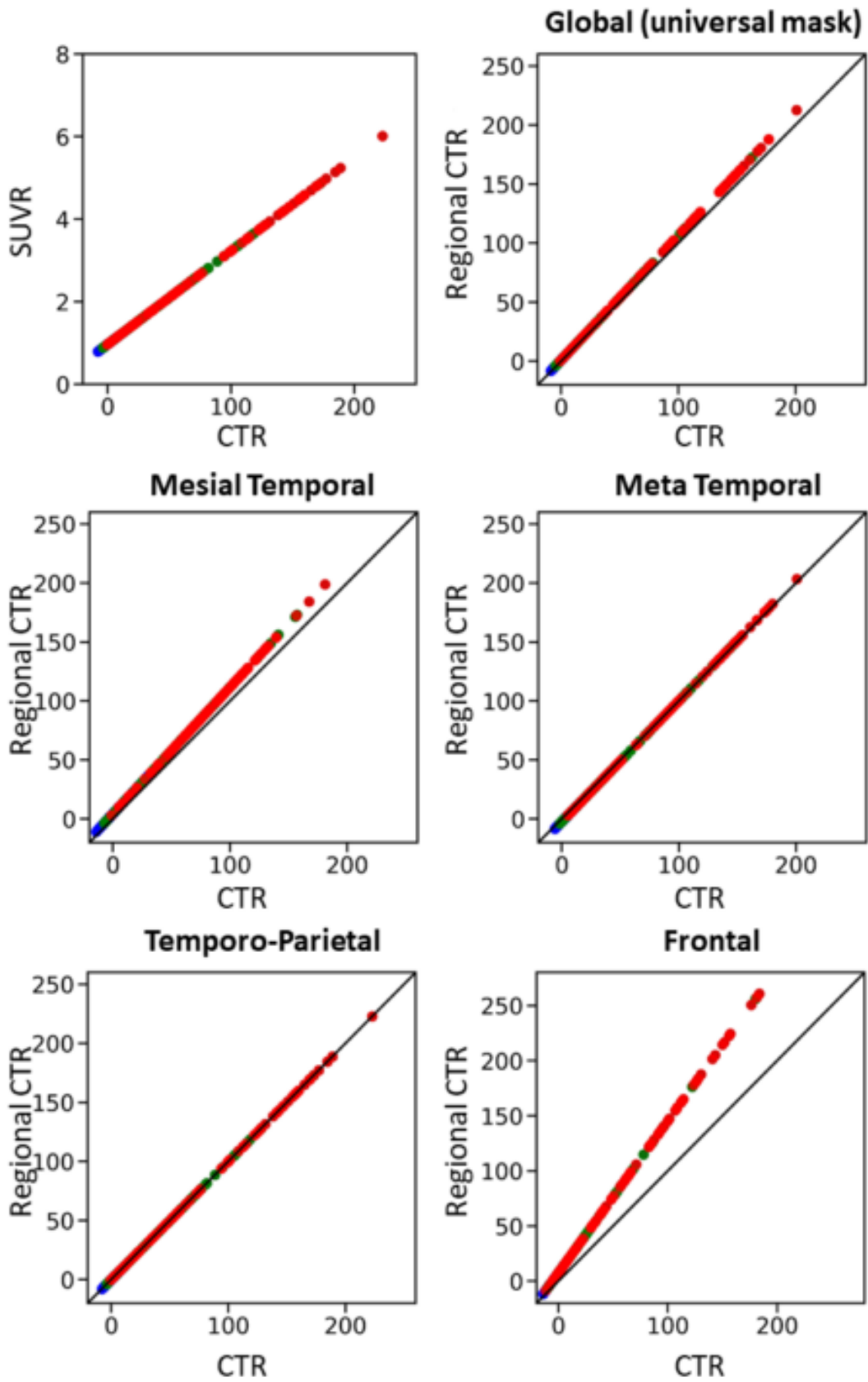


Figure 2: comparison between SUVR and CTR, CTR and regional CTR. (blue HC, green MCI and red AD)

P54 Tau accumulation across the Alzheimer's disease continuum: an 18F-MK6240 AIBL study

Natasha Krishnadas^{1,2}, Vincent Doré^{2,3}, Jo Robertson⁴, Larry Ward⁴, Christopher Fowler⁴, Colin L Masters⁴, Pierrick Bourgeat⁵, Jurgen Fripp⁵, Victor L Villemagne⁶, Christopher C Rowe^{1,2,4}

¹Florey Department of Neurosciences & Mental Health, The University of Melbourne, Melbourne, AU

²Department of Molecular Imaging & Therapy, Austin Health, Melbourne, AU

³Health and Biosecurity Flagship, The Australian eHealth Research Centre, Melbourne, AU

⁴Florey Institute of Neurosciences & Mental Health, Melbourne, AU

⁵Health and Biosecurity Flagship, The Australian eHealth Research Centre, Brisbane, AU

⁶Department of Psychiatry, University of Pittsburgh, Pittsburgh, PA, US

Background: Tau PET imaging enables longitudinal observation of tau accumulation in Alzheimer's disease (AD). ¹⁸F-MK6240 is a high affinity tracer for the paired helical filaments of tau in AD. Despite sparse longitudinal natural history data, ¹⁸F-MK6240 is widely used in clinical trials. This study aimed to evaluate the natural history of tau accumulation, and the impact of disease stage and reference region on the rates of regional change.

Methods: One hundred and eighty-four participants: 89 cognitively unimpaired (CU) beta-amyloid negative (Ab-), 44 CU Ab+, and 51 cognitively impaired Ab+ (26 with mild cognitive impairment [MCI] and 25 with dementia) had annual ¹⁸F-MK6240 scans for one to four years (median 1.48). Regional standardised uptake value ratios (SUVR) were generated. Two reference regions were examined: cerebellar cortex and eroded subcortical white matter.

Results: CU Ab- participants had very low rates of tau accumulation in the mesial temporal lobe (MTL). In CU Ab+, a significantly higher rate of accumulation was seen in the MTL (particularly the amygdala), extending into inferior temporal lobes. MTL tau accumulation plateaued in the MCI Ab+, where the rate of accumulation was greatest in the lateral temporal, parietal, and lateral occipital cortex. Accumulation was global in the AD Ab+, except for a plateau in the MTL. The eroded subcortical white matter reference region showed no significant advantage over the cerebellar cortex, and appeared prone to spill-over in AD participants. Data fitting suggested approximately two decades to accumulate tau to typical AD levels.

Conclusions: Tau accumulation occurs slowly at a similar rate to that reported for Ab. Rates vary according to brain region, disease stage, and tend to plateau at high levels. Rates of tau accumulation are best measured in the MTL and inferior temporal cortex in preclinical AD, and in large neocortical areas, excluding the MTL in MCI/ AD.

Keywords: Tau, positron emission tomography (PET), longitudinal, Alzheimer's disease, 18F-MK6240

P55 Multi-modal analysis of myelin and neurofilament light chain in individuals at risk for Alzheimer's disease using MRI, PET, and CSF biomarker assessments

Kao Lee Yang¹, Doug Dean III^{2,3,4}, Tobey Bethausen¹, Cynthia Carlsson^{1,5,6}, Sterling Johnson^{1,4,5}, Kaj Blennow⁷, Henrik Zetterberg⁷, Andrew Alexander^{2,4,8}, Barbara Bendlin^{1,5}

¹Wisconsin Alzheimer's Disease Research Center, University of Wisconsin, Madison, WI, US

²Waisman Center, University of Wisconsin, Madison, WI, US

³Department of Pediatrics, University of Wisconsin, Madison, WI, US

⁴Department of Medical Physics, University of Wisconsin, Madison, WI, US

⁵Wisconsin Alzheimer's Institute, University of Wisconsin, Madison, WI, US

⁶Geriatric Research Education and Clinical Center, William S. Middleton Veterans Hospital, Madison, WI, US

⁷The Sahlgrenska Academy at the University of Gothenburg, Gothenburg, Sweden

⁸Department of Psychiatry, University of Wisconsin, Madison, WI, US

Background: Myelin alterations (Dean et al, 2017) and axonal degeneration (Merluzzi et al, 2019) are detectable among individuals harboring Alzheimer's disease (AD) pathology. However, the extent to which myelin degeneration may associate with axonal injury in AD is unknown. Here, we tested the association between myelin content and axonal degeneration using neuroimaging and fluid biomarker analysis. Given that axonal degeneration may be accelerated by tangle pathology, we also tested for an interaction between myelin and tau pathology on axonal degeneration.

Methods: Seventy-four cognitively-unimpaired individuals from the Wisconsin Alzheimer's Disease Research Center and Wisconsin Registry for Alzheimer's Prevention were selected based on completion of one multicomponent relaxometry (mcDESPOT) MRI scan and one lumbar puncture. mcDESPOT myelin water fraction (MWF) maps were used to quantify myelin content. Axonal degeneration was indexed by CSF neurofilament light chain (NfL) protein concentration, and tau pathology was indexed via [18F]MK-6240 PET. We used Pearson correlation analysis to test the linear relationship between MWF and NfL. Additionally, we used multiple regression analysis to test for a main effect of MWF on NfL, and a MWF*tau interaction, controlling for amyloid (CSF Ab42/Ab40), years between biomarker acquisition, and age. Results were considered significant at unadjusted $p < 0.05$.

Results: Myelin content negatively correlated with NfL concentration in the forceps minor ($r(72) = -0.37$, $p = 0.001$) and inferior fronto-occipital fasciculus ($r(72) = -0.25$, $p = 0.03$), shown in the Figure. No regression models reached significance.

Conclusions: Lower myelin content in tracts projecting to frontal brain regions associated with higher NfL in the expected direction, suggesting that myelin degeneration may be associated with axonal degeneration. However, when accounting for AD pathology and age, the relationship was not significant. Further, interactions between myelin and tau pathology were not observed. Longitudinal studies are needed to better determine the temporal trajectory of myelin and axonal degeneration in the context of accruing AD pathology.

Table. Characteristics of participants

Characteristics	N=74
Female	70.3% (n=52)
Age at MRI scan, years	64.6 ± 5.57
APOE4 positivity	37.8% (n=28)
Years between MRI & LP	3.32 ± 1.90
CSF Aβ42/Aβ40 ratio	0.07 ± 0.01
Tau PET-positive	8.1% (n=6)
White matter tracts, <i>MWF</i>	
Uncinate fasciculus	0.16 ± 0.06
Fornix	0.05 ± 0.03
Inferior fronto-occipital Fasciculus	0.16 ± 0.05
Inferior longitudinal Fasciculus	0.22 ± 0.06
Cingulum bundle	0.16 ± 0.05
Forceps minor	0.19 ± 0.04
Forceps major	0.19 ± 0.03

Values are provided as mean±standard deviation unless noted otherwise.

Time between MRI scan and lumbar puncture (LP) was calculated from taking the absolute value difference in age of the participant at the time of each procedure. APOE4 positivity was determined through carriage of at least one ε4 allele. A positive tau burden was determined through [F-18]MK-6240 PET scans with SUVR ≥ 1.27 in bilateral entorhinal cortex. Amyloid burden was determined through ratio of CSF Aβ42/Aβ40. Abbreviations: MRI = magnetic resonance imaging; MWF = myelin water fraction; CSF = cerebrospinal fluid; PET = positron emission tomography; SUVR = standardized uptake value ratio; Aβ = amyloid-beta; APOE4 = apolipoprotein E epsilon 4 allele.

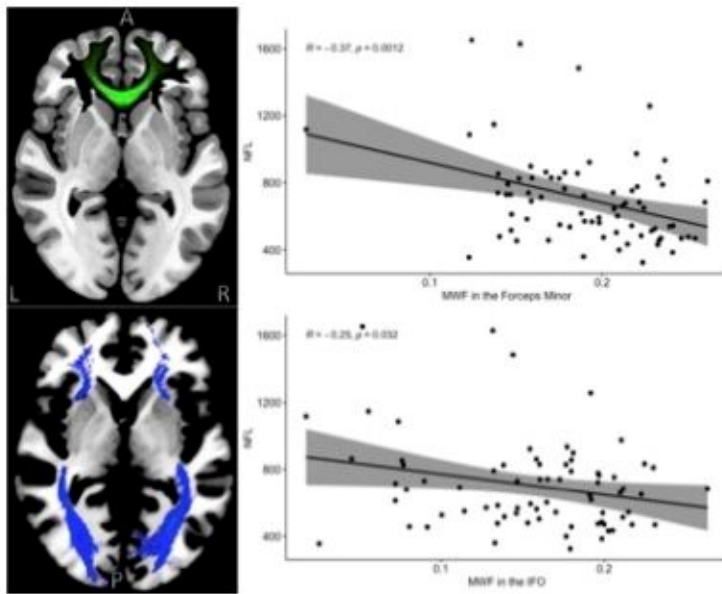


Figure. Correlations between myelin content and NFL

The top left panel shows the forceps minor (in green). The top right panel depicts the linear relationship between myelin water fraction (MWF) in the forceps minor and neurofilament light chain (NFL). The bottom left panel shows the inferior fronto-occipital fasciculus (IFO) in blue. The bottom right panel depicts the correlation between MWF in the IFO and NFL. In both white matter tracts, higher myelin content was correlated with lower NFL concentration, suggesting myelin degeneration may be associated with greater axonal degeneration.

Keywords: myelin, white matter, neurofilament light chain, neuroimaging

P56 The gut microbiota metabolite trimethylamine n-oxide is associated with white matter degeneration on the Alzheimer's disease continuum

Jason Moody¹, Margo Heston¹, Katie Zarbock^{2,3}, Kaj Blennow^{4,5}, Henrik Zetterberg^{4,5,6,7,8}, Federico Rey², Tyler Ulland³, Barbara Bendlin¹

¹Wisconsin Alzheimer's Disease Research Center, University of Wisconsin-Madison, Madison, WI, US

²Department of Bacteriology, University of Wisconsin-Madison, Madison, WI, US

³Department of Pathology and Laboratory Medicine, University of Wisconsin-Madison, Madison, WI, US

⁴Department of Psychiatry and Neurochemistry, Institute of Neuroscience and Physiology, Sahlgrenska Academy, University of Gothenburg, Mölndal, Sweden

⁵Clinical Neurochemistry Laboratory, Sahlgrenska University Hospital, Mölndal, Sweden

⁶Department of Neurodegenerative Disease, UCL Institute of Neurology, London, UK

⁷UK Dementia Research Institute, UCL, London, UK

⁸Hong Kong Center for Neurodegenerative Diseases, Hong Kong, CN

Purpose: Trimethylamine *N*-oxide (TMAO), a pro-inflammatory metabolite impacted by the gut microbiome, is elevated in individuals with mild cognitive impairment (MCI) and Alzheimer's disease (AD) and associated with cerebrospinal fluid (CSF) markers of AD pathology. Neurite density index (NDI) and return to origin probability (RTOP) are two diffusion-weighted imaging (DWI) markers that have shown promise for characterizing microstructural neurodegeneration in AD. Recently, our group used *ex vivo* DWI to show that the oral administration of TMAO led to widespread reductions in NDI in transgenic mice.

To correlate TMAO levels and white matter degeneration in human AD, we assessed the relationships between CSF TMAO and DWI parameters and potential mediation by AD pathology among 244 aging adults.

Methods: 10 AD, 25 MCI, and 209 cognitively unimpaired (CU) participants (Table 1) were imaged with multi-shell DWI and T2 FLAIR. TMAO, amyloid-beta_{42/40} (A β _{42/40}), phosphorylated tau (pTau181), and neurofilament light chain (NfL), were determined in CSF collected via lumbar puncture. NDI and RTOP were extracted from the corpus callosum, cingulum, uncinate fasciculus, superior longitudinal fasciculus, and fornix. Linear regression was used to assess the relationships between TMAO and DWI metrics, and a mediation analysis was performed to determine whether A β _{42/40}, pTau, and NfL mediated these relationships. Results were corrected for age, sex, *APOE* $\epsilon 4$ status, white matter hyperintensities, and multiple comparisons (Bonferroni).

Results: Elevated TMAO levels were associated with decreased RTOP in the superior longitudinal fasciculus and decreased NDI and RTOP in the cingulum (Figure 1). No CSF AD biomarkers were found to mediate these relationships.

Discussion: Because NDI and RTOP serve as markers for neurite density and tissue restriction, respectively, our results suggest that increases in TMAO may exacerbate neurodegeneration along the AD continuum. Future work will examine TMAO relationships with amyloid and tau PET as well as consider other metabolites.

Table 1 – Demographics

Status	Males	Females	Age (yrs.) - M(SD)
AD	4	6	71.8 (8.1)
MCI	13	12	74.3 (11.4)
CU	70	139	64.7 (8.0)

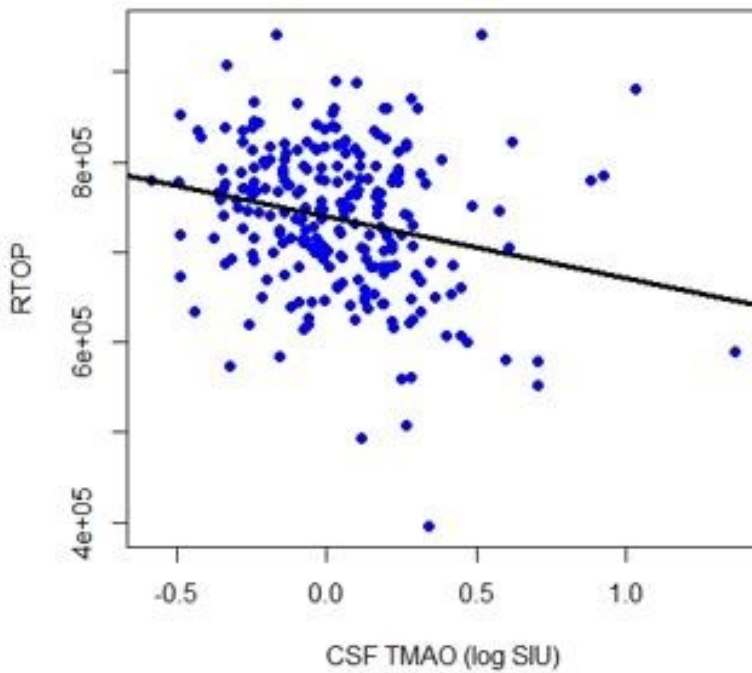
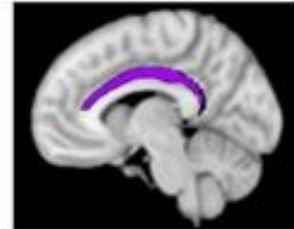
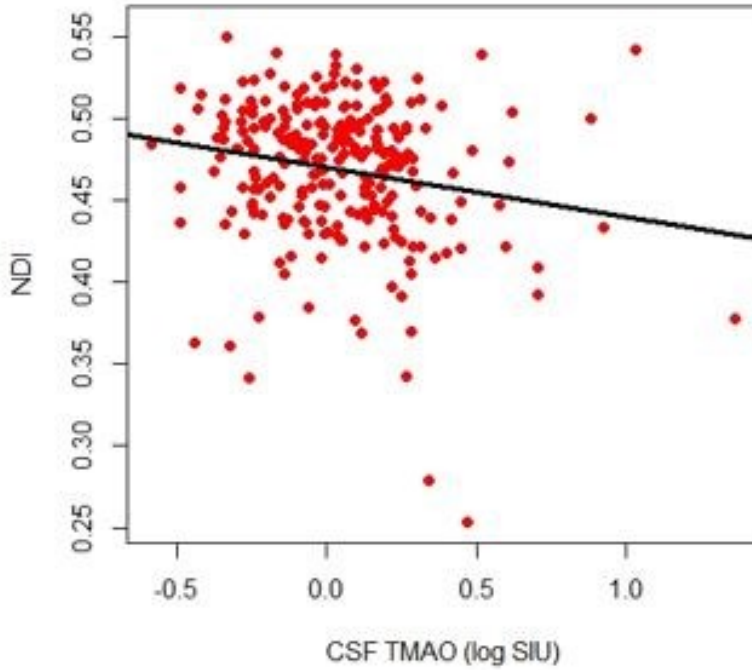


Figure 1

Keywords: gut microbiome, trimethylamine n-oxide, neurodegeneration, white matter, diffusion mri

P57 In vivo measures of fibrillar beta-amyloid pathology limits cognitive plasticity in healthy aging: A multi-center intervention study.

Gerard Bischof^{1,2}, Tim Fellerhoff^{1,3}, Kathrin Giehl^{1,2}, Alexander Drzezga^{1,2,4}

¹University of Cologne, University Hospital of Cologne, Department of Nuclear Medicine, Multimodal Neuroimaging Group, Cologne, Germany, Cologne, Germany

²Research Center Juelich, Institute for Neuroscience and Medicine II, Molecular Organization of the Brain, Juelich, Germany, Juelich, Germany

³Medical Faculty, Heinrich Heine University Düsseldorf, Germany, Duesseldorf, Germany

⁴German Center for Neurodegenerative Diseases, Bonn/Cologne, Germany, Bonn/Cologne, Germany

Experience-dependent cognitive plasticity can be elicited through cognitive training well into later decades of life. Although some prerequisites (education, intelligence) and limitations (age, genetic disposition) towards the extent of cognitive plasticity have been discussed, the impact of molecular age-related changes in form of fibrillar amyloid pathology on plasticity has yet to be investigated.

Here, seventy-six healthy older adults (Age (mean) = 68.5, Age (SD) = 5.8) were enrolled in a multicenter cognitive intervention study. Participants completed twelve 60-minute cognitive training sessions, consisting of validated computerized tasks designed to train executive function, memory, attention and processing speed. A neuropsychological test battery was administered at baseline, post-training, and after three-months (follow-up). Outcome measures included training improvement (i.e., performance slope over training sessions), immediate improvement on transfer tasks (difference score in *untrained* neuropsychological tests from baseline-to post-training = transfer) and maintenance of transfer effects until follow-up (difference score in *untrained* neuropsychological tests post-training -to follow up = long-term transfer)

Additionally, Positron-Emission Tomography (PET) using ¹⁸F-Florbetaben to image fibrillary beta-amyloid plaques was performed. Global standard-uptake value ratios (SUVR) were computed. General linear models to assess the influence of global SUVR on intervention outcome measures controlling for age, education and general intelligence were conducted.

We observed significant negative effects of global amyloid on training improvement, where individuals with higher SUVRs showed significant less training improvement. Similarly, significant amyloid deposition was negatively associated with transfer maintenance until follow-up. Interestingly, immediate transfer improvement at post-testing was not related to amyloid deposition.

We show that global amyloid deposition in cognitively healthy participants can limit the ability to benefit from cognitive training. Additionally, long-term maintenance of cognitive training effects is degraded by increased amyloid deposition. Our results show, that although cognitive training can elicit cognitive plasticity in healthy older adults, this cognitive plasticity can be limited by amyloid pathology.

Keywords: Beta-amyloid PET, Cognitive Training, Intervention, Plasticity

P58 One Year Longitudinal Change of Tau Accumulation on [¹⁸F]PI-2620 PET in Alzheimer Spectrum

Minyoung Oh¹, Seung Jun Oh¹, Sang Ju Lee¹, Jungsu S. Oh¹, Seung Yeon Seo¹, Jee Hoon Roh², Jae-Hong Lee², Jae Seung Kim¹

¹Department of Nuclear Medicine, Asan Medical Center, University of Ulsan College of Medicine, Seoul, Korea

²Department of Neurology, Asan Medical Center, University of Ulsan College of Medicine, Seoul, Korea

Purpose: We tracked longitudinal changes in tau accumulation in patients with early and late onset A β ⁺ mild cognitive impairment and Alzheimer's disease (EO+ and LO+) using [¹⁸F]PI-2620 PET.

Methods: At baseline, 54 participants (9 A β ⁻ cognitively normal [NC-], 22 LO+, 23 EO+) underwent [¹⁸F]PI-2620 and [¹⁸F]florbetaben PET. And 44 participants (70.8 \pm 8.9y, M:F=14:30, 7 NC-, 20 LO+, 17 EO+) completed 1yr follow up(FU). Standardized uptake value ratios(SUVR) of [¹⁸F] PI-2620 PET were determined by cerebral to inferior cerebellar ratio corrected for partial volume effect. We also investigated a correlation between the progression of tau accumulation and cognitive decline.

Results: At baseline, global SUVR in NC-, LO+ and EO+ were 0.96 \pm 0.07, 1.23 \pm 0.41 and 1.86 \pm 0.87 (p=0.002 for LO+ vs. EO+) for [¹⁸F]PI-2620 and 1.21 \pm 0.06, 1.71 \pm 0.22 and 1.75 \pm 0.20 for [¹⁸F] florbetaben (p=0.55 for LO+ vs. EO+). For regional SUVR of [¹⁸F]PI-2620, EO+ showed higher SUVR in Braak IV (2.02 \pm 0.86 vs. 1.52 \pm 0.68, p=0.023) and V (1.98 \pm 1.15 vs. 1.15 \pm 0.43, p=0.001) areas than LO+. Whereas, there was no significant difference in regional SUVR of [¹⁸F]florbetaben. During 1yr FU, global cortical tau accumulated rapidly on EO+ (0.27 \pm 0.33, 12.5%) than LO+ (0.09 \pm 0.14, 7.0%) globally. It was most significant in Braak V area (0.33 \pm 0.41, 13.9%) in EO+ and Braak III area (0.15 \pm 0.25, 8.2%) in LO+. Both EO+ and LO+ showed rapid deterioration in verbal memory than in NC- (p=0.007, 0.025 for each), tau accumulation correlated with deterioration of verbal memory in EO+(r=-0.885, p<0.001), but not in LO+(r=0.016, p=0.943). Atrophic change of hippocampus dose not showed significant correlation with tau accumulation on both groups.

Conclusions: Tau accumulation measured by [¹⁸F] PI-2620 in EO+ showed rapid accumulation in parietal cortex and correlated with deterioration of verbal memory. It suggests that [¹⁸F] PI-2620 PET is potential biomarker for selecting therapeutic target and monitoring treatment effect for tau targeting treatment.

Keywords: tau, PET, EOAD, LOAD

P59 The role of vascular pathology in the association between amyloid- β and tau in cognitively unimpaired individuals

Emma Coomans^{1,2}, Danielle van Westen³, Alexa Pichet Binette³, Olof Strandberg³, Nicola Spotorno³, Sebastian Palmqvist³, Erik Stomrud³, Rik Ossenkoppele^{3,4,5}, Oskar Hansson³

¹Radiology & Nuclear Medicine, Vrije Universiteit Amsterdam, Amsterdam UMC location VUmc, Amsterdam, The Netherlands

²Amsterdam Neuroscience, Brain Imaging, Amsterdam, The Netherlands

³Clinical Memory Research Unit, Lund University, Lund, Sweden

⁴Alzheimer Center Amsterdam, Neurology, Vrije Universiteit Amsterdam, Amsterdam UMC location VUmc, Amsterdam, The Netherlands

⁵Amsterdam Neuroscience, Neurodegeneration, Amsterdam, The Netherlands

Background: Although cerebrovascular pathology often co-exists with Alzheimer's disease pathology, it remains incompletely understood to what extent vascular pathology can contribute to the progression of Alzheimer's disease pathology. We investigated whether the presence of cerebrovascular pathology measured on MRI (white matter hyperintensities [WMH] and cerebral microbleeds [CMB]) modified the association between amyloid- β (A β) and both cross-sectional and longitudinal tau in cognitively unimpaired (CU) individuals.

Methods: We included 306 CU participants from the Swedish BioFINDER-2 cohort with [¹⁸F]flutemetamol (A β)-PET and longitudinal [¹⁸F]RO-948 (tau)-PET. We extracted A β -PET SUVR in a global region-of-interest and tau-PET SUVR in a temporal meta-region-of-interest. Global WMH volume was calculated using the lesion segmentation tool in SPM and log-transformed to improve normality. The presence of CMB's was dichotomized into absent (0 CMB's) or present (≥ 1 CMB's). We performed linear mixed models with longitudinal tau-PET as outcome, and a 3-way interaction between time, A β -PET and WMH volume or presence of CMB's as predictor (separate models) corrected for age, sex and APOE- $\epsilon 4$ carriership.

Results: Participant characteristics are shown in **Table-1**. No significant difference was observed in WMH volume between A β -positive (3.86 \pm 5.04) and A β -negative participants (3.25 \pm 5.45, $p=0.39$), but a trend-level effect was observed for more CMB's in A β -positive (17.3%) compared to A β -negative participants (8.6%, $p=0.055$). We observed a significant interaction between higher WMH volumes and higher A β with greater cross-sectional tau ($\beta=0.18$ [CI: 0.04-0.32], $p=0.01$), but not longitudinal tau ($\beta=0.01$ [CI: -0.02-0.04], $p=0.53$). For CMB's, we observed a significant interaction between having ≥ 1 CMB's and higher A β load with both greater cross-sectional tau ($\beta=0.63$ [CI: 0.33-1.00], $p<0.001$) and longitudinal tau ($\beta=0.12$ [CI: 0.05-0.19], $p=0.002$)(**Fig-1**).

Discussion: In CU, vascular pathology may modify the association between A β and tau by accelerating tau accumulation in the presence of A β . Further research including regional information of vascular pathology is needed to better understand this relationship.

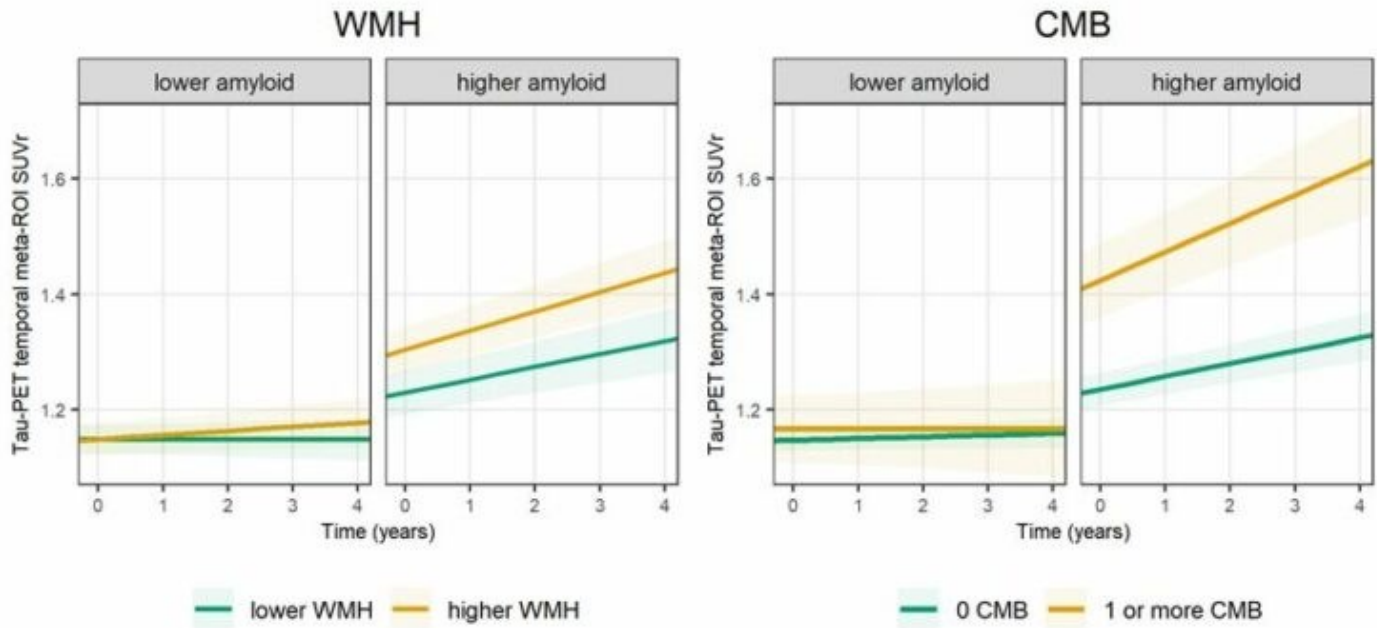
Table 1 Demographics

	Cognitively unimpaired (CU) participants		
	Total group	A β negative	A β positive
N	306	224	82
Age (baseline), years	68.80 \pm 9.99	67.56 \pm 10.07	72.17 \pm 9.00*
Sex, n female (%)	168 (54.9)	122 (54.5)	46 (56.1)
APOE ϵ4 status, n carrier (%)	134 (43.8)	75 (33.5)	59 (72.0)*
Education, years	12.40 \pm 3.48	12.51 \pm 3.29	12.09 \pm 3.94
MMSE	28.89 \pm 1.24	28.99 \pm 1.15	28.61 \pm 1.44*
Aβ-PET global SUVR	0.54 \pm 0.14	0.47 \pm 0.02	0.72 \pm 0.15*
WMH volume, mL	3.41 \pm 5.34	3.25 \pm 5.45	3.86 \pm 5.04
CMB, n present (%)	33 (11.0)	19 (8.6)	14 (17.3)
No. tau-PET scans	2.28 \pm 0.55	2.24 \pm 0.51	2.39 \pm 0.62*
Tau-PET follow-up time, years	2.20 \pm 0.81	2.18 \pm 0.80	2.25 \pm 0.82
Tau-PET temporal meta-ROI SUVR	1.18 \pm 0.16	1.15 \pm 0.10	1.26 \pm 0.24*

Shown are mean \pm standard deviation unless specified otherwise. WMH volume and CMB were both missing for n=5 (non-overlapping) participants.

* Significant difference between A β negative and A β positive participants at $p < 0.05$.

Figure 1 Interaction effects of A β pathology and vascular pathology on trajectories of tau pathology



Plotted are results from linear mixed models (longitudinal tau \sim time*A β *WMH/CMB + age*time + sex*time + ϵ 4-carrier*time). Separate models for WMH and CMB were performed. For visualization, longitudinal tau trajectories for low and high A β , WMH and CMB are shown. Low A β reflects the mean SUVR of A β -negative CU (0.47), high A β reflects the mean SUVR of A β -positive CU (0.72). Low WMH reflects the mean log-transformed WMH of CU participants below the WMH-average (0.29), high WMH reflects the mean log-transformed WMH of CU participants above the WMH-average (1.9). For CMB, results for participants without CMB's and participants with ≥ 1 CMB is shown.

Keywords: Vascular pathology, amyloid-beta, tau, MRI, PET

P60 Dual biomarker amyloid PET for improved subtype and stage inference

Catherine J Scott^{1,2}, William Coath², John C Dickson¹, Sarah J McQuaid¹, David M Cash², Jonathan M Schott²

¹Institute of Nuclear Medicine, University College London Hospitals NHS Foundation Trust, London, UK

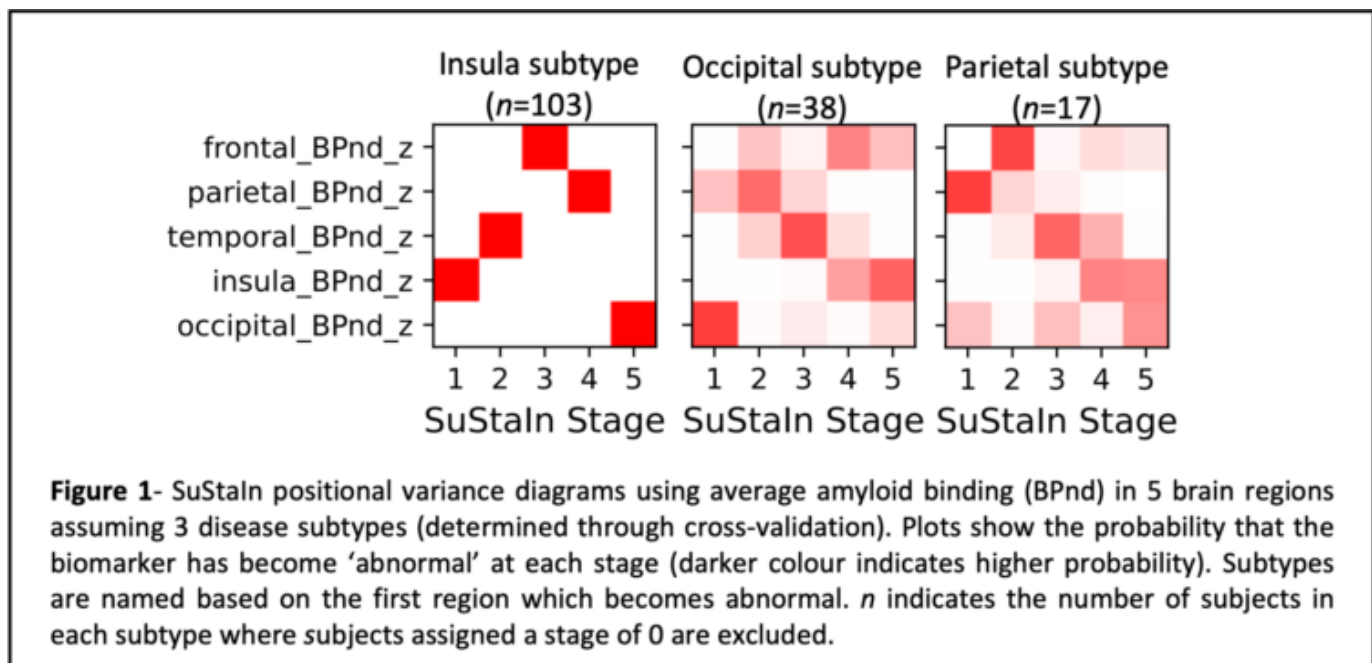
²Dementia Research Centre, UCL Queen Square Institute of Neurology, University College London, London, UK

Background: Regional measures of amyloid PET binding have been shown to be useful biomarkers for disease subtype and stage inference (SuStaIn), elucidating the accumulation of amyloid with disease progression. However, amyloid PET data can provide a second biomarker of tracer delivery if imaging is performed immediately post-injection. Tracer delivery is correlated with blood flow and this work aims to determine whether combining tracer delivery (R1) and amyloid binding (BPnd) can improve subtype and stage modelling.

Methods: The data was derived from Insight46, a neuroimaging sub-study of the Medical Research Council National Survey of Health and Development (n=412), and AVID2, a study of patients with a differential diagnosis of Alzheimer’s Disease (n=15). Subjects underwent a dynamic 60-minute PET/MR scan following 18F-Florbetapir injection. PET frames were reconstructed using NiftyPET, and regional averages derived from T1 parcellations were analysed using the simplified reference tissue model implemented in NiftyPAD. The R1 and BPnd values for 5 cortical regions were then converted into z-scores, assuming single and bi-modal distributions respectively, and input into SuStaIn (pySuStaIn).

Results: When applying SuStaIn to BPnd alone, figure 1 shows good concordance with the parietal and occipital subtypes reported in a study using regional standardised uptake value ratios (SUVRs). However, a standard frontal subtype is not present and instead an insula first ordering is found. When R1 is included, figure 2, the insula subtype shows blood flow changes which resemble the ordering of the frontal subtype found in the literature, suggesting that the pattern identified using SUVR may be influenced by blood flow. Figure 2 also demonstrates less pronounced R1 changes in the parietal subtype and minimal R1 changes in the occipital group.

Conclusion: Using R1 and BPnd as separate biomarkers within SuStaIn yields additional information that may better characterise the disease progression patterns identified than BPnd alone.



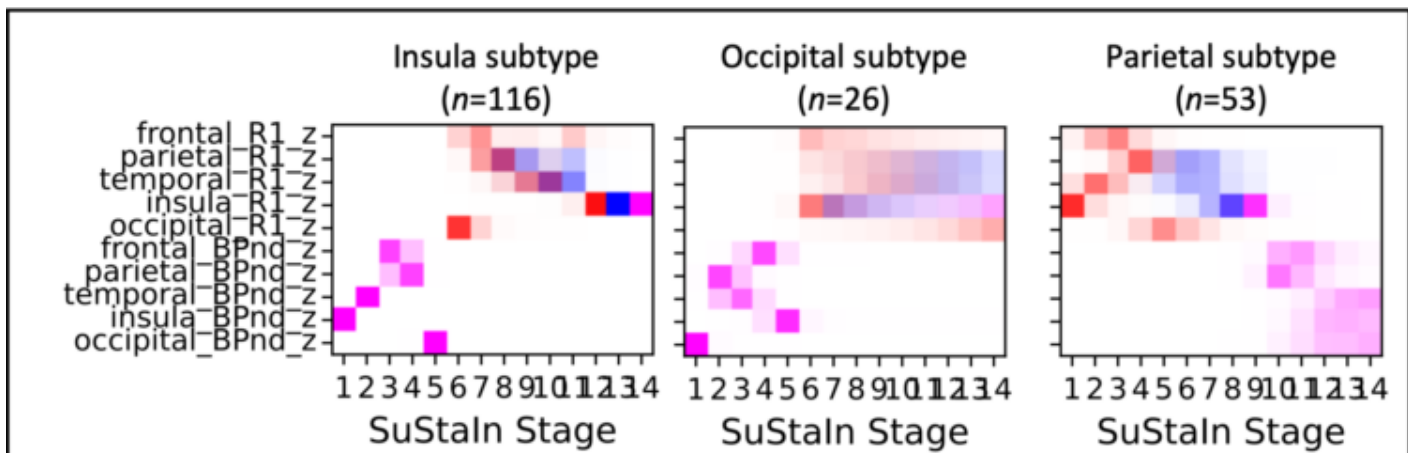


Figure 2- SuStaln positional variance diagrams using both amyloid binding (BPnd) & tracer delivery (R1) in 5 brain regions, assuming 3 subtypes (determined through cross-validation). Plots show the probability that the biomarker has become 'abnormal' at each stage (darker colour indicates higher probability, different colours indicate z-score). Subtypes are named based on the first region which becomes abnormal in BPnd. *n* indicates the number of subjects in each subtype where subjects assigned a stage of 0 are excluded.

Keywords: amyloid, modelling, progression, blood flow

P61 Standardization of Tau PET using the CenTauR Scale: Preliminary findings from BioFINDER-2 using [18F]RO948 and [18F]Flortaucipir

Antoine Leuzy^{1,2,3}, Vincent Doré^{4,5}, Gregory Klein⁶, Suzanne Baker⁷, Maria C. Carillo⁸, Arnaud Charil⁹, Emily C. Collins^{10,11}, Jessica Collins¹², Samantha Budd Haerberlein¹², Nick Henscheid¹³, Eric Hostetler¹⁴, Makoto Higuchi¹⁵, Matthew Hutchinson¹², Leonardo Iacarino^{10,11}, Michael C. Irizarry⁹, William J. Jagust¹⁶, Keith A. Johnson^{17,18}, Yashmin Karten³, Hartmuth C. Kolb¹⁹, Brian Lopresti²⁰, Rik Ossenkoppele^{1,21}, Tharick Pascoal²², Ioannis Pappas^{23,24}, Michael J. Pontecorvo^{10,11}, Gil Rabinovici^{25,26}, Lars Lau Raket^{1,27}, Sandra Sanabria Bohorquez²⁸, Ziad Saad¹⁹, Andrew W. Stephens²⁹, Sulantha Mathotaarachchi², Mark A. Mintun^{10,11}, Sudhir Sivakuraman³, Ruben Smith^{1,30}, Christopher C. Rowe^{5,31,32}, Victor L. Villemagne^{4,22}, Oskar Hansson^{1,33}

¹Clinical Memory Research Unit, Department of Clinical Sciences, Lund University, Malmö, Sweden;

²Cerveau Technologies Inc, Knoxville, TN;

³Critical Path for Alzheimer's Disease (CPAD) Consortium, Critical Path institute, Tucson, AZ;

⁴Health and Biosecurity Flagship, The Australian eHealth Research Centre, CSIRO, Victoria, Australia;

⁵Department of Molecular Imaging & Therapy, Austin Health, Victoria, Australia;

⁶F. Hoffmann-La Roche Ltd, Basel, Switzerland;

⁷Department Lawrence Berkeley National Laboratory, United States;

⁸Alzheimer's Association Chicago Illinois USA;

⁹Eisai, Inc., Woodcliff Lake, New Jersey, USA;

¹⁰Avid Radiopharmaceuticals, Philadelphia, PA, USA;

¹¹Eli Lilly and Company, Indianapolis, IN 46285, USA;

¹²Biogen, Cambridge, Massachusetts;

¹³Critical Path Institute, Tucson, AZ, USA

¹⁴Merck & Co., Inc. West Point, PA 19486, USA;

¹⁵Department of Functional Brain Imaging, Institute for Quantum Medical Science, National Institutes for Quantum Science and Technology, Chiba, Japan

¹⁶University of California Berkeley; Lawrence Berkeley National Laboratory

¹⁷Harvard Medical School, Department of Radiology, Boston, MA, USA

¹⁸Gordon Center for Medical Imaging, Massachusetts General Hospital, Boston, MA, US

¹⁹Janssen, San Diego, California

²⁰Department of Radiology, University of Pittsburgh School of Medicine, US

²¹VU University Medical Center, Neuroscience Campus Amsterdam, Amsterdam, The Netherlands

²²Department of Neurology and Psychiatry, University of Pittsburgh School of Medicine, Pittsburgh, PA, USA

²³Department of Psychology, Helen Wills Neuroscience Institute, University of California, Berkeley, Berkeley, California, USA

²⁴Department of Neurology, VA Northern California Health Care System, Martinez, California, USA

²⁵Department of Neurology, Memory and Aging Center, Weill Institute for Neurosciences, University of California, San Francisco

²⁶Department of Radiology & Biomedical Imaging, University of California, San Francisco

²⁷Novo Nordisk A/S, Søborg, Denmark; ²⁸Clinical Imaging Group, Genentech, Inc., South San Francisco, CA, USA

²⁹Life Molecular Imaging GmbH, Berlin, Germany

³⁰Department of Neurology, Skåne University Hospital, Lund, Sweden

³¹Department of Medicine The University of Melbourne Melbourne Victoria Australia

³²Australian Dementia Network, University of Melbourne, Parkville, Victoria, Australia

³³Memory Clinic, Skåne University Hospital, Lund, Sweden

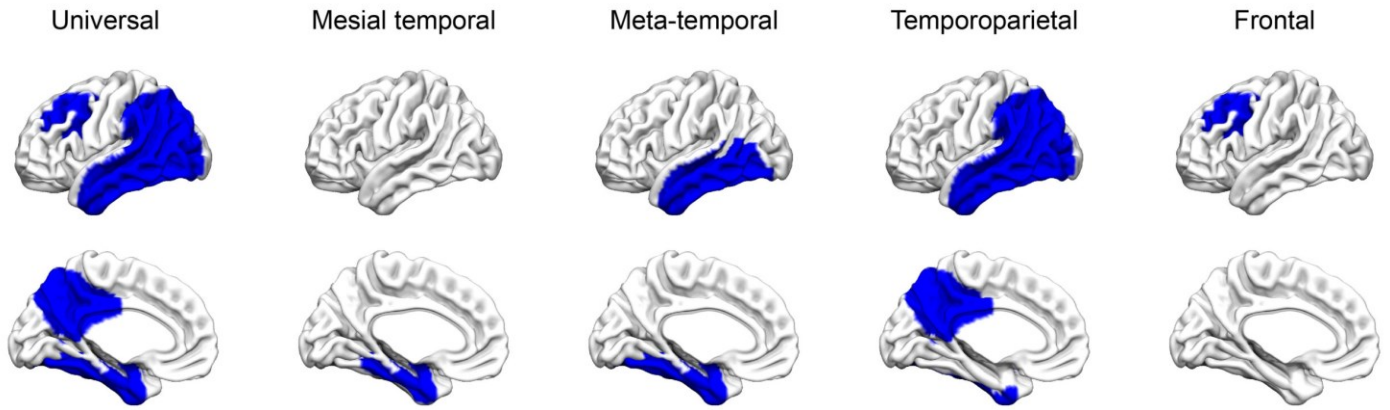
Objectives: To test the feasibility of using a Centiloid-like approach (CenTauR) with tau positron emission tomography (PET) in order to harmonize tau PET outcome data.

Methods: Using data from BioFINDER-2 (^{18}F RO948) and the Avid A05 cohort (^{18}F flortaucipir), we defined inclusion criteria for 0 and 100 anchor points: CenTauR-0, cognitively unimpaired (CU), amyloid PET negative (<10 Centiloids); CenTauR-100, amyloid PET positive (>50 Centiloids), typical Alzheimer’s disease (AD) pattern on tau PET visual read, age <65 and MMSE >20. Based on these criteria, we included 36 CU (CenTauR-0) and 30 AD CenTauR-100) from BioFINDER-2 and 29 CU (CenTauR-0) and 25 AD dementia (CenTauR-100) from the Avid cohort. ^{18}F RO948 and ^{18}F flortaucipir data was acquired 70 to 90 and 80-100 minutes postinjection, respectively. SUVR values were calculated using the inferior cerebellar cortex as the reference region. A head-to-head (^{18}F RO948 and ^{18}F flortaucipir within 30 days) cohort consisting of 37 individuals (5 CU, 24 AD and 8 non-AD) was also included. ROIs included (Figure 1) a universal tau-PET ROI—based on the intersection of tracer specific (^{18}F flortaucipir, ^{18}F MK-6240, ^{18}F -PI2620, ^{18}F PM-PBB3, ^{18}F GTP1 and ^{18}F RO948) masks that had been derived by subtracting average of CU images from the average AD image—as well as four subregions delineated within this ROI (medial temporal, meta-temporal, temporoparietal and frontal) (Doré et al., 2022). In order to convert SUVR values into CenTauRs, we adapted Centiloid equations (Figure 2). The relationship between CenTauRs for ^{18}F RO948 and ^{18}F flortaucipir was assessed within each ROI using coefficient of determination (R^2).

Results: High R^2 values (average 0.962) were observed between ^{18}F RO948 and ^{18}F flortaucipir CenTauRs across the five included ROIs (universal [global], 0.972; medial temporal, 0.967; meta-temporal, 0.968; temporoparietal, 0.967; frontal, 0.923) (Figure 3).

Conclusions: Preliminary findings suggest that the CenTauR approach may prove suitable for harmonization of tau PET outcome data.

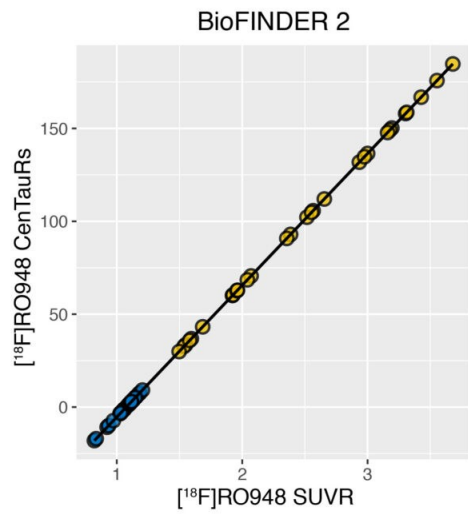
Figure 1. Universal tau PET ROI and subregions



Doré et al., 2022

Figure 2. Example conversion of SUVR to CenTauRs using the Universal ROI

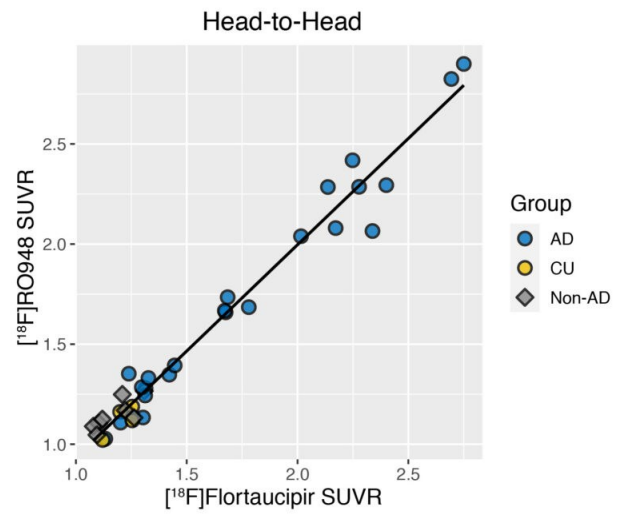
A. Using [¹⁸F]RO948 as standard



Convert RO948 SUVR to CenTauRs

$$\text{CenTauR} = 100 * [\text{SUVR}_{\text{IND}} - \text{Avg. SUVR CenTauR-0}] / (\text{Avg. SUVR CenTauR-100} - \text{Avg. SUVR CenTauR-0})$$

$$\text{Eq}_1. y = 70.931x - 76.288$$



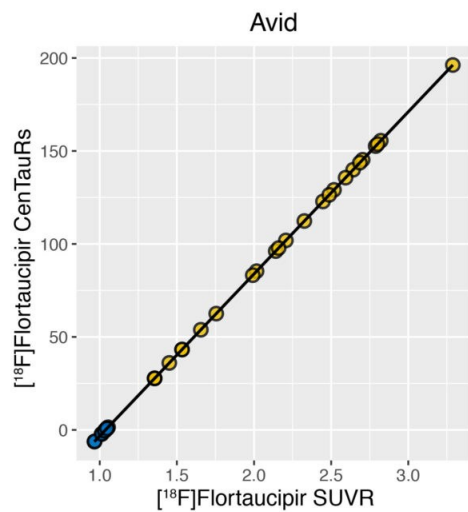
Convert Flortaucipir SUVR to equivalent RO948 SUVR
(^{RO948-Calc}Flortaucipir SUVR)

$$\text{Eq.2. } y = 1.0621x - 0.1273$$

$$\text{RO948-CalcFlortaucipir SUVR} = (\text{Flortaucipir SUVR}_{\text{IND}} - \text{Flortaucipir intercept}) / \text{Flortaucipir slope}$$

Convert ^{RO948-Calc}Flortaucipir SUVR to RO948 CenTauRs using Eq. 1

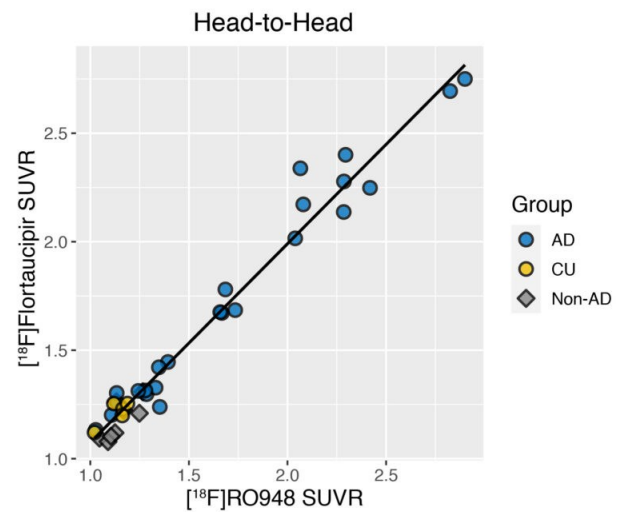
B. Using [¹⁸F]flortaucipir as standard



Convert flortaucipir SUVR to CenTauR

$$\text{CenTauR} = 100 * [\text{SUVR}_{\text{IND}} - \text{Avg. SUVR CenTauR-0}] / (\text{Avg. SUVR CenTauR-100} - \text{Avg. SUVR CenTauR-0})$$

$$\text{Eq}_1. y = 87.20x - 90.497$$



Convert RO948 SUVR to equivalent flortaucipir SUVR
(^{Flortaucipir-Calc}RO948 SUVR)

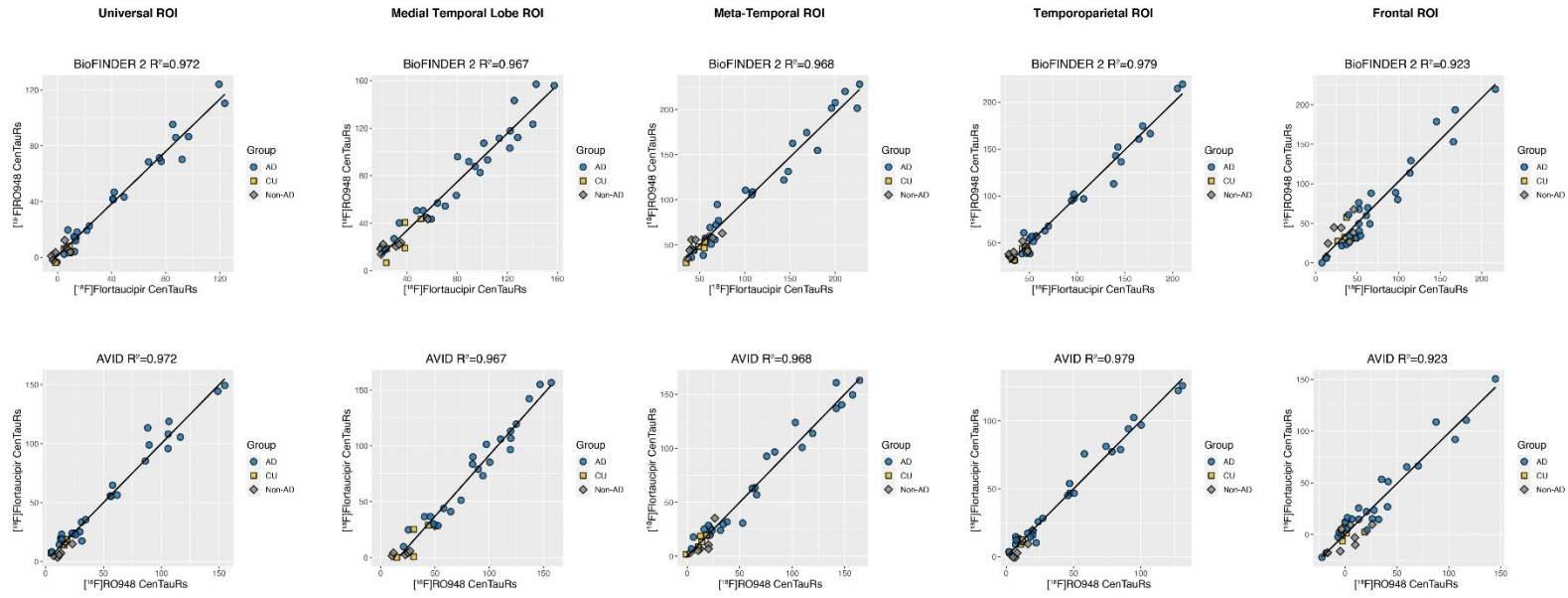
$$\text{Eq.2. } y = 0.9152x + 0.16$$

$$\text{Flortaucipir-CalcRO948 SUVR} = (\text{RO948 SUVR}_{\text{IND}} - \text{RO948 intercept}) / \text{RO948 slope}$$

Convert ^{Flortaucipir-Calc}RO948 SUVR to Flortaucipir CenTauR

$$\text{Eq}_1. y = 87.20x - 90.497$$

Figure 3. Correlations between CenTauR values across ROIs using [¹⁸F]RO948 (top row) and [¹⁸F]flortaucipir (bottom row) as standards



Keywords: Tau, PET, CenTauR, Centiloid, Standardization

P62 Plasma GFAP and NFL are correlated with measures of global cognition in EOAD and EOnonAD

Ralitsa V. Kostadinova¹, Dustin B. Hammers¹, Paige E. Logan¹, Mohit K. Manchella^{1,7}, Sára Nemes¹, Anna M. Fagan², Tatiana M. Foroud¹, Henrik Zetterberg³, Joel H. Kramer⁴, Paul S. Aisen⁸, Maria C. Carrillo⁵, Gil D. Rabinovici⁴, Brad C. Dickerson⁶, Liana G. Apostolova¹, Jeffrey L. Dage¹

¹Indiana University School of Medicine, Indianapolis, IN, US

²Washington University School of Medicine, St. Louis, MO, US

³The Sahlgrenska Academy, University of Gothenburg, Gothenburg, Sweden

⁴University of California, San Francisco, San Francisco, CA, US

⁵Alzheimer's Association, Chicago, IL, US

⁶Massachusetts General Hospital, Harvard Medical School, Boston, MA, US

⁷University of Southern Indiana, Evansville, IN, US

⁸University of Southern California, Keck School of Medicine, Los Angeles, CA, US

Background: Historically, Alzheimer's disease (AD) biomarkers have been used to identify the presence of pathology and have been shown to change well ahead of symptom onset. Here we investigate how select plasma biomarkers are associated with global cognitive measures in early-onset AD (EOAD) and early-onset non AD (EOnonAD).

Method: The current sample included 367 Longitudinal Early-Onset AD Study (LEADS) participants (aged 41 to 65) categorized as amyloid PET-positive EOAD, amyloid PET-negative EOnonAD, or cognitively normal (CN). Each participant had global cognitive (Mini-Mental State Examination [MMSE], Montreal Cognitive Assessment [MoCA], Clinical Dementia Rating Scale sum of boxes [CDR-SB], and ADAS-Cog13) and plasma biomarkers measured on the Simoa-HDx using the N4PE kit (A β 42:40, Neurofilament light protein [NfL], and glial fibrillary acidic protein [GFAP]) assessments at baseline. Phosphorylated Tau measures were not available at the time of this analysis. Partial correlations between cognitive measures and biomarkers were conducted accounting for demographic variables. Fisher r-to-z transformations were run to assess the ability of plasma biomarkers to identify cognitive decline, and compare their performance in different diagnostic groups.

Results: Partial correlations showed moderate associations between cognitive variables and plasma GFAP and NfL ($r=.42-.50$, $p<.001$), and mild associations with A β 42:40 ($r=.25-.33$, $p<.001$). In the pooled sample, all correlations were significant. When split into diagnostic groups, the NfL and GFAP correlations were significant in both EOAD and EOnonAD, but not CN. A β 42:40 correlations were generally non-significant within specific diagnostic groups. There were no significant differences in the associations of plasma GFAP and NfL with different cognitive endpoints.

Conclusions: Across the whole population, all three plasma biomarker measures showed significant associations with cognitive performance. Significant differences between the global cognitive measures were not observed. The correlation for A β 42:40 was only observed in the pooled sample. NfL and GFAP showed similar effects in the pooled, EOAD, and EOnonAD groups.

Keywords: biomarkers, early-onset, cognition

P63 Comparisons of plasma biomarkers with ¹⁸F-Florzolotau PET in AD continuum – a pilot study

Kuo-Lun Huang¹, Ing-Tsung Ing-Tsung^{2,3}, Kun-Ju Lin^{2,3}, Chien-Hung Huang¹

¹Department of Neurology, Linkou Chang Gung Memorial Hospital, Taoyuan, TW

²Department of Nuclear Medicine and Molecular Imaging Center, Linkou Chang Gung Memorial Hospital, Taoyuan, TW

³Healthy Aging Research Center and Department of Medical Imaging and Radiological Sciences, College of Medicine, Chang Gung University, Taoyuan, TW

Introduction: Both plasma beta-amyloid (A β) and pTau181 protein and ¹⁸F-Florzolotau tau PET have been shown the potential to detect Alzheimer's disease (AD) pathology. In this study, we would like to investigate the correlations between plasma biomarkers and Tau PET imaging as well as their association with cognitive performance.

Method: Eighteen amyloid-negative cognitive unimpaired (CU) subjects and 17 amyloid-positive patients with mild cognitive impairment (MCI) or dementia due to AD were recruited for ¹⁸F-Florbetapir PET, ¹⁸F-Florzolotau PET, plasma collection and cognitive evaluation within 3 months. ¹⁸F-Florbetapir PET was visually rated for amyloid positivity adjudication. Standardized uptake value ratios (SUVR) of ¹⁸F-Florzolotau PET were calculated for global cortical uptake and regional Braak-Braak (BB) stages I/II, III/IV, and V/VI. Plasma A β 42/40 ratio and pTau181 were analyzed. Mini Mental State Examination (MMSE) and sum of boxes of Clinical Dementia Rating (CDR-SOB) were evaluated.

Results: When discriminating between amyloid-negative CU and amyloid-positive MCI/AD subjects, the areas under curve (AUCs) were significant for A β 42/40 ratio (0.79), pTau181 (0.95), and ¹⁸F-Florzolotau BB III/IV regional SUVR (0.83). For all participants, global ¹⁸F-Florzolotau SUVR was correlated with A β 42/40 ratio ($r=-0.46$, $p=0.03$) and pTau181 ($r=0.60$, $p<0.01$). Similar trends of ¹⁸F-Florzolotau SUVR were also noted in BB III/IV area with A β 42/40 ratio ($r=-0.49$, $p=0.02$) and pTau181 ($r=0.60$, $p<0.01$), as well as BB V/VI area with A β 42/40 ratio ($r=-0.46$, $p=0.03$) and pTau181 ($r=0.60$, $p<0.01$). After adjusting for age and education, ¹⁸F-Florzolotau global SUVR and regional BB III/IV & V/VI SUVRs were correlated with MMSE and CDR-SOB scores, while plasma A β 42/40 ratio and pTau181 were only associated with CDR-SOB scores.

Conclusion: Both plasma A β 42/40 ratio, pTau181 and ¹⁸F-Florzolotau PET can differentiate CU subjects from MCI/AD patients. ¹⁸F-Florzolotau SUVR was correlated with plasma A β 42/40 ratio and pTau181, especially in regional BB III/IV area. Plasma A β 42/40 ratio, pTau181 and ¹⁸F-Florzolotau SUVR were associated with cognitive performance.

Keywords: A β 42/40 ratio, pTau181, ¹⁸F-Florzolotau, plasma biomarker, Alzheimer's disease

P64 Validating Tau PET Staging Schemes in Relation to Cognitive Outcomes

Dustin Hammers¹, Joshua Lin¹, Paige Logan¹, Shannon Risacher², Adam Schwarz³, Liana Apostolova¹

¹Indiana University School of Medicine, Department of Neurology, Indianapolis, IN, US

²Indiana University School of Medicine, Radiology and Imaging Sciences, Indianapolis, IN, US

³Takeda Pharmaceuticals Ltd., Cambridge, MA, US

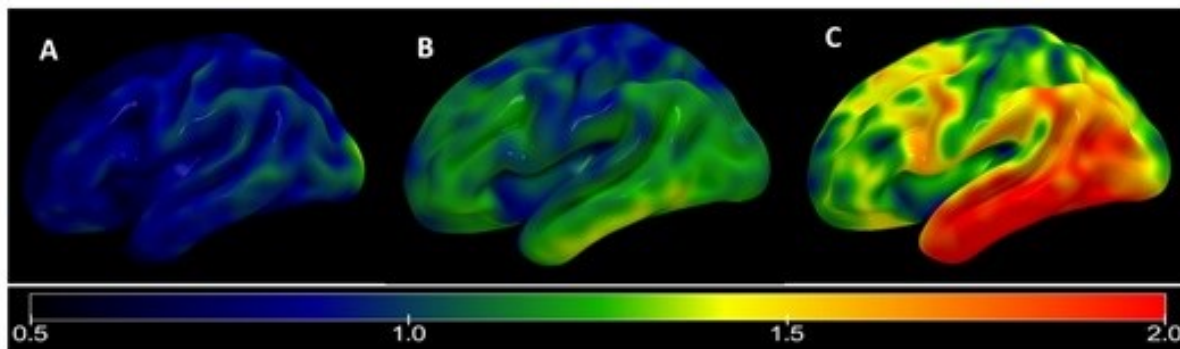


Figure 1. Mean right hemispheric flortaucipir SUVR maps of participants with normal cognition, MCI, and AD in ADNI. A. Tau maps for a participant classified as tau negative by both Schwarz and Chen pathologic staging schemes. B. Tau map for participant classified as tau positive by Chen staging scheme and tau negative by Schwarz staging scheme. C. Tau map for participant classified as tau positive by both Schwarz and Chen staging schemes. Abbreviations: SUVR = standardized uptake value ratio, MCI = Mild Cognitive Impairment, AD = Alzheimer's disease, ADNI = Alzheimer's Disease Neuroimaging Initiative.

Background: The NIA-AA Research Framework definition of Alzheimer's disease (AD) requires the dichotomization of both amyloid and tau pathology. Unlike amyloid, however, the relative novelty of tau-PET imaging has resulted in there being no consensus yet on methods to categorize tau-PET scans into "positive" or "negative". The current study sought to establish multi-modal criterion validity for the use of two different tau pathologic staging schemes.

Method: Tau positivity (T+) and negativity (T-) were calculated from 465 participants across the AD spectrum using pathologic staging schemes from Schwarz et al. (2018) and Chen et al. (2021), with T+ being classified as \geq Stage 4 in Schwarz's TOC model and \geq Stage 1 in Chen's model. Memory subtests from ADNI battery were compared between biomarker status groups using MANCOVA, and with regards to how well they discriminated samples with (T+) and without (T-) tau pathology using ROC-AUC curves. Comparison of effect between the two staging schemes were additionally conducted.

Results: Lower learning and memory subtest scores – from RAVLT, Logical Memory, and ADAS-Cog Word Recall subtests – were observed for the T+ group than the T- group for both Schwarz and Chen staging schemes. Memory subtest scores also displayed fair receiver operator characteristics when differentiating those with and without tau pathology for the Schwarz scheme, though operator characteristics were poor when using the Chen scheme. Differences in effect size were non-significant when accounting for 95% CIs, though false positive rates were highly discrepant (54% Chen, 32% Schwarz).

Conclusions: These results provide support for multi-modality criterion validity of both tau pathologic staging schemes, though false positive rates for Chen's scheme is concerning. Future work to refine these schemes is encouraged, as well as consideration of other staging schemes to further validate the use of tau +/- dichotomization for the NIA-AA Research Framework.

Keywords: Alzheimer's Disease, tau-PET imaging, memory, neuropsychology

P65 Shared variance between FDG metabolism and PiB tracer delivery is not predictive of cognitive decline in preclinical AD

Danielle Mayblyum^{1,2}, Zahra Shirzadi¹, J. Alex Becker¹, Jasmeer Chhatwal¹, Michelle Farrell¹, Heidi Jacobs¹, Nicolas Guehl¹, Georges El Fakhri¹, Reisa Sperling^{1,3}, Julie Price¹, Keith Johnson^{1,3}, Aaron Schultz¹, Bernard Hanseeuw^{1,4}

¹Massachusetts General Hospital, Boston, MA, US

²Drexel College of Medicine at Tower Health, Reading, PA, US

³Brigham and Women's Hospital, Boston, MA, US

⁴Cliniques Universitaires Saint-Luc, Brussels, Belgium

Background: (FDG) metabolism is a clinically validated biomarker. Specifically, entorhinal hypometabolism is associated with subsequent cognitive decline in preclinical AD. Perfusion images, obtained from dynamic PiB-PET scans, are correlated with FDG, and show potential as a proxy for glucose metabolism. We investigated whether PiB-R1, a perfusion measure of relative tracer delivery, was associated with FDG metabolism and could predict subsequent cognitive decline in preclinical AD.

Methods: We analyzed dynamic PiB-PET and FDG-PET from 239 clinically normal participants (Table.1). We calculated PiB-R1 using MRTM in the same 36 FreeSurfer-defined regions-of-interest (ROI) using cerebellar gray as reference and uncorrected for partial volume effects. First, we explored correlations between PiB-R1 and FDG-PET data between-regions within-subjects, then between-subjects for each ROI. Second, we predicted changes in the Preclinical Alzheimer's Cognitive Composite (PACC-5) using either PiB-R1 or FDG data, covarying age, sex, and education. Analyses were repeated in individuals with high-PiB separately.

Results: PiB-R1 images were strongly correlated with FDG from the same participant (mean between-regions $R^2=0.80$, $CI_{95}=[0.66-0.94]$), indicating that FDG metabolism depends on the perfusion of each ROI. Between-subjects however, the correlation between FDG metabolism and PiB-R1 in each ROI was significant but weaker (mean between-subjects $R^2=0.40$, $CI_{95}=[0.19-0.60]$). Specifically, the correlation between entorhinal FDG and R1 was $R^2=0.48$ ($p<0.001$, Fig.1), showing that less than half the FDG variance between-subjects was explained by perfusion.

FDG metabolism predicted subsequent cognitive decline in 12 ROI. In high-PiB individuals, entorhinal FDG predicted cognitive decline (Est.=0.87, $p=0.042$, Fig.2) and remained significant after adjusting for entorhinal R1. In contrast, PiB-R1 predicted cognitive decline in different regions than FDG and didn't significantly predict decline in high-PiB individuals in any region.

Conclusion: PiB-R1 and FDG data aren't equivalent when predicting cognitive decline in preclinical AD. Longitudinal imaging studies are needed to better understand the dynamics between metabolic and perfusion measures.

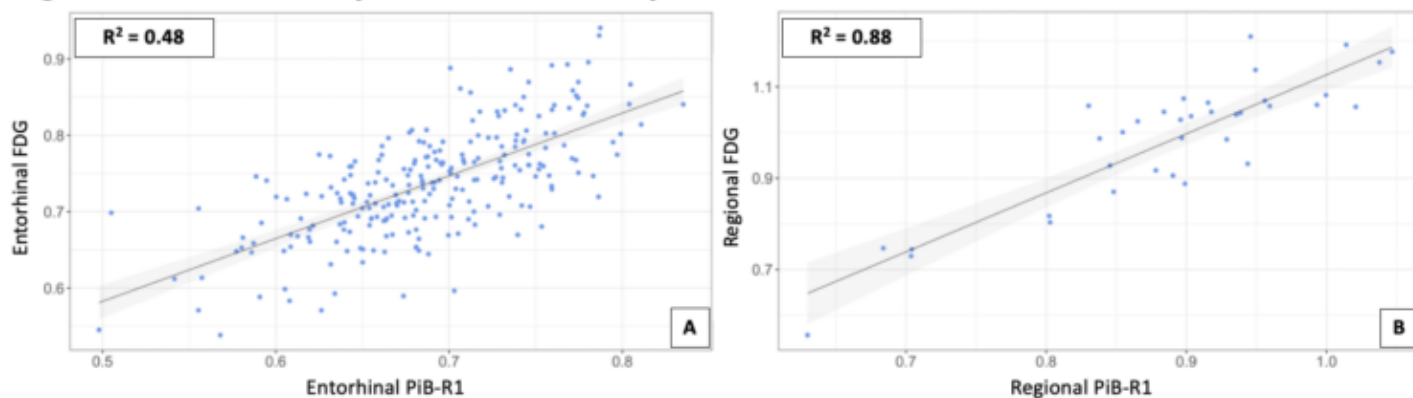
Table 1. Participant Demographics

	All Subjects	Low PiB	High PiB
N	239	181	58
Age	72.74 ± 7.22 (51.75-88.75)	71.97 ± 7.39 (51.75-88)	75.13 ± 6.12 (59.75-88.75)*
APOE E4 status (%)	67 (28.4)	31 (17.4)	36 (62.1)
Education	15.71 ± 3.02 (8-20)	15.60 ± 3.02 (8-20)	16.07 ± 3.01 (8-20)
Females N (%)	137 (57.3)	102 (56.4)	35 (60.3)
MMSE	29.01 ± 1.12 (25-30)	29.08 ± 1.13 (25-30)	28.79 ± 1.07 (26-30)
PACC5 Score	0.02 ± 0.67 (-2.39-2.06)	0.04 ± 0.67 (-2.15-2.06)	-0.04 ± 0.69 (-2.39-1.30)
PACC5 Slope	-0.09 ± 0.20 (-1.04-0.56)	-0.04 ± 0.15 (-1.01-0.56)	-0.22 ± 0.26 (-1.04-0.11)**
PiB FLR DVR	1.17 ± 0.19 (0.95-1.98)	1.08 ± 0.05 (0.95-1.2)	1.47 ± 0.17 (1.22-1.98)**
EC FDG SUVR	0.74 ± 0.07 (0.54-0.94)	0.74 ± 0.07 (0.55-0.94)	0.72 ± 0.07 (0.54-0.93)*
PiB EC R1	0.69 ± 0.06 (0.50-0.84)	0.69 ± 0.06 (0.50-0.84)	0.68 ± 0.06 (0.54-0.80)

Mean ± SD (min-max); p < 0.01*, p < 0.001**

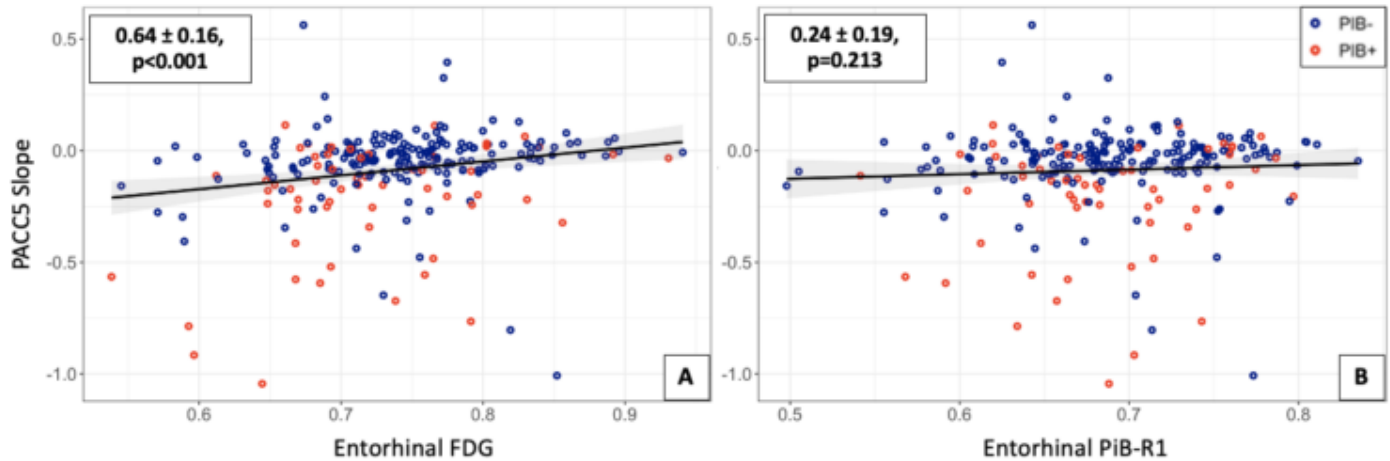
MMSE: mini-mental state exam; PACC5: preclinical Alzheimer’s cognitive composite 5; PiB: Pittsburgh Compound B; FLR: composite with frontal, lateral temporal, and retrosplenial cortices; DVR: distribution volume ratio; SUVR: standard uptake value ratios

Figure 1. Between-subject and within-subject correlations



Legend: (A) Between-subjects correlation showing the association between entorhinal R1 and FDG in each subject. (B) Within-subject correlation for one participant is shown and looks at the association between regional R1 and FDG.

Figure 2. Entorhinal FDG/R1 predicting PACC decline (one line of fit)



Legend: (A) Entorhinal FDG significantly predicted subsequent PACC5 decline in the entire sample, which we did not see with entorhinal R1 (B). FDG Hypometabolism in the following regions was also predictive of cognitive decline in the entire sample: inferior temporal, amygdala, inferior parietal, lateral orbitofrontal, rostral anterior cingulate, middle temporal, caudal anterior cingulate, hippocampus, isthmus cingulate, pars orbitalis, and insula ($p < 0.05$). PiB-R1 signal in the transverse temporal and pars opercularis were the only regions predictive of cognitive decline ($p < 0.05$).

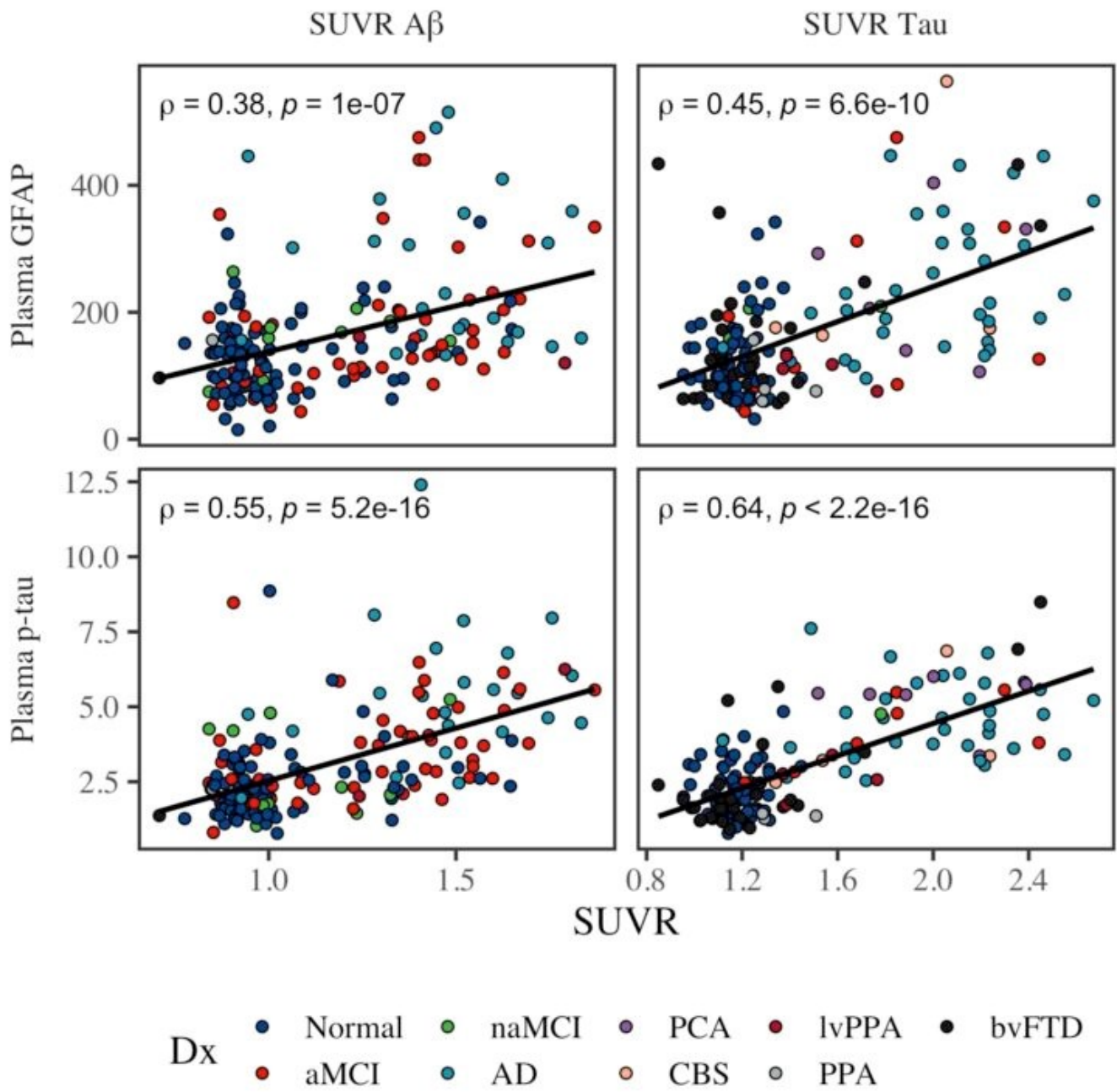
Keywords: R1, PiB, FDG, cognitive decline

P66 Amyloid and tau PET are associated with plasma phosphorylated tau 181 and glial fibrillary acidic protein in a sample of heterogeneous dementia syndromes

Katheryn Cousins¹, Jeffrey Phillips¹, Sandhitsu Das¹, Elizabeth Fulop¹, Ilya Nasrallah¹, Kyra O'Brien¹, Corey McMillan¹, David Irwin¹, Lauren Massimo¹, Murray Grossman¹, David Wolk¹

¹University of Pennsylvania, Philadelphia, PA, US

In a clinically diverse neurodegenerative disease sample, we evaluated the association of the plasma biomarkers phosphorylated tau 181 (p-tau₁₈₁) and glial fibrillary acidic protein (GFAP) with tau (flortaucipir) and amyloid (florbetaben) positron emission tomography (PET). Participants were clinically diagnosed with normal cognition (n=99); Alzheimer's disease (AD) spectrum syndromes, including amnesic mild cognitive impairment (MCI; n=52), AD dementia (n=51), posterior cortical atrophy (n=6), and logopenic variant primary progressive aphasia (n=6); and frontotemporal dementia (FTD) syndromes (non-amnesic MCI, n=11; behavioral variant FTD, n=30; corticobasal syndrome, n=4; and other primary progressive aphasia, n=4). All participants (n=263) had plasma assayed using single molecule array (Simoa); subsets had amyloid (n=181) and tau (n=169) PET. Standardized uptake value ratios (SUVRs) were quantified in inferior temporal cortex for tau PET and as a global composite for amyloid PET. Linear models regressed A β and tau SUVRs on both GFAP and p-tau₁₈₁ (plasma was negative square-root transformed), covarying for age, plasma-to-PET interval, and sex. In the full sample, amyloid PET was associated with both p-tau₁₈₁ ($\beta=1.1$, $p=2.9e-13$) and GFAP ($\beta=4.1$, $p=0.00000071$); tau PET was associated with both p-tau₁₈₁ ($\beta=1.6$, $p=1.8e-14$) and GFAP ($\beta=9.0$, $p=3.6e-10$). In AD-spectrum cases, amyloid PET was associated with p-tau₁₈₁ ($\beta=1.1$, $p=0.00000015$) and GFAP ($\beta=5.5$, $p=0.00018$); tau PET was associated with p-tau₁₈₁ ($\beta=1.6$, $p=0.0091$) and GFAP ($\beta=8.2$, $p=0.00019$). In FTD-spectrum cases, amyloid PET was associated with neither p-tau₁₈₁ ($p=0.53$) nor GFAP ($p=0.52$); tau PET was associated with p-tau₁₈₁ ($\beta=1.2$, $p=0.00011$) and GFAP ($\beta=5.4$, $p=0.04$). In normal participants, A β PET was associated with p-tau₁₈₁ ($\beta=0.5$, $p=0.015$) but not GFAP ($p=0.35$); tau PET was associated with neither (both $p>0.55$). Overall, plasma measures of p-tau₁₈₁ and GFAP were highly consistent with PET imaging of AD biomarkers, particularly among participants with likely AD neuropathologic change. Among normal and non-AD participants, plasma and PET markers were less consistent.



Plasma-PET correlations.

Keywords: Plasma, tau, amyloid-beta, glial fibrillary acidic protein, frontotemporal dementia

P67 Combined and independent effects of hyperphosphorylation of tau on microglial activation

Nesrine Rahmouni^{1,2}, Joseph Therriault^{1,3}, Cécile Tissot^{1,3}, Andrea L. Benedet⁴, Nicholas J. Ashton⁴, Gallen Triana-Baltzer⁵, Firoza Z. Lussier⁶, Stijn Servaes¹, Arthur C. Macedo^{1,3}, Jenna Stevenson¹, Alyssa Stevenson¹, Peter Kunach^{1,3}, Jaime Fernandez-Arias^{1,3}, Yi-Ting Wang^{1,3}, Serge Gauthier^{1,3}, Hartmuth C. Kolb⁵, Thomas K. Karikari^{6,7}, Henrik Zetterberg^{4,8}, Kaj Blennow^{4,8}, Tharick A. Pascoal⁶, Pedro Rosa-Neto^{1,3}

¹Translational Neuroimaging Laboratory, McGill Research Centre for Studies in Aging, Montreal, QC, Canada

²Department of Psychiatry, Faculty of Medicine, McGill University, Montreal, QC, Canada

³Department of Neurology and Neurosurgery, Faculty of Medicine, McGill University, Montreal, QC, Canada

⁴Department of Psychiatry and Neurochemistry, Institute of Neuroscience and Physiology, The Sahlgrenska Academy, University of Gothenburg, Molndal, Sweden

⁵Department of Neurodegenerative Disease, UCL Institute of Neurology, London, UK

⁶Department of Neurology and Psychiatry, University of Pittsburgh School of Medicine, Pittsburgh, PA, US

⁷Wallenberg Centre for Molecular Medicine, University of Gothenburg, Gothenburg, Sweden

⁸Clinical Neurochemistry Laboratory, Sahlgrenska University Hospital, Molndal, Sweden

Aims: Microglial activation is an important component of the immune response in the Alzheimer's disease (AD) brain and has been shown to follow a similar propagation pattern to tau tangle accumulation. However, the effects of tau hyperphosphorylation on microglial activation remain to be demonstrated. Our aim was to investigate to what extent plasma phosphorylated tau (pTau) 181, 217 and 231 concentrations are associated with microglial activation indexed by [¹¹C]PBR28 PET.

Methods: We included 131 individuals from TRIAD cohort: 91 cognitively unimpaired (CU) and 40 cognitively impaired (CI) individuals. Different plasma pTau biomarkers (pTauX) were quantified: pTau181, pTau217 and pTau231. Microglial activation, tau accumulation and amyloid (A β) deposition were assessed via [¹¹C]PBR28-PET, [¹⁸F]MK6240-PET and [¹⁸F]AZD4694-PET, respectively. Regression models evaluated the relationship between plasma pTauX and [¹¹C]PBR28, at the voxel and ROI levels.

Results: Positive associations were found between p-tau biomarkers in plasma and [¹¹C]PBR28 across the AD spectrum, and in the CU subset group in the precuneus, the posterior cingulate and medial prefrontal cortices. *T*-values were higher in the linear regression across the AD spectrum (Figure1). These associations survived corrections for multiple comparisons. Adjusting these associations for tau-PET and A β -PET did not modulate their magnitude in the CU subset group, while affecting the associations along the AD spectrum (Figure2).

Conclusion: Tau phosphorylation constitutes an integral step in the AD process, with a potential role in microglial activation. The present study shows that neuroinflammation depends on pTau-X and tau tangles in both the CU subset and across the AD spectrum, as microglial activation increases as a function of combined tau and pTau-X. Our findings corroborate the idea that neuroinflammation plays a significant role in AD-related changes.

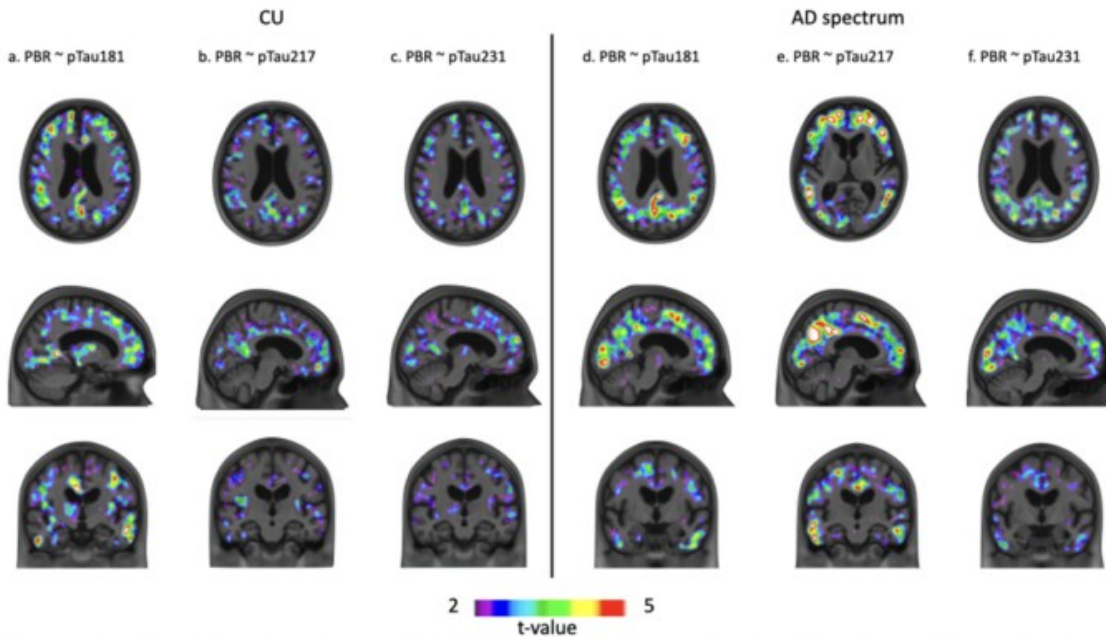


Figure 1: Phosphorylated tau 181, 217, 231 are associated with microglial activation in cognitively unimpaired (CU) individuals and across the Alzheimer’s Disease spectrum *a, d*. Associations between plasma pTau181 concentration and microglial activation adjusted for age and sex in the CU group and across the AD spectrum, respectively. *b, e*. Associations between plasma pTau217 concentration and microglial activation adjusted for age and sex in the CU group and across the AD spectrum, respectively. *c, f*. Associations between plasma pTau231 concentration and microglial activation adjusted for age and sex in the CU group and across the AD spectrum, respectively.

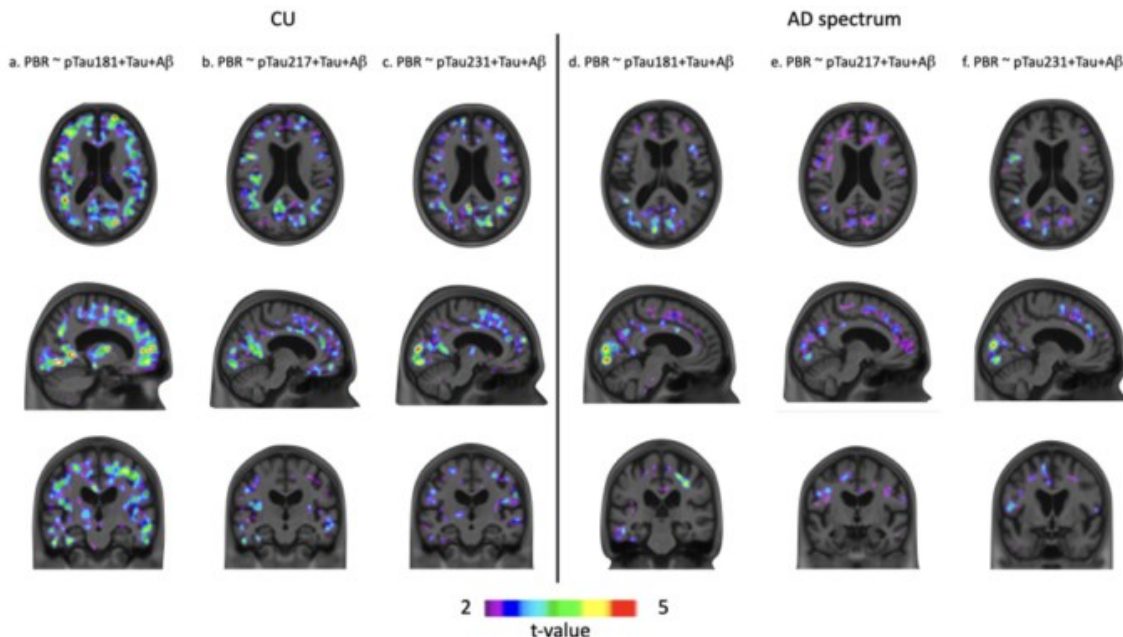


Figure 2: Phosphorylated tau 181, 217, 231 drive microglial activation in cognitively unimpaired individuals (CU), while tau accumulation drives microglial activation in later stages of Alzheimer’s disease. *a, d*. Associations between plasma pTau181 and microglial activation adjusted for age, sex, [¹⁸F] AZD4694-amyloid-PET and [¹⁸F]MK6240-tau-PET in the CU group and across the AD spectrum, respectively. *b, e*. Associations between plasma pTau217 and microglial activation adjusted for age, sex, [¹⁸F] AZD4694-amyloid-PET and [¹⁸F]MK6240-tau-PET in the CU group and across the AD spectrum, respectively. *c, f*. Associations between plasma pTau231 and microglial activation adjusted for age, sex, [¹⁸F] AZD4694-amyloid-PET and [¹⁸F]MK6240-tau-PET in the CU group and across the AD spectrum, respectively.

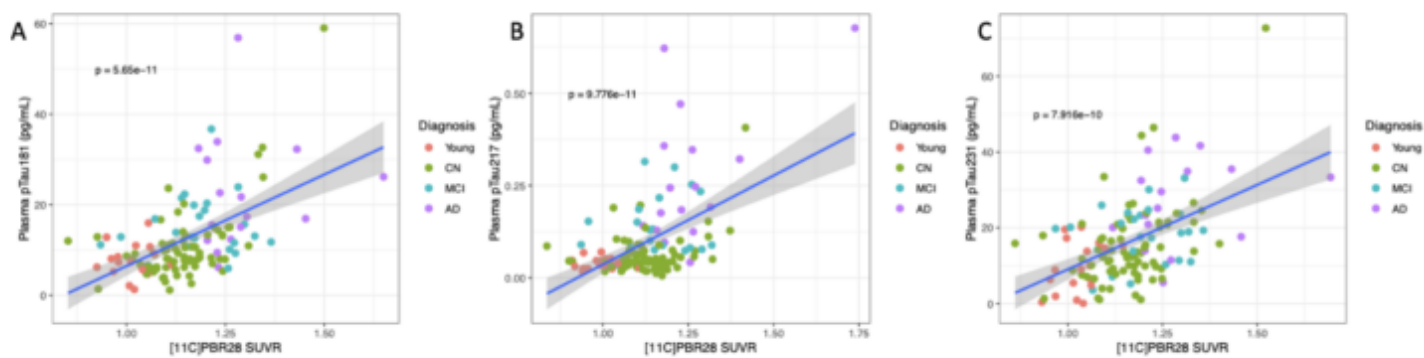


Figure 3: Correlation plots (N=132). Linear regression models evaluated the correlation between concentrations of plasma pTau181 (A), plasma pTau217 (B) and plasma pTau231 (C) and microglial activation indexed by PET using [¹¹C] PBR28 ROI SUVR.

Keywords: Alzheimer's disease, p-tau, tau, microglia, biomarkers

P68 Cognitive impairment is more closely associated with the regional extension of F18MK6240 tau-PET signal than with PET signal intensity or CSF tau measures

Bernard Hanseeuw^{1,2}, Thomas Gerard¹, Vincent Malotaux¹, Lise Colmant¹, Lisa Quenon¹, Adrian Ivanoiu¹, Renaud Lhommel¹

¹*Cliniques Universitaires Saint-Luc, Brussels, Belgium*

²*Massachusetts General Hospital, Boston, MA, US*

Background: Tau imaging is increasingly available in Memory Clinics, but the clinical value of this biomarker is not yet determined. We hypothesized that the regional extension of tau-PET signal would better predict cognition and discriminate symptomatic AD from clinically normal (CN) older adults than cerebrospinal fluid (CSF) or global PET measures.

Methods: We analyzed ^{F18}MK6240 tau-PET imaging from 84 participants including 42CN and 42 symptomatic AD. Standard Uptake Volume ratios (SUVr) used cerebellar gray as reference. We calculated the total tau brain load (TTBL) as the percentage of neocortical voxels with SUVr>1.3 (corresponding to the P95 of voxels in low-A β CN), providing an index of the regional extension of tau pathology. Analyses were repeated in the Braak-region I-II, providing a more regional tau brain load (RTBL). Cognition was assessed using an average of z-scores evaluating four different cognitive domains. Forty-five participants had CSF sampling (A β -42, total-tau, and p-tau¹⁸¹). Age-adjusted partial correlations were computed between, PET, CSF, and cognition data.

Results: TTBL (age-adjusted R²=0.68), RTBL (R²=0.59), neocortical SUVr (R²=0.61), and all CSF measures (max R²=0.25 for p-tau¹⁸¹) were associated with lower cognition (Fig.1). TTBL remained associated with cognition when adjusting for CSF p-tau¹⁸¹ (TTBL: adjusted-R²=0.49, p<0.001; p-tau¹⁸¹: R²=0.08, p=0.06) or SUVr (TTBL: adjusted-R²=0.17, p<0.001; SUVr: R²=0.002, p=0.72), demonstrating that tau extent best predicted cognition. ROC curves confirmed the superiority of extent measures to discriminate between symptomatic AD and CN (Fig.2). RTBL (BraakI-II) slightly outperformed TTBL because of increased sensitivity (Fig.3). RTBL (Braak \geq III-IV) was similar to TTBL.

Conclusion: The regional extent of tau pathology as measured with ^{F18}MK6240 is more strongly associated with the severity of cognitive impairment than quantitative measurements neglecting regional information such as CSF or a global PET-SUVr measure. Symptomatic AD is best discriminated from CN using a regional extent measure in the Braak-region I-II.

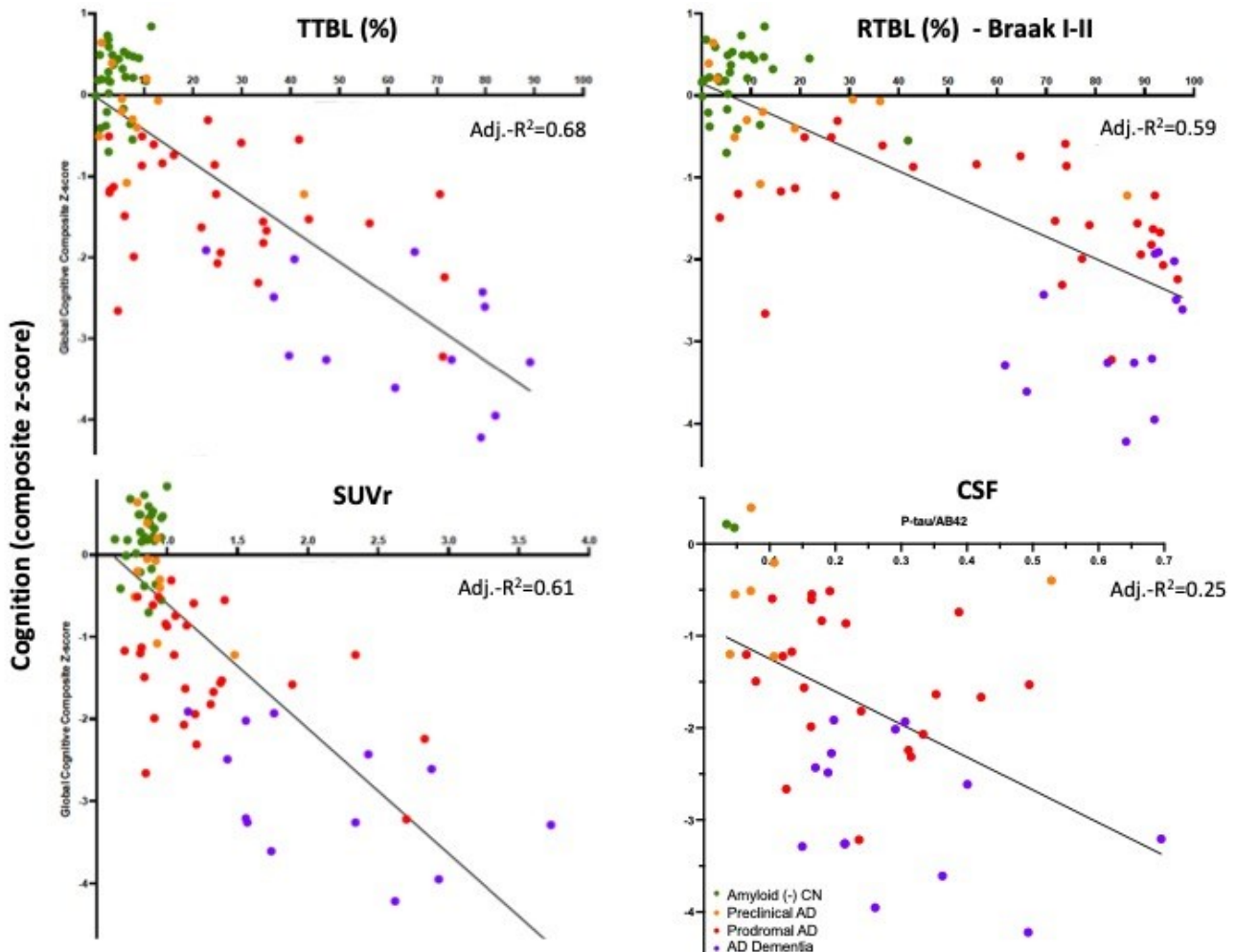


Fig.1

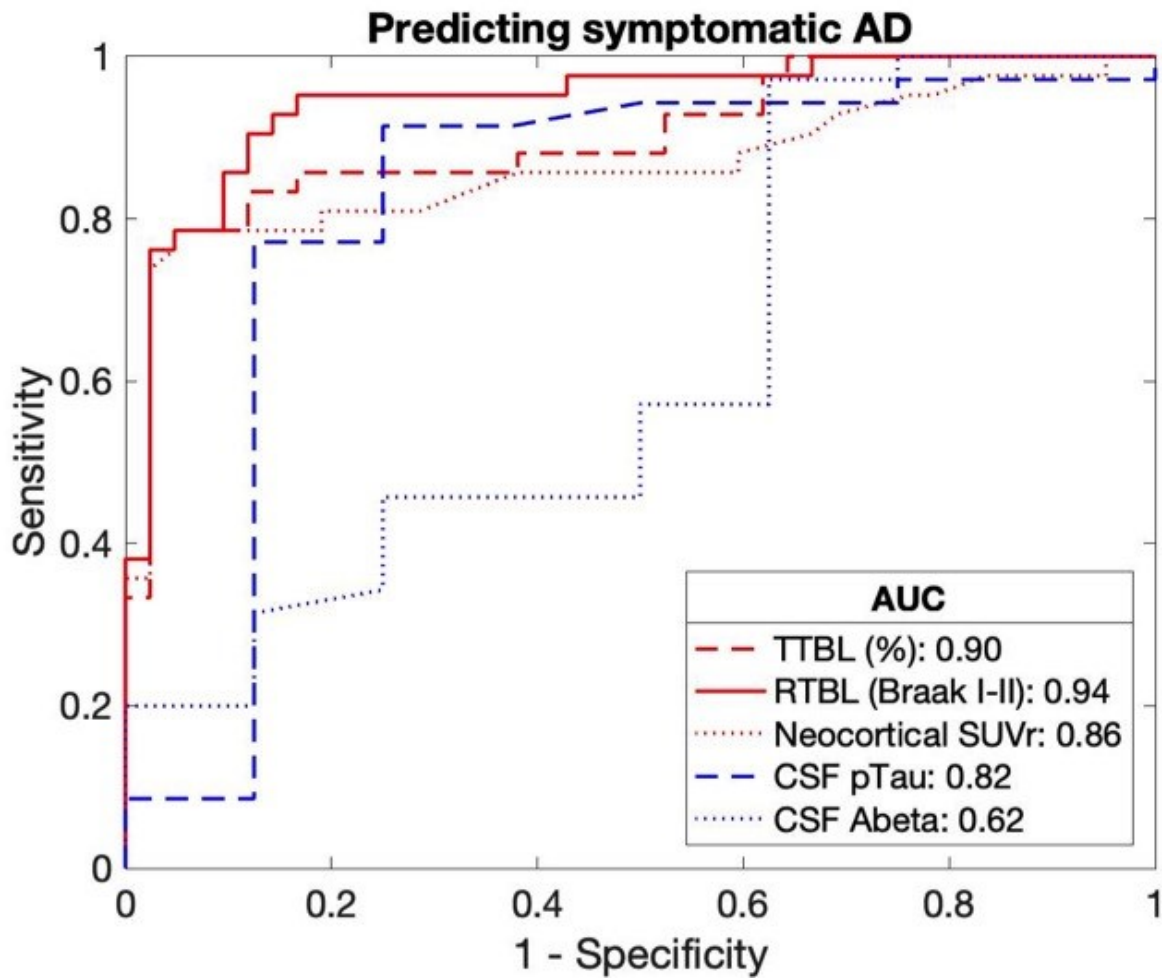


Fig.2

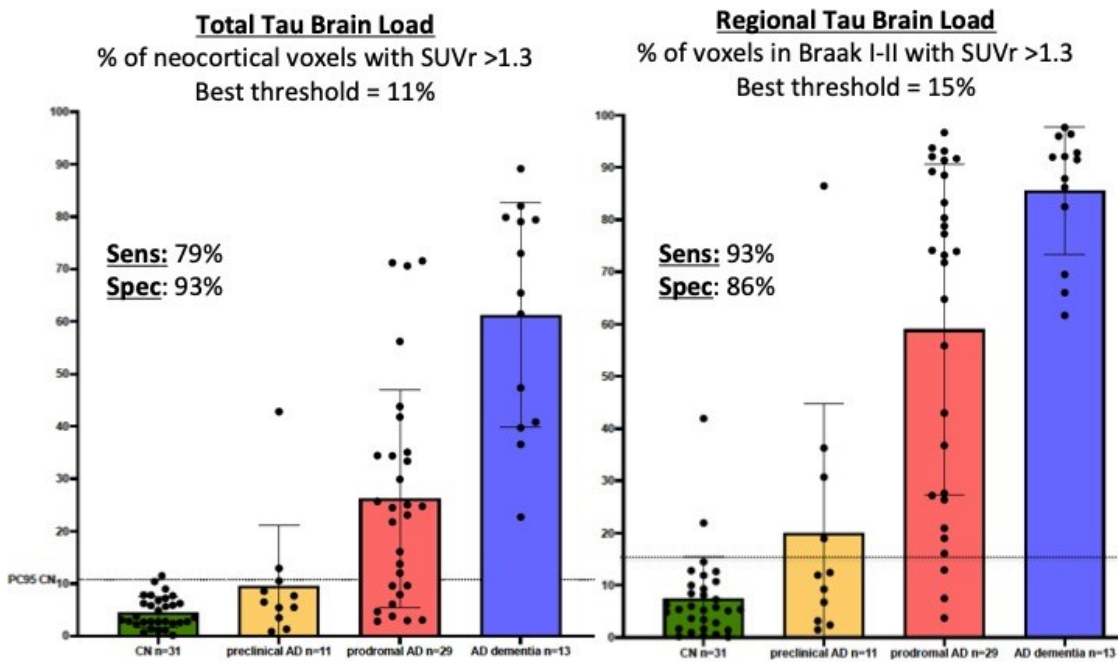


Fig.3

P69 Disentangling spatial-temporal remote interaction between tau and Amyloid- β proteins in different stages of tau aggregations

Seyed Hani Hojjati¹, Farnia Feiz¹, Siddharth Nayak¹, Jacob Shteingart¹, Sindy Ozoria¹, Antonio Fernández¹, Davangere P. Devanand², José A. Luchsinger², Yaakov Stern², Qolamreza R. Razlighi¹

¹Weill Cornell Medicine, New York, NY, US

²Columbia University Irving Medical Center, New York, NY, US

Background: The presence of Amyloid- β ($A\beta$), and tau proteins, are the two major proteins involved in the pathogenesis of AD. Spatial discrepancies between these two proteins across the brain regions are well-documented. However, interaction between these two proteins in the early and late stages of aggregations is still illusive.

Methods: We aimed to investigate the remote interaction between tau and $A\beta$ uptakes by using 557 elderly 67.15 ± 5.99 (436 healthy control (HC) and 94 mild cognitive impairments (MCI)) amyloid and tau positron emission tomography (PET) scans. In this study for the first time, we took advantage of 48 young individuals' 29.36 ± 4.73 tau-PET scans to find the regional cut-points for 68 cortical regions in the brain. We performed agglomerative clustering to identify groups with unique spatial characteristics which resulted in four different groups (see Figure 1); Next, a regional multiple linear regression model is performed for each group to detect remote interaction between each target region of tau and all other regions $A\beta$ (controlling for gender, age, and intracranial volume).

Results: First, we show that the left/right entorhinal cortex tau is the hub of remote interaction with $A\beta$ in several cortical regions in the early stage of aggregation (Figure 2: groups 1). Second, we identify tau in two MTL regions (left/right entorhinal, and para-hippocampal) demonstrating highest remote interaction with cortical $A\beta$ (Figures 2 and 3: groups 2 and 3) in early stage of the disease, whereas no remote interaction was found in the later stage (Figures 2 and 3: groups 4 and 5).

Conclusion: Our results provide evidence for remote interaction between cortical accumulation of $A\beta$ and MTL tau during the early stage of the disease, as it has been proposed by Amyloid cascade hypothesis. Furthermore, this remote interaction attenuates significantly in the later stage of the disease.

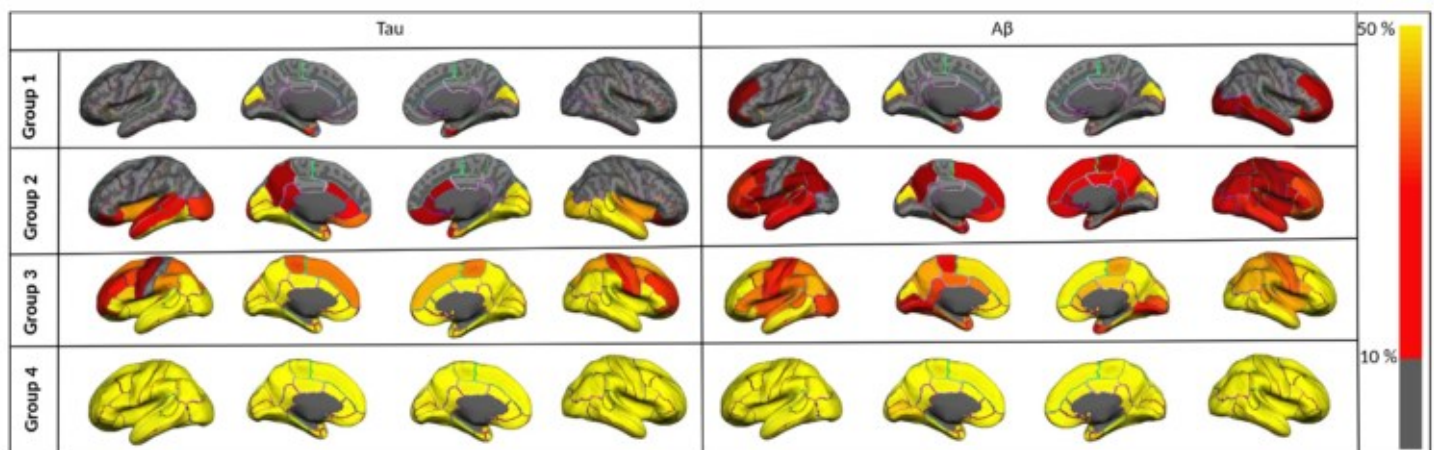


Figure 1. Illustrating the region-wise probabilistic atlas of Tau (left column) and $A\beta$ (right column) pathologies throughout the entire cerebral cortex obtained in four participant groups. The probability of observing $A\beta$ and tau at each region is color-coded with a heat color map and overlaid on a semi-inflated cortical surface of the MNI152 template.

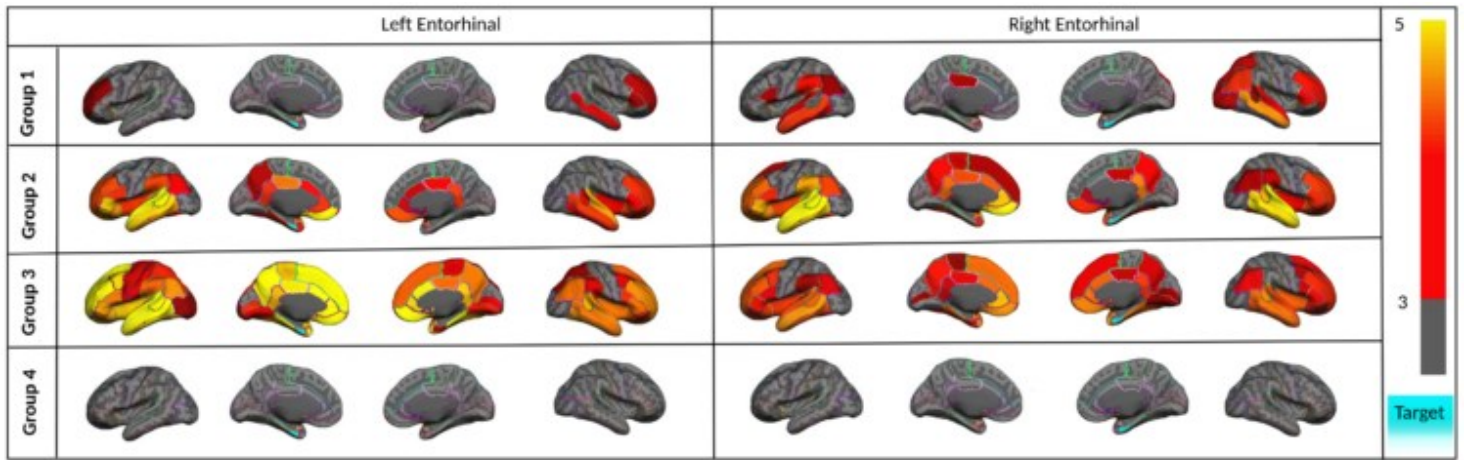


Figure 2. Region-wise statistical map (t-value) of association between left Entorhinal (left column) and right Entorhinal (right column) tau as target regions and regional A β in other 67 ROIs obtained in four groups of participants. The t-value at each region is color-coded with red or yellow colors representing increasing positive t-values and light blue representing the target region and overlaid on the semi-inflated cortical surface of the MNI152 template.

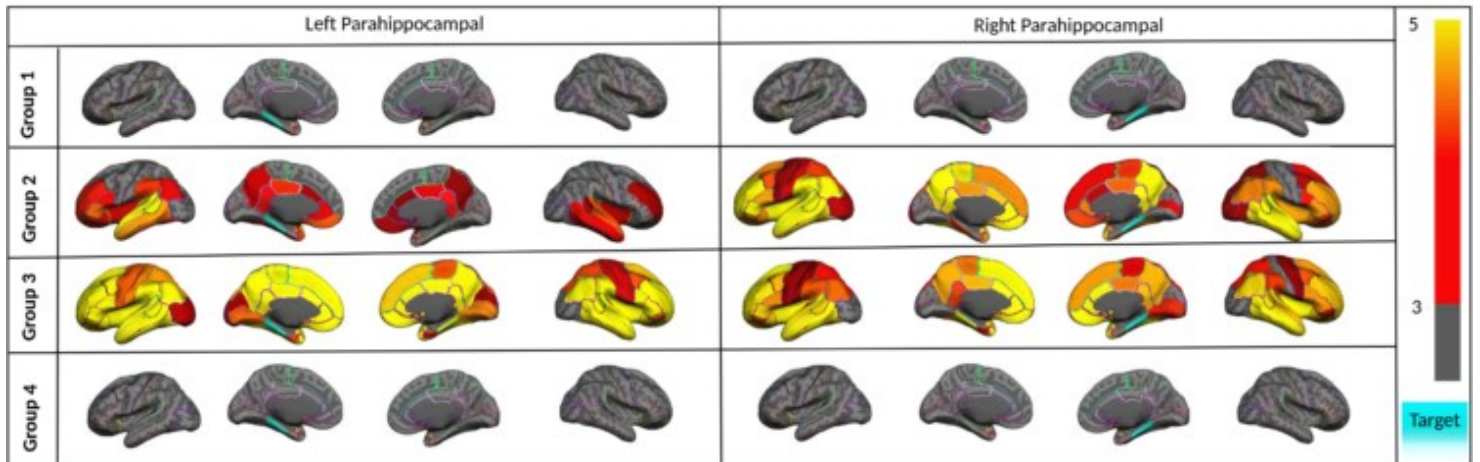


Figure 3. Region-wise statistical map (t-value) of association between left Parahippocampal (left column) and right Parahippocampal (right column) tau as target regions and regional A β in other 67 ROIs obtained in four groups of participants. The t-value at each region is color-coded with red or yellow colors representing increasing positive t-values and light blue representing the target region and overlaid on the semi-inflated cortical surface of the MNI152 template.

Keywords: Tau, Amyloid- β , Remote Interaction, entorhinal, and para-hippocampal

P70 Predictors of Discordance Between Pre-PET Clinical Diagnosis and Amyloid-PET Results in the Imaging Dementia—Evidence for Amyloid Scanning (IDEAS) Study

Jeremy Tanner^{1,2,10}, Renaud La Joie^{1,10}, Lucy Hanna³, Leonardo Iaccarino^{1,10}, Isabel Allen⁴, Barry Siegel⁵, Bruce Hillner⁶, Rachel Whitmer^{7,8}, Constantine Gatsonis^{3,11}, Maria Carrillo⁹, Gil Rabinovici^{1,10}

¹Memory and Aging Center, University of California San Francisco, San Francisco, CA, US

²Biggs Institute for Alzheimer's and Neurodegenerative Diseases, University of Texas Health San Antonio, San Antonio, TX, US

³Center for Statistical Sciences, Brown University School of Public Health, Providence, RI, US

⁴Department of Epidemiology and Biostatistics, University of California San Francisco, San Francisco, CA, US

⁵Edward Mallinckrodt Institute of Radiology, Washington University School of Medicine in St Louis, St. Louis, MO, US

⁶Department of Medicine, Virginia Commonwealth University, Richmond, VA, US

⁷Division of Research, Kaiser Permanente, Oakland, CA, US

⁸Department of Public Health Sciences, University of California Davis, Davis, CA, US

⁹Alzheimer's Association, Chicago, IL, US

¹⁰Weill Institute for Neurosciences, University of California San Francisco, San Francisco, CA, US

¹¹Department of Epidemiology, Brown University School of Public Health, Providence, RI, US

Objective: To characterize clinical situations where amyloid PET would be most valuable by identifying predictors associated with discordance between clinical diagnosis pre-PET and amyloid-PET results in IDEAS.

Methods: IDEAS participants who completed both pre/post-PET visits were included in the analysis (n=11,829, age 76±6, 51% female, 88% White, MMSE 24.5±5). Specialists documented clinical diagnosis before and after PET. Diagnosis-PET discordance was defined as either an AD diagnosis pre-PET with negative amyloid-PET, or a non-AD diagnosis pre-PET with positive amyloid-PET. Univariate logistic regressions were performed to compare predictors of discordance versus concordance in the total sample and in subgroups stratified by pre-PET diagnosis (AD/non-AD).

Results: Diagnosis-PET discordance occurred in 40% of total participants (n=4732), including 36% with AD pre-PET diagnosis and negative amyloid-PET (n=3323/9115) and 52% with non-AD pre-PET diagnosis and positive amyloid-PET (n=1409/2714). In the total sample (**Figure 1**), predictors associated with greater discordance included non-White race (Black/African American: OR 1.26; 95%CI [1.04-1.53]; Asian: (1.62[1.23-2.13]) and more medical comorbidities (each comorbidity: 1.07[1.05-1.07]). Predictors associated with less discordance included older age (5-year increase: 0.91[0.89-0.94]), female sex (0.91[0.85-0.98]), greater disease severity (0.70[0.65-0.75]), greater disease duration (≥3yr: 0.64[0.59-0.69]), greater physician diagnostic confidence (0.89[0.86-0.89]), AD medication use (0.64[0.59-0.69]), family history of dementia (0.89[0.81-0.97]), greater physician time(≥50%) in dementia care (0.92[0.86-0.99]), use of image quantification (0.90[0.81-0.99]), and comparison to other imaging modalities (0.90[0.82-0.97]). Subgroup analyses (**Figure 2**) revealed additional predictors associated with greater discordance in those diagnosed with AD include Hispanic ethnicity (1.35[1.10-1.66]), living alone (1.16[1.04-1.30]), and non-English primary language (1.22[1.01-1.47]).

Discussion: Amyloid-PET may be more valuable to confirm AD diagnosis in participants who are early in the disease course, younger, from underrepresented racial/ethnic groups, live alone, have multiple medical comorbidities, and lack a suggestive family history. The results suggest that using image quantification, multimodal imaging, and highly specialized providers may reduce the risk of discordance.

Figure 1 – Predictors of Diagnosis-PET Discordance in Total Sample

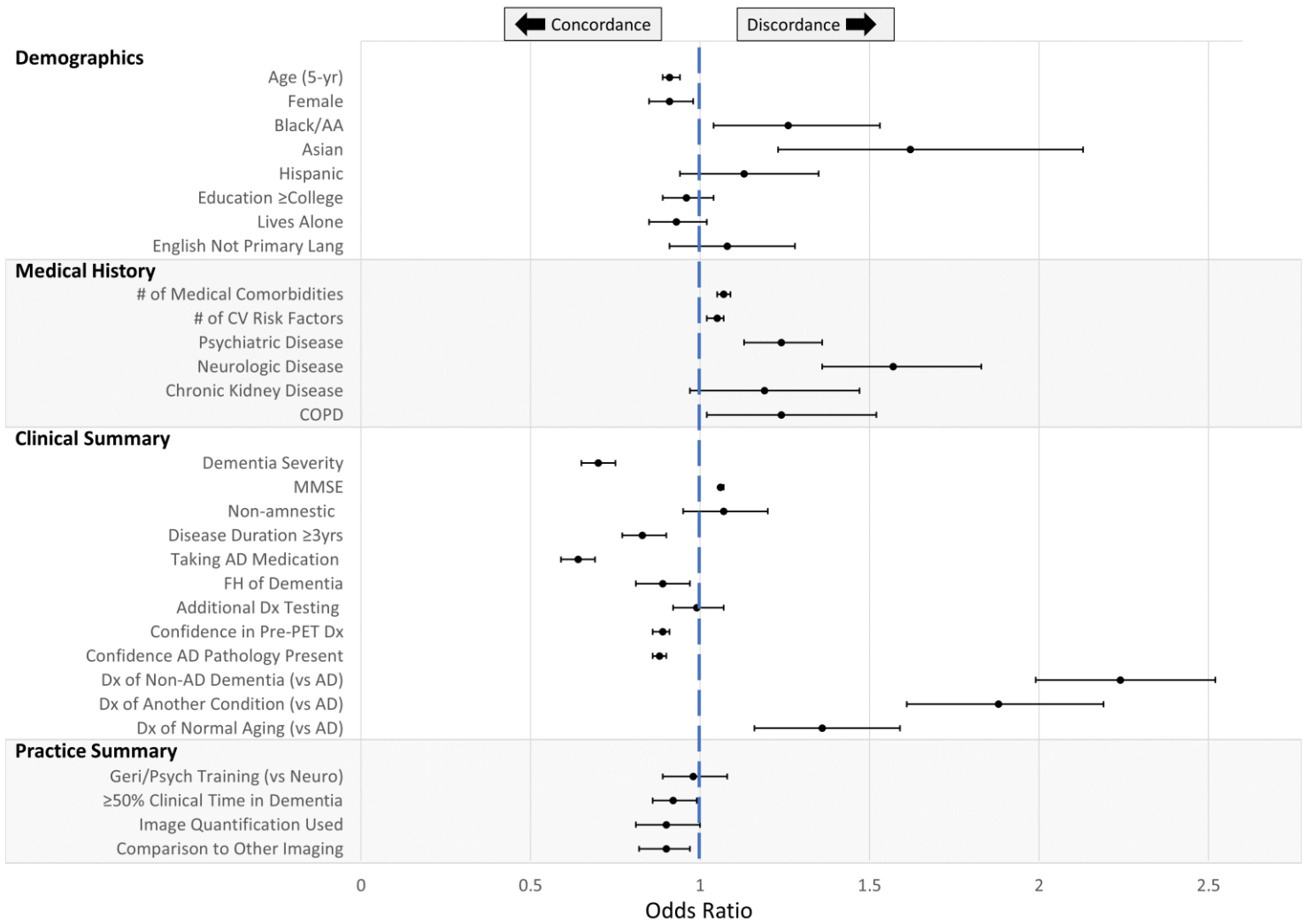
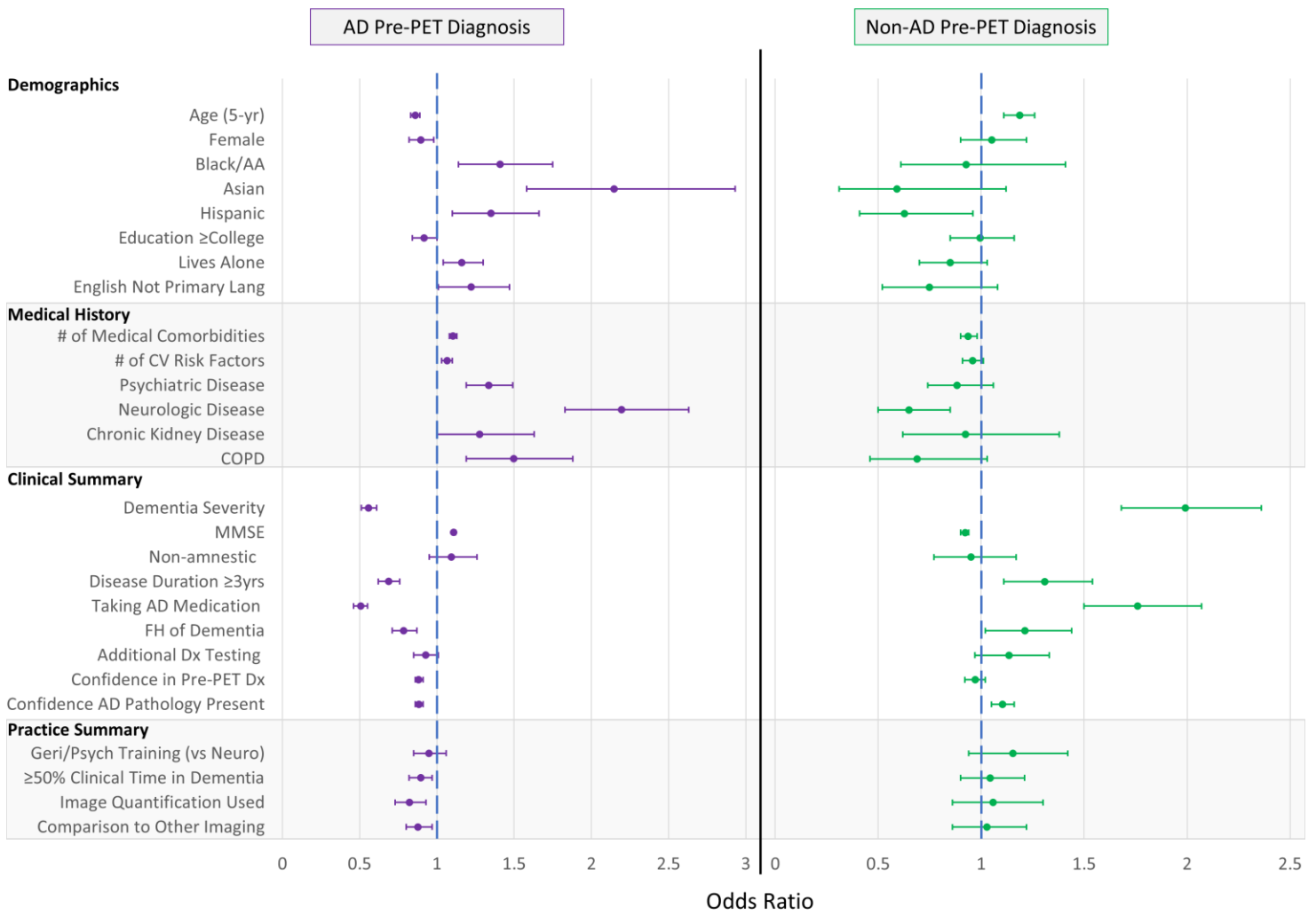


Figure 2 – Predictors of Diagnosis-PET Discordance by Pre-PET Diagnostic Group



Keywords: Amyloid PET, Alzheimer's Disease, clinical diagnosis

P71 Mid-life atherosclerotic cardiovascular disease risk score and late-life AT(N) measures

Anum Saeed¹, YueFang Chang¹, Sarah Royse¹, Brian Lopresti¹, Beth Snitz¹, Victor Villemagne¹, Steven Reis¹, Oscar Lopez¹, Ann Cohen¹

¹University of Pittsburgh School of Medicine, Pittsburgh, PA, US

Introduction: CVD risk factors in mid-life have been associated with cognitive decline and late-life dementia. Atherosclerosis and arteriosclerosis are both implicated in incident dementia however their association with Alzheimer's disease (AD) neuropathology remains elusive. We investigated whether mid-life atherosclerotic cardiovascular disease risk score is associated with late-life AT(N) measures.

Methods: Participants >65y enrolled in the Heart Strategies Concentrating on Risk Evaluation (Heart SCORE) study between 2003-2005 (mid-life) underwent brain MRI and PET scans in 2018-2022 (late-life) to detect and quantify amyloid (A, PiB-PET) and tau (T, AV-1451 PET) deposition and cortical thickness (N). The 10-year ASCVD risk score was categorized in mid-life as borderline (5%-7.4%), intermediate (7.5%-19.9%), or high ($\geq 20\%$). Logistic regression was used to calculate OR (95% CI) for association of A, T, or N with mid-life ASCVD risk.

Results: In 135 participants (mean age 79y), mid-life ASCVD risk showed no significant association with A and T, while N demonstrated a graded association with increasing mid-life ASCVD risk categories (OR, ASCVD high vs low risk% 11.00 [2.82-47.49]; $p < 0.05$) after mean 16y follow up. The N measure was mainly driven by Black race (OR 10.07 [3.25-36.39]) and age (OR 1.24 [1.10-1.41]); all $p < 0.05$.

Conclusions: In this asymptomatic, diverse cohort, 10y ASCVD risk was predictive of late-life Neurodegeneration but not of Amyloid or Tau; driven mainly by Black race and older age. A simple mid-life ASCVD risk calculation may predict of late-life neurodegeneration, particularly in Black participants. These data suggest that ASCVD risk and amyloid and tau pathology may have two mechanistically distinct pathways- Further mechanistic studies are warranted to explore the association of ASCVD risk, N and cognitive performance and to interrogate the race related differences to ASCVD risk and AD.

Keywords: PiB-PET, Tau-PET, AT(N), MRI, Cardiovascular disease

P72 A clinical diagnosis of Alzheimer's disease and CSF-based tau positivity are both associated with lower locus coeruleus metabolism

Elouise A. Koops¹, Joyita Dutta^{1,2}, J. Alex Becker¹, Maxime Van Egroo³, Joost M. Riphagen¹, Prokopis C. Prokopiou¹, Bernard J. Hanseeuw¹, Reisa A. Sperling⁴, Georges El Fakhri¹, Keith A. Johnson^{1,4}, Heidi I.L. Jacobs^{1,3}

¹*Gordon Center for Medical Imaging, Department of Radiology, Massachusetts General Hospital, Harvard Medical School, Boston, MA, USA., Boston, MA, US*

²*Department of Electrical and Computer Engineering, University of Massachusetts Lowell, Lowell, USA., Lowell, MA, US*

³*Faculty of Health, Medicine and Life Sciences, School for Mental Health and Neuroscience, Alzheimer Centre Limburg, Maastricht University, Maastricht, The Netherlands., Maastricht, The Netherlands*

⁴*Department of Neurology, Brigham and Women's Hospital, Massachusetts General Hospital, Harvard Medical School, Boston, MA, USA., Boston, MA, US*

Background. The locus coeruleus (LC) is one of the earliest brain structures to accumulate tau pathology, one of the neuropathologic hallmarks of Alzheimer's disease (AD). Significant loss of LC volume and cell count were observed with AD progression based on Braak staging and clinical diagnosis. As AD progresses, both tau pathology and significant cell loss may result in changes in the metabolic turnover of the LC. We investigated differences in LC glucose metabolism across AD clinical diagnostic and biomarker groups.

Methods. Using an in-house developed joint-entropy algorithm to quantify Positron Emission Tomography (PET) signal within small brain regions, we investigated the LC FDG-PET signal of 295 participants from the ADNI-1 and ADNI-GO cohort who were equally distributed across the CSF amyloid (A) and ptau (T) biomarker groups (Table 1; Fig 1A). ANCOVA was used to investigate group differences in LC metabolism based on diagnostic categories and amyloid and tau positivity. Post-hoc Tukey contrasts corrected for multiple comparisons in subsequent pairwise analyses. Age, sex, and education were included as covariates.

Characteristic	A-T-, N = 99 ¹	A+T-, N = 98 ¹	A+T+, N = 98 ¹	p-value ²
Diagnosis				0.6
CN	60 (60.6%)	33 (33.7%)	13 (13.3%)	
MCI	37 (37.4%)	48 (49.0%)	51 (52.0%)	
AD	2 (2.0%)	17 (17.3%)	34 (34.7%)	
Sex				0.5
Male	53 (53.5%)	59 (60.2%)	51 (52.0%)	
Female	46 (46.5%)	39 (39.8%)	47 (48.0%)	
CSF Amyloid Beta	1,539.9 (198.8)	714.8 (216.0)	670.7 (183.0)	<0.001
CSF pTau	18.8 (4.5)	18.3 (5.6)	41.4 (15.1)	<0.001
MMSE	28.6 (1.5)	27.5 (2.6)	25.8 (2.9)	<0.001
CDR SOB				<0.001
cognitively unimpaired	54 (54.5%)	32 (32.7%)	13 (13.3%)	
minimal cognitive impairment	43 (43.4%)	45 (45.9%)	48 (49.0%)	
very mild dementia	1 (1.0%)	12 (12.2%)	25 (25.5%)	
mild dementia	1 (1.0%)	9 (9.2%)	12 (12.2%)	
Education level	16.2 (2.5)	16.6 (2.5)	15.8 (2.8)	0.090
APOE e4 alleles				<0.001
0	80 (80.8%)	50 (51.0%)	33 (33.7%)	
1	18 (18.2%)	39 (39.8%)	47 (48.0%)	
2	1 (1.0%)	9 (9.2%)	18 (18.4%)	

¹n (%); Mean (SD)

²Kruskal-Wallis rank sum test;

Pearson's Chi-squared test;

One-way ANOVA

Table 1. Participant characteristics. Per biomarker group, the mean and standard deviation are given for CSF beta-amyloid, pTau, MMSE score, and education level. Percentages per biomarker group are depicted for diagnosis, Sex, CDR SOB, and APOE 4 alleles. The threshold for CSF-based biomarker positivity was <1100 pg/ml for amyloid and >27 pg/ml for phosphorylated tau (Roche Elecsys Assay). *Abbreviations: CSF = cerebrospinal fluid, MMSE = Mini Mental State Examination, CDR SOB = Clinical Dementia Rating Scale sum of boxes score, APOE = Apolipoprotein E.*

Results: Lower LC FDG-PET signal was observed in the group with both amyloid and tau-positivity compared to the other groups ($p < 0.0001$; Fig 1B). Pair-wise differences between the diagnostic groups did not survive correction for multiple comparisons (Fig 1C). Combining biomarker and diagnostic status, we observed lower LC metabolism in A+T+ MCI and AD groups compared to MCI A-T-, MCI A+T-, CN A-T-, and CN A+T- ($p < 0.001$; Fig 2).

Figure 1. Processing pipeline to obtain LC FDG-PET signal per biomarker and diagnostic group. (A) The Keren mask, dilated with an anisotropic Gaussian kernel to account for the low spatial resolution of PET scans, and an in-house developed LC mask, based on 7 Tesla magnetization transfer-weighted turbo flash (MT-TFL) images were used to extract the LC FDG-PET signal. The processing consisted of co-registration of the FreeSurfer-processed T1 anatomical images, registering the FDG-PET images (referenced to cerebellar gray) and LC templates to T1-space. The average signal of the LC was extracted from the MRI-PET joint entropy deblurred FDG-PET images for the dilated Keren and 7T MT-TFL-based masks. The results were similar for both masks, and subsequent analyses were performed with the 7T MT-TFL mask, which is restricted to the rostral LC. (B) For the biomarker groups, there was a significant overall group difference in mean LC metabolism ($F(1,290)=26.22$ (1), $p < 0.0001$). Follow-up pair-wise Tukey post hoc analyses indicated that the group with positive amyloid and tau levels (A+T+) had significantly lower LC metabolism compared to the amyloid positive and tau negative (A+T-) group ($T=4.61$, $p < 0.0001$) and the amyloid and tau negative (A-T-) group ($T=5.19$, $p < 0.0001$). (C) For the diagnostic groups, there was a significant overall group difference in mean LC metabolism ($F(1,290)=5.69$, $p=0.0177$). Pair-wise differences between the diagnostic groups did not survive correction for multiple comparisons. *Abbreviations: LC JEP SUVr = locus coeruleus joint-entropy PET deblurring algorithm corrected signal referenced to the cerebellar cortex. CN = cognitively normal, MCI = mild cognitive impairment, AD = Alzheimer's disease. The asterisks indicate significant differences: $p < 0.001$ ***.*

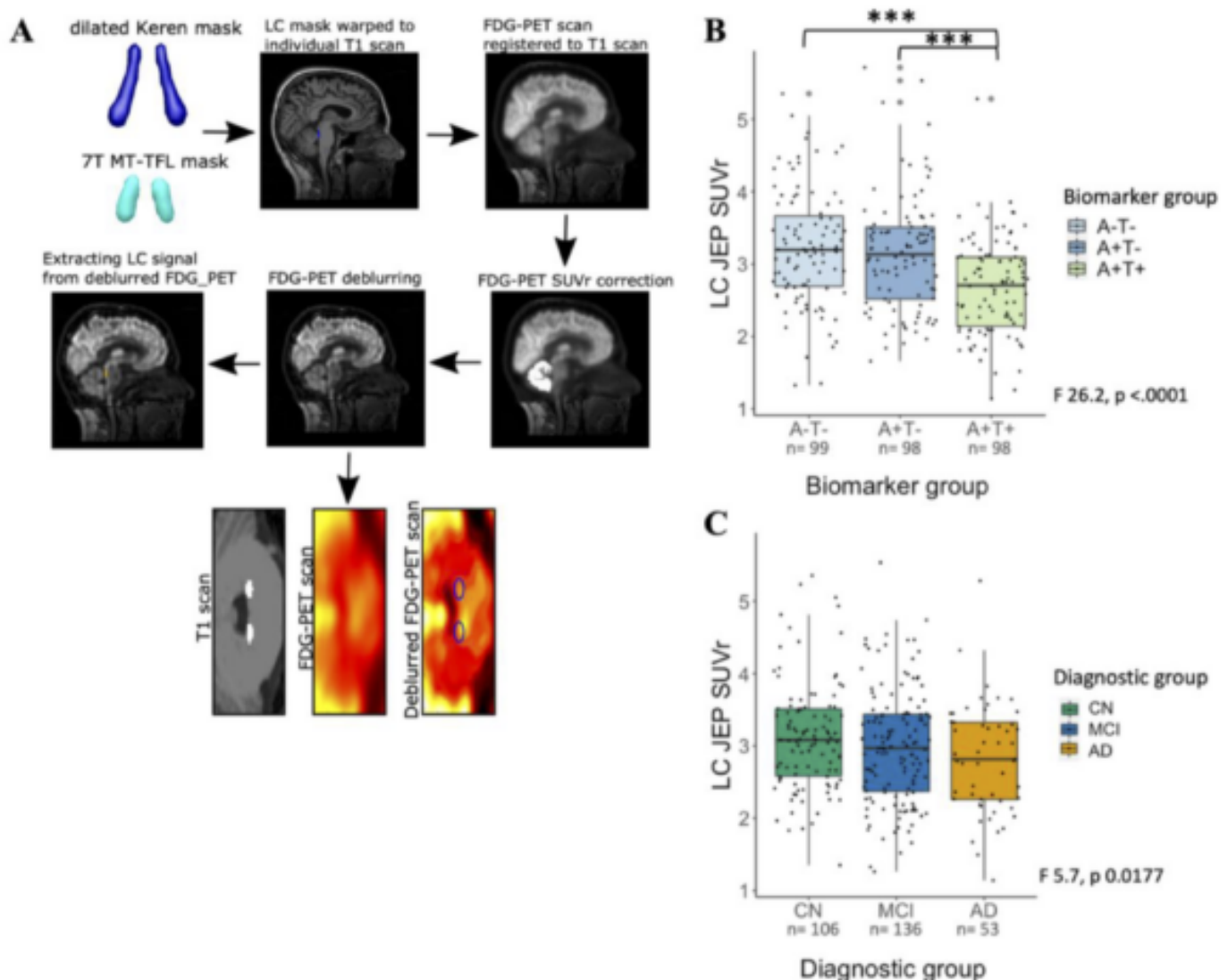
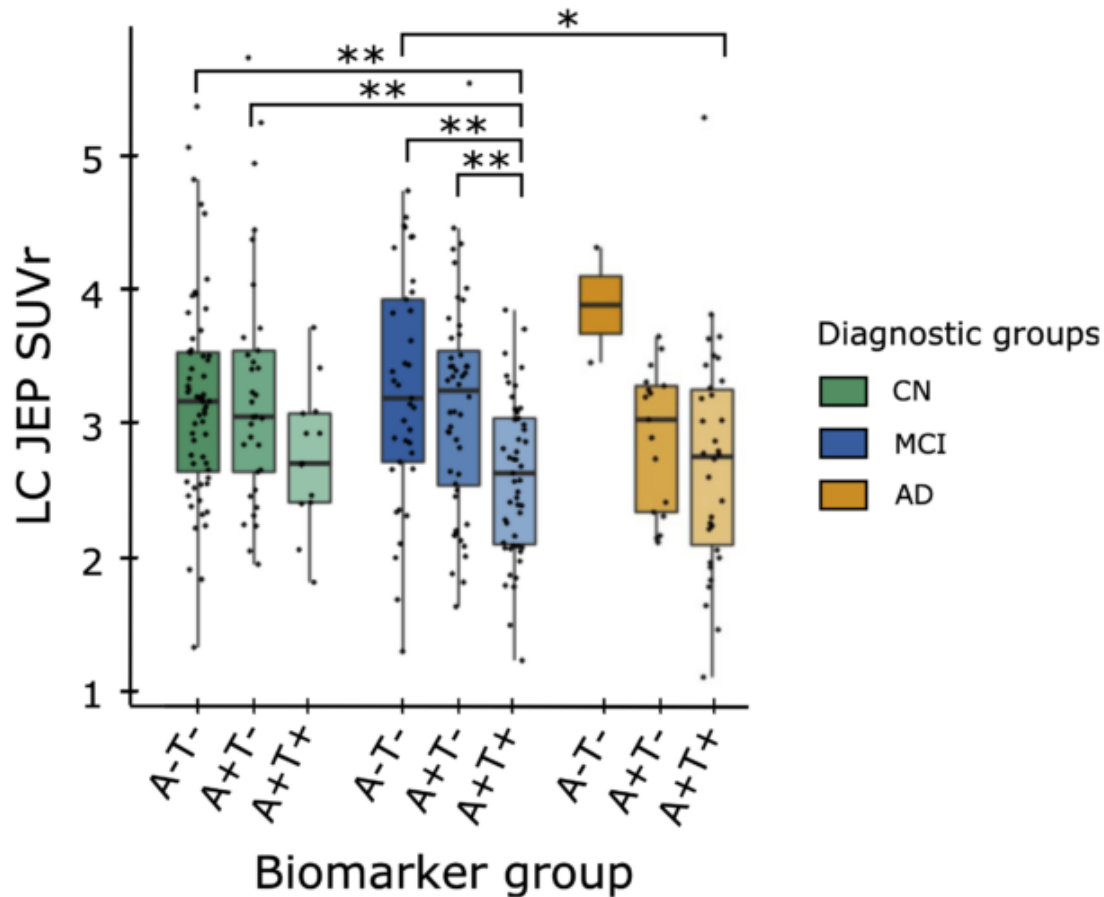


Figure 2. LC FDG-PET signal for the diagnostic groups by biomarker status. A significant overall group difference in mean LC metabolism ($F(8,283)=4.55$ (8), $p < 0.0001$) was detected when grouping participants according to both diagnostic and biomarker status. Follow-up pair-wise Tukey analyses indicated that the group with mild cognitive impairment (MCI) and positive amyloid and tau levels (A+T+) had significantly lower LC metabolism compared to the other MCI groups (MCI A-T-: $T=3.89$, $p < 0.01$; MCI A+T-: $T=3.67$, $p < 0.01$) and compared to the tau negative control groups (CN A-T-: $T=3.81$, $p < 0.01$; CN A+T-: $T=3.57$, $p < 0.01$). Lastly, the AD group with positive amyloid and tau levels (AD A+T+) had significantly lower LC metabolism than the amyloid and tau negative MCI group ($T=3.18$, $p=0.037$). *Abbreviations: LC JEP SUVr = locus coeruleus joint-entropy PET deblurring algorithm corrected signal referenced to the cerebellar cortex. CN = cognitively normal, MCI = mild cognitive impairment, AD = Alzheimer's disease. The asterisks indicate significant differences: < 0.01 **, < 0.05 *.*



Conclusion. To the best of our knowledge, this is the first study relating in-vivo spatially specific measures of LC metabolism to AD-related biomarker status. Low LC metabolism was most pronounced in those with evidence of underlying AD pathologic change and cognitive impairment. Future work needs to investigate whether low LC glucose metabolism in the various stages of AD corresponds to distinct trajectories of cognitive decline or protein accrual.

Keywords: Biomarkers, Alzheimer's disease, locus coeruleus, CSF, FDG-PET.

Thursday, January 12, 2023 - 10:45 am - 11:50 am

Podium Session

SESSION VI: Heterogeneity in the AD cascade

Thursday, January 12, 2023		
10:45 am – 11:50 am	SESSION VI: HETEROGENEITY IN THE AD CASCADE	CHAIRS: Heidi Jacobs, PhD, <i>Massachusetts General Hospital</i> Susan Landau, PhD, <i>University of California, Berkeley</i>
10:45	Introduction	Chairs
10:50	Longitudinal increases in tau emerge alongside early amyloid change in Down syndrome	Matt Zammit, PhD, <i>University of Wisconsin-Madison</i>
11:05	Cross-sectional and longitudinal associations between amyloid- and tau-PET in early-onset Alzheimer's Disease: update from the LEADS study	Nidhi Mundada, PhD, <i>University of California, San Francisco</i>
11:20	Amyloid PET Burden Predicts Longitudinal Cognitive Trajectories in a Heterogeneous ADRD Cohort	Kyan Younes, PhD, <i>Stanford University</i>
11:35	Variations in gamma-secretase function across PSEN1 pathogenic variants strongly predict the clinical, cognitive, and biomarker progression of autosomal dominant Alzheimer's disease	Stephanie Schultz, PhD, <i>Massachusetts General Hospital</i>
11:50	Discussion	

Longitudinal increases in tau emerge alongside early amyloid change in Down syndrome

Matt Zammit¹, Tobey Betthausen¹, Andrew McVea¹, Charles Laymon², Dana Tudorascu², Ann Cohen², Sterling Johnson¹, Sigan Hartley¹, Alexander Converse¹, Davneet Minhas², Shahid Zaman³, Beau Ances⁴, Chester Mathis², William Klunk², Benjamin Handen², Bradley Christian¹

¹University of Wisconsin-Madison, Madison, WI, US

²University of Pittsburgh, Pittsburgh, PA, US

³University of Cambridge, Cambridge, UK

⁴Washington University in St. Louis, St. Louis, MO, US

Background: Understanding the natural history of AD biomarkers is necessary for inclusion of individuals with Down syndrome (DS) in clinical interventions aimed at amyloid and tau clearance. This study compares longitudinal amyloid and tau PET to determine when tau emerges following A+.

Methods: 177 adults with DS underwent PET and MR imaging as part of the ABC-DS. 119 individuals had 2-5 PiB scans, while 92 had two AV-1451 scans. A β burden was measured using Amyloid Load (A β _L) and Centiloids (CL) (A+ = 13.3A β _L = 18.0CL). ROIs encompassing the Braak staging of tau pathology were parcellated from the MRI using FreeSurfer v5.3.0. Sampled iterative local approximation (SILA) was applied to A β _L/CL vs. age data to model amyloid trajectories and provide individual-level estimates of A+ onset age and A+ duration at tau scan. Longitudinal tau change was then compared to A+ duration.

Results: All participants with A+ duration > 0 years had rapidly accumulating A β trajectories (mean(SD) rate: 3.1(0.93)A β _L/yr, 6.9(2.1)CL/yr; Fig.1). APOE E4 carriers had mean A+ onset age of 40.1(4.89)years while non-carriers reached A+ at 41.6(5.93)years. Elevated tau was observed in all Braak regions following A+ and longitudinal tau rapidly increased with respect to A+ duration (Fig.2). Tau increases in Braak regions I-III were observed 0-2.5 years following A+ with medium to large effect sizes (Cohen's d > 0.5), while Braak regions IV-VI saw increases between 2.5-5 years (Tables 1&2). Nearly all A+ individuals had positive rates of AV-1451 change in the medial temporal lobe.

Discussion: This study is the first to evaluate longitudinal tau PET in a large DS cohort. Early tau accumulation in DS was uniformly observed within 2.5 years following A+, much earlier than observed in LOAD. These findings highlight the early onset of tau relative to amyloid in DS and indicate that a strategy of early tau intervention is necessary for this population.

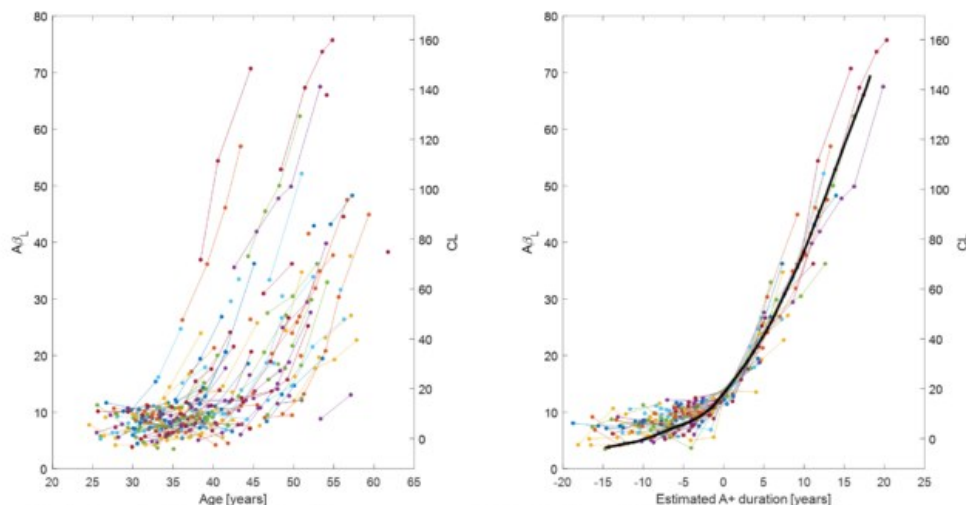


Fig 1. Longitudinal A β _L/CL with respect to age (left). SILA modeled fit of A β _L/CL with respect to estimated A+ duration (right).

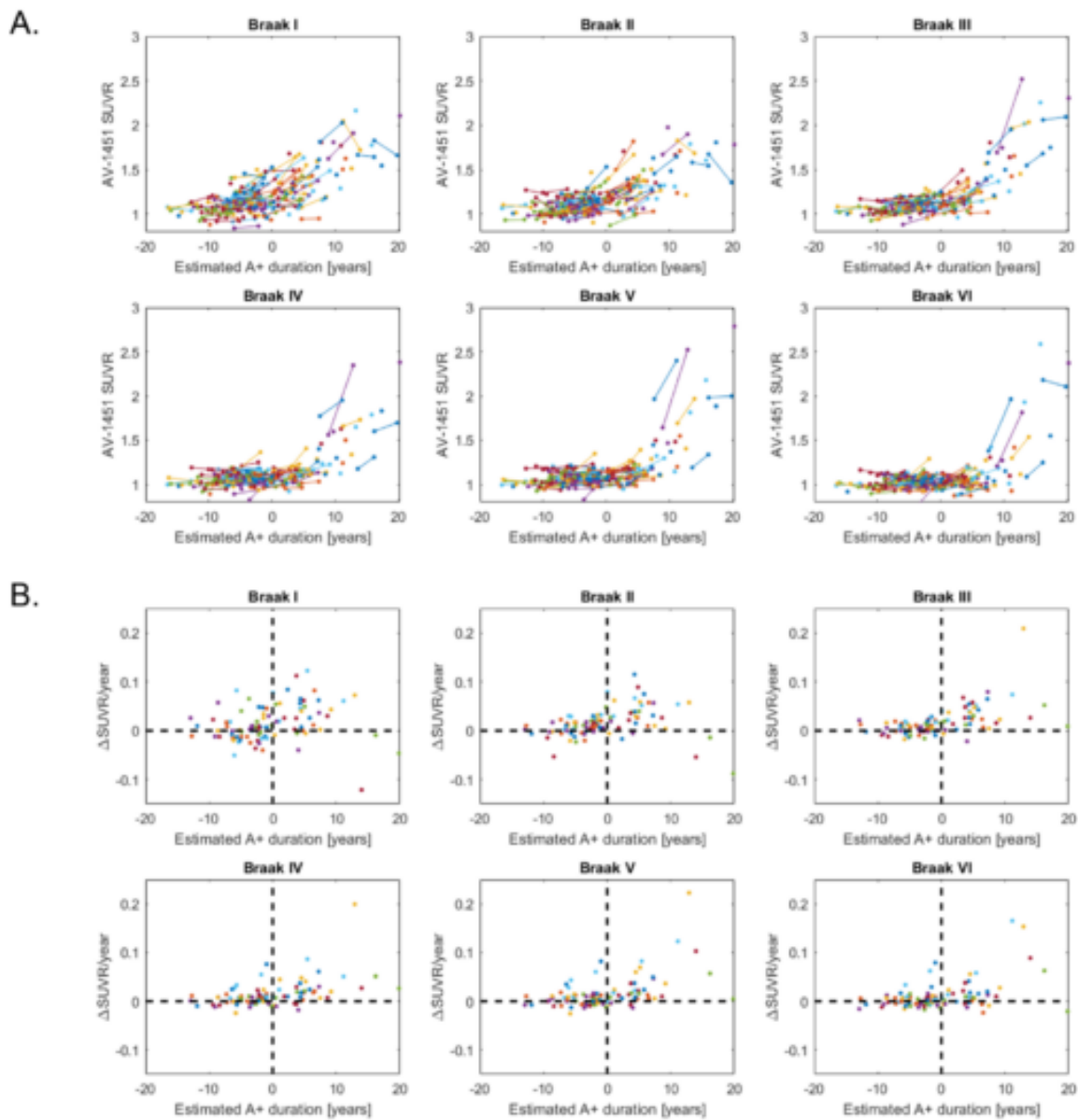


Fig 2. A. AV-1451 SUVR with respect to A+ duration across the Braak stage regions of tau pathology for each participant (N=169). Connected lines represent participants with longitudinal amyloid and tau scans. **B.** Longitudinal rates of tau change with respect to A+ duration for each participant (N=92). Plotted points represent the longitudinal rate of tau change observed at the most recent scan. Decreases in Braak regions I-II for A+ individuals may be attributed to choroid plexus binding. Braak I: Entorhinal cortex. Braak II: Hippocampus. Braak III: Amygdala, parahippocampal, fusiform & lingual gyri. Braak IV: Middle & inferior temporal gyri, thalamus, anterior, posterior & isthmus cingulate, insula, temporal pole. Braak V: superior frontal, orbitofrontal, middle frontal, lateral occipital, superior temporal & transverse temporal gyri, frontal pole, pars opercularis, pars orbitalis, pars triangularis, parietal lobe, pallidum, precuneus. Braak VI: Pericalcarine cortex, cuneus, postcentral, precentral & paracentral gyri.

Table 1. Longitudinal rates of tau change (annualized % change presented as mean [95% CI]) across each Braak stage region of tau pathology with respect to A+ duration (years). Early tau increases were observed within 2.5 years following A+.

A+ duration	N	A β burden	Braak I	Braak II	Braak III	Braak IV	Braak V	Braak VI
<0 years	56	8.68 A β _t /7.61 CL	0.46[0.14, 0.78]	0.73[0.54, 0.93]	0.53[0.40, 0.66]	0.66[0.45, 0.87]	0.59[0.36, 0.83]	0.38[0.14, 0.62]
0-2.5 years	8	15.1 A β _t /22.2 CL	3.7[2.8, 4.7]	2.2[1.3, 3.1]	1.5[1.0, 2.0]	1.1[0.55, 1.7]	0.73[0.41, 1.1]	0.64[0.31, 0.98]
2.5-5 years	12	20.6 A β _t /34.7 CL	2.4[1.6, 3.3]	3.4[2.8, 4.1]	2.9[2.4, 3.5]	1.3[0.82, 1.8]	1.6[1.1, 2.1]	1.5[0.95, 2.1]
5-10 years	11	29.7 A β _t /55.3 CL	3.4[2.6, 4.3]	3.3[2.7, 3.9]	3.1[2.5, 3.7]	2.8[2.2, 3.4]	3.0[2.4, 3.7]	1.1[0.55, 1.7]
>10 years	5	52.4 A β _t /107 CL	-0.23[-1.9, 1.4]	-0.38[-1.9, 1.2]	4.4[2.6, 6.3]	4.7[2.9, 6.6]	6.2[4.3, 8.1]	7.3[5.2, 9.5]

Table 2. Effect size (Cohen's d [95% CI]) between baseline and follow-up AV-1451 SUVR for each Braak stage region. For an A+ duration of 0-2.5 years, medium to large effect sizes were observed for Braak regions I-III. For an A+ duration of 2.5-5 years, medium to large effect sizes were observed in all Braak stage regions.

A+ duration	Braak I	Braak II	Braak III	Braak IV	Braak V	Braak VI
<0 years	0.12[-0.25, 0.49]	0.29[-0.083, 0.66]	0.3[-0.073, 0.67]	0.27[-0.10, 0.64]	0.24[-0.13, 0.61]	0.14[-0.23, 0.51]
0-2.5 years	1.0[-0.062, 2.0]	0.63[-0.39, 1.6]	0.84[-0.20, 1.9]	0.59[-0.42, 1.6]	0.41[-0.59, 1.4]	0.37[-0.63, 1.4]
2.5-5 years	0.53[-0.29, 1.3]	0.69[-0.14, 1.5]	1.1[0.22, 2.0]	0.61[-0.22, 1.4]	0.78[-0.060, 1.6]	0.64[-0.19, 1.5]
5-10 years	0.75[-0.12, 1.6]	1.0[0.098, 1.9]	1.3[0.27, 2.1]	1.2[0.27, 2.1]	1.2[0.27, 2.1]	0.43[-0.42, 1.3]
>10 years	-0.017[-1.3, 1.2]	-0.092[-1.3, 1.2]	1.0[-0.36, 2.3]	0.81[-0.51, 2.1]	0.88[-0.45, 2.2]	0.77[-0.55, 2.0]

Keywords: Tau, Amyloid, Longitudinal, Trajectories, Down syndrome

Cross-sectional and longitudinal associations between amyloid- and tau-PET in early-onset Alzheimer's Disease: update from the LEADS study

Nidhi Mundada¹, Renaud La Joie¹, Leonardo Iaccarino^{1,2}, Sarah Ackley³, David Soleimani-Meigooni¹, Ehud Zeltzer¹, Charles Windon¹, Jeremy Tanner¹, Courtney Lawhn Heath³, Ranjani Shankar¹, Alinda Amuiri¹, Paul Aisen⁴, Ani Eloyan⁵, Robert Koeppe⁶, Maria Carrillo⁷, Bradford Dickerson⁸, Liana Apostolova⁹, Gil Rabinovici¹

¹Memory and Aging Center, Department of Neurology, University of California San Francisco, San Francisco, CA, US

²Eli Lilly and Company, Indianapolis, IN, US

³University of California San Francisco, San Francisco, CA, US

⁴Alzheimer's Therapeutic Research Institute, University of Southern California, San Diego, CA, US

⁵Department of Biostatistics, Center for Statistical Sciences, Brown University, Providence, RI, US

⁶Department of Radiology, University of Michigan, Ann Arbor, MI, US

⁷Medical & Scientific Relations Division, Alzheimer's Association, Chicago, IL, US

⁸Department of Neurology, Massachusetts General Hospital and Harvard Medical School, Boston, MA, US

⁹Department of Neurology, Indiana University School of Medicine, Indianapolis, IN, US

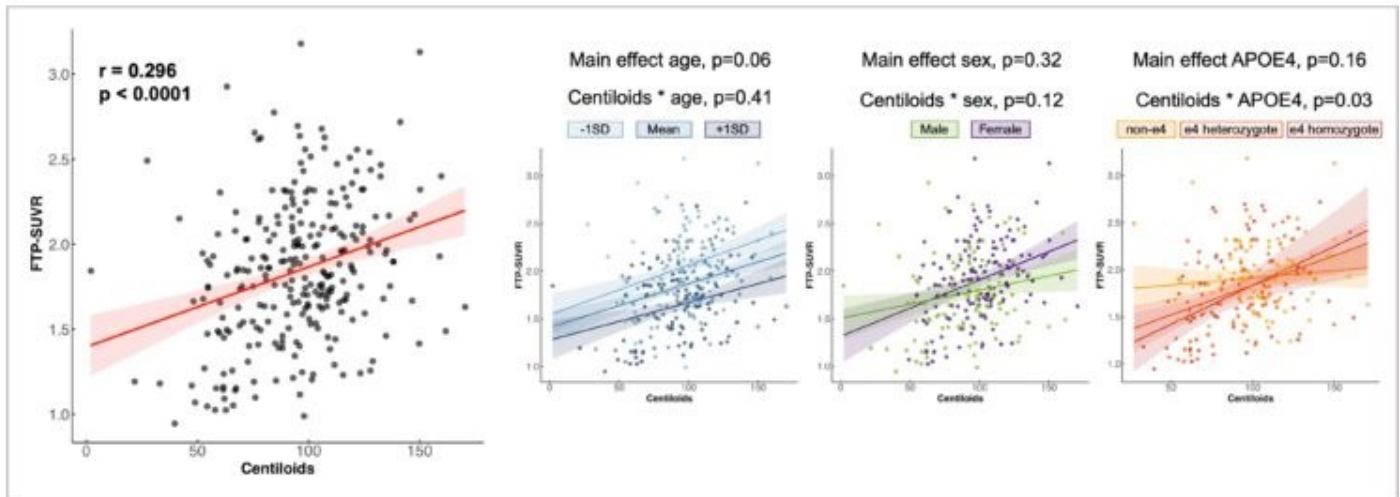
Objective: We aimed to describe amyloid/tau-PET relationships in patients with sporadic Early Onset AD (EOAD) using cross-sectional and longitudinal data from the Longitudinal Early-onset Alzheimer's Disease Study (LEADS).

Methods: In October 2022, we selected LEADS patients who fulfilled the following criteria: 1) clinical diagnosis of MCI or mild dementia, 2) available baseline amyloid-PET (¹⁸F-florbetaben/FBB), tau-PET (¹⁸F-fortaucipir/FTP), and structural MRI, 3) positive amyloid-PET based on a process including visual read and quantification. Image acquisition, quality control, and processing followed ADNI protocols. FBB-PET Centiloids (CLs) and mean cortical FTP-SUVR were extracted in native space using FreeSurfer. Cross-sectional analyses were performed using general linear models; longitudinal analyses were performed using linear mixed effect models with random intercepts using all available scans (between 1 and 4 scans per patient, details in figures).

Results: Our cohort included 266 EOAD patients; mean age at baseline 59.2±4.1y (range:46-65), mean MMSE 21.6±5.2; 53.3% female and 55% APOE4 carriers (40% heterozygotes, 15% homozygotes). Cross-sectionally, Centiloids and FTP-SUVR were mildly correlated ($r=0.29$, $p<.001$); this relationship was stronger in APOE4 carriers, but not modulated by age or sex (Fig 1). 118 patients had longitudinal amyloid-PET (Fig 2 for details on number of timepoints and duration of follow-up). On average, Centiloids increased by ~4.7 CLs/year (95%CI=[3.8-5.6]); the rate of Centiloid change was not modulated by age, sex, or APOE4 (Fig 2). Longitudinal tau-PET was available in 110 patients (Fig 3) and showed cortical FTP increases of ~0.07 SUVR/year (95%CI=[0.05,0.08]), independent of sex, APOE4 or baseline Centiloids. However, patients' age impacted longitudinal tau-PET, with younger patients showing greater FTP-SUVR increase over time (Fig 3).

Conclusions: In symptomatic patients with EOAD, amyloid- and tau-PET are modestly correlated at baseline, and both continue to increase longitudinally. Even within this group of patients between 46 and 65yo, patients' age showed a specific association with tau-PET signal.

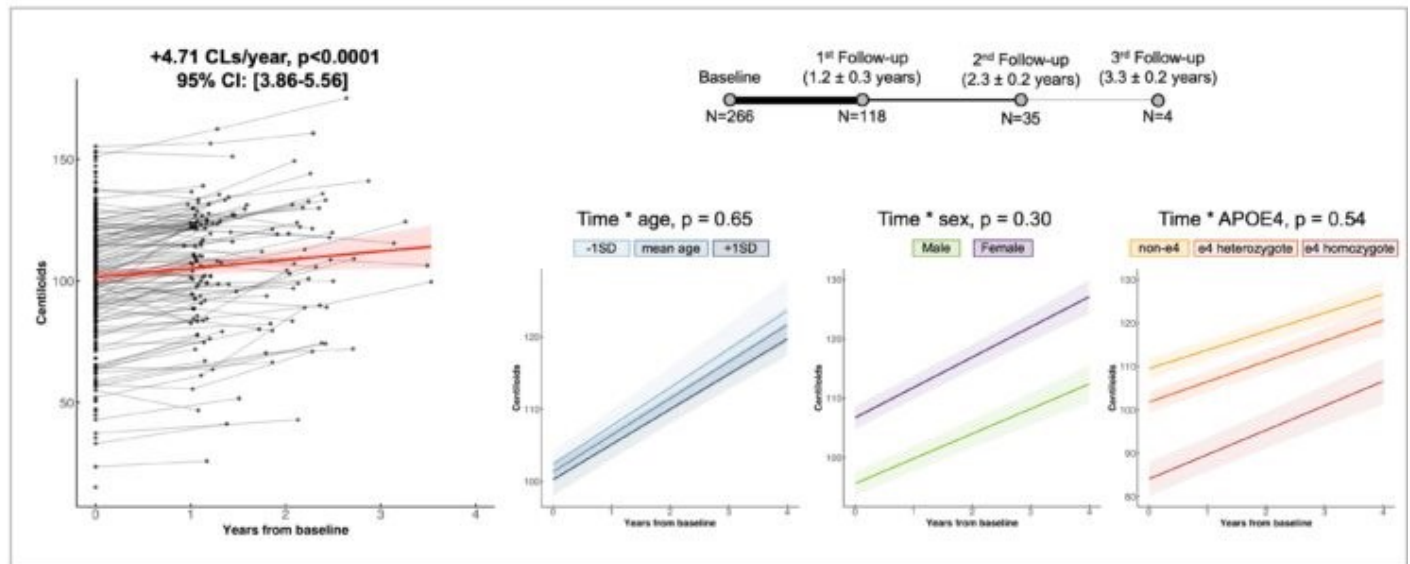
Fig 1: Cross-sectional association between FBB- and FTP-PET



PET scans were scaled using whole cerebellum as reference region for FBB-PET and inferior cerebellar for FTP-PET. Total cortical FTP-SUVR is used as a dependent variable in all models. Smaller panels show Centiloids and a specific variable (e.g., age) as independent variables and their corresponding interaction with Centiloids (e.g., Centiloids * age).

β 's represent estimated change in SUVR for 1 year increase ($\beta_{\text{age}} = -0.03$) or for females compared to males ($\beta_{\text{sex-female:male}} = 0.19$)
 Post-hoc tests for APOE4 showed significant effects on FTP-SUVR: $\beta_{\text{APOE4-1:0}} = -0.56$, $p=0.018$; $\beta_{\text{APOE4-2:0}} = -0.75$, $p=0.007$

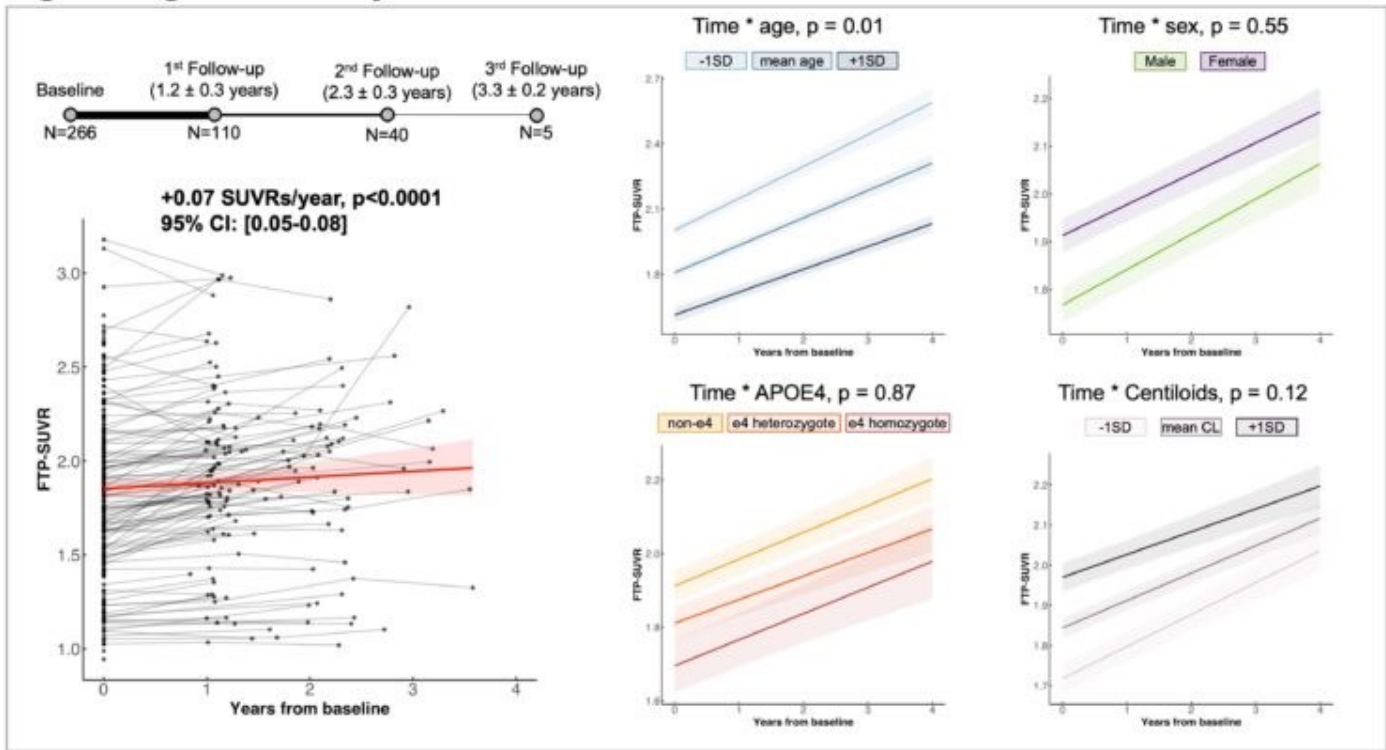
Fig 2: Longitudinal Analysis of FBB-PET



FBB-PET scans were scaled using a composite reference region which includes whole cerebellum, brainstem and eroded white matter. Centiloids are used as a dependent variable in all linear mixed effect models. Smaller panels show the effect of age, sex, and APOE4 on the rate of Centiloid changes using interaction terms with time.

Age = 60 ± 4.2 .

Fig 3: Longitudinal Analysis of FTP-PET



FTP-PET scans were scaled using inferior cerebellar grey. Total cortical FTP-SUVR is used as a dependent variable in all linear mixed effect models. Smaller panels show the effect of age, sex, APOE4, and baseline Centiloids on the rate of tau-PET changes using interaction terms with time.
 Age = 60 ± 4.2 ; FBB-CLs = 95 ± 27

Keywords: early-onset Alzheimer's Disease, amyloid-PET, tau-PET, cross-sectional, longitudinal

Amyloid PET Burden Predicts Longitudinal Cognitive Trajectories in a Heterogeneous ADRD Cohort

Kyan Younes¹, Emily Johns¹, Shubhabrata Mukherjee², Christina B. Young¹, Gabriel Kennedy¹, Hillary A. Vossler¹, Victor W. Henderson^{1,3}, Kathleen L. Poston¹, Tobey J. Betthausen⁴, Bill Bevis⁴, William M. Brooks⁵, Jeffrey M. Burns⁵, Stephen A. Coombes⁶, Charles DeCarli⁷, Frank DiFilippo^{1,8}, Ranjan Duara⁶, Audrey Fan⁷, Laura E. Gibbons², Todd Golde⁶, Sterling C. Johnson⁴, Rebecca Lepping⁵, James Leverenz⁸, Sean McDougall⁷, Emily Rogalski⁹, Elizabeth Sanders², Jaiashre Sridhar⁹, Andrew J. Saykin¹⁰, Anjali Sridharan⁴, Emily H. Trittschuh^{11,12}, David Vaillancourt⁶, Eric Vidoni⁵, Wei-en Wang⁶, Jesse Mez¹³, Timothy J Hohman¹⁴, Duygu Tosun¹⁵, Sarah Biber¹⁵, Walter A. Kukull¹⁶, Paul Crane², Elizabeth Mormino¹

¹Department of Neurology and Neurological Sciences, Stanford University, Stanford, CA, US

²Department of Medicine, The University of Washington, Seattle, WA, US

³Department of Epidemiology and Population Health, Stanford University, Stanford, CA, US

⁴Wisconsin Alzheimer's Disease Research Center, University of Wisconsin School of Medicine and Public Health, Madison, WI, US

⁵University of Kansas Alzheimer's Disease Center, University of Kansas Medical Center, Kansas, KS, US

⁶Florida Alzheimer's Disease Research Center, University of Florida, Gainesville, FL, US

⁷Alzheimer's Disease Center, University of California Davis Medical Center, Davis, CA, US

⁸Cleveland Alzheimer's Disease Research Center, Cleveland, OH, US

⁹Mesulam Center for Cognitive Neurology and Alzheimer's Disease, Feinberg School of Medicine, Northwestern University, Chicago, IL, US

¹⁰Indiana Alzheimer's Disease Research Center, Indiana University School of Medicine, Indianapolis, IN, US

¹¹Department of Psychiatry and Behavioral Science, University of Washington, Seattle, WA, US

¹²VA Puget Sound Health Care System, Geriatric Research Education and Clinical Center, Seattle, WA, US

¹³Department of Neurology, Boston University, Boston, MA, US

¹⁴Vanderbilt Memory and Alzheimer's Center, Vanderbilt University Medical Center, Nashville, TN, US

¹⁵Department of Radiology and Biomedical Imaging, University of California San Francisco, SAN FRANCISCO, CA, US

¹⁶Department of Epidemiology, National Alzheimer's Coordinating Center, University of Washington, Seattle, WA, US

Background: Cerebral amyloid-positivity predicts cognitive decline in aging and Alzheimer's disease (AD). However, previous work often excluded individuals with common comorbidities and focused on specific amnesic clinical presentations, thereby limiting generalizability.

Objectives: Investigate the prognostic value of amyloid PET in a large, demographically-diverse, multi-center, heterogeneous cohort of Clinically Unimpaired (CU) and Clinically Impaired (CI) participants from the national Alzheimer's Disease Research Center program.

Methods: 868 multi-site amyloid PET scans were analyzed using an MRI-Free pipeline. Late-frame data were extracted according to the optimal window for each ligand. Standardized Uptake Value Ratios were created by summing late-frame data, normalized using the whole cerebellum, and converted to centiloids. We conducted Gaussian Mixture Models within each amyloid dataset to derive the probability of amyloid positivity, which we used as a measure of amyloid PET burden. We examined cross-sectional and prospective longitudinal associations between cognition and amyloid burden with linear mixed models. Models were conducted separately for the CU and CI controlling for age, sex, ethnicity/race, and education. Outcome measures were harmonized composite memory, executive, and language scores (Mukherjee et al.,2022).

Results: We identified 223 CI (median follow-up=2 and IQR=1.9 years) and 645 CU (Median follow-up= 1.7 and IQR= 3.5 years) participants (Table 1). The CI group included varying suspected etiologies thought to be the primary cause of impairment (AD, alpha-synucleinopathy, vascular, etc). Among CI, increased probability of amyloid positivity was

related to worse cross-sectional memory and language, as well as prospective decline in memory, executive function, and language (Table 2). For CU, increased probability of amyloid positivity was related to worse cross-sectional memory and language, as well as prospective memory decline.

Conclusion: Amyloid PET burden is associated with cross-sectional and longitudinal cognitive decline in both CU and CI groups. Amyloid burden is an important prognostic marker in a heterogenous clinical cohort.

	CU		MCI (n = 146)					Dementia (n = 77)					
		AD	Syn	FTLD	Driving Cognitive Impairment	Neuro/Gen	Psyc	VBI	AD	Syn	FTLD	Driving Cognitive Impairment	Psyc
Count	648	87	15	1	27	8	8	60	10	4	1	1	1
Amyloid+ (%)	22.99	68.96	40.00	0.00	22.22	50.00	37.50	88.33	60.00	0.00	0.00	0.00	0.00
Age mean (sd)	72.7 (7.09)	73.0 (8.51)	70.0 (9.71)	66.6 (0)	75.5 (9.29)	68.2 (1.70)	69.7 (4.71)	72.3 (8.51)	66.0 (8.70)	61.9 (2.40)	70.3 (0)	44.4 (0)	90.2 (0)
Sex M/F	211/434	42/45	13/2	1/	15/12	3/5	5/3	31/29	8/2	1/3	1/1	1/1	1/
Education mean (sd)	16.1 (3.07)	16.2 (2.99)	17.4 (1.95)	20 (0)	15.4 (2.85)	15.4 (3.63)	16.1 (1.45)	15.5 (3.20)	17 (2.49)	15.2 (2.57)	12 (0)	12 (0)	23 (0)
Ethnicity/Race													
Hispanic White	53	19	2		13	4	3	16					1
Non-Hispanic American Indian	9	1											
Non-Hispanic Asian	11	1					1	1					
Non-Hispanic Black	53	9	13	1	14	3	4	1	10	4	1	1	
Non-Hispanic White	514	55				1		40					
Other	5	2						2					

	Memory composite β (SE) [95% CI]	Executive composite β (SE) [95% CI]	Language composite β (SE) [95% CI]
Clinically Unimpaired			
Intercept	-0.51 *** (0.11) [-0.74, -0.28]	-0.65 *** (0.11) [-0.88, -0.42]	-0.78 *** (0.12) [-1.03, -0.5]
Age	-0.39 *** (0.03) [-0.46, -0.31]	-0.31 *** (0.03) [-0.38, -0.24]	-0.24 *** (0.03) [-0.32, -0.16]
Time	-0.10 (0.07) [-0.25, 0.04]	-0.30 *** (0.06) [-0.42, -0.18]	-0.16 ** (0.06) [-0.29, -0.04]
Sex	0.24 *** (0.06) [0.10, 0.37]	-0.07 (0.06) [-0.20, 0.06]	0.28 *** (0.07) [0.14, 0.42]
Education	0.24 *** (0.03) [0.17, 0.3]	0.34 *** (0.036) [0.27, 0.41]	0.25 *** (0.03) [0.17, 0.32]
Amyloid Probability	-0.11 *** (0.03) [-0.18, -0.05]	-0.02 (0.032) [-0.09, 0.03]	-0.09 ** (0.034) [-0.16, -0.02]
Time x Age	-0.11 *** (0.02) [-0.16, -0.06]	-0.04* (0.02) [-0.08, -0.003]	-0.03 (0.02) [-0.08, 0.003]
Time x Sex	-0.05 (0.04) [-0.14, 0.03]	-0.01 (0.03) [-0.08, 0.061]	-0.04652 (0.03) [-0.12, 0.02]
Time x Education	0.008 (0.023) [-0.03, 0.05]	0.02 (0.019) [-0.01, 0.06]	0.004 (0.019) [-0.03, 0.04]
Time x Amyloid Probability	-0.05 ** (0.02) [-0.09, -0.01]	-0.009 (0.01) [-0.04, 0.02]	-0.02 (0.017) [-0.06, 0.008]
Impaired (MCI and Dementia)			
Intercept	0.39 *** (0.11) [0.17, 0.61]	0.01 (0.14) [-0.25, 0.28]	0.08 (0.15) [-0.21, 0.37]
Age	-0.16 ** (0.05) [-0.27, -0.06]	-0.09 (0.06) [-0.22, 0.03]	-0.29 *** (0.07) [-0.43, -0.14]
Time	-0.05 (0.07) [-0.19, 0.08]	-0.29 *** (0.08) [-0.46, -0.12]	-0.28 *** (0.075) [-0.42, -0.13]
Sex	-0.19 (0.10) [-0.39, 0.004]	-0.02 (0.13) [-0.27, 0.22]	0.03 (0.14) [-0.22, 0.30]
Education	0.04 (0.05) [-0.05, 0.14]	0.19 ** (0.06) [0.07, 0.31]	0.05 (0.06) [-0.07, 0.18]
Cognitive Diagnosis [#]	-1.44 *** (0.11) [-1.65, -1.23]	-1.38 *** (0.13) [-1.64, -1.12]	-1.13 *** (0.14) [-1.42, -0.85]
Amyloid Probability	-0.36 *** (0.05) [-0.46, -0.26]	-0.10 (0.06) [-0.22, 0.01]	-0.14* (0.06) [-0.27, -0.02]
Time x Age	-0.12 *** (0.03484) [-0.18, -0.05]	0.02 (0.042) [-0.06, 0.10]	-0.05 (0.03) [-0.13, 0.01]
Time x Sex	-0.18 ** (0.06) [-0.31, -0.05]	-0.03 (0.08) [-0.19, 0.11]	0.04 (0.07) [-0.09, 0.18]
Time x Education	-0.04 (0.03) [-0.11, 0.02]	-0.08* (0.04) [-0.17, -0.002]	-0.02 (0.03) [-0.10, 0.04]
Time x Cognitive Diagnosis [#]	-0.27 *** (0.07) [-0.42, -0.12]	-0.29 ** (0.09) [-0.48, -0.10]	-0.32 *** (0.08) [-0.48, -0.15]
Time x Amyloid Probability	-0.12 *** (0.03) [-0.18, -0.06]	-0.17 *** (0.03) [-0.2, -0.09]	-0.15 *** (0.03) [-0.21, -0.08]

Keywords: Amyloid PET, heterogeneity, neurodegenerative disease, Alzheimer`s disease, cognitive composite scores, NACC data.

Variations in gamma-secretase function across PSEN1 pathogenic variants strongly predict the clinical, cognitive, and biomarker progression of autosomal dominant Alzheimer's disease

Stephanie Schultz¹, Lei Liu², Aaron Schultz¹, Colleen Fitzpatrick¹, Raina Levin¹, Jean-Pierre Bellier², Alan Renton⁴, Nelly Joseph-Mathurin³, Ricardo Allegri⁵, Tammie Benzinger³, Sarah Berman⁶, Helena Chui⁷, Anne Fagan³, Martin Farlow⁸, Nick Fox⁹, Gregory Day¹⁰, Clifford Jack¹¹, Jason Hassenstab³, Mathias Jucker¹², Robert Koeppe¹³, Jae-Hong Lee¹⁴, Allan Levey¹⁵, Johannes Levin¹⁶, Ralph Martins¹⁷, Hiroshi Mori¹⁸, James Noble¹⁹, Richard Perrin³, Pedro Rosa-Neto²⁰, Stephen Salloway²¹, Raquel Sanchez-Valle²², Peter Schofield²³, Chengjie Xiong³, John Morris³, Brian Gordon³, Celeste Karch³, Eric McDade³, Keith Johnson¹, Randall Bateman³, Dennis Selkoe², Jasmeer Chhatwal^{1,2}

¹Massachusetts General Hospital, Boston, MA, US

²Brigham and Women's Hospital, Boston, MA, US

³Washington University in St. Louis School of Medicine, St. Louis, MO, US

⁴Icahn School of Medicine at Mount Sinai, New York, NY, US

⁵INEBA, Buenos Aires, AR

⁶University of Pittsburgh, Pittsburgh, PA, US

⁷University of Southern California, Los Angeles, CA, US

⁸Indiana Alzheimer's Disease Research Center, Indianapolis, IN, US

⁹UCL, London, UK

¹⁰Mayo Clinic, Jacksonville, FL, US

¹¹Mayo Clinic, Rochester, MN, US

¹²German Center for Neurodegenerative Diseases (DZNE), Tuebingen, Germany

¹³University of Michigan, Ann Arbor, MI, US

¹⁴University of Ulsan College of Medicine, Seoul, Korea

¹⁵Emory Goizueta Alzheimer's Disease Research Center, Atlanta, GA, US

¹⁶German Center for Neurodegenerative Diseases (DZNE), Munich, Germany

¹⁷Edith Cowan University, Joondalup, AU

¹⁸Osaka City University Medical School, Osaka, Japan

¹⁹Columbia University, New York, NY, US

²⁰McGill University, Montreal, QC, Canada

²¹Butler Hospital, Providence, RI, US

²²Institut d'Investigacions Biomediques, Barcelona, Spain

²³Neuroscience Research Australia, Randwick, AU

Background: Despite the high penetrance of autosomal dominant Alzheimer's disease (ADAD) variants, striking heterogeneity in age at symptom onset (AAO) and biomarker trajectories is seen in different ADAD mutations. Most ADAD mutations are in *PSEN1*, the catalytic core of the γ -secretase complex, and *PSEN1* variants directly bias the balance of longer, aggregation-prone A β peptides relative to shorter, non-aggregating peptides (Figure 1A). We hypothesized that the phenotypic heterogeneity in ADAD may be partially explained by mutation-specific differences in production of longer vs. shorter A β , as measured in a novel mammalian cell model system.

Methods: 162 *PSEN1* variants were co-transfected with APP into HEK293 cells lacking endogenous *PSEN1/2*. Immunoassays quantified A β -37, 38, 40, 42, and 43 production by each variant. An A β -production composite that maximized prediction of AAO was developed using 107 variants not represented in DIAN and was then applied to 55 *PSEN1* variants having clinical, cognitive and biomarker data within DIAN (n=190 participants; Figure 2A).

Results: The cell model-derived A β composite was highly predictive of AAO across the 162 variants examined (r[53]=0.61, p=6.03e-07; Figure 1B). Among the 55 variants represented in DIAN, the cellular-derived A β composite was

strongly associated with all biomarker and cognitive measures (adjusted for age, sex, and family membership), including PiB-PET ($p=2.33e-07$; Figure 2B-C), CSF A β 42/40 ($p=2.88e-05$), CSF ptau-181 ($p=2.73e-06$), hippocampal volume ($p=3.94e-10$), and MMSE ($p=2.28e-04$; Figure 3A-D).

Conclusions: Cellular measures of A β production across *PSEN1* variants were strongly predictive of AAO and core cognitive and biomarker measures. These findings elucidate the critical quantitative link between γ -secretase dysfunction and ADAD phenotypes and a potential molecular cause for the biomarker and clinical heterogeneity observed among *PSEN1* variants. The approach here also represents a tool to account for heterogeneity in ADAD clinical trials and to assess the pathogenicity of *PSEN1* variants of unknown significance or with limited family history.

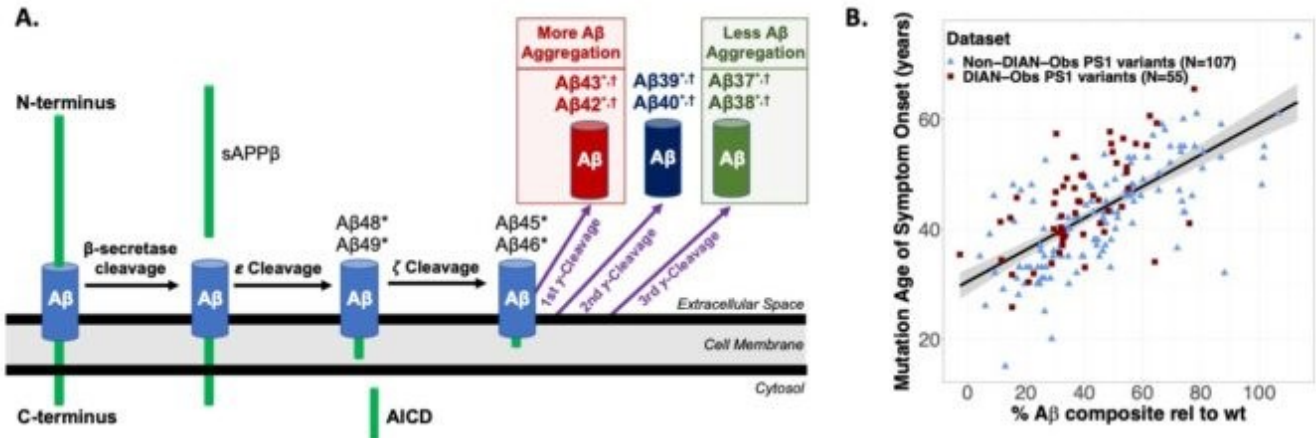


Figure 1. Cell-based mutation-specific A β composite predicts age of symptom onset in corresponding *PSEN1* pathogenic variant carriers. A) Schematic showing γ secretase processivity (left to right). Following ϵ - and ζ cleavage of APP, successive γ -cleavages of the APP transmembrane domain fragment release several A β peptides of decreasing lengths depending on the number of sequential γ -cleavage events. Longer A β peptides (esp. A β 42 & A β 43) are more amyloidogenic/pathogenic compared to shorter A β peptides (A β 37 & A β 38). B) 162 *PSEN1* (PS1) variants (107 not included in DIAN-Obs, 55 with available clinical, cognitive, and imaging data from DIAN-Obs) were assessed in a cell model system for the relative amounts of A β peptides produced by each variant (please see Figure 2 for further detail). A single summary measure of pathologic A β production (A β composite, expressed as % relative to wild type) was developed to maximize prediction of age at symptom onset (AAO) among the 107 variants examined previously in Liu et al., 2022 (B, blue triangles). This same composite was also highly predictive of AAO in 55 *PSEN1* variants represented in the DIAN-Obs (B, red squares). Note that AAO for DIAN-Obs participants is averaged across available values for a given variant, and data points are jittered to facilitate blinding.

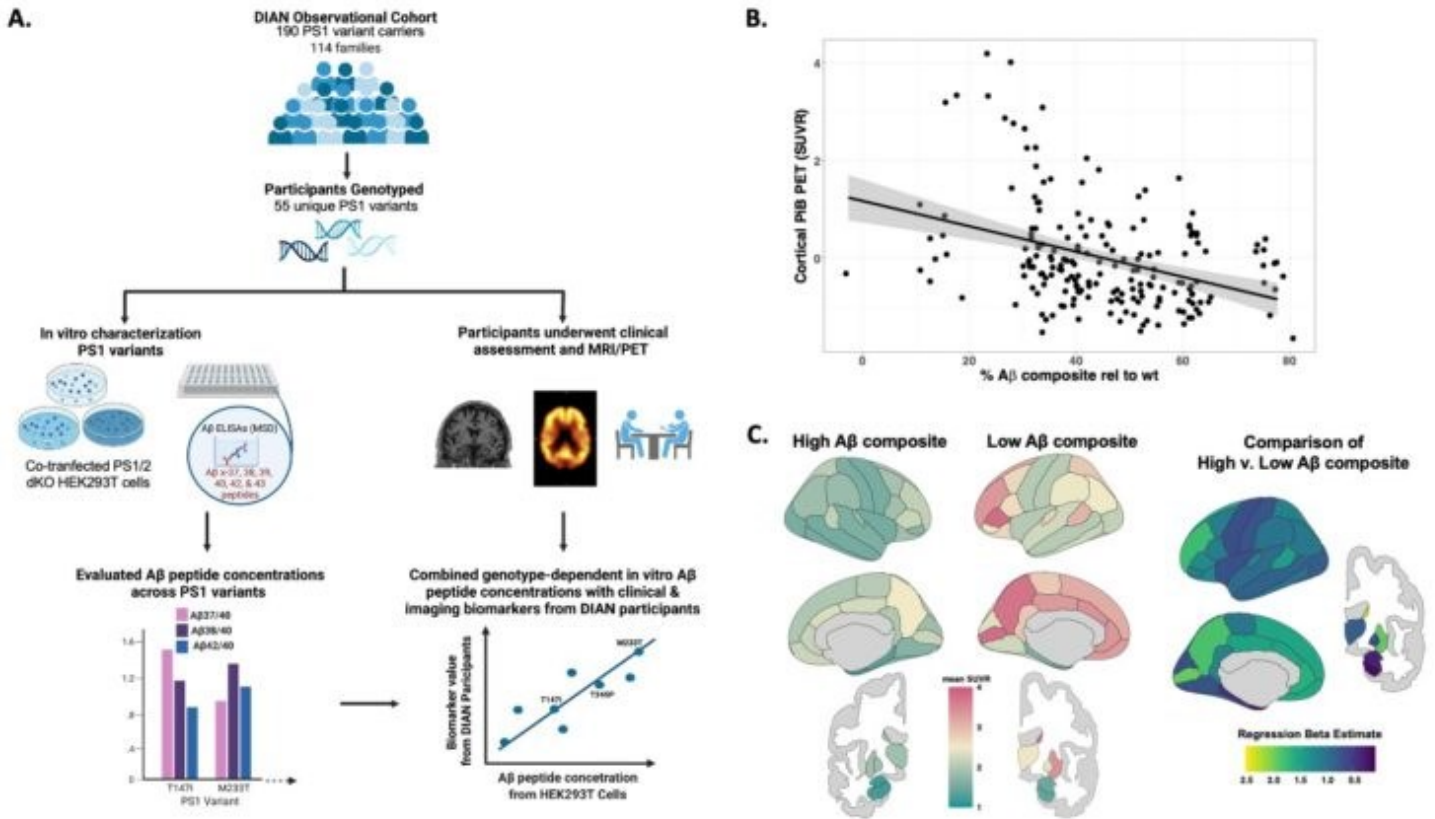


Figure 2. Cell model based Aβ composite is predictive of *in vivo* Aβ burden in *PSEN1* pathogenic variant carriers participating in DIAN. A) Schematic summarizing cell-based and *in vivo* methods. The *in vitro* cell model is based on transient transfections of HEK293 cells lacking endogenous *PSEN1/2* (dKO) with plasmids coding for wild-type (wt) *PSEN1* or one of the known pathogenic variants together with wild-type human APP. Conditioned media harvested from the transfected HEK cells was assayed for Aβ-37, 38, 40, 42 and 43. These data were compared with cross-sectional amyloid PET data (C11-PiB) from DIAN participants carrying the corresponding pathogenic variants. B) Association between age-adjusted cortical composite PiB-PET SUVR and Aβ composite (% relative to wild-type). C) Comparison of mean regional PiB-PET SUVR from individuals in the Lowest (most pathogenic) and Highest (least pathogenic) cell-based Aβ composite tertiles, as well as regression estimates from linear mixed effects models examining differences in regional PiB-PET in the Low versus High Tertile groups. These models are adjusted for age, sex, and family membership. Mean Aβ composite (% relative to wt) score for Low and High tertile groups corresponds to 26.6% and 64.4% of wild-type *PSEN1*, respectively.

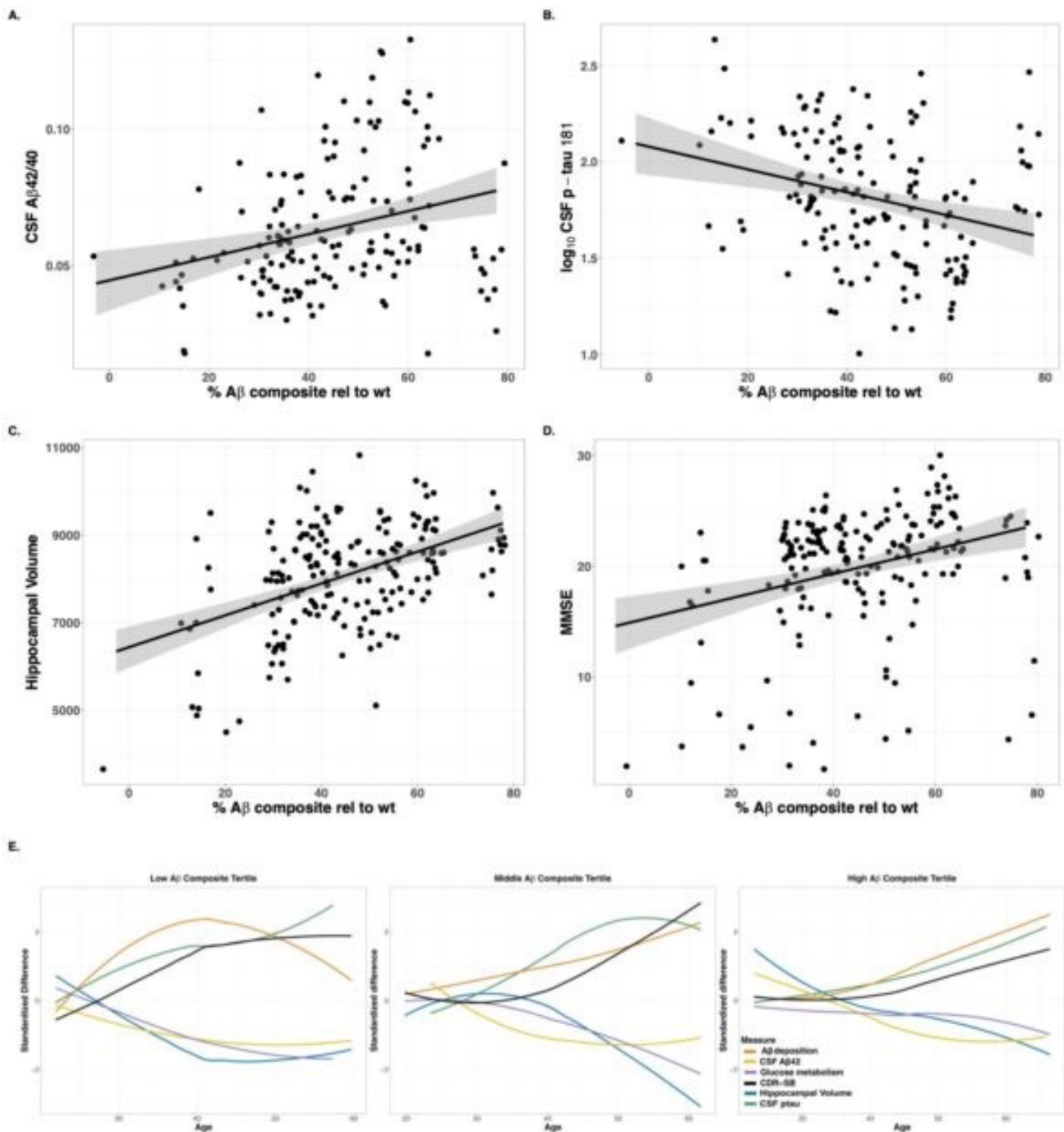


Figure 3. Cell model derived Aβ composite is associated with *in vivo* biomarker and cognitive measures in *PSEN1* pathogenic variant carriers. Associations between the cell model derived Aβ composite (% relative to wt) and cross-sectional, age-adjusted CSF Aβ_{42/40} values (A), age-adjusted CSF log₁₀ ptau-181 values (B), age and total intracranial volume-adjusted hippocampal volume (C), and age-adjusted Mini Mental State Examination scores (MMSE; D) are shown. (E) Aβ composite tertiles showing distinct biomarker and cognitive trajectories. Normalized cross-sectional biomarker and cognitive differences between *PSEN1* pathogenic variant carriers and non-carriers are plotted relative to age fitted with LOESS using participant data from DIAN-Obs.

Keywords: *PSEN1*, gamma-secretase, multimodal, translational, amyloid

Thursday, January 12, 2023 - 01:15 pm - 02:35 pm

Podium Session

SESSION VII: Tau PET and MRI: multimodality insights

Thursday, January 12, 2023		
1:15 pm – 2:35 pm	SESSION VII: TAU PET AND MRI: MULTIMODALITY INSIGHTS	CHAIRS: Annie Cohen, PhD , <i>University of Pittsburgh</i> Beth Mormino, PhD , <i>Stanford University</i>
1:15	Introduction	Chairs
1:20	Mapping tau accumulation to the functional and structural organization of the brain in Alzheimer's disease	Julie Ottoy, PhD, <i>University of Toronto</i>
1:35	Baseline tau PET shows stronger associations with cognitive and behavioral changes over time than cortical thickness	Ellen Singleton, PhD, <i>Lund University</i>
1:50	A Central Role of Locus Coeruleus in the Initial Spatiotemporal Progression of Tau and its Contribution to Cognition	Elisenda Bueicheku, PhD, <i>Massachusetts General Hospital/Harvard Medical School</i>
2:05	Tau Propagation in the Brain Olfactory Circuits Contributes to Smell Perception Changes in Aging	Ibai Diez, PhD, <i>Massachusetts General Hospital/Harvard Medical School</i>
2:20	Medial temporal lobe subregional microstructure measured with ultra-high resolution diffusion imaging as a biomarker for early tau pathology and memory impairment	Jenna Adams, PhD, <i>University of California, Irvine</i>
2:35	Discussion	

Mapping tau accumulation to the functional and structural organization of the brain in Alzheimer's disease

Julie Ottoy^{1,2}, Min Su Kang^{1,2}, Reinder Vos de Wael³, Bo-yong Park^{3,4,5}, Gleb Bezgin^{2,6}, Firoza Lussier², Nesrine Rahmouni², Jenna Stevenson², Jean-Paul Soucy³, Serge Gauthier², Boris Bernhardt³, Sandra Black^{1,7}, Pedro Rosa-Neto², Maged Goubran^{1,8}

¹LC Campbell Cognitive Neurology Unit, Hurvitz Brain Sciences Program, Sunnybrook Research Institute, University of Toronto, Toronto, ON, Canada

²Translational Neuroimaging laboratory, McGill Centre for Studies in Aging, Montreal, QC, Canada

³McConnell Brain Imaging Centre, Montreal Neurological Institute and Hospital, McGill University, Montreal, QC, Canada

⁴Department of Data Science, Inha University, Incheon, Korea

⁵Center for Neuroscience Imaging Research, Institute for Basic Science, Suwon, Korea

⁶Neuroinformatics for Personalized Medicine lab, Montreal Neurological Institute, McGill University, Montreal, QC, Canada

⁷Department of Medicine (Division of Neurology), University of Toronto, Toronto, ON, Canada

⁸Department of Medical Biophysics, University of Toronto, Toronto, ON, Canada

Introduction: Alzheimer's disease affects brain networks. However, traditional understanding of pathology spread through networks suffered from functional/structural connectivity being studied in isolation, low-resolution brain atlases, or simplified linear analyses. We addressed these limitations by leveraging smooth spatial transitions ('gradients') of connectivity and tau imaging data to better understand the link between brain connectivity and tau spread.

Methods: 213 participants from TRIAD underwent diffusion-weighted MRI, rs-functional MRI, and ¹⁸F-MK6240 tau-PET (baseline and subset 1-y follow-up). Participants were grouped by disease stage: 103/35 A β -/+ cognitively normal and 75 cognitively impaired A β +. The MRI-connectivity matrices and (Δ)tau-PET covariance matrices were subjected to non-linear dimensionality reduction to extract the orthogonal components ('gradients') explaining maximum variance per modality and disease stage. We correlated functional/structural connectivity gradients (G_{FUNC} , G_{STRUC}) with tau-PET gradients at baseline (G_{TAU}) and 1-y change ($G_{\Delta\text{TAU}}$). We showed partial correlations between a cognitive battery and tau SUVR in discretized spatial clusters along the primary G_{FUNC} or G_{STRUC} .

Results: At baseline, $G_{1\text{TAU}}$ significantly related to $G_{1\text{FUNC}}$ in cognitively impaired (**Fig.1A**). $G_{2\text{TAU}}$ (explaining less variance in tau-PET compared to $G_{1\text{TAU}}$) significantly related to $G_{1\text{STRUC}}$ (**Fig.1B**), in both cognitively normal A β + and impaired groups. Furthermore, the regions with highest between-group differences in tau SUVR also showed the highest between-group differences in connectivity gradients. These findings support a link between tau distribution and network (re-)organization in AD. Longitudinally, $G_{1\Delta\text{TAU}}$ and $G_{2\Delta\text{TAU}}$ showed distinct patterns of tau accumulation (temporal/posterior- vs. DMN-focused) (**Fig.2A**). While $G_{1\Delta\text{TAU}}$ related closely to structural connectivity and Braak staging, $G_{2\Delta\text{TAU}}$ related to functional connectivity (**Fig.2**). Lastly, cognitive performance was dependent on tau load within specific networks along G_{FUNC} .

Conclusion: We showed distinct pathways of transneuronal tau accumulation along functional or structural connections that may vary with disease stage and tau epicenter. Connectome gradients may provide a novel approach to study spatial heterogeneity in tau spread.

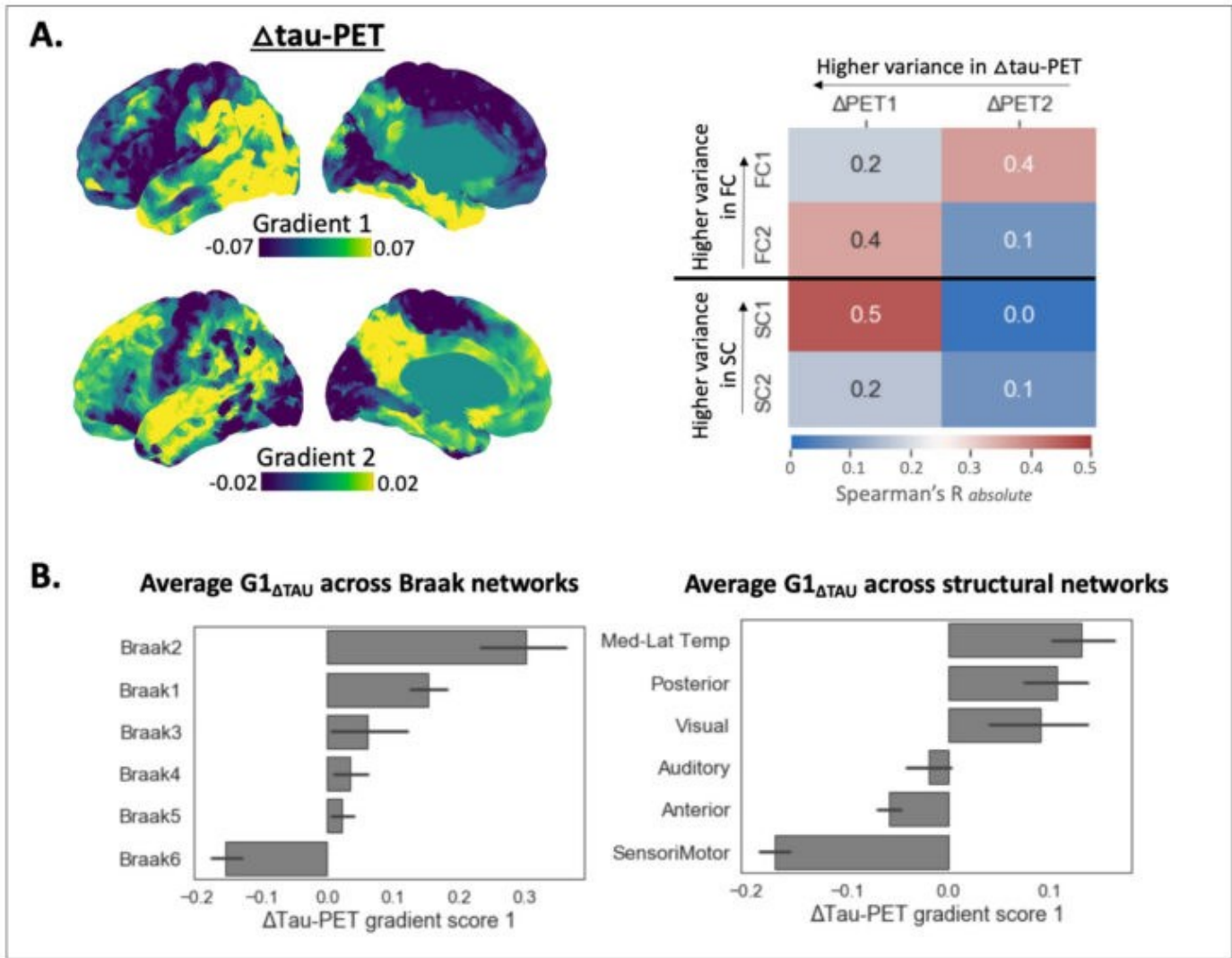


Figure 2. Longitudinal results of $\Delta\text{tau-PET}$ gradients and their association with connectivity in $A\beta^+$. A) The primary and secondary gradients of longitudinal tau-PET (51 and 13% variance, respectively) and their correlations with FC and SC gradients. Δtau was extracted as follow-up minus baseline SUVR and adjusted for the time difference between scans (420 ± 79 days, $N=39$ $A\beta^+$). B) The primary tau-PET gradient scores were averaged across networks to visualize their propagation along the Braak stages.

Keywords: Connectivity; Alzheimer's disease; tau; imaging; Braak staging

Baseline tau PET shows stronger associations with cognitive and behavioral changes over time than cortical thickness

Ellen Singleton¹, Alexa Pichet Binette¹, Olof Strandberg¹, Erik Stomrud^{1,3}, Rik Ossenkoppele^{1,2,3}, Oskar Hansson^{1,3}

¹Clinical Memory Research Unit, Department of Clinical Sciences, Lund University, Malmö, Sweden, Lund, Sweden

²Alzheimer Center Amsterdam, Department of Neurology, Amsterdam Neuroscience, Vrije Universiteit Amsterdam, Amsterdam UMC, Amsterdam, The Netherlands, Amsterdam, The Netherlands

³Memory Clinic, Skåne University Hospital, Lund, Sweden, Lund, Sweden

Objective: To examine the associations between regional tau PET SUVR and cortical thickness at baseline and cognitive and behavioral changes over time.

Methods: We included 1030 participants from the Swedish BioFINDER-2 study, of whom n=547 were cognitively unimpaired amyloid-negative individuals (CU A-), n=157 were amyloid-positive cognitively unimpaired individuals (CU A+), n=326 were amyloid-positive cognitively impaired individuals (CI A+, n=167 with MCI and n=159 with AD dementia) (Table 1). All underwent tau PET with [18F]RO948 and structural MRI. The average follow-up time was 1.63(1.29) years. Linear mixed models with random intercepts and fixed slopes, adjusted for age, sex and education, were performed to examine the associations between tau PET SUVR and cortical thickness in temporoparietal, frontal and occipital regions and the MMSE, modified PACC5 (mPACC5), memory domain z-score and Mild Behavioral Inventory (MBI) total score. FDR-correction was performed to account for multiple testing.

Results: In the CU A- group, lower cortical thickness was related to more decline on MMSE and mPACC5 especially in the temporoparietal region, while there were no associations with tau PET (Figure 1A). In the CU A+ group, higher tau PET levels are related to more decline on all cognitive and behavioral outcomes than cortical thickness (Figure 1B). In the CI A+ group, the same pattern (tau PET > cortical thickness) was observed, with even more pronounced stronger effects with tau PET than cortical thickness (Figure 1C).

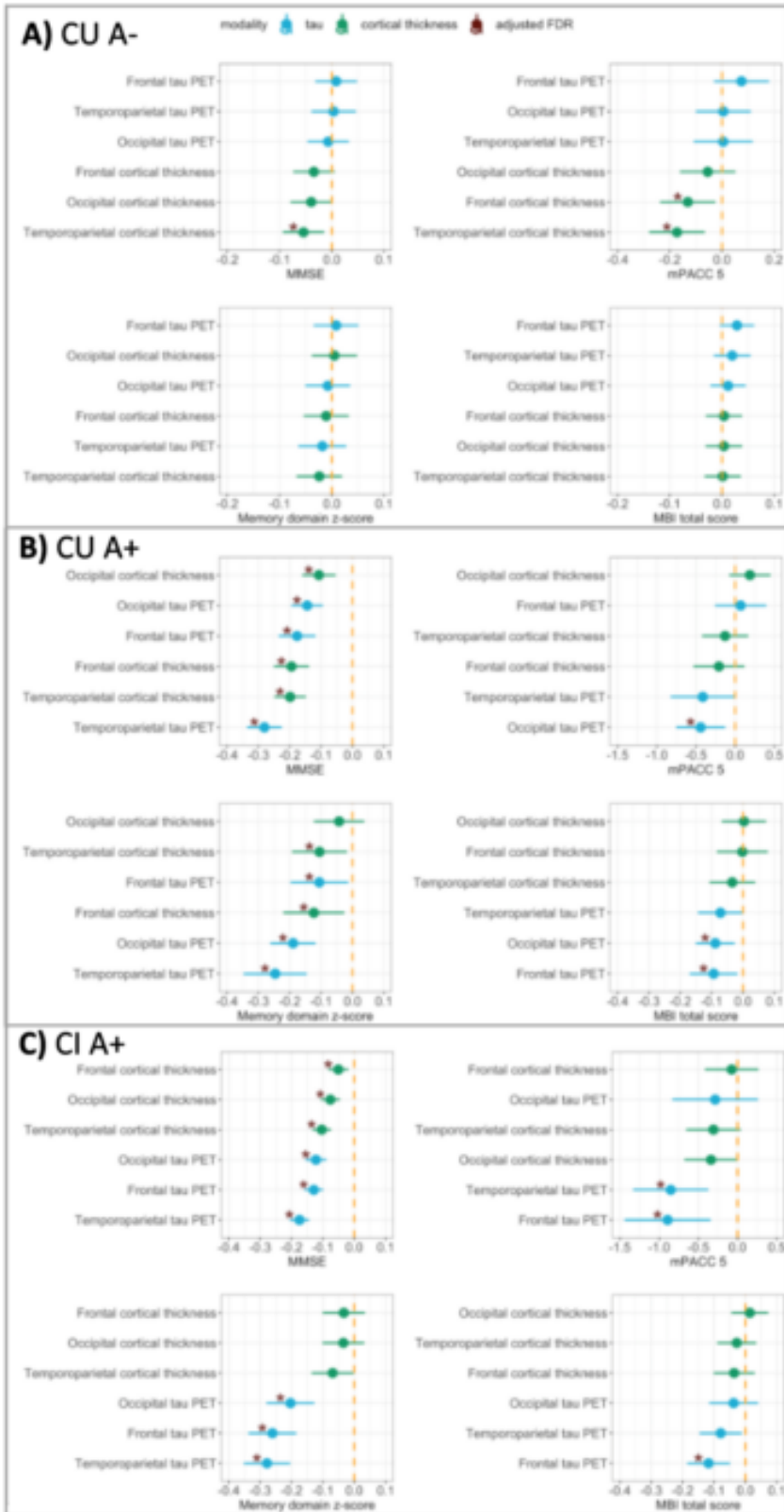
Conclusions: Our findings suggest that tau PET at baseline is more strongly associated with cognition and behavioral changes over time than cortical thickness in AD. Future work should investigate the potential mediating effect of (change in) cortical thickness on the relationship between tau PET at baseline and cognition and behavior over time.

Table 1. Demographic characteristics of study participants

	CU A- (N=547)	CU A+ (N=157)	CI A+ (N=326)	p-value
Gender, % Female	254 (46 %)	73 (46 %)	168 (52 %)	1.00
Age	61 (\pm 15)	72 (\pm 9.7)	73 (\pm 7.1)	<0.001
Education (years)	13 (\pm 3.4)	13 (\pm 3.7)	13 (\pm 4.4)	0.237
MMSE	29 (\pm 1.1)	29 (\pm 1.3)	24 (\pm 4.6)	<0.001
mPACC 5	-0.46 (\pm 3.4)	-3.0 (\pm 3.9)	-15 (\pm 6.1)	<0.001
Memory domain z-score	0.0079 (\pm 1.4)	-0.77 (\pm 1.4)	-4.1 (\pm 1.8)	<0.001
MBI total score	8.3 (\pm 6.0)	9.8 (\pm 6.0)	16 (\pm 11)	0.0178
CSF AB42/40 ratio	0.11 (\pm 0.018)	0.055 (\pm 0.019)	0.047 (\pm 0.013)	<0.001
Tau PET Temporo Parietal Lobe	1.1 (\pm 0.097)	1.2 (\pm 0.27)	1.7 (\pm 0.63)	<0.001
Tau PET Occipital Lobe	1.1 (\pm 0.086)	1.2 (\pm 0.16)	1.5 (\pm 0.55)	<0.001
Tau PET Frontal Lobe	1.0 (\pm 0.090)	1.0 (\pm 0.13)	1.2 (\pm 0.38)	0.00194
Cortical Thickness Temporoparietal Lobe	2.5 (\pm 0.11)	2.4 (\pm 0.11)	2.3 (\pm 0.13)	<0.001
Cortical Thickness Occipital Lobe	2.0 (\pm 0.086)	2.0 (\pm 0.093)	1.9 (\pm 0.11)	0.00323
Cortical Thickness Frontal Lobe	2.4 (\pm 0.10)	2.4 (\pm 0.10)	2.3 (\pm 0.12)	<0.001

Legend: CU A- = cognitively unimpaired amyloid negative individuals, CU A+ = cognitively unimpaired amyloid positive individuals, CI A+ = cognitively impaired amyloid positive individuals, MMSE = mini-mental state examination, mPACC = modified preclinical Alzheimer cognitive composite, MBI = Mild Behavioral Inventory, CSF = cerebrospinal fluid. Tau PET values are depicted as SUVRs and cortical thickness as mm. Values are depicted as Mean (SD) unless otherwise specified.

Figure 1. Beta coefficients of the associations between baseline tau and cortical thickness on cognition and behavior over time across diagnostic groups



Legend: CU A- = cognitively unimpaired amyloid negative individuals, CU A+ = cognitively impaired amyloid negative individuals, CI A+ = cognitively impaired amyloid positive individuals, MMSE = mini-mental state examination, mPACC = modified preclinical Alzheimer cognitive composite, MBI = Mild Behavioral Inventory, FDR = false discovery rate. Tau PET values are depicted as SUVRs and cortical thickness as mm.

Keywords: Cognition, Behavior, Tau PET, MRI, Alzheimer's disease

A Central Role of Locus Coeruleus in the Initial Spatiotemporal Progression of Tau and its Contribution to Cognition

Elisenda Bueichekú^{1,2}, Ibai Diez^{1,2,3}, Chan-Mid Kim^{1,2}, Alex Becker^{1,2}, Elouise A. Koops^{1,2}, Kenneth Kwong^{2,3}, Kathryn V. Papp^{2,4,6}, David H. Salat^{2,3,5}, Dorene M. Rentz^{2,4,6}, Reisa A. Sperling^{2,4,6}, Keith A. Johnson^{1,2,6}, Jorge Sepulcre^{1,2,3}, Heidi I. L. Jacobs^{1,2,7}

¹*Gordon Center for Medical Imaging, Department of Radiology, Massachusetts General Hospital, Boston, MA 02114, USA., Boston, MA, US*

²*Harvard Medical School, Boston, MA 02115, USA., Boston, MA, US*

³*The Athinoula A. Martinos Center for Biomedical Imaging, Department of Radiology, Massachusetts General Hospital, Boston, MA 02129, USA., Boston, MA, US*

⁴*Center for Alzheimer Research and Treatment, Department of Neurology, Brigham and Women's Hospital, Boston, MA 02115, USA., Boston, MA, US*

⁵*Neuroimaging Research for Veterans Center, VA Boston Healthcare System, Boston, MA, USA, Boston, MA, US*

⁶*Department of Neurology, Massachusetts General Hospital, Boston, MA 02114, USA., Boston, MA, US*

⁷*Faculty of Health, Medicine and Life Sciences, School for Mental Health and Neuroscience, Alzheimer Centre Limburg, Maastricht University, 6200 MD Maastricht, Netherlands., Maastricht, The Netherlands*

Introduction: Misfolded tau protein, an Alzheimer's Disease (AD) hallmark, accumulates decades before the emergence of cognitive decline. Autopsy and neuroimaging studies support the locus coeruleus (LC) as an early site of tau and its contribution to disease progression. However, whether tau in LC precedes cortical tau deposition remains unclear. Understanding the topography of tau progression and the biological factors making specific neuronal systems prone to AD-related pathology is essential to target interventions appropriately. We examined the spatiotemporal relationships between LC integrity and cortical tau accumulation and its relevance to cognition.

Method: We combined longitudinal LC-integrity (T1-TSE-imaging) and tau pathology (18F-FTP-PET) data from 77 adults (Fig1A). We used whole-brain voxel-wise GLM analysis to investigate the relationship between baseline LC-integrity (inverted signal) and longitudinal tau accumulation and compared the correlation distributions in both directions. Robust regression analysis was used to examine whether the observed tau spreading pathway predicts PACC5 performance at follow-up. Using AHBA, the biological backgrounds underlying the connectomic-genetic relationships related to LC were explored using a whole-brain region-wise transcriptomic similarity analysis.

Results: Correlations between baseline LC-integrity and follow-up tau were stronger than the inverse correlations, indicative of lower LC-integrity preceding tau accumulation in MTL (Fig1B-C). Longitudinal tau accumulation in the LC-MTL axis is associated with lower cognitive performance (Fig2). Common neurogenetic profiles exist between LC and MTL/limbic regions, supporting a shared connectomic-transcriptomic substrate. The genetic profile displays specific biological functions in protein transport regulation and lipid biosynthetic processes (Fig3).

Conclusion: Our results suggest that changes in LC-integrity may occur before tau spreads into the MTL, which jointly contributes to lower cognitive performance. The neurogenetic profiles can provide a biological framework for identifying individuals more likely to be at risk for AD disease progression. Future developments could examine the intersection between amyloid and LC-related tau progression in the context of AD.

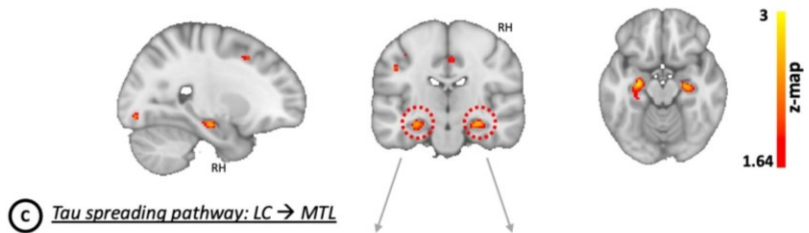
Figure 1. LC integrity predicts tau spreading in subsequent years. (A) The table summarizes the participants' demographic information, including mean values for locus coeruleus (LC) integrity, global amyloid, and cognition assessments. (B) Baseline LC integrity (inverted signal) was used as a predictor of longitudinal tau accumulation at the whole-brain voxel-wise level, finding associations between LC and bilateral hippocampus and left amygdala (p -value <0.05 cluster-corrected). (C) Each distribution represents the longitudinal relationship between LC integrity and the tau signal from the voxels within the left or the right medial temporal lobe (MTL) clusters surviving the multiple comparisons correction from the previous analysis. These distributions were compared using t-statistics. Our results support LC integrity reductions precede abnormal tau accumulation in MTL structures.

(A) Characteristics of the sample

	Baseline	Follow-up
n (% females)	77 (65%)	
Mean age (SD)	66.98 (13.09)	69.69 (7.64)
Mean years of education (SD)	15.96 (2.66)	
Mean MMSE (SD)	29.08 (1.21)	28.79 (1.17)
CDR: n = 0 n = 0.5	74 3	71 6
Mean LC integrity (SD)	1.33 (0.05)	1.30 (0.04)
Mean PIB (SD)	1.26 (0.2)	1.32 (0.23)
Mean PACC5 (SD)	0.37 (0.70)	0.28 (0.80)

Abbreviations: CDR = Clinical Dementia Rating (CDR = 0, no impairment; CDR = 0.5, questionable impairment); LC = locus coeruleus; MMSE = Mini-Mental State Examination; n = total number of individuals; PACC5 = Preclinical Alzheimer's Cognitive Composite; PIB = Pittsburgh Compound-B amyloid quantification; SD = standard deviation.

(B) Spatiotemporal relation between LC integrity and tau



(C) Tau spreading pathway: LC → MTL

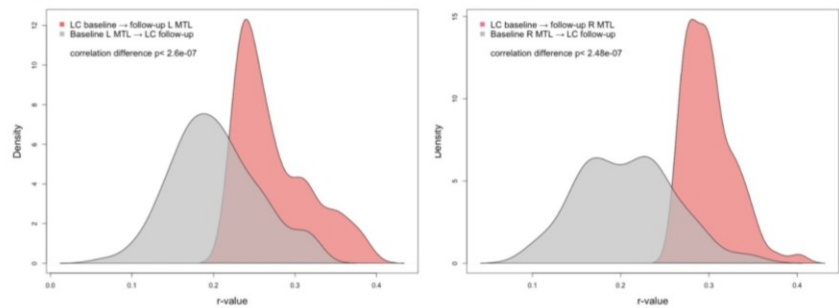
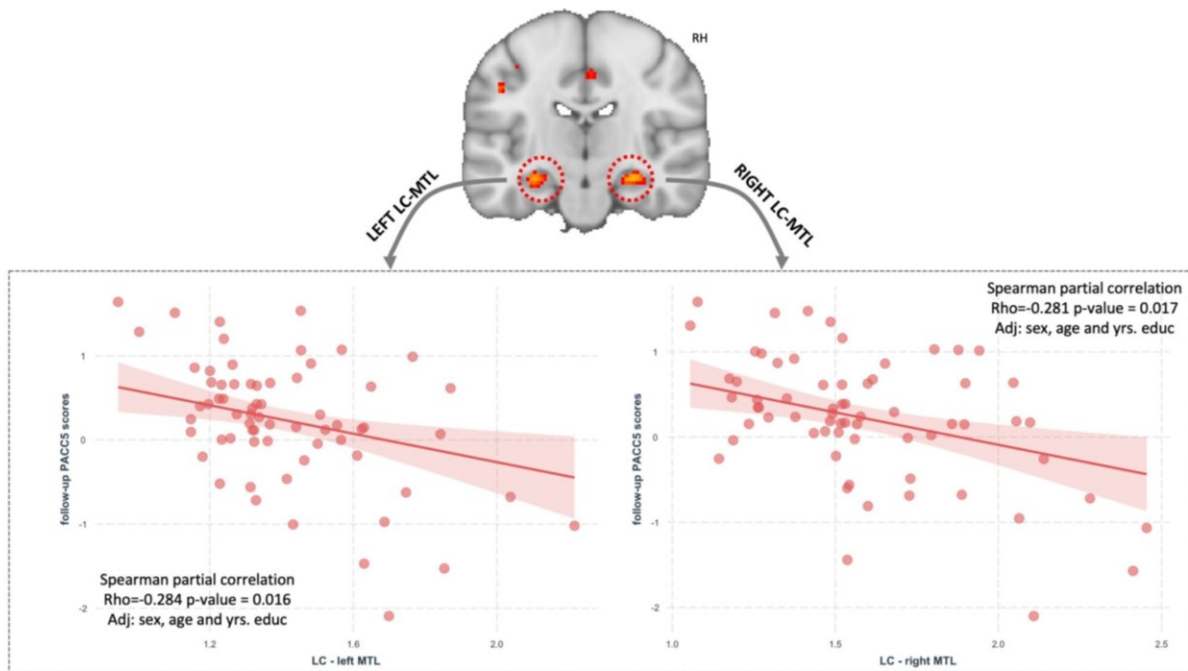
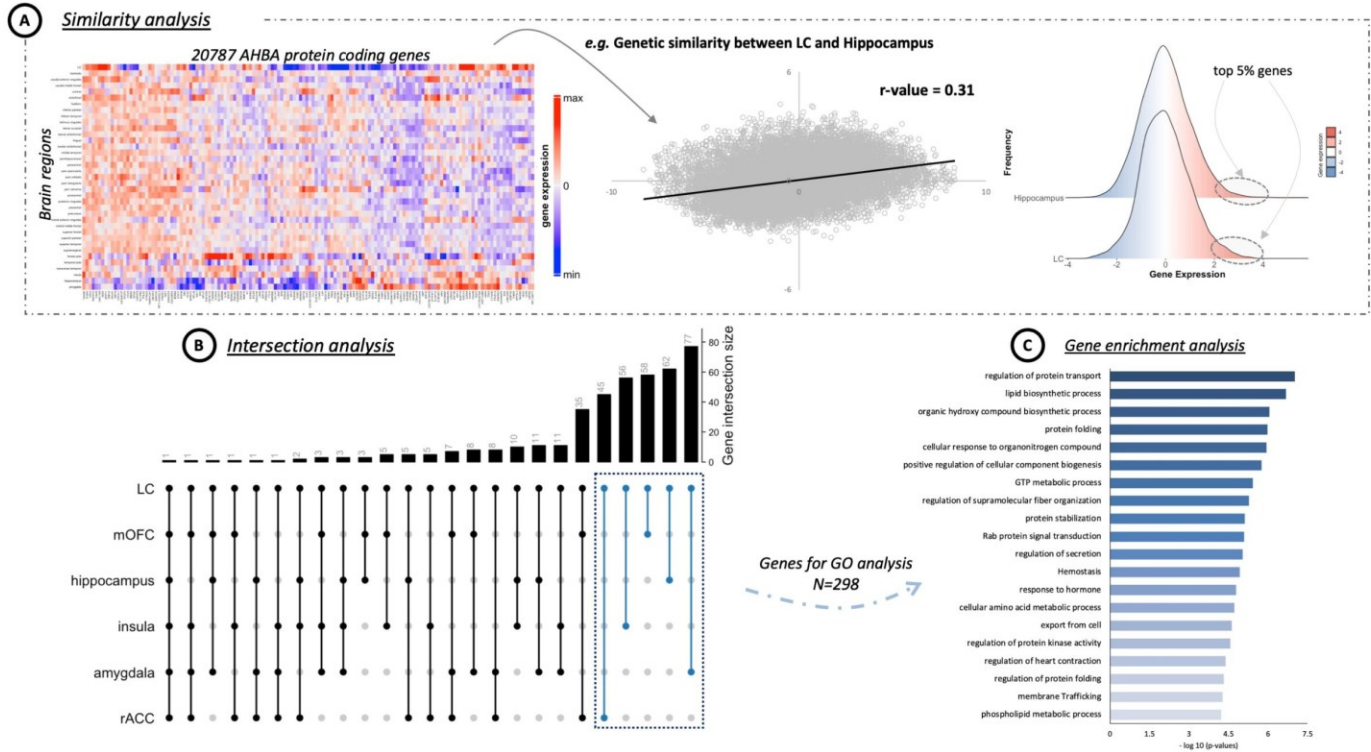


Figure 2. The decline in cognition is predicted by the biological link between LC and MTL. Evidence supports that worse locus coeruleus (LC) integrity (in baseline) predicts higher tau accumulation in the medial temporal lobe (MTL) years later, and that this biological association is accompanied by lower cognitive performance as measured by the Preclinical Alzheimer's Cognitive Composite (PACC5), which includes the Mini-Mental State Examination (MMSE), the Logical Memory Delayed Story Recall, the Digit-Symbol Substitution Test, recall from the Free and Cued Selective Reminding Test (FCSRT), and the Category Fluency Task (CAT). Note that the LC integrity signal is inverted; therefore, higher signal values indicate worse LC integrity.



The plots reflect the effect of LC-MTL in predicting follow-up PACC5 adjusting by sex, age and years of education.

Figure 3. Neurogenetic approach exploring common genetic background across the brain. (A) A whole-brain region-wise phenotypic-transcriptomic similarity analysis using the Allen Human Brain Atlas (AHBA) was conducted correlating LC to 68 regions from the Desikan-Killiany cortical parcellation, the hippocampus and the amygdala (left panel). The analysis revealed that the genetic profile of LC is similar to that of the hippocampus, amygdala, insula, medial orbitofrontal cortex (mOFC), and rostral anterior cingulate cortex (rACC) (middle panel). The genes with the highest genetic expression (top 5%) within these six regions were selected for subsequent analysis (right panel). (B) An intersection analysis was used to define common protein-coding genes between LC and each of the other regions, aggregating genes involving LC plus one region (N=298 protein-coding genes). (C) Gene ontology (GO) enrichment analysis revealed that the biological functions related to these genes – which are highly expressed in early AD-affected regions – regulate protein transport and lipid biosynthetic processes.



Keywords: Aging, Locus Coeruleus, Hippocampus, Tau-PET, Alzheimer's Disease

Tau Propagation in the Brain Olfactory Circuits Contributes to Smell Perception Changes in Aging

Ibai Diez^{1,2}, Laura Ortiz-Terán^{1,3}, Thomas Ng⁴, Mark W. Albers⁵, Gad Marshall⁶, William Orwig⁷, Chan-mi Kim¹, Elisenda Bueichekú¹, Victor Montal¹, Jonas Olofsson⁸, Patrizia Vannini^{2,6}, Georges ElFahkri¹, Reisa Sperling^{2,5,6}, Keith Johnson¹, Heidi I.L. Jacobs¹, Jorge Sepulcre^{1,2}

¹*Gordon Center for Medical Imaging, Department of Radiology, Massachusetts General Hospital, Harvard Medical School, Boston, MA, US*

²*Athinoula A. Martinos Center for Biomedical Imaging, Department of Radiology, Massachusetts General Hospital, Harvard Medical School, Charlestown, MA, US*

³*Department of Radiology, Beth Israel Deaconess Medical Center, Harvard Medical School, Boston, MA, US*

⁴*Division of Nuclear Medicine and Molecular Imaging, Department of Radiology, Massachusetts General Hospital, Harvard Medical School, Boston, MA, US*

⁵*Department of Neurology, Massachusetts General Hospital, Harvard Medical School, Boston, MA, US*

⁶*Department of Neurology, Brigham and Women's Hospital, Harvard Medical School, Boston, MA, US*

⁷*Harvard University, Department of Psychology, Cambridge, MA, US*

⁸*Stockholm University, Department of Psychology, Stockholm, Sweden*

The prompt and direct access of the olfactory afferents to memory-related cortical systems has inspired theories about the potential role of the olfactory systems as an entry point for infectious or environmental agents triggering cortical neurodegeneration. Postmortem studies have repeatedly shown neurofibrillary tangles in the olfactory system at early preclinical stages of Alzheimers disease (AD), leading to olfactory deficits in AD patients, years before cognitive symptoms appear. While some views propose that pathological aggregates reach the olfactory system from the brainstem and medial temporal lobe (MTL), there are also hypotheses suggesting a primary implication of the olfactory organs, from where a later pathology spreading occurs toward the MTL. In this study, we used longitudinal flortaucipir PET, diffusion MRI, and olfaction identification measures of 89 cognitively normal older adults (age 73.82±8.44; 56% females) to investigate the role of the olfactory system in tau progression and to evaluate olfactory measure as a proxy for tau spreading in the brain. We observed that odor identification deficits were associated with aging, cognitive decline, brain atrophy, and tau accumulation (Fig1). Our results suggest a secondary role of the olfactory system derived from tau spreading from MTL, as well as evidence for the strong predictive power of olfactory measures in the characterization of the longitudinal progression of tau (Fig2). Additionally, a link between odor perception-related genes and tau was found, including the identification of genes affecting both olfaction and different domains of AD pathology (Fig3): tau, amyloid, cognition decline, atrophy, etc. This study offers several new observations regarding the relationship between odor discrimination changes, neurodegeneration, genetics, and tau spreading pathways in the olfactory system during aging. While olfactory measures have been observed to predict tau progression strongly, more research will be needed to understand better the genetic intersection between the olfactory system and tau spreading.

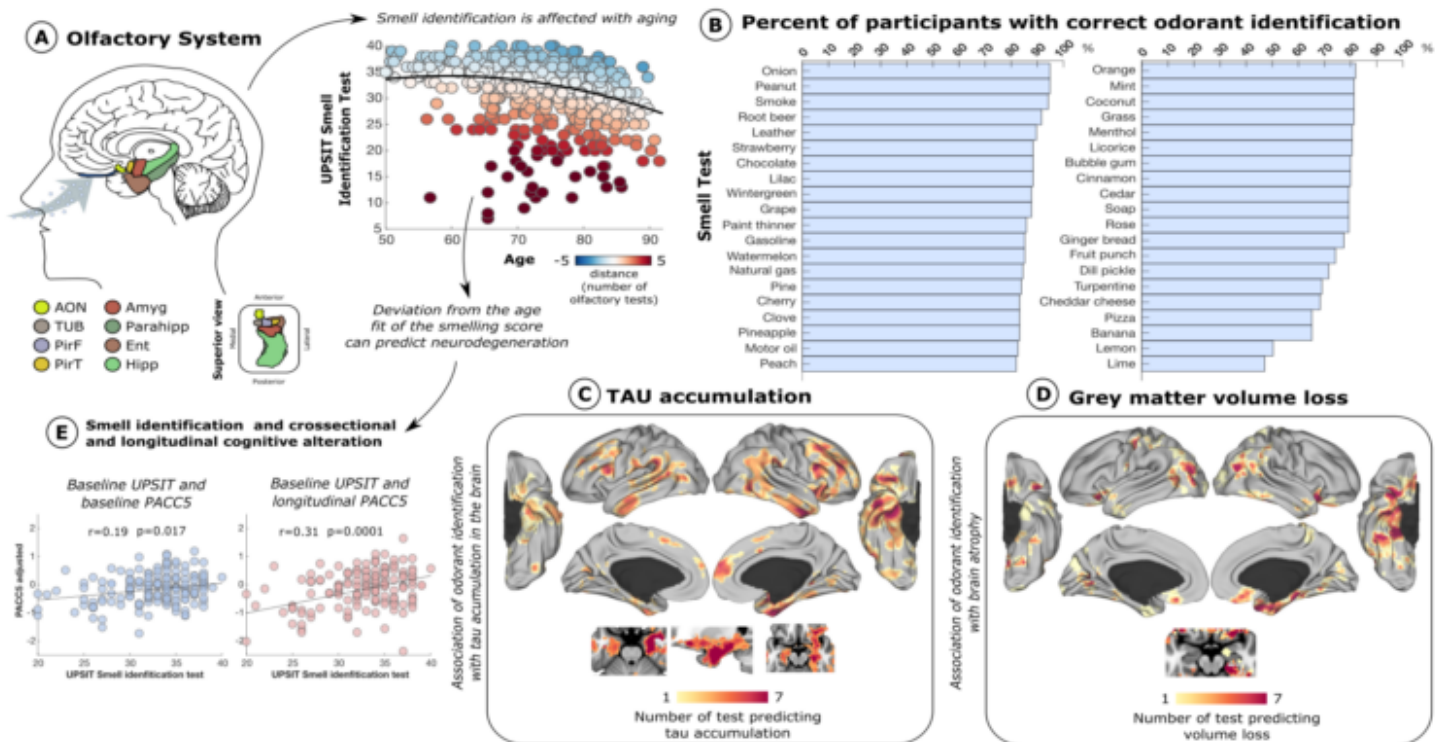


Fig. 1 | Olfactory system disfunction in healthy aging and its association to neurodegeneration. (A) Primary olfactory regions of the brain and smell identification ability in healthy aging are displayed. The colors in the scatterplot represents the deviation of the estimated smell identification test of each participant based on their age. (B) Sorted bar plot of the percentage of participants correctly identifying the 40 odorants composing UPSIT test. (C,D) Amount of odorants able to distinguish high accumulation of tau and atrophy at voxel level. (E) Association between smell identification at baseline and cognitive performance both at baseline and after ~ 2.5 years. AON - anterior olfactory nucleus, TUR - olfactory tubercle, PirF - frontal piriform cortex, PirT - temporal piriform cortex, Ent - entorhinal, Amyg – amygdala, and Hipp – hippocampus.

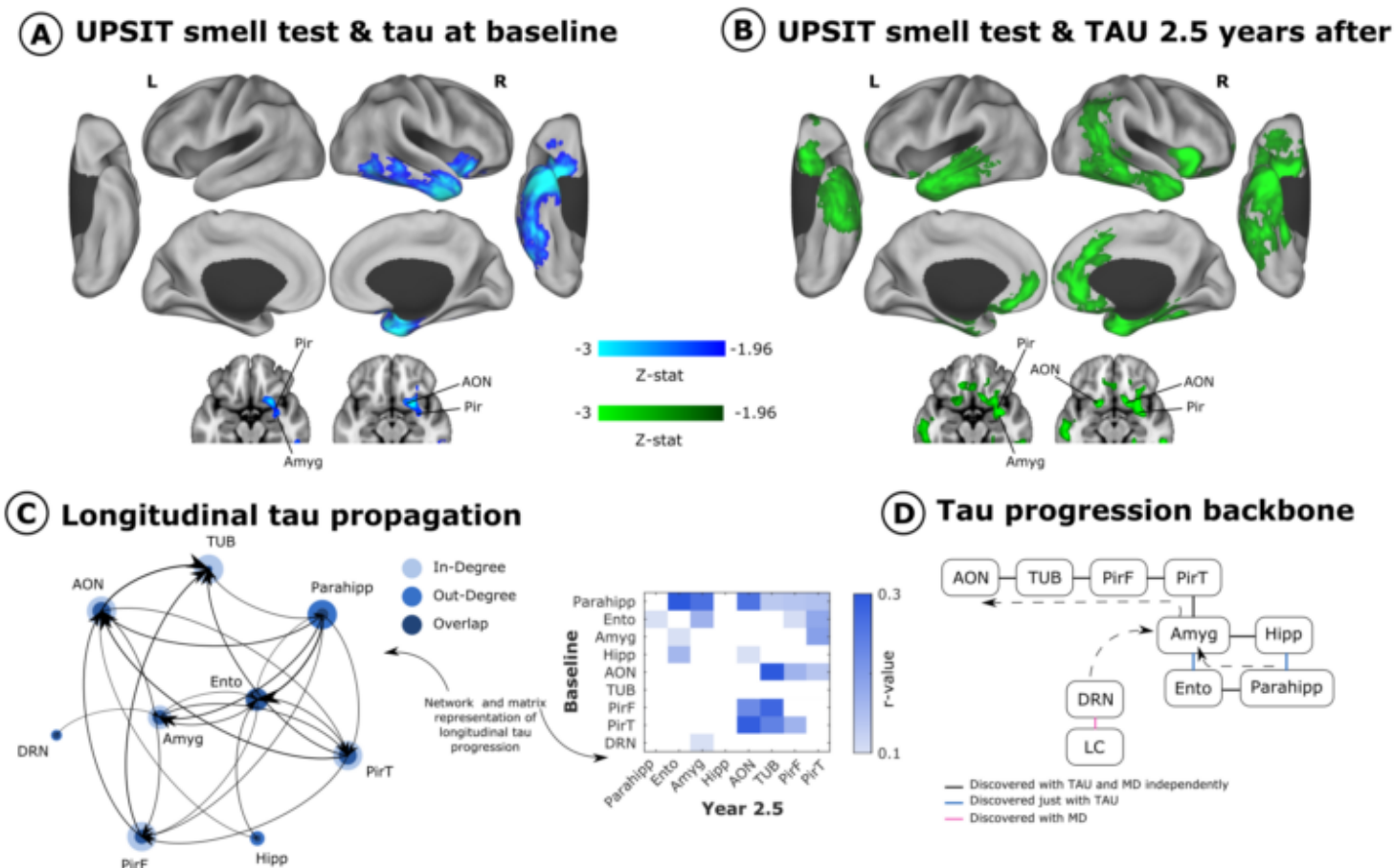


Fig. 2 | Smell identification test association with tau accumulation and spreading. (A) Z-stat of the association between UPSIT smell identification test with baseline tau deposition. (B) Z-stat of the association between baseline UPSIT smell identification test and tau accumulation ~2.5 years after. Only results surviving to multiple comparisons are displayed. (C) Bipartite graph between baseline and longitudinal tau accumulation showing a progression of tau from medial temporal regions towards the olfactory system. Mean diffusivity (MD) of the dorsal raphe nucleus was also included. The node size represents the weighted degree, amount of out and in tau. (D) Tau progression backbone between olfactory and medial temporal regions computed with conditional independent testing. Arrows were drawn based on directionality results obtained from bipartite longitudinal graph.

AHBA based gene co-expression groups of sensory perception of smell (390 genes)

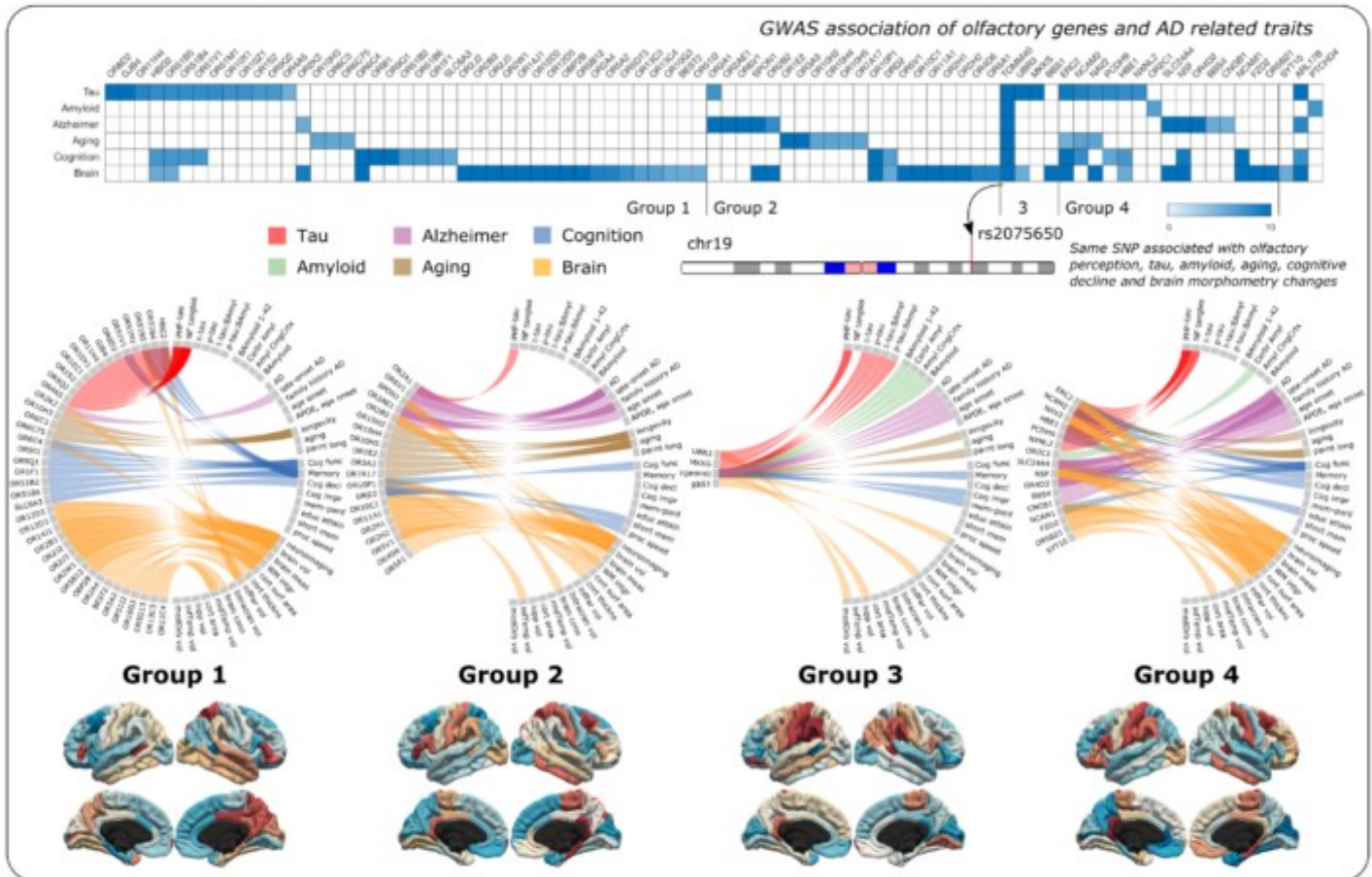
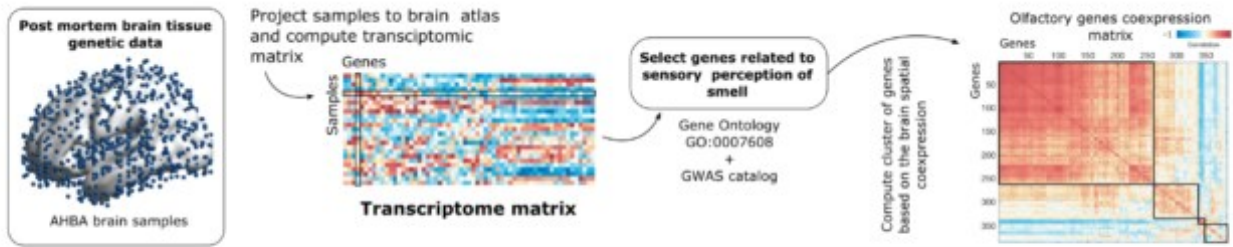


Fig. 3 | Co-expression of genes related to olfactory perception and associated neurodegenerative traits. Allen Human Brain transcriptome Atlas was projected to Desikan cortical parcellation and the spatial brain co-expression between 390 genes annotated as sensory perception of smell was computed. Using hierarchical clustering 4 groups of genes with similar co-expression were identified. Genecard Suite was used to compute bipartite networks associating olfactory genes with traits related to neurodegeneration. For each group a circular diagram is shown with the associations and their mean brain expression. These associations were classified in 5 domains: tau, amyloid, Alzheimer, aging, cognition, and brain morphometry. For visualization purposes the brain maps of the mean expression of each cluster where z-scored separately for each hemisphere. A matrix representing the association of each gene with each domain is also displayed.

Keywords: Olfactory system, Tau Spreading, Aging, Alzheimer's disease

Medial temporal lobe subregional microstructure measured with ultra-high resolution diffusion imaging as a biomarker for early tau pathology and memory impairment

Jenna Adams¹, Steven Granger¹, Lisa Taylor¹, Soyun Kim¹, Theresa Harrison², Alyssa Harris¹, Liv McMillan¹, Luis Colon-Perez¹, David Keator¹, Michael Yassa¹

¹University of California, Irvine, Irvine, CA, US

²University of California, Berkeley, Berkeley, CA, US

Background: Detecting the earliest consequences of tau pathology on neuronal integrity is critical to understanding how tau leads to memory decline. Here, we applied novel ultra-high-resolution diffusion MRI (dMRI) to test whether cellular integrity of gray matter within medial temporal lobe (MTL) subregions, measured with mean diffusivity (MD), is related to tau pathology and memory in cognitively normal older adults (OA).

Method: Twenty-three OA (70.3 ± 6.6 years, 57% female) from the Biomarker Exploration in Aging, Cognition, and Neurodegeneration (BEACoN) study received ultra-high-resolution dMRI (Zoomit scans focused on MTL; $0.67 \times 0.67 \times 3$ mm) and 18F-MK6240-PET to measure tau pathology. MD maps were generated from dMRI using FSL DTIfit. High-resolution T1- and T2-weighted MRIs were processed with Automated Segmentation of Hippocampal Subfields (ASHS) to extract hippocampal subfield and MTL ROIs for MD and volume. Mean 18F-MK6240 SUVR (90-110 min, inferior cerebellar gray reference) was quantified for entorhinal cortex (EC) and hippocampus. Correlations between imaging biomarkers and object mnemonic discrimination performance were examined, controlling for age, sex, education, and PET-MRI interval.

Results: Increased EC MK6240 SUVR was strongly associated with increased MD within EC ($r=0.61, p=0.004$) and transentorhinal cortex ($r=0.72, p<0.001$). Increased hippocampal MK6240 SUVR was associated with increased dentate gyrus (DG) MD ($r=0.64, p=0.003$; Fig1A). These associations persisted when controlling for regional volume ($p<0.02$). Volume was not correlated with MK6240 SUVR except in EC (Fig1B). Increased MK6240 SUVR in EC and hippocampus was associated with worse mnemonic discrimination ($p<0.05$, Fig2A). In DG and CA3, increased MD (Fig2B), but not volume (Fig2C), was associated with worse mnemonic discrimination.

Conclusions: Increased MD, reflecting less restricted diffusion within gray matter and possibly decreased cellularity, is strongly associated with tau pathology and hippocampal memory deficits in OA, even in the absence of frank volume loss. Our preliminary findings suggest MD may be a more sensitive biomarker of early neurodegeneration than traditional volume measures.

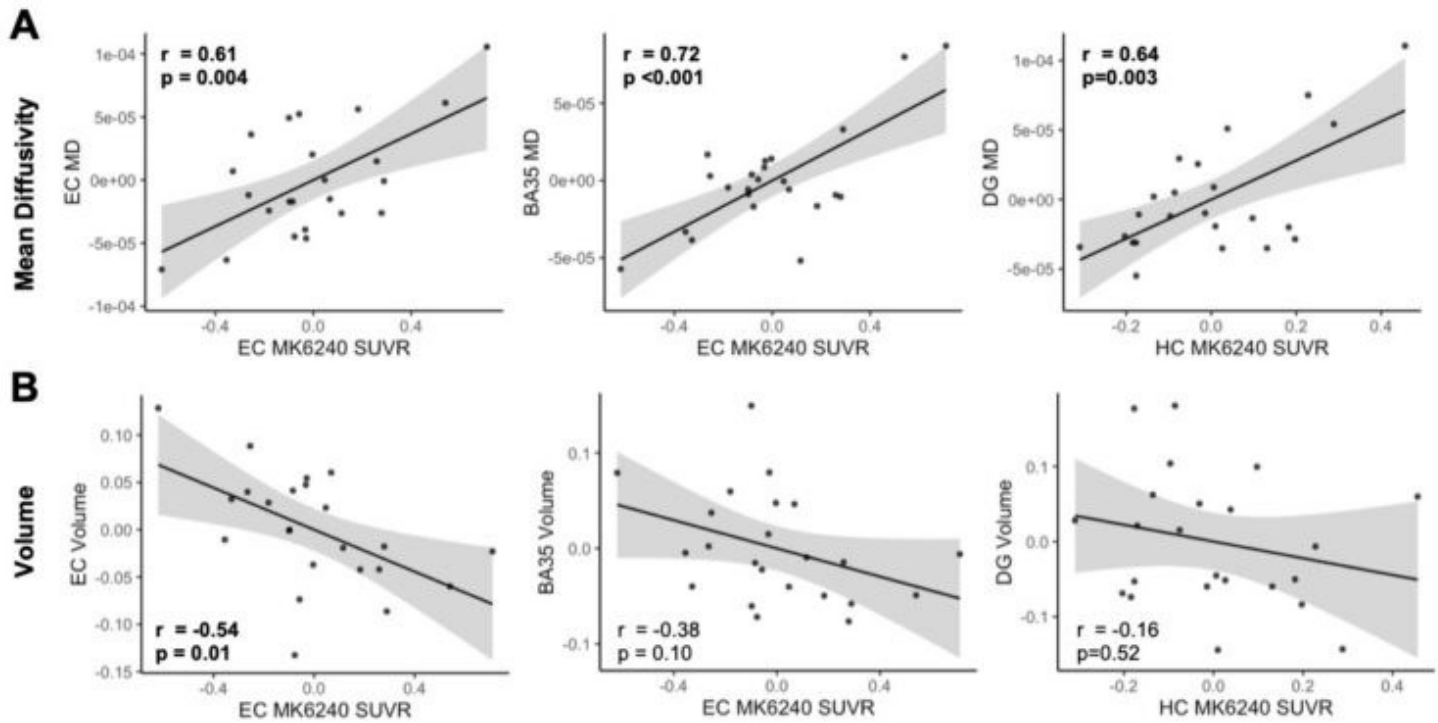


Figure 1. Relationships between tau pathology (18F-MK6240 SUVR) and regional measures of mean diffusivity (MD) and volume. (A) Higher MK6240 SUVR in entorhinal cortex (EC) was strongly associated with greater MD in EC and transentorhinal cortex (BA35), while higher MK6240 SUVR in hippocampus (HC) was strongly associated with higher MD within dentate gyrus (DG), reflecting decreased cellularity of these regions. **(B)** Regional volumes were normalized by total intracranial volume. Relationships between MK6240 SUVR and volume of BA35 and DG were not significant, while the relationship between EC MK6240 SUVR and EC MD was significant though not as strong as with MD. Controlling for volume, all associations between MK6240 SUVR and MD remained significant ($p < 0.02$). All associations controlled for age, sex, and time between PET and diffusion scans. Scatter plots represent the residual values.

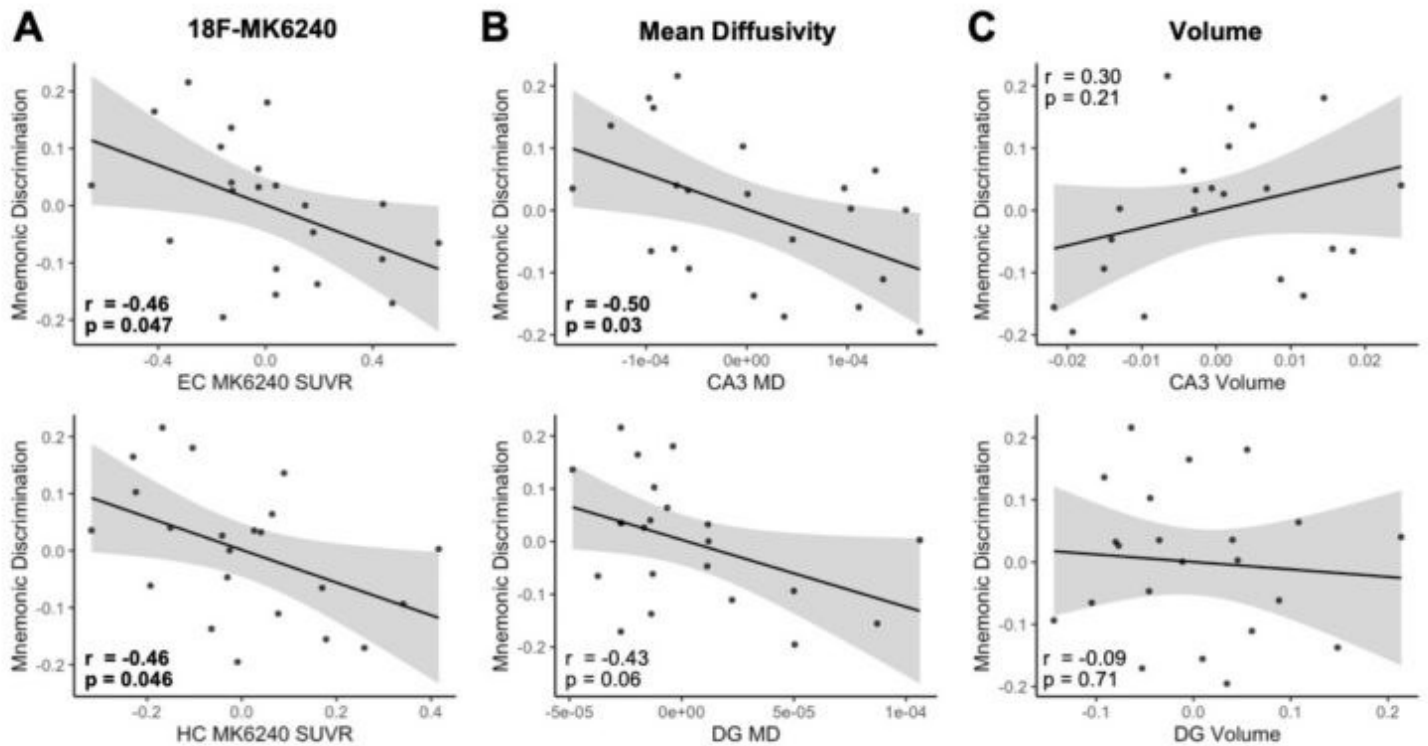


Figure 2. Relationships between mnemonic discrimination, tau pathology (18F-MK6240 SUVR) and structural measures of regional integrity. Cognitively normal older adult participants performed an object mnemonic discrimination task, reflecting hippocampal pattern separation ability in dentate gyrus (DG)/CA3, that probed their ability to distinguish between highly similar lure stimuli and exact repeats of stimuli. The lure discrimination index was used as the outcome measure. **(A)** Higher MK6240 SUVR in entorhinal cortex (EC) and hippocampus (HC) was associated with worse mnemonic discrimination performance. **(B)** Worse mnemonic discrimination performance was associated with higher mean diffusivity (MD), reflecting decreased cellularity, in CA3 and a trend-level relationship in DG, two regions critical for pattern separation. **(C)** Traditional measures of regional volume, normalized for intracranial volume, did not show associations with mnemonic discrimination performance. All associations controlled for age, sex, and education. Scatter plots represent the residual values.

Keywords: tau, mean diffusivity, diffusion imaging, medial temporal lobe, memory

Thursday, January 12, 2023 - 03:00 pm - 03:45 pm

KEYNOTE: On making neuroimaging studies more equitable, inclusive, and relevant

Monica Rivera-Mindt

Fordham University

Thursday, January 12, 2023 - 04:30 pm - 05:20 pm

Podium Session

SESSION VIII: Lifestyle and lived experiences

Thursday, January 12, 2023

4:30 pm – 5:20 pm	SESSION VIII: LIFESTYLE AND LIVED EXPERIENCES	CHAIRS: Gil Rabinovici, MD, <i>University of California, San Francisco</i> Tobey Betthausen, PhD, <i>University of Wisconsin-Madison</i>
4:30	Introduction	Chairs
4:35	African American racialization modifies the association between apolipoprotein-E4 and amyloid deposition	Sarah Royse, PhD, University of Pittsburgh
4:50	Cardiovascular risk and AD biomarkers in unimpaired older adults: A comparison of U.S. POINTER and ADNI	Susan Landau, PhD, University of California, Berkeley
5:05	Association between mid-life social factors and estimated late life amyloid burden: the Atherosclerosis Risk in Communities (ARIC)-PET study	Renee Groechel, PhD, NINDS
5:30	Discussion	

African American racialization modifies the association between apolipoprotein-E4 and amyloid deposition

Sarah Royse^{1,2}, Beth Snitz³, Alexandria Reese², Rebecca Roush³, Ilyas Kamboh^{4,5}, Brian Lopresti², Oscar Lopez^{3,4}, James Becker^{3,4,6}, Ann Cohen⁴

¹Department of Epidemiology, University of Pittsburgh, Pittsburgh, PA, US

²Department of Radiology, University of Pittsburgh, Pittsburgh, PA, US

³Department of Neurology, University of Pittsburgh, Pittsburgh, PA, US

⁴Department of Psychiatry, University of Pittsburgh, Pittsburgh, PA, US

⁵Department of Human Genetics, University of Pittsburgh, Pittsburgh, PA, US

⁶Department of Psychology, University of Pittsburgh, Pittsburgh, PA, US

Introduction: The apolipoprotein (*APOE*)**E4* and *APOE***2* alleles confer comparatively attenuated risk and protection, respectively, of clinical Alzheimer's disease (AD) in African Americans (AA) versus non-Hispanic whites (nHW). It is unknown if this is also reflected in AD pathological burden. We tested differences between AA and nHW in the associations of *APOE***4* and *APOE***2* alleles with [¹¹C]Pittsburgh Compound-B (PiB) and [¹⁸F]Flortaucipir (FTP) standardized uptake value ratios (SUVRs).

Methods: We collected blood samples, PiB scans, and T1 MRIs in 148 AA (63.8 ± 8.54 years, 105F/43M) and 204 nHW (69.5 ± 8.59 years, 121F/83M) participants ranging from cognitively normal to AD. We also collected FTP scans in a subset of 38 AA (73.7 ± 4.05 years, 30F/8M) and 92 nHW (73.5 ± 4.96 years, 56F/36M) participants. MRIs were processed using FreeSurfer v7.1 to sample PET images for calculating composite SUVRs for global PiB and medial temporal FTP. Two-site *APOE* polymorphisms were determined using TaqMan assays. Associations of *APOE***4* and *APOE***2* alleles with PiB SUVR and FTP SUVR were tested in linear models stratified by racialized group, controlling for age, sex, and education; if stratified results differed, we tested allele-by-racialized group interactions. We repeated analyses excluding participants aged <65 years.

Results: Compared to nHW, AA had a higher proportion of both *APOE***4* (p=0.03) and *APOE***2* (p=0.02) carriers and exhibited lower PiB SUVRs (p<0.0001). *APOE***4* was significantly associated with higher PiB SUVR in nHW (β=0.30, p<0.0001), but not in AA (β=-0.0008, p=0.96); *APOE***4* allele-by-racialized group interaction was significant (p=0.0002). In contrast, neither *APOE***4* nor *APOE***2* was associated with FTP SUVR in AA (p≥0.29) or nHW (p≥0.09). Excluding participants <65 years did not change results.

Conclusions: The association of *APOE***4* with Aβ deposition differs between AA and nHW. These results suggest that current understanding of AD pathophysiology may not be generalizable to AA populations.

Keywords: *APOE*, amyloid, tau, racialization

Cardiovascular risk and AD biomarkers in unimpaired older adults: A comparison of U.S. POINTER and ADNI

Susan Landau¹, Theresa Harrison¹, Tyler Ward¹, Robert Koeppe², Suzanne Baker³, Prashanthi Vemuri⁴, Samuel Lockhart⁵, Danielle Harvey⁶, Youngkyoo Jung⁶, Laura Lovato⁵, Arthur Toga⁷, Joseph Masdeu⁸, Hwamee Oh⁹, Darren Gitelman¹⁰, Neelum Aggarwal¹¹, Heather Snyder¹², Laura Baker⁵, Charles DeCarli⁶, William Jagust¹

¹University of California, Berkeley, Berkeley, CA, US

²University of Michigan, Ann Arbor, MI, US

³Lawrence Berkeley National Laboratory, Berkeley, CA, US

⁴Mayo Clinic, Rochester, MN, US

⁵Wake Forest School of Medicine, Winston-Salem, NC, US

⁶University of California, Davis, Davis, CA, US

⁷University of Southern California, Los Angeles, CA, US

⁸Houston Methodist, Houston, TX, US

⁹Brown University, Providence, RI, US

¹⁰Advocate Aurora Health, Chicago, IL, US

¹¹Rush University Medical Center, Chicago, IL, US

¹²Alzheimer's Association, Chicago, IL, US

A key focus of the U.S. Study to Protect Brain Health Through Lifestyle Intervention to Reduce Risk (U.S. POINTER) is enrollment of unimpaired older individuals with characteristics that increase risk for memory decline (e.g. sedentary lifestyle, suboptimum diet, family history of memory impairment, hypertension), and a subset of individuals undergo PET and MRI. Here, we compared currently enrolled U.S. POINTER neuroimaging participants (N=544, ~54% of the anticipated sample) to a comparable subsample from the Alzheimer's Disease Neuroimaging Initiative (N=388) at baseline in order to investigate how greater at-risk characteristics in U.S. POINTER influence cardiovascular risk (Framingham risk score (FRS)), biomarkers (amyloid/tau PET, hippocampal volume, and white matter hyperintensities (WMH)), and cognition.

U.S. POINTER imaging participants were younger than those in ADNI (68.6+/-5.0yrs vs 70.7+/-4.4yrs), more likely to be female (65% vs 58%) and from under-represented groups (27% vs 15%), and had lower education (14.7+/-3.3yrs vs 16.7+/-2.3yrs). Controlling for these variables, the cohorts did not differ on FRS, systolic blood pressure, amyloid, or WMH, but POINTER had higher body mass indices (BMI), and poorer cognitive status (global CDR, CDRsb), while ADNI had more hippocampal atrophy and greater likelihood of abnormal temporal tau (Table). Although associations between FRS, amyloid, tau, and cognition were similar overall between cohorts, high FRS in ADNI was associated with temporal tau positivity, whereas the reverse relationship was observed for POINTER (p=0.02; Figure). In addition, elevated temporal tau (but not FRS) was associated with poorer CDRsb in ADNI, whereas in POINTER, higher FRS (but not tau) was associated with poorer CDRsb (cohort X tau status; p=0.05).

Despite substantial differences in recruitment and enrollment criteria, POINTER and ADNI did not differ on amyloid or cardiovascular risk measures, but did differ on tau and cognition. Future research will examine how complex inter-relationships between risk factors and biomarkers may influence cognition.

	US POINTER imaging	ADNI	cohort difference	
N	544	388		
Age (yrs)	68.6+/-5.0	70.7+/-4.4	*	
Sex (%female)	66%	58%	*	
Education (yrs)	14.7+/-3.3	16.7+/-2.3	*	
Non-white race (%)	27%	15%	*	
Global CDR 0.5 (%)	21%	8%	*	
CDR sum of boxes	0.20 +/- 0.35	0.12 +/- 0.33	*	
Cardio-vascular risk	Body mass index	29.9 +/- 5.3	28.0 +/- 5.5	*
	Systolic blood pressure	131 +/- 16	133 +/- 16	
	Framingham risk score	16.2 +/- 3.6	16.5 +/- 3.7	
Biomarkers	Amyloid PET (CL)	17 +/- 25	21 +/- 29	
	Amyloid PET (% positive)	29%	34%	
	Entorhinal tau (% positive)	18%	15%	
	Temporal tau (% positive)	14%	23%	*
	White matter hyperintensities (adj)	1.00 +/- 0.69	1.03 +/- .79	
	Hippocampal volume, mm3 (adj)	8092 +/- 698	7765 +/- 766	*

Table. Significant differences between POINTER and ADNI (adjusted for age, sex, and education for risk and biomarker variables) are shown.

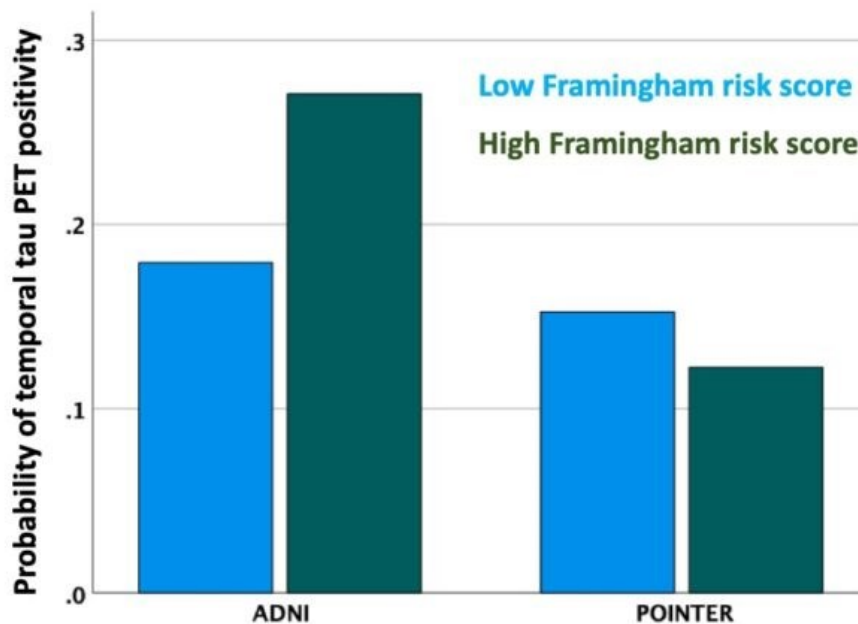


Figure. Logistic regression model results are shown illustrating a cohort X FRS status interaction ($p=0.02$) such that higher FRS was associated with greater likelihood of positive temporal tau status in ADNI while the reverse was true in POINTER. Model results were adjusted for age, sex, and education, and amyloid. Abnormal amyloid was associated with a greater likelihood of positive temporal tau status in both cohorts (not shown), but amyloid did not influence the relationship between FRS and tau for either cohort.

Keywords: cardiovascular risk, amyloid, tau, lifestyle

Association between mid-life social factors and estimated late life amyloid burden: the Atherosclerosis Risk in Communities (ARIC)-PET study

Renee C. Groechel¹, Silvia Koton^{2,3}, Anna M. Kucharska-Newton⁴, Pamela L. Lutsey⁵, Thomas H. Mosley Jr.⁶, Priya Palta⁷, A. Richey Sharrett³, Keenan A. Walker⁸, Dean F. Wong⁹, Rebecca F. Gottesman¹

¹National Institute of Neurological Disorders & Stroke Intramural Research Program, National Institutes of Health, Bethesda, MD, US

²Department of Nursing, The Stanley Steyer School of Health Professions, Tel Aviv University, Tel Aviv, IL

³Department of Epidemiology, Johns Hopkins University School of Public Health, Baltimore, MD, US

⁴Department of Epidemiology, University of North Carolina Gillings School of Global Public Health, Chapel Hill, NC, US

⁵Division of Epidemiology and Community Health, University of Minnesota School of Public Health, Minneapolis, MN, US

⁶Department of Medicine, University of Mississippi Medical Center, Jackson, MS, US

⁷Department of Neurology, University of North Carolina at Chapel Hill, Chapel Hill, NC, US

⁸National Institute on Aging Intramural Research Program, National Institutes of Health, Baltimore, MD, US

⁹Department of Radiology, Washington University, St. Louis, MO, US

Introduction: Research has shown social engagement is beneficial to longevity and well-being in older adults. However, the mechanism by which social engagement may impact Alzheimer's disease progression in later life is unclear. Because we believe social engagement is more likely to influence cognitive performance and not underlying disease pathogenesis, we proposed there would *not* be an association between measures of social support and isolation in mid-life with late life brain amyloid deposition, measured using florbetapir positron emission tomography (PET).

Methods: Data from 316 non-demented participants were collected from the Atherosclerosis Risk in Communities (ARIC)-PET study. Social support and isolation were evaluated categorically by interviews (Visit 2; 1990 – 1992). Brain amyloid was evaluated with florbetapir PET (Visit 5; 2011-2013). Elevated amyloid burden was defined as standardized uptake value ratio (SUVR) > 1.2 in the global cortex. Logistic regression models were used to assess the independent associations of social support and isolation, each, with elevated SUVR. Models were adjusted for demographics, ApoE4 status, marital/occupational status, and vascular risk factors (all measured at visit 2). Formal tests to assess whether sex or race modified the association between each social factor and SUVR were conducted with interaction terms.

Results: Intermediate/low social support and moderate risk of isolation, compared to high social support and low risk of isolation, were each respectively associated with lower odds of elevated SUVR after adjusting for covariates. There was no evidence for effect modification by sex or race.

Conclusion: In this cohort of non-demented older adults, unexpectedly, intermediate/low levels of social support and moderate risk of isolation were each associated with lower odds of elevated brain amyloid. Associations were independent of potential confounders. Further studies evaluating social engagement in mid-life are needed to strengthen our understanding as to how selection bias and survivorship may influence findings from longitudinal studies.

Table 1. Adjusted Odds Ratios for Association of Mid-Life Social Support and Social Isolation with Elevated Amyloid Burden (Global Cortex Florbetapir SUVR > 1.2) (n = 316)

	Model 1 OR (95% CI)	Model 2 OR (95% CI)	Model 3 OR (95% CI)
Social Support (ISEL-SF)			
High (Score ≥ 42) n = 103	Reference	Reference	Reference
Intermediate (Score 36 - 41) n = 109	0.46 (0.25 – 0.84)*	0.46 (0.25 – 0.85)*	0.44 (0.23 – 0.82)**
Low (Score ≤ 35) n = 104	0.41 (0.22 – 0.77)**	0.41 (0.22 – 0.77)**	0.38 (0.20 – 0.74)**
Social Isolation (Lubben Social Network Scale)			
Low risk (Score ≥ 31) n = 257	Reference	Reference	Reference
Moderate risk (Score 26 - 30) n = 39	0.37 (0.17 – 0.81)*	0.34 (0.15 – 0.77)**	0.28 (0.12 – 0.67)**
High risk (Score 21 – 25) n = 13	0.66 (0.20 – 2.17)	0.64 (0.19 - 2.17)	0.52 (0.14 – 1.93)
Isolated (Score ≤ 20) n = 7	1.85 (0.36 - 9.59)	1.84 (0.35 - 9.55)	1.37 (0.28 - 6.87)

* $P \leq 0.05$; ** $P \leq 0.01$. Abbreviations: CI = confidence interval; ISEL-SF = Interpersonal Support Evaluation List-Short Form; OR = odds ratio; SUVR = standardized uptake value ratio

The ISEL-SF was used to assess social support and is scored 0-48 with higher scores indicating greater social support. The Lubben Social Network Scale was used to measure social isolation and is scored 0-50 with higher scores indicating a lower risk of isolation. Categorical distributions (tertiles for ISEL-SF and quartiles for Lubben Social Network Scale) were based upon cut-offs commonly used in the literature. Model 1 adjusted for age, race, sex, APOE ε4 status (carrier vs non-carrier), and education level; model 2 adjusted for model 1 covariates, occupational status (employed outside the home vs not), and marital status (married vs not married); model 3 adjusted for model 2 covariates and vascular risk factors (hypertension, obesity, total cholesterol, diabetes, and current drinking/smoking status).

Keywords: amyloid, social support, isolation, cognitive reserve, PET

Friday, January 13, 2023 - 09:00 am - 10:20 am

Podium Session

SESSION IX: Longitudinal change in tau and amyloid markers

Friday, January 13, 2023		
9:00 am – 10:20 am	SESSION IX: LONGITUDINAL CHANGES IN TAU AND AMYLOID MARKERS	CHAIRS: Keith Johnson, MD, Massachusetts General Hospital William Jagust, MD, University of California, Berkeley
9:00	Introduction	Chairs
9:05	Longitudinal tau accumulation is associated with faster memory decline in typical aging and preclinical Alzheimer's disease	Corrina Fonseca, PhD, <i>University of California, Berkeley</i>
9:20	The use of plasma markers to predict tau accumulation in a stage-specific manner	Cécile Tissot, PhD, <i>McGill University</i>
9:35	Temporal dynamics of plasma pTau217 and amyloid PET in preclinical AD	Karly Cody, PhD, <i>University of Wisconsin-Madison</i>
9:50	Longitudinal changes in Alzheimer's disease-related plasma biomarkers in relation to changes in PiB PET measures of brain amyloid	Murat Bilgel, PhD, <i>NIA</i>
10:05	Longitudinal bidirectional associations between sleep and Alzheimer's pathology in At-Risk Cognitively Unimpaired Older Adults	Bery Mohammediyan, MSc, <i>McGill University</i>
10:20	Discussion	

Longitudinal tau accumulation is associated with faster memory decline in typical aging and preclinical Alzheimer's disease

Corrina S. Fonseca¹, Suzanne L. Baker², William J. Jagust¹, Theresa M. Harrison¹

¹Helen Wills Neuroscience Institute, University of California, Berkeley, Berkeley, CA, US

²Lawrence Berkeley National Laboratory, Berkeley, CA, US

Background: Cross-sectional tau has been linked to brain and cognitive outcomes in cognitively normal older adults. Here we used longitudinal data to investigate the relationships between change in tau, amyloid, brain structure, and memory.

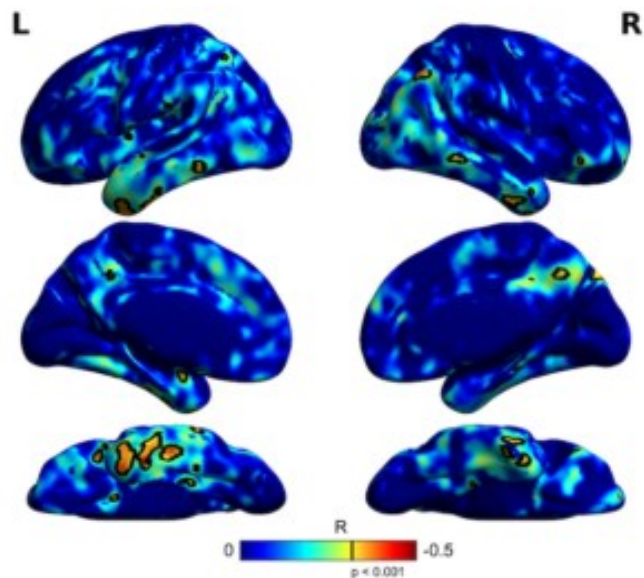
Methods: 78 cognitively normal older adults (age = 76.1 ± 5.6) underwent longitudinal FTP, PiB PET, structural MRI, and cognitive assessment. Longitudinal slopes for each measure were estimated using linear mixed effects models. Voxel-wise FTP slope maps were generated to explore whole-brain associations with structure and memory. ROIs included the entorhinal cortex (EC), a temporal meta-ROI (meta-ROI), and hippocampal volume. Elastic net regression was used to select the best predictors of memory decline and the relationships were subsequently plotted using linear models. Analyses were performed using the whole cohort and within PiB- and PiB+ groups separately.

Results: Faster memory decline was associated with greater voxel-wise FTP slope in temporal and parietal regions, with significant clusters across the whole cohort and within PiB- and PiB+ groups separately (Figure 1). Elastic net regression models predicting memory decline selected higher EC FTP slope and lower meta-ROI thickness slope across all groups, whereas higher meta-ROI FTP slope and PiB slope were only selected in groups containing PiB+ subjects (Figures 2 & 3). FTP (regional or voxel-wise) was not associated with regional cortical thickness slope or volume slope.

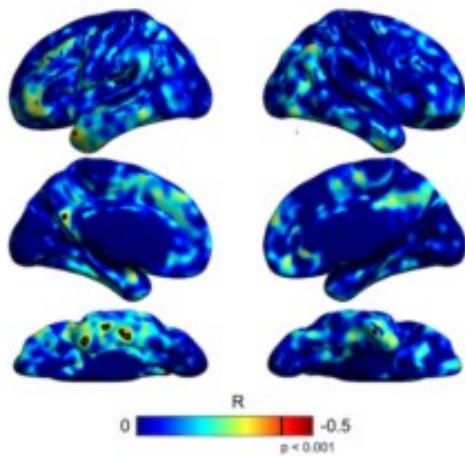
Conclusions: In typical aging (PiB-), longitudinal EC tau accumulation & neocortical thinning predicted memory decline; in preclinical AD (PiB+), memory decline was also associated with greater neocortical tau and global amyloid accumulation. The relationship between longitudinal tau and memory decline in both typical aging and preclinical AD was robust to analytical method. Our results suggest potential shared (EC tau accumulation & cortical thinning) and differential (neocortical tau & amyloid accumulation) mechanisms of memory decline in typical aging and preclinical AD.

A.

Full Group
n = 78

**B.**

PiB-
n = 44

**C.**

PiB+
n = 34

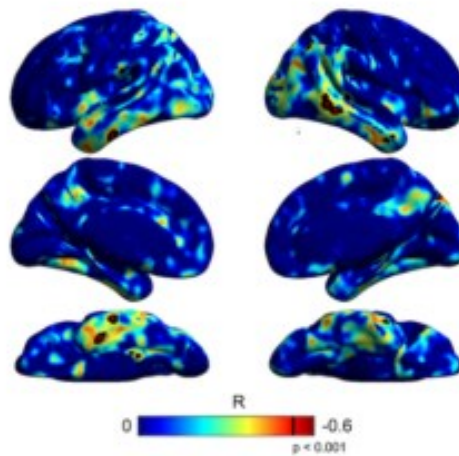



Figure 1. Voxel-wise relationships between memory slope & FTP slope. Significant clusters of higher voxel-wise FTP slope emerged in bilateral inferior & lateral temporal & right medial & inferior parietal regions as associated with faster memory decline in the full group (A). Smaller but significant clusters in the lateral & inferior temporal regions emerged in groups subset by baseline PiB status (threshold PiB DVR=1.065). Significant clusters in PiB+ group were larger than in the PiB- group (B-C). The black line indicates clusters significant at cluster threshold $p_{unc} < 0.001$.

Elastic Net Regression Coefficients Predicting Memory Slope

	Full group	PiB-	PiB+
EC Tau Slope	-28.3	-24.3	-18.1
Meta-ROI Tau Slope			-2.4
PiB Slope	-8.5		-2.5
EC Thickness Slope	14.9	10.8	
Meta-ROI Thickness Slope	634.3	74.5	1324.6
EC Volume Slope			
Meta-ROI Volume Slope			
Hippocampal Volume Slope			
Age			
Edu			
Sex			



1000
β Coefficients
-30

Figure 2. Elastic net regression coefficients predicting memory slope. Elastic net regression models predicting memory slope were run for the full group & groups subset by baseline PiB status. EC FTP slope and Meta-ROI thickness slope were selected in all three elastic net models. Meta-ROI FTP slope was selected only in the PiB+ group model. Global PiB slope was selected for the full group & PiB+ models. EC thickness was selected in the full group & PiB- group. Volume slopes & demographic measure coefficients were reduced to zero in all models.

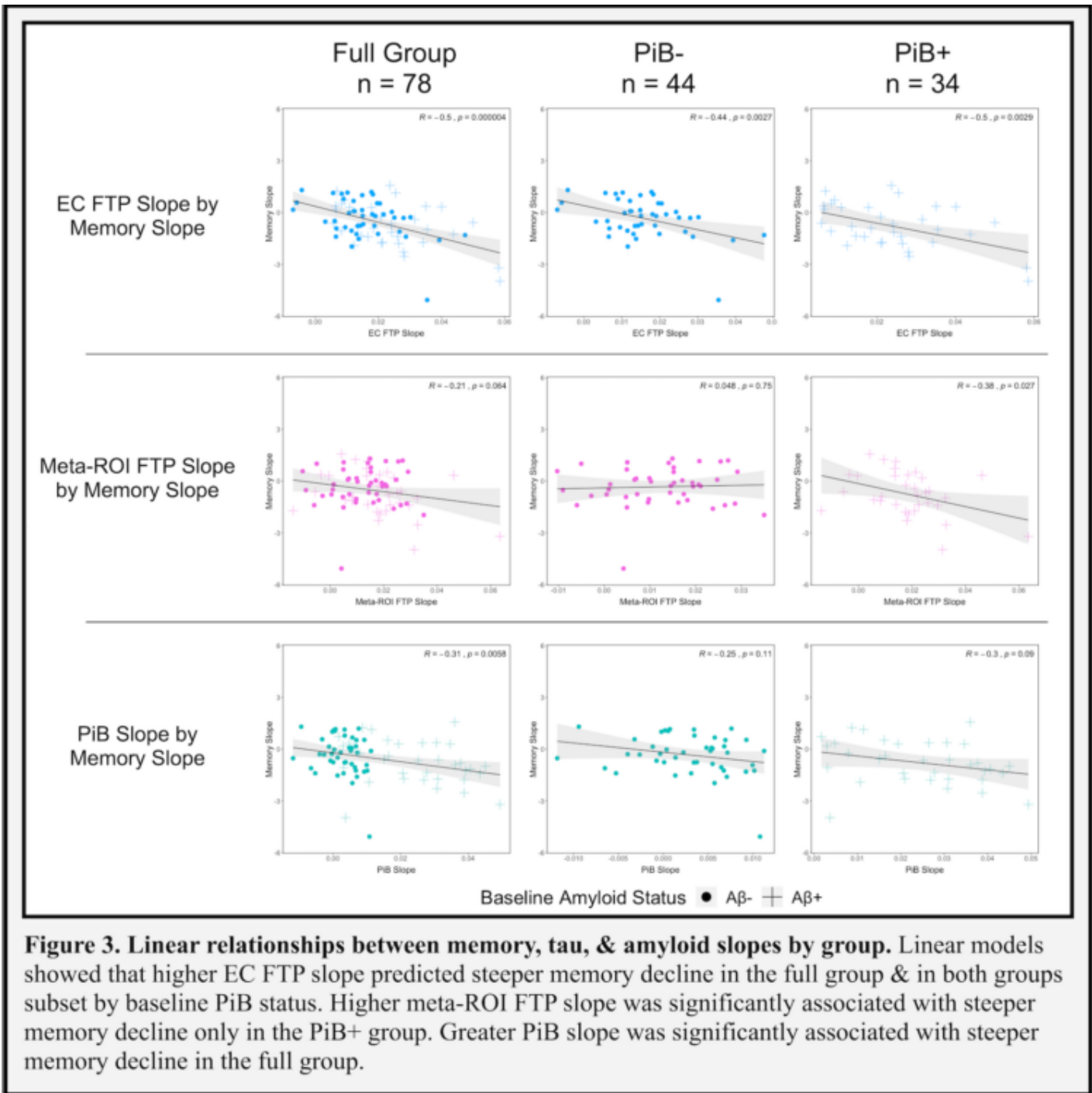


Figure 3. Linear relationships between memory, tau, & amyloid slopes by group. Linear models showed that higher EC FTP slope predicted steeper memory decline in the full group & in both groups subset by baseline PiB status. Higher meta-ROI FTP slope was significantly associated with steeper memory decline only in the PiB+ group. Greater PiB slope was significantly associated with steeper memory decline in the full group.

Keywords: tau, flortaucipir, memory decline, typical aging, Alzheimer's disease

The use of plasma markers to predict tau accumulation in a stage-specific manner

Cécile Tissot¹, Joseph Therriault¹, Nesrine Rahmouni¹, Stijn Servaes¹, Arthur C. Macedo¹, Yi-Ting Wang¹, Jenna Stevenson¹, Anniina Snellman², Juan Lantero Rodriguez³, Alyssa Stevenson¹, Jaime Fernandez-Arias¹, Firoza Lussier⁴, Sulantha Mathotaarachchi¹, Mira Chamoun¹, Gleb Bezgin¹, Peter Kunach¹, Hartmuth Kolb⁵, Gallen Triana-Baltzer⁵, Serge Gauthier¹, Thomas Karikari³, Andrea L. Benedet³, Kaj Blennow³, Henrik Zetterberg³, Tharick Pascoal⁴, Nicholas Ashton³, Pedro Rosa-Neto¹

¹McGill University, Montreal, QC, Canada

²Turku PET Center, Turku, FI

³University of Gothenburg, Gothenburg, Sweden

⁴University of Pittsburgh, Pittsburgh, PA, US

⁵Neuroscience Biomarkers Janssen Research & Development, La Jolla, CA, US

Aims: Plasma markers of tau, such as phosphorylated (pTau) or total tau detect the protein levels in the blood. They could potentially be useful in the clinical and clinical trial settings to assess changes in tau over time. Our aim was to investigate whether plasma pTau epitopes and N-terminal tau fragment (NTA) predict future accumulation of tau-PET in specific regions.

Methods: We included cognitively unimpaired, mild cognitive impairment and AD participants from the TRIAD cohort. Tau progression was calculated as the relative change (Δ) in [¹⁸F]MK6240. We conducted linear regressions between plasma levels at baseline and Δ [¹⁸F]MK6240, in Braak regions I/II, III/IV and V/VI and voxel-wise. Finally, we assessed which plasma marker was the best predictor of tau accumulation at specific Braak stages by comparing β -values of the linear regressions between plasma markers (z-scores) and Δ [¹⁸F]MK6240, correcting for age and sex.

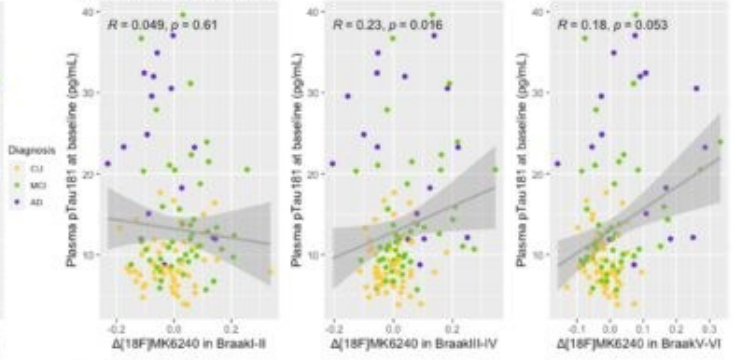
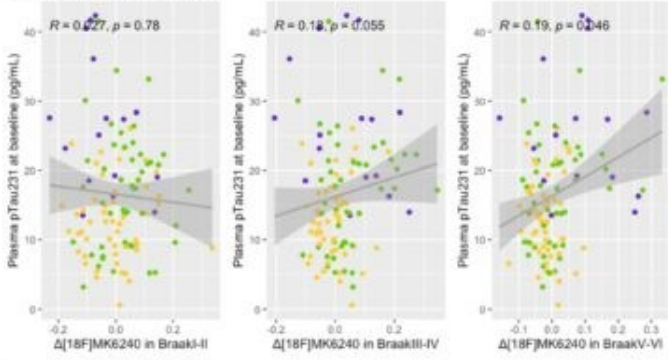
Results: We observed significant positive correlations between baseline plasma pTau181, 231, 217 and NTA with Δ BraakIII/IV and Δ BraakV/VI (Figure1). Voxel-wise analyses showed a positive relationship between Δ [¹⁸F]MK6240 and plasma pTau231 in the anterior cingulate, and medial frontal, pTau181 in the frontal and superior temporal lobes, pTau217 in the frontal, cingulate, and cuneus, NTA in the cuneus, medial frontal, paracentral and precentral gyri (Figure 2). Finally, among the significant associations, the stronger β -value was for plasma NTA for both Δ BraakIII/IV and Δ BraakV/VI (Figure3).

Conclusion: Plasma biomarkers are great predictors of future tau accumulation in regions outside of the medial temporal lobe (BraakIII and above). Plasma pTau217 and NTA predicted a more widespread accumulation of tau. Plasma NTA was the best predictor of early tau and late tau. Plasma markers could be useful at predicting future tau accumulation, at a stage-specific level.

Figure1: Linear regressions between plasma markers at baseline and [18F]MK6240 relative change in Braak regions

A: Plasma pTau231

B: Plasma pTau181



C: Plasma pTau217

D: Plasma NTA

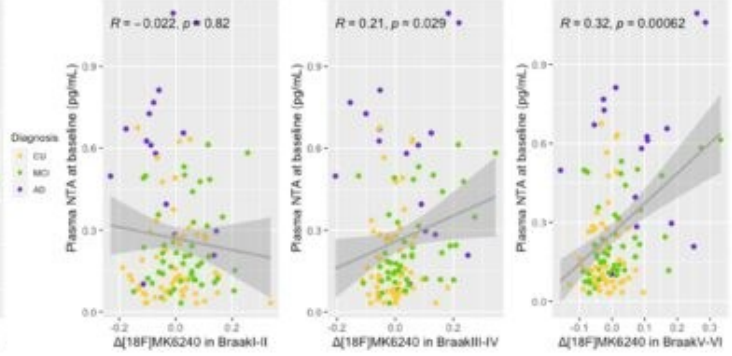
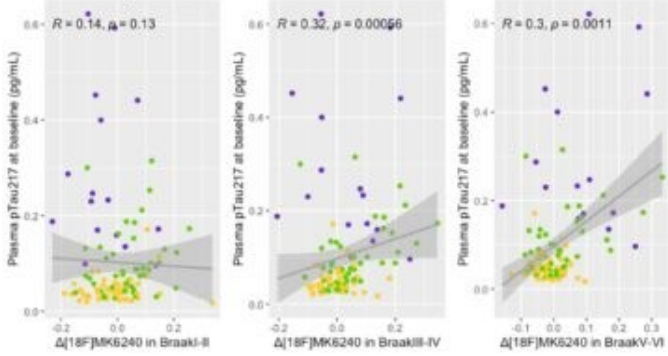


Figure2: Voxel-wise regression between plasma markers at baseline and relative changes in [18F]MK6240

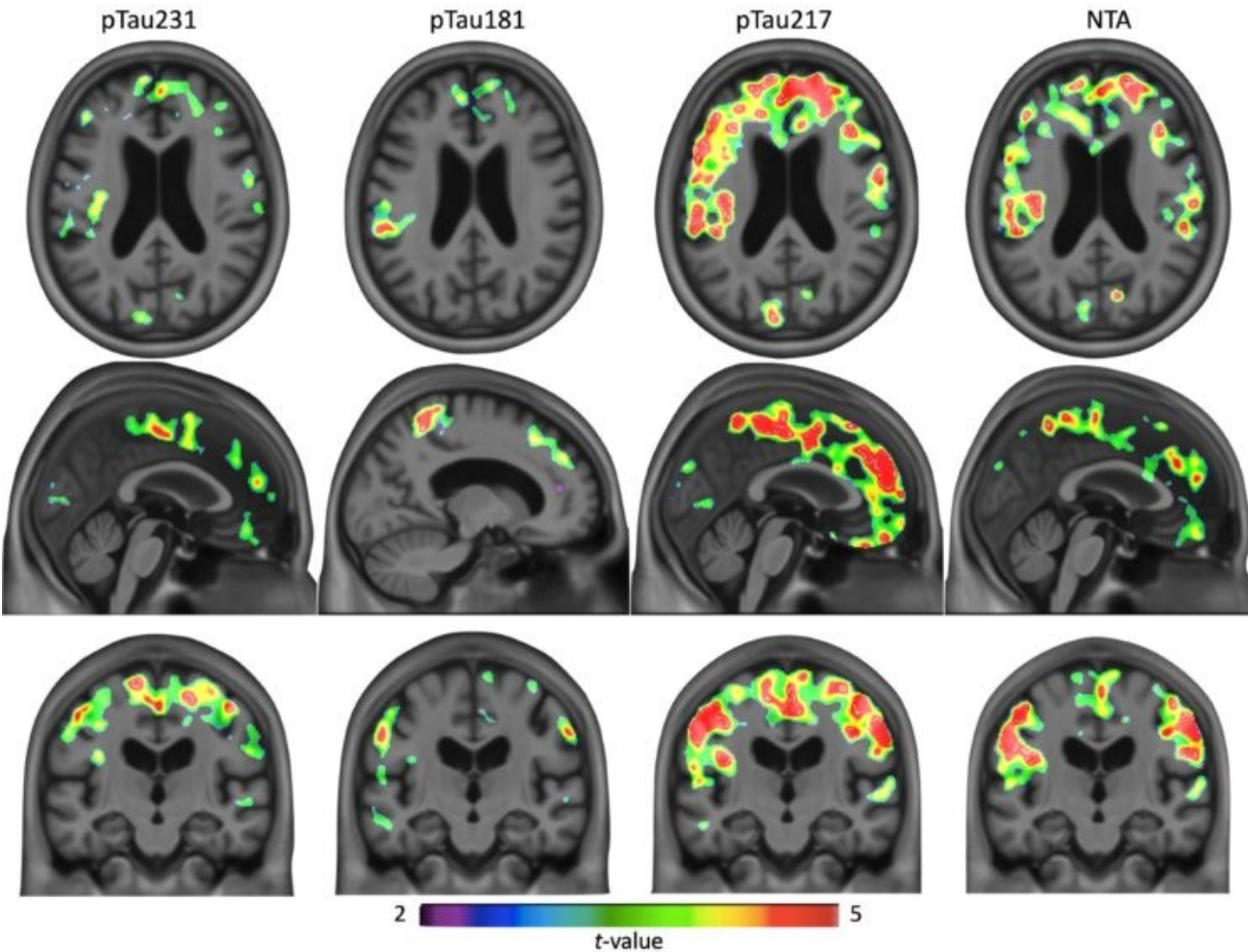
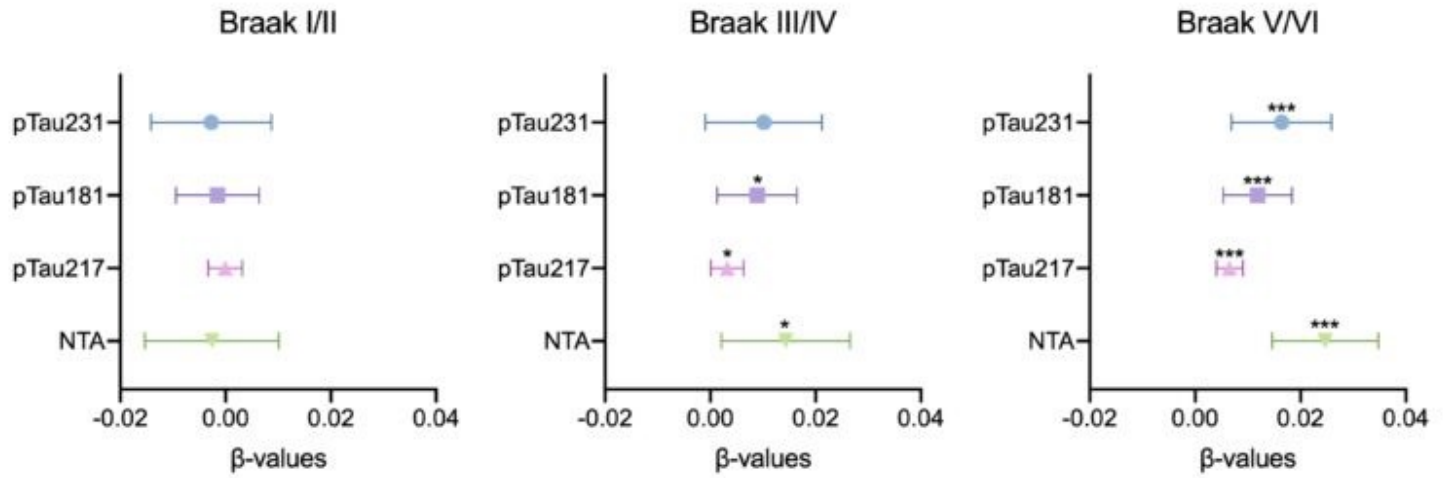


Figure3: β -values of regression analyses



Keywords: plasma, positron emission tomography, tau, prediction, phosphorylated tau.

Temporal dynamics of plasma pTau₂₁₇ and amyloid PET in preclinical AD

Karly Cody^{1,2}, Rebecca Langough^{1,2,3}, Shorena Janelidze⁵, Bradley Christian^{1,4}, Sterling Johnson^{1,2,3}, Oskar Hansson⁶, Tobey Betthausen^{1,2,4}

¹Wisconsin Alzheimer's Disease Research Center, University of Wisconsin-Madison, Madison, WI, US

²Department of Medicine, School of Medicine and Public Health, University of Wisconsin-Madison, Madison, WI, US

³Wisconsin Alzheimer's Institute, Madison, WI, US

⁴Department of Medical Physics, School of Medicine and Public Health, University of Wisconsin-Madison, Madison, WI, US

⁵Clinical Memory Research Unit, Department of Clinical Sciences, Malmö, Lund University, Lund, Sweden

⁶Memory Clinic, Skåne University Hospital, Malmö, Sweden

Objective: The goal of this work is to characterize the time between detecting pathological change in amyloid PET and plasma phosphorylated tau₂₁₇ (pTau₂₁₇) in preclinical AD.

Methods: Participants (N=172; mean (SD) age=69.4 (6.6) years; 159 unimpaired, 9 MCI, 3 dementia, 1 impaired non-AD) from the Wisconsin Registry for Alzheimer's Prevention were selected if they had plasma pTau₂₁₇ and PiB PET results available. Plasma pTau₂₁₇ was quantified using an immunoassay on the Meso Scale Discovery platform (Lilly Research Laboratories). Cortical PiB DVR (Logan, k_2' =0.149 min⁻¹, cerebellum GM reference region) was calculated from dynamic PiB imaging and averaged across eight brain regions. Two thresholds representing confident longitudinal accumulators and possible accumulators were defined by applying group-based trajectory modeling to participants with ≥ 2 observations for each biomarker (pTau₂₁₇, n=162; PiB, n=155). Sampled iterative local approximation (SILA) was used to model longitudinal PiB and pTau₂₁₇ trajectories in these subsets, and to estimate biomarker onset ages and biomarker positive time for all participants with at least one PiB and pTau₂₁₇ measurement.

Results: 34.9% (60/172) participants were observed PiB(+) and pTau₂₁₇(+), 14.5% (25/172) were PiB(+) and pTau₂₁₇(-), 3.5% (6/172) were PiB(-) and pTau₂₁₇(+), and 47% (81/172) were PiB(-) and pTau₂₁₇(-). SILA-aligned spaghetti plots (**Figure 1**) showed consistent accumulation patterns with greater pTau₂₁₇ variability. Plots of pTau₂₁₇ vs. years PiB(+) and PiB DVR vs. years pTau₂₁₇(+) suggested PiB(+) typically preceded plasma pTau₂₁₇(+) with a mean (SD) time from PiB(+) onset to pTau₂₁₇ onset of 4.3 (5.8) years in those that became positive for both biomarkers (**Figure 2**).

Conclusions: Amyloid PET and plasma pTau₂₁₇ are amenable to temporal modeling. AD pathology detected by amyloid PET typically precedes plasma pTau₂₁₇ by ~4 years, but this time difference ranges considerably between individuals. Future work will investigate predictors of this temporal offset and relationships with cognitive trajectories.

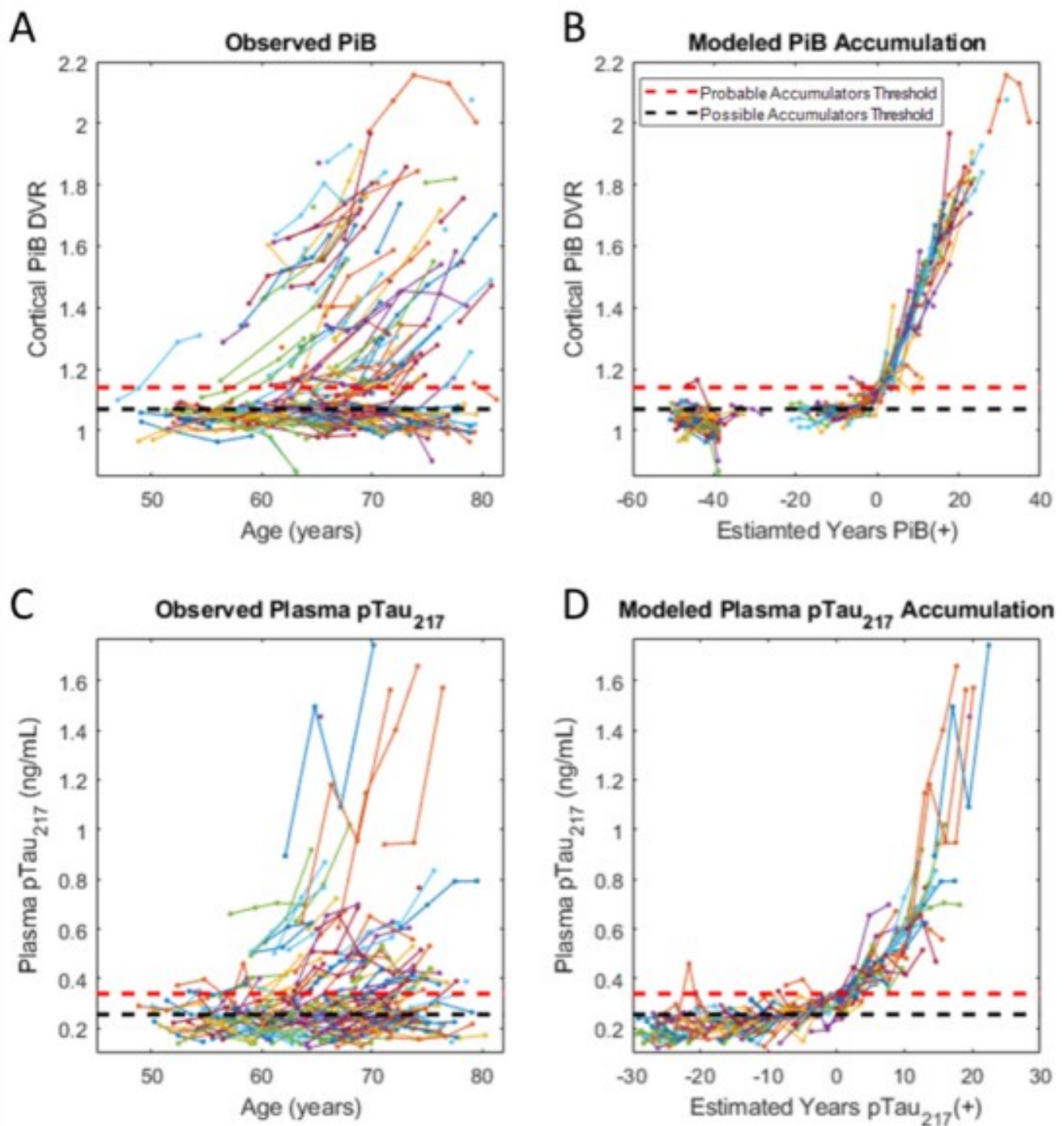


Figure 1. Observed cortical PiB DVR (A) and plasma pTau₂₁₇ (C) as a function of age and the resultant PiB (B) and pTau₂₁₇ (D) accumulation trajectories from the SILA model. SILA models were trained on the subset of participants with any observation exceeding the possible accumulators threshold (PiB DVR >1.07 (3.4 Centiloids); pTau₂₁₇ >0.26 pg/mL). Zero years for modeled PiB and plasma pTau₂₁₇ timelines were defined as the point the model intersected the probable accumulators threshold for each biomarker (PiB DVR = 1.14 (14.1 Centiloids); pTau₂₁₇ = 0.34 pg/mL).

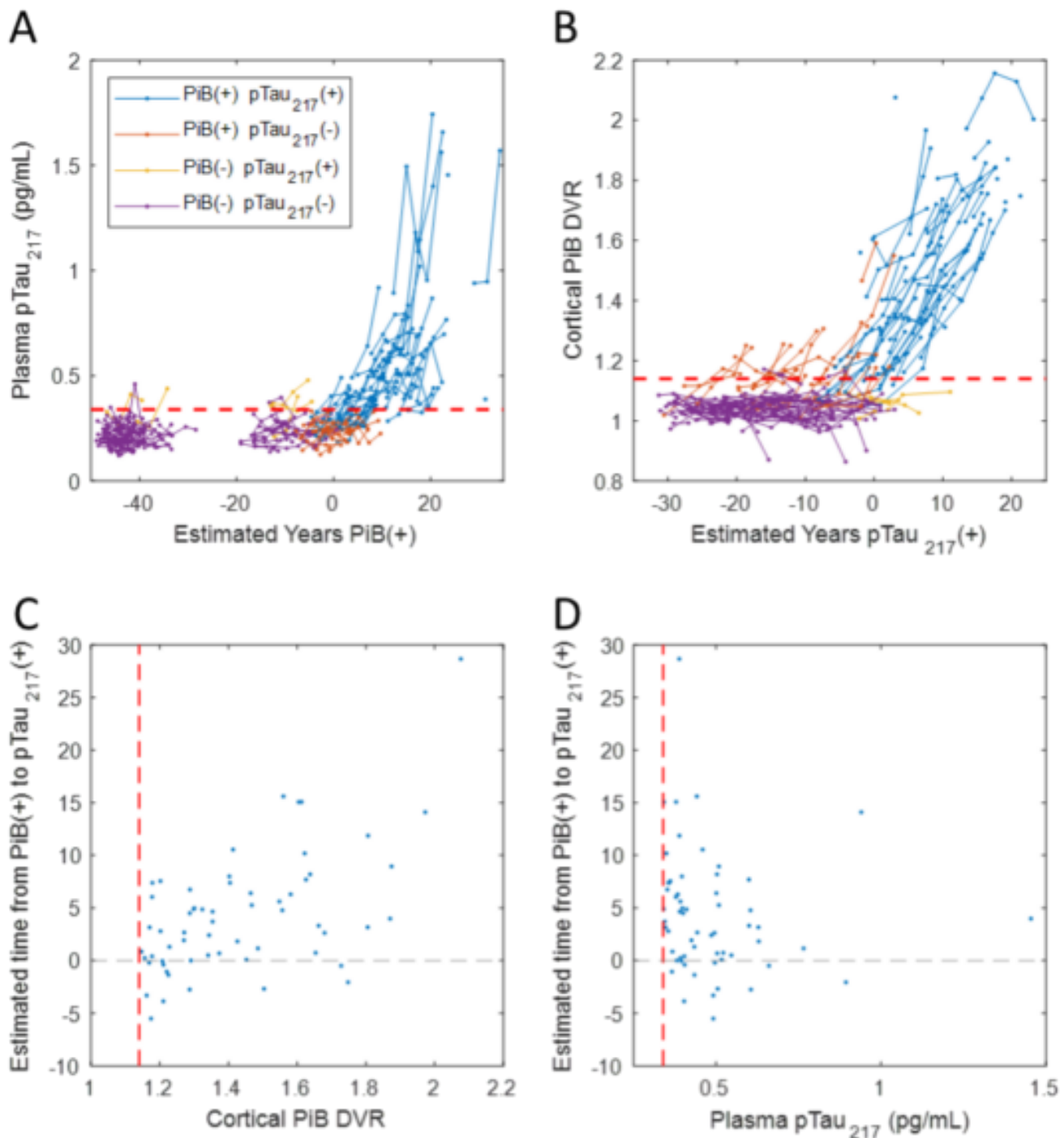


Figure 2. Plasma pTau₂₁₇ as a function of estimated years PiB(+) (A) and cortical PiB DVR as a function of estimated years pTau₂₁₇(+) (B) suggested that individuals typically became PiB(+) positive before becoming pTau₂₁₇(+). The estimated difference between PiB(+) and pTau₂₁₇(+) is shown as a function of Cortical PiB DVR (C) and plasma pTau₂₁₇ (D) for the group that was observed to be positive on both biomarkers. Results suggest that PiB(+) typically precedes pTau₂₁₇(+) by ~4 years on average but with considerable inter-individual heterogeneity in this timing.

Longitudinal changes in Alzheimer's disease-related plasma biomarkers in relation to changes in PiB PET measures of brain amyloid

Murat Bilgel¹, Yang An¹, Keenan Walker¹, Abhay Moghekar², Nicholas Ashton³, Przemysław Kac³, Thomas Karikari³, Kaj Blennow³, Henrik Zetterberg³, Bruno Jedynak⁴, Madhav Thambisetty¹, Susan Resnick¹

¹*Laboratory of Behavioral Neuroscience, National Institute on Aging, Baltimore, MD, US*

²*Department of Neurology, Johns Hopkins University School of Medicine, Baltimore, MD, US*

³*Department of Psychiatry and Neurochemistry, Institute of Neuroscience and Physiology, The Sahlgrenska Academy, University of Gothenburg, Mölndal, Sweden*

⁴*Department of Mathematics and Statistics, Portland State University, Portland, OR, US*

Introduction: Understanding longitudinal plasma biomarker trajectories in relation to changes in brain amyloid can help devise strategies for assessing disease progression.

Methods: We used longitudinal plasma ($A\beta_{40}$, $A\beta_{42}$, NfL, and GFAP measured using Quanterix Simoa Neurology-4-plex-E assay and p-tau181 and p-tau231 measured using Simoa assays developed in-house at the University of Gothenburg) and amyloid PiB PET biomarker data for 199 participants from the Baltimore Longitudinal Study of Aging to investigate the association between rates of change in pairs of biomarkers using bivariate linear mixed effects models and the temporal ordering of changes using a progression score (PS) model. Participants were cognitively normal at baseline with a 6.1-year median follow-up duration.

Results: Plasma measures with the highest and lowest longitudinal stabilities were GFAP (intraclass correlation coefficient=0.78, 95% CI=[0.72–0.82]) and NfL (0.48 [0.4–0.55]), respectively. Global PiB DVR had the highest stability over time (0.96 [0.94–0.97]).

Pairs of biomarkers with statistically significant positive correlations in their rates of change were p-tau181/ $A\beta_{42}$ and p-tau231/ $A\beta_{42}$, GFAP and NfL, GFAP and global PiB DVR, and NfL and global PiB DVR (Figure 1).

The PS model accounts for individual differences in the onset of biomarker changes by estimating a time-shift per individual to better align biomarker measurements (Figure 2). The PS model suggests that change in $A\beta_{42}/A\beta_{40}$ precedes the change in global PiB DVR by as much as four decades, with the change in the remaining plasma biomarkers occurring closer in time to, and along with, brain amyloid accumulation (Figure 3).

Discussion: Plasma biomarkers may reflect changes that begin decades prior to brain changes but show more variability over time than brain PET measures of amyloid. Further studies are needed to determine if these changes can be reliably detected at the individual level and may be useful in predicting future risk of developing disease.

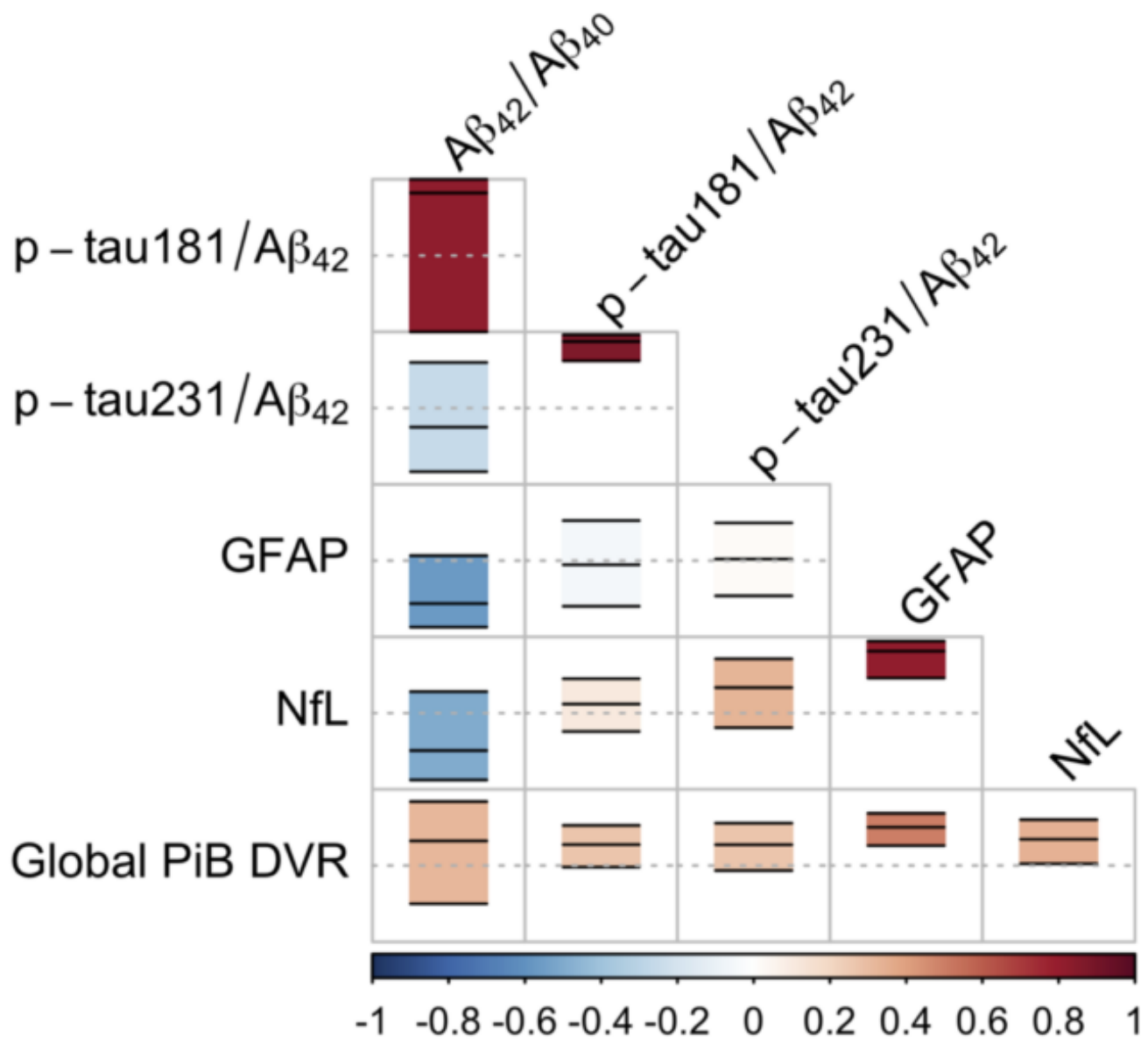


Figure 1. Pairwise correlations among rates of change of plasma and PiB PET measures, as assessed using the random effect correlation matrix estimated in the bivariate linear mixed effects models. The rectangle in each cell indicates the 95% confidence interval of the correlation estimate, which is shown with a black solid line inside the rectangle. Dashed horizontal lines correspond to a correlation of 0. Color indicates the correlation estimate.

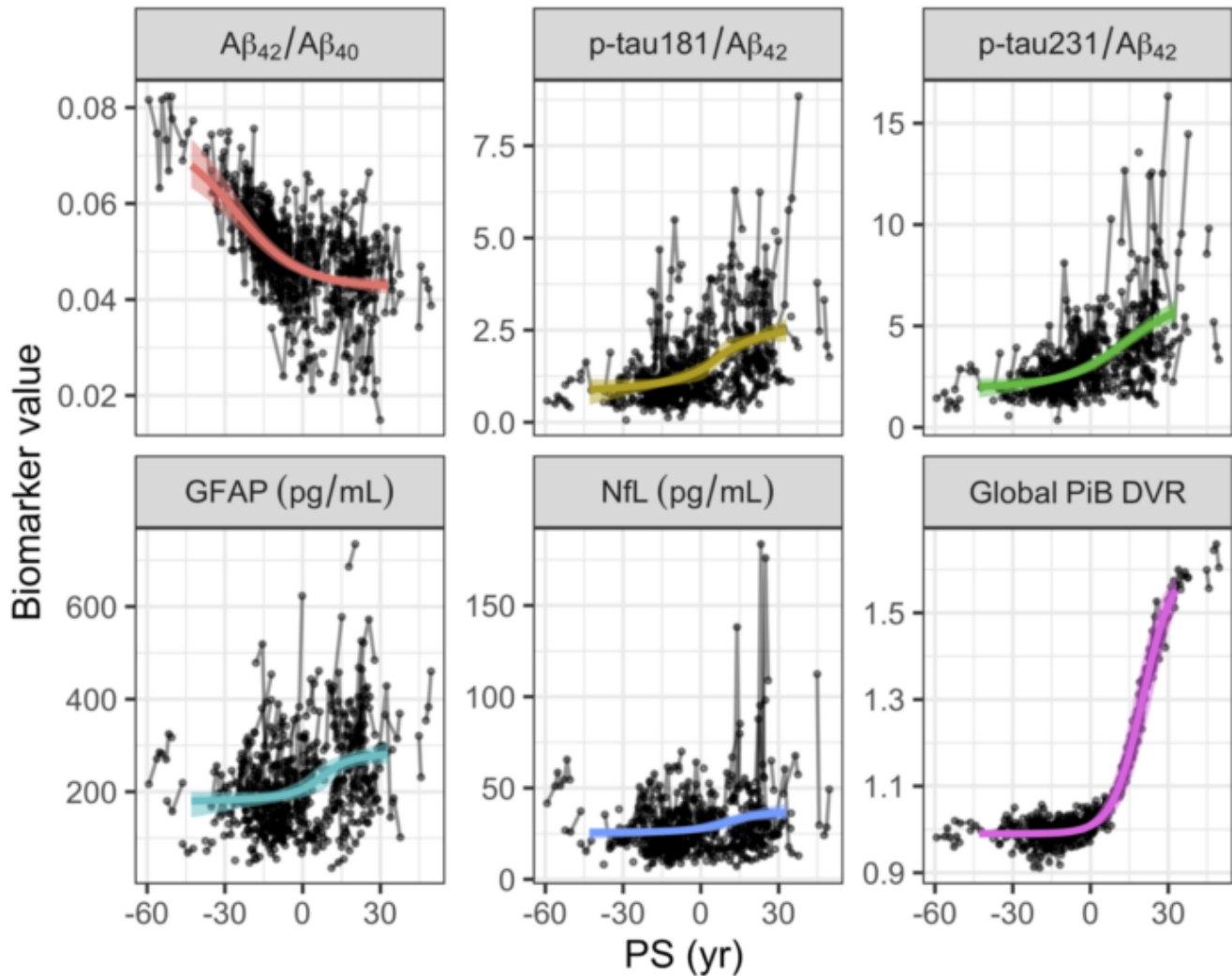


Figure 2. Biomarker trajectories estimated after alignment of individual-level longitudinal data using the progression score (PS) model, superimposed on observed data. Bands indicate the 95% confidence intervals for the trajectory estimates. At last visit, both PS and the subject-specific time shift parameter were higher for individuals with mild cognitive impairment or dementia compared to cognitively normal individuals, suggesting that higher PS is indicative of greater disease severity. (PS = 0 is an arbitrary point without any intrinsic meaning. Since PS is time-shifted age, it is in the units of years. PS value corresponding to a global PiB DVR of 1.06, which is the PiB positivity threshold, is 8.4.)

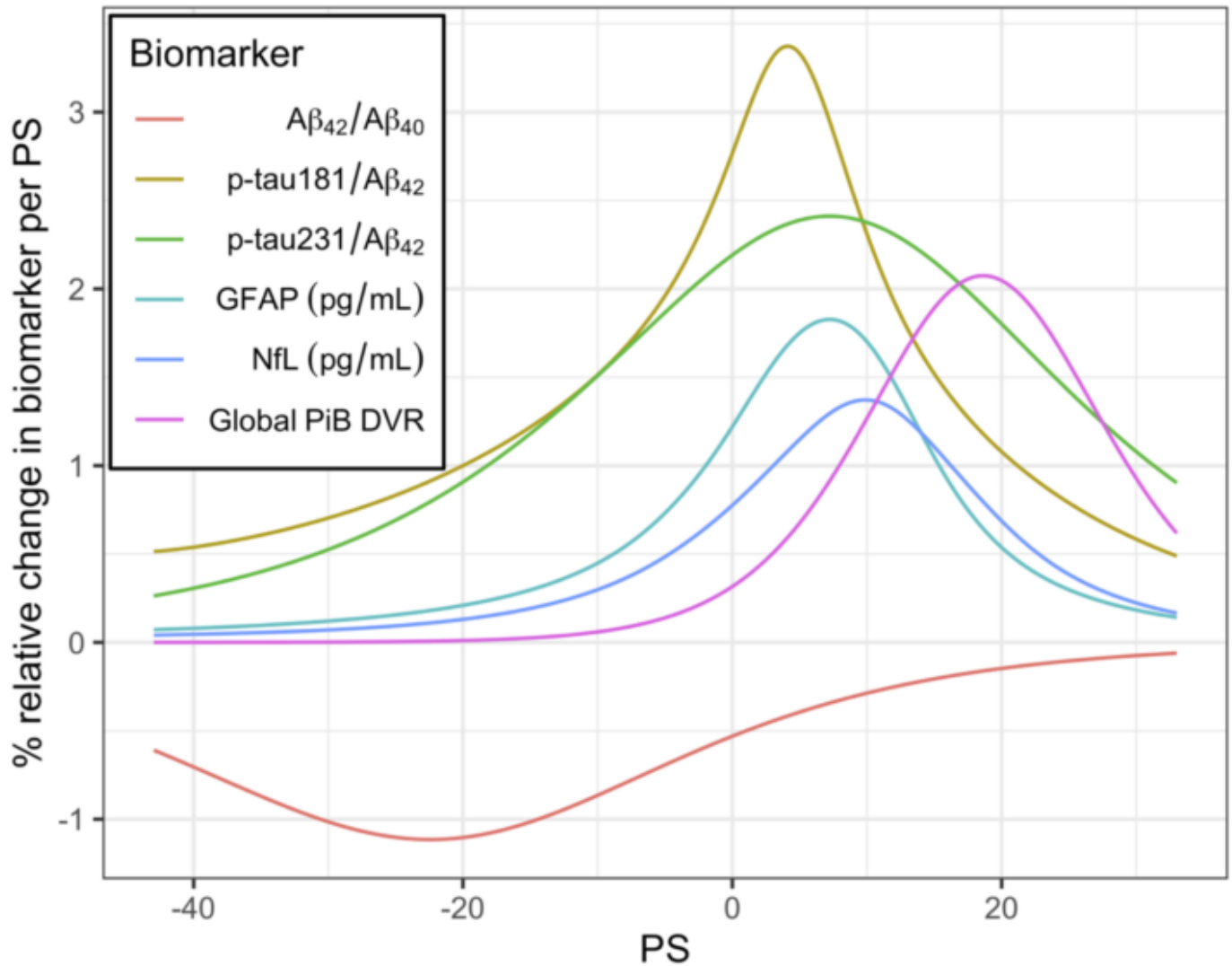


Figure 3. Percent relative change in biomarkers per PS as a function of PS. Relative change peaks earliest for $A\beta_{42}/A\beta_{40}$ and latest for global PiB DVR. Absolute relative change in $A\beta_{42}/A\beta_{40}$ is capped at around 1%, whereas other plasma biomarkers exhibit greater changes. This suggests that it might be more difficult to detect individual-level longitudinal change in plasma $A\beta_{42}/A\beta_{40}$ relative to other proteins.

Keywords: longitudinal, plasma, PiB

Longitudinal bidirectional associations between sleep and Alzheimer's pathology in At-Risk Cognitively Unimpaired Older Adults

Bery Mohammediyani^{1,2}, Andrée-Ann Baril^{1,2}, Frédéric St-Onge^{1,2}, Valentin Ourry^{1,2}, Julie Carrier³, Jean-Paul Soucy^{1,2}, John Breitner^{1,2}, Judes Poirier^{1,2}, Sylvia Villeneuve^{1,2}

¹Douglas Mental Health University Institute, Montreal, QC, Canada

²Department of Psychiatry, Faculty of Medicine, McGill University, Montreal, QC, Canada

³Department of Psychology, University of Montreal, Montreal, Montreal, QC, Canada

Background: Increasing evidence suggests a link between sleep and late-life Alzheimer's disease (AD) pathology. We investigated bidirectional longitudinal associations between sleep quality and amyloid- β ($A\beta$) and tau burden in a cohort of cognitively unimpaired participants with a family history of AD.

Methods: We included 205 PREVENT-AD participants with available sleep data who underwent $A\beta$, [¹⁸F] NAV-4694, and tau, [¹⁸F] Flortaucipir, positron emission tomography (PET). Longitudinal PET scans were available for 80 participants (follow-up: 4.4 \pm 0.24y) and longitudinal sleep data were available for 213 participants (follow-up: 1.03 \pm 0.19y). We assessed sleep quality subjectively using the Pittsburgh sleep quality index (PSQI) global score and objective sleep using 7-day actigraphy including sleep period, efficiency, and fragmentation. We used linear regression models to examine cross-sectional associations. Linear mixed effect (LME) models were performed to test for longitudinal associations with baseline sleep measures used as predictors of change in pathology and repeated with baseline pathology used as a predictor of change in sleep quality.

Results: Higher PSQI scores, reflecting worse sleep quality, were associated with higher baseline tau levels in the entorhinal cortex and in a temporal meta-ROI ($p=0.005$, $R^2=0.08$, $\beta=0.01$; $p=0.003$, $R^2=0.07$, $\beta=0.01$ respectively). Higher baseline PSQI scores were also associated with faster entorhinal and meta-ROI tau accumulation over time ($p=0.006$, $R^2=0.08$, $\beta=0.01$; $p=0.007$, $R^2=0.06$, $\beta=0.01$ respectively, Figure 1). Finally, individuals with increased tau at baseline in the entorhinal cortex and meta-ROI showed faster worsening in sleep quality compared to individuals with no or less pathology ($p=0.022$, $R^2=0.04$, $\beta=2.80$; $p=0.012$, $R^2=0.04$, $\beta=3.21$ (Figure 2) respectively). We found no association between PSQI and $A\beta$ burden, or between actigraphy measures and AD pathology.

Conclusion: Sleep impairments in older age could contribute to tau pathology accumulation, which could in turn disrupt sleep further. Treating sleep disturbances may therefore serve in delaying tau burden and slowing down disease progression.

Figure.1

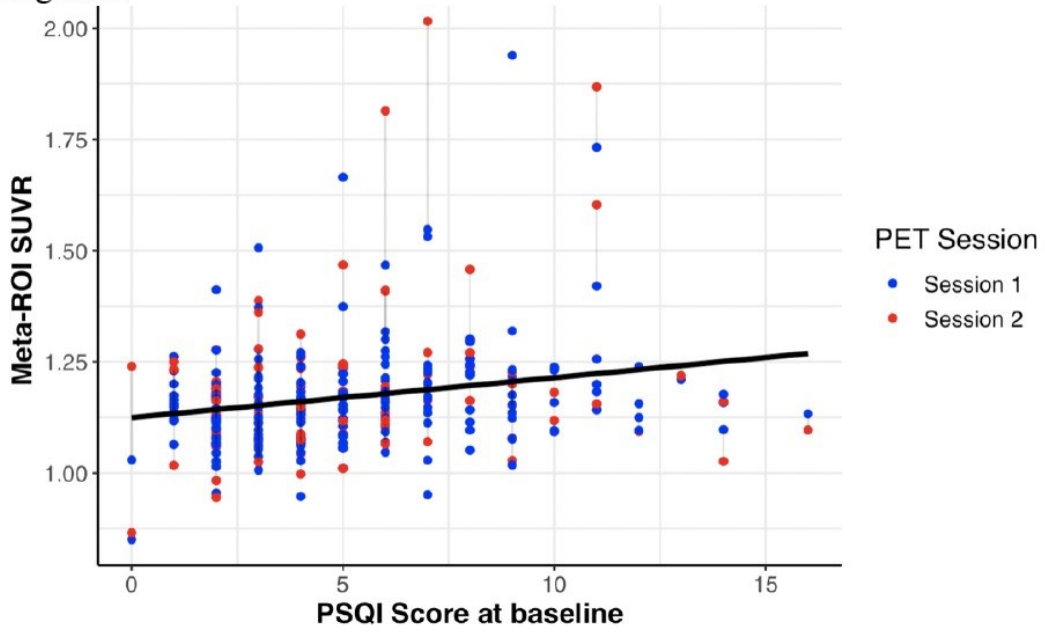
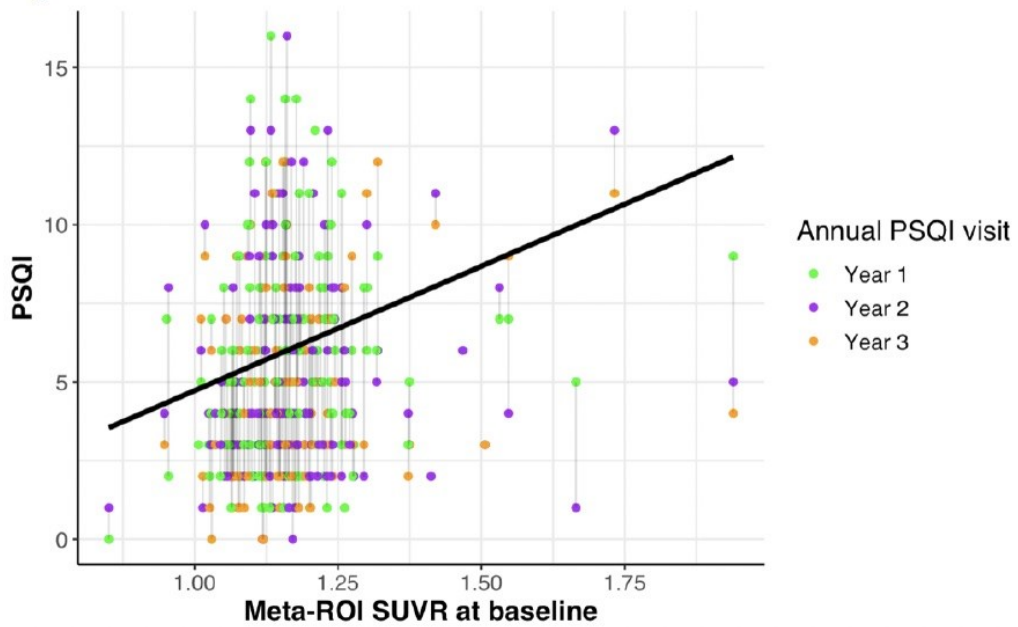


Figure. 2



Keywords: amyloid, tau, sleep, Alzheimer's disease, imaging

POSTER SESSION 3A

Friday, January 13, 2023		
10:45 am – 11:30 am	Poster Session 3A	
73	Motion and partial volume corrections in dynamic [18F]-MK6240 PET imaging	Tiss Gong Lois Becker Thibault Guehl Xia Normandin Ouyang Johnson El Fakhri
74	Encoding, consolidation and retrieval deficits are differentially shaped by tau and atrophy in the Alzheimer’s disease spectrum	Fernandez Therriault Lussier Bezgin Tissot Servaes Wang Matotharachchi Stevenson Rahmouni Kang Pallen Kunach Quispialaya Margherita-Poltronetti Pascoal Rosa-Neto
75	Comorbid medical conditions, anxiety, and amyloid- β pathology in cognitively unimpaired older adults	Abiose Young Winer Deters Mormino
76	Defining and characterizing neocortical tau resistance in preclinical Alzheimer’s disease	Buckley Klinger Boyle Coughlan Hanseeuw Yang Amariglio Rentz Townsend Farrell Jacobs Shirzadi Yau Price Chhatwal Schultz Hohman Donohue Properzi Johnson Sperling
77	Development and evaluation of image preprocessing pipelines for the Centiloid method	Luo Minhas Rubenstein Situ Royse Ances Christian Cohen Handen Klunk Tudorascu Zamon Laymon
78	Cognitively estimated disease time: Associations with amyloid and tau burden in the Harvard Aging Brain Study	Townsend Properzi Betthausen Klinger Boyle Coughlan Hanseeuw Yang Amariglio Farrell Jacobs Shirzadi Yau Price Chhatwal Rentz Johnson Sperling Schultz Buckley
79	Synergistic interaction between sex, amyloid and phosphorylated tau predicts the longitudinal progression of tau tangles	Wang Therriault Servaes Tissot Fernandez Arias Rahmouni Macedo Stevenson Stevenson Haeger Hosseini Nazneen Rosa-Neto
80	[18F]PI-2620 binding patterns in patients with suspected AD- and FTLT-tauopathies	Blazhenets Soleimani-Meigooni Thomas Brendel Vento VandeVrede Heuer Ljubenkov Rojas Chen Iaccarino Mundada Litvan Grossman Boeve Pantelyat Tartaglia Irwin Dickerson Baker Boxer Rabinovici La Joie
81	Regional analysis of change in synaptic density over time by cognitive status	DiFilippo Mcvea Mclachlan Pasquesi Davenport-Sis Jonaitis Ennis Betthausen Engle Johnson Bendlin Christian
82	Regional tau profiles in early tau pathology populations	Kotari Morris Svaldi Southekal Lu Pontecorvo Collins Shcherbinin Neuroimaging Initiative
83	[18F]MK-6240 tau-PET in an A β -enriched sample from the 1946 British birth cohort - Insight 46	Coath Markiewicz Modat Scott Malone Thomas Dickson Schöll Ourselin Richards Fox Cash Schott
84	Longitudinal trajectories of depressive symptoms and regional amyloid accumulation (PiB PET) in clinically normal older adults	Munro Farrell Hanseeuw Buckley Properzi Vannini Amariglio Quiroz Blacker Rentz Sperling Johnson Marshall Gatchel

85	Improving sub-threshold PiB fidelity using relative radioligand delivery	Properzi Shirzadi Buckley Klinger Hanseeuw Amariglio Rentz Farrell Price Chhatwal Marshall Gatchel Johnson Sperling Schultz
86	Improved prediction of preclinical cognitive decline using amyloid PET spatial extent	Farrell Thibault Becker Price Hanseeuw Buckley Papp Jacobs Rentz Sperling Johnson
87	18F-MK-6240 Tau PET as a Potential Biomarker for Chronic Traumatic Encephalopathy	Alosco Mundada La Joie Asken Nowinski Smith Culhane Shankar Amuri Pettway Iaccarino Windon Tripodis Mercier Kowall Stein Grinberg McKee Stern Miller Mez Killiany Rabinovici
88	Psychosis and tau burden across the AD continuum	Johnson* Ziaggi* Huey, MD Kreisl, MD Talmasov, MD Lao, PhD
89	Classifying cognitive resilience to differing levels of Alzheimer's disease pathology	Boyle Townsend Klinger Coughlan Hanseeuw Yang Amariglio Farrell Jacobs Shirzadi Yau Price Chhatwal Schultz Hohman Donohue Properzi Rentz Johnson Sperling Buckley
90	Cerebrospinal fluid neurofilament light predicts increased amyloid, tau, and decreased grey matter density	Manchella Logan Dage Hammers Nemes Kostadinova Eloyan Mundada La Joie Iaccarino Fagan Foroud Zetterberg Koeppe Aisen Carrillo Rabinovici Dickerson Apostolova
91	Unhealthy white matter connectivity in African American and non-Hispanic white older adults	Royse Snitz Hengenius Huppert Roush Cisneros Potopenko Becker Cohen Shaaban
92	Locus coeruleus integrity as neural substrate providing resilience against cognitive decline in the face of Alzheimer's disease pathology	Jacobs Papp Buckley Riphagen Hanseeuw Boyle Donovan Rentz Sperling Johnson
93	Lower locus coeruleus integrity predicts diminished practice effects in cognitively normal older individuals	Smegal Schneider Jutten Rentz Johnson Sperling Papp Jacobs
94	PET-based Braak staging predicts neuropsychiatric burden in the Alzheimer's disease continuum	Macedo Tissot Therriault Servaes Rahmouni Fernandez-Arias Z. Lussier Stevenson Wang Quispialaya Socualaya Nazneen Ali Hosseini Kunach Haeger Stevenson Vitali A. Pascoal Rosa-Neto
95	A computational model to study the combined effect of neuronal connectivity loss and tauopathy progression	Rahimabadi Soucy Benali
96	Simulated dose reduction in longitudinal [18F]MK-6240 PET	McLachlan McVea DiFilippo Schöll Betthausen Johnson Christian
97	Regional amyloid change improves prediction of future tau progression over global metrics	Thibault Farrell Properzi Mayblyum Hanseewu Healy Price Becker Sperling Johnson
99	Rates of tau PET accumulation along the amyloid timeline in Alzheimer's disease	Cody Langhough Christian Betthausen Johnson
100	Body mass index, pathological tau, and cognition in preclinical AD: Could women with high BMI be protected?	Wang Sundermann Buckley Reas McEvoy Banks

101	Amyloid drives later tau accumulation for fast progressors in early Braak stages	Servaes Therriault Tissot Lussier Bezgin Wang Stevenson Rahmouni Stevenson Pallen Kunach Fernandez Arias Cassa Macedo Hosseini Pascoal Gauthier Rosa-Neto
102	Brain-wide and AD-risk genetic expression: A descriptive study	Hobbs McCullough Millar Gordon
103	Behavioral brain networks underlying the effect of Alzheimer's pathology on cognition	Ziontz Harrison Jagust
104	Exploration of 18F-Florzolotau tau PET distribution patterns using machine learning approach in AD	Huang Lee Lin Huang Hsu Chang Huang Hsiao
105	The interplay of vascular disease, peripheral interleukin-6, beta-amyloid, and memory in older adults	Rizvi Adams Sathishkumar Kim Larson McMillan Brickman Mapstone Thomas Greenia Corrada Kawas Yassa
106	Gut microbiome composition is associated with cortical amyloid burden in a preclinical human cohort	Heston González Betthausen Johnson Asthana Knight Kaddurah-Daouk Rey Bendlin
107	Study on MR-free template-based spatial normalization for Tau PET Image Quantitation using 18F-Florzolotau	Lee Huang Lin Huang Huang Wu Chang Hsiao
108	β -Amyloid in World Trade Center responders: Result indicate age-related toxic encephalopathy mediated by an immunogenic amyloid response	Clouston Vaska Huang Kritikos Zhou
109	[18F]MK-6240 PET/MRI Test-Retest performance in cognitively normal elderly subjects	Lois Fanglu Fu Salvatore Huell Izquierdo Garcia Garimella Dickerson Johnson Catana Price

P73 Motion and partial volume corrections in dynamic [^{18}F]-MK6240 PET imaging

Amal Tiss^{1,2}, Kuang Gong^{1,2}, Cristina Lois^{1,2}, Alex Becker^{1,2,3}, Emma Thibault^{1,2,3}, Nicolas Guehl^{1,2}, Ye Xia¹, Marc Normandin^{1,2}, Jinsong Ouyang^{1,2}, Keith Johnson^{1,2,3}, Georges El Fakhri^{1,2}

¹Gordon Center for Medical Imaging, Department of Imaging, Massachusetts General Hospital, Boston, MA, US

²Radiology Department, Harvard Medical School, Boston, MA, US

³Department of Neurology, Massachusetts General Hospital, Boston, MA, US

The accumulation of tau protein has been linked to the cognitive decline seen in Alzheimer's disease (AD). [^{18}F]-MK6240 is a novel tracer developed to achieve high binding affinity and selectivity to tau protein. However, dynamic PET quantitation is significantly compromised by partial volume effect and motion. To address these concerns, we propose a novel kernel-based reconstruction with data-driven motion and partial volume corrections (MC/PVC).

The PET data are saved in list-mode format and partitioned into separate frames according to established protocols. In each frame, motion estimation is achieved through image registration of ultra-short (~3.6s) snaps and then applied to each measurement in the event-by-event list-mode reconstruction algorithm. Subsequently, we use the high-resolution MPRAGE image as a prior with patch-based correspondence. This representation is embedded in the list-mode reconstruction to generate a PVC image, with intra-frame MC. We apply this novel framework to one subject with mild cognitive impairment and compare our method with the conventional approach (no PVC and frame-to-frame alignment for MC). We adopt an MRTM2 kinetic model to calculate the distribution volume ratio (DVR) in key brain regions for AD, using the cerebellum grey matter as reference. We also generate voxel-wise DVR images for both the conventional and proposed methods.

Figure 1 shows the axial and sagittal views of voxel-wise DVR overlaid on corresponding MR images (Left) and reports DVR values in tau-rich brain regions (Right) for the conventional approach and after MC/PVC. The proposed method yielded qualitatively better images (reduced signal in the cerebellum) and a 12% average increase in DVR. Figure 2 shows an image corrupted by intra-frame motion, confirmed by estimated registration parameters. Motion correction removes the blurring.

MC/PVC yields better images in subjects prone to motion and with high tau uptake.

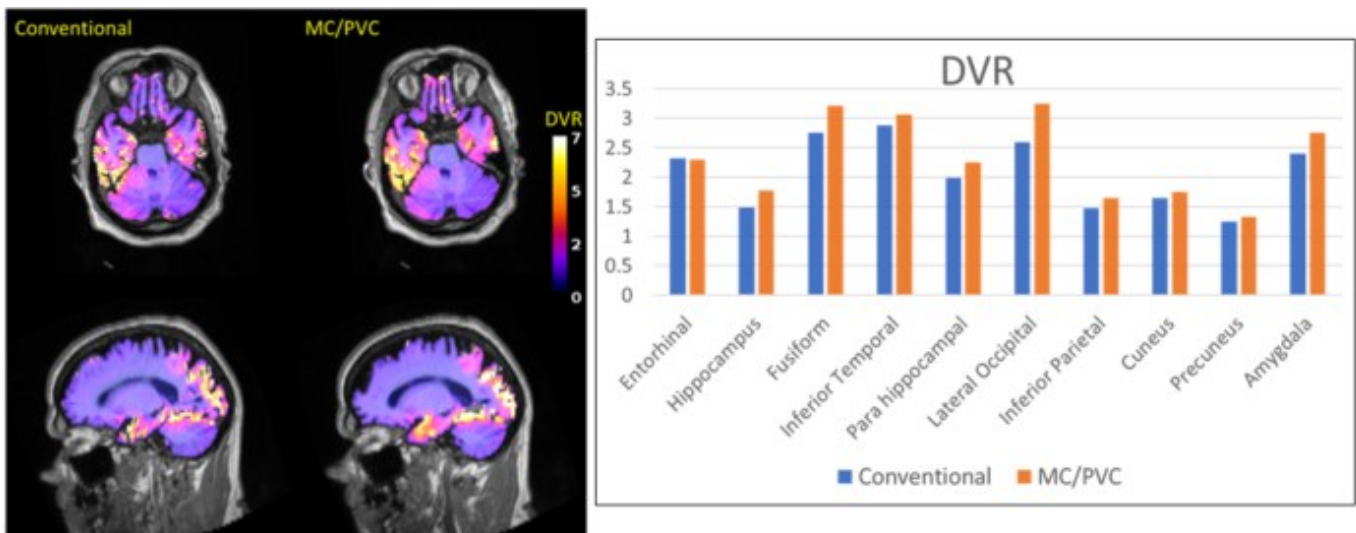


Figure 1: Voxel-wise DVR images and region-based DVR values for the conventional and the proposed methods.

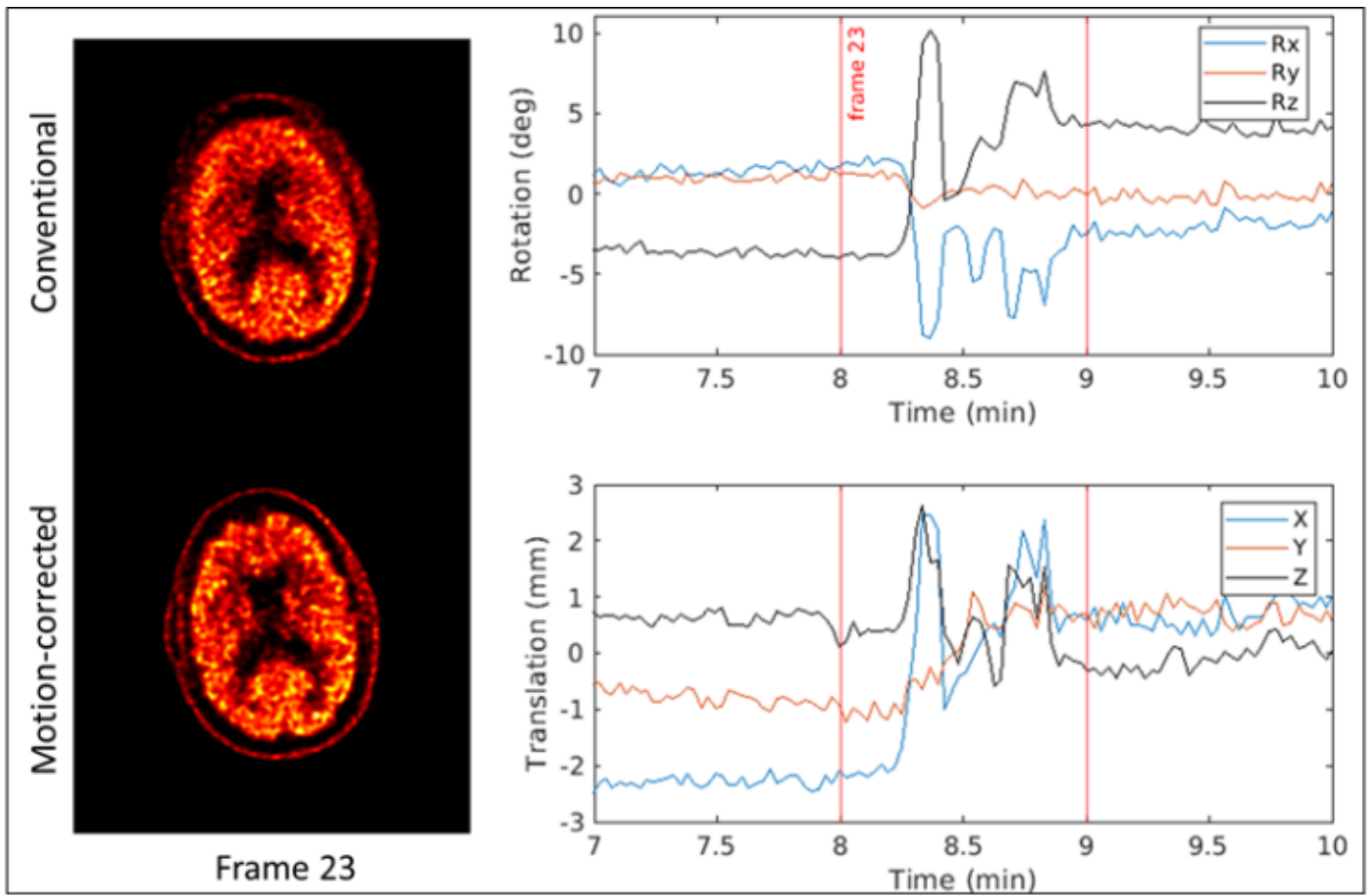


Figure 2: The 23rd frame (8-9min post tracer injection) from the conventional pipeline is blurred. The transformation parameters obtained by the motion estimation step confirm the presence of notable intra-frame motion. The motion-corrected image shows no motion-related blurring.

Keywords: motion correction, partial volume correction, dynamic tau imaging, [18F]-MK6240, MRTM2

P74 Encoding, consolidation and retrieval deficits are differentially shaped by tau and atrophy in the Alzheimer's disease spectrum

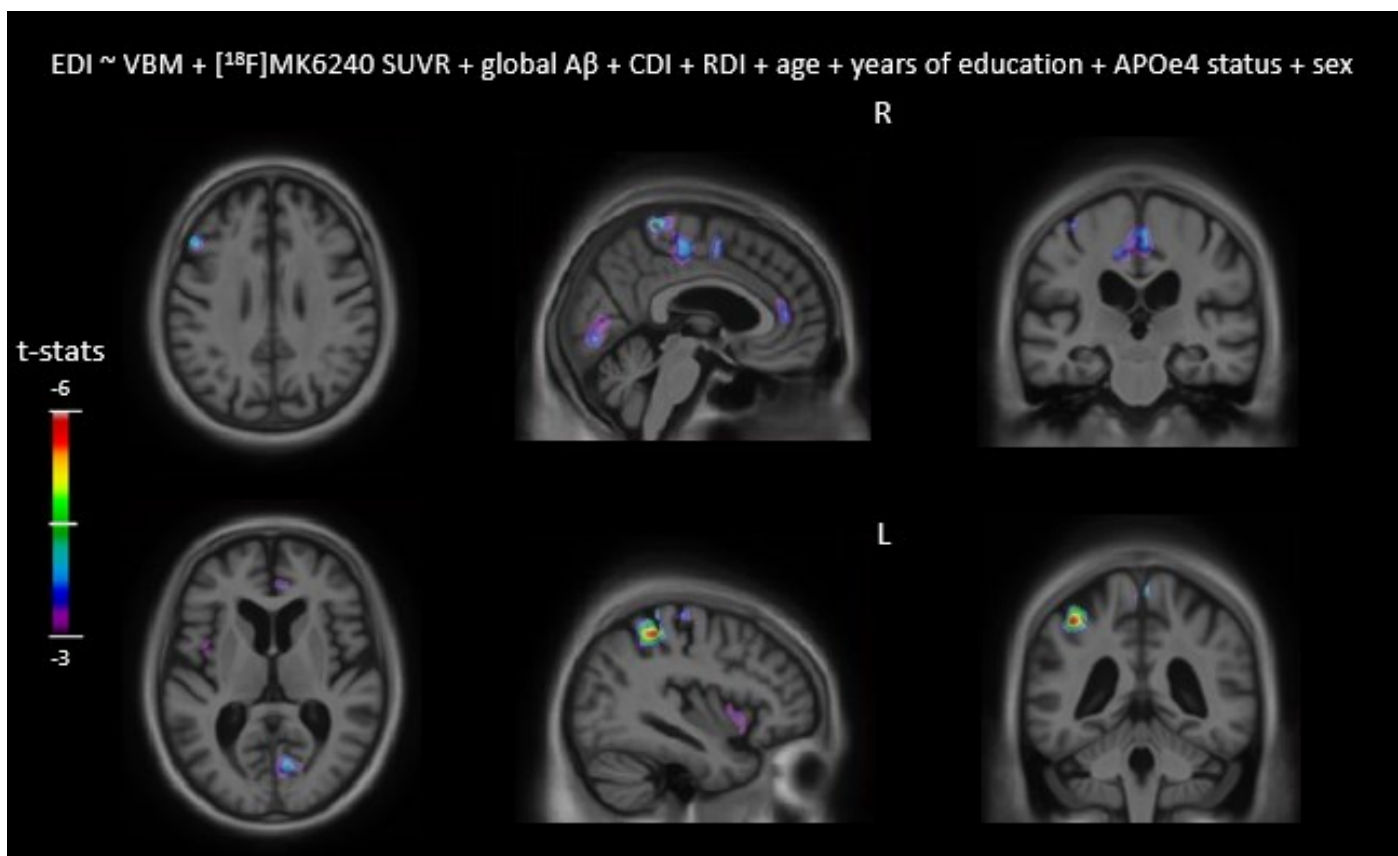
Jaime Fernandez^{1,2}, Joseph Therriault^{1,2}, Firoza Lussier^{1,3}, Gleb Bezgin¹, Cécile Tissot^{1,2}, Stijn Servaes^{1,2}, Yi-Ting Wang^{1,2}, Sulantha Matotharachchi¹, Jenna Stevenson², Nesrine Rahmouni^{1,2}, Min Su Kang⁴, Vanessa Pallen², Peter Kunach¹, Kely Quispialaya^{1,2}, Nina Margherita-Poltronetti², Tharick Pascoal³, Pedro Rosa-Neto^{1,2}

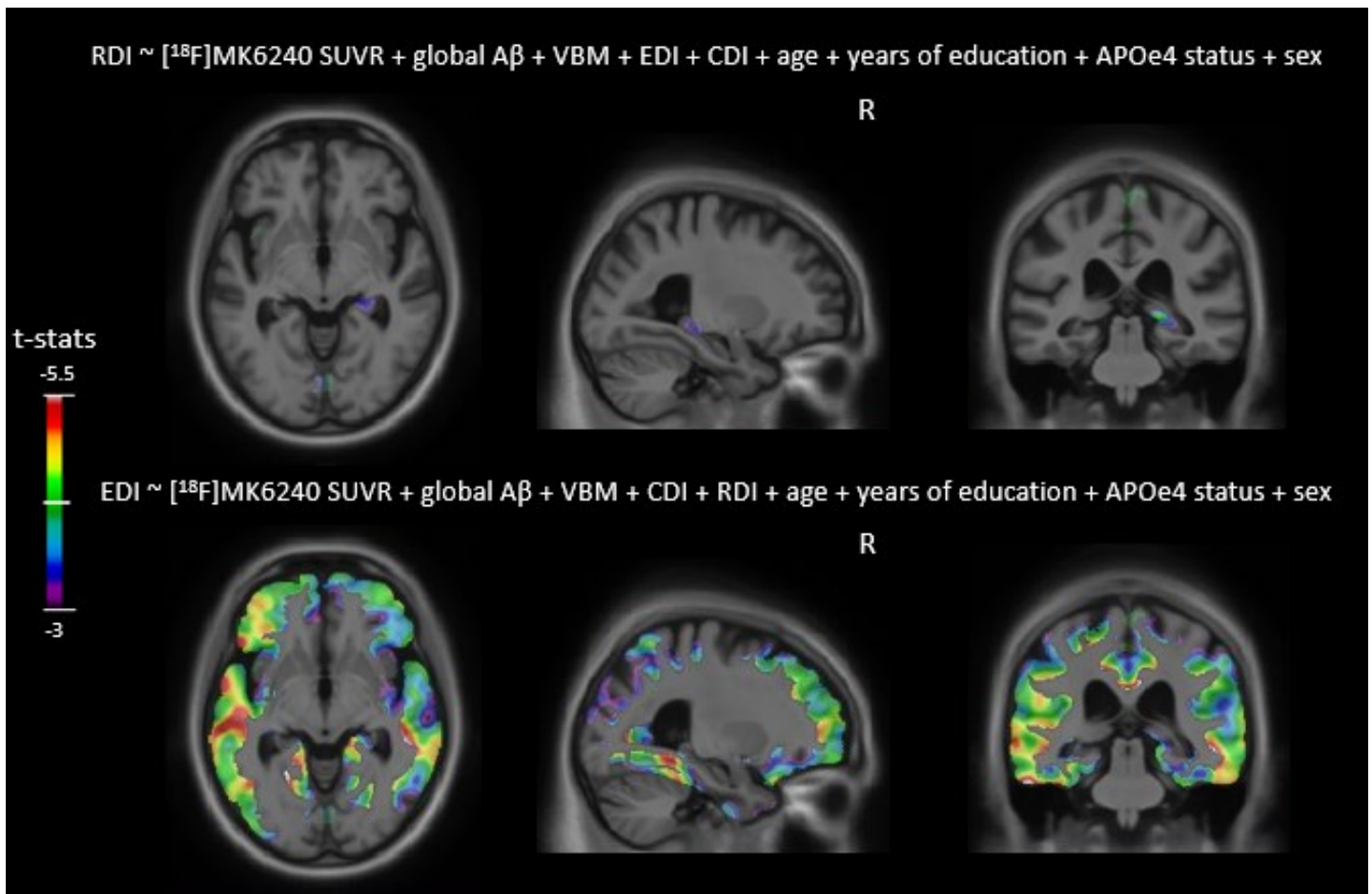
¹Translational Neuroimaging Laboratory, Montreal Neurological Institute, McGill University, Montreal, QC, Canada

²McGill University Research Centre for Studies in Aging, Verdun, QC, Canada

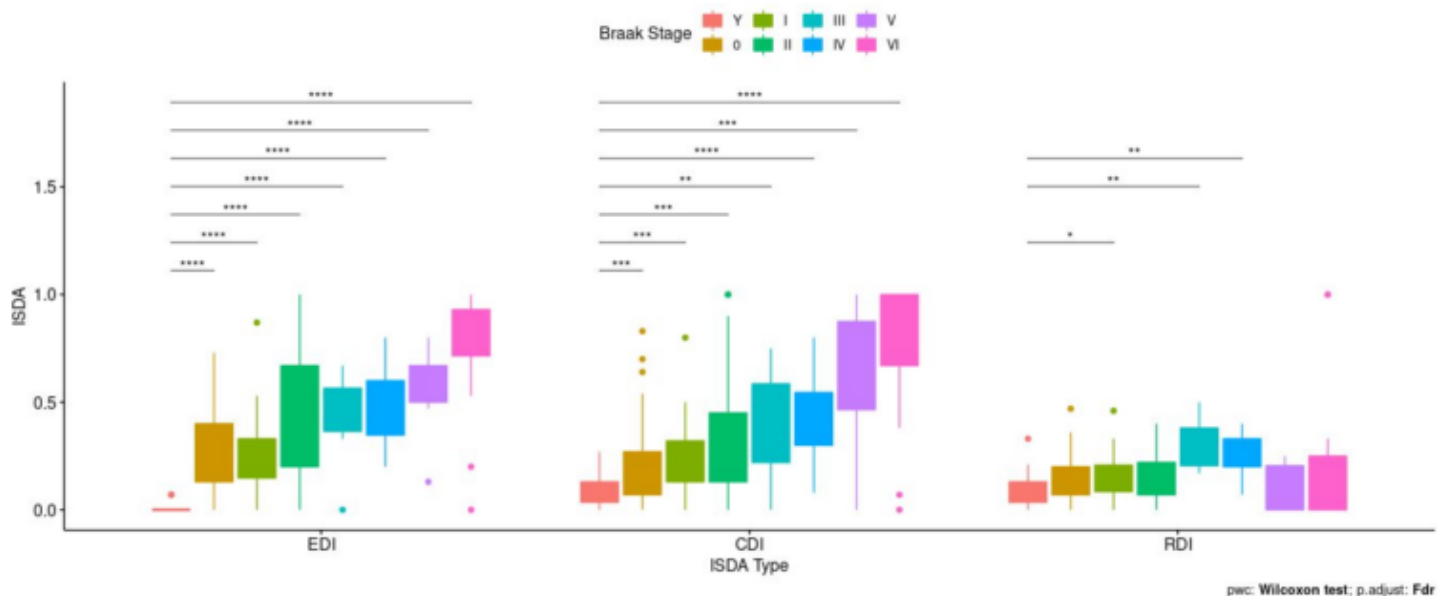
³Department of Psychiatry, University of Pittsburgh, Pittsburgh, PE, US

⁴Sunnybrook Health Sciences Centre, Toronto, ON, Canada





Anova, $F(11.81, 416.55) = 18.58, p < 0.0001, \eta_p^2 = 0.18$



Background: Memory processing has been classically divided into encoding, consolidation and retrieval stages. In Alzheimer's disease, some research suggests that memory decline results from encoding deficits. We aimed to explore memory stages of processing across the Alzheimer's disease spectrum and their association with ATN biomarkers.

Methods: Structural MRI, amyloid PET ($[^{18}F]AZD4694$) and tau PET ($[^{18}F]-MK6240$) scans were acquired for 33 young (<26y.o.) participants, 146 cognitively unimpaired elderly (CU), 40 MCI $A\beta^+$ patients and 32 AD $A\beta^+$ patients. MRI were segmented into probabilistic grey (GM) and white (WM) maps, non-linearly registered to the ADNI template using Dartel and smoothed with an 8mm FWHM gaussian kernel. Encoding, consolidation and retrieval scores were

derived from the RAVLT using the item-specific deficit approach. We used nonparametric comparisons and voxel-wise analyses to explore our hypotheses.

Results: All memory processes declined at old age, particularly encoding. Further decline was significant from PET-Braak stage II onwards for encoding and consolidation, and at PET-Braak III and IV for retrieval. At late stages, encoding and consolidation decline sharply. Retrieval deficits were associated with tau load in R pHC, and some posterior medial areas. Encoding associated with tau in neocortical frontal and temporal regions predominantly on the left hemisphere. Encoding deficits were also related to smaller brain volumes in some neocortical areas. No significant associations were found with amyloid PET and between consolidation and biomarkers.

Conclusions: our results indicate that encoding is the process most affected by age. Encoding and consolidation deficits can be detected at PET-Braak II when compared to healthy elderly, while retrieval remains unchanged until PET-Braak III. However, only retrieval associates with accumulation of tau in early PET-Braak stage regions, while encoding relates to tau and brain volume in neocortical regions. Late PET-Braak stages steep decline in encoding and preservation of retrieval may indicate encoding deficits' takeover.

Keywords: memory stages, tau PET, early decline, PET-Braak, Alzheimer's disease

P75 Comorbid medical conditions, anxiety, and amyloid- β pathology in cognitively unimpaired older adults

Olamide Abiose¹, Christina B. Young¹, Joseph Winer¹, Kacie Deters², Elizabeth Mormino¹

¹Stanford University School of Medicine Department of Neurology & Neurological Sciences, Stanford, CA, US

²University of California Los Angeles Department of Integrative Biology & Physiology, Los Angeles, CA, US

OBJECTIVES: Comorbid medical conditions are common in Alzheimer's disease (AD) and can influence disease severity. We examined the extent to which they influence early amyloid- β pathology and cognition.

Methods: We analyzed data from 4479 clinically unimpaired older adults in the A4/LEARN study who underwent florbetapir PET imaging. Current symptoms and/or disorders across fourteen disease categories were summed to calculate the total number of concurrent medical conditions. Individual disease categories were binarized when used to predict amyloid- β pathology. Anxiety symptoms were captured by the State-Trait Anxiety Inventory (STAI), and cognition was measured by the digit symbol substitution test. We used linear regression analyses controlling for age, sex, and ethnoracial group when predicting amyloid burden or comorbidity; we further controlled for years of education when predicting cognitive performance.

Results: There was a significant relationship between the concurrent medical conditions and amyloid PET SUVR ($\beta = 0.003$, $p < 0.0001$). Psychiatric ($\beta = 0.019$, $p = 0.003$), cardiovascular ($\beta = 0.012$, $p = 0.033$), dermatologic ($\beta = 0.018$, $p = 0.015$), and musculoskeletal ($\beta = 0.019$, $p = 0.001$) symptoms and disorders were significantly associated with amyloid PET SUVR values. A number of lifestyle factors were associated with the concurrent medical conditions; however, only sleep ($\beta = -0.007$, $p = 0.013$) and anxiety symptom severity predicted amyloid- β pathology ($\beta = 0.003$, $p = 0.004$). Amyloid PET SUVR ($\beta = -3.000$, $p < 0.0001$), anxiety symptoms ($\beta = -0.105$, $p = 0.009$), and medical conditions ($\beta = -0.155$, $p < 0.0001$) exhibited independent effects on cognition within the same model; additionally, medical conditions and amyloid- β pathology interacted to significantly predict digit symbol performance ($\beta = 0.296$, $p = 0.038$).

Conclusions: These findings suggest that amyloid- β , anxiety symptoms, and concurrent medical conditions may reflect distinct, yet overlapping, biological pathways relevant to cognition and dementia risk.

Keywords: amyloid PET, anxiety, comorbidity, cognition, epidemiology

P76 Defining and characterizing neocortical tau resistance in preclinical Alzheimer's disease

Rachel Buckley¹, Hannah Klinger, Rory Boyle, Gillian Coughlan, Bernard Hanseeuw, Hyun-Sik Yang, Rebecca Amariglio, Dorene Rentz, Diana Townsend, Michelle Farrell, Heidi Jacobs, Zahra Shirzadi, Wai-Ying Yau, Julie Price, Jasmeer Chhatwal, Aaron Schultz, Timothy Hohman, Michael Donohue, Michael Properzi, Keith Johnson, Reisa Sperling

¹Massachusetts General Hospital, Department of Neurology, Boston, MA, US

²Vanderbilt University Medical Center, Department of Neurology, Nashville, TN, US

³Massachusetts General Hospital, Department of Radiology, Boston, MA, US

⁴Brigham and Women's Hospital, Department of Neurology, Boston, MA, US

⁵University of Southern California, Keck School of Medicine, San Diego, CA, US

Background: Topographical staging of tauopathy in preclinical Alzheimer's disease (AD) posits early deposition in the entorhinal region (medial temporal lobe; MTL) followed by spread to adjacent neocortical (NEO) regions, like the inferior temporal gyri. Predictive models support a temporal cascade of tau deposition as baseline MTL tau robustly predicts NEO tau accumulation¹⁻³. In clinically normal (CN) Ab⁺, elevated tau in both MTL and NEO is associated with faster rates of progression to dementia relative to those with only elevated MTL tau⁴. What remains unclear is frequency and profile of neocortical tau resistance (defined as MTL+/NEO-) in CN Ab⁺.

Methods: To define tau-PET thresholds, we selected all participants from ADNI, A4 and HABS with Flortaucipir-PET scans (n=1259). Using two-component Gaussian mixture models with a posterior probability of 50%⁵, we identified tau-abnormality thresholds for entorhinal (MTL+) and inferior temporal (NEO+) distributions of tau-PET SUVrs. Due to unequal sample sizes, we used non-parametric group comparisons to determine demographic differences.

Results: We found a partial volume corrected SUVr threshold of 1.44 and 1.45 for MTL+ and NEO+, respectively (see Fig.1). CN Ab⁺ were identified as MTL-/NEO- (n=308;63%), MTL+/NEO- (neocortical tau resistant; n=265;5%) and MTL+/NEO+ (n=155;32%). Only 5% of CNAb⁺ were defined as MTL+/NEO- (see Fig.2). MTL+/NEO- showed a higher proportion of APOEε4, more years of education, lower cross-sectional PACC performance and higher global PiB-PET burden (Fig.3). The MTL-/NEO- and MTL+/NEO- did not differ markedly from one another, excepting that MTL-/NEO- included all Asian participants.

Conclusion: Our preliminary findings suggest that resistance to neocortical tau in CN Ab⁺ exists in 5% of our sample, aligning with other prevalence estimates in independent cohorts⁶. Given the complexities with determining tau-PET thresholds⁷, our approach to identifying NEO+ may be too conservative. We will explore different definitions of tau resistance and seek to validate its plausibility via clinical progression and longitudinal tau-PET data.

Figure 1.

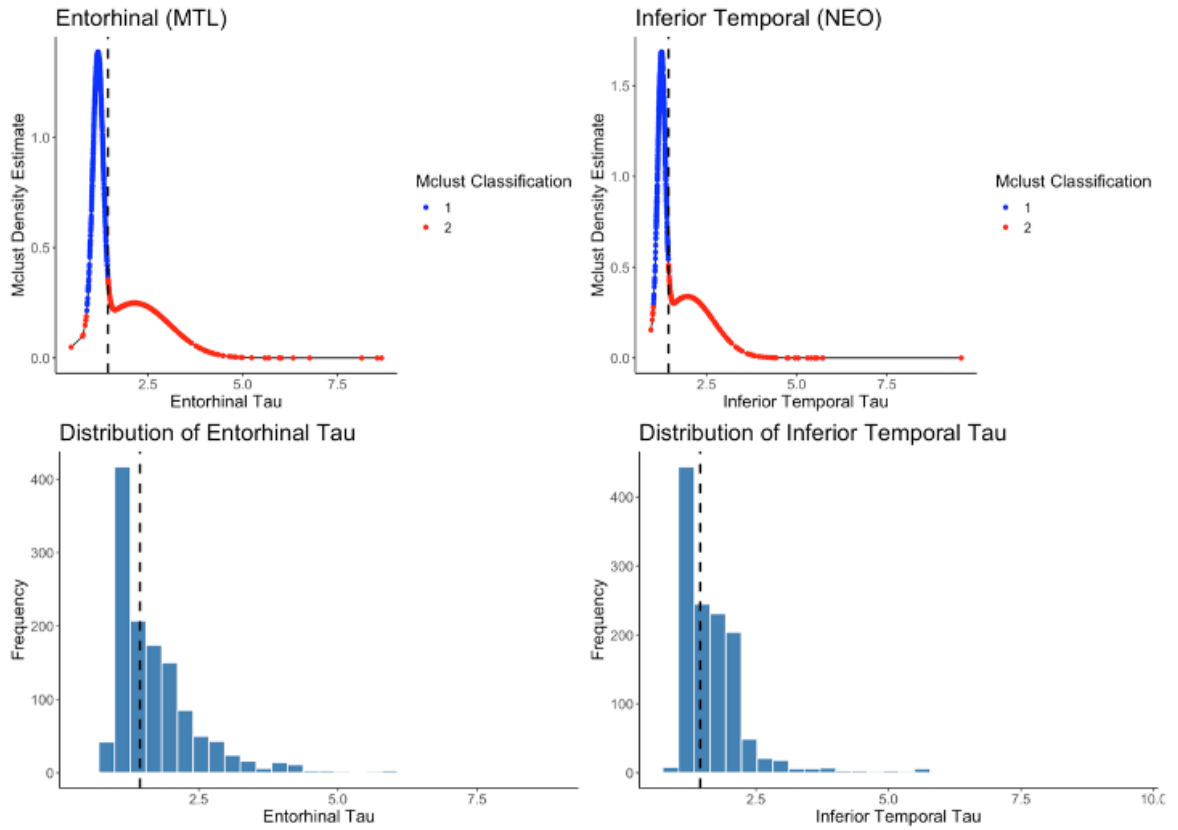


Figure 2.

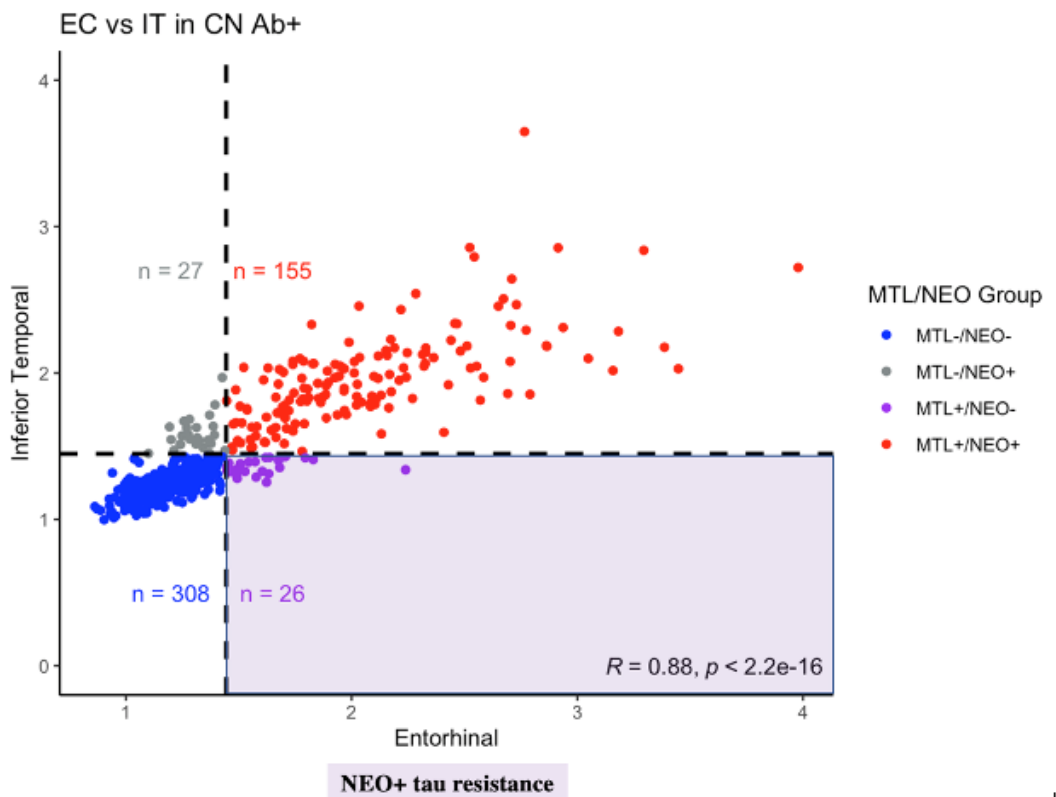


Figure 3.

MTL-/NEO-
 vs.
MTL+/NEO-
 No differences between these groups,
 EXCEPT, that **MTL+/NEO-** exhibits a
 greater frequency of APOEε4 carriers
 than both other groups
 All Asian participants sit in the
MTL-/NEO- group
MTL+/NEO-
 vs.
MTL-/NEO-
MTL+/NEO+
 More years of education, Higher
 PiB FLR burden in **MTL+/NEO-**,
 but lower cross-sectional PACC
 than **MTL-/NEO-** and
MTL+/NEO+

Table of CN Ab+ Individuals without MTL-/NEO+ Group

Characteristic	MTL-/NEO-, N = 308 ¹	MTL+/NEO-, N = 26 ¹	MTL+/NEO+, N = 155 ¹	p-value ²
Age	72.50 (5.09)	72.12 (4.36)	79.76 (7.79)	<0.001
Sex				0.6
F	173 (56.17%)	15 (57.69%)	95 (61.29%)	
M	135 (43.83%)	11 (42.31%)	60 (38.71%)	
Education	16.01 (2.86)	17.00 (2.51)	16.53 (2.49)	0.025
APOE				0.055
e4+	179 (58.69%)	19 (82.61%)	82 (56.16%)	
e4-	126 (41.31%)	4 (17.39%)	64 (43.84%)	
Race				<0.001
White	280 (92.11%)	26 (100.00%)	137 (89.54%)	
Black or African American	7 (2.30%)	0 (0.00%)	16 (10.46%)	
Asian	17 (5.59%)	0 (0.00%)	0 (0.00%)	
Ethnicity				0.073
Not Hispanic or Latino	298 (98.35%)	25 (96.15%)	145 (94.77%)	
Hispanic or Latino	5 (1.65%)	1 (3.85%)	8 (5.23%)	
Baseline PACC	0.19 (0.73)	0.00 (0.99)	0.49 (0.73)	<0.001
Closest PACC	0.18 (0.73)	-0.07 (0.91)	0.39 (0.77)	0.001
Closest PIB	1.34 (0.15)	1.44 (0.15)	1.37 (0.21)	0.009
Entorhinal Tau	1.17 (0.12)	1.60 (0.17)	2.07 (0.47)	<0.001
Inferior Temporal Tau	1.22 (0.09)	1.35 (0.05)	1.96 (0.32)	<0.001

¹Mean (SD); n (%)

²Kruskal-Wallis rank sum test; Pearson's Chi-squared test; Fisher's exact test

Keywords: Amyloid, Tau, Resistance, PET

P77 Development and evaluation of image preprocessing pipelines for the Centiloid method

Weiquan Luo¹, Davneet Minhas¹, Ethan Rubenstein², David Situ³, Sarah Royse^{1,4}, Beau Ances⁵, Bradley Christian⁶, Ann Cohen⁷, Benjamin Handen⁷, William Klunk⁷, Dana Tudorascu⁷, Shahid Zamon⁸, Charles Laymon^{1,3}

¹Department of Radiology, University of Pittsburgh, Pittsburgh, PA, US

²Department of Computer Science, University of Pittsburgh, Pittsburgh, PA, US

³Department of Bioengineering, University of Pittsburgh, Pittsburgh, PA, US

⁴Department of Epidemiology, University of Pittsburgh, Pittsburgh, PA, US

⁵Department of Neurology, Washington University, St. Louis, MO, US

⁶Department of Radiology, University of Wisconsin, Madison, WI, US

⁷Department of Psychiatry, University of Pittsburgh, Pittsburgh, PA, US

⁹Department of Psychiatry, University of Cambridge, Cambridge, UK

Background: The Centiloid method (Klunk-2015) provides a standardized procedure to quantify brain amyloid. The method entails registration of PET to MR and warping to a template and requires adequate MR and PET image quality. In the Neurodegeneration in Aging Down Syndrome (NiAD) study, we observe a higher Centiloid processing failure rate (Figure 1) in the Down Syndrome (DS) cohort compared to non-DS subjects, due to MR motion artifacts and morphology. Our goal is to improve the success rate of DS Centiloid by developing (1) rigorous quality-assurance (QA) criteria and (2) alternative pipelines that are interchangeable with the standard pipeline.

Method: QA procedures were developed by characterizing the degree to which visually apparent registration/normalization deficiencies affect Centiloid score. To improve the success rate, we developed 6 pipelines by adding 4 preprocesses into the standard pipeline: automated MR/template origin matching (reset origin), N4 bias correction, co-registration using a smoothed PET image, and MR skull-stripping. We ran all pipelines on Standard Centiloid GAAIN (n=79) and NiAD PiB-PET and T1 MRI (n=319) datasets. Results were rated as pass/fail using the new QA procedures. Regression analyses between the Centiloid values obtained using the standard and modified pipelines were performed. Following the reproducibility criteria of Klunk-2015, regression results were evaluated to determine the compatibility of modified pipelines with the standard pipeline.

Results: From the regression analysis (Figure 2) using the GAAIN dataset, all modified pipelines met reproducibility criteria (Table 1). Using the NiAD data, 5 out of 6 pipelines met reproducibility criteria, with the 6th pipeline's slope off by 0.006. By combining the results from 6 pipelines, the success rate for processing NiAD scans increased from 68.0% (standard pipeline) to 95.3%.

Conclusion: Compatibility of the standard and five modified pipelines is established. Additional preprocessing steps significantly improve the success rate of Centiloid processing for DS imaging.

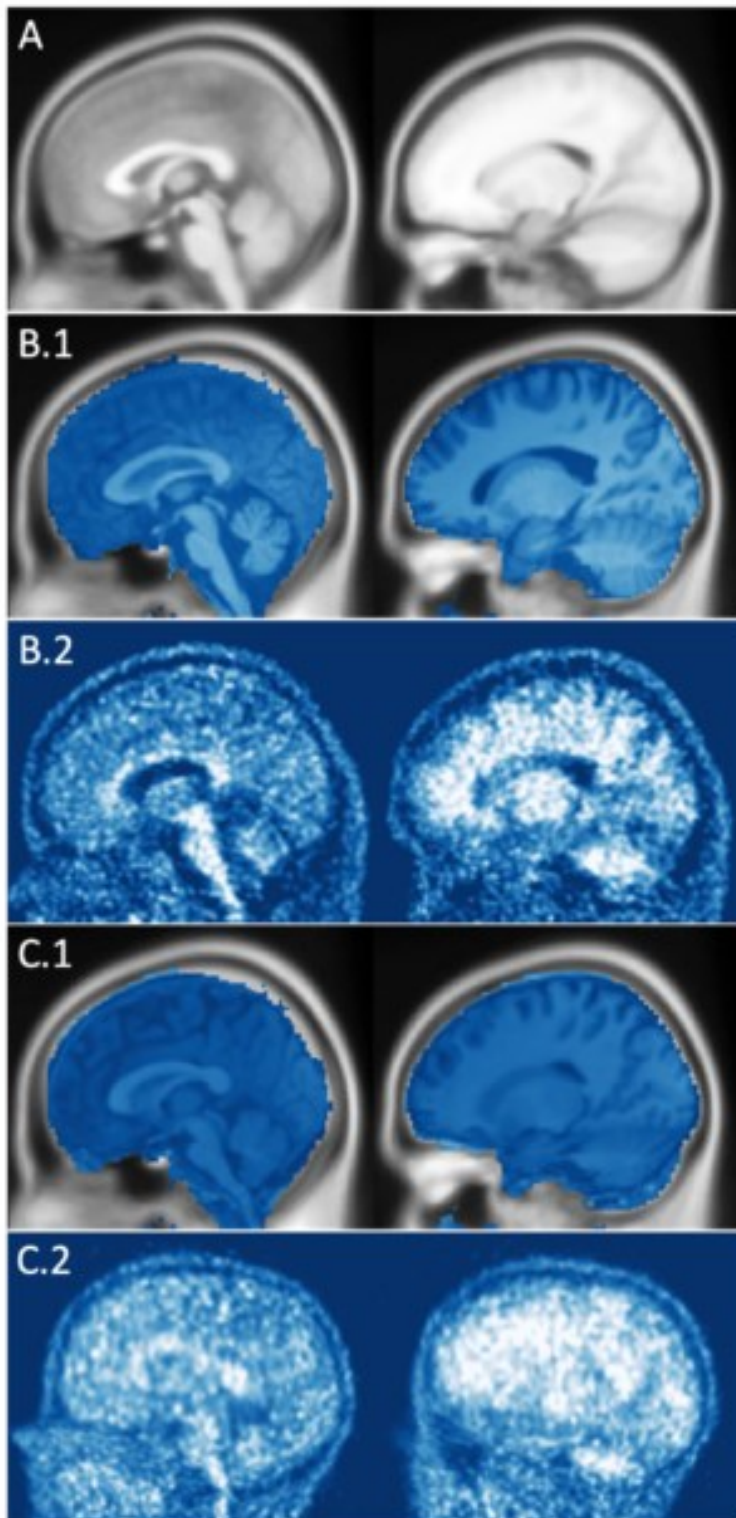


Figure 1. examples for warped MR and PET images in MNI template space: MNI template (A); MR (B.1) with good normalization and PET (B.2) with good co-registration of a same subject; MR (C.1) with bad normalization and PET (C.2) with bad co-registration of a same subject.

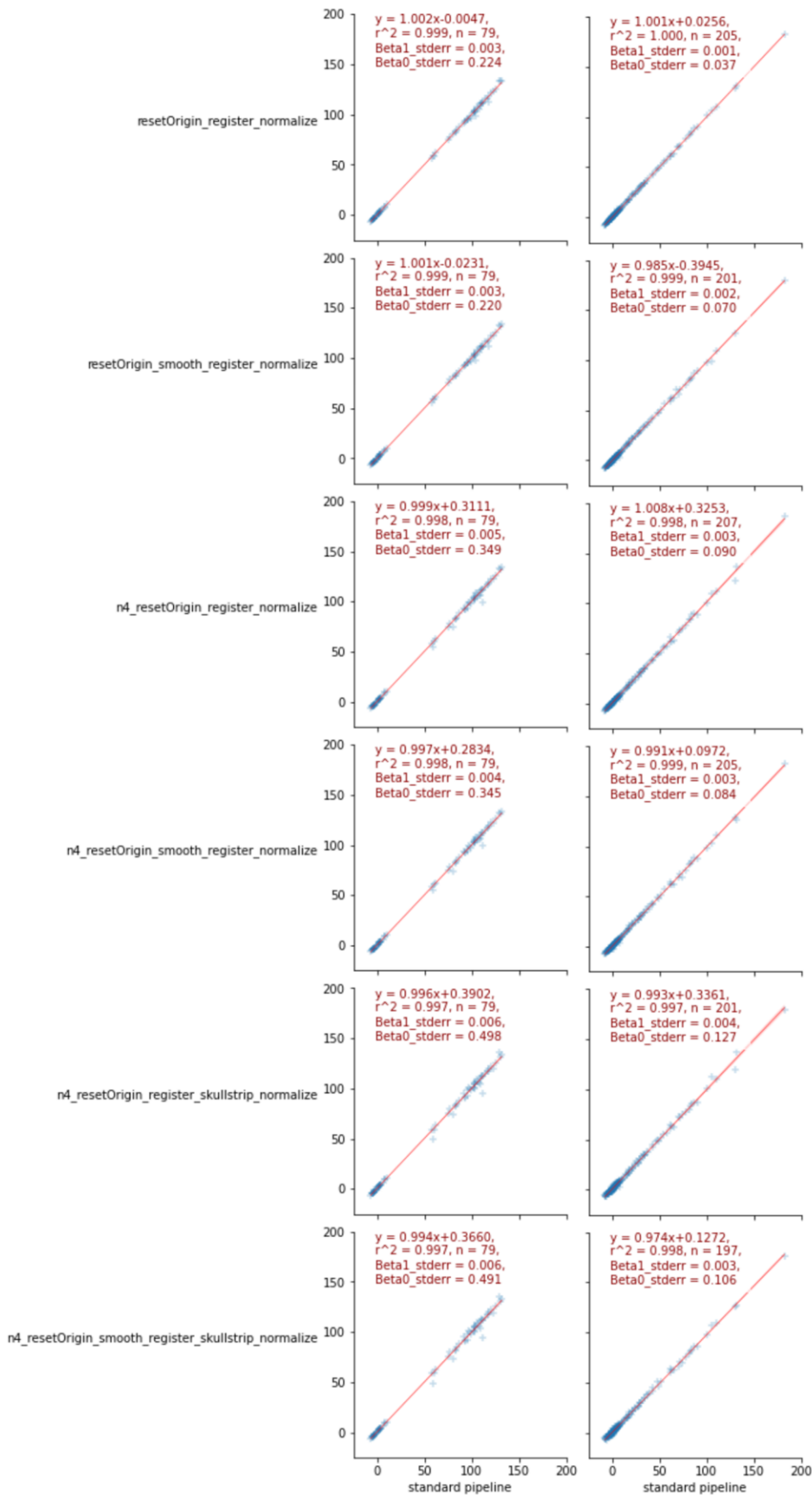


Figure 2: Linear regression results comparing Centiloid values from the standard pipeline (x-axis) to the each of modified pipelines (y-axis). Results are shown for GAAIN dataset (first column) and NiAD dataset (second column). The regression models show in each subplot with additional statistics: sample size (n), r squared (r^2), standard error of estimate slope (slope_sterr) and intercept (intercept_sterr)

Table 1: Linear regression parameters and R-squared between the standard pipeline and each of the modified pipelines for the GAAIN dataset and the NiAD dataset. For the NiAD data, regression was performed using those scans that passed the QA procedure. Green entries indicate that the reproducibility criteria described in *Alzheimers Dement.* 2015 Jan; 11(1): 1–15.e4 (Klunk-2015) were met: slope between 0.98 and 1.02, intercept between -2 and 2, and R-squared greater than 0.98.

pipeline_as_x	GAAIN			NiAD (QA)		
	slope	intercept	R2	slope	intercept	R2
resetOrigin_register_normalize	1.002	-0.005	0.999	1.001	0.026	1.000
resetOrigin_smooth_register_normalize	1.001	-0.023	0.999	0.985	-0.395	0.999
n4_resetOrigin_register_normalize	0.999	0.311	0.998	1.008	0.325	0.998
n4_resetOrigin_smooth_register_normalize	0.997	0.283	0.998	0.991	0.097	0.999
n4_resetOrigin_register_skullstrip_normalize	0.996	0.390	0.997	0.993	0.336	0.997
n4_resetOrigin_smooth_register_skullstrip_normalize	0.994	0.366	0.997	0.974	0.127	0.998

Keywords: PET, Centiloid, Amyloid

P78 Cognitively estimated disease time: Associations with amyloid and tau burden in the Harvard Aging Brain Study

Diana Townsend¹, Michael Properzi, Tobey Betthausen, Hannah Klinger, Rory Boyle, Gillian Coughlan, Bernard Hanseeuw, Hyun-Sik Yang, Rebecca Amariglio, Michelle Farrell, Heidi Jacobs, Zahra Shirzadi, Wai-Ying Yau, Julie Price, Jasmeer Chhatwal, Dorene Rentz, Keith Johnson, Reisa Sperling, Aaron Schultz, Rachel Buckley

¹Department of Neurology, Massachusetts General Hospital, Boston, MA, US

²University of Wisconsin School of Medicine and Public Health, Madison, WI, US

³Department of Radiology, Massachusetts General Hospital, Boston, MA, US

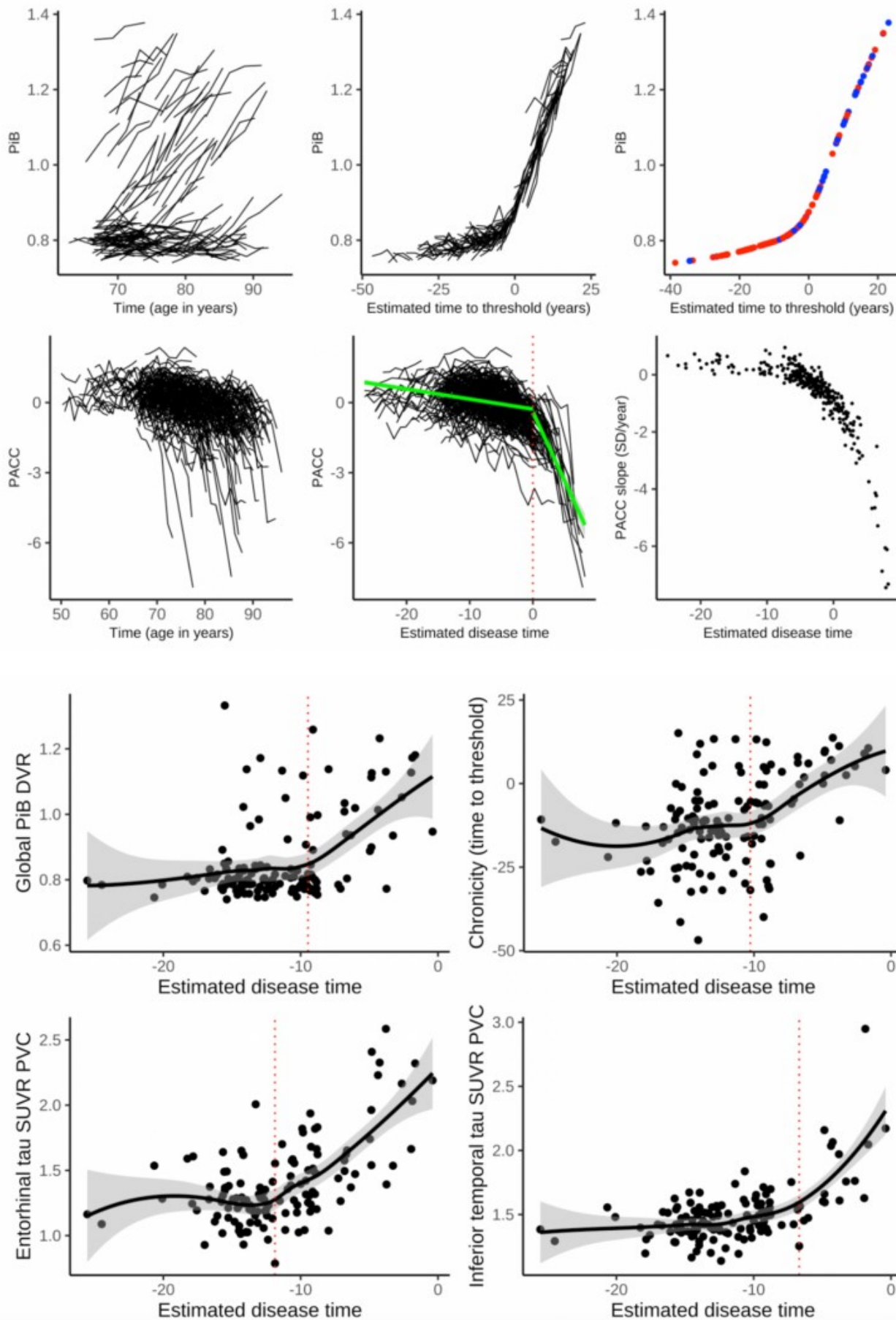
⁴Department of Neurology, Brigham and Women's Hospital, Boston, MA, US

Background: Sporadic Alzheimer's disease (AD) dementia is characterized by heterogeneous onset and course. In observational studies of preclinical AD, the estimation of an individual's placement on a cognitive continuum is obscured by an arbitrary 'baseline'. Optimizing longitudinal cognitive trajectories can distill many observations into a single metric that reflects an estimated disease time (EDT). Our goal was to examine associations between EDT (Fig1.bottom) and baseline neocortical A β , time to A β + threshold (Fig1.top), and tau burden in initially clinically normal older adults.

Methods: We identified 135 participants from the Harvard Aging Brain Study (age_{mean}: 72years(7.6SD); Female:62%) with >3 neuropsychological assessments, PiB-PET acquisitions, Flortaucipir-PET acquisitions, and diagnostic follow-up. To define disease time, we used iterative non-linear least-squares optimization to define a curvilinear function that described the group-level PACC trajectory. Each participant's PACC trajectory was subsequently located on the curve using trust-region-reflective non-linear least-squares optimization (Fig.1bottom) and anchored at zero by the inflection point of cognitive-decline acceleration identified by piecewise linear mixed-effects models. We then examined piecewise linear regression associations between the EDT metric and time to A β + (Fig.1top), and cross-sectional measures of neocortical A β PiB-PET DVR, entorhinal cortex (EC) and inferior temporal (IT) FTP-PET SUV_r (PVC).

Results: Piecewise regression revealed knots in the data where associations between EDT and AD biomarkers became significant. Associations with EC-tau were significant at -11.9 years EDT from cognitive-inflection, while A β burden and chronicity became significant at -9.4 and -10.3years EDT, respectively (Fig.2). Higher levels of IT-tau were associated with EDT temporally later at -6.7years EDT (Fig.2D).

Discussion: Our EDT metric recapitulated the expected temporal trend of AD biomarker associations with cognitive decline onset in the order of: EC tau-PET>A β -PET>time to A β -PET+>IT tau-PET. Notably, considerable heterogeneity of biomarker signal is evident along the EDT, opening the door for future analyses that further explore between-subject heterogeneity in EDT.



Keywords: cognition, amyloid, tau, PET

P79 Synergistic interaction between sex, amyloid and phosphorylated tau predicts the longitudinal progression of tau tangles

Yi-Ting Wang^{1,2,3}, Joseph Therriault^{1,2,3}, Stijn Servaes^{1,2,3}, Cécile Tissot^{1,2,3}, Jaime Fernandez Arias^{1,2,3}, Nesrine Rahmouni^{1,2,3}, Arthur Macedo^{1,2,3}, Jenna Stevenson^{1,2,3}, Alyssa Stevenson^{1,2,3}, Arlette Haeger^{1,2,3}, Ali Hosseini^{1,2,3}, Tahniah Nazneen^{1,2,3}, Pedro Rosa-Neto^{1,2,3}

¹McGill Centre for Studies in Aging, Montreal, QC, Canada

²Translational Neuroimaging Laboratory, Montreal, QC, Canada

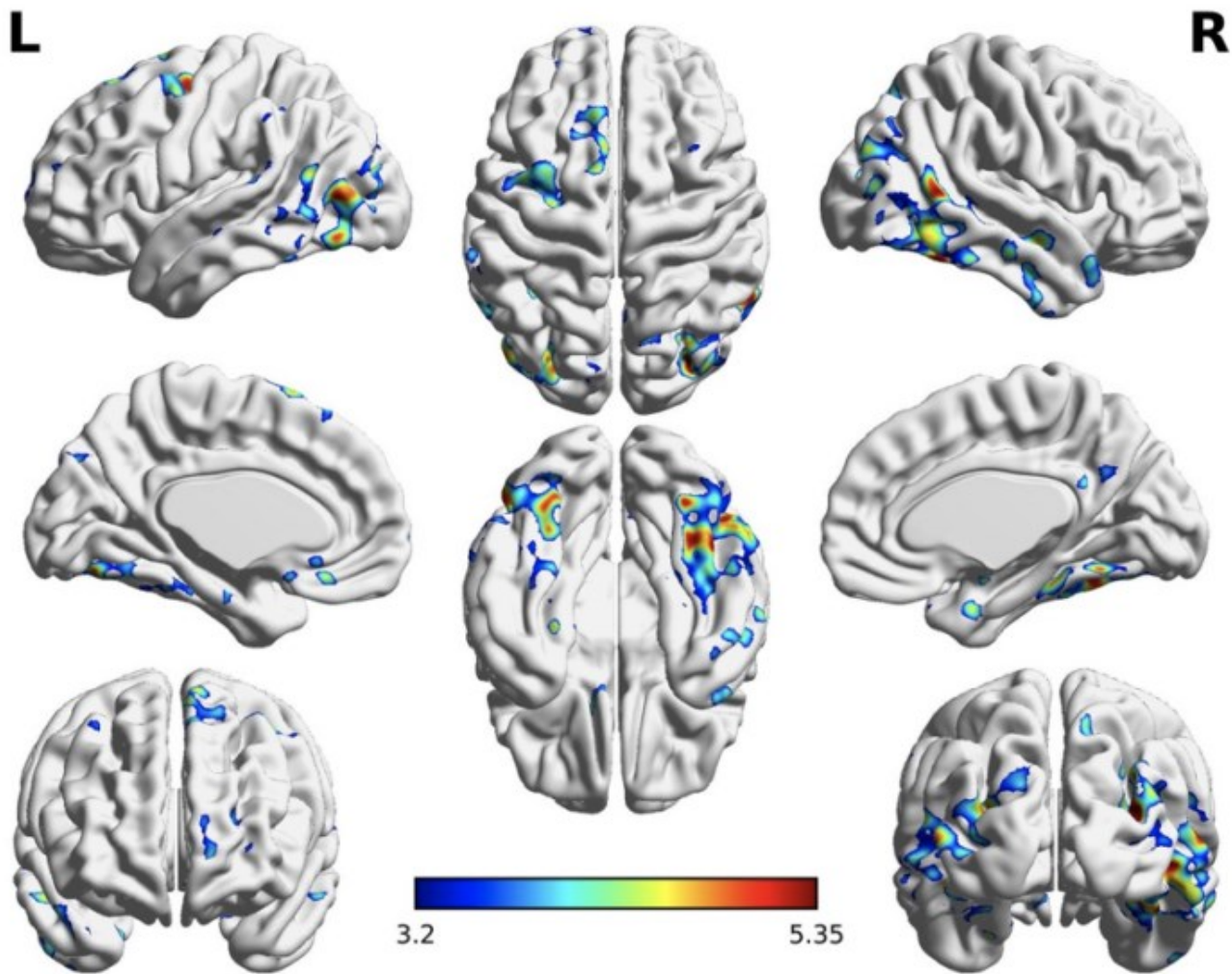
³McGill University, Montreal, QC, Canada

Background: The high prevalence of Alzheimer's dementia in females have long puzzled researchers in the field. Despite similar amyloid levels, females show higher load of neurofibrillary tangles. Previous literature proposed that amyloid- β (A β) and phosphorylated tau (p-tau) synergism accelerates biomarker abnormalities. However, it remains to be answered whether this synergism is the driving force behind faster tau progression in females.

Methods: In this study, we assessed 241 participants (mean age= 68.5 y.o., female n=143; male n=98) from TRIAD cohort at McGill Centre for Studies in Aging. Cerebral A β and tau deposition were assessed with positron emission tomography (PET) radiotracers [¹⁸F]AZD4694 ([¹⁸F]NAV4694) and [¹⁸F]MK6240 respectively. Cerebrospinal fluid (CSF) p-tau181 were also measured. Regression and voxel-based models with interaction terms were used to evaluate baseline tau load (n=241) and tau change rate (performed in a subgroup comprising 98 individuals who underwent two-year follow-up PET scans) as a function of sex and baseline biomarkers (A β and p-tau).

Results: We found that the synergism between sex, neocortical A β load and CSF p-tau181, rather than their main effects, was associated with the tau accumulation rate (Table 1). Furthermore, voxel-based analysis revealed that this synergism was most associated with tau increase in medial temporal and inferior parietal regions (Figure 1). Baseline tau load was only associated with main effects of the three parameters but not their synergistic interaction.

Conclusion: Together, the present results support that tau progression is driven by the synergistic interaction rather than a merely additive effect between sex, A β and p-tau.



Longitudinal tau progression is driven by the synergistic interaction between sex, $A\beta$ and p-tau. Age, APOE carriage status and clinical diagnosis were used as covariates in the model. Results were corrected for multiple comparisons using FDR cluster threshold of $P < 0.001$.

	Estimate	SE	t-Stat	p-Value
Sex (Female)	-0.0718	0.0424	-1.693	0.095
APOE carriage status	0.0320	0.0254	1.260	0.212
Age	0.0071	0.0142	0.497	0.621
Symptomatic (MCI/AD)	0.0190	0.0307	0.618	0.538
Neocortical Amyloid	-0.0068	0.0046	-1.481	0.143
CSF ptau181	-0.0094	0.0086	-1.088	0.280
Two-way Interaction				
Sex (Female) * Neocortical Amyloid	0.0136	0.0051	2.652	0.010
Sex (Female) * CSF ptau181	0.0280	0.0098	2.842	0.006
Neocortical Amyloid * CSF ptau181	0.0010	0.0004	2.307	0.024
Three-way Interaction				
Sex (Female) * Neocortical Amyloid * CSF ptau181	-0.0017	0.0005	-3.593	0.0006

Keywords: tau progression, phosphorylated tau, amyloid- β , sex difference, synergism

P80 [18F]PI-2620 binding patterns in patients with suspected AD- and FTLD-tauopathies

Ganna Blazhenets¹, David N. Soleimani-Meigooni¹, Wesley Thomas², Matthias Brendel³, Stephanie Vento¹, Lawren VandeVrede¹, Hilary W. Heuer¹, Peter Ljubenkov¹, Julio Rojas¹, Miranda Chen¹, Leonardo Iaccarino¹, Nidhi Mundada¹, Irene Litvan⁴, Murray Grossman⁵, Brad Boeve⁶, Alex Pantelyat⁷, Carmela Tartaglia⁸, David J. Irwin⁵, Brad C. Dickerson⁹, Suzanne L. Baker², Adam L. Boxer¹, Gil D. Rabinovici^{1,10,11}, Renaud La Joie¹

¹Memory and Aging Center, Department of Neurology, University of California, San Francisco, CA, US

²Lawrence Berkeley National Laboratory, Berkley, CA, US

³Department of Nuclear Medicine, University Hospital of Munich, LMU Munich, Munich, Germany

⁴University of California, San Diego, San Diego, CA, US

⁵Penn FTD Center, University of Pennsylvania, Philadelphia, PA, US

⁶Mayo Clinic, Rochester, MN, US

⁷Johns Hopkins University School of Medicine, Baltimore, MD, US

⁸University of Toronto, Toronto, ON, Canada

⁹Massachusetts General Hospital, Boston, MA, US

¹⁰Weill Institute for Neurosciences, University of California, San Francisco, CA, US

¹¹Department of Radiology and Biomedical Imaging, University of California, San Francisco, CA, US

Introduction: This multicenter study characterizes binding patterns of [18F]PI-2620 tau PET in patients with suspected AD- and FTLD-tau and explores its diagnostic value over various time windows.

Methods: N=27 (4-Repeat Tauopathy Neuroimaging Initiative, 4RTNI-2) and N=19 (UCSF-ADRC) patients underwent [18F]PI-2620 PET. N=19 amyloid-negative cognitively unimpaired controls (HC) from various cohorts were used as a control group (Table.1). Scans were acquired 30-60 minutes p.i.; SUVR maps (reference: inferior cerebellum) were created for the full acquisition and 10-min truncated windows (30-40, 35-45, ...). Voxel-wise *W*-score (age- and sex-adjusted) maps were computed to quantify binding relative to HC. Mean SUVR in eroded WM, temporal meta-ROI, globus pallidus (GP), and dentate nuclei (DN) were extracted for full and truncated windows.

Results: Patients with suspected AD (A β + MCI or AD dementia) showed high-intensity temporoparietal-predominant binding. At the group level, patients with clinical diagnoses that are more associated with FTLD-tau (PSP-RS, CBS, nfvPPA) exhibited tracer retention in basal ganglia that exceeded that of HCs, and the highest level of tracer retention was seen in PSP-RS (Fig.1A). At the individual level, patients with suspected FTLD-tau demonstrated heterogeneous striatal binding (Fig.1B). Compared to HC, AD and PSP-RS patients exhibited higher uptake in the temporal meta-ROI and GP, respectively (Fig.2). Truncated window analyses indicated a washout from all regions except the temporal meta-ROI, with significant group differences in tracer dynamic (time window*group, p 's<0.03). ROC-AUC for differentiating AD from HC was 0.93 for all time windows using temporal meta-ROI. Separation between FTLD-tau and HC using GP non-significantly improved with time: AUC=0.75 at 30-40-min versus 0.83 at 50-60-min acquisition (bootstrap p >0.1).

Conclusions: [18F]PI-2620 shows intense and consistent binding in AD, but lower intensity, heterogenous and rapidly reversible binding in non-AD tauopathies. Further work is needed to delineate the substrate and utility of [18F]PI2620 PET outside of the AD continuum.

Table 1. Demographic and clinical characteristics of the cohort.

Group	n	Age [years]	Male	PSP-RS Score	CDR	MMSE
HC	19	68 ± 10	32%	-	0.0 ± 0.0	29 ± 1
PSP-RS	12	70 ± 8	75%	30 ± 14	1.0 ± 0.5***	23 ± 3**
CBS	7	69 ± 5	29%	24 ± 17	0.4 ± 0.2	27 ± 3
nfvPPA	9	72 ± 6	67%	10 ± 8	0.6 ± 0.4*	22 ± 4*
Aβ+ MCI/D	13	73 ± 10	54%	0 ± 0	1.0 ± 0.7***	18 ± 8***
Aβ- MCI/D	5	69 ± 5	40%	2 ± 1	0.5 ± 0.0	26 ± 4

HC, healthy controls; PSP-RS, progressive supranuclear palsy with Richardson's syndrome; CBS, corticobasal syndrome; nfvPPA, non-fluent/agrammatic variant of primary aphasia; Aβ, amyloid status; MCI/D, mild cognitive impairment, or dementia; CDR-tot, clinical dementia rating total score; MMSE, mini-mental state examination. Significance of difference compared to HC: *** - $p < 0.001$; ** - $p < 0.01$; * - $p < 0.5$. Clinical information was not available for every participant.

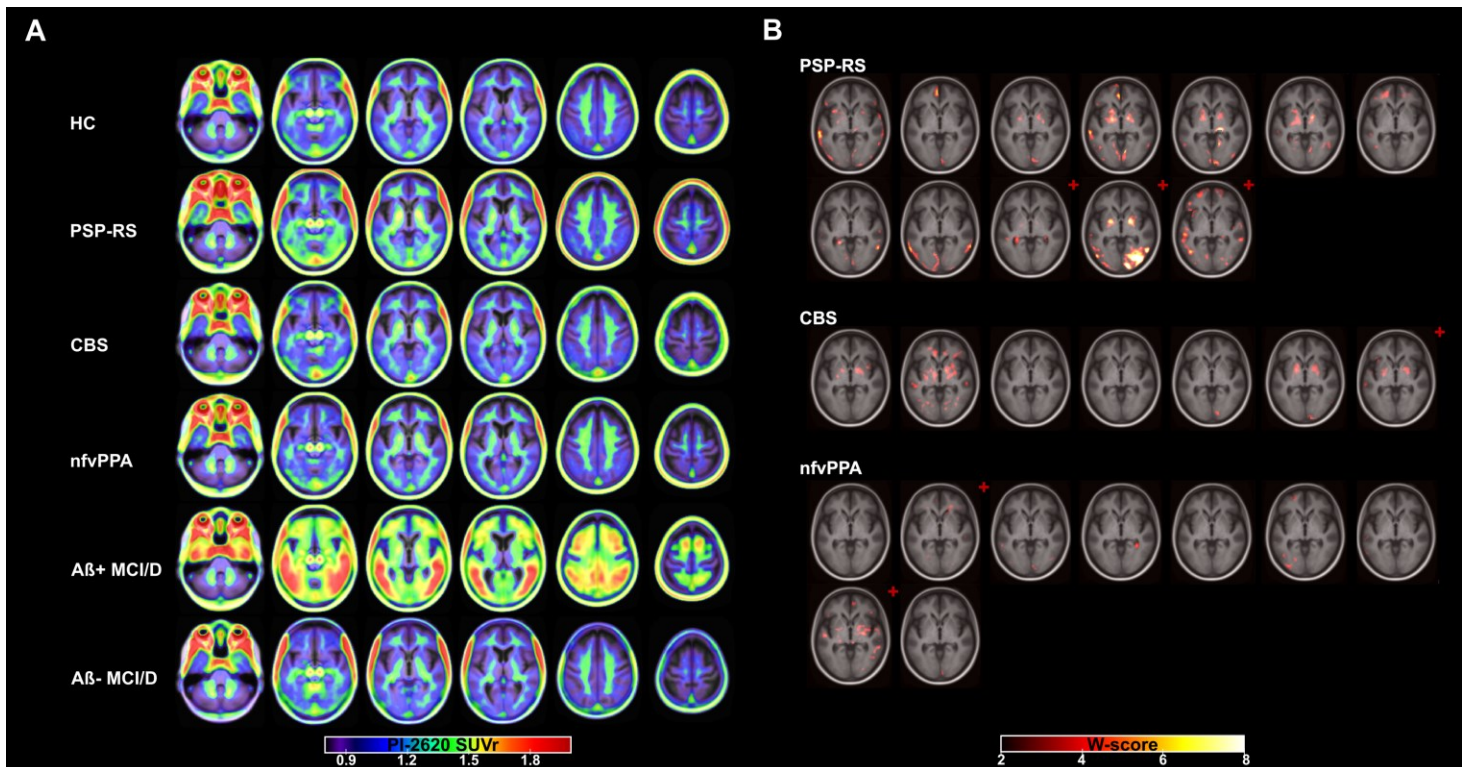


Figure 1. Results of the voxel-wise data analysis. (A) Group-averaged PI-2620 SUVR maps for each of the diagnostic groups. (B) W -score (age- and sex-adjusted) maps for each individual patient with suspected FTLD-tau pathology thresholded at $W > 2$, which corresponds to tracer uptake that is 2 SD above HC. Displayed are axial slices at the level of globus pallidus, with the W -score map overlaid on top of an MRI template. The red crosses indicate amyloid positive status. HC, healthy controls; PSP-RS, progressive supranuclear palsy with Richardson's syndrome; CBS, corticobasal syndrome; nfvPPA, non-fluent/agrammatic variant of primary aphasia; Aβ, amyloid status; MCI/D, mild cognitive impairment, or dementia.

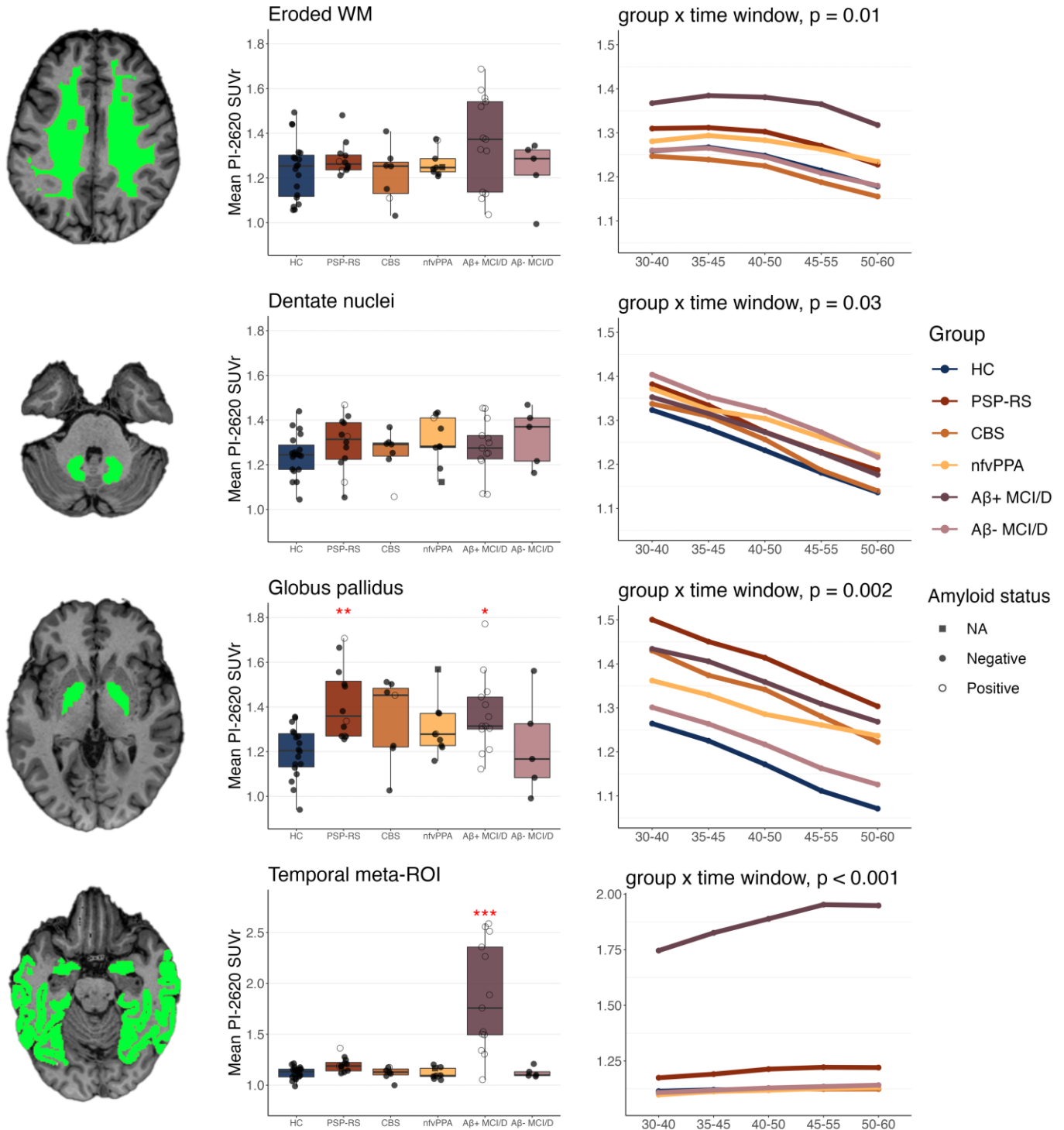


Figure 2. Results of the region of interest analysis. Each row shows an example of the region of interest defined in individual's native space and overlaid onto their corresponding MRI, followed by the group distribution of the SUVR values in the selected region. The last column reflects the change in group averaged SUVR over acquisition time. Stars indicate significance of difference in pairwise comparison to HC (age and sex adjusted): *** - $p < 0.001$; ** - $p < 0.01$; * - $p < 0.05$. P-value indicates significance of interaction between time and group calculated by linear mixed effects model. HC, healthy controls; PSP-RS, progressive supranuclear palsy with Richardson's syndrome; CBS, corticobasal syndrome; nfvPPA, non-fluent/agrammatic variant of primary aphasia; A β , amyloid status; MCI/D, mild cognitive impairment, or dementia.

P81 Regional analysis of change in synaptic density over time by cognitive status

Alexandra DiFilippo¹, Andrew Mcvea¹, Max Mclachlan¹, Mary-Elizabeth Pasquesi¹, Nancy Davenport-Sis¹, Erin Jonaitis¹, Gilda Ennis¹, Tobey Betthausen¹, Jonathan Engle¹, Sterling Johnson¹, Barbara Bendlin¹, Bradley Christian^{1,2}

¹University of Wisconsin-Madison School of Medicine and Public Health, Madison, WI, US

²University of Wisconsin-Madison Waisman Center, 53711, WI, US

Introduction Synaptic density loss has been observed in Alzheimer's disease (AD), but prior studies have mostly been restricted to post-mortem analyses where advanced disease pathology is already present. Little work has been done evaluating longitudinal synaptic density changes in older unimpaired and prodromal AD groups. Synaptic vesicle protein SV2A is expressed ubiquitously in the presynaptic terminals of neurons in gray matter and is the target of the PET radiotracer [¹¹C]UCB-J which is used to image synaptic density *in vivo*. Here, we examined longitudinal change in synaptic density among individuals with and without cognitive impairment.

Methods Participants (N=84) were recruited from the Wisconsin Alzheimer's Disease Research Center and the Wisconsin Registry for Alzheimer's Prevention studies (Table 1) to undergo longitudinal evaluations including cognitive testing and PET imaging: [¹¹C]PiB for amyloid load, [¹⁸F]MK-6240 for neurofibrillary tau burden, and [¹¹C]UCB-J to image synaptic density. The analyses performed here includes N=18 participants with longitudinal [¹¹C]UCB-J imaging. Synaptic density was quantified LGA DVR_{CS} in 12 Freesurfer (v7)-defined bilateral composite regions of interest that are known to be sensitive to AD pathology and neurodegeneration.

Results No notable changes in [¹¹C]UCB-J DVR_{CS} per year were observed in any region for either the impaired or unimpaired cognitive groups.

Conclusion In this analysis of longitudinal synaptic density changes in an older adult group with and without cognitive impairment, no significant change in synaptic density was observed in any brain region. However, group sizes were small and longitudinal data acquisition is ongoing to evaluate the relationship between amyloid load, tau burden, cognitive impairment, and the temporal course of synaptic density loss in Alzheimer's disease. Determining longitudinal trajectories of synaptic density loss is expected to inform upon abnormal trajectories and risk of cognitive decline, as well as provide normative data for earlier identification of dementia risk.

Table 1 Demographics and test results of study sample

	Cognitively Unimpaired	Cognitively Impaired
Participants (n)	13	5
Sex (F/M)	10/3	1/4
Age at Baseline (years)	67.9 (6.5) (58-81)	66.8 (3.8) (63-72)
Interscan Interval (years)	2.2 (0.5)	2.1 (0.3)
Amyloid +/-	2/11	1/4
PACC	-0.17 (1.02)	-0.99 (0.58)

Data are mean (SD) (range) for continuous variables. Interscan interval is the time in between [¹¹C]UCB-J scans. Amyloid positivity (A+) established if global [¹¹C]PiB DVR > 1.19 (25 CL) during the study period. PACC = Preclinical Alzheimer's Cognitive Composite score.

Table 2 [¹¹C]UCB-J DVR change in each ROI / year by cognitive group

Region	Cognitively Unimpaired (n = 13)		Cognitively Impaired (n = 5)	
Hippocampus	0.00	[-0.06, 0.04]	-0.02	[-0.07, 0.03]
Entorhinal	-0.01	[-0.07, 0.05]	0.00	[-0.08, 0.08]
Parahippocampus	0.00	[-0.05, 0.04]	0.01	[-0.06, 0.08]
Amygdala	-0.01	[-0.06, 0.05]	0.01	[-0.06, 0.08]
Prefrontal	0.00	[-0.07, 0.08]	0.02	[-0.05, 0.9]
Lateral Temporal	-0.01	[-0.07, 0.06]	0.01	[-0.8, 0.11]
Posterior Cingulate	0.01	[-0.07, 0.10]	0.02	[-0.8, 0.12]
Pericentral	0.01	[-0.07, 0.10]	0.01	[-0.04, 0.06]
Lateral Parietal	0.00	[-0.07, 0.08]	0.01	[-0.08, 0.10]
Lateral Occipital	0.00	[-0.06, 0.05]	0.01	[-0.09, 0.11]
Medial Occipital	0.01	[-0.06, 0.08]	0.00	[-0.10, 0.10]
Cerebellum	0.00	[-0.06, -0.06]	-0.03	[-0.11, 0.04]

Data are mean [¹¹C]UCB-J DVR change per year [95% confidence interval].

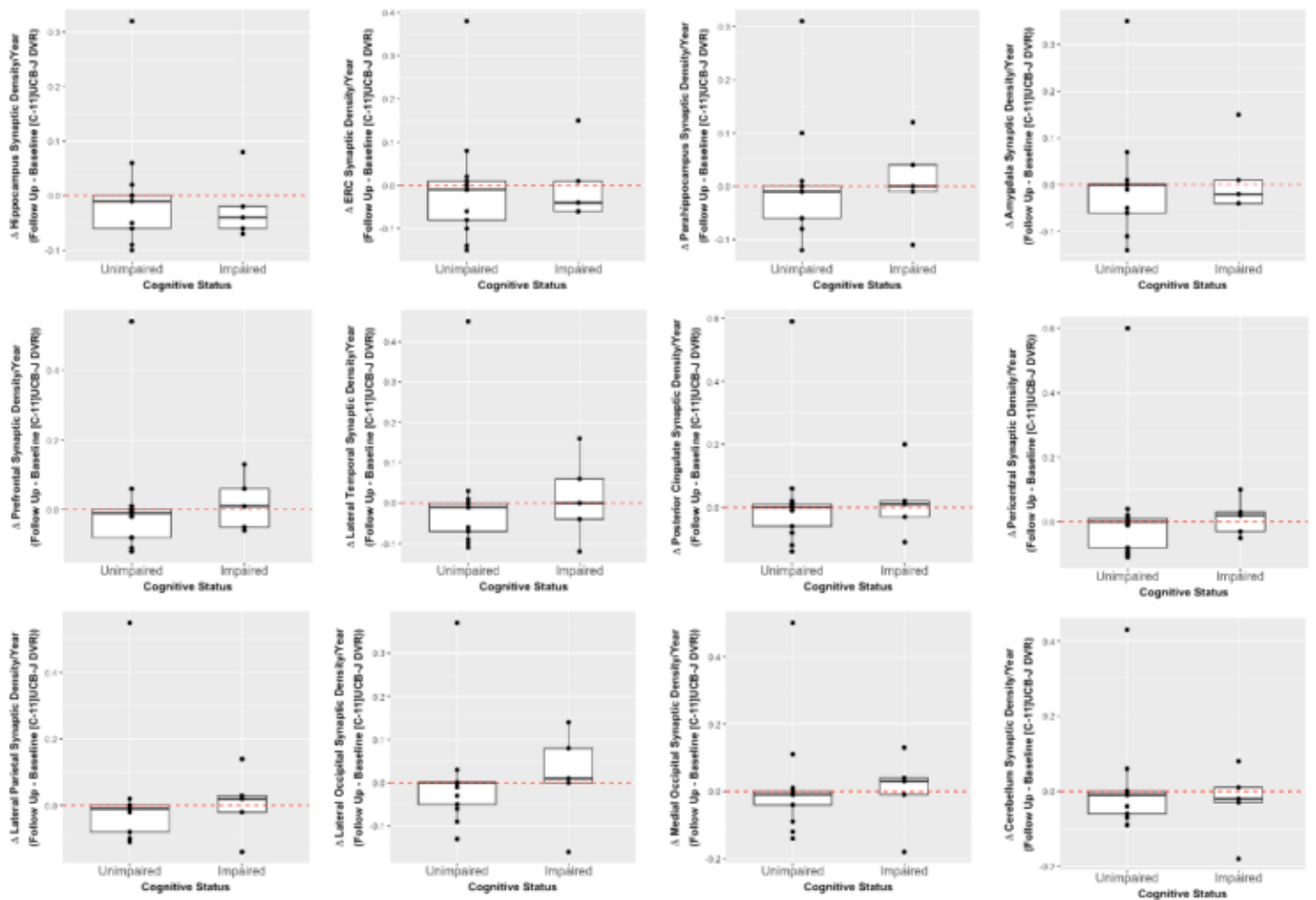


Figure 1 Difference in UCB-J DVR_{CS} per year in 12 Freesurfer-generated composite ROIs for each cognitive group. Synaptic density was quantified using LGA DVR_{CS} (centrum semiovale reference region) in 12 Freesurfer (v7)-defined bilateral composite ROIs that are known to be sensitive to AD pathology and neurodegeneration (Desikan-Killiany atlas). No notable changes in synaptic density were identified in any region of interest nor cognitive group.

Keywords: synapse, UCB-J, longitudinal, PET

P82 Regional tau profiles in early tau pathology populations

Vikas Kotari¹, Amanda Morris¹, Diana Otero Svaldi¹, Sudeepti Southekal¹, Ming Lu¹, Michael Pontecorvo¹, Emily Collins¹, Sergey Shcherbinin¹, For the Alzheimer's Disease Neuroimaging Initiative²

¹Eli Lilly and Company, Indianapolis, IN, US

²Alzheimer's Disease Neuroimaging Initiative (ADNI), , US

Background: The cross-sectional and longitudinal regional tau patterns at early states of tau pathology are critical for understanding Alzheimer's disease pathophysiology and for disease-modifying therapies^{1,2}. We sought to compare regional tau profiles of two cohorts, representative of early tau pathology. Furthermore, we examined whether participants' baseline characteristics influence cross-sectional and longitudinal tau PET patterns.

Methods: First cohort included 64 amyloid positive (A β +), clinically unimpaired participants (CU A+) from ADNI database. Second cohort included 88 A β +, clinically impaired participants from three clinical trials (18-F-AV1451-A05 Exploratory/ Confirmatory and EXPEDITION 3) with sub-threshold neo-cortical tau SUVR (CI A+/T-). We estimated flortaucipir SUVR and annualized mean change adjusted for age and baseline value from 35 cortical and sub-cortical regions using cerebellum-crus reference region. Longitudinal SUVR and signal-to-noise ratio (SNR, mean change divided by the standard deviation) was compared across regions.

Results: While there were significant differences ($p < 0.001$) in mean age, MMSE, and amyloid levels between cohorts, similar baseline global cortical tau level was observed (Table 1). Overall, we noticed similar ordering in magnitude of regional SUVRs at baseline. Entorhinal cortex and inferior temporal gyrus SUVR values were higher in the CI A+/T- group (Figure 1). Longitudinally, fusiform, inferior, middle temporal, bankstss, and inferior parietal gyri had substantially higher change and SNR in both cohorts. Bankssts and precuneus SUVR change was significantly higher in the CI A+/T- cohort (Figure 2). Our analysis suggests that the baseline group-level neo-cortical tau SUVR might play a key role in determining baseline and longitudinal regional tau patterns for a given population.

Conclusion: Two A β + early tau populations with similar mean global tau level, but different amyloid level and clinical phenotype showed similar regional patterns. These findings are useful in determining regional tau PET endpoints in interventional trials targeting early tau populations, although further examinations with larger datasets are required.

Table 1. Demographics of subjects

	ADNI cognitively unimpaired (CU) A β + participants CU A+	Cognitively impaired A β + "T-" patients ¹ in Avid and Lilly clinical trials ² CI A+T-
N	64	88
Follow-up period	20.8 (8.6)	18
Age, mean (SD)*	71.8 (5.5)	76.9 (7.5)
Gender (F / M)	35/ 29	33 / 55
MMSE, mean (SD)*	29.0 (1.2)	24.7 (2.9)
Amyloid level, CL, mean (SD)*	59.0 (30.3) N = 61	84.1 (38.4) N = 86
Tau level, Cortical VOI -CC, mean (SD)	1.072 (0.1)	1.046 (0.1)
<i>APOE4</i> Carrier Percentage	58.7%	58.6%

¹"T-" is determined quantitatively using the cut point for cortical Composite with cerebellar-crus (CC) reference. ²Participants from A05E, A05C, and EXPEDITION 3 trials are included; Data are represented as mean (S.D), CU= Cognitively unimpaired, CI = Cognitively impaired, A β = beta amyloid group.

Baseline mean \pm SD SUVR-CC

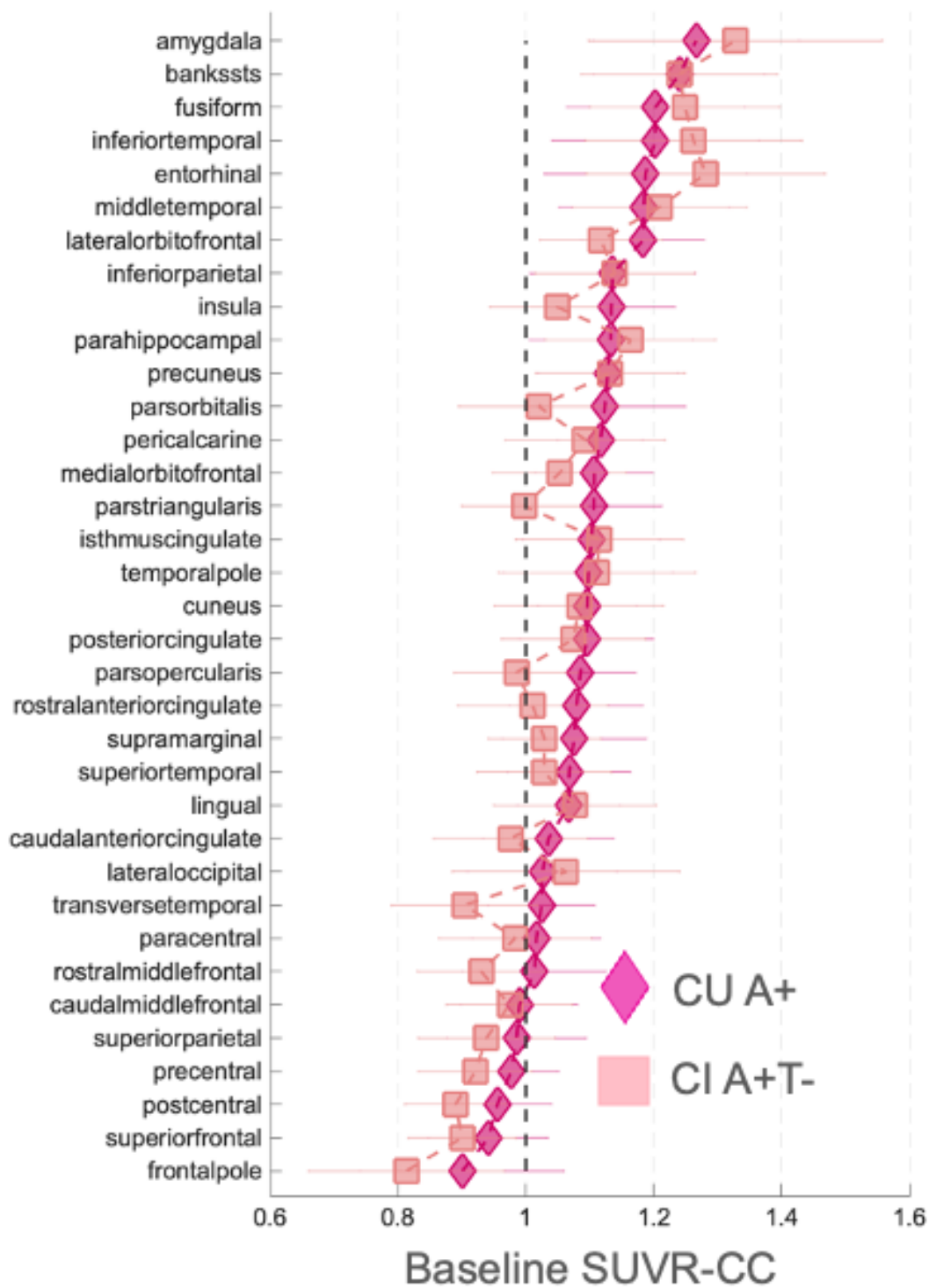


Figure 1. Waterfall plot showing the baseline regional tau profiles of CU A+ and CI A+/T- studies.

Annual rate of LS mean change \pm SE for CU A+ and CI A+/T-

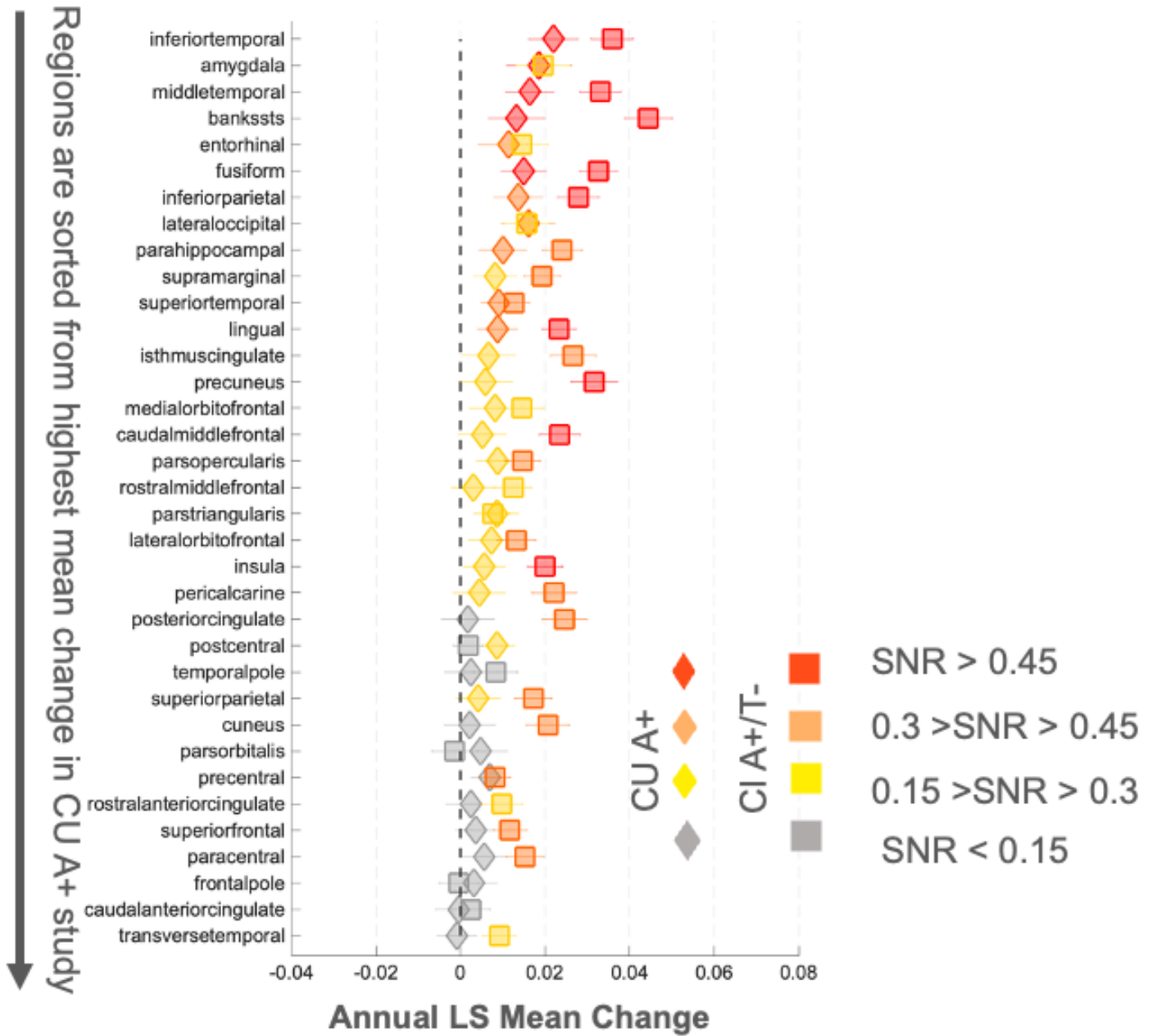


Figure 2. Waterfall plot showing the annual LS mean change \pm SE regional tau profiles of CU A+ and CI A+/T- studies.

Keywords: Early Tau Pathology, Tau Progression, Tau PET endpoints, Clinical Trials, Preclinical AD

P83 [18F]MK-6240 tau-PET in an A β -enriched sample from the 1946 British birth cohort - Insight 46

William Coath¹, Pawel J Markiewicz², Marc Modat³, Catherine J Scott^{1,4}, Ian B Malone¹, David L Thomas¹, John Dickson⁴, Michael Schöll^{1,5}, Sebastien Ourselin³, Marcus Richards⁶, Nick C Fox^{1,7}, David M Cash^{1,7}, Jonathan M Schott¹

¹Dementia Research Centre, UCL Queen Square Institute of Neurology, University College London, London, UK

²Centre for Medical Image Computing, Department of Medical Physics and Biomedical Engineering, University College London, London, UK

³King's College London, School of Biomedical Engineering & Imaging Sciences, London, UK

⁴Institute of Nuclear Medicine, University College London Hospitals, London, UK

⁵Wallenberg Centre for Molecular and Translational Medicine, University of Gothenburg, Gothenburg, Sweden

⁶MRC Unit for Lifelong Health and Ageing at University College London, London, UK

⁷UK Dementia Research Institute at University College London, London, UK

Aim: We investigated imaging biomarkers of A β and neurodegeneration in relation to tau-PET positivity in a preclinical birth cohort.

Methods: Cognitively normal individuals in the Insight 46 NSHD neuroimaging sub-study were scanned on combined PET/MR with [18F]florbetapir A β -PET at age ~70 years and again at ~73 years. A sub-sample enriched for A β -positive individuals is currently being assessed with [18F]MK-6240 tau-PET at age ~76 years. For this interim analysis, MK-6240 images were reconstructed 90-110 minutes post-injection and co-registered with T1-weighted MRI. Anatomical areas were parcellated on the T1 to form Braak stage regions. Standard uptake value ratios (SUVRs) were calculated using an inferior cerebellar grey reference without partial volume correction. Tau-PET positivity (Tau+) was defined using Gaussian mixture modelling in each region. Participants were assigned to “Tau-”, “Early” (Braak I-II) or “Advanced” (Braak III-VI) groups; and differences in baseline A β (Centiloids), A β accumulation (Centiloids/year) and hippocampal atrophy (%/year) were investigated with Mann-Whitney U tests.

Results: Analysis included 54 individuals (M/F=36/18). Baseline MMSE ranged between 28-30 and 48% were A β + (Centiloid \geq 13, whole cerebellum reference) by age 73 years. All individuals conformed to the Braak stage hierarchy (Figure 1). Figure 2 shows baseline A β , A β accumulation and hippocampal atrophy for Tau- (N=38), Early (N=11) and Advanced (N=5) groups. Baseline Centiloid was elevated in the Early group compared to Tau- (95% CI: 0.5,41.2). Compared to Tau- participants, the Advanced group showed increased baseline A β (32.6,65.0), A β accumulation (0.9,6.8) and hippocampal atrophy (0.9,3.5). Compared to the Early group, hippocampal atrophy was significantly higher in the Advanced group (0.3,3.4).

Conclusion: In this preliminary analysis, participants with tau in advanced Braak regions at age 76 had increased baseline and accumulation of A β aged 70-73 compared to Tau- participants. Neurodegeneration was evident between 3-6 years prior to tau scanning in individuals where tau has spread beyond Braak I-II.

MK-6240 SUVR Braak stages for each individual aged ~76

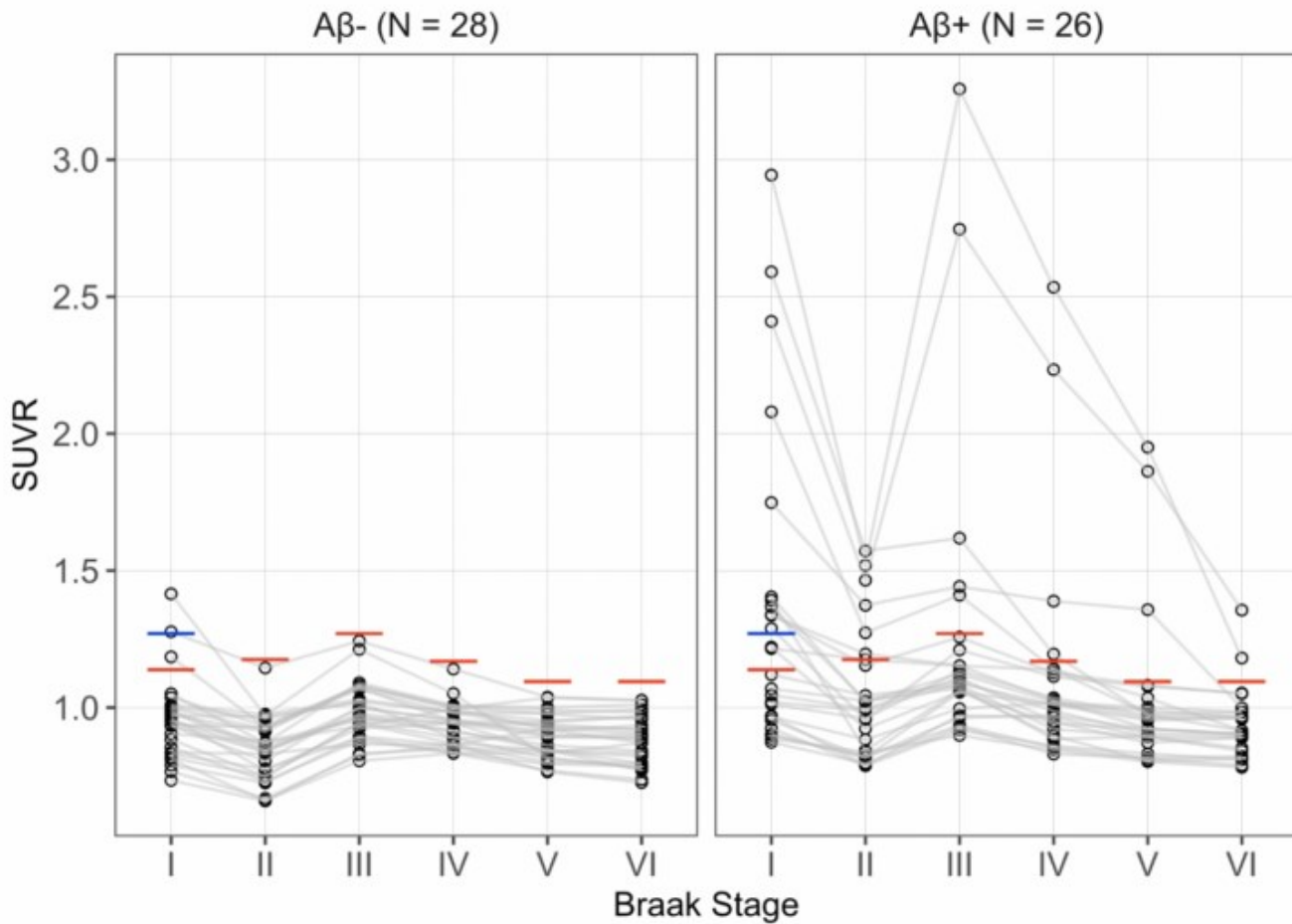


Figure 1. Participants are grouped by Aβ-PET positivity at either ~70 or ~73 years old ($\text{Centiloid} \geq 13$). Red lines represent cutpoints from Gaussian-mixture modelling on all individuals with the cutpoint at 99th percentile of the lower distribution, for every region two components were selected using Bayesian information criterion. The blue line is the Braak I cutpoint of 1.27 from Betthausen et al. (2020). Points from the same participant are connected.

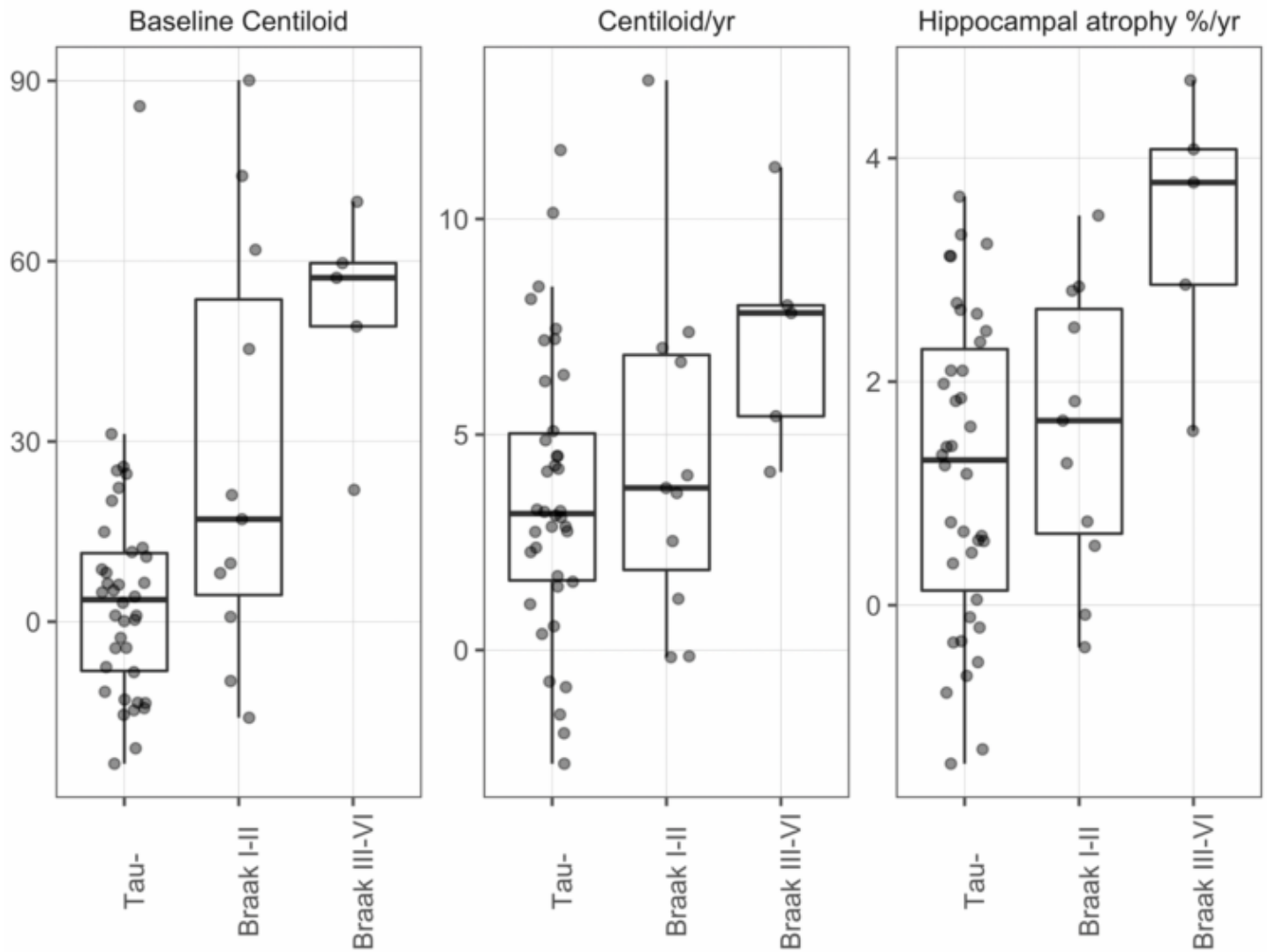


Figure 2. Box plots of baseline A β Centiloid (at age ~70 years), Centiloid accumulation and hippocampal atrophy (between ~70 to ~73 years) grouped by Braak stage at age ~76 years: tau negative (Tau-; N=38), Braak I-II (N=11) or Braak III-VI (N=5).

Keywords: Tau-PET, preclinical, Alzheimer's disease, Amyloid-PET

P84 Longitudinal trajectories of depressive symptoms and regional amyloid accumulation (PiB PET) in clinically normal older adults

Catherine Munro¹, Michelle Farrell^{2,5}, Bernard Hanseeuw^{2,3}, Rachel Buckley², Michael Properzi², Patrizia Vannini^{1,2}, Rebecca Amariglio^{1,2}, Yakeel T. Quiroz^{2,4}, Deborah Blacker^{2,6,7}, Dorene Rentz^{1,2}, Reisa Sperling^{1,2}, Keith Johnson^{1,2}, Gad Marshall^{1,2}, Jennifer Gatchel^{2,8}

¹Brigham and Women's Hospital, Boston, MA, US

²Massachusetts General Hospital, Boston, MA, US

³Institute of Neuroscience, Université Catholique de Louvain, Brussels, Belgium

⁴Grupo de Neurociencias de Antioquia, Universidad de Antioquia, Medellin, CO

⁵Athinoula A. Martinos Center for Biomedical Imaging, Charlestown, MA, US

⁶Harvard University, Boston, MA, US

⁷Department of Epidemiology, Harvard T. H. Chan School of Public Health, Boston, MA, US

⁸McLean Hospital, Belmont, MA, US

Background: Depression is an early neuropsychiatric symptom of Alzheimer's disease (AD) and has been linked to higher cortical amyloid burden in preclinical AD. We sought to examine whether specific regional amyloid accumulation in areas subserving mood may lead to increased depressive symptoms over time.

Methods: 288 cognitively-unimpaired participants with no/subclinical depressive symptoms at baseline (mean age=73.6; mean years follow-up=7.06) were included from the Harvard Aging Brain Study with annual Geriatric Depression Scale (GDS) assessment and MRI/PiB-PET every three years (mean=3.44 scans). PiB slopes were calculated for FreeSurfer-defined bilateral ROIs implicated in emotional control: amygdala, medial and lateral orbitofrontal cortices (mOFC, IOFC), superior and middle frontal cortices, anterior cingulate (ACC), posterior cingulate (PCC), and isthmus cingulate (IC). Separate linear mixed-effects models assessed whether ROI PiB slope predicted longitudinal GDS scores, covarying for age, sex, and education, and random intercept/slope, adjusted for multiple comparisons. Sub-analyses in 151 participants below the cortical PIB threshold at baseline were conducted to examine whether regional amyloid is already linked to depressive symptoms during the earliest stages of accumulation.

Results: Increasing GDS over time was associated with steeper PiB slopes in the mOFC and IC (see Table 1/graphic for statistics). Similar results were seen in the low-FLR group, with additional significant relationships in the IOFC, middle frontal cortex, and ACC.

Conclusions: In a cohort of cognitively-unimpaired older adults without depression at baseline, increasing depressive symptoms over time were associated with amyloid accumulation in frontal, isthmus, and anterior cingulate regions. This suggests that the emergence of depressive symptoms in older adults may be associated with the earliest stages of amyloid accumulation in areas necessary for mood/emotional control. Results shed light on the neurobiology of depressive symptoms and underscore the importance of monitoring new and increasing symptoms when screening for AD.

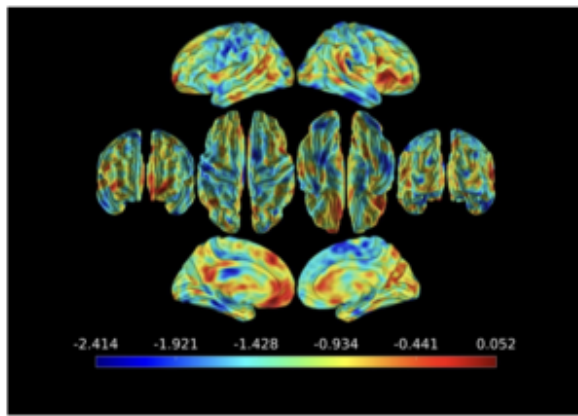


Figure 1 (above): Vertex-wise map visualizing the results of linear mixed-effects models (t score) examining the interaction between GDS slope and time compared to longitudinal PiB PET values ($p < 0.01$).

Table 1 (right): Results of linear mixed-effects models using the interaction between PiB PET and time to predict longitudinal GDS scores, covarying for age, sex, and education.
 * indicates significance at $p < 0.05$; all p-values in the table have been adjusted for multiple comparisons using an FDR correction.

Model: longitudinal GDS~amyloid slope*time+(sex +edu +age)*time				
	Whole Sample (n=218)		Low FLR at baseline (<0.86; n=154)	
mOFC	$\beta=4.05$ $p=0.008^*$ SE=1.22	$t=3.32$ 95%CI= [1.66-6.45]	$\beta=9.50$ $p=0.002^*$ SE=1.78	$t=5.35$ 95%CI= [6.01-12.98]
IOFC	$\beta=1.82$ $p=0.205$ SE=1.19	$t=1.52$ 95%CI= [-0.52-4.16]	$\beta=3.49$ $p=0.040^*$ SE=1.56	$t=2.24$ 95%CI= [0.43-6.54]
Middle frontal	$\beta=2.64$ $p=0.096$ SE=1.33	$t=1.98$ 95%CI= [0.03-5.26]	$\beta=7.39$ $p=0.002^*$ SE=2.08	$t=3.55$ 95%CI= [3.31-11.47]
Superior frontal	$\beta=(-)0.03$ $p=0.982$ SE=1.35	$t=(-)0.02$ 95%CI= [-2.67-2.61]	$\beta=1.22$ $p=0.531$ SE=1.95	$t=0.63$ 95%CI= [-2.61-5.05]
ACC	$\beta=2.36$ $p=0.053$ SE=1.02	$t=2.32$ 95%CI= [0.37-4.36]	$\beta=5.29$ $p=0.002^*$ SE=1.54	$t=3.43$ 95%CI= [2.27-8.31]
IC	$\beta=4.05$ $p=0.040^*$ SE=1.57	$t=2.58$ 95%CI= [0.98-7.13]	$\beta=10.82$ $p=0.002^*$ SE=2.19	$t=4.93$ 95%CI= [6.51-15.12]
PCC	$\beta=(-)0.71$ $p=0.746$ SE=1.36	$t=(-)0.52$ 95%CI= [-3.39-1.97]	$\beta=3.20$ $p=0.083$ SE=1.71	$t=1.87$ 95%CI= [-0.16-6.55]
Amygdala	$\beta=(-)0.81$ $p=0.746$ SE=1.80	$t=(-)0.45$ 95%CI= [-4.34-2.72]	$\beta=(-)3.03$ $p=0.170$ SE=2.10	$t=(-)1.44$ 95%CI= [-7.14-1.09]

Keywords: amyloid, depression, neuropsychiatric symptoms, longitudinal, positron emission tomography

P85 Improving sub-threshold PiB fidelity using relative radioligand delivery

Michael Properzi¹, Zahra Shirzadi^{1,2}, Rachel Buckley^{1,2,3}, Hannah Klinger¹, Bernard Hanseeuw^{1,2,4}, Rebecca Amariglio^{1,2,3}, Dorene Rentz^{1,2,3}, Michelle Farrell^{1,2}, Julie Price^{1,2}, Jasmeer Chhatwal^{1,2,3}, Gad Marshall^{1,2,3}, Jennifer Gatchel^{1,2}, Keith Johnson^{1,2}, Reisa Sperling^{1,2,3}, Aaron Schultz^{1,2}

¹Massachusetts General Hospital, Boston, MA, US

²Harvard Medical School, Boston, MA, US

³Brigham and Women's Hospital, Boston, MA, US

⁴Université Catholique de Louvain, Brussels, Belgium

Background: Relative radioligand delivery in PET imaging is a potential source of bias in metrics of pathological burden in Alzheimer's disease. The R1 metric, as derived from the multilinear reference tissue model (MRTM) of PET kinetics, is an estimate of this relative delivery. We propose that it can be used to increase signal clarity in sub-threshold β -amyloid (A β) PET burden estimation. Sub-threshold A β PET signal is dominated by noise, and as such, improvements in the signal to noise ratio in this area of the distribution will provide significant benefits in its concordance with pathology, and ability to predict future accumulation.

Methods: 308 subjects from the Harvard Aging Brain Study, and associated studies of Aging, underwent C11 Pittsburgh Compound-B (PiB) imaging in a 60 minute full-dynamic acquisition. Metrics of AD-related A β burden were derived using Logan Plotting (DVR) in Frontal, Lateral, and Retrosplenial (FLR) regions. A 40-60 minute window was used for derivation/calculation of DVR metrics. R1 values, extracted from MRTM, were used as an adjustment factor on participants with low A β burden (A β -), using per-region linear models. Baseline DVR and R1 adjusted DVR were then compared in their ability to predict PiB accumulation and change in PACC (covarying for demographics).

Results: Adjusting for R1 improved the ability of sub-threshold baseline PiB DVR to predict the future accumulation of Amyloid (Figure1A t:1.06->t:3.26) and future cognitive decline (Figure1B t:-1.42->t:-3.08), relative to unadjusted PiB DVR. Adjusting for R1 attenuated sex differences in sub-threshold PiB (Figure2A t:-4.49->t:-1.37), while age associations were found after adjustment (Figure2C t:0.48->t:3.80). There was no sex*age interaction in either metric.

Conclusion: Correcting for relative tracer delivery using R1 provides a small but significant improvement to the fidelity of A β -PET DVR in sub-threshold subjects, suggesting that correcting for relative tracer delivery in PET metrics increases concordance with pathological burden when specific binding is low.

Figure1: Longitudinal Prediction improvements after adjustment for R1. Plots A and B show baseline PiB DVR predicting PiB accumulation before and after adjusting for R1. Linear Mixed Effects models included covariates of age and sex. Plots C and D show Linear mixed effects model estimates of baseline PiB DVR predicting PACC change (covarying for age sex and education) became significant after adjusting for R1 in sub-threshold PiB subjects. |

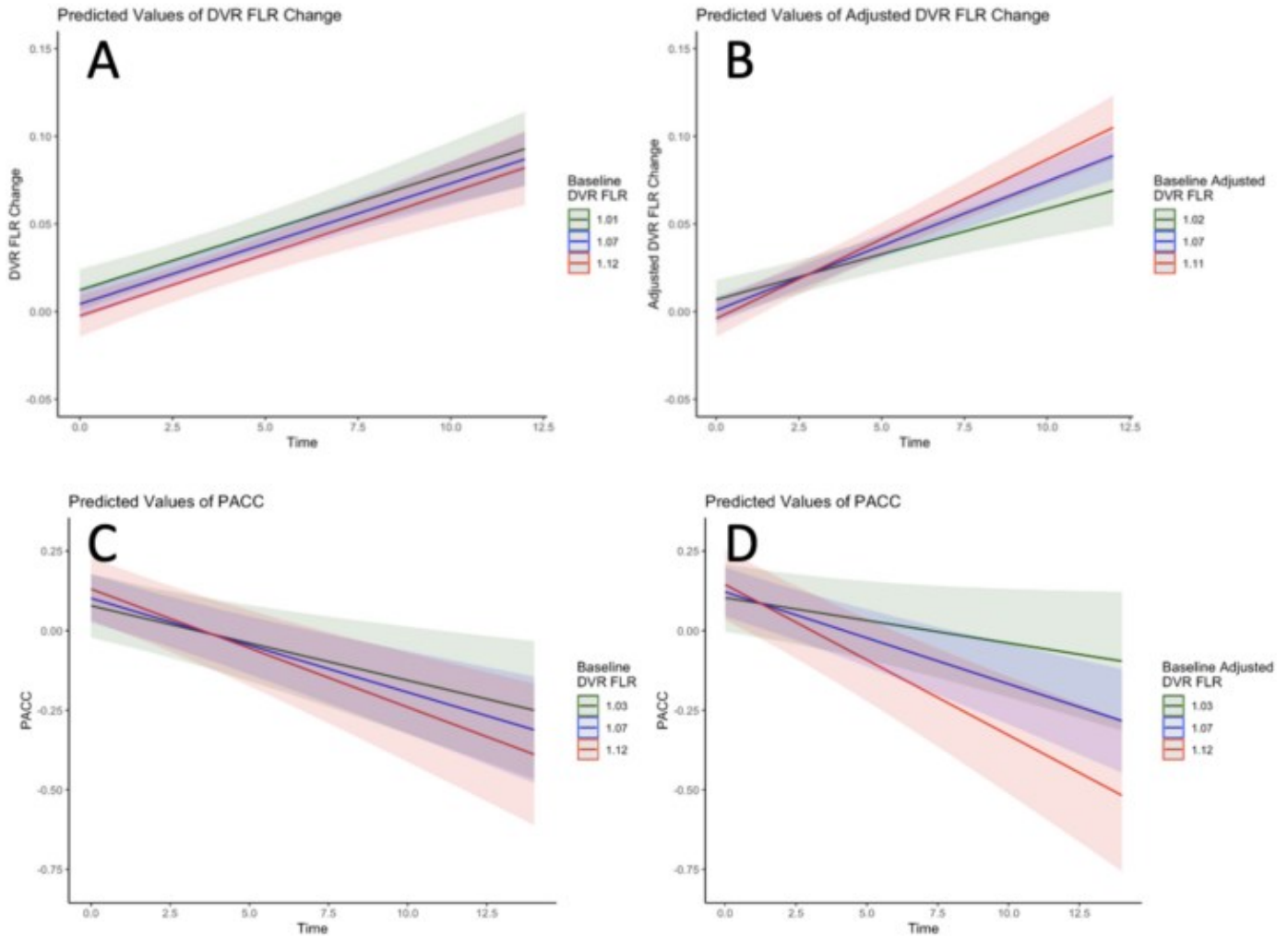


Figure2: Cross-Sectional characteristics of sub-threshold PiB DVR before and after adjusting for R1. Plot A highlights the removal of the significant sex association in PiB DVR after adjustment. Plot B shows that although there are changes to the e4 effects on sub-threshold DVR, they remain non-significant after R1 adjustment. A significant main effect of age on sub-threshold PiB DVR is found after R1 adjustment. Plot D shows that corrected and uncorrected sub-threshold DVRs are correlated with an R-squared of 0.69.

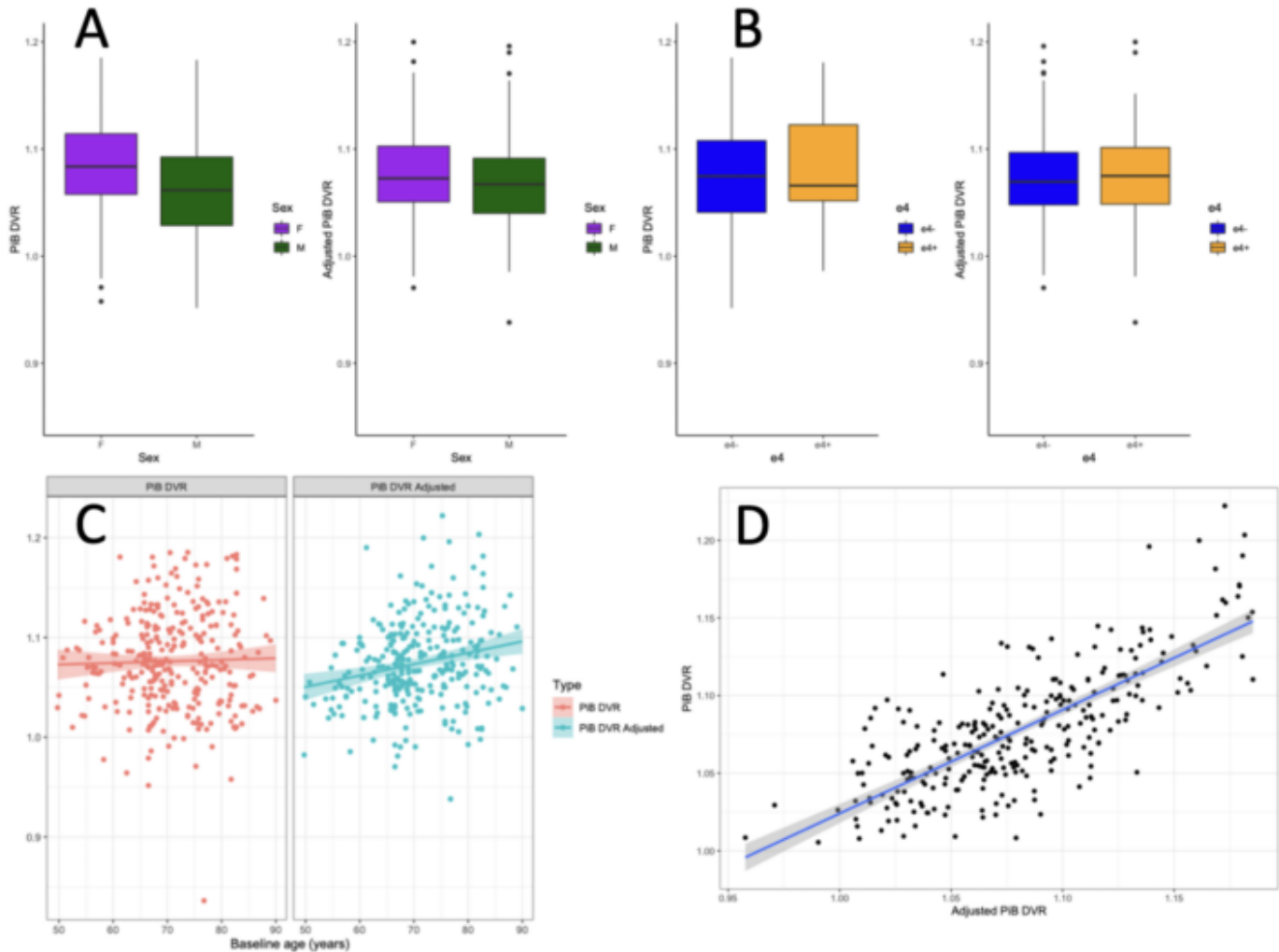
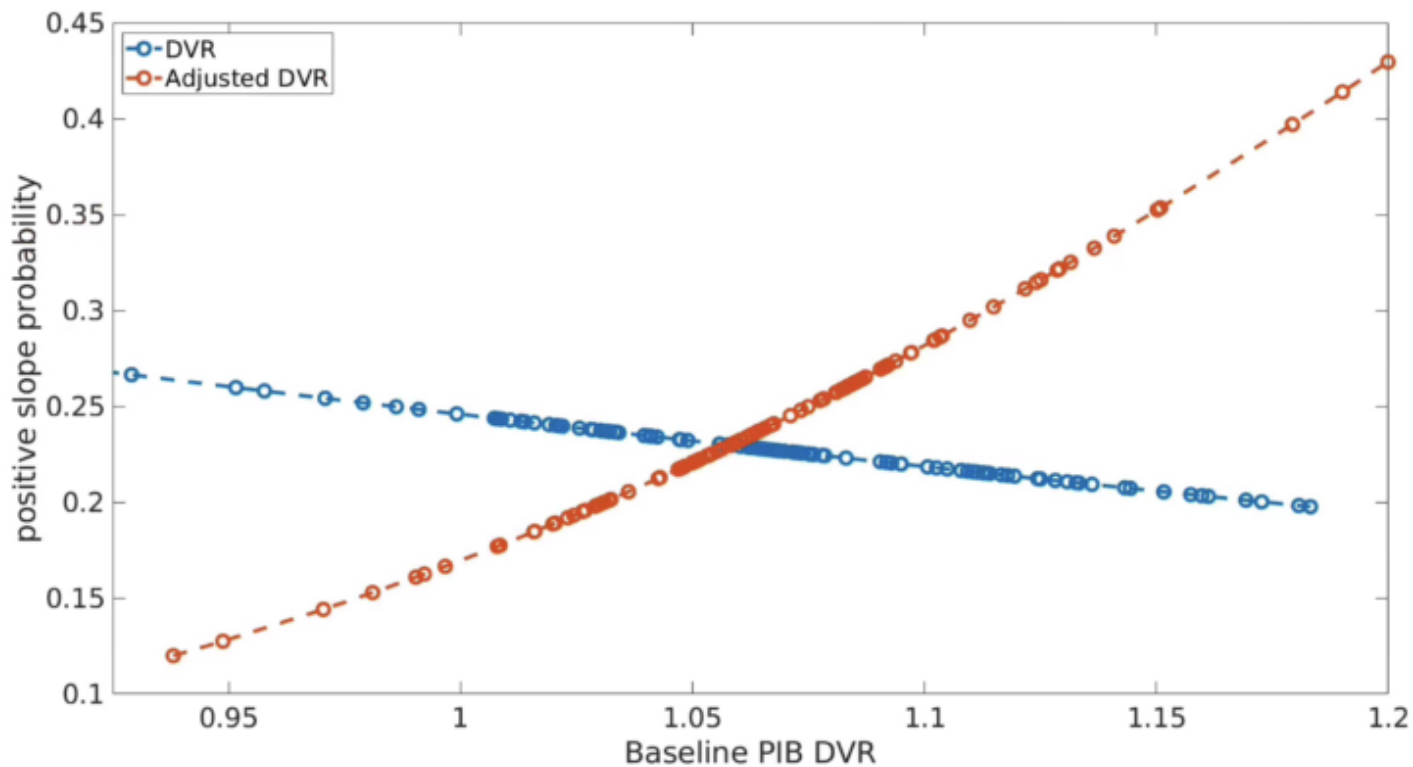


Figure3: Probability of reliable positive PiB slope increase as baseline DVR increase after R1 Adjustment. logistic regressions predicting slope increases above 0.01 DVR per year (top quartile of slopes) showed an increase in probability as baseline DVR increases only after adjusting for R1, suggesting less regression to the mean, and more meaningful signal, in sub-threshold DVR after adjustment.



Keywords: PET, PIB, R1

P86 Improved prediction of preclinical cognitive decline using amyloid PET spatial extent

Michelle E. Farrell¹, Emma G. Thibault¹, J. Alex Becker¹, Julie C. Price¹, Bernard J. Hanseeuw^{1,3}, Rachel F. Buckley^{1,2,4}, Kathryn V. Papp^{1,2}, Heidi I.L. Jacobs¹, Dorene M. Rentz^{1,2}, Reisa A. Sperling^{1,2}, Keith A. Johnson^{1,2}

¹Massachusetts General Hospital, Harvard Medical School, Boston, MA, US

²Brigham & Women's Hospital, Harvard Medical School, Boston, MA, US

³Cliniques Universitaires Saint-Luc, Université Catholique de Louvain, Brussels, Belgium

⁴Florey Institute of Neuroscience and Mental Health, University of Melbourne, Melbourne, AU

Objective: To evaluate whether an alternative PET spatial extent metric (how far A β has spread throughout the cortex) improves prediction of preclinical cognitive decline compared with a traditional magnitude-based metric of mean cortical A β -PET retention.

Methods: 266 clinically normal participants were included from Harvard Aging Brain Study with up to 10 years of annual cognitive follow-up (median=4.68 years). A β burden (Fig.1) was quantified using magnitude (mean cortical PIB DVR, also expressed in Centiloids) and spatial extent (% of cortical ROIs above their ROI-specific DVR thresholds). Separate linear mixed effects models assessed baseline 1) A β magnitude and 2) spatial extent as predictors of the Preclinical Alzheimer Cognitive Composite (PACC5) over time, before 3) directly comparing the contributions of magnitude and extent in the same model and 4) assessing the ability of A β extent/magnitude to predict PACC5 change while accounting for tau, measured with inferior temporal (IT) flortaucipir SUVR.

Results: Baseline spatial extent explained more variance in PACC5 over time than baseline magnitude ($\eta^2=28\%$ vs. $\eta^2=22\%$, $p<.001$) and only spatial extent was significant when modeled together. Spatial extent was more strongly linearly associated with the rate of subsequent cognitive decline (Fig.2B) compared with a more binary cognitive impact of high A β magnitude (Fig.2A). Spatial extent also enabled detection of early, subtle changes in PACC over time in those below the PIB DVR threshold (Fig.2C-D). While accounting for IT tau pathology, A β spatial extent (Fig.3), but not magnitude remained independently associated with cognitive decline.

Conclusions: A β spatial extent is more strongly associated with future cognitive decline than a traditional magnitude-based approach, suggesting how far A β has spread is more biologically relevant to cognitive functioning than the amount of A β . Measuring spatial extent may provide new insight in A β 's role in preclinical AD and improve design of the next generation of AD prevention trials.

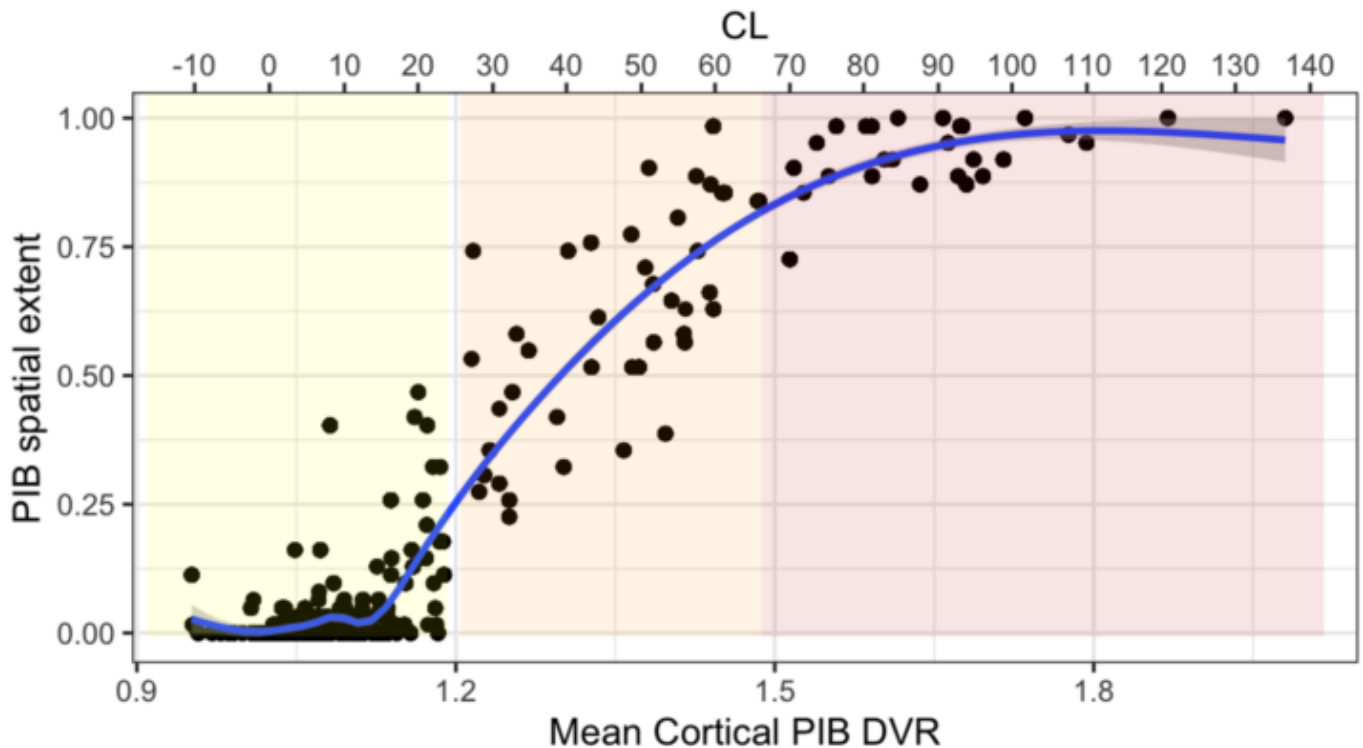


Figure 1. Magnitude vs. spatial extent of A β burden. Two alternative A β burden measures are plotted expressing the magnitude (x-axis) and spatial extent (y-axis) of A β in HABS participants. Contrasting the traditional magnitude measure of mean cortical PIB DVR (also translated to CL scale on the top axis for generalizability) with PIB spatial extent (the proportion of cortical ROIs with elevated local PIB ROI DVR) provides insight into how A β spreads through the cortex. At a low magnitude of A β burden (<math>< 25</math> CL, yellow range), PIB spatial extent shows superior dynamic range and signal-to-noise, allowing for earlier detection of A β than possible with mean cortical PIB DVR and thus the potential to detect early A β -related cognitive changes. At a moderate magnitude of A β burden (CL 25-70, orange range), there is considerable individual variability in spatial extent (~23-100%) that allows it to provide information about an individual's A β burden that is distinct from the magnitude information afforded by mean cortical PIB DVR. It is only at high magnitudes of A β burden (CL >70) that individuals reach full cortical spatial extent.

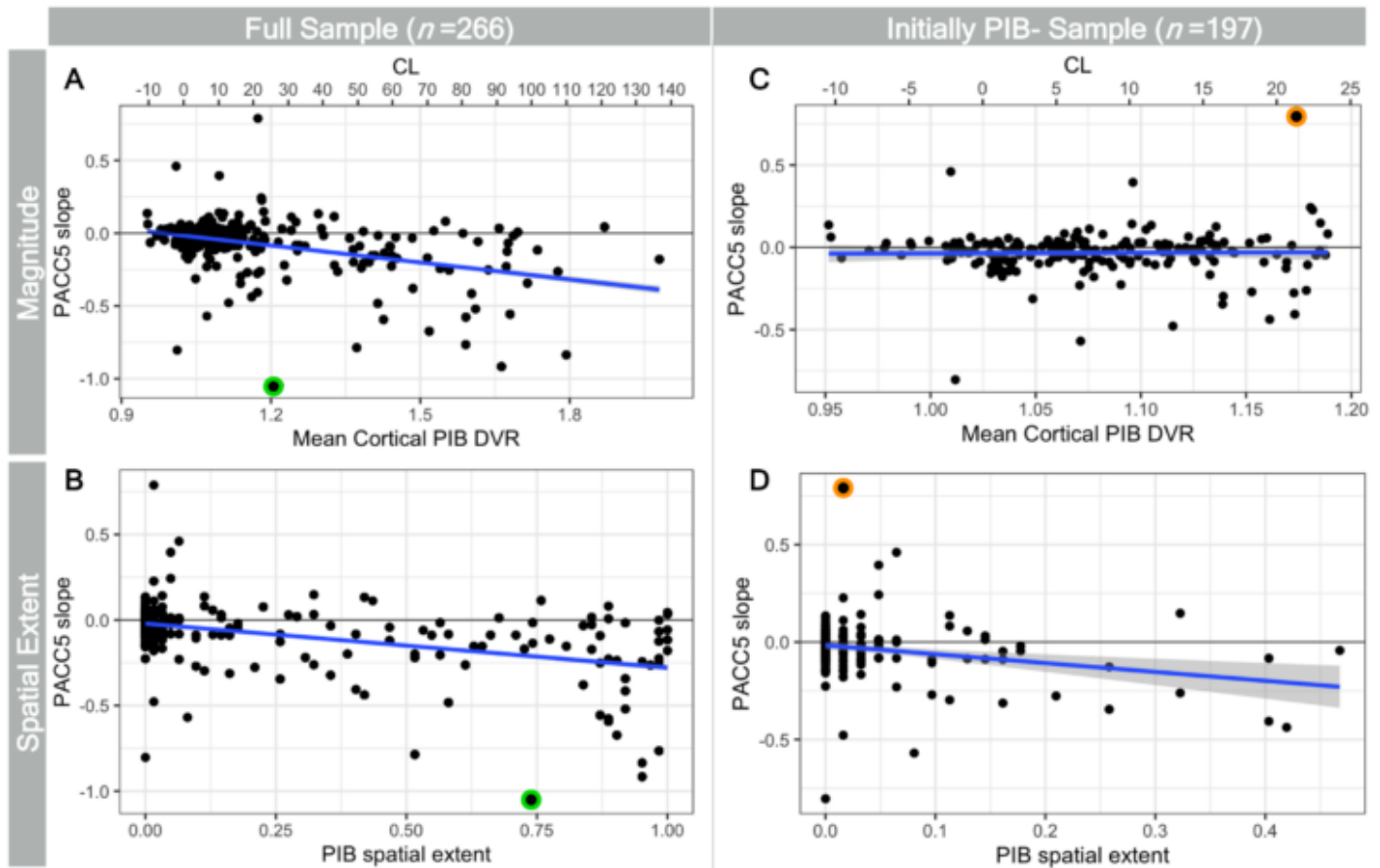


Figure 2. A β spatial extent exhibits more linear association with future cognitive decline than the magnitude of A β burden. Baseline A β magnitude (mean cortical PIB DVR/CL, top row) and spatial extent (bottom row) are plotted against PACC5 slope over up to the next 10 years in the full sample (left column) and within the subsample of individuals that would be considered PIB- at baseline based on the mean cortical PIB DVR threshold (right column). In both the full and initially PIB- samples, spatial extent is a better predictor of cognitive decline. Using the average magnitude of A β burden exhibits more of a threshold relationship with cognitive decline, such that the likelihood of cognitive decline increases in those with high PIB magnitude but there is not a clear association between the amount of A β and the rate of PACC5 decline. Adding continuous mean cortical DVR does not significantly improve prediction of PACC decline ($\chi^2=1.78$, $p=.41$) over a model using a binary PIB+/PIB- group based on the mean cortical PIB DVR threshold of 1.19. In contrast, spatial extent exhibits a more linear, dose-response relationship such that as the proportion of the cortex with elevated A β increases there is a corresponding increase in the rate of future cognitive decline, with a significant improvement in the linear prediction of PACC decline over both continuous magnitude/mean cortical PIB DVR ($\chi^2=16.6$, $p<.001$) and binary PIB+/PIB- groups ($\chi^2=17.8$, $p<.001$). Notably, the individual with the highest rate of cognitive decline (green outline) has a low magnitude of A β burden but high spatial extent, demonstrating how the improved linearity of the A β -cognition relationship with spatial extent allows for better prediction of the risk of cognitive decline in preclinical AD. In initially mean cortical PIB- adults, C) there is no relationship between increasing magnitude of PIB DVR and cognitive decline, but D) higher spatial extent is associated with greater PACC5 decline. Spatial extent is more effective at differentiating signal from noise at low A β burden, as exemplified by an individual (orange outline) with relatively high mean cortical PIB DVR but very low spatial extent that exhibits increased PACC5 over time.

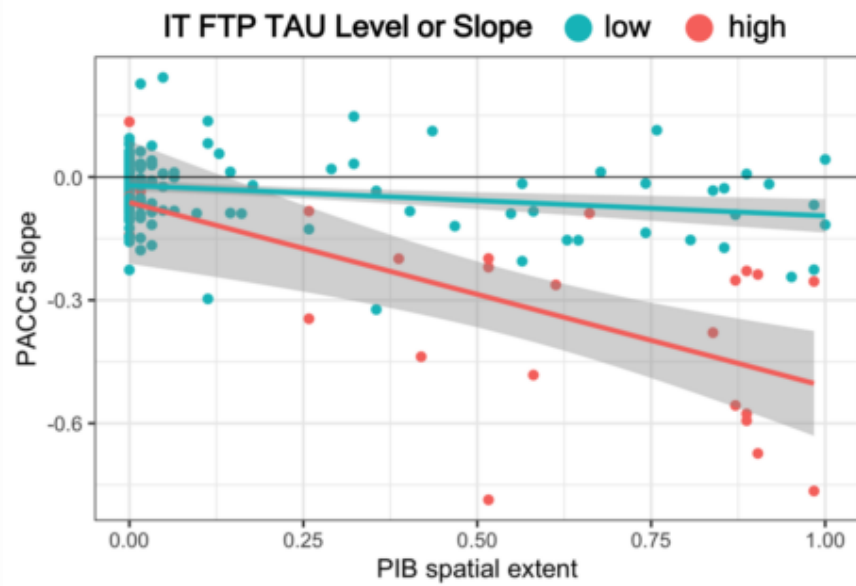


Figure 3. Distinct A β extent-related trajectories of preclinical cognitive decline with and without tau pathology. The relationship between A β spatial extent and PACC5 decline is grouped by the presence or absence of neocortical tau pathology in the IT. To ensure we are fully accounting for tau pathology, individuals were considered to have high tau if IT FTP SUVR was elevated (SUVR>1.38) or high rates of IT tau slope were detected (slope>.025 SUVR per year). Individuals with high IT tau (*red*) exhibited steeper PACC decline, and the rate of decline accelerated with increasing baseline A β spatial extent. Though more subtle, declines in PACC5 were still observed with increasing spatial extent in the absence of IT tau pathology (*blue*).

Keywords: Early detection, longitudinal, cognition, spatial extent, preclinical

P87 18F-MK-6240 Tau PET as a Potential Biomarker for Chronic Traumatic Encephalopathy

Michael Alosco¹, Nidhi Mundada², Renaud La Joie², Breton Asken³, Chris Nowinski⁶, Karen Smith², Julia Culhane¹, Ranjani Shankar², Alinda Amuiri², Erika Pettway¹, Leonardo Iaccarino², Charles Windon², Yorghos Tripodis⁴, Gustavo Mercier^{1,5}, Neil Kowall¹, Thor Stein¹, Lea Grinberg², Ann McKee¹, Robert Stern¹, Bruce Miller², Jesse Mez¹, Ron Killiany¹, Gil Rabinovici²

¹Boston University Chobanian & Avedisian School of Medicine, Boston, MA, US

²University of California San Francisco, San Francisco, CA, US

³University of Florida, Gainesville, FL, US

⁴Boston University School of Public Health, Boston, MA, US

⁵Boston Medical Center, Boston, MA, US

⁶Concussion Legacy Foundation, Boston, MA, US

Background: An accurate *in vivo* diagnosis of chronic traumatic encephalopathy (CTE) is not yet attainable due to lack of validated biomarkers. ¹⁸F-MK-6240 binds to CTE p-tau by autoradiography and tissue binding assays (K_d=1.5 nM). We report results from a proof-of-concept study investigating ¹⁸F-MK-6240 tau PET in people at high risk for CTE.

Methods: Twenty-three male former National Football League (NFL) players with subjective cognitive concerns (mean age=57.5, SD=7.04; 12, 52.2% Black) completed tau (MK-6240) and amyloid (florbetapir) PET. Controls included 36 cognitively normal males without traumatic brain injury history (unknown contact sport history) from the Wisconsin Registry for Alzheimer's Prevention (mean age=66.3, SD=6.3; mean MMSE=29.6, SD=0.5). Using cerebellar gray matter reference, 70-90 min MK-6240 SUVR images were created. W-score (age-adjusted z-scores) maps were generated using the controls. W-score>1.65 defined high binding voxels. SUVR and w-score maps were qualitatively assessed. Independent t-tests evaluated group differences in SUVRs.

Results: Of 21/23 NFL players with consensus diagnoses, 5 (23.8%) had normal cognition, 11 (52.4%) had mild cognitive impairment, and 5 (23.8%) had dementia. All NFL players had a negative florbetapir PET based on visual read. There was variable MK-6240 uptake across cases, including some with no signal, many with MTL uptake, and a few showing focal frontal uptake. A subset had both MTL and low intensity frontal uptake (**Figure 1**). Approximately 13/23 NFL players had supra-threshold MTL binding (**Figure 2A**). NFL players had higher SUVRs compared with controls in the parahippocampal gyrus (p=0.035) and trend-level increase in entorhinal cortex (p=0.063) (**Figure 2B-C**). Visual interpretation and quantification of cortical uptake was complicated by off-target meningeal binding.

Conclusions: MK-6240 might have utility for detection of high stage CTE. Off-target meningeal binding is problematic for interpretation of cortical uptake. Data collection is ongoing and includes acquisition of longitudinal MK-6240 scans in those with elevated baseline signal.

Figure 1. Former National Football League player with medial temporal lobe and superior frontal MK-6240 uptake. Images are displayed in neurological orientation. Left and right are SUVR and W-score maps, respectively, of a former National Football League (NFL) player with MK-6240 binding in the medial temporal lobes (MTL) (top rows). Images show low intensity, focal regions of binding in superior frontal cortex (bottom rows). W-score maps were generated (right) and are based on age-adjusted z-scores derived using the unimpaired men and a threshold of 1.65 determined the number of voxels with abnormal tracer uptake. Arrows demonstrate highest w-scores in R MTL and L frontal cortex.

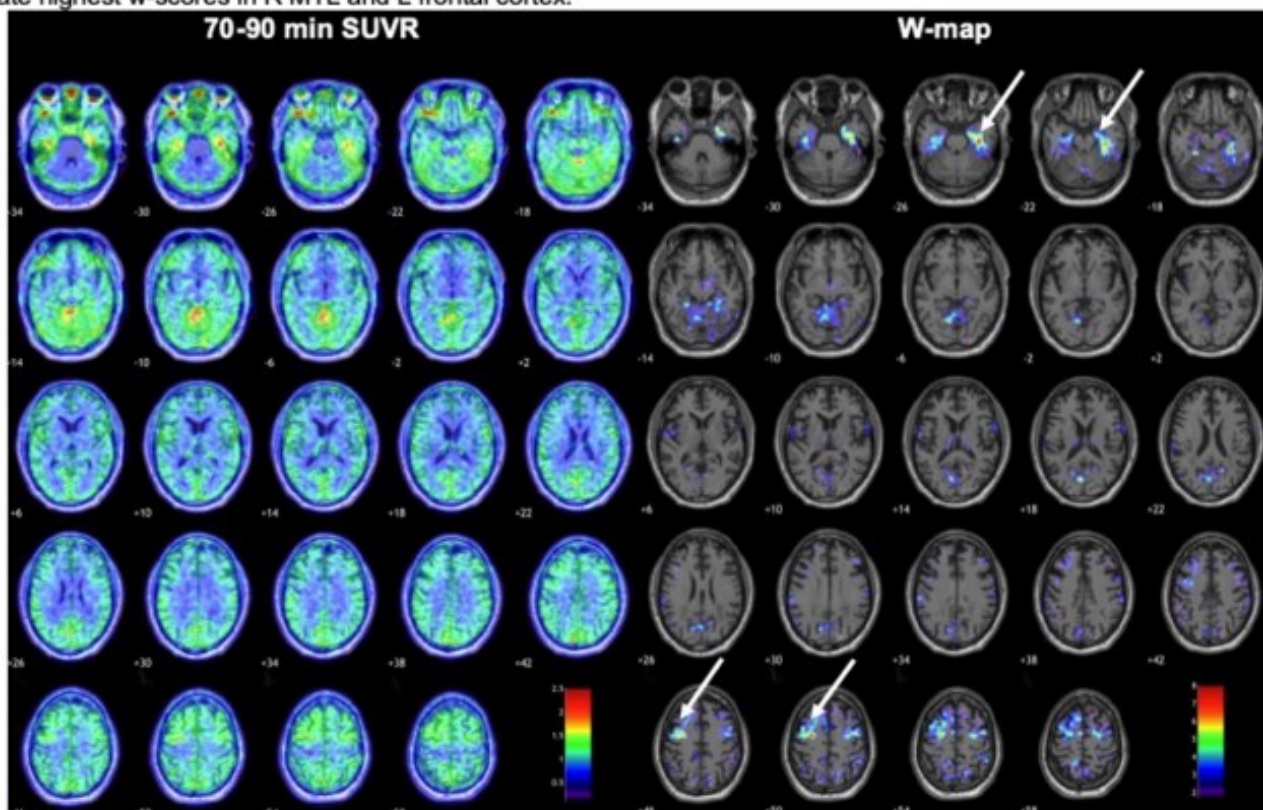
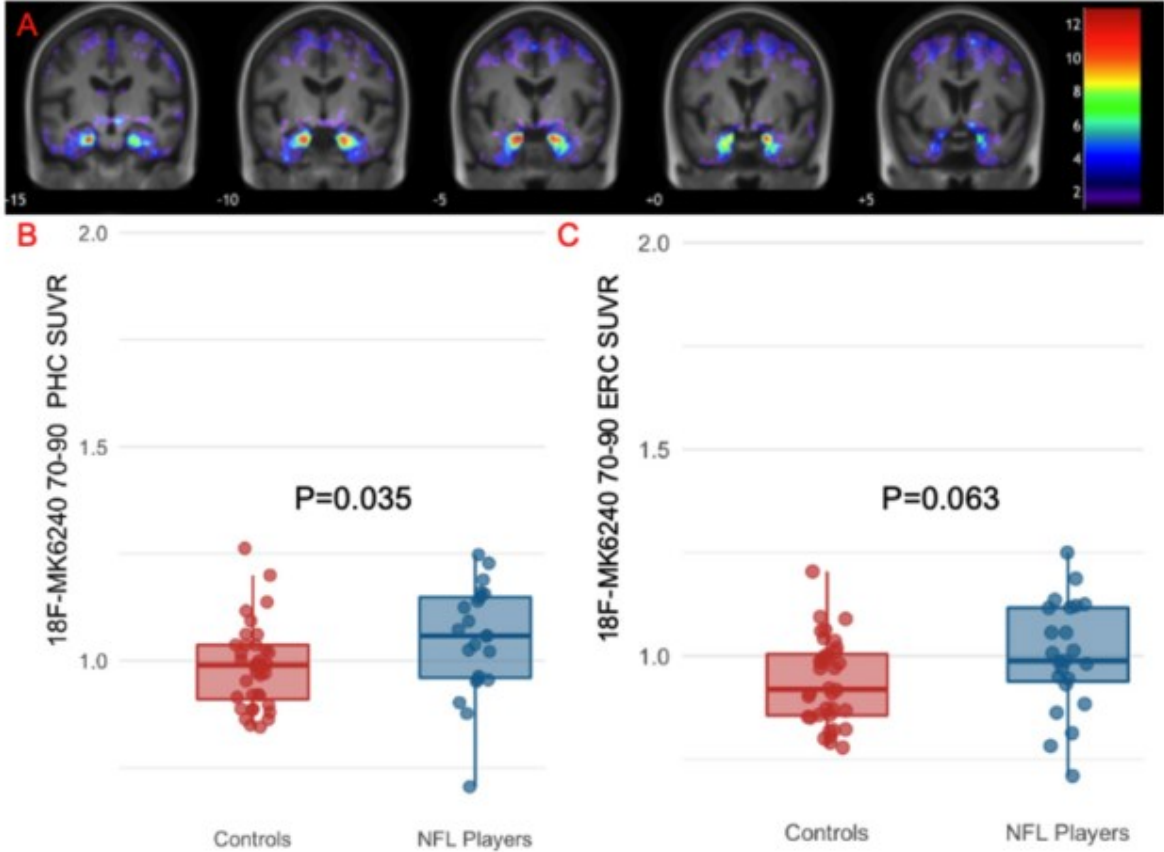


Figure 2. Medial temporal lobe MK-6240 binding in symptomatic former National Football League players. (A) Frequency maps of MK-6240 binding in the MTL. Images show the number of former NFL players who have high binding defined by a w-score >1.65. Bottom are box plots comparing parahippocampal gyrus (B) and entorhinal cortex (C) SUVRs between the 23 former NFL players and the 36 cognitively unimpaired men without a history of traumatic brain injury from the Wisconsin Registry for Alzheimer's Prevention.



Keywords: Chronic traumatic encephalopathy; tau PET; MK-6240; Alzheimer's disease

P88 Psychosis and tau burden across the AD continuum

Aubrey S. Johnson*², Galen Ziaggi*, Edward D. Huey, MD, William C. Kreisl, MD, Daniel Talmasov, MD, Patrick J. Lao, PhD

²Columbia University Irving Medical Center, New York, NY, US

*The first two authors contributed equally.

Introduction: Psychosis is a debilitating symptom cluster occurring in some Alzheimer's Disease (AD) patients, and is defined by the presence of delusions and/or hallucinations. Previous studies suggest that psychosis in AD patients is associated with increased tau burden and accelerated cognitive decline. We sought to assess differences in tau burden between cognitively impaired patients with psychosis (I+P) and those without psychosis (I-P).

Methods: Thirty-five ADNI participants with psychosis (I+P; 46% CDR0.5, 37% CDR1, 14% CDR2, 3% CDR3, 74±7.5yr old, 57% women, 15±2.3yr education, 89% White) and 35 without psychosis were matched by CDR, age, sex, education, and race (I-P; 46% CDR0.5, 37% CDR1, 14% CDR2, 3% CDR3, 75±7.3yr old, 57% women, 16±2.6yr education, 91% White). [18F]-AV1451 PET data were processed according to ADNI methods. Our I+P group was defined based on any endorsement of hallucinations or delusions on either Neuropsychiatric Inventory (89%) or Neuropsychiatric Inventory-Questionnaire (11%). Tau burden was compared in a paired t-test between I+P and I-P groups in Braak stage regions as well as individual regions including the amygdala, hippocampus, and frontal, temporal, and parietal lobes.

Results: There was no significant difference in tau burden between I+P and I-P groups in Braak I-VI regions, or frontal, temporal and parietal lobes. Tau burden in the amygdala was elevated in I+P compared to I-P (2.11 [1.87, 2.34]; p=0.047).

Discussion: Tau burden in the amygdala may be a potential biomarker of psychosis across the AD continuum. Future voxelwise analyses can confirm the spatial specificity of psychosis on tau burden within the composite regions explored here. Given that early psychosis in AD is associated with faster cognitive decline, these results could inform future research into early biomarker regions.

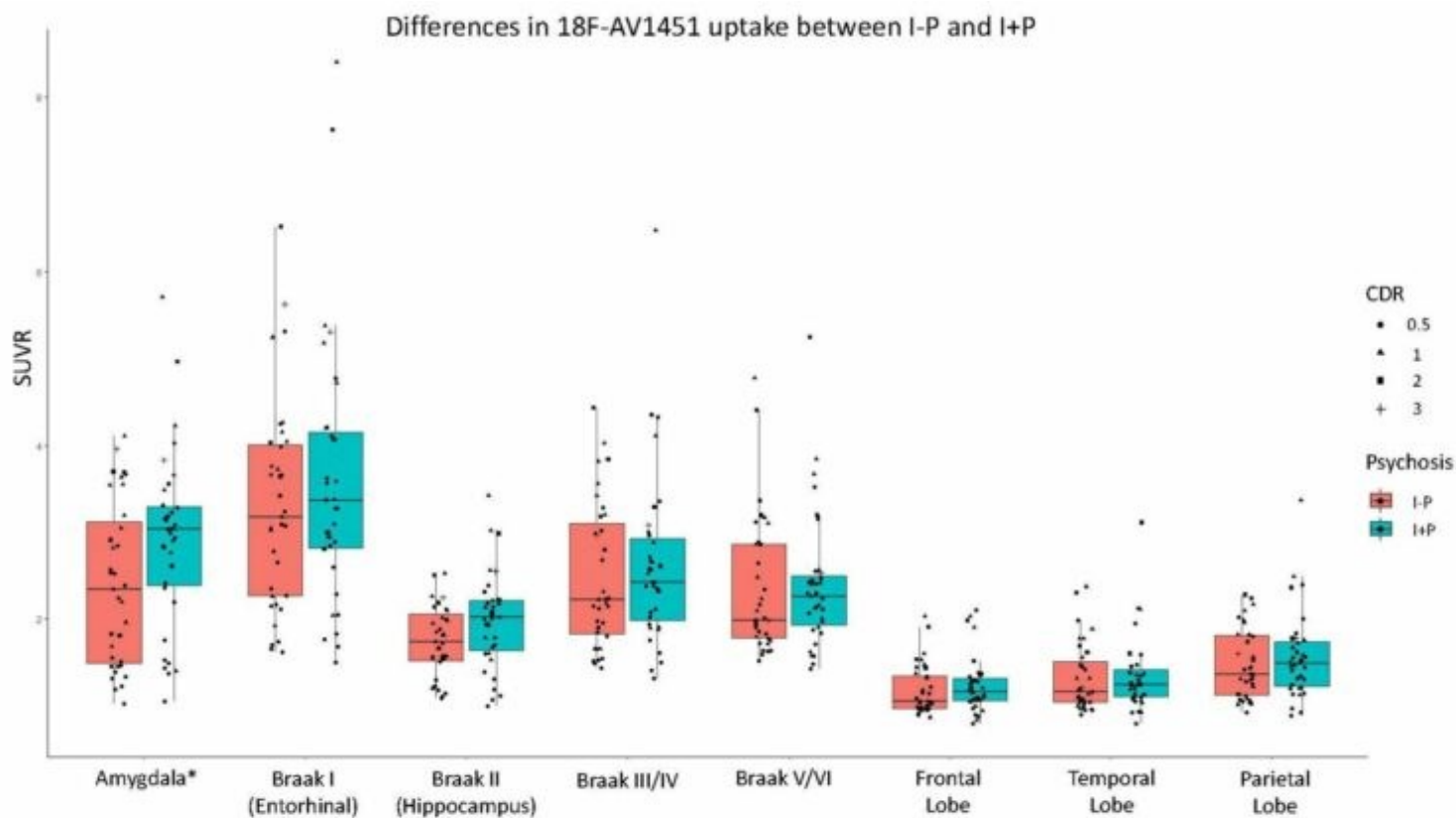


Figure 1 The difference in [F18]-AV1451 uptake between groups was found to be significant in the amygdala ($p=0.047$). No significant difference was found in Braak I, Braak II, Braak III/IV, Braak V/VI, frontal lobe, temporal lobe, or parietal lobe.

Keywords: Tau, Psychosis

P89 Classifying cognitive resilience to differing levels of Alzheimer's disease pathology

Rory Boyle¹, Diana Townsend¹, Hannah Klinger¹, Gillian Coughlan¹, Bernard Hanseeuw^{1,2}, Hyun-Sik Yang³, Rebecca Amariglio^{1,3}, Michelle Farrell¹, Heidi Jacobs¹, Zahra Shirzadi¹, Wai-Ying Yau¹, Julie Price¹, Jasmeer Chhatwal^{1,3}, Aaron Schultz¹, Timothy Hohman⁴, Michael Donohue⁵, Michael Properzi¹, Dorene Rentz^{1,3}, Keith Johnson^{1,3}, Reisa Sperling^{1,3}, Rachel Buckley^{1,3}

¹Massachusetts General Hospital, Harvard Medical School, Charlestown, MA, US

²Institute of Neuroscience, UCLouvain, Louvain-la-Neuve, Belgium

³Brigham and Women's Hospital, Harvard Medical School, Boston, MA, US

⁴Vanderbilt Memory & Alzheimer's Center, Vanderbilt University Medical Center, Nashville, TN, US

⁵Alzheimer's Therapeutic Research Institute, Keck School of Medicine, University of Southern California, Los Angeles, CA, US

Background: Some individuals remain cognitively unimpaired despite possessing substantial AD pathology. This may be explained by cognitive resilience (CR), a property of the brain that enables better-than-expected cognition despite pathology/neurodegeneration. Conventional CR measures have been critiqued. We present a novel method for classifying CR by modeling cognitive trajectories, accounting for levels of Ab and tau, across the whole continuum of pathology.

Methods: We identified 247 participants from the Harvard Aging Brain Study (HABS) with baseline Pittsburgh Compound-B[PiB]-PET, Flortaucipir[tau]-PET data, and 2 timepoints of Preclinical Alzheimer's Cognitive Composite (PACC) data. Latent class mixture models (LCMMs) classified longitudinal PACC trajectories into two groups (resilient vs. not-resilient), accounting for baseline age, sex, and global PiB-PET DVR (CR to Ab) or age, sex, global PiB-PET and entorhinal tau-PET SUVR (CR to Ab+tau). LCMMs used a non-linear beta link function. Non-parametric tests compared resilient vs not-resilient groups on CR-related lifestyle/risk factors.

Results: LCMMs classified 35% (n=87) as CR to Ab and 47% (n=117) as CR to Ab+tau (see Fig. 1). CR groups had more stable cognitive trajectories even at higher levels of Ab and Ab+tau (see Fig. 2). CR to Ab+tau was the best-fitting model (AIC=969 vs. AIC for CR to Ab=999). CR groups had lower proportions of subsequent MCI/Dementia diagnoses than not-resilient groups but did not differ on CR-related lifestyle or risk factors (see Table 1). **Conclusion:** Preliminary findings suggest that LCMMs accurately classify individuals as CR to AD pathology, with 14% of CR individuals showing elevated Ab and tau levels. This approach may be more sensitive than sociobehavioral 'CR-proxies' (e.g. education). CR to AD pathology was best defined using Ab and tau, as per model fit, reflecting the proximity of tau deposition to cognitive decline. This highlights the importance of including tauopathy in definitions of CR.

Characteristic ¹	CR to Aβ			CR to Aβ+tau		
	Not Resilient N = 160 ²	Resilient N = 87 ²	p-value ³	Not Resilient N = 130 ²	Resilient N = 117 ²	p-value ³
Age (Baseline)	72.74 (9.93)	73.13 (7.21)	0.9	72.59 (9.88)	73.19 (8.05)	0.6
Sex			0.6			0.6
F	94 (59%)	54 (62%)		80 (62%)	68 (58%)	
M	66 (41%)	33 (38%)		50 (38%)	49 (42%)	
Progression to MCI/Dementia	21 (13%)	0 (0%)	<0.001	17 (13%)	4 (3.4%)	0.007
APOE e4 Status			0.4			0.2
e4-	117 (74%)	60 (69%)		97 (76%)	80 (68%)	
e4+	41 (26%)	27 (31%)		31 (24%)	37 (32%)	
Years of Education	16.04 (2.91)	16.32 (2.96)	0.4	16.04 (2.96)	16.26 (2.89)	0.6
AMNART VIQ	121.89 (8.14)	122.36 (8.25)	0.5	121.82 (8.08)	122.32 (8.30)	0.4
DMN FC	0.26 (0.07)	0.26 (0.07)	0.5	0.26 (0.07)	0.26 (0.07)	0.6
FPN FC	0.27 (0.05)	0.27 (0.05)	0.7	0.27 (0.05)	0.27 (0.05)	0.8
Steps per Day	5,843.31 (3,072.91)	5,492.42 (2,664.20)	0.6	5,966.55 (3,070.09)	5,458.91 (2,771.12)	0.3
Social Engagement	7.67 (4.05)	7.26 (4.34)	0.4	7.54 (4.24)	7.53 (4.00)	0.8

¹ AMNART VIQ = American National Adult Reading Test Verbal Intelligence Quotient; DMN FC = Default Mode Network Functional Connectivity; FPN FC = Frontoparietal Network Functional Connectivity
² Mean (SD); n (%)
³ Wilcoxon rank sum test; Pearson's Chi-squared test

Table 1

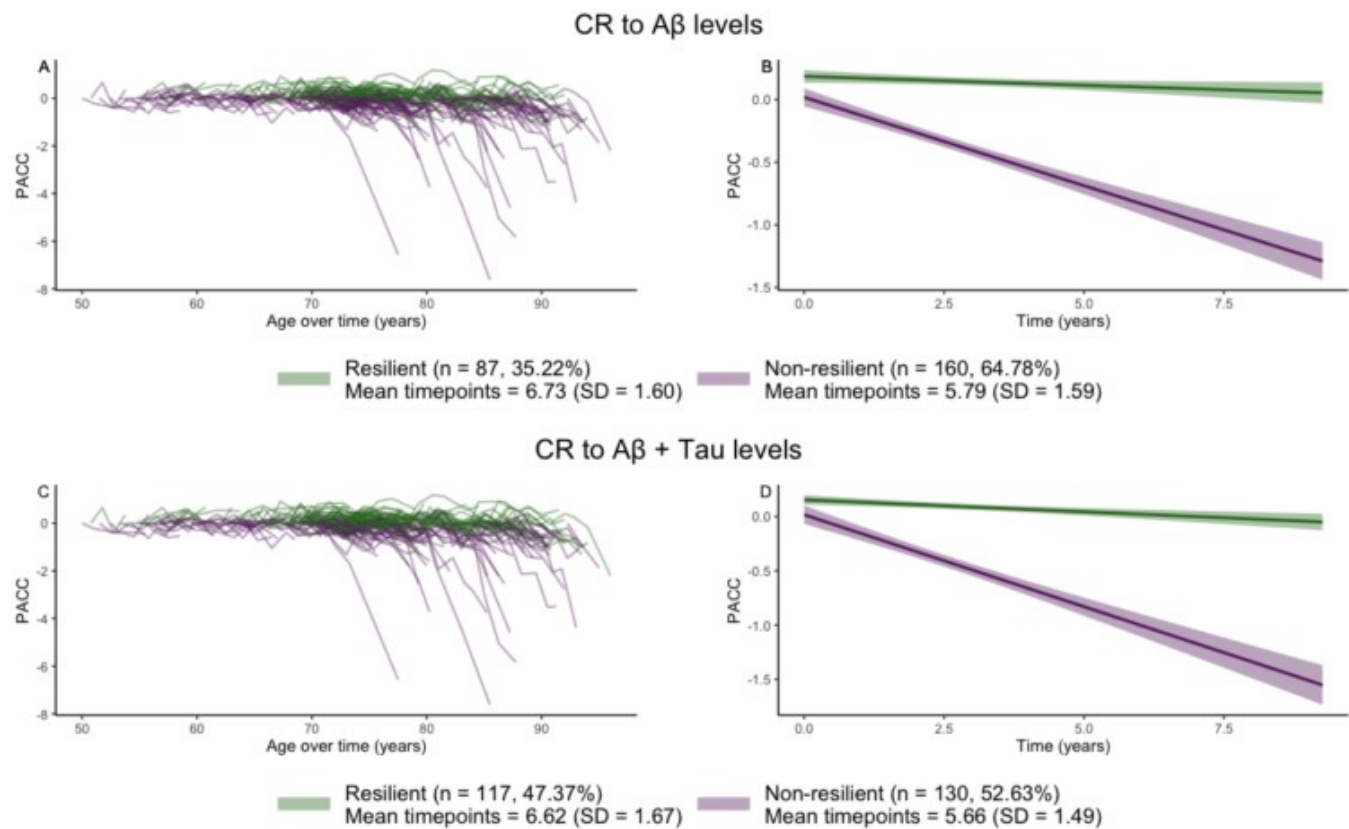


Figure 1

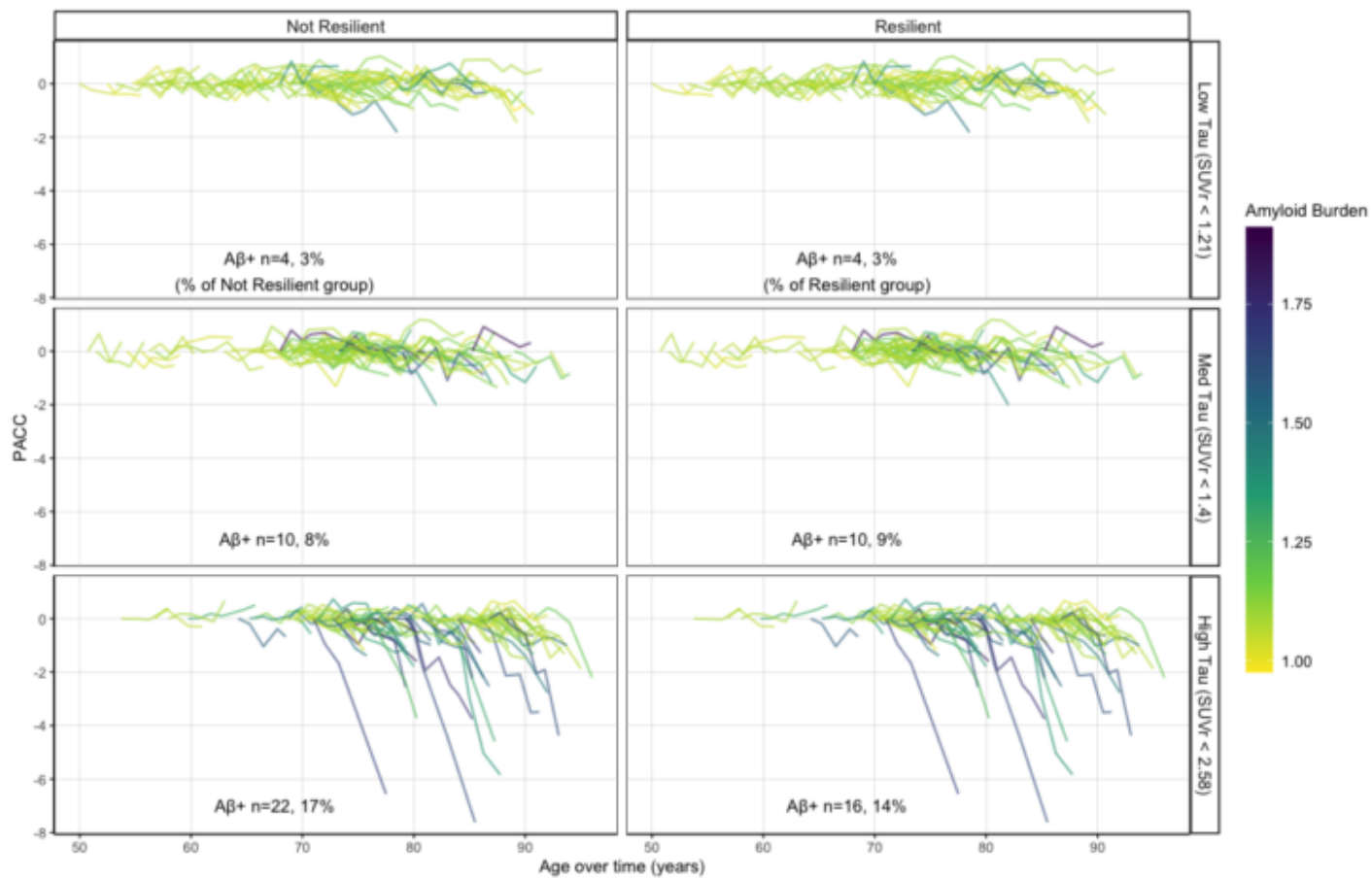


Figure 2

Keywords: Cognitive Resilience; Amyloid; Tau; PET; Cognitive Trajectories

P90 Cerebrospinal fluid neurofilament light predicts increased amyloid, tau, and decreased grey matter density

Mohit Manchella^{1,2}, Paige Logan¹, Jeffrey Dage¹, Dustin Hammers¹, Sára Nemes¹, Ralitsa Kostadinova¹, Ani Eloyan³, Nidhi Mundada⁴, Renaud La Joie⁴, Leonardo Iaccarino⁴, Anne Fagan⁵, Tatiana Foroud¹, Henrik Zetterberg⁶, Robert Koeppe⁷, Paul Aisen⁸, Maria Carrillo⁹, Gil Rabinovici⁴, Bradford Dickerson¹⁰, Liana Apostolova¹

¹Indiana University School of Medicine, Indianapolis, IN, US

²University of Southern Indiana, Evansville, IN, US

³Brown University, Providence, RI, US

⁴University of California, San Francisco, San Francisco, CA, US

⁵Washington University School of Medicine in St. Louis, St. Louis, MO, US

⁶The Sahlgrenska Academy, University of Gothenburg, Gothenburg, Sweden

⁷University of Michigan Medical School, Ann Arbor, MI, US

⁸Keck School of Medicine of University of Southern California, Los Angeles, CA, US

⁹Alzheimer's Association, Chicago, IL, US

¹⁰Massachusetts General Hospital, Harvard Medical School, Boston, MA, US

Background: Neurofilament Light chain (NfL), a neuron-specific cytoskeletal protein released into extracellular fluid following axonal injury, has been identified as a proxy for neurodegenerative diseases. Few studies describe associations between cerebrospinal fluid (CSF) NfL concentration and deposition of amyloid, tau, and grey matter density (GMD) in early-onset Alzheimer's Disease (EOAD). We explored the association of CSF NfL concentration with GMD, amyloid and tau burden in the Longitudinal Early-Onset Alzheimer's Disease Study (LEADS).

Methods: We analyzed baseline CSF data of 83 EOAD, 23 amyloid-negative early-onset cognitively impaired (EOnonAD) participants and 22 cognitively normal (CN) LEADS participants with available MRI, amyloid, and tau PET data. Voxel-wise multiple linear regressions of GMD, florbetaben, and flortaucipir imaging yielded statistical maps with CSF NfL concentration as the predictor. Hierarchical regression was employed, sequentially adding covariates in the following blocks:

Model 1: age, sex

Model 2: age, sex, Apolipoprotein (*APOE*)-*e4* status

Model 3: age, sex, *APOE-e4* status, Mini-Mental State Examination (MMSE)

Results: Increasing CSF NfL concentration is associated with greater tau burden in both the EOAD and pooled (Figure 1), as well as with amyloid accumulation and decreased GMD in the pooled samples only for models 1 and 2 (Figure 2). These effects diminished in model 3 after controlling for MMSE. The EOAD cohort showed regional association of CSF NfL with GMD in the left hemisphere which did not survive cluster-wide correction and no association of NfL with florbetaben (maps not shown).

Conclusions: CSF NfL concentration shows significant associations with tau deposition in the EOAD cohort. Our findings also suggest that the strength of the association of CSF NfL concentration with tau, amyloid, and GMD is dependent on disease severity.

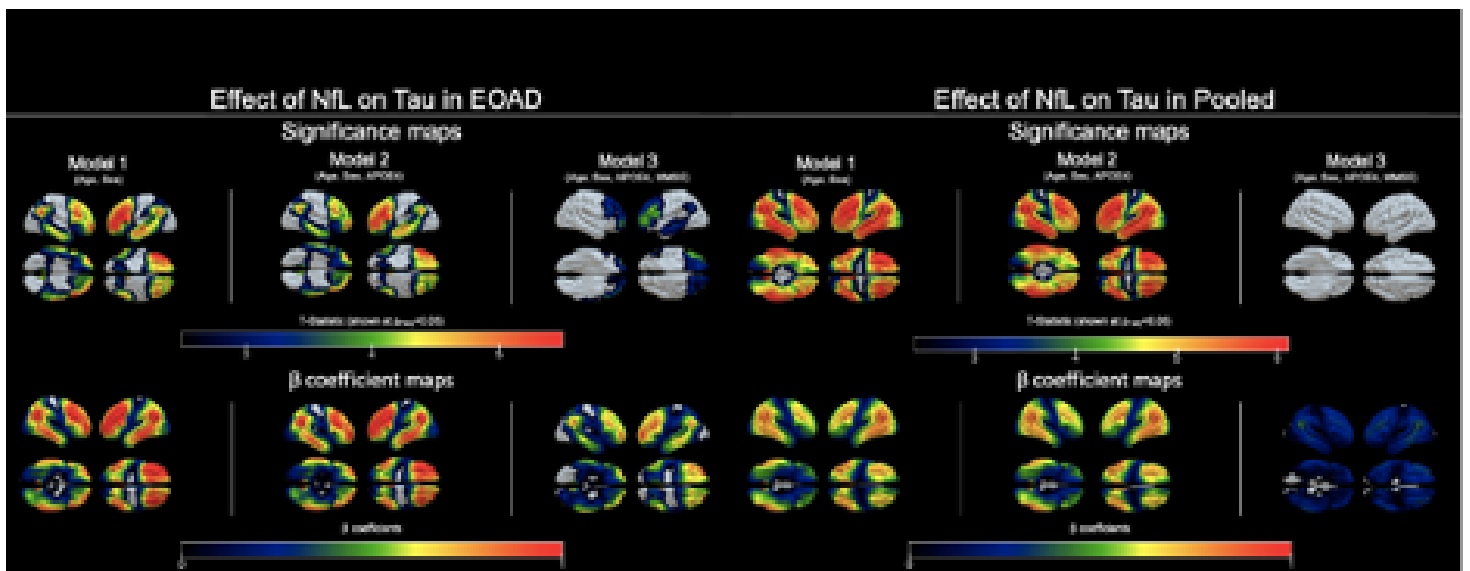


Figure 1. Voxel-wise multiple linear regression statistical maps showing the effect of CSF NFL on tau deposition in EOAD (left) and pooled (right). Statistical significance maps are displayed on top row with respective beta coefficient maps on bottom row. Covariates included in each model are listed in parentheses. Cluster corrected images shown rendered in Surf Ice at a family-wise error correction of $p < 0.05$

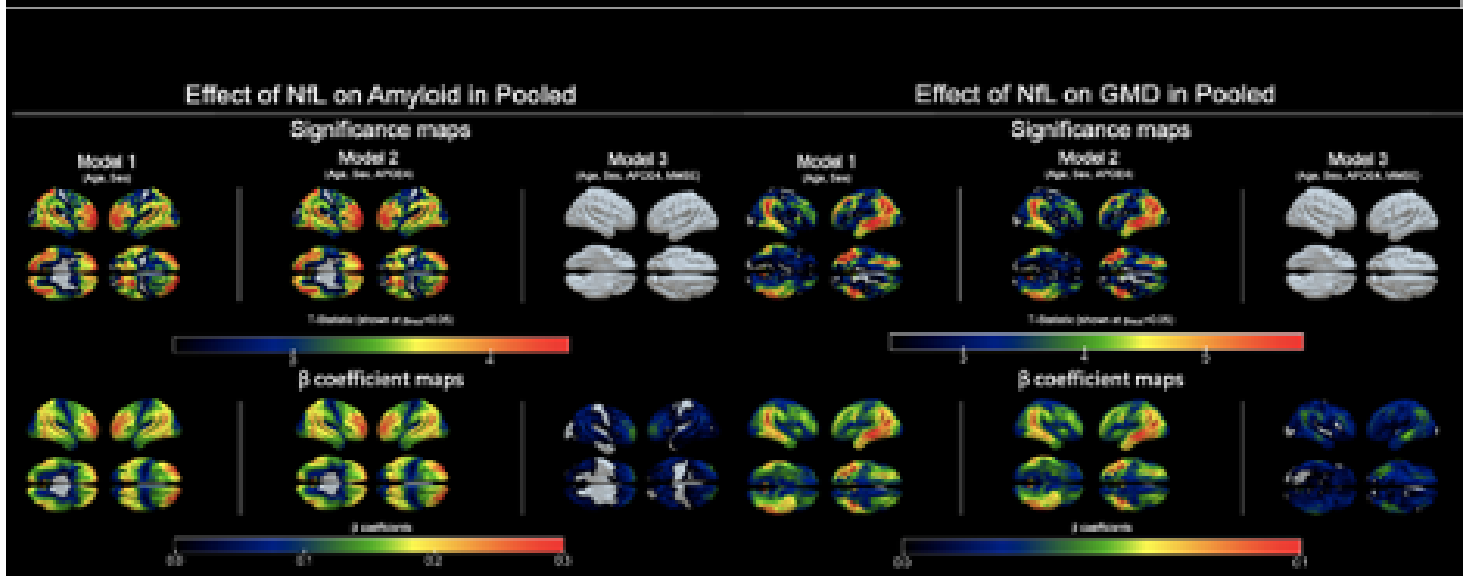


Figure 2. Voxel-wise multiple linear regression statistical maps showing the effect of CSF NFL on amyloid accumulation (left) and brain atrophy (right) in pooled cohort. All GMD models were corrected for intracranial volume. Statistical significance maps are displayed on top row with respective beta coefficient maps on bottom row. Covariates included in each model are listed in parentheses. Cluster corrected images shown rendered in Surf Ice at a family-wise error correction of $p < 0.05$

Keywords: Early-onset, CSF, NFL, imaging

P91 Unhealthy white matter connectivity in African American and non-Hispanic white older adults

Sarah Royse^{1,2}, Beth Snitz³, James Hengenius¹, Theodore Huppert⁴, Rebecca Roush³, Geraldine Cisneros⁵, Katey Potopenko⁵, James Becker^{3,5,6}, Ann Cohen⁶, C. Elizabeth Shaaban¹

¹Department of Epidemiology, University of Pittsburgh, Pittsburgh, PA, US

²Department of Radiology, University of Pittsburgh, Pittsburgh, PA, US

³Department of Neurology, University of Pittsburgh, Pittsburgh, PA, US

⁴Department of Electrical Engineering, University of Pittsburgh, Pittsburgh, PA, US

⁵Department of Psychology, University of Pittsburgh, Pittsburgh, PA, US

⁶Department of Psychiatry, University of Pittsburgh, Pittsburgh, ND, US

Introduction: Greater white matter hyperintensity (WMH) burden in African Americans (AA) versus non-Hispanic whites (nHW) may drive Alzheimer's disease (AD) disparities. Emerging evidence suggests that WMH may impair structural connectivity and that WMH and AD pathology could influence one another. We tested if unhealthy white matter connectivity (UWMC) in AD pathology-vulnerable regions is related to cognition and if these associations differ between AA and nHW.

Methods: We conducted Montreal Cognitive Assessments (MoCA) and T1, T2, and diffusion weighted imaging (DWI) scans in 100 AA (61.4 ± 7.7 years, 71F/29M, 29.0% cognitively impaired) and 101 nHW (65.8 ± 9.6 years, 63F/38M, 24.8% cognitively impaired) participants. We defined regions-of-interest (ROIs) and WMH with T1 and T2 scans, respectively. We used DWI scans to generate full-brain connectomes, with which we determined (1) ROI-to-ROI connections, (2) connections passing through WMH, and (3) the percent of total connections passing through WMH for each ROI pair (UWMC). In beta-amyloid (A β)- and tau-vulnerable regions separately, we tested associations of UWMC and MoCA score in individual regression models overall, racialized group-stratified analyses, and overall with UWMC-by-racialized group interaction terms.

Results: MoCA scores were lower in AA than nHW ($p=0.0001$). UWMC in eleven A β -vulnerable regions was negatively associated with MoCA ($p<0.003$); in five of these, AA exhibited worse UWMC than nHW ($p<0.04$). UWMC in four tau-vulnerable regions was negatively associated with MoCA ($p<0.01$); in three of these, AA showed worse UWMC than nHW ($p<0.05$). UWMC and MoCA associations differed between racialized groups in five A β -vulnerable regions ($p<0.004$) and four tau-vulnerable regions ($p<0.04$). Interactions were non-significant ($p\geq 0.06$).

Conclusion: UWMC in AD-vulnerable regions is associated with worse cognition. While AA generally exhibited more UWMC and lower MoCA scores than nHW, the strength of associations did not differ between racialized groups. Thus, UWMC may partially account for higher AD burden in AA.

Keywords: white matter, cognition, racialization

P92 Locus coeruleus integrity as neural substrate providing resilience against cognitive decline in the face of Alzheimer's disease pathology

Heidi IL Jacobs^{1,2}, Kathryn V Papp^{2,3,4}, Rachel F Buckley^{2,3}, Joost M Riphagen^{1,2}, Bernard J Hanseeuw^{1,2,5}, Rory T Boyle^{2,3}, Nancy Donovan^{2,4,6}, Dorene M Rentz^{2,4}, Reisa A Sperling^{2,3,4}, Keith A Johnson^{1,2,4}

¹Massachusetts General Hospital, Gordon Center for Medical Imaging, Boston, MA, US

²Harvard Medical School, Boston, MA, US

³Massachusetts General Hospital, Department of Neurology, Boston, MA, US

⁴Brigham and Women's Hospital, Department of Neurology, Boston, MA, US

⁵Cliniques Universitaires Saint-Luc, Department of Neurology, Brussels, Belgium

⁶Brigham and Women's Hospital, Department of Psychiatry, Boston, MA, US

Introduction: Previous autopsy work suggested that higher neuronal density in the locus coeruleus (LC) provides neural reserve against cognitive decline in dementia. Imaging studies indicated that higher LC MRI-signal, reflecting neuronal integrity, was associated with better memory performance and lower levels of Alzheimer's disease (AD)-related pathology. Here, we aimed to evaluate whether in vivo measurements of LC integrity reflect resilience against cognitive decline among individuals with elevated beta-amyloid.

Methods: We included 144 cognitively normal individuals from the Harvard Aging Brain Study (n=144; mean age:72.6 years, 63% female, CDR=0, Table 1) who underwent 3T LC-imaging, Beta-amyloid (PiB) and tau (FTP)-PET imaging and serial cognitive assessments (mean:2.7 years (SD:1.4)). LC intensity was derived from the normalized signal of 5-voxel-clusters. Hippocampal volume was quantified by FreeSurfer and adjusted for intracranial volume. Tau was assessed in the entorhinal and inferior temporal cortex, referenced to cerebellar cortex and partial volume corrected (PVC). Beta-amyloid status was ascertained using a previously established cut-off (1.324 DVR PVC; Table 1). Latent class mixture modeling identified 2 groups of different trajectories on PACC5-performance over time (age, sex and education-adjusted). Bootstrapped linear regressions compared LC integrity and brain measures across PiB negative and positive individuals in these cognitive trajectory groups (age-adjusted).

Table 1: Demographics of the cohort

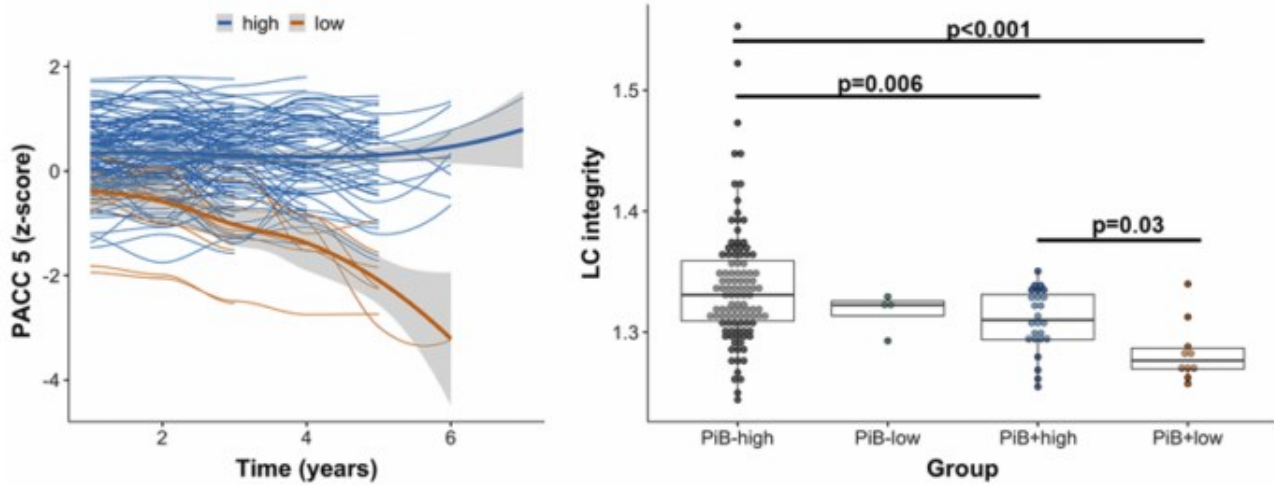
	Aβ- (n=109)	Aβ+ (n=35)	p-value (t-test/χ ²)
Age (years)	71.5 (9.52)	77.4 (8.22)	-3.59***
Female (n, %)	70 (64%)	21 (60%)	0.06
Education (years)	16.0 (2.87)	16.9 (2.55)	-1.63
APOE – ε4 (n, %)	15 (14%)	22 (63%)	32.07***
MMSE (total score)	29.1 (1.27)	29.0 (1.0)	0.35
PACC5 (z-score)	0.31 (0.71)	0.15 (0.65)	1.19
LC integrity	1.34 (0.05)	1.30 (0.03)	5.16***
Hipp volume (mm ³)	7468.35 (864.55)	6977.00 (800.46)	3.09**
Cognitive follow-up time	2.70 (1.37)	2.65 (1.35)	0.08

Note: Mean and standard deviation are provided for continuous measures and proportions for dichotomous variables. Abbreviation: MMSE = Mini-Mental State Examination; LC = Locus coeruleus; Hipp = Hippocampal volume (adjusted for intracranial volume); **:p<0.01; ***:p<0.001.

Results: Two PACC-5 groups were identified: stable high performers (high) and decliners (low), resulting in PiB-/high (n=105), PiB-/low (n=4), PiB+/high (n=25) and PiB+/low (n=10) groups (Figure 1). PiB+/high was older and had higher

EC and IT tau compared to PiB-/high. The PiB-/low received the lowest education. LC integrity was highest in the PiB-/high, and LC integrity was higher in the PiB+/high compared to the PiB+/low (Figure 1; $p < 0.05$).

Figure 1: Identification of cognitive trajectories and relationship with LC integrity and brain measures



	PiB-high (n=105)	PiB-low (n=4)	PiB+high (n=25)	PiB+low (n=10)
Age (years)	71.1 (9.36)	81.7 (9.04)	76.4 (8.45)	80.2 (7.28)
Female (n, %)	68 (65%)	2 (50%)	17 (68%)	4 (40%)
APOE-ε4 (n, %)	15 (14%)	0 (0%)	16 (64%)	6 (60%)
Education (years)	16.2 (2.82)	12.8 (2.22)	16.7 (2.69)	17.3 (2.21)
Hipp volume (mm ³)	7510 (825)	6400 (1294)	7133 (811)	6588 (658)
Entorhinal FTP (SUVR, PVC)	1.26 (0.25)	1.59 (0.23)	1.41 (0.32)	1.67 (0.30)
Inferior temporal FTP (SUVR, PVC)	1.41 (0.16)	1.52 (0.17)	1.58 (0.36)	1.55 (0.12)
LC integrity	1.34 (0.05)	1.32 (0.02)	1.31 (0.03)	1.28 (0.02)

Note: Top left: Identified groups of PACC-5 performance over time. Top right: LC integrity across the four groups (higher integrity is better). Bottom: table describing the groups differences in demographics and brain measures. Abbreviation: LC = Locus coeruleus; Hipp = Hippocampal volume (adjusted for intracranial volume); FTP=Flortaucipir; SUVR = standardized uptake value ratio; PVC= partial volume correction.

Discussion: Maintenance of optimal cognitive performance over the course of six years in individuals with preclinical AD is associated with better LC integrity. Future work will assess factors contributing to LC health.

Keywords: Locus coeruleus, cognition, resilience, amyloid

P93 Lower locus coeruleus integrity predicts diminished practice effects in cognitively normal older individuals

Lindsay Smegal¹, Christoph Schneider¹, Roos Jutten², Dorene Rentz^{2,3}, Keith Johnson^{1,2}, Reisa Sperling^{2,3}, Kathryn Papp^{2,3}, Heidi Jacobs^{1,4}

¹*Gordon Center for Medical Imaging, Department of Radiology, Massachusetts General Hospital/ Harvard Medical School, Boston, MA, US*

²*Department of Neurology, Massachusetts General Hospital and Harvard Medical School, Boston, MA, US*

³*Department of Neurology, Brigham and Women's Hospital and Harvard Medical School, Boston, MA, US*

⁴*Faculty of Health, Medicine and Life Sciences, School for Mental Health and Neuroscience, Alzheimer Centre Limburg, Maastricht University, Maastricht, The Netherlands*

Background: The locus coeruleus (LC), the primary source of norepinephrine (NE) in the brain and one of the initial subcortical regions of hyperphosphorylated tau aggregation in Alzheimer's disease (AD), has important implications in learning through repeated exposure to the same material. Practice effects (PE) are used to detect subtle changes in preclinical AD, where diminished PE have been associated with greater amyloid burden, tau deposition in the entorhinal cortex, and cognitive decline. We investigated the relationship between LC integrity, an indicator of LC health, and PE.

Methods: Seventy-six cognitively normal participants from the Harvard Aging Brain Study (age= 77.1 ± 4.8 , 62% female, MMSE= 29 ± 1.3 ; Figure 1) completed monthly at home computerized cognitive composite (C3) assessments for up to 12 months, which incorporated a face-name learning task (FNLT) and behavioral pattern separation task (BPSO). A composite measure (C2) consisting of the FNLT and BPSO was created. Participants also underwent dedicated 3T LC-imaging at the start of the assessments. Adjusting for age, sex, and years of education, robust linear regressions were used to associate LC integrity with baseline C2 performance and linear mixed effect models with random slope and intercept were used to investigate change in C2 accuracy and C2 task response time over 12 months.

Results: At baseline, there was no association between C2 performance and LC integrity. For the longitudinal data, we observed that individuals with lower LC integrity exhibited diminished PE relative to those with higher LC integrity ($p=0.049$; Figure 2). Furthermore, we found that individuals with lower LC integrity showed slower response times compared to those with greater LC integrity ($p=0.004$).

Conclusions: These findings suggest that lower LC integrity is associated with diminished PE and provides a marker of cognitive decline. Further studies are needed to investigate how these findings relate to tau pathology progression.

Figure 1. Baseline demographics and characteristics of the studied population (mean \pm SD)

	<i>N</i> = 76
Age (years)	77.1 \pm 4.84 (range = 68– 88.5)
Sex (N)	47F/ 29M
Years of Education	16.8 \pm 2.53
Global CDR (N)	72 CDR = 0/ 4 CDR = 0.5
PiB status (N)	55 PiB–/ 21 PiB+
MMSE score	29 \pm 1.27
PACC5 score	0.25 \pm 0.74
LC integrity	1.3 \pm 0.05

Abbreviations: CDR, Clinical Dementia Rating scale; PiB, Pittsburgh Compound B, MMSE, Mini-Mental State Examination; PACC5, Preclinical Alzheimer's Cognitive Composite-5; LC, Locus coeruleus.

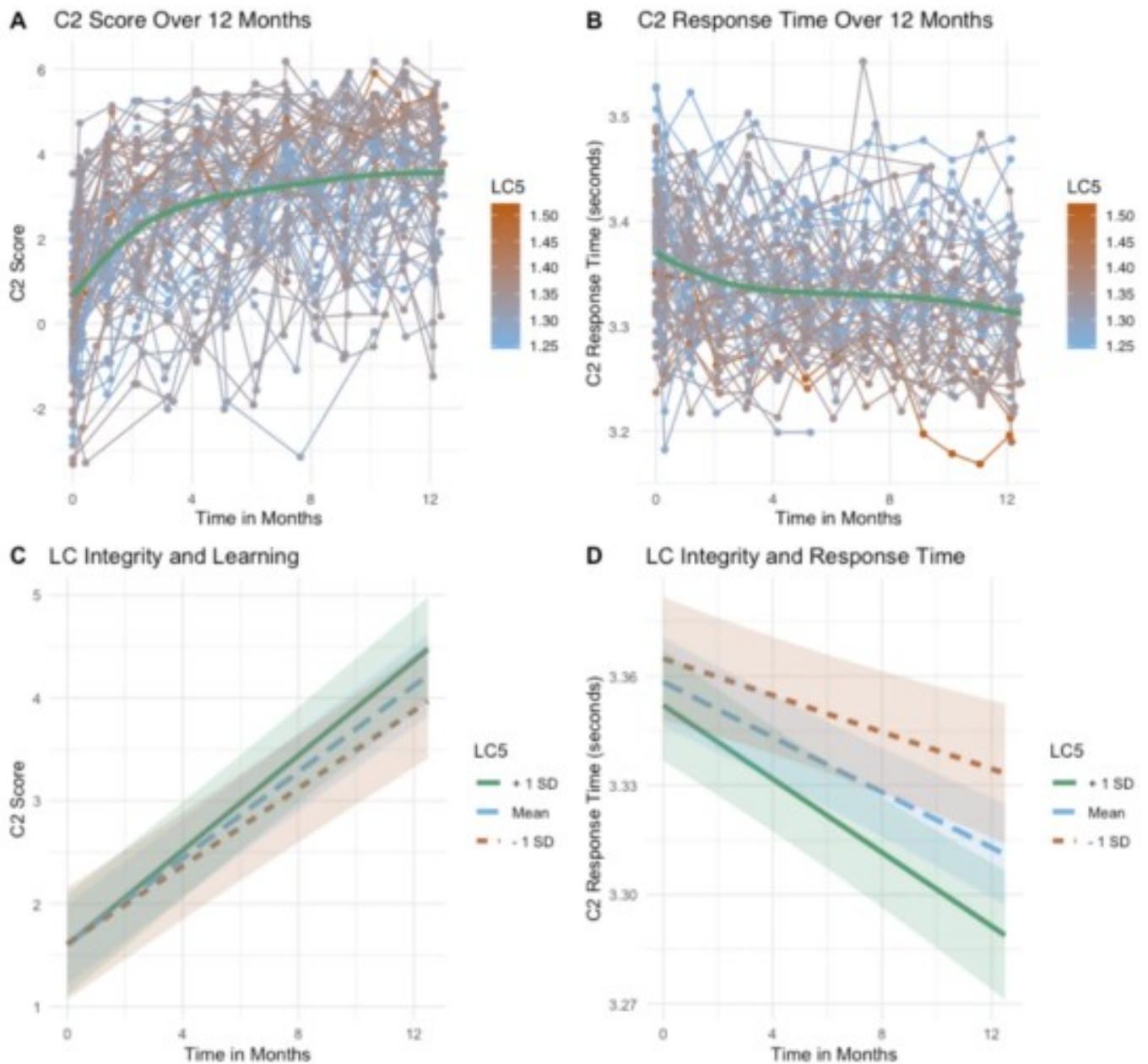


Figure 2. **A:** Individual participant performance on the C2 over 12 months, demonstrating overall improvement over time. **B:** Individual participant response times on the C2 over 12 months, demonstrating faster response times over time, where participants had no time constraints. **C:** There was an overall strong practice effect in the whole sample which showed an interaction with LC integrity, where participants with lower LC integrity showed diminished practice effects. **D:** The same effect shown in plot C was observed with response times, with an inverse sign, where participants with lower LC integrity had slower response times.

Keywords: Alzheimer's disease, locus coeruleus integrity, MRI, practice effects, remote assessment

P94 PET-based Braak staging predicts neuropsychiatric burden in the Alzheimer's disease continuum

Arthur C. Macedo^{1,2}, Cécile Tissot^{1,2}, Joseph Therriault^{1,2}, Stijn Servaes^{1,2}, Nesrine Rahmouni^{1,2}, Jaime Fernandez-Arias^{1,2}, Firoza Z. Lussier^{1,2}, Jenna Stevenson^{1,2}, Yi-Ting Wang^{1,2}, Kely Quispialaya Socualaya^{1,2}, Tahnia Nazneen^{1,2}, Seyyed Ali Hosseini^{1,2}, Peter Kunach^{1,2}, Arlette Haeger¹, Alyssa Stevenson¹, Paolo Vitali^{1,2}, Tharick A. Pascoal³, Pedro Rosa-Neto^{1,2}

¹Translational Neuroimaging Laboratory, The McGill University Research Centre for Studies in Aging, Montreal, QC, Canada

²Department of Neurology and Neurosurgery, McGill University, Montreal, QC, Canada

³Department of Neurology and Psychiatry, University of Pittsburgh, Pittsburgh, PA, US

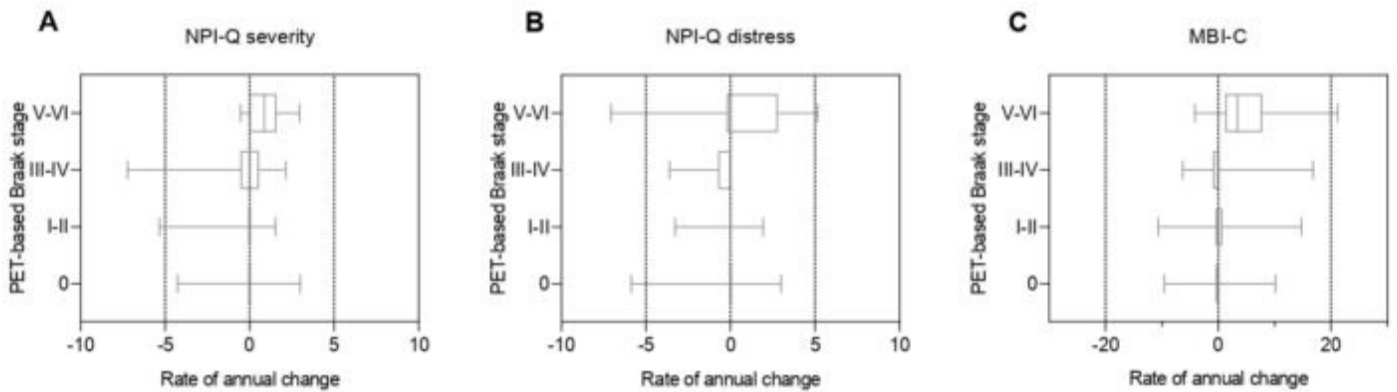


Figure 2

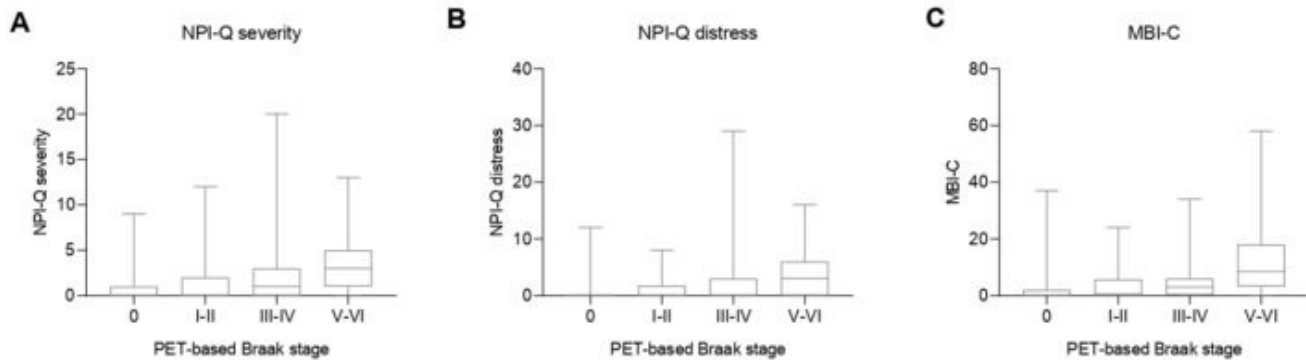


Figure 1

	NPI-Q severity baseline score		NPI-Q distress baseline score		MBI-C baseline score		NPI-Q severity annual rate of change		NPI-Q distress annual rate of change		MBI-C annual rate of change	
	Beta (95% CI)	p-value	Beta (95% CI)	p-value	Beta (95% CI)	p-value	Beta (95% CI)	p-value	Beta (95% CI)	p-value	Beta (95% CI)	p-value
PET-based Braak stages I-II	0.49 (-0.47-1.46)	0.313	0.26 (-0.88-1.40)	0.658	1.78 (-0.08-0.23)	0.177	0.06 (-0.62-0.49)	0.819	0.01 (-0.64-0.66)	0.973	-0.37 (-1.95-1.20)	0.177
PET-based Braak stages III-IV	1.74 (0.51-2.96)	0.006	1.91 (0.47-3.36)	0.0097	3.83 (-0.08-0.14)	0.024	-0.35 (-1.10-0.39)	0.348	-0.29 (-1.18-0.59)	0.517	-0.28 (-2.45-1.89)	0.024
PET-based Braak stage V-VI	2.61 (1.51-3.72)	<0.0001	3.03 (1.73-4.33)	<0.0001	10.63 (-0.007-0.17)	<0.0001	0.99 (0.29-1.68)	0.006	0.83 (-0.006-1.67)	0.051	4.93 (3.04-6.82)	<0.0001
Age	-0.03 (-0.08-0.03)	0.312	-0.02 (-0.08-0.05)	0.577	-0.06 (-0.007-0.007)	0.400	-0.008 (-0.05-0.03)	0.704	0.02 (-0.03-0.07)	0.517	-0.00004 (-0.12-0.12)	0.999
Sex (male)	-0.36 (-1.16-0.44)	0.379	-0.18 (-1.13-0.77)	0.704	-1.47 (-0.11-0.07)	0.163	0.22 (-0.26-0.70)	0.364	-0.29 (-0.87-0.28)	0.310	-0.14 (-1.21-1.50)	0.836

Table 1

Background: In the Alzheimer's disease (AD) continuum, neuropsychiatric symptoms (NPS) correlate with tau deposition in the brain as measured by positron emission tomography (PET). Here, we aim to track the progression of the neuropsychiatric burden through the AD continuum using the PET-based Braak staging framework. Specifically, we investigate the association of PET-based Braak stages with NPS measures and assess whether PET-based Braak staging can predict annual change in NPS.

Methods: We evaluated 164 cognitively unimpaired individuals, 56 amyloid- β positive ($A\beta^+$) individuals with mild cognitive impairment, and 50 $A\beta^+$ individuals with AD dementia. Participants underwent [^{18}F]AZD4694 $A\beta$ PET and [^{18}F]MK6240 tau-PET, were assigned a PET-based Braak stage at baseline and were followed for a mean (s.d.) of 1.98 (0.60) years. NPS symptoms were investigated using the Mild Behavioral Impairment Checklist (MBI-C) and the Neuropsychiatric Inventory Questionnaire (NPI-Q) severity and distress domains. Multiple linear regressions assessed the association of PET-based Braak stages with baseline NPS measures and with the annual rate of change on the NPS scores.

Results: At baseline, the participants' scores in all scales increased following the progression of PET-based Braak stages (Figure 1A-C). Cross-sectionally, higher scores in the NPI-Q severity, the NPI-Q distress and the MBI-C were significantly associated with PET-based Braak stages III-IV and V-VI (Table 1). Furthermore, PET-based Braak stages V-VI predicted a significant annual increase in the NPI-Q severity and MBI-C scores (Figure 2A-C; Table 1), but not in the NPI-Q distress domain.

Conclusions: These findings suggest that the informant-reported NPS presence and burden increases with the progression of tau accumulation, from PET-based Braak III to VI. Moreover, PET-based Braak staging appears to be a good predictor of the progression of the NPS severity. These results also corroborate the clinical significance of the PET-based Braak staging framework.

Keywords: Alzheimer's disease; Braak stages; Positron emission tomography; Neuropsychiatric symptoms

P95 A computational model to study the combined effect of neuronal connectivity loss and tauopathy progression

Arsalan Rahimabadi^{1,2}, Jean-Paul Soucy^{1,3}, Habib Benali^{1,2}

¹*PERFORM Centre, Concordia University, Montreal, QC, Canada*

²*Department of Electrical and Computer Engineering, Concordia University, Montreal, QC, Canada*

³*Montreal Neurological Institute, Montreal, QC, Canada*

Introduction: Aggregation and spreading of misfolded tau proteins play central roles in the development of tauopathies, which gradually leads to neuronal network degeneration. Moreover, the alteration of the neuronal network may mutually influence tau pathology progression. Here, we built an in-silico model to capture the mutual effect between tauopathy aggravation and neuronal connectivity loss (NCL).

Methods: To model the spatiotemporal evolution of toxic-tau species concentration in the brain, we use the Fisher-KPP reaction-diffusion equation where the diffusion operator is replaced by the graph Laplacian. The brain network is also modeled as a weighted undirected graph in which the strength of each link between two nodes depends on the concentrations of toxic-tau species at both nodes. Specifically, we multiplied the strength of each link connecting two nodes by a decreasing function of the concentrations at both to mimic the pathological situation in which tauopathy progression and neuronal connectivity strength are inversely correlated. All defined decreasing functions have the same parameter, called here the NCL coefficient, whose increase exacerbates the neuronal network degeneration in the in-silico model. The other two parameters of the suggested model are the aggregation and spreading coefficients, which are equivalent to the reaction and diffusion coefficients of the Fisher-KPP equation, respectively.

Results: The simulation results of two in-silico experiments for which the model was initialized by some nonzero concentration of toxic-tau species at the right entorhinal node has been presented in Figures 1 and 2. The tauopathy propagation in the experiment with the zero NCL coefficient was faster compared to that of the experiment with a nonzero NCL coefficient at the earlier stages. See Figure 3.

Conclusions: The proposed model helps us to investigate both tauopathy progression and neuronal degeneration simultaneously. For future work, we aim to include the impact of Amyloid-Beta as another hallmark of Alzheimer's disease.

*The simulation results of the proposed model
without considering neuronal connectivity loss*

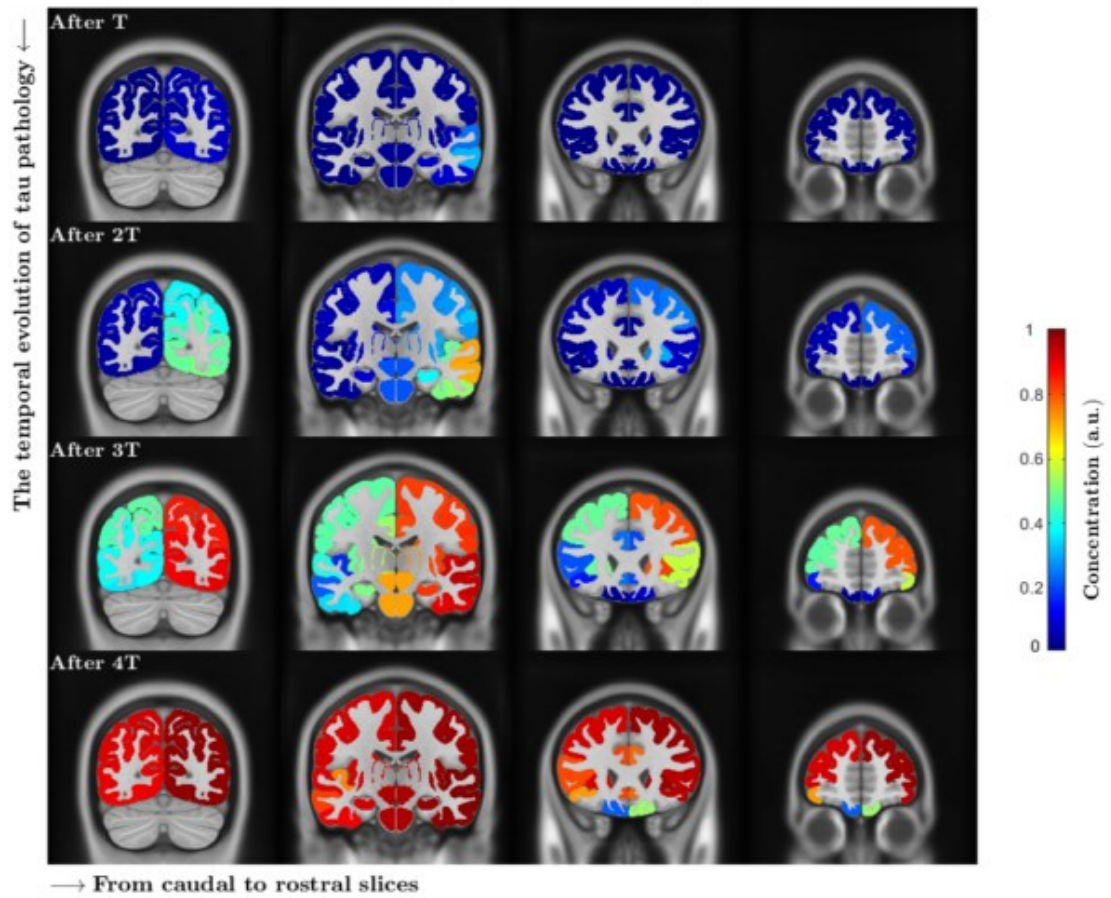


Figure 1. It demonstrates the in silico spatiotemporal evolution of tau pathology when the neuronal connectivity loss coefficient was set to zero. The aggregation and spreading coefficients were also set to 0.5 and 2.5, respectively. The time interval T is 5 years.

*The simulation results of the proposed model
with considering neuronal connectivity loss*

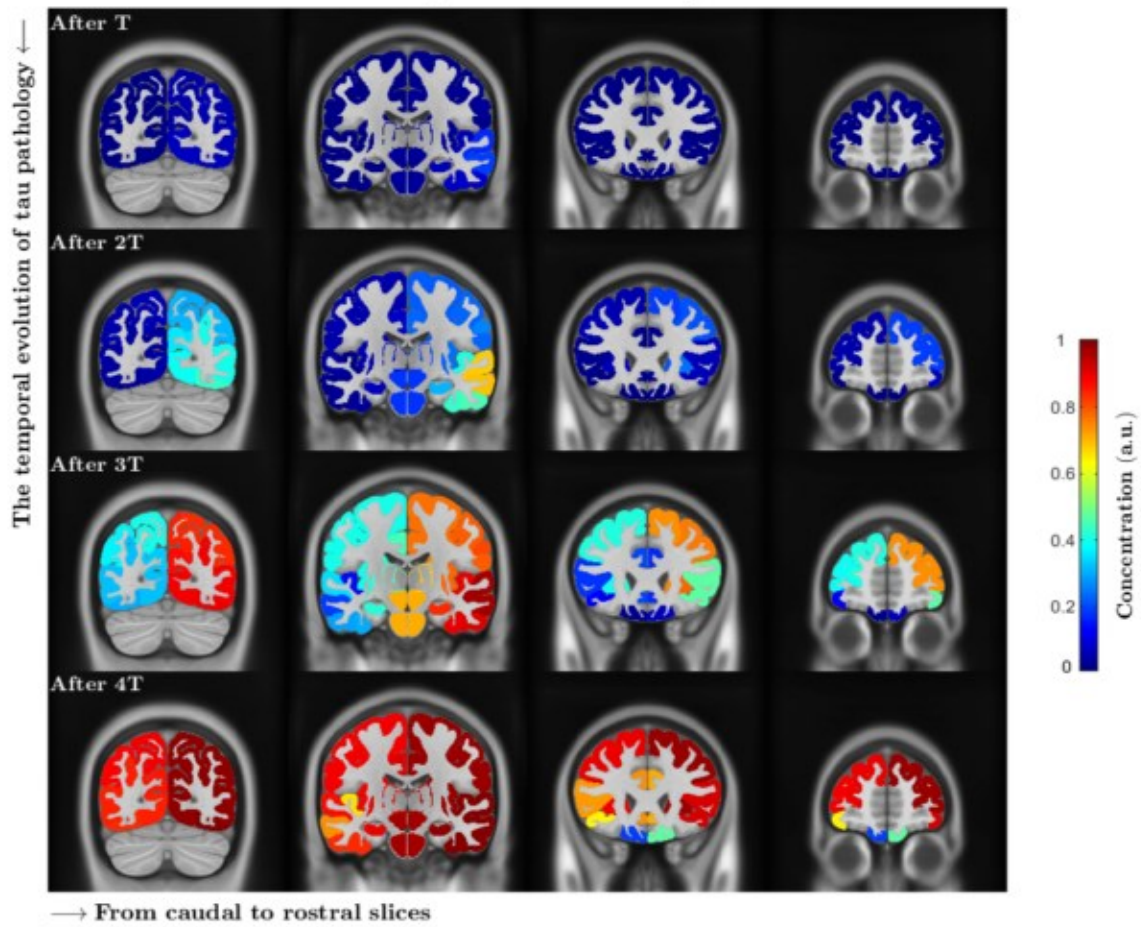


Figure 2. It shows the in silico spatiotemporal evolution of tau pathology when the neuronal connectivity loss coefficient was set to the nonzero value 13. The aggregation and spreading coefficients were also set to 0.5 and 2.5, respectively. The time interval T is 5 years.

The difference between the outputs of the two in silico experiments
without and with considering neuronal connectivity loss



Figure 3. It indicates the relative spatiotemporal evolution of tau pathology in the in silico experiment for which the neuronal connectivity loss has not happened with respect to that for which the neuronal connectivity loss has occurred. The time interval T is 5 years.

Keywords: computational models, tauopathies, neuronal atrophy

P96 Simulated dose reduction in longitudinal [18F]MK-6240 PET

Max McLachlan¹, Andrew McVea¹, Alexandra DiFilippo¹, Michael Schöll^{5,6,7}, Tobey Betthausen^{1,2,3}, Sterling Johnson^{2,3,4}, Bradley Christian^{1,2}

¹Department of Medical Physics, University of Wisconsin – Madison, School of Medicine and Public Health, Madison, WI, US

²Wisconsin Alzheimer's Disease Research Center, University of Wisconsin-Madison, Madison, WI, US

³Department of Medicine, University of Wisconsin-Madison, School of Medicine and Public Health, Madison, WI, US

⁴Wisconsin Alzheimer's Institute, Madison, WI, US

⁵Department of Psychiatry and Neurochemistry, University of Gothenburg, Gothenburg, Sweden

⁶Dementia Research Centre, Department of Neurodegenerative Disease, UCL Institute of Neurology, London, UK

⁷Department of Medical Physics and Biomedical Engineering, Sahlgrenska University Hospital, Gothenburg, Sweden

Background: Decreasing the injected dose of PET radiotracers is desirable in longitudinal tau PET studies, but the effect of reducing injected dose between baseline and follow-up scans on calculating longitudinal rates of tau change is not well understood. This study examines the extent to which reducing injected dose from baseline to follow-up [18F]MK-6240 scans affects longitudinal SUVR change. This is achieved by simulating dose reduction in follow-up scans by removing photon events from the original unreduced listmode files.

Methods: 6 participants (3 Amyloid+/Tau+ and 3 Amyloid-/Tau-) were scanned with [18F]MK-6240 PET at baseline (TP1) and at follow-up (TP2), ~2 years later. The TP2 listmode data was reduced to 50% of the original injected dose using the Siemens LMChopperStar algorithm, which randomly eliminates 50% of all PET photon events. Analysis for each participant considered three scans: TP1 unreduced, TP2 unreduced, and TP2 50% reduced. Images were summed 70-110min, smoothed with a 4mm Gaussian kernel, and registered to MNI space. SUVR (inferior cerebellum reference region) was calculated in Braak-associated regions. Longitudinal SUVR change from unreduced TP1 was compared between the unreduced and 50% reduced TP2 scans.

Results: 50% dose reduction resulted in comparatively noisier images (**Figure 1**). Longitudinal SUVR changes for A+/T+ and A-/T- groups are listed in **Table 1**. Simulated 50% dose reduction of TP2 generally resulted in slightly lower annualized SUVR change, but differences between SUVR change per year calculated using unreduced and reduced injected dose were low, with confidence intervals overlapping zero for most regions and for both groups.

Discussion: Both groups showed low variation in longitudinal SUVR change across dose reduction. Most regions demonstrated a 95% confidence interval containing no difference in SUVR change across reduction. Further investigation must consider larger longitudinal sample sizes and smaller dose reductions to determine the feasibility of implementing low dose protocols.

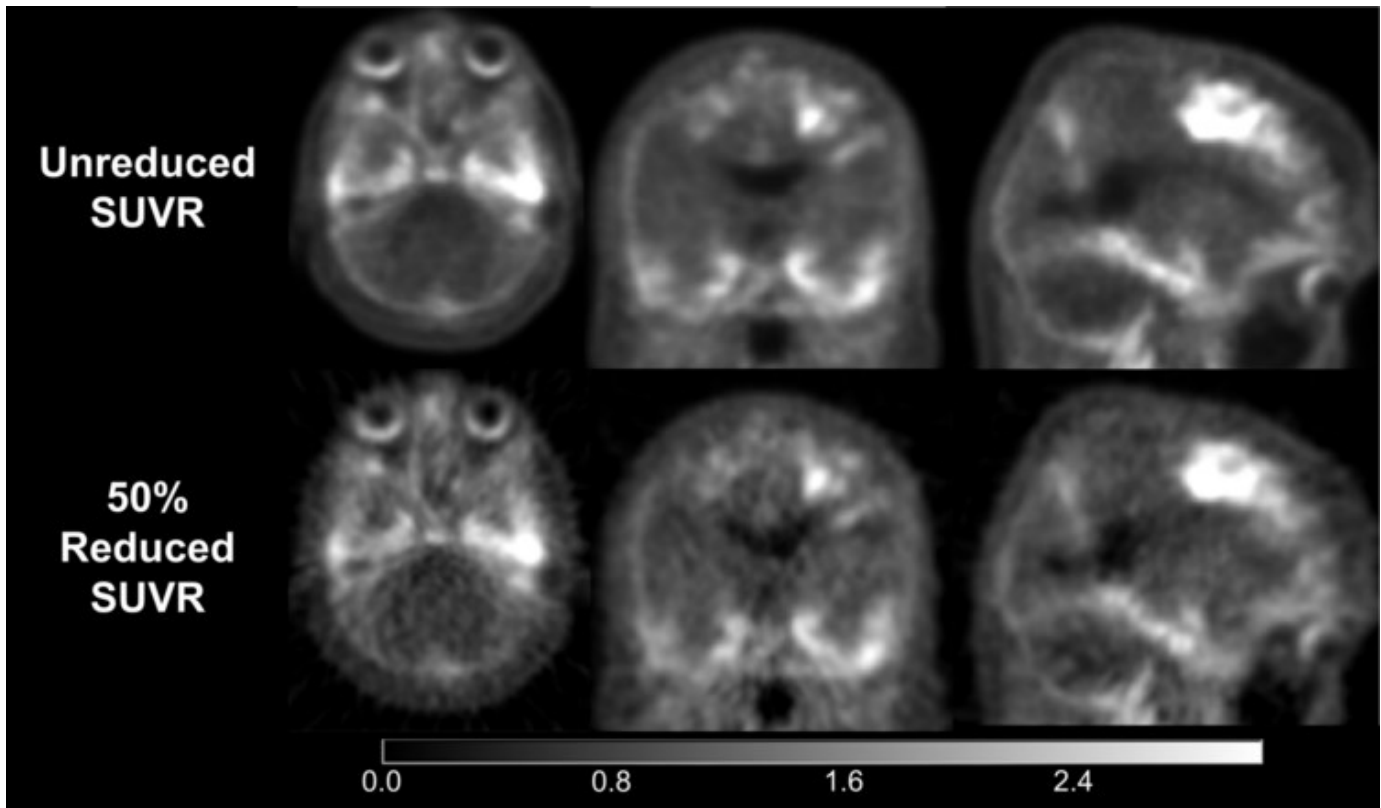


Figure 1 – Unreduced (top) and 50% reduced (bottom) SUVR images for a A+/T+ participant, registered in MNI space.

	Baseline SUVR (mean [95% C.I.])	Unreduced Long. Change (SUVR/yr) (mean [95% C.I.])	50% Reduced Long. Change (SUVR/yr) (mean [95% C.I.])	Difference in Long. Change (SUVR/yr) (mean [95% C.I.])
A+/T+ Participants				
Entorhinal Cortex	1.6680 [1.5441, 1.7919]	0.0526 [0.0146, 0.0906]	0.0513 [0.0298, 0.0728]	-0.0013 [-0.0182, 0.0156]
Hippocampus	1.2965 [1.1246, 1.4683]	0.0614 [0.0349, 0.0879]	0.0485 [0.0210, 0.0760]	-0.0130 [-0.0294, 0.0034]
Temporal Fusiform Gyrus	1.4567 [1.2514, 1.6620]	0.0540 [-0.0056, 0.1136]	0.0462 [-0.0066, 0.0989]	-0.0078 [-0.0170, 0.0014]
Inferior and Middle Temporal Gyri	1.5570 [1.0822, 2.0318]	0.0499 [0.0243, 0.0755]	0.0372 [0.0237, 0.0508]	-0.0127 [-0.0248, -0.0006]
Insular Cortex	1.0110 [0.9575, 1.0644]	0.0050 [-0.0298, 0.0397]	0.0048 [-0.0283, 0.0379]	-0.0002 [-0.0087, 0.0083]
A-/T- Participants				
Entorhinal Cortex	1.0926 [1.0274, 1.1578]	-0.0035 [-0.0358, 0.0288]	-0.0204 [-0.0459, 0.0050]	-0.0169 [-0.0239, -0.0099]
Hippocampus	0.9627 [0.8346, 1.0909]	-0.0242 [-0.0587, 0.0104]	-0.0288 [-0.0623, 0.0047]	-0.0046 [-0.0057, -0.0036]
Temporal Fusiform Gyrus	1.1160 [0.9999, 1.2322]	-0.0204 [-0.0677, 0.0269]	-0.0252 [-0.0627, 0.0123]	-0.0048 [-0.0166, 0.0070]
Inferior and Middle Temporal Gyri	1.1935 [1.0710, 1.3161]	-0.0257 [-0.0680, 0.0167]	-0.0256 [-0.0634, 0.0123]	0.0001 [-0.0050, 0.0052]
Insular Cortex	0.9983 [0.9079, 1.0888]	-0.0336 [-0.0684, 0.0011]	-0.0298 [-0.0658, 0.0062]	0.0038 [0.0008, 0.0068]

Table 1 – Regional SUVR data, separated by amyloid and tau status. All ROIs were segmented using the Harvard-Oxford atlas registered in MNI space. Longitudinal (Long.) change is determined from the difference between regional SUVR at TP2 and TP1, divided by the time between scans. Differences in longitudinal change compare the calculated annualized SUVR rates between unreduced and 50% reduced treatments of the TP2 scan.

Keywords: PET, Tau, Amyloid, dose, simulation

P97 Regional amyloid change improves prediction of future tau progression over global metrics

Emma Thibault¹, Michelle Farrell¹, Michael Properzi¹, Danielle Mayblyum¹, Bernard Hanseewu^{1,3}, Brian Healy^{1,2}, Julie Price¹, J. Alex Becker¹, Reisa Sperling^{1,2}, Keith Johnson^{1,2}

¹Massachusetts General Hospital, Boston, MA, US

²Brigham and Women's Hospital, Boston, MA, US

³Université Catholique de Louvain, Brussels, Belgium

Background: The presence of global amyloid (A β) pathology appears to be necessary but not sufficient to predict extensive spread of tau pathology into the neocortex in the near future. We hypothesize that using A β change in salient regions can improve prediction of future neocortical tau proliferation.

Methods: 220 clinically normal individuals from the Harvard Aging Brain Study (HABS) aged 61-92 underwent longitudinal Pittsburgh Compound B (PIB) and Flortaucipir (FTP) PET. We evaluated regional change in amyloid burden over 3 years and subsequent tau accumulation over a non-overlapping period of 2.2 \pm 2.1 years (Figure 1). Tau ROIs expected to accumulate (tROIs) were defined a priori (inferior temporal (IT), amygdala (AM), entorhinal cortex (ERC)), as well as a negative control (pericalcarine (PC)). First, linear mixed effects (LME) models were constructed to assess the contributions of age and global amyloid measures (baseline PIB \pm , DVR, DVR slope) on tau SUVR change in each tROI. Akaike's Information Criteria (AIC) was used to identify the optimal age-global A β base models for predicting tau proliferation. Next, we evaluated whether the inclusion of antecedent regional A β change (ROI PIB slope) improved the predictive capacity of each age-global A β base model for subsequent tau rise.

Results: Optimized age-global A β base models (Table 1) for ERC, AM and IT included main effects of age and baseline global amyloid (both PIB status and DVR) and time*PIB Status for IT and left AM. Only age predicted tau SUVR in the PC. Addition of antecedent regional PIB change to tROI base models revealed an association between PIB rise in adjacent temporal ROIs (Figure 2) and subsequent rise in IT FTP SUVR.

Conclusions: Regional A β change provides useful insight into subsequent tau proliferation and can improve identification of those likely to accumulate neocortical tau.

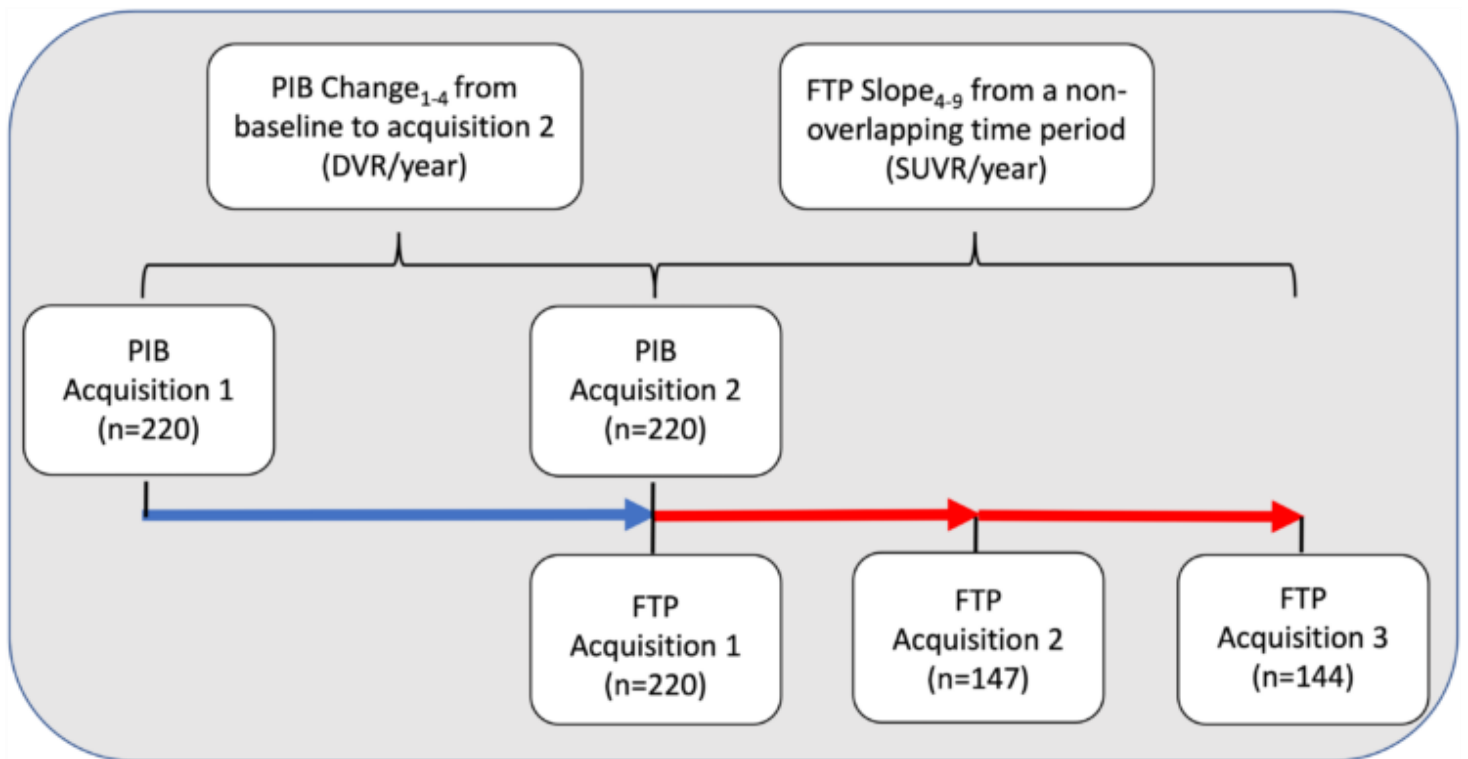


Figure 1. Study schematic. Amyloid change was generated in all HABS subjects with two amyloid timepoints within our window of interest and with at least one successive timepoint of tau. Tau slopes were then evaluated in a subsequent, non-overlapping time period. Amyloid slopes were extracted from PIB acquisitions at timepoints one and two of participation in the Harvard Aging Brain Study (DVR/year). Tau slopes were derived from FTP acquisitions at timepoints two, three, and four (SUVR/year).

		Main Effects				Interactions with Time			
		Age	Global Amyloid			Age	Global Amyloid		
ROI	Hemi		+/-	DVR	DVR Slope		+/-	DVR	DVR Slope
IT	L	■	■	■			■		
	R	■	■	■			■		
AM	L	■	■	■			■		
	R	■	■	■					
ERC	L	■	■	■					
	R	■	■	■					
PC	L	■							
	R	■							

Table 1. Optimal age-global A β base models for predicting tau proliferation over time.

Table 1 summarizes the results of analyses to generate base age-global A β models for predicting tau proliferation in ERC, IT, AM, and the negative control region (pericalcarine-PC). For each tau ROI, a series of LME models were conducted to determine whether age and three different measures of global amyloid (baseline PIB +/-, baseline PIB DVR, PIB DVR slope) predicted FTP tau SUVR over time (with sex as a covariate). We first assessed the age effects (main effect and interaction with time), with all tauROIs showing age main effects such that older age was associated with higher FTP SUVR but no age*time effects indicating older individuals did not exhibit higher rates of change for any tauROI. Next we added global A β status (PIB +/- based on a global PIB DVR>1.19, approximately 25 Centiloid), and found significant main effects for ERC, AM and IT but not the PC control region, such that PIB+ individuals had higher ERC, AM and IT FTP SUVR. Global A β status also significantly interacted with time for bilateral IT and left AM, with PIB+ individuals exhibiting greater IT and left AM tau proliferation over time. We confirmed that the addition of these global A β status effects significantly improved model prediction of tau SUVR over time in each tROI by using ANOVA to demonstrate a significant reduction in the Akaike's Information Criteria (AIC). We also found that the main effect (but not time interaction) of continuous global PIB DVR significantly contributed to the tau prediction model for ERC, AM, and IT, such that higher magnitudes of global A β burden were associated with higher tau SUVR even after accounting for A β positivity. The antecedent global DVR slope did not contribute to the prediction of tau proliferation for any tROI. In summary, three sets of base models for predicting tau from age and global A β were derived: 1) Main effects of age, global PIB positivity and global PIB DVR on ERC and right AM; 2) Main effects of age, global PIB positivity and global PIB DVR and the time*global PIB positivity interaction for IT and left AM; 3) Age only for the PC control region.

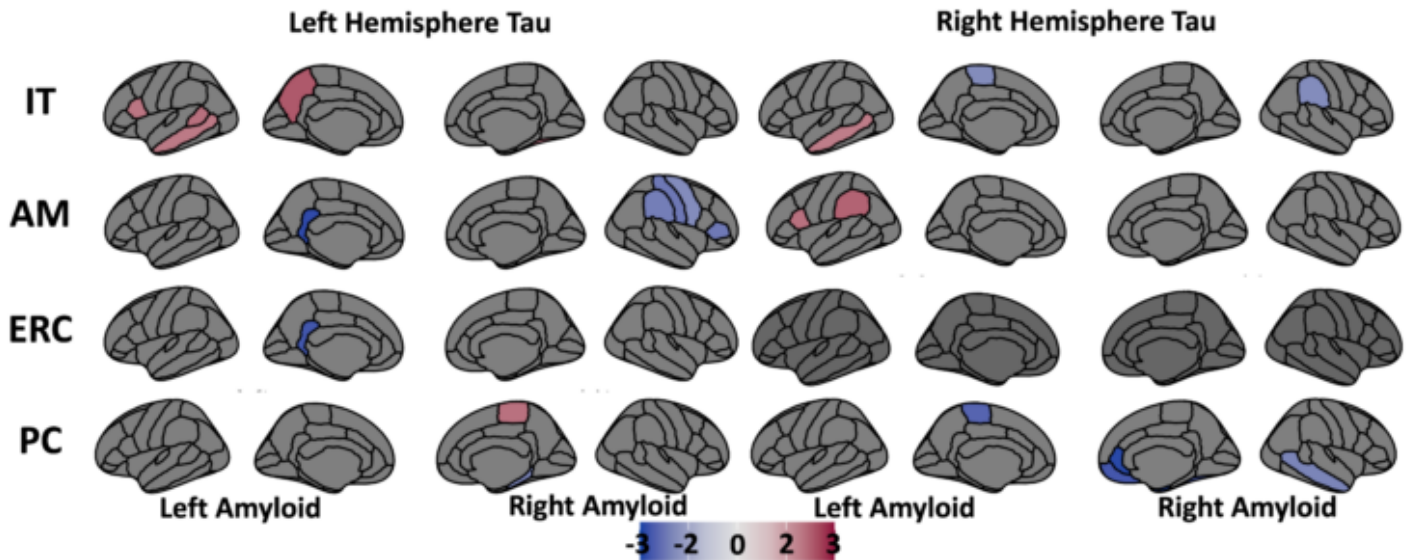


Figure 2. Improved prediction of tau SUVR using antecedent regional PIB slope. ROI PIB slope₁₋₄ main effects and interactions were added to the base model for each ROI and AIC was tested to determine whether prediction of the tROI was improved. For all significantly improved models, t-statistics are shown for the time*ROI PIB slope₁₋₄ effects. Increasing Left IT tau SUVR over time was associated with prior increases in A β in nearby temporal cortices (middle temporal, banks of the superior temporal sulcus, and fusiform) as well as precuneus and pars opercularis. Increasing FTP tau over time in the right IT was similarly predicted by high rates of A β accumulation in the middle temporal cortex. Limited associations were observed between prior PIB slope and FTP tau increase over time in AM, ERC, and PC.

Keywords: Amyloid, tau, PET, accumulation, prediction

P99 Rates of tau PET accumulation along the amyloid timeline in Alzheimer's disease

Karly Cody^{1,2}, Rebecca Langhough^{1,2,3}, Bradley Christian^{1,4}, Tobey Betthausen^{1,2,4}, Sterling Johnson^{1,2,3}

¹Wisconsin Alzheimer's Disease Research Center, University of Wisconsin-Madison, Madison, WI, US

²Department of Medicine, School of Medicine and Public Health, University of Wisconsin-Madison, Madison, WI, US

³Wisconsin Alzheimer's Institute, Madison, WI, US

⁴Department of Medical Physics, School of Medicine and Public Health, University of Wisconsin-Madison, Madison, WI, US

Background: This work examined the magnitude and spatial burden of regional tau change in individuals spanning the amyloid timeline.

Methods: Individuals (N=190, 68.2±6.3 years, 165 unimpaired, 13 MCI, 12 dementia; Table 1) from University of Wisconsin AD research cohorts underwent serial amyloid and tau PET (tau follow-up: Median(Range), 2.3 yrs (1.0-4.4yr)). Cortical ¹¹C-PiB DVR and sampled iterative local approximation was used to estimate amyloid time at tau PET. Tau burden was quantified using ¹⁸F-MK-6240 SUVR (70-90 min, inferior cerebellar GM reference region). Annualized change and percent change in ¹⁸F-MK-6240 SUVR were estimated in regions approximating NFT neuropathological staging and exploratory regions of interest (ROIs). A maximum NFT stage (i.e., highest tau positive NFT ROI) was defined at each tau visit. Rates of tau accumulation were assessed relative to baseline NFT stage and amyloid time.

Results: Tau accumulation rates varied according to brain region and baseline tau deposition (Figure 1). Individuals with tau contained to NFT I/II at baseline had the highest rates of tau accumulation in NFT I (5.1%); those at baseline NFT stage III/IV had the highest accumulation rates in NFT III (7.3%), NFT IV (10.1%), and NFT V (7.7%) ROIs. Subjects with widespread baseline tau, NFT stage V/VI, had no evidence of accumulation in early NFT ROIs and had the highest accumulation rate in NFT V (6.4%) and NFT VI (6.0%) (Table 2). Detection of elevated tau generally followed the hierarchical pattern of NFT staging, such that with increasing time from A+ onset, the spatial extent of detectable tau progressed from early to late NFT stages (Figure 2).

Conclusions: Overall, rates of tau accumulation varied based on baseline tau patterns of elevation and amyloid time. The highest magnitude of ¹⁸F-MK-6240 SUVR accumulation progressed from the entorhinal cortex to outside the medial temporal lobe across the amyloid timeline.

Table 1. Participant characteristics at baseline tau PET

Characteristic	N	N = 190 ¹
Age (years)	190	68.16 (6.29)
Cohort	190	
ADRC		19 (10%)
ALERT		20 (11%)
WRAP		151 (79%)
Clinical Diagnosis	190	
Dementia		12 (6.3%)
MCI		13 (6.8%)
Normal		165 (87%)
Sex	190	
Female		119 (63%)
Male		71 (37%)
No. APOE e4 alleles	168	
0		102 (61%)
1		55 (33%)
2		11 (6.5%)
Duration of tau follow-up	190	2.40 (0.56)
Amyloid status	190	77 (41%)

¹ Mean (SD); n (%)

Table 2. Annualized Percent Change in Tau PET

Characteristic	N	Baseline NFT Stage				p-value ²
		Tau-, N = 156 ¹	NFT I/II, N = 13 ¹	NFT III/IV, N = 8 ¹	NFT V/VI, N = 13 ¹	
NFT I Annualized % Change	190	0.72 (4.75)	5.14 (4.16)	3.87 (5.75)	0.75 (5.30)	0.002
NFT II Annualized % Change	190	1.18 (4.26)	3.39 (3.72)	1.40 (2.84)	-0.62 (3.93)	0.14
NFT III Annualized % Change	190	0.43 (3.50)	3.44 (2.72)	7.33 (4.14)	4.99 (4.20)	<0.001
NFT IV Annualized % Change	190	0.49 (3.72)	3.66 (2.76)	10.06 (7.63)	5.01 (5.94)	<0.001
NFT V Annualized % Change	190	0.06 (3.24)	2.20 (2.73)	7.73 (8.39)	6.36 (4.34)	<0.001
NFT VI Annualized % Change	190	-0.04 (3.24)	0.76 (2.23)	2.08 (3.28)	6.00 (3.53)	<0.001
Temporal Meta-ROI Annualized % Change	190	0.60 (3.88)	4.06 (2.58)	9.29 (6.09)	4.90 (5.92)	<0.001
MTL Annualized % Change	190	1.16 (4.27)	4.41 (3.82)	2.60 (4.22)	-0.06 (4.30)	0.028
ITG Annualized % Change	190	0.68 (4.01)	4.31 (2.96)	11.50 (7.82)	5.03 (6.79)	<0.001

¹ Mean (SD)

² Kruskal-Wallis rank sum test

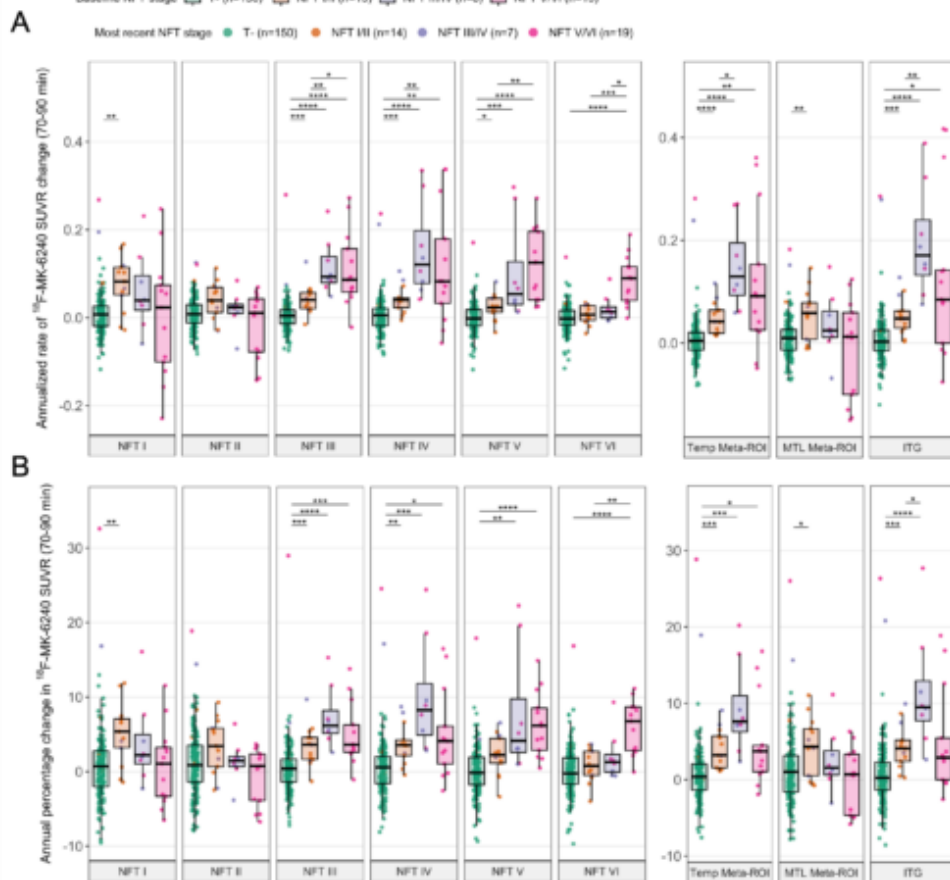


Figure 1. Annualized rate of change and percent change in ¹⁸F-MK-6240 SUVR in NFT and exploratory composite ROIs. In accordance with stereotypical staging of tau pathology based on neuropathological findings, we used volume-weighted bilateral composite regions of interest (ROIs) approximating the anatomical definitions of Braak neurofibrillary tangle (NFT) stages: (NFT I, entorhinal cortex; NFT II, hippocampus; NFT III, temporal portion of the fusiform gyrus, amygdala, posterior parahippocampal gyrus, and lingual gyrus; NFT IV, inferior and middle temporal gyri, posterior cingulate, and insular cortex; NFT V, orbitofrontal, superior frontal, middle frontal, frontal pole, frontal medial, superior temporal, superior parietal, lateral occipital, occipital portion of the fusiform, subcallosal, anterior cingulate, supramarginal, angular, precuneus, cuneus, and planum temporale; NFT VI, Heschl's gyrus, precentral, postcentral, and calcarine cortex). A maximum NFT stage (ie. highest tau positive NFT ROI) was defined at baseline and the most recent visit. Additionally, we examined three exploratory ROIs: a temporal meta-ROI including the entorhinal cortex, amygdala, parahippocampal gyrus, fusiform gyrus, inferior and middle temporal gyri; a medial temporal lobe (MTL) composite ROI including the entorhinal cortex, hippocampus, and amygdala; and an inferior temporal gyrus (ITG) ROI.

Boxplots showing the (A) annual tau SUVR change and (B) annual percent tau change across NFT ROIs and exploratory ROIs in groups based on NFT stage at baseline. Boxplots depict the median (horizontal bar) and IQR (hinges), and observed points are colored by maximum NFT stage at most recent visit. Across all ROIs (except NFT II), the rate of accumulation differed by baseline NFT stage (Kruskal-Wallis test, all $p < .01$). Mann-whitney U *post hoc* groupwise comparisons indicated significant step-wise increases in tau accumulation rates across baseline NFT stage groups in regions extending outside of the MTL (NFT IV-VI). Overall, rates of tau accumulation were highest in regions of elevated tau at baseline. Significance was adjusted for multiple comparisons using Bonferroni-correction. * $p < .05$, ** $p < .01$, *** $p < .001$, **** $p < .0001$.

A Longitudinal tau PET change by amyloid time

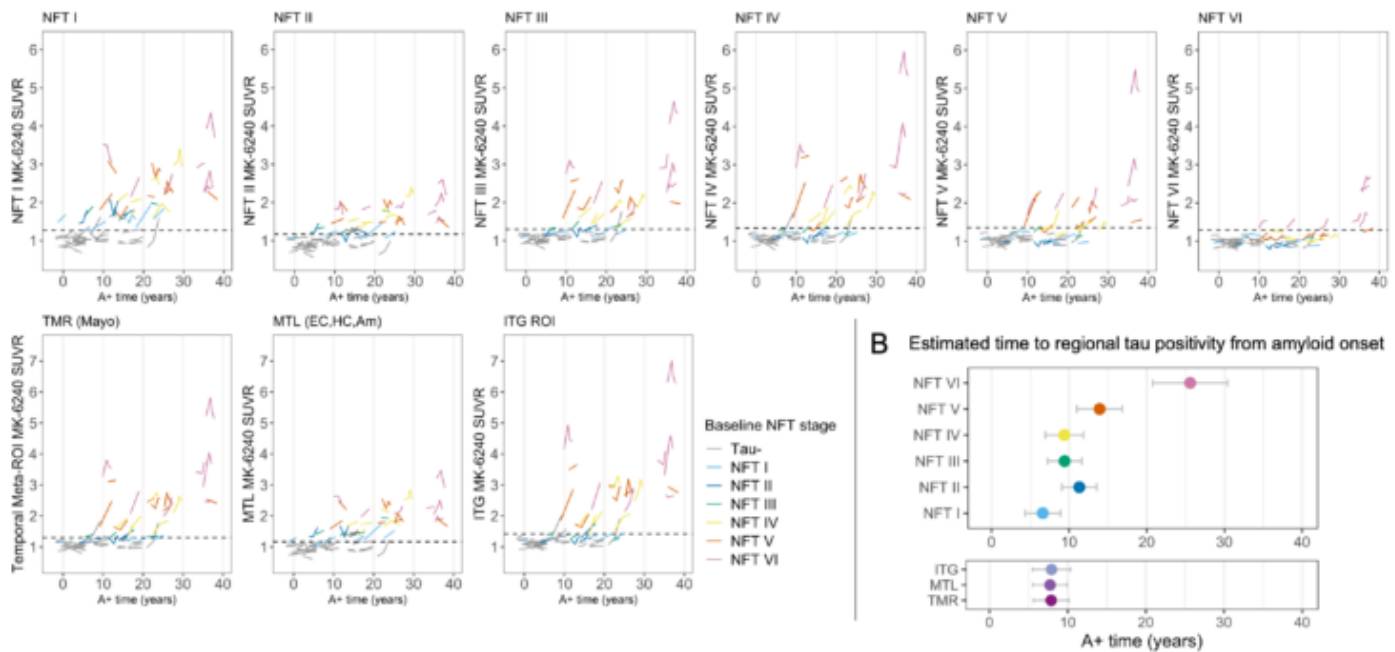


Figure 2. Regional tau PET as a function of amyloid time among A+ individuals (n=85 subjects; n= 198 tau PET observations) (A) Spaghetti plots indicating the observed relationship between ^{18}F -MK-6240 SUVR ROIs and amyloid time (i.e., estimated years A+) among A+ individuals. The threshold for tau positivity is represented as the horizontal dashed line and was defined as 2.5 standard deviations above the mean of young (<60 years), CU A- participants in each respective ROI. Individuals are color coded by their baseline NFT stage (i.e., highest tau positive NFT ROI at baseline). **(B)** A linear mixed effects model (random intercept) was used to model the association between regional tau PET signal and amyloid time. Figure B shows a summary of the predicted amyloid time at tau ROI positivity, including predicted 95% confidence intervals (Wald interval). The time from A+ onset to estimated tau positivity varied within and across tau ROIs. On average, the timepoints of detectable tau follow the stereotypical pattern of tau staging as time from amyloid onset increases.

Keywords: Amyloid, Tau, PET, Timing

P100 Body mass index, pathological tau, and cognition in preclinical AD: Could women with high BMI be protected?

Xin Wang¹, Erin Sundermann², Rachel Buckley³, Emilie Reas¹, Linda McEvoy⁴, Sarah Banks^{1,2}

¹Department of Neurosciences, University of California, San Diego., La Jolla, CA, US

²Department of Psychiatry, University of California, San Diego., La Jolla, CA, US

³Department of Neurology, Massachusetts General Hospital/Harvard Medical School., Boston, MA, US

⁴Department of Radiology, University of California, San Diego., La Jolla, CA, US

Background: The association between body mass index (BMI) and Alzheimer's disease (AD) is controversial. Sex-specific relationships between obesity and AD pathology have been reported, with women showing an advantage when having high BMI. However, this is the first study to investigate the sex-specific relationships between BMI and tau levels and Preclinical Alzheimer's Cognitive Composite (PACC) in preclinical AD.

Methods: We included 340 cognitively unimpaired amyloid-positive individuals (202 women, 138 men) from the Anti-Amyloid Treatment in Asymptomatic Alzheimer's Disease (A4) study who were self-identified as non-Hispanic white, had 18F-flortaucipir PET data and completed neuropsychological tests: PACC. Participants were categorized as: normal-weight (BMI<25), overweight (BMI:25-30) and obese (BMI≥30). Tau Standardized Uptake Value Ratio (SUVR) was generated using the inferior cerebellum grey matter as the reference region. Linear regression models assessed the interaction effects of sex and BMI categories on tau SUVR (BRAAK1 stage region and a composite meta-temporal region) and PACC and each individual component, adjusting for age and education. Significant BMI by sex interactions were probed via sex-stratified analyses. All *P* values were not corrected for multiple comparisons.

Results: There were significant interaction effects of sex and BMI categories on tau SUVR (BRAAK1 and meta-temporal region) and PACC components: Free and Cued Selective Reminding Test-Free + Total Recall (FCSRT96) and Mini-Mental State Examination (MMSE) (Table 1). After sex-stratification, overweight and obese women showed less tau burden and better performance on the FCSRT96 than normal-weight women (Figure 1 and 2A), while obese men showed poorer MMSE performance than normal-weight men (Figure 2B).

Conclusions: Our results showed that women with high BMI have an advantage in verbal memory and less tau pathology than women in the normal BMI range. Future studies focusing on the mechanism for this relationship may inform sex-specific interventions for AD prevention.

Table 1 Interaction coefficients of BMI_categories and sex on tau PET and PACC and its components

	BMI_categories x Sex		
	Estimate	SE	P value
Outcome: Tau PET			
BRAAK1_SUVR	-0.053	0.025	0.031*
META_TEMPORAL_SUVR	-0.038	0.017	0.027*
Outcome: Cognitive Performance			
PACC	0.602	0.349	0.085
MMSE	0.358	0.147	0.015*
LMDR	-0.010	0.150	0.947
DSC	-0.072	0.133	0.590
FCSRT96	0.326	0.141	0.022*

Interaction coefficients of BMI categories and sex on tau SUVR in the BRAAK1 and meta-temporal region and PACC and individual components. SE: Standard Error; PACC: Preclinical Alzheimer Cognitive Composite; MMSE: Mini-Mental State Examination; LMDR: Logical Memory Delayed Recall; DSC: Digit-Symbol Coding Test; FCSRT96: Free and Cued Selective Reminding Test-Free + Total Recall. $P < 0.05$: *.

Figure 1 Tau SUVR comparison between BMI categories grouped by sex

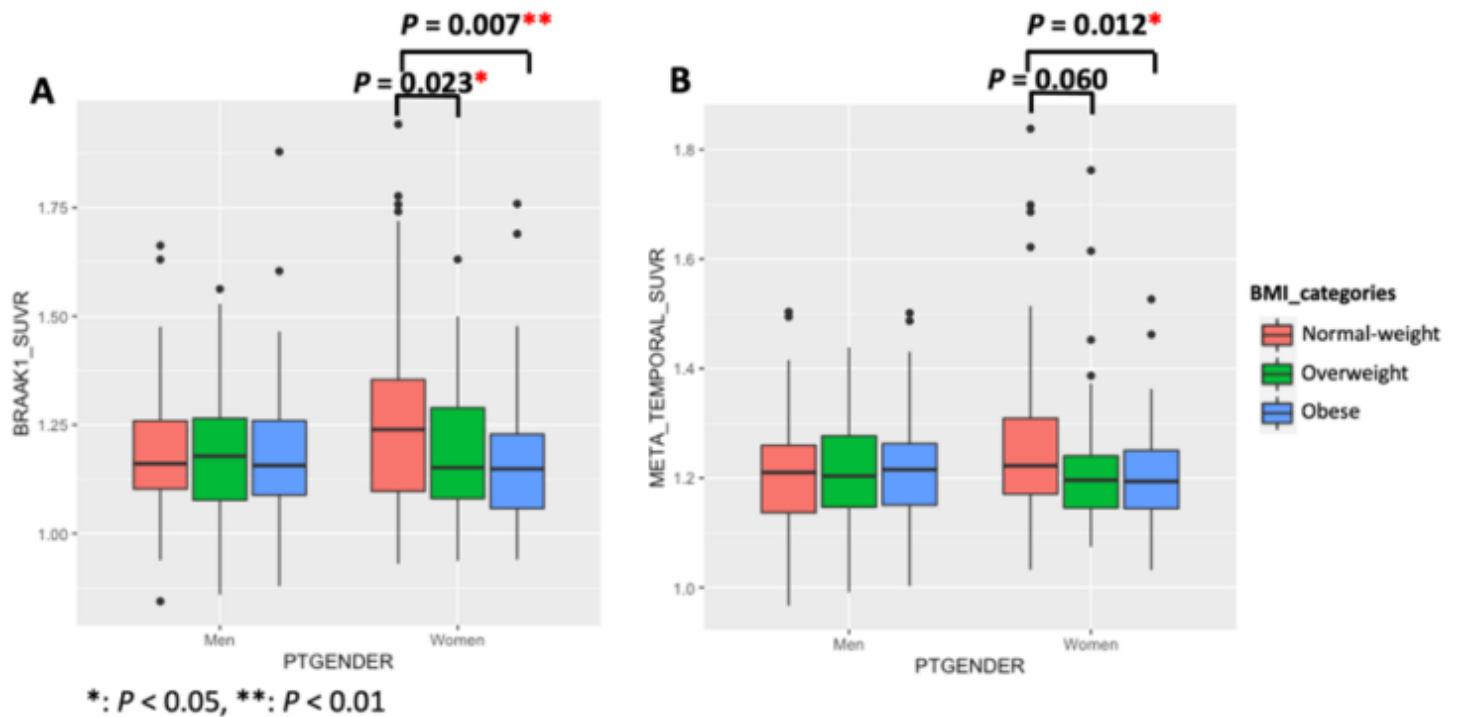
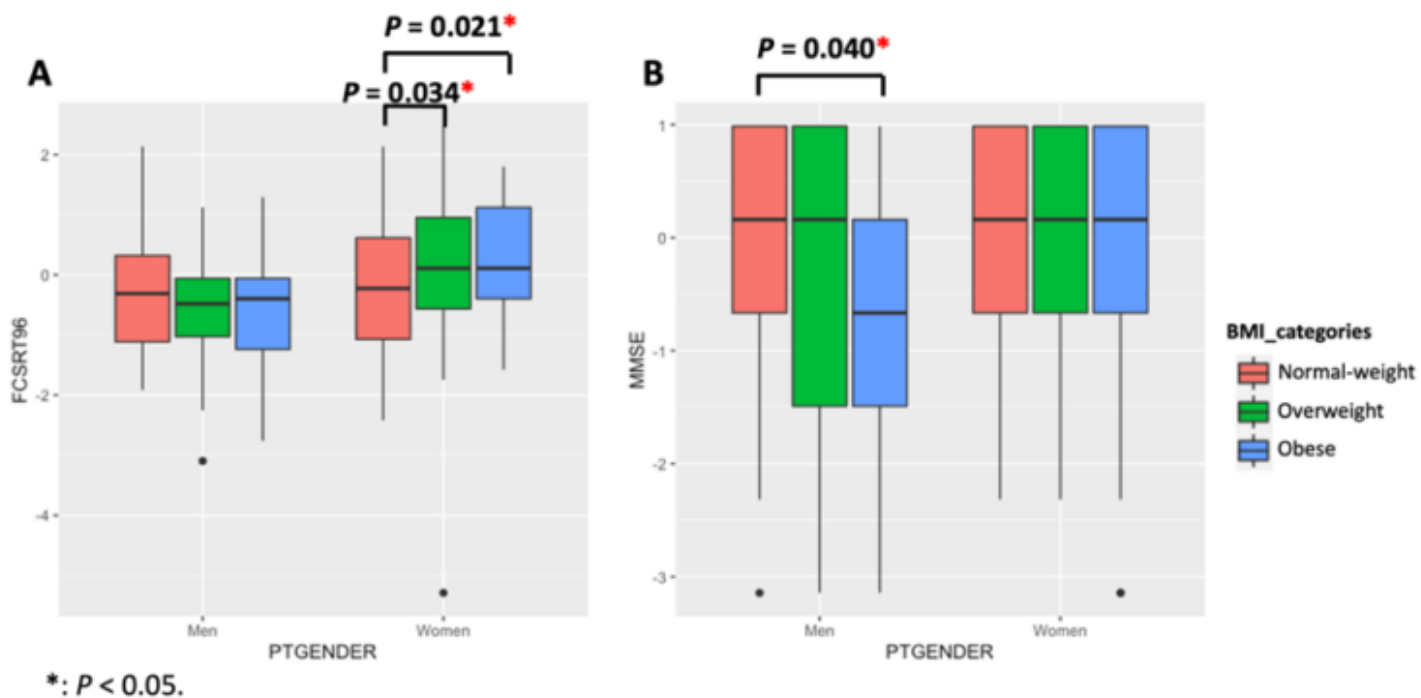


Figure 2 FCSRT96 and MMSE comparison between BMI categories grouped by sex



Keywords: Body mass index, tau pathology, cognition, sex differences, preclinical AD.

P101 Amyloid drives later tau accumulation for fast progressors in early Braak stages

Stijn Servaes^{1,2}, Joseph Therriault^{1,2}, Cécile Tissot^{1,2}, Firoza Lussier^{1,2,3}, Gleb Bezgin^{1,2}, Yi-Ting Wang^{1,2}, Jenna Stevenson^{1,2}, Nesrine Rahmouni^{1,2}, Alyssa Stevenson^{1,2}, Vanessa Pallen^{1,2}, Peter Kunach^{1,2}, Jaime Fernandez Arias^{1,2}, Arthur Cassa Macedo^{1,2}, Seyyed Ali Hosseini^{1,2}, Tharick Ali Pascoal³, Serge Gauthier^{1,2}, Pedro Rosa-Neto^{1,2}

¹Translational Neuroimaging Laboratory, McGill Research Centre for Studies in Aging, Montreal, QC, Canada

²Department of Neurology and Neurosurgery, Faculty of Medicine, McGill University, Montreal, QC, Canada

³Department of Neurology and Psychiatry, University of Pittsburgh School of Medicine, Pittsburgh, PA, US

Objectives: Accumulation of tau neurofibrillary tangles in Alzheimer's disease (AD) follows a stereotypical pattern – known as Braak staging - as suggested by post-mortem and tau-PET imaging studies. As individuals show different rates of tau accumulation, depending on their initial stage, this potentially biases drug effects on tau pathology over time. We hypothesized that amyloid would be a driving force behind tau deposition in later Braak regions for those that were at earlier stages of the disease.

Methods: Individuals in Braak stage 1 (n = 17), 2 (n = 39), 3 (n = 3) or 4 (n = 10) with baseline and follow-up were recruited from the Translational Biomarkers of Aging and Dementia (TRIAD) cohort. All individuals underwent amyloid ([¹⁸F]AZD4694) and tau ([¹⁸F]MK6240) PET imaging. Differences in standardized uptake value ratios between the two timepoints in Braak I-IV were used to separate fast accumulators of tau from slow accumulators, using the standard deviation of a Young group (n = 13).

Pearson R's were calculated between tau deposition in Braak regions V-VI and the neocortical amyloid load at baseline, within both these groups. Furthermore, a voxelwise analysis was performed to identify specific regional differences while correcting for age, sex and presence of ApoE4.

Results: Fast accumulators of tau had higher baseline levels of amyloid in the neocortex. Furthermore, the level of tau deposition in Braak region V and VI was associated with the amyloid load in the neocortex, but only in the fast accumulator group (figure 1). This was confirmed in a voxelwise analysis, after correcting for control variables (figure 2).

Conclusion: Tau deposition in later Braak regions is associated with a higher amyloid load in individuals in earlier Braak stages that accumulate tau at a more rapid rate.

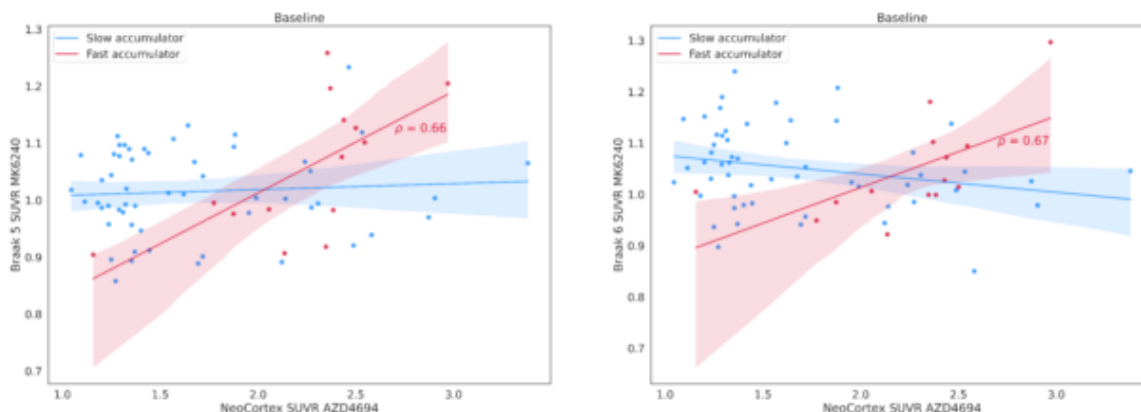


Figure 1

$\tau \sim \text{amyloid} + \text{sex} + \text{age} + \text{apoe}$

Slow accumulator

Fast accumulator

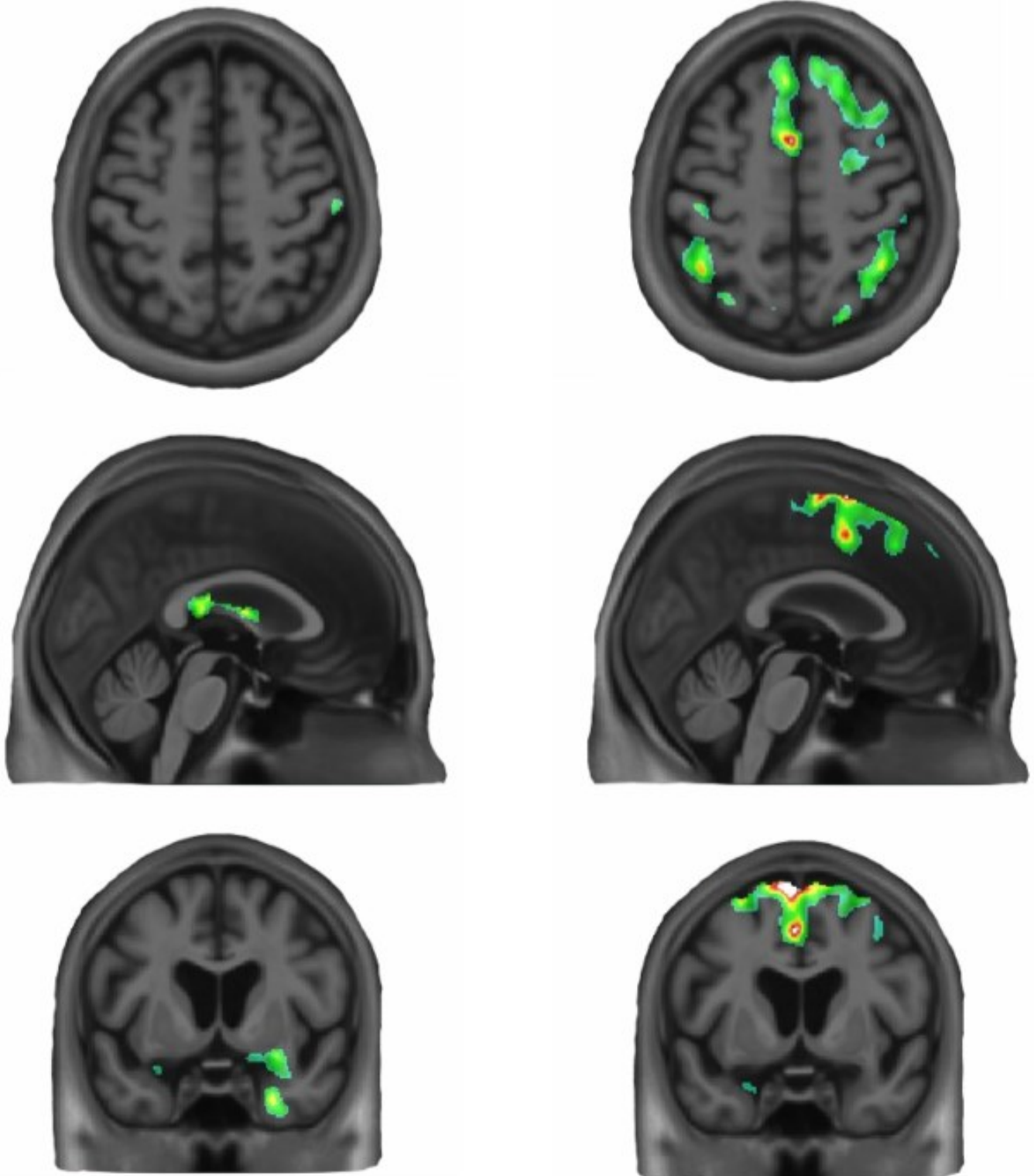


Figure 2

Keywords: amyloid, tau, braak, pet

P102 Brain-wide and AD-risk genetic expression: A descriptive study

Diana Hobbs¹, Austin McCullough¹, Peter Millar¹, Brian Gordon¹

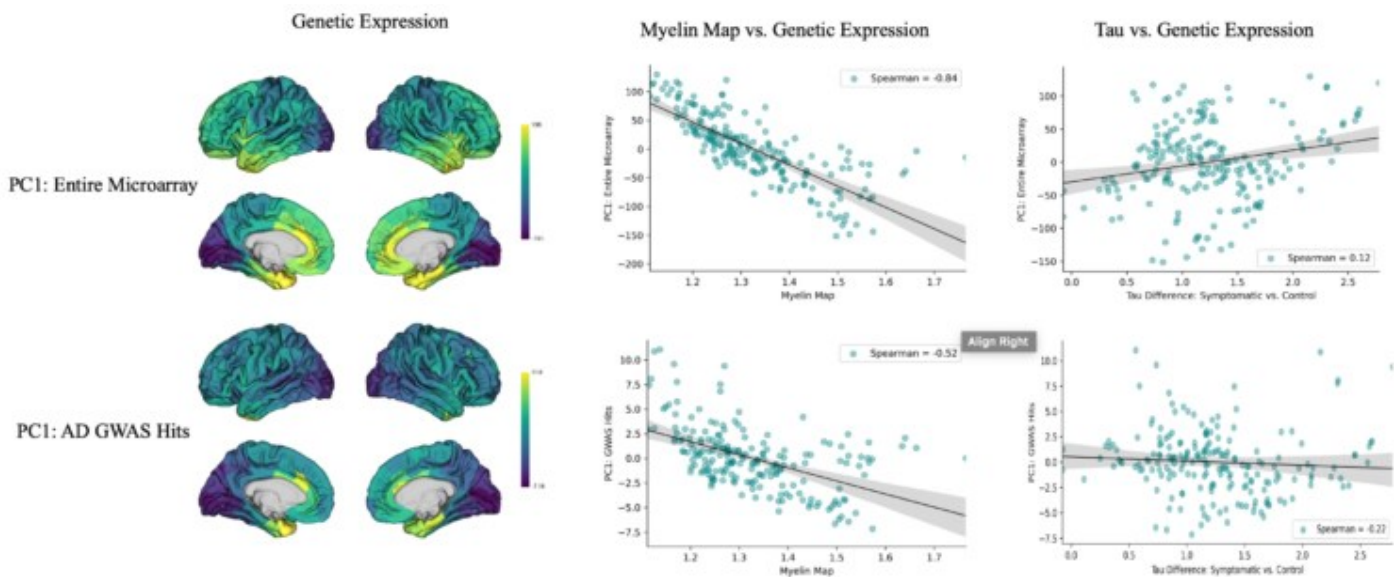
¹Washington University in St. Louis, St. Louis, MO, US

Imaging transcriptomics is a technique used to assess biological underpinnings of regional neuroimaging characteristics. Myelin, for example, is a well-known neuroimaging marker that captures patterns of genetic expression (Burt et al., 2018). We can additionally measure the relationship between pathology and its specific genetic pattern. Tau-containing neurofibrillary tangles are characteristic of Alzheimer disease (AD); however, little is known about their imaging transcriptome. The aim of this study was to assess the cortico-spatial representation of AD-risk genes to that of tau deposition.

Brain-wide genetic expression from the Allen Human Brain Atlas as well as the top prioritized genes from genome-wide significant loci for AD (Kunkle et al., 2019) were parcellated into 200 regions of interest (ROIs) from the Schaefer cortical atlas. The first principal components for the entire microarray and specific AD-risk genes were computed and compared to myelin maps as well as differences in tau-deposition between controls and those symptomatic for AD.

The first principal component of brain-wide (Fig. 1A) and AD-risk (Fig. 1B) genetic expression were mapped onto 200 Schaefer ROIs. The relationships between myelin mappings and the entire microarray ($r = 0.84$, Fig. 1C) or AD-risk genes ($r = -0.52$, Fig. 1D) show moderate to strong associations. The difference in tau deposition between those symptomatic for AD and controls was less strong in relation to brain-wide genetics ($r = -0.12$, Fig. 1E) and AD-specific gene hits ($r = -0.22$, Fig. 1F).

Myelin is a higher-order structure with well documented patterns of genetic expression, a finding supported by the strong associations in our data. We expected a stronger association between AD-risk genes and tau deposition; however, this was not identified in our results. This could be due to lack of representation from the microarray collection. Further analyses would be beneficial to better understand this question.



Keywords: alzheimer disease, tau pathology, imaging transcriptomics, genetic expression

P103 Behavioral brain networks underlying the effect of Alzheimer's pathology on cognition

Jacob Ziontz¹, Theresa Harrison¹, William Jagust^{1,2}

¹Helen Wills Neuroscience Institute, University of California Berkeley,, Berkeley, CA, US

²Lawrence Berkeley National Laboratory, Berkeley, CA, US

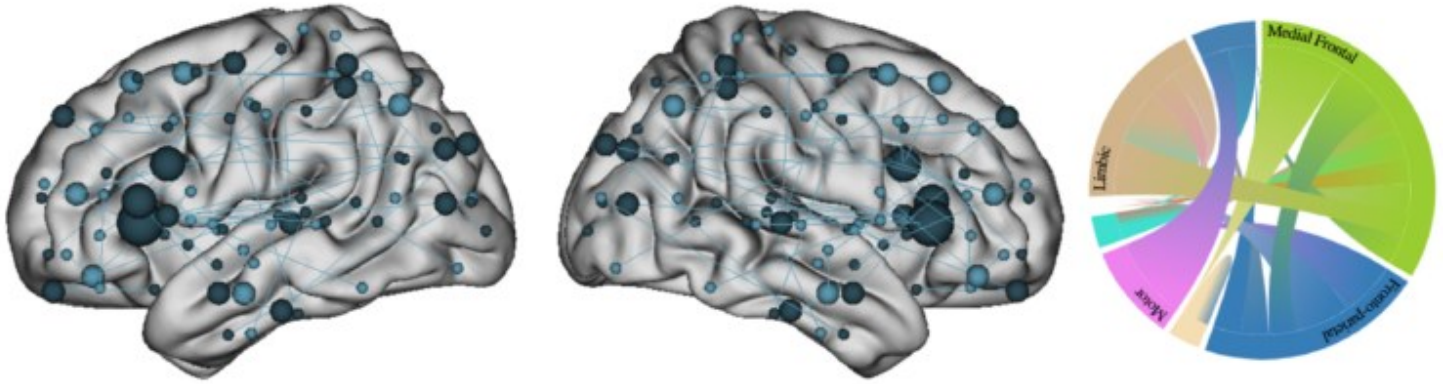
Background: Tau pathology is associated with impaired cognitive function in both aging and Alzheimer's disease (AD), but the mechanisms by which tau and cognition are linked remain unclear. We hypothesized that strength of behaviorally-defined functional brain networks would in part explain the relationship between tau and cognitive performance.

Method: Resting state fMRI was collected in 120 cognitively normal older adults from the Berkeley Aging Cohort Study (BACS; 77.6 ± 6.4 yrs), with $n=94$ receiving FTP and PiB PET. A replication sample of 172 cognitively normal and MCI individuals from ADNI3 with rsfMRI and FTP PET were also included. Functional connectivity (FC) for each ROI-ROI pair of a 246-region atlas was computed, and LASSO+BIC regression of these values against episodic memory (EM) and executive function (EF) composite measures was used to select a highly sparse subset of connections. Overall network strength was computed as the sum of FC values for all selected ROI-ROI pairs.

Result: In BACS, EM and EF networks were identified, comprising connections between limbic, temporal, and frontal regions (Figure 1). Adjusting for age and sex, lower EM network strength was associated with greater meta-temporal ROI tau ($b=-4.05$, $p=.014$), as well as an interaction between greater global Ab and tau ($b=-12.02$, $p=.025$; Figure 2). Causal mediation analysis revealed the effect of meta-ROI tau on EM performance was mediated by EM network strength ($b=-0.802$, $p=.017$; Figure 3), but not by the EF-defined control network. In the ADNI replication sample, meta-ROI tau was related to lower strength of both EM- ($r=-0.2$, $p=.01$) and EF-defined networks ($r=-.22$, $p=0.006$).

Conclusion: Greater tau and Ab pathology was associated reduced network strength, and network strength was observed to mediate the relationship between tau pathology and cognition. Behavioral brain networks may thus be a key mechanism in the effect of AD pathology on cognitive function.

Episodic Memory Network



Executive Function Network

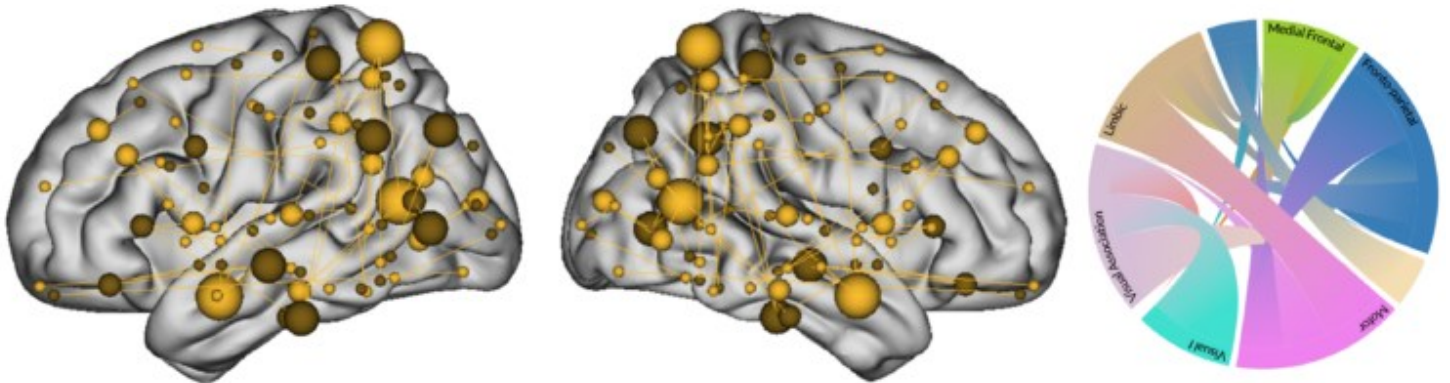


Figure 1. Visualization of behavioral brain networks from LASSO+BIC analysis defined with episodic memory (top) and executive function (bottom) composite measures. Nodes are centered within ROIs with size corresponding to the number of connections to each region.

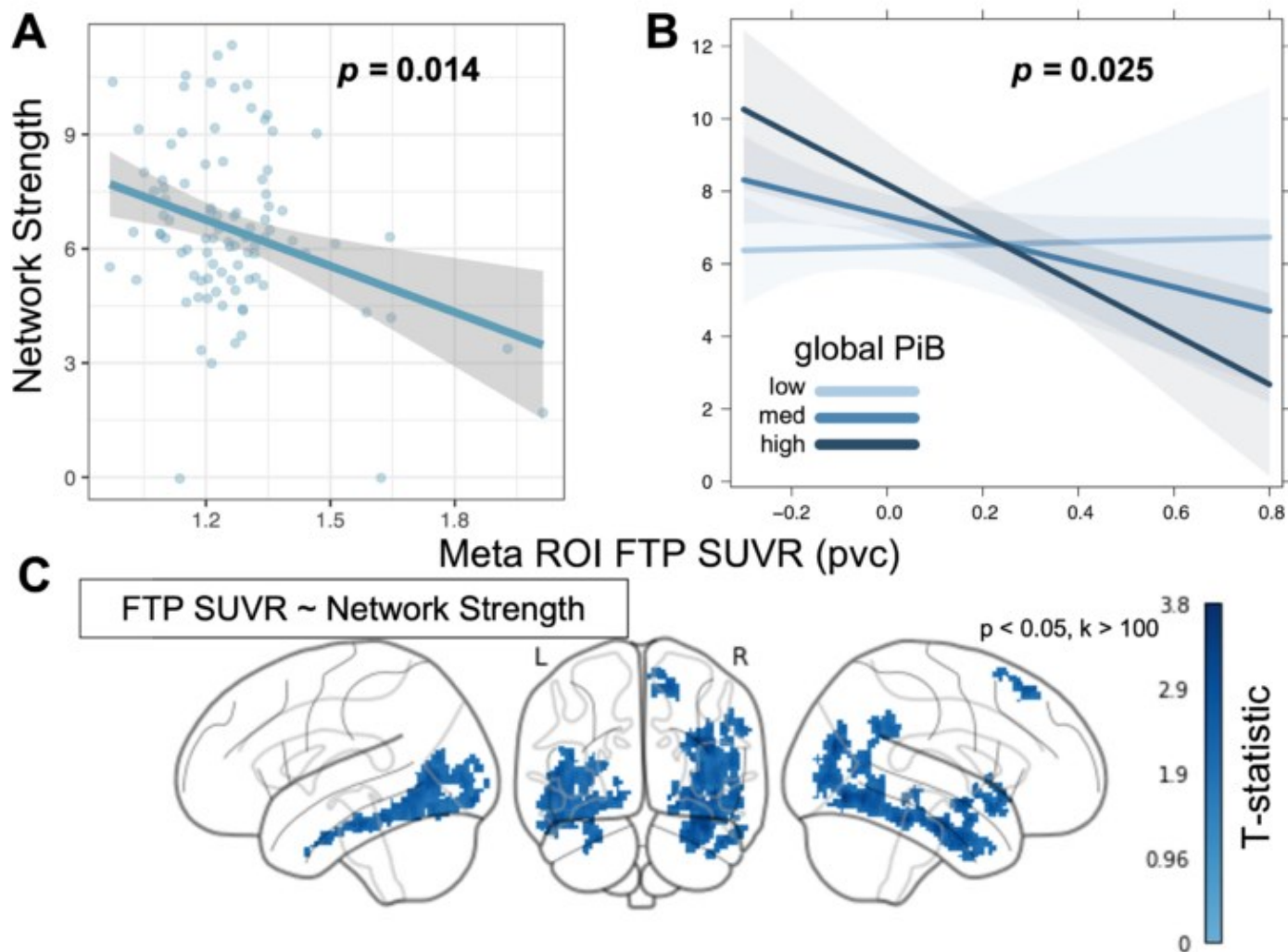


Figure 2. Episodic memory network strength is associated with AD pathology. (A) Adjusting for age, sex, and years of education and global $A\beta$, greater meta-temporal ROI tau is associated with lower overall network strength. (B) In a separate model, network strength is associated with an interaction between global $A\beta$ and meta ROI tau. (C) A voxelwise analysis of the relationship between tau PET SUVR and network strength confirms that the meta ROI region captures tau relevant for network strength.

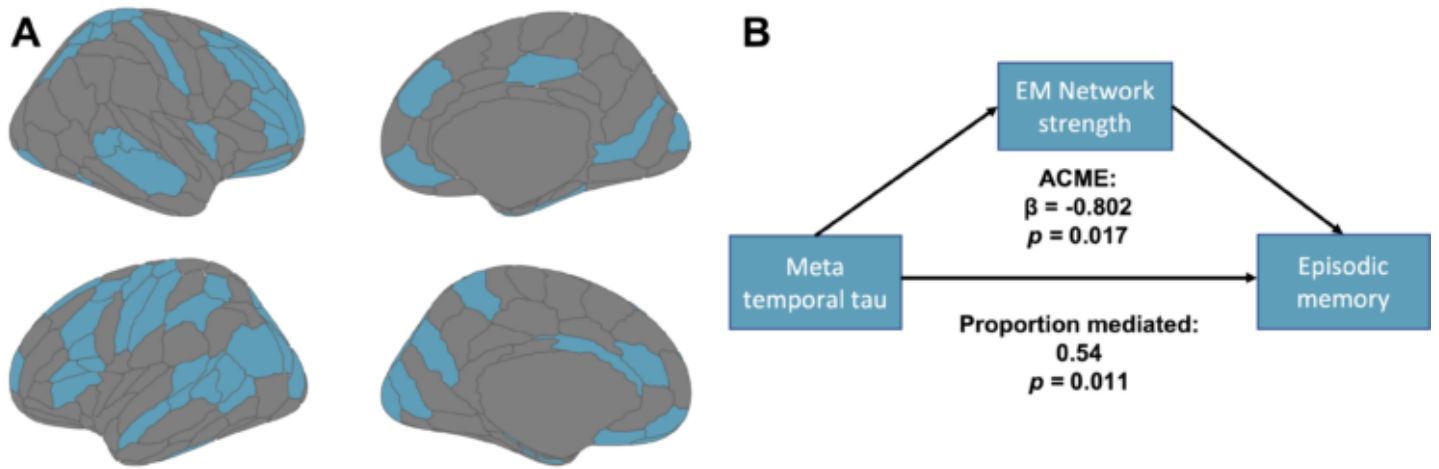


Figure 3. Network mediation of tau-cognition relationship. (A) Visualization of regions comprising the episodic memory network. (B) Episodic memory (EM) network strength shows a significant Average Causal Mediating Effect (ACME) of the association between meta-ROI tau and episodic memory performance.

Keywords: Networks, fMRI, tau, memory, executive function

P104 Exploration of 18F-Florzolotau tau PET distribution patterns using machine learning approach in AD

Shao-Yi Huang¹, Zih-Ning Lee¹, Kun-Ju Lin^{1,2}, Chin-Chang Huang³, Jung-Lung Hsu³, Chiung-Chih Chang⁴, Kuo-Lun Huang³, Ing-Tsung Hsiao^{1,2}

¹Medical Imaging & Radiological Sciences and Healthy Aging Research Center, Chang Gung University, Taoyuan, TW

²Molecular Imaging Center and Nuclear Medicine, Chang Gung Memorial Hospital, Taoyuan, TW

³Neurology, Chang Gung Memorial Hospital, Taoyuan, TW

⁴Neurology, Chang Gung Memorial Hospital, Kaohsiung, TW

Purpose: This work aims to explore the tau distribution patterns in AD by utilizing machine learning approaches on tau-PET images using 18F-Florzolotau and also investigated the differences in clinical characteristics among different tau patterns.

Materials and methods: A total of 32 NC, 37 MCI, and 144 A subjects were included in this study. They all underwent T1-MRI, 18F-Florzolotau and neuropsychological testing. Image preprocessing was performed using PMOD 3.7. MR-based spatial normalization was first conducted, and SUVR (standard uptake value ratio) quantification was then calculated with the inferior cerebellum cortex as the reference region and followed by a z-score standardization. Before applying clustering model, the number of clusters was optimized based on Davies-Bouldin and Silhouette-value criteria. Afterward, the agglomerative hierarchical clustering was applied to classify PET images into 4 clusters. For each subtype, voxel-wise analysis was performed on the SUVR images by SPM12 as comparison to normal controls. Additionally, the difference in the cognitive performance and disease severity among the four subtypes was also investigated.

Results: Four distinct tau patterns were derived (Fig.1). From voxel-wise analysis, tau distribution in subtype 1 was with limbic-dominant tau pattern (15.8%). In subtype 2, tau was primarily distributed in frontal region (15.2%), while the predominant tau accumulation in subtype 3 was in the medial-temporal lobe (39.76%). For the subtype 4, tau aggregation was spread out across the whole neocortex (29.24%). For clinical performance, there was a significant MMSE difference between subtype 1 and 4, while no significant difference between subtype 2 and 3.

Conclusions: Using the 18F-Florzolotau PET imaging, four possible distinct variants in tau topography were observed in this preliminary study, and the predominant tau deposition region differ for each subtype, as well as the clinical feature. Future work will include more samples for studying group difference from the distribution patterns and clinical features.

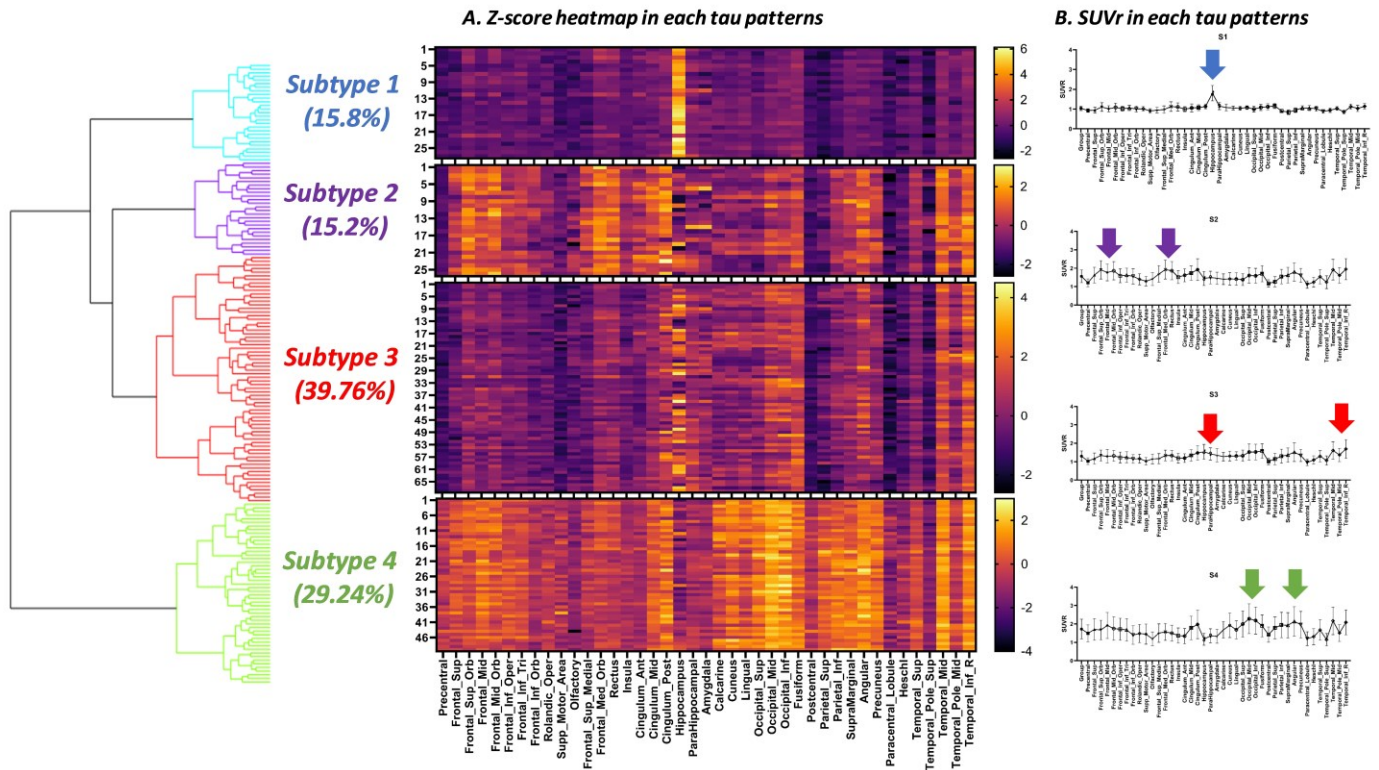


Figure 1. Four ^{18}F -Florzolotau tau PET distribution patterns derived from the agglomerative hierarchical clustering. Figure 1A displayed z-score heatmaps in 4 tau distribution patterns. SUVr in VOIs of each patterns were shown in Figure 1B. Arrows refer to the main tau accumulation regions in 4 distinct tau patterns.

Keywords: Alzheimer's disease, 18F-Florzolotau, tau distribution, machine learning

P105 The interplay of vascular disease, peripheral interleukin-6, beta-amyloid, and memory in older adults

Batool Rizvi¹, Jenna Adams¹, Mithra Sathishkumar¹, Soyun Kim¹, Myra Larson¹, Liv McMillan¹, Adam Brickman², Mark Mapstone¹, Elizabeth Thomas¹, Dana Greenia¹, Maria Corrada¹, Claudia Kawas¹, Michael Yassa¹

¹University of California, Irvine, Irvine, CA, US

²Columbia University, New York, NY, US

White matter hyperintensities (WMH) are a marker of small vessel cerebrovascular disease and are known to promote memory impairment in older adults. Neuroinflammatory processes, which can be assessed by cytokines such as interleukin-6 (IL-6), have been implicated in memory, vascular disease, and amyloid- β (A β) burden. Here, we tested whether WMH in the posterior cerebral artery (PCA), which perfuses posterior and medial temporal regions, are associated with IL-6 independently of A β status. Furthermore, we investigated whether these markers would be related to specific memory domains.

147 older adults (mean 75.54 \pm 10.25 years, 62.6% female) were included. PCA WMH volumes were derived from T2-FLAIR images using ANTs. A β was assessed with 18F-florbetapir-PET and A β status was determined using a threshold of global SUVR > 1.11. IL-6 was measured in plasma using immunofluorescence. Participants completed object (MDT-O), spatial (MDT-S), and temporal (MDT-T) versions of a mnemonic discrimination task. Using linear regressions, we tested for associations between PCA WMH, IL-6, A β , and MDT scores. All models adjusted for age and sex; education was included in models assessing MDT.

IL-6 was positively associated with PCA WMH (b=27.8, p=0.019), while negatively associated with FBP mean SUVR (b=-0.529, p=0.005). When A β status was included in the model, IL-6 was associated with PCA WMH independently of A β status (b=33.6, p=0.008). A β status did not moderate the association of IL-6 with PCA WMH (b=-16.8, p=0.616). PCA WMH were related to MDT-S (b=-0.003, p=0.021), and MDT-O (b=-0.003, p=0.018). FBP mean SUVR was related to only MDT-T (b=-0.189, p=0.018). IL-6 was not related to MDT performance.

We found that IL-6 levels were related to PCA-defined WMH independently of amyloid status. This suggests that inflammation is directly associated with cerebrovascular disease and this association is not impacted by amyloid burden. Future work should understand the roles processes including tau and neurodegeneration in this pathway mediating memory impairment.

Keywords: white matter hyperintensities, memory, inflammation, amyloid, vascular disease

P106 Gut microbiome composition is associated with cortical amyloid burden in a preclinical human cohort

Margo Heston^{1,2}, Antonio González³, Tobey Betthausen^{1,2}, Sterling Johnson^{1,2,4}, Sanjay Asthana^{1,2}, Rob Knight^{3,5,6,7}, Rima Kaddurah-Daouk^{8,9,10,11}, Federico Rey¹², Barbara Bendlin^{1,2,4}

¹Wisconsin Alzheimer's Disease Research Center, Madison, WI, US

²Division of Geriatrics, Department of Medicine, University of Wisconsin School of Medicine and Public Health, Madison, WI, US

³Department of Pediatrics, University of California, San Diego, La Jolla, CA, US

⁴Wisconsin Alzheimer's Institute, Madison, WI, US

⁵Center for Microbiome Innovation, University of California, San Diego, La Jolla, CA, US

⁶Department of Bioengineering, University of California, San Diego, La Jolla, CA, US

⁷Department of Computer Science & Engineering, University of California, San Diego, La Jolla, CA, US

⁸Department of Psychiatry and Behavioral Sciences, Duke University, Durham, NC, US

⁹Department of Medicine, Duke University, Durham, NC, US

¹⁰Duke Institute of Brain Sciences, Duke University, Durham, NC, US

¹¹Duke University Medical Center, Durham, NC, US

¹²Department of Bacteriology, University of Wisconsin-Madison, Madison, WI, US

Background: Altered gut microbiome composition is present in Alzheimer's disease (AD) dementia, and we have identified microbial associations with cerebrospinal fluid biomarkers of amyloid and tau before cognitive impairment. These findings and studies in germ-free mice suggest a possible role for the microbiome early in AD, however the links between intestinal microbes and AD pathology remain poorly characterized in humans. Here we tested whether the gut microbiome is related to cortical amyloid burden by evaluating bacterial species-level relationships with respect to global [C-11]PiB (DVR 0-70 minute dynamic scan) in a cognitively unimpaired human cohort.

Methods: 112 cognitively unimpaired participants (Table 1) completed [C-11]PiB PET and fecal sample collection. Amyloid burden was indexed as an average of eight bilateral cortical regions, and the v4 region of microbial 16S rRNA was sequenced to assess composition in previously frozen stool. Differentials, or log-fold changes in microbial relative abundance, were calculated using multinomial regression (*songbird*) and ranked across a global [C-11]PiB DVR gradient, controlling for age, sex, *APOE* risk score, and Bristol Stool Scale score.

Results: Species in the phylum *Actinobacteria* were associated with higher amyloid burden, while species in the phylum *Bacteroidetes* were associated with lower amyloid burden. These results and additional associations are shown in Fig. 1. Furthermore, several *Firmicutes* species were positively associated with amyloid. Species from the family *Ruminococcaceae* were associated with both higher and lower amyloid.

Conclusions: In a preclinical cohort, we established microbial variability associated with amyloid burden indexed via global [C-11]PiB DVR, and yielded species-level insight to prior correlations identified across the AD continuum. Future work will use metagenomic analysis to investigate the highly ranked *Clostridiales* species (Fig. 2), and will use amyloid chronicity to determine whether microbiome composition is associated with projected age of amyloid positivity onset.

Table 1. Cognitively unimpaired participant characteristics

Characteristic	N = 124 ¹
Age (years)	66.76 (6.15)
Sex	
Female	81 (65%)
Male	43 (35%)
APOE	
E2-E2	0 (0%)
E2-E3	12 (9.8%)
E2-E4	1 (0.8%)
E3-E3	67 (54%)
E3-E4	38 (31%)
E4-E4	5 (4.1%)
Unknown	1
BMI	28.44 (5.70)
Amyloid positive	23 (19%)
Age difference: fecal collection and PiB scan (years)	-0.29 (1.50)

¹n (%); Mean (SD)

Figure 1. Species ranks for *Actinobacteria* and *Bacteroidetes* phyla across [C-11]PiB DVR. As discussed in Morton et al. Nat Comm 2019, the y-axis is the log-fold change known up to some bias constant *K*.

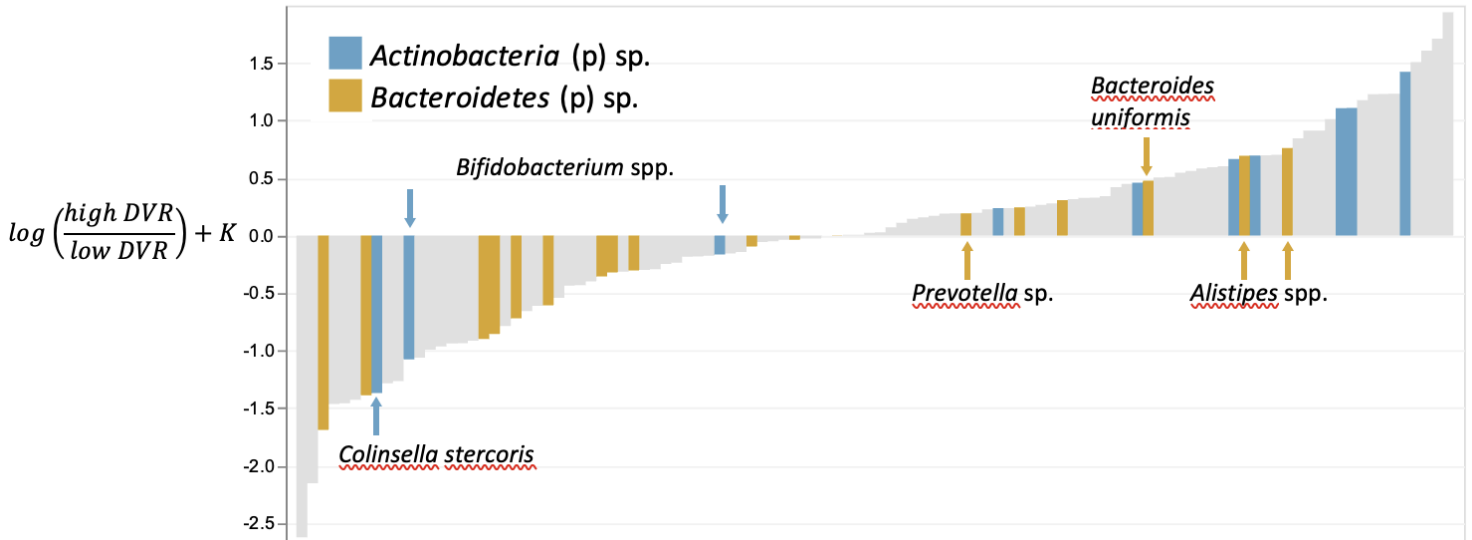
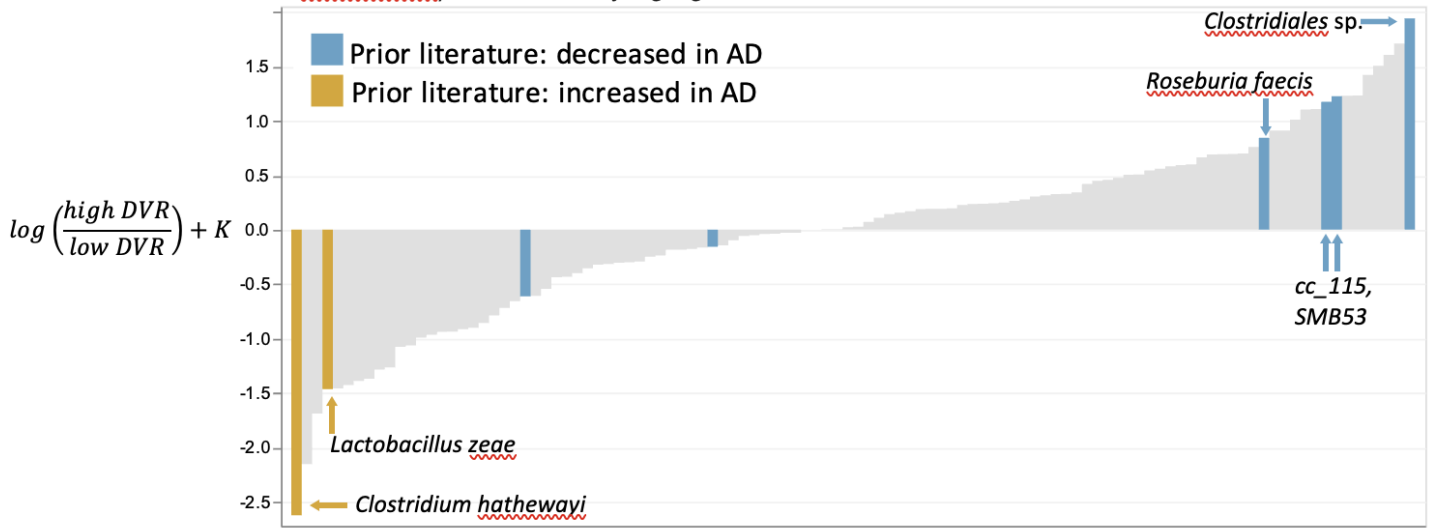


Figure 2. Species ranks for phylum *Firmicutes* across [C-11]PiB DVR. Highlighted species exhibit trends that contradict prior findings across the AD continuum (e.g., *Roseburia* relative abundance was reported as lower in AD, but here is associated with higher amyloid burden). Highest and lowest ranked species (members of order *Clostridiales*) are additionally highlighted.



Keywords: gut microbiome, global [C-11]PiB DVR, preclinical human cohort, observational study, multinomial regression

P107 Study on MR-free template-based spatial normalization for Tau PET Image Quantitation using 18F-Florzolotau

Zih-Ning Lee¹, Shao-Yi Huang¹, Kun-Ju Lin^{1,2}, Chin-Chang Huang³, Kuo-Lun Huang³, Hsiu-Chuan Wu³, Chiung-Chih Chang⁴, Ing-Tsung Hsiao^{1,2}

¹Medical Imaging & Radiological Sciences and Healthy Aging Research Center, Chang Gung University, Taoyuan, TW

²Molecular Imaging Center and Nuclear Medicine, Chang Gung Memorial Hospital, Taoyuan, TW

³Neurology, Chang Gung Memorial Hospital, Taoyuan, TW

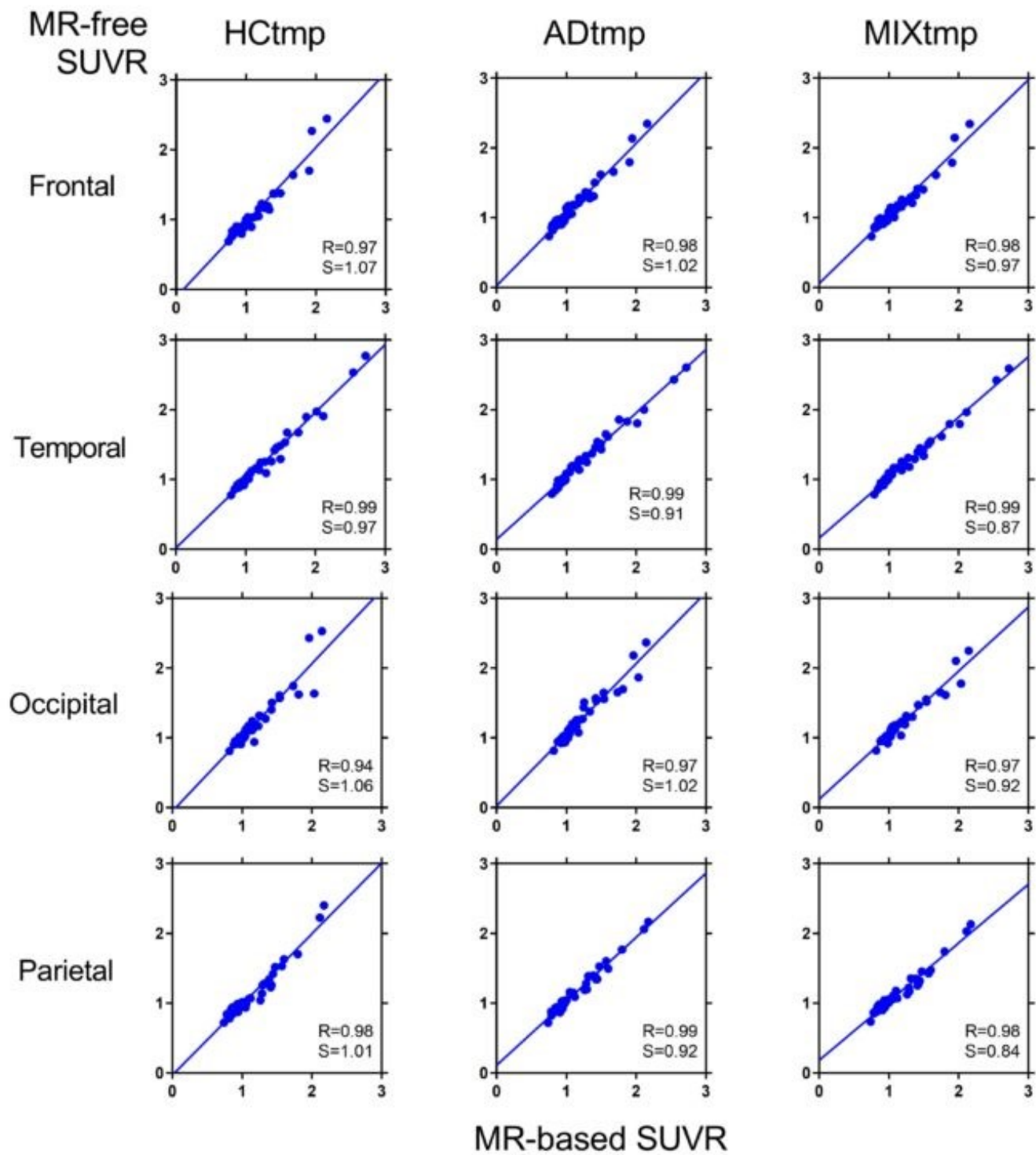
⁴Neurology, Chang Gung Memorial Hospital, Kaohsiung, TW

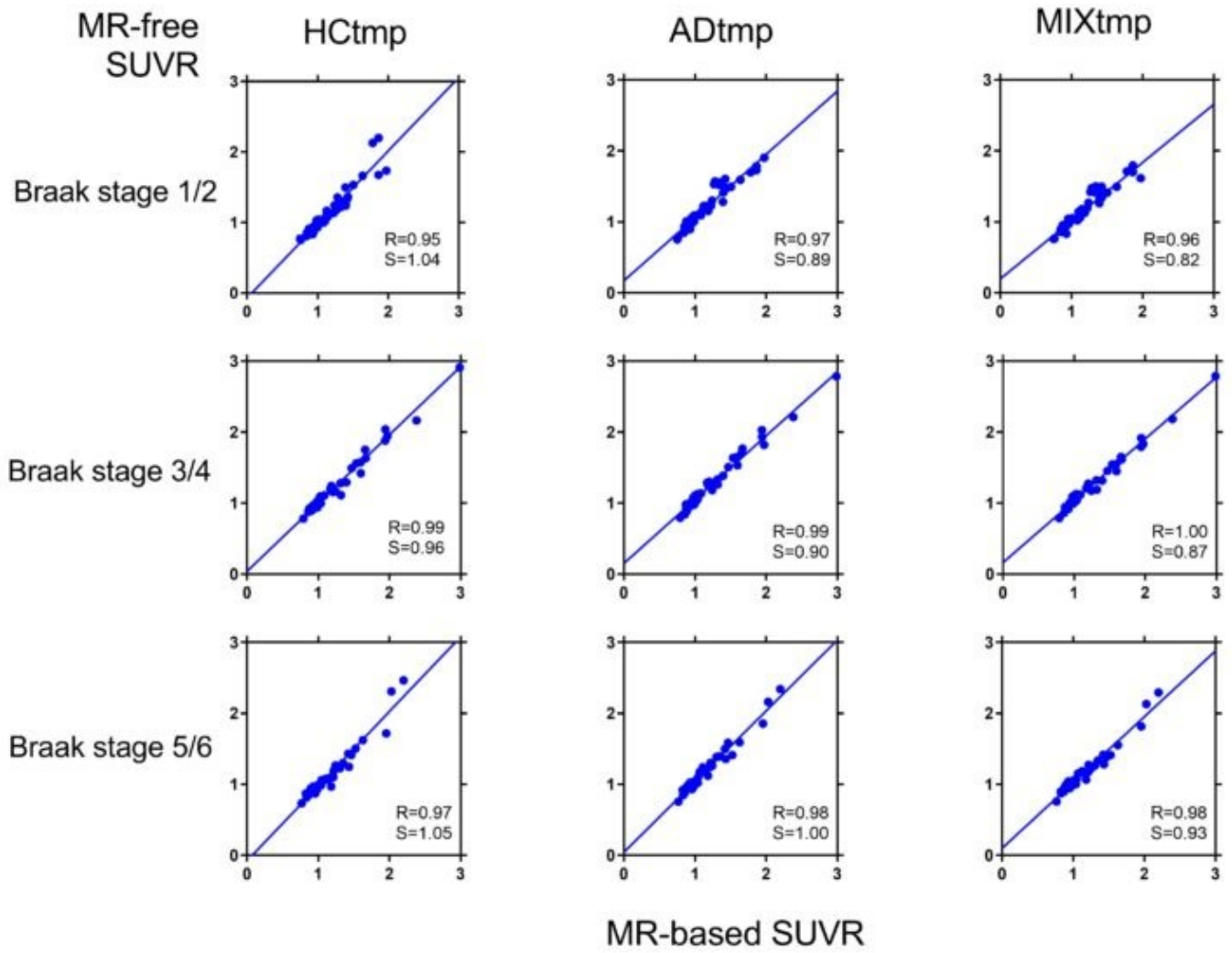
Aim: To construct and study the performance of MR-free templates for the quantitation of 18F-Florzolotau imaging in Alzheimer diseases (AD) patients and normal controls (NC).

Methods: A total of 46 NC and 42 AD subjects with both 18F-Florzolotau PET and MRI scans were further divided into two cohorts for MR-free template construction (22 NC, 22 AD) and validation (24 NC, 20 AD). For the MR-free template construction, three MR-free PET templates were constructed from the NC (NCtmp), AD (ADtmp), and all subjects (mixture of NC and AD) in the first cohort (MIXtmp). All PET images were spatially normalized to MNI space using template-based approach from MR template (MNItmp) and three MR-free PET templates. Regional SUV_r for frontal, temporal, parietal and occipital lobe volumes of interest (VOIs) and Braak-like VOIs were computed using inferior cerebellar cortex as reference region.

Results: In general, the regional SUV_r's for both NC and AD groups generated from each MR-free PET template and those from the MR-based method are highly correlated in the cortical regions ($r=0.94\sim0.99$, Fig.1), and in the Braak VOIs ($r=0.95\sim1.00$, Fig.2). Among all three PET templates, the quantitation from MIXtmp is with the highest correlation for all PET quantitation. For the SUV_r difference as compared to MNItmp, NCtmp generated the least SUV_r difference for NC subjects, while ADtmp for AD subjects. Nevertheless, the SUV_r difference from MIXtmp is between NCtmp and Adtmp for all subjects. Moreover, the slope of the linear regression between PET templates and MR template is slightly lower than 1.0 and that indicates underestimation from PET templates.

Conclusion: Three MR-free PET templates were constructed and studied. Preliminary result indicates their feasibility for tau PET quantitation when MRI is not available. Future study will include more samples to study the reliability of these templates in tau PET quantitation.





Keywords: Tau PET quantitation, MR-free template, ^{18}F -Florzolotau, Alzheimer's disease

P108 β -Amyloid in World Trade Center responders: Result indicate age-related toxic encephalopathy mediated by an immunogenic amyloid response

Sean Clouston¹, Paul Vaska¹, Chuan Huang¹, Minos Kritikos¹, Juin Zhou¹

¹*Stony Brook University, Stony Brook, NY, US*

Background: The objective of the present neuroimaging study was to examine whether symptoms of neurotoxic cognitive impairment (CI) in World Trade Center responders were consistent with cortical β -Amyloid deposition consistent with an immunologic response to neurotoxic infiltrate.

Method: World Trade Center (WTC) responders were eligible for this study if they were aged 44-65, were eligible to complete the neuroimaging protocol. Participants were excluded if they had a history of psychosis, head trauma, or neurological conditions. Cases were matched to controls based on age, race/ethnicity, sex, occupation, education, and history of chronic PTSD. PET/MRI images were acquired simultaneously on a 3T Siemens Biograph 80-120 minutes after intravenous injection of 300 MBq [¹⁸F]-Neuraceq radiotracer. T1-weighted magnetization prepared rapid gradient echo were collected to facilitate signal localization and measure neurodegeneration. Amyloid burden was calculated twice, using the ADRD-Centiloid score, and using mean SUVR in cortical regions previously identified in the WTC signature (SUVR_{WTC}). T-tests compared responders with CI to cognitively unimpaired (CU) responders.

Results: Neuroimaged responders were aged 55.8±5.24 years old, and nine were female. We found no association between CI and Amyloid-Centiloid (P=0.341) but identified elevated SUVR_{WTC} (P=0.039). SUVR_{WTC} was associated with 8/9 cognitive measures (Figure 1) and focal associations emerged between most cognitive measures and amyloid with focal results in the accumbens, isthmus cingulate, and precuneus. Regional volume (%TIV) was associated with amyloid in the amygdala ($r=-0.65$, P<0.001) and isthmus cingulate ($r=-0.37$, P=0.043). WTC exposure duration was associated with increased amyloid in the pars triangularis ($r=0.50$, P=0.003), lateral orbitofrontal ($r=0.43$, P=0.012), and inferior temporal lobe ($r=0.39$, P=0.026). SUVR_{WTC} was associated with elevated SUVR in 21/34 cerebral regions (Figure 1).

Conclusions: Our study identified low-grade amyloidosis in regions of interest with evidence of cortical atrophy in WTC responders. Results may support the presence of immunogenic amyloidosis.

Keywords: World Trade Center, toxic encephalopathy, Amyloid, neuraceq,

P109 [18F]MK-6240 PET/MRI Test-Retest performance in cognitively normal elderly subjects

Cristina Lois^{1,2}, Jessie Fanglu Fu^{2,3}, Andrew Salvatore³, Derek Huell³, David Izquierdo Garcia^{2,3}, Arun Garimella³, Bradford Dickerson^{2,3}, Keith Johnson^{1,2}, Ciprian Catana^{2,3}, Julie Price^{2,3}

¹Gordon Center for Medical Imaging, Massachusetts General Hospital, Boston, MA, US

²Harvard Medical School, Department of Radiology, Boston, MA, US

³Athinoula A. Martinos Center for Biomedical Imaging, Massachusetts General Hospital, Boston, MA, US

Background: Understanding the test-retest variability (T-RT) of quantitative PET measurements is key for the accurate interpretation of results. T-RT of [18F]MK-6240, a tau-PET ligand, has been reported for: **1**) binding potential (BP_{ND}) and standardized-uptake value (SUV) tissue ratio (SUVR) T-RT were 14% and 6%, respectively, in tau-rich regions in an Alzheimer's disease (AD) subject-dominant sample with retest 3-21 days after test [1]; **2**) Longer-term 6-month SUVR T-RT was 2% in the grey matter in cognitively normal (CN) subjects, and no significant differences between 6 month and 2-year extracerebral (EC) uptake [2].

Aim: To assess [18F]MK-6240 T-RT of SUV in potential reference regions; of relative delivery (R1), SUVR, and distribution volume ratios (DVR) in target regions; and of SUVR in EC, in a sample largely consisting of elderly CN (eCN) subjects.

Methods: Thirteen participants (10 eCN, 3 AD; **Table 1**) underwent [18F]MK-6240 PET/MRI (Biograph-mMR), and eight (7eCN, 1 AD) underwent retest PET/MRI within 22±10 days. Brain region segmentations were generated using FreeSurfer. Four reference regions (REF_{ROIS}) were evaluated using SUV_{90-110min}. Four target regions (TARGET_{ROIS}) were evaluated using SUVR_{90-110min}, DVR (MRTM2), and R1. EC was evaluated using R1. Partial volume correction was applied to target region SUVR_{90-110min}. T-RT (%) was estimated as $100 * |(Test-Retest)| / (Test+Retest) / 2$.

Results/Conclusions: SUV₉₀₋₁₁₀ T-RT was similar across REF_{ROIS} (8-10%, **Table 2**). TARGET_{ROIS} SUVR T-RT were 4-6%, and increased to 7-10% when applying PVC. TARGET_{ROIS} DVR T-RT and R1 T-RT were similar to SUVR T-RT. EC SUVR exhibited high T-RT variability (~13%).

Our results are consistent with prior reports and provide further evidence of acceptable T-RT in low-signal eCN subjects. High T-RT in the EC signal should be taken into account, particularly in longitudinal studies, as it may affect TARGET_{ROIS} signal.

[1] Salinas et al. J Cereb Blood Flow Metab. 2020;40(11):2179-2187.

[2] Vanderlinden et al. Eur J Nucl Med Mol Imaging. 2022;49(13):4580-4588.

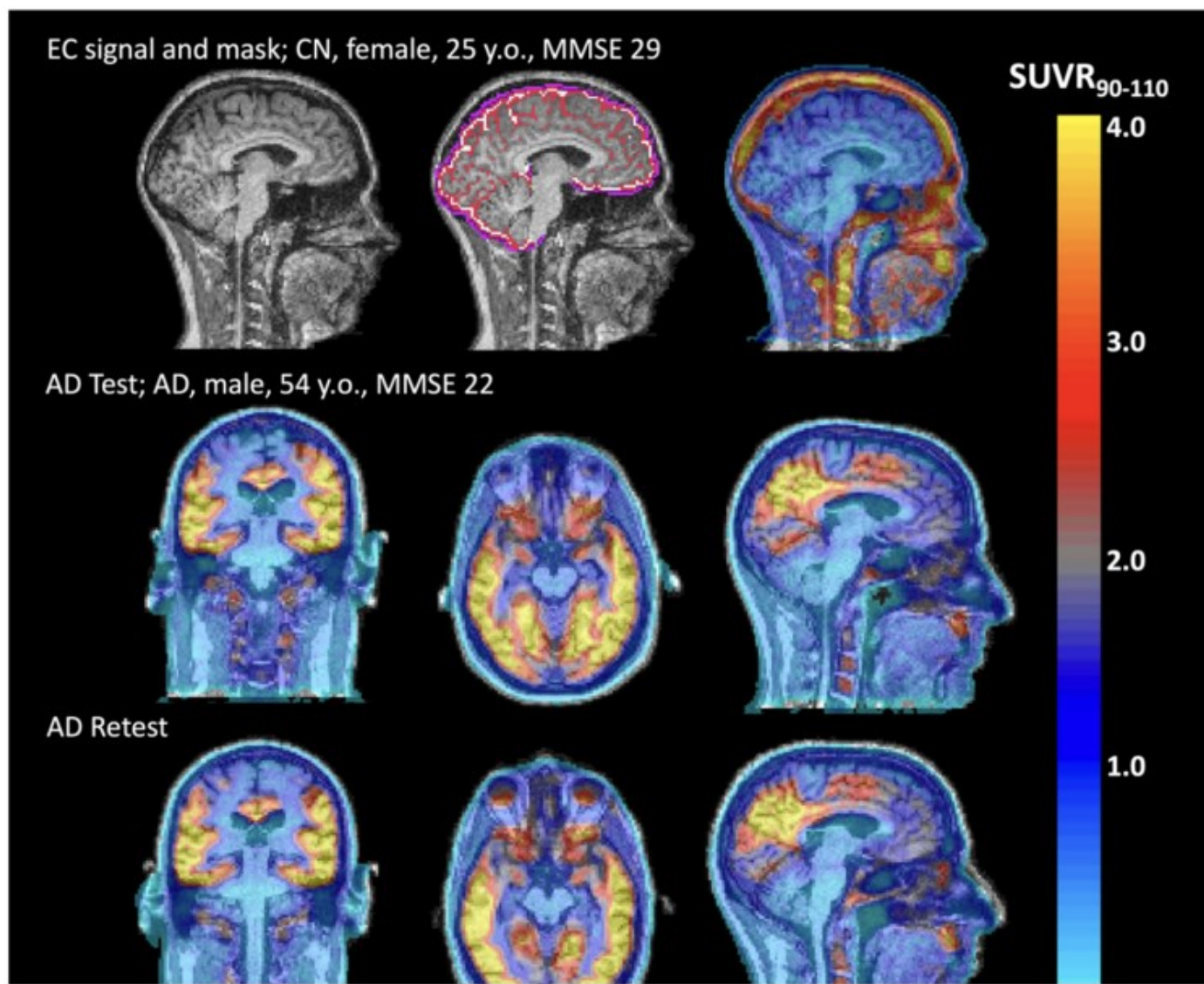
Table 1. Subject Demographics

	eCN	AD	T-RT eCN	T-RT AD
N	10	3	7	1
Age (years)	68±6	58±6	67±8	54
Sex (F/M)	3 / 7	1 / 2	2 / 5	0 / 1
MMSE	29±2	19±2	29±2	22

Table 2: Target region outcome measures (SUVR, SUVR PVC, DVR, R1) and corresponding T-RT variability (%). Reference region SUV T-RT variability shown at the bottom.

<i>REF_{ROI}</i> <u>CerGM</u>	Entorhinal	Hippocampus	Inferior Temporal	Precuneus	EC
SUVR					
<u>eCN</u>	1.1±0.2	0.8±0.1	1.1±0.1	0.9±0.1	1.4±0.6
AD	1.8±0.5	1.0±0.2	2.5±1.0	2.3±1.5	1.3±0.6
SUVR PVC					
<u>eCN</u>	1.2±0.4	0.8±0.2	1.2±0.2	0.8±0.1	n/a
AD	2.2±0.6	1.0±0.2	3.6±1.3	4.4±2.3	n/a
DVR					
<u>eCN</u>	1.0±0.2	0.9±0.1	1.0±0.1	0.9±0.1	n/a
AD	1.7±0.5	1.1±0.2	2.5±1.0	2.7±1.4	n/a
R1					
<u>eCN</u>	0.7±0.1	0.9±0.2	0.9±0.1	1.1±0.1	n/a
AD	0.6±0.04	0.78±0.04	0.63±0.01	0.76±0.04	n/a
SUVR T-RT (%)					
<u>eCN</u>	3.9±4.7	6.3±3.0	5.9±4.5	5.3±3.0	12.1±15.2
SUVR PVC T-RT (%)					
<u>eCN</u>	7.3±5.6	9.3±4.9	9.9±10.3	9.7±6.2	n/a
DVR T-RT (%)					
<u>eCN</u>	5.0±3.1	4.5±3.2	4.8±3.0	3.4±2.5	n/a
R1 T-RT (%)					
<u>eCN</u>	4.8±4.6	6.7±4.3	6.9±3.9	4.2±5.2	n/a
	<u>CerGM</u>	<u>CerGM3mm</u>	<u>WholeCer</u>	<u>WM</u>	
SUV T-RT (%)	8.4±4.4	9.4±3.9	8.6±4.1	9.9±4.5	

Figure 1. [^{18}F]MK-6240 SUVR_{90-110} PET images (CerGM3mm reference) overlaid on simultaneously acquired structural MRI. Top row: Example subject with high EC signal and used EC mask. Middle row: Example AD subject baseline PET. Bottom row: Same AD subject Retest PET.



Keywords: [^{18}F]MK-6240, tau, PET imaging, Test-Retest, Extracerebral signal

Friday, January 13, 2023 - 11:30 am - 01:50 pm

Podium Session

SESSION X: Fluid biomarkers in AD

CHAIRS: Donna Wilcock, Henrik Zetterberg, Henrik Zetterberg

Friday, January 13, 2023		
11:30 am – 1:50 pm	SESSION X: FLUID BIOMARKERS IN AD	CHAIRS: Henrik Zetterberg, MD, PhD, <i>University of Gothenburg</i> Donna Wilcox, PhD, <i>University of Kentucky College of Medicine</i>
11:30	Introduction	Chairs
11:35	Plasma p-tau217 ratios associated with amyloid and tau PET measures in preclinical AD: Findings from the AHEAD 3-45 Study screening data	Reisa Sperling, MD, <i>MGH/Harvard Medical School</i>
11:50	Plasma biomarkers as stand-alone tests to rule out Alzheimer's disease	Joseph Therriault, PhD, <i>McGill University</i>
12:05	Comparative performance of three plasma A β 42/A β 40 and two plasma p-tau181 assays versus amyloid-PET imaging status	Alicia Algeciras-Schimnich, PhD, <i>Mayo Clinic, Rochester</i>
12:20	Prognostic utility of plasma p217+tau vs amyloid and tau PET in the Alzheimer continuum	Azadeh Feizpour, PhD, <i>Austin Health</i>
12:35	Associations of blood biomarkers with early-onset Alzheimer's disease pathology	Paige Logan, PhD, <i>Indiana University School of Medicine</i>
12:50	Associations between amyloid PET, CSF pTau, and plasma biomarkers in memory clinic patients	Marina Bluma, PhD, <i>Karolinska University</i>
1:05	Discussion	

Plasma p-tau217 ratios associated with amyloid and tau PET measures in preclinical AD: Findings from the AHEAD 3-45 Study screening data

Reisa Sperling^{1,5}, Oliver Langford^{2,5}, Robert Rissman^{2,5}, Aaron Schultz^{1,5}, Emma Thibault¹, Michael Donohue^{2,5}, Rema Raman^{2,5}, Sara Abdel-Latif^{2,5}, Matthew Meyer³, Kristopher Kirmess³, Joel Braunstein³, Michael Irizzary⁴, Jin Zhou⁴, Chad Swanson⁴, Paul Aisen^{2,5}, Keith Johnson^{1,5}, Team AHEAD 3-45 Study⁵

¹Mass General Brigham, Harvard Medical School, Boston, MA, US

²Alzheimer Therapeutic Research Institute, University of Southern California, San Diego, CA, US

³C2N Diagnostics, St. Louis, MO, US

⁴Eisai and Co., Nutley, NJ, US

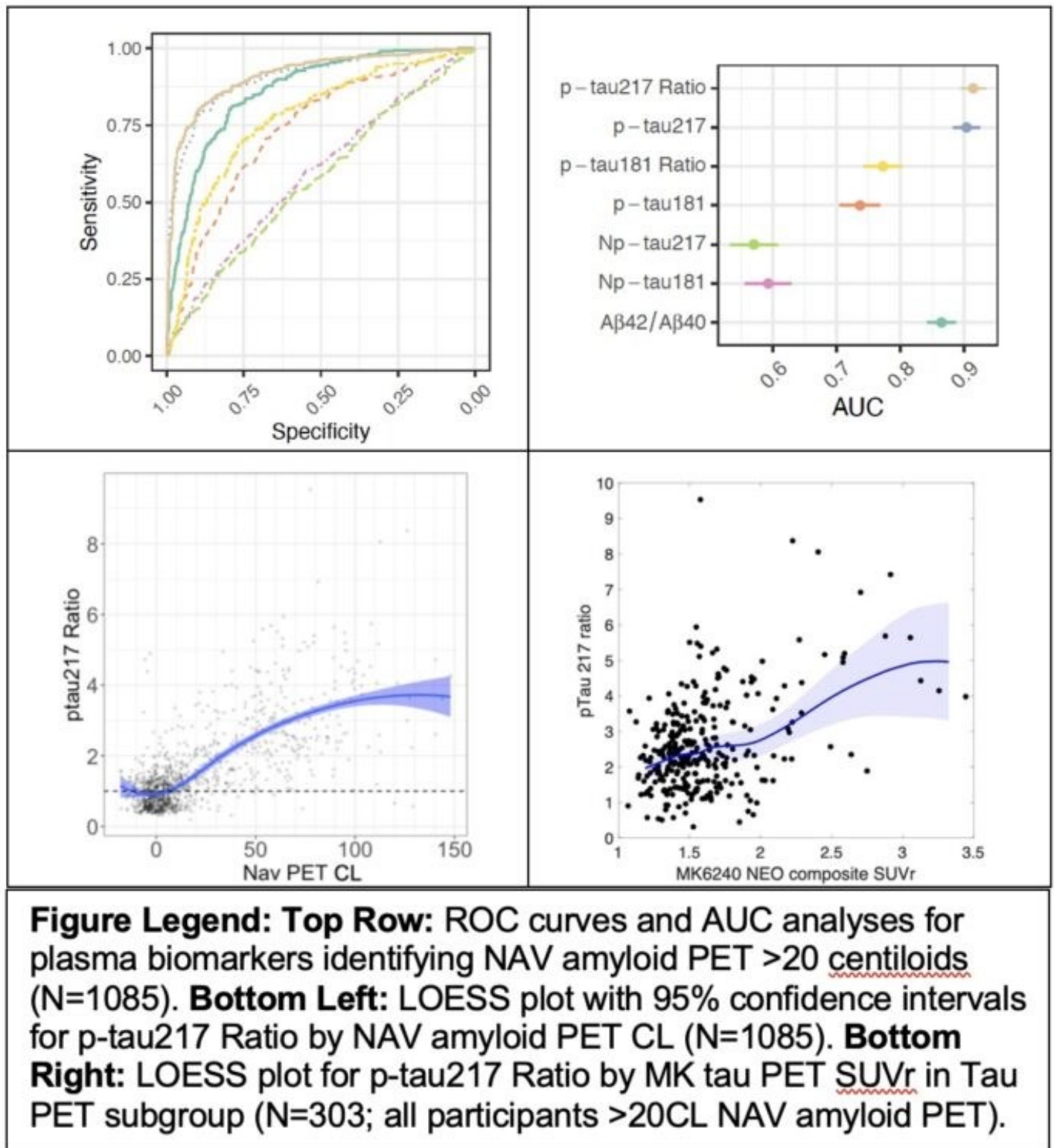
⁵Alzheimer's Clinical Trial Consortium, San Diego, CA, US

Background: The AHEAD 3-45 Study recently implemented screening plasma biomarkers to evaluate the association with amyloid and tau PET measures in preclinical AD.

Methods: Cognitively unimpaired participants (N=1085; age 55-80) screening for AHEAD underwent cognitive testing (PACC-5), plasma collection and 18F-NAV4694 amyloid PET. A subset of amyloid eligible participants (>20centiloids (CL) on NAV) underwent 18F-MK6240 tau PET (N=303). Plasma amyloid (A β 42/40) and ratios of phosphorylated and non-phosphorylated forms of tau181 (p-tau181r) and tau217 (p-tau217r) were quantified by C₂N Diagnostics using mass spectrometry. NAV PET CL were quantified in a cortical composite template by InVivo. Individual FreeSurfer anatomic regions of interest were used to define two tau PET composites: medial temporal allocortex (MTL) and inferolateral temporal/parietal neocortex (NEO). We conducted ROC analyses for plasma biomarkers against amyloid status defined by NAV PET>20CL and regression analyses for continuous variables to investigate the relationship among plasma, PET and cognition.

Results: The AUCs for identifying NAV >20CL for plasma A β 42/40=0.87 (95% CI; 0.84, 0.89); p-tau181r=0.74 (95% CI; 0.71, 0.77); and p-tau217r=0.91(95% CI; 0.90, 0.93). When examining relationships across the full range of amyloid, p-tau217r began to increase at approximately 11CL (see Figure). P-tau217r correlated with tau PET SUVR in both MTL (R=0.35;p<0.0001) and NEO (R=0.43;p<0.0001) composites. NEO tau PET composite was associated with screening PACC-5 (β =-0.18;p=0.0006); no association with cognition was observed with NAV CL, MTL tau PET, p-tau181r, or p-tau217r in the >20CL subset.

Conclusions: Our findings suggest p-tau217r can accurately identify amyloid status and begins to rise prior to 20CL on amyloid PET. P-tau217r is also associated with tau PET, although further work is needed across the full continuum to define cutpoints for specific trial eligibility. Neocortical tau PET was associated with screening cognition even within the restricted range of preclinical AD and may prove useful for tracking very early cognitive decline.



Keywords: plasma, amyloid PET, tau PET, preclinical AD, clinical trial

Plasma biomarkers as stand-alone tests to rule out Alzheimer's disease

Joseph Therriault², Andrea Lessa Benedet², Nicholas Ashton², Thomas Karikari³, Armand Gonzalez³, Marta Mila-Aloma³, Marc Suarez-Calvet², Henrik Zetterberg², Kaj Blennow¹, Pedro Rosa-Neto

¹*McGill University, Montreal, QC, Canada*

²*University of Gothenburg, Gothenburg, Sweden*

³*Barcelona Beta Centre, Barcelona, Spain*

Background: Blood-based biomarkers promise to revolutionize the diagnosis of Alzheimer's disease (AD). However, their interpretation at the individual-level and the situations requiring confirmatory testing with CSF or PET are poorly understood.

Methods: We assessed the screening capability of plasma biomarkers for AD in observational cohorts consisting of cognitively unimpaired individuals, individuals with mild cognitive impairment (MCI), AD or other neurodegenerative diseases. Abnormality for plasma biomarkers was predefined based on externally-validated thresholds from independent cohorts. We calculated predictive values of individual plasma biomarkers for amyloid-beta positivity and for biologically-defined AD, with PET, CSF or neuropathology used as reference standards. We furthermore evaluated whether the combination of plasma biomarkers resulted in higher predictive value for AD.

Findings: Data were collected from 2202 individuals from observational research studies, memory clinics and multicentre studies. Due to high false positive rates, the positive predictive values of plasma biomarkers for AD were below 60% for all biomarkers in all settings. In the TRIAD, ALFA+ and memory clinic cohorts, plasma p-tau217 had a negative predictive value above 97% (95%CI: 96%-100%) (Figure1). Combining plasma biomarkers together did not result in better negative predictive values for biological AD. In ADNI, where only p-tau181 was available, negative predictive values for biological AD exceeded 94% (Figure2).

Interpretation: Because of the low positive predictive value of blood biomarkers and high false positive rate, CSF or PET will be needed for individuals who are plasma biomarker positive to determine the presence of AD. However, blood biomarkers are highly useful for identifying individuals without AD. Plasma p-tau217 in particular may provide sufficient negative predictive value to be used as a stand-alone test to rule out AD in the differential diagnosis of cognitive impairment.

Baseline mean \pm SD SUVR-CC

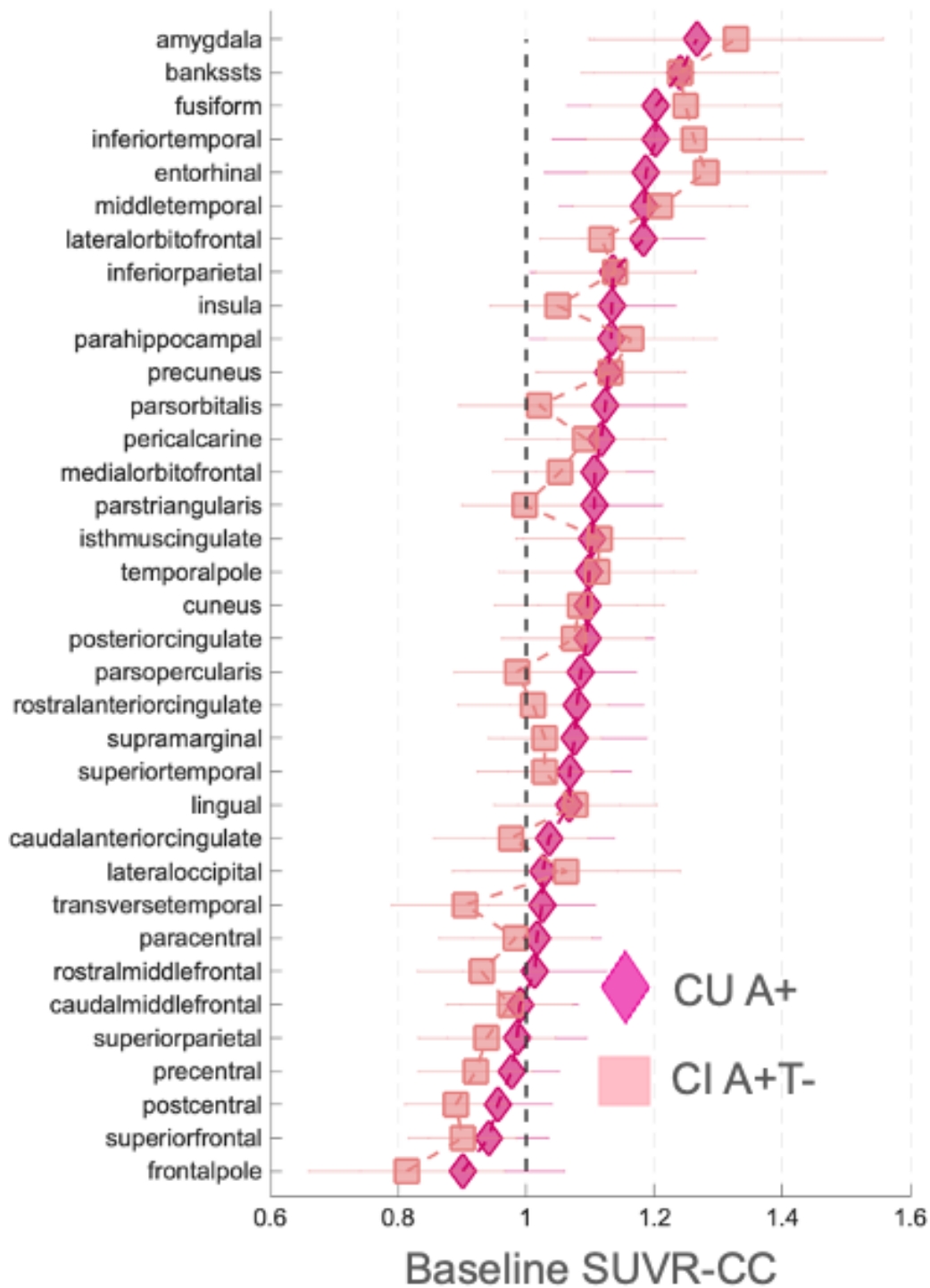


Figure 1. Waterfall plot showing the baseline regional tau profiles of CU A+ and CI A+/T- studies.

Figure1:

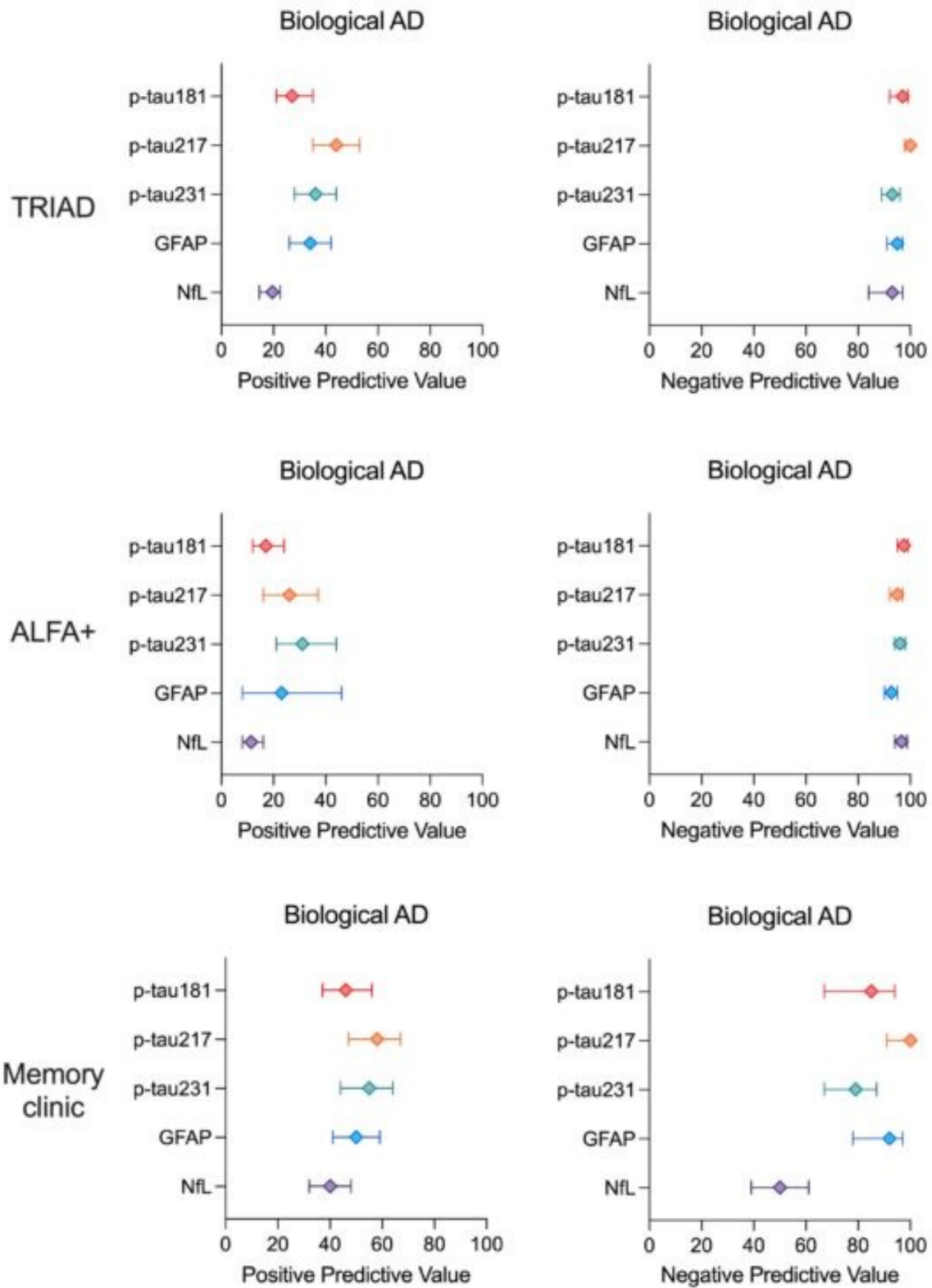


Figure2:

Annual rate of LS mean change \pm SE for CU A+ and CI A+/T-

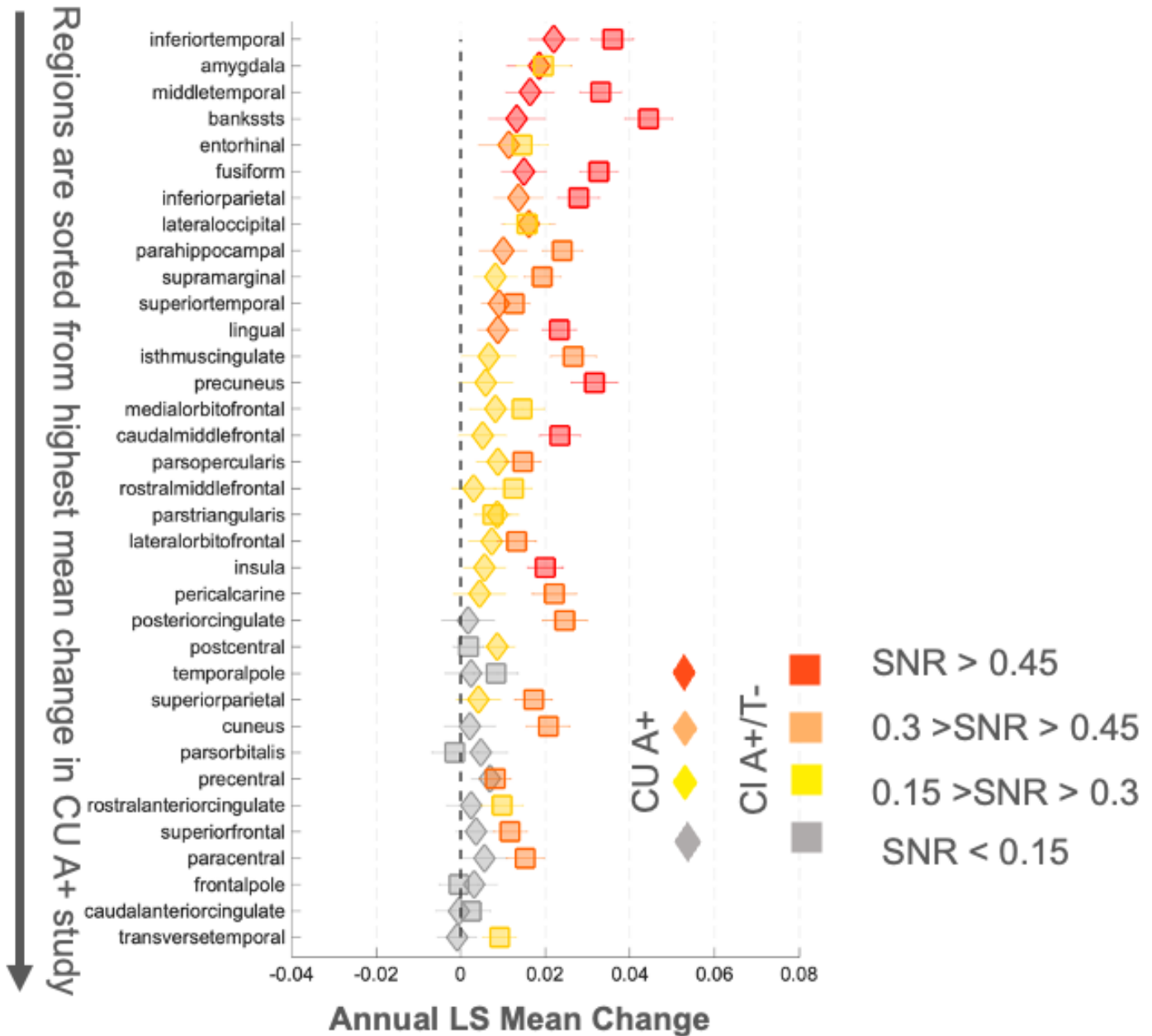
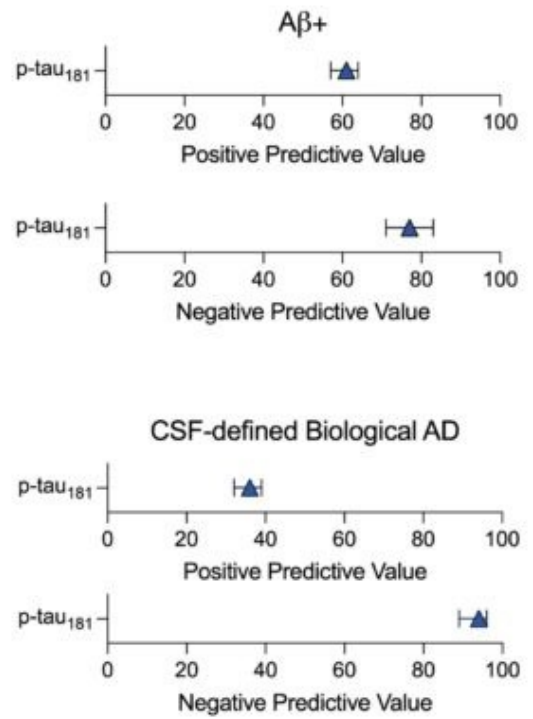
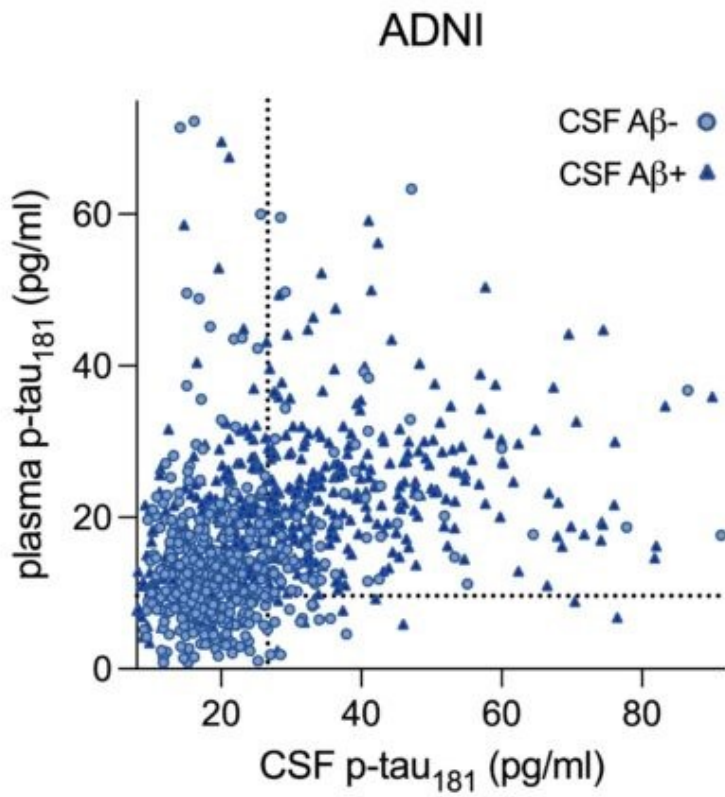


Figure 2. Waterfall plot showing the annual LS mean change \pm SE regional tau profiles of CU A+ and CI A+/T- studies.



Keywords: Plasma, p-tau, diagnosis, amyloid-beta, tau

Comparative performance of three plasma A β 42/A β 40 and two plasma p-tau181 assays versus amyloid-PET imaging status

Daniel Figdore¹, Joshua Bornhorst¹, Jeremy Syrjanen¹, Jonathan Graff-Radford¹, David Knopman¹, Prashanthi Vemuri¹, Randall Bateman², Clifford Jack Jr¹, Ronald Petersen¹, Alicia Algeciras-Schimmich¹

¹Mayo Clinic, Rochester, MN, US

²Washington University School of Medicine, St. Louis, MO, US

Background: Alzheimer's disease (AD) blood-based markers (BBMs) may revolutionize the detection of brain amyloid pathology irrespective of the clinical stage of the disease. The clinical robustness of assay for BBMs for the detection of amyloid pathology is presently an area of intense study. This study describes a comparative evaluation of three A β 42/A β 40 and two p-tau181 assays versus amyloid-PET imaging.

Methods: Participants with a cognitive unimpaired (CU) (n=112) or MCI/AD dementia (n=34) diagnosis were from the Mayo Clinic Study of Aging. Plasma A β 42/A β 40 concentrations were measured by two immunoassays (Fujirebio Lumipulse and Quanterix Simoa) and a mass spectrometry (MS) assay (Washington University). Additionally, plasma pTau181 concentrations were measured using Fujirebio and Quanterix immunoassays. Amyloid-PET imaging was performed with Pittsburg Compound B, and a SUVR cutoff of 1.48 was used for positive (n=69) or negative (n=77) classification.

Results: The strongest correlation of A β 42/A β 40 with amyloid-PET SUVR was observed with the A β 42/A β 40 MS (Spearman's correlation (ρ) = -0.61, $P < .0001$) followed by the Fujirebio A β 42/A β 40 (ρ = -0.55, $P < .0001$); Quanterix A β 42/A β 40 showed the weakest correlation (ρ = -0.22, $P = 0.0079$). The MS and Fujirebio A β 42/A β 40 showed the best performance for detection of a positive amyloid-PET with AUCs of 0.84 (95%CI 0.77-0.90) and 0.81 (95%CI 0.75-0.88), respectively, whereas Quanterix A β 42/A β 40 AUC was 0.58 (95%CI 0.49-0.68). Correlations between amyloid-PET SUVR and the two pTau181 immunoassays were essentially identical (Quanterix, ρ = 0.38, $P < .0001$; Fujirebio, ρ = 0.37, $P < .0001$). The pTau181 assays exhibited AUCs of 0.73 (95%CI 0.64-0.81) for Quanterix, and 0.72 (95%CI 0.64-0.80) for Fujirebio.

Conclusion: This is the first comparative description of the performance of the Fujirebio A β 42/A β 40 assay. For identifying the presence of amyloid-PET positivity the Fujirebio and WashU MS A β 42/A β 40 assays showed the best performance, with both pTau181 and Quanterix A β 42/A β 40 immunoassays having lower performance.

Keywords: plasma A β 42/A β 40, plasma pTau181, amyloid-PET

Prognostic utility of plasma p217+tau vs amyloid and tau PET in the Alzheimer continuum

Azadeh Feizpour^{1,5}, Vincent Doré^{1,2}, James D. Doecke³, Ziad S. Saad⁴, Gallen Triana-Baltzer⁴, Natasha Krishnadas^{1,5}, Christopher Fowler⁵, Larry Ward⁵, Ralph N. Martins^{7,8}, Colin L. Masters⁵, Victor L. Villemagne^{1,9}, Jurgen Fripp³, Hartmuth C. Kolb⁴, Christopher C. Rowe^{1,5,6}

¹Department of Molecular Imaging & Therapy, Austin Health, Melbourne, Victoria, Melbourne, AU

²The Australian e-Health Research Centre, CSIRO, Melbourne, Victoria, Melbourne, AU

³The Australian e-Health Research Centre, CSIRO, Brisbane, Queensland, Brisbane, AU

⁴Neuroscience Biomarkers, Janssen Research and Development, La Jolla, La Jolla, CA, US

⁵The Florey Institute of Neuroscience and Mental Health, Melbourne, Victoria, Melbourne, AU

⁶Florey Department of Neuroscience and Mental Health, The University of Melbourne, Melbourne, Victoria, Melbourne, AU

⁷Edith Cowan University, Perth, Perth, AU

⁸McCusker Alzheimer's Research Foundation, Nedlands, Perth, Perth, AU

⁹Department of Psychiatry, University of Pittsburgh, Pittsburgh, Pittsburgh, PA, US

Introduction We evaluated the association of plasma p217+tau with longitudinal cognition and its comparative performance to amyloid- β (A β) and tau PET in predicting prospective cognitive decline.

Methods 153 cognitively unimpaired (CU) and 50 cognitively impaired (CI) participants underwent baseline p217+tau SIMOA assay, ¹⁸F-MK6240 tau-PET and ¹⁸F-NAV4694 A β -PET with neuropsychological follow-up (MMSE, CDR-SB, AIBL-PACC) over 2.4 ± 0.8 years. The association of baseline biomarkers with cognitive decline was evaluated. Sample size to detect a 30% slowing in cognitive decline in a 2-year trial and selection cost using p217+tau (pT+) were compared to A β -PET (A+) and tau-PET (T+) with and without p217+tau pre-screening.

Results In the CI, plasma p217+tau predicted change in MMSE ($\beta = -0.55, p < 0.001$) and CDR-SB ($\beta = 0.61, p < .001$) with effect size larger than A β Centiloid (MMSE $\beta = -0.48, p = 0.002$; CDR-SB $\beta = 0.43, p = .004$) but smaller than tau_{MetaT} SUVR (MMSE: $\beta = -0.62, p < .001$; CDR-SB: $\beta = 0.65, p < .001$). In the CU, only tau_{MetaT} SUVR predicted change in AIBL-PACC ($\beta = -0.22, p = 0.008$). Screening CI for pT+ led to 24% reduction in sample size compared to screening with PET for A+ and 6-13% compared to T+ (different regions). This translated to an 80% test cost-saving assuming p217+tau costed one-fifth of PET. In a trial requiring PET T+ or A+, pT+ pre-screening followed by PET would cost more in the CI group with AD prevalence of 70%, compared to 35% cost-saving in the CU group with preclinical AD prevalence of 25%.

Conclusion Substantial cost reduction can be achieved using p217+tau alone to select participants with CI for a trial, compared to selection by PET. Pre-screening with p217+tau followed by PET provides cost-saving in preclinical trials but is questionable in MCI/AD trials.

Keywords: Plasma biomarker, Neuroimaging, Cognitive Decline, Tau PET, Amyloid- β PET

Associations of blood biomarkers with early-onset Alzheimer's disease pathology

Paige E. Logan¹, Jeffery L. Dage¹, Dustin B. Hammers¹, Ani Eloyan², Mohit K. Manchella^{1,3}, Sára Nemes¹, Ralitsa V. Kostadinova¹, Nidhi Mundada⁴, Renaud La Joie⁴, Leonardo Iaccarino^{4,10}, Anne M. Fagan⁶, Tatiana M. Faroud¹, Henrik Zetterberg¹¹, Robert A. Koeppe⁷, Paul S. Aisen⁵, Maria C. Carrillo⁸, Gil D. Rabinovici⁴, Bradford C. Dickerson⁹, Liana G. Apostolova¹

¹Indiana University School of Medicine, Indianapolis, IN, US

²Brown University, Providence, RI, US

³University of Southern Indiana, Evansville, IN, US

⁴University of California, San Francisco, San Francisco, CA, US

⁵Alzheimer's Therapeutic Research Institute, University of Southern California, San Diego, CA, US

⁶Washington University School of Medicine, St. Louis, MO, US

⁷University of Michigan, Ann Arbor, MI, US

⁸Alzheimer's Association, Chicago, IL, US

⁹Massachusetts General Hospital, Harvard Medical School, Boston, MA, US

¹⁰Avid Radiopharmaceuticals, Philadelphia, PA, US

¹¹The Sahlgrenska Academy, University of Gothenburg, Gothenburg, Sweden

Introduction: Increased levels of glial fibrillary acidic protein (GFAP) and neurofilament light (NfL) in plasma have been associated with late-onset Alzheimer's Disease (AD). GFAP and NfL are indicators of astrocytosis and neurodegeneration, respectively. Our goal was to demonstrate the utility of these biomarkers in early-onset AD (EOAD) and investigate their associations with gray matter density (GMD), amyloid and tau burden.

Methods: EOAD participants from the Longitudinal EOAD study (LEADS) with available baseline plasma GFAP and NFL, MRI, amyloid and tau PET data were included (n=183). Voxel-wise multiple linear regression models of T1-weighted MRI, amyloid and tau PET images yielded statistical maps with GFAP or NFL as the predictors, displayed at a family-wise error correction of $p < 0.05$. Covariates were hierarchically added: Model 1: age, sex; Model 2: age, sex and *APOE-ε4*; Model 3: age, sex, *APOE-ε4* and MMSE.

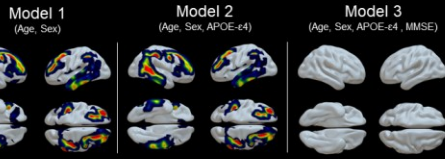
Results: Increasing levels of GFAP were significantly associated with greater GM atrophy in models 1-2, amyloid burden in model 1 only and tau burden in models 1-3. While still significant, the association with tau burden was attenuated in model 3. Once controlled for MMSE, the association with GMD was no longer significant (Figure 1). Increasing levels of NFL were significantly associated with greater GM atrophy in models 1-3, amyloid burden in models 1-2 and tau burden in models 1-3. While still significant, the association with GMD and tau burden was attenuated in model 3 (Figure 2). Additionally, GFAP's effect did not survive when controlled for NfL, but NfL showed a strong effect independent of GFAP.

Conclusion: These results suggest that GFAP and NfL are strongly associated with GM atrophy, tau burden and disease severity in EOAD, but lack strong association with amyloidosis. Further, the association of NfL with EOAD pathology seems independent of GFAP, while the opposite was not true.

Effect of GFAP in EOAD

Gray Matter Density

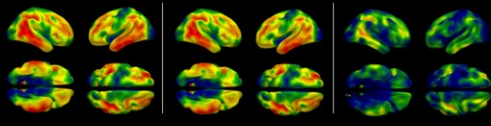
Significance maps



T-Statistic (shown at $p_{FWE} < 0.05$)



β coefficient maps



β coefficients



Amyloid PET

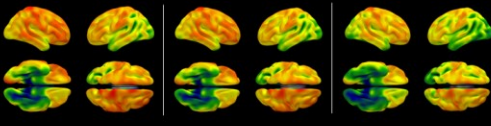
Significance maps



T-Statistic (shown at $p_{FWE} < 0.05$)



β coefficient maps

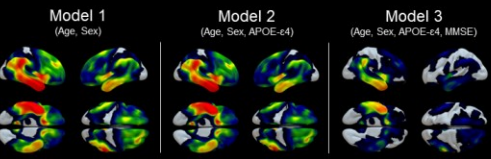


β coefficients



Tau PET

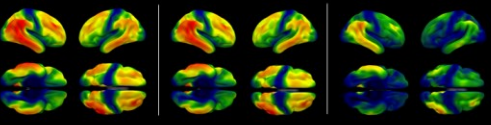
Significance maps



T-Statistic (shown at $p_{FWE} < 0.05$)



β coefficient maps



β coefficients

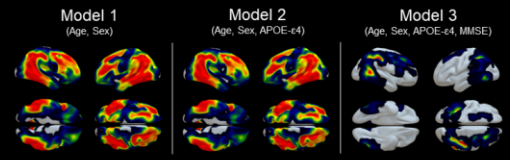


Figure 1. Voxel-wise multiple linear regression statistical maps showing the effect of GFAP on GMD and amyloid and tau PET in EOAD for each model. Significance maps are on the top row and their respective beta coefficient maps are on the bottom row in each panel. Covariates for each model are listed in parenthesis. All GMD models were also controlled for ICV. FWE cluster-corrected images shown were rendered in Surf-ice. ICV: intracranial volume; FWE: family-wise error.

Effect of NfL in EOAD

Gray Matter Density

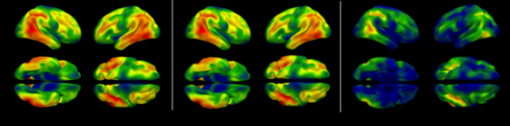
Significance maps



T-Statistic (shown at $p_{FWE} < 0.05$)



β coefficient maps

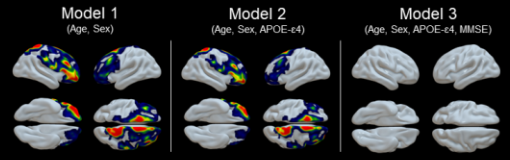


β coefficients



Amyloid PET

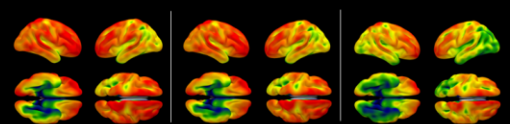
Significance maps



T-Statistic (shown at $p_{FWE} < 0.05$)



β coefficient maps

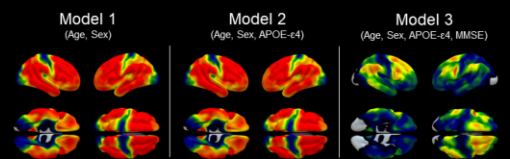


β coefficients



Tau PET

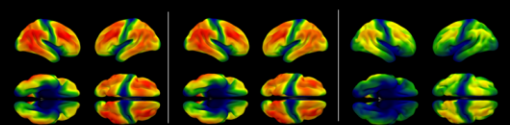
Significance maps



T-Statistic (shown at $p_{FWE} < 0.05$)



β coefficient maps



β coefficients



Figure 2. Voxel-wise multiple linear regression statistical maps showing the effect of NfL on GMD and amyloid and tau PET in EOAD for each model. Significance maps are on the top row and their respective beta coefficient maps are on the bottom row in each panel. Covariates for each model are listed in parenthesis. All GMD models were also controlled for ICV. FWE cluster-corrected images shown were rendered in Surf-ice. ICV: intracranial volume; FWE: family-wise error.

Keywords: early-onset, GFAP, NfL, Amyloid-PET, Tau-PET

Associations between amyloid PET, CSF pTau, and plasma biomarkers in memory clinic patients

Marina Bluma¹, Marco Bucci^{1,2}, Nicholas J. Ashton³, Irina Savicheva⁴, Anna Sandebring-Matton¹, Guglielmo Di Molfetta³, Josef Panec³, Kaj Blennow³, Henrik Zetterberg³, Agneta Nordberg^{1,2}

¹Department of Neurobiology, Care Sciences and Society, Division of Clinical Geriatrics, Center for Alzheimer Research, Karolinska University, Stockholm, Sweden

²Theme Inflammation and Aging, Karolinska University Hospital, Stockholm, Sweden

³Department of Psychiatry and Neurochemistry, Institute of Neuroscience and Physiology, Sahlgrenska Academy, University of Gothenburg, Mölndal, Sweden

⁴Medical Radiation Physics and Nuclear Medicine, Karolinska University, Stockholm, Sweden

Background: Earlier studies have yielded contradictory findings in respect to association of plasma biomarkers with tau and amyloid pathology. With this study we aim to examine relationship between amyloid PET and CSF pTau with plasma biomarkers in a cohort of tertiary clinic patients.

Methods: Plasma GFAP, pTau181, pTau231, A β 42/A β 40, and NFL and CSF pTau181 were measured in 126 patients (age=65 \pm 8 (mean \pm SD), 70F/56M, MMSE=25.5 \pm 3), admitted to the Memory Clinic, Theme Inflammation and Aging, Karolinska University Hospital, Stockholm in Sweden, and referred to [¹⁸F]flutemetamol amyloid PET after extensive clinical assessment. PET images were preprocessed with the rPOP pipeline for PET-only datasets. Plasma A β 42, A β 40, NfL, GFAP were measured using N4PE assay, whereas pTau181 and pTau231 with in-house assays. To assess the relationship between the biomarkers we run multiple linear regression and dominance analysis to compare the relative importance of the predictors.

Results: We found significant association of plasma GFAP ($p < 0.01$) and pTau231 ($p < 0.05$), but not of plasma NFL, pTau181, and A β 42/A β 40 ($p > 0.05$) with [¹⁸F]flutemetamol uptake (after controlling for sex, age, and CSF pTau). Plasma pTau231 was also significantly associated with CSF pTau ($p < 0.05$). Dominance analysis has shown that the relative importance of the variables (i.e., amyloid PET, demographics (sex, age), and CSF pTau181) for prediction of GFAP values followed the order: amyloid > demographics (age + sex) > CSF pTau; whereas for pTau231 it was: CSF pTau > amyloid > demographics.

Conclusion: In a clinical cohort of patients, we found differing associations between plasma GFAP and pTau231 with amyloid PET and CSF pTau, but not to other plasma biomarkers. Amyloid burden contributed most in explaining variance in GFAP, but not in pTau231, where contribution of CSF pTau was higher. These results suggest GFAP as a potential marker pathological processes associated with amyloid pathology, whereas in pTau231 -to both amyloid and tau pathology.

Keywords: plasma, GFAP, amyloid PET, pTau231

Friday, January 13, 2023 - 02:30 pm - 03:15 pm

KEYNOTE: Biofluids and imaging: two sides of the same coin

Thomas Karikari

University of Pittsburgh

Recent advances in plasma biomarkers are improving the simplicity, accessibility and cost-effectiveness of assessing biological evidence of Alzheimer's disease (AD) and related dementias. These biomarkers have shown good agreements with their neuroimaging alternatives. In fact, imaging markers remain the methods of choice to validate new plasma biomarkers. However, plasma biomarkers only have good (but not strong) concordances with their neuroimaging counterparts. For example, plasma phosphorylated-tau (p-tau) have stronger correlations with amyloid beta (Ab) positron emission tomography (PET) than tau-PET, despite both p-tau and tau-PET designated as tau (T) markers in the AT(N) framework.

In this keynote, I will discuss new evidence that explains this anomalous observation. I will also describe a novel biofluid biomarker of soluble tau aggregation that correlates stronger with tau PET signal and neurofibrillary tangle load at autopsy, and thus could be a better surrogate marker of tau aggregation when compared with p-tau. Furthermore, I will present biochemical evidence to explain why some plasma p-tau biomarkers (e.g., p-tau181, p-tau217 and p-tau231) have stronger associations between themselves and with Ab pathology compared with other p-tau epitopes (including p-tau396).

Other aspects of the talk will focus on novel plasma p-tau biomarkers. For example, plasma p-tau212 is an AD-specific biomarker whose performances often parallel those of plasma p-tau217. Additionally, clinical and biological validation of a new non-phosphorylated tau assay (referred to as brain-derived tau [BD-tau]) that outperforms plasma neurofilament light and total-tau as an AD-specific neurodegeneration biomarker with potential to complete the AT(N) framework will be discussed.

In summary, plasma and neuroimaging markers are complementary tools for the early detection and continuous monitoring of AD.

Friday, January 13, 2023 - 04:15 pm - 05:05 pm

Podium Session

SESSION XI: Plasma with other modalities

Friday, January 13, 2023		
4:15 pm – 5:05 pm	SESSION XI: PLASMA WITH OTHER MODALITIES	CHAIR: Thomas Karikari, PhD, <i>University of Pittsburgh</i> Suzanne Schindler, MD, PhD, <i>Washington University</i>
4:15	Introduction	Chairs
4:20	Plasma biomarkers associated with cortical brain structure and multi-domain cognition in Alzheimer's disease and Parkinson's disease	Gillian Coughlan, PhD, <i>Massachusetts General Hospital</i>
4:35	Relationships of blood insulin with brain structures and plasma A β 42 to A β 40 ratio in a multi-ethnic cohort of older adults	Brandon Hall, MSc, <i>University of Southern California</i>
4:50	Unique biological pathways associated with plasma ptau species and AD PET: an imaging-transcriptomic study	Min Su Kang, PhD, <i>Sunnybrook Research Institute</i>
5:05	Discussion	

Plasma biomarkers associated with cortical brain structure and multi-domain cognition in Alzheimer's disease and Parkinson's disease

Gillian Coughlan¹, Peter Zhukovsky², Erlan Sanchez³, Sandra Black³, Doug Munoz³, Rachel Buckley¹, Mario Masellis³

¹Massachusetts General Hospital/Harvard Medical School, Boston, MA, US

²The Centre for Addiction and Mental Health, Toronto, CA

³Sunnybrook Health Sciences, Toronto, CA

Introduction: Plasma biomarkers of phosphorylated-tau(p-tau), astrocytosis and axonal damage offer a reliable means of identifying and measuring multiple pathological processes *in-vivo*. How these biomarkers are associated with cortical brain structure and cognition within, and across, disorders is unclear. Leveraging the Ontario Neurodegenerative Disease Research Initiative, we examined the cross-sectional association between plasma biomarkers, cortical thickness(CT), and multi-domain cognition.

	Overall, N = 290 ¹	HC-NC, N = 43 ¹	PD-NC, N = 48 ¹	PDMCI/PDD, N = 78 ¹	ADMCI/ADD, N = 121 ¹	p-value ²
Sex						<0.001
Male	172 (59%)	11 (26%)	35 (73%)	61 (78%)	65 (54%)	
Female	118 (41%)	32 (74%)	13 (27%)	17 (22%)	56 (46%)	
Age	68.96 (7.31)	66.94 (6.06)	65.89 (5.77)	68.50 (6.22)	71.19 (8.22)	<0.001
Education(yrs)	15.53 (2.81)	16.33 (2.08)	15.81 (2.63)	15.27 (2.73)	15.30 (3.10)	0.2
Left Handed						0.7
Right	267 (92%)	38 (88%)	44 (92%)	74 (95%)	111 (92%)	
Left	21 (7.2%)	5 (12%)	4 (8.3%)	4 (5.1%)	8 (6.6%)	
Ambidextrous	2 (0.7%)	0 (0%)	0 (0%)	0 (0%)	2 (1.7%)	
MOCA Score	24.84 (3.24)	28.11 (1.43)	27.48 (1.86)	24.85 (2.51)	22.79 (2.90)	<0.001
Disease stage						<0.001
MCI	137 (55%)	0 (NA%)	0 (0%)	52 (67%)	85 (70%)	
Dementia	62 (25%)	0 (NA%)	0 (0%)	26 (33%)	36 (30%)	
NC	48 (19%)	0 (NA%)	48 (100%)	0 (0%)	0 (0%)	

¹n (%), Mean (SD)
²Pearson's Chi-squared test, Kruskal-Wallis rank sum test, Fisher's exact test

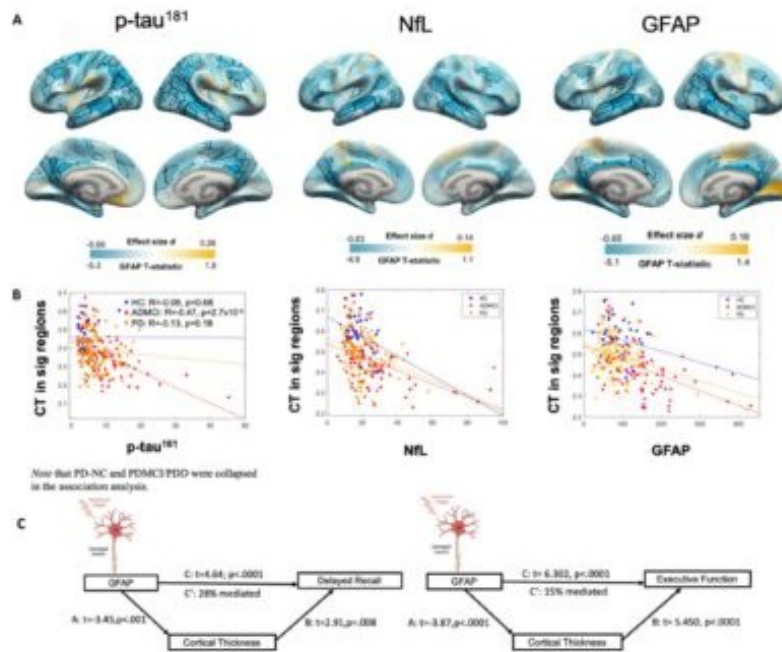
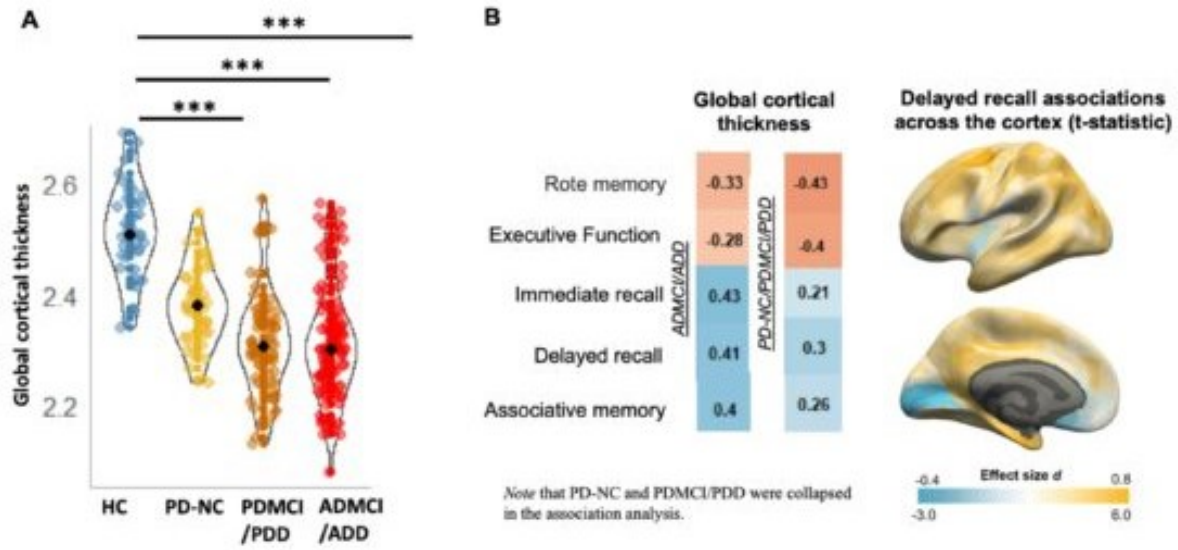
Table

Method: A total of 290 participants clinically diagnosed with Alzheimer's disease (AD) or Parkinson's disease (PD) and healthy controls (HC) were included (MeanAge=68.96[41% women; 35% APOE4carriers]). Four groups were formed(Table): i)AD with mild cognitive impairment or dementia(ADMCI/ADD; N=121), ii)PD with MCI or dementia(PDMCI/PDD; N=78), iii)PD with normal cognition(PD-NC; N=48) and HC(N=43). PDMCI/PDD and PD-NC were collapsed for association analyses(N=126). Plasma measures of p-tau¹⁸¹, glial fibrillary acidic protein(GFAP) and Neurofilament light chain(NfL), alongside FreeSurfer-derived CT were included. A neuropsychological battery was administered. All models were adjusted for age, sex, and socioeconomic status.

Results: There was a main effect of group on global CT, with patient groups exhibiting a significant reduction relative to HC(Fig1A). CT was associated with memory and executive function, even when stratified by group(ADMCI/ADD vs PD-NC/PDMCI/PDD; Figure1). Region-wise analysis showed a significant group*p-tau¹⁸¹ interaction on CT, with widespread p-tau¹⁸¹-related reductions in ADMCI/ADD only. GFAP was associated with a reduction in lateral temporal and medial parietal regions, with no group*GFAP interaction. CT mediated 28-14% of the association between GFAP and delayed memory(95%CI:0.12–0.42) and GFAP and executive function(95%CI:0.06-0.26; Figure2).

Conclusion: P-tau¹⁸¹ is associated with cortical reductions in AD, but not PD. Consistent with the transdiagnostic approach, GFAP, a measure of astrocytosis, played a significant role in reduced CT across both AD and PD, with implications for the severity of cognitive impairment. These results inform the pathological pathways underlying cognition and highlight transdiagnostic approaches to treatment via neuroinflammation control.

Figure 1 A-B Figure 2A-C



Keywords: Alzheimer's disease, Parkinson's disease, Plasma GFAP, Plasma p-tau181, Cortical thickness

Relationships of blood insulin with brain structures and plasma A β 42 to A β 40 ratio in a multi-ethnic cohort of older adults

Brandon Hall¹, Koral Wheeler¹, Meral Tubi¹, Nalini Hazra², Arthur Toga³, Leigh Johnson⁵, Raul Vintimilla⁵, Rocky Vig⁵, Sid O'Bryant⁵, Meredith Braskie¹

¹*Imaging Genetics Center, Mark and Mary Stevens Neuroimaging and Informatics Institute, Keck School of Medicine, University of Southern California, Los Angeles, CA, US*

²*Univeristy College London, London, UK*

³*Laboratory of Neuro Imaging USC Stevens Neuroimaging and Informatics Institute Keck School of Medicine of USC University of Southern California, Los Angeles, CA, US*

⁴*Department of Psychiatry, Neurology, and Epidemiology and Biostatistics University of California San Francisco, San Francisco, CA, US*

⁵*Institute for Translational Research University of North Texas Health Science Center, Fort Worth, TX, US*

⁶*Imaging Midtown Medical Imaging, Fort Worth, TX, US*

Objective: Type 2 diabetes (T2DM) is associated with elevated blood insulin and, by unknown mechanisms, Alzheimer's disease (AD). We evaluated how blood insulin related to plasma A β 42/A β 40 ratio (A β ratio) and cortical thickness in AD-relevant brain regions across diagnoses (cognitively unimpaired, mild cognitive impairment (MCI), dementia; diabetic, non-diabetic).

Methods: We acquired T1-weighted MRI images (3T) for 1088 subjects with blood insulin measures from the Health and Aging Brain - Health Disparities cohort (684 F, mean age 65.9 \pm 8.6; 892 cognitively unimpaired, 143 MCI, 53 AD; 817 non-diabetics, 271 diabetics; 558 Mexican American, 530 non-Hispanic white). Cortical thickness in previously-determined AD-relevant regions (fusiform, entorhinal, middle temporal, and inferior temporal gyri) was derived using Freesurfer v5.7. We used R v4.2 to perform separate multiple linear regressions between cortical thickness in each region and 1) A β ratio 2) fasting blood insulin, covarying for age, education, gender, ethnicity, cognitive and diabetic diagnoses. We examined the interactions of 1) insulin and diabetic status 2) insulin and cognitive diagnosis 3) insulin and APOE4 positivity, with A β ratio and cortical thickness. In a subset of 1080 subjects with available A β ratio, we tested whether A β ratio mediated the relationship between blood insulin and fusiform thickness. We used the false discovery rate for multiple comparison correction.

Results: Higher insulin was associated with lower fusiform thickness ($B = -1.2 \times 10^{-2}$, $p = 2.5 \times 10^{-3}$) and lower A β ratio ($B = -0.09$, $p = 6.8 \times 10^{-3}$), the latter suggesting greater brain amyloid. These relationships did not differ by cognitive or diabetic diagnosis. Insulin's direct effect on fusiform thickness was significant ($p = 0.02$) and partially mediated by A β ratio ($p = 0.04$).

Discussion: The relationship between higher blood insulin and thinner fusiform across cognitive diagnoses is partially mediated by the A β ratio. These results support a possible role of insulin in AD-related fusiform pathology.

Keywords: biomarkers, Alzheimer's, diabetes, insulin, APOE4

Unique biological pathways associated with plasma ptau species and AD PET: an imaging-transcriptomic study

Min Su Kang^{1,2}, Julie Ottoy^{1,2,3}, Gleb Bezgin³, Nesrine Rahmouni⁴, Jenna Stevenson⁴, Andrea Benedet⁵, Nicholas Ashton⁵, Thomas Karikari⁵, Gassan Massarweh³, Jean-Paul Soucy³, Mario Masellis⁶, Kaj Blennow^{5,7}, Henrik Zetterberg^{5,7,8,9}, Sandra Black^{2,6}, Pedro Rosa-Neto^{3,4}, Maged Goubran^{1,2,10}

¹Artificial Intelligence and Computational Neurosciences lab, Sunnybrook Research Institute, University of Toronto, Toronto, ON, Canada

²LC Campbell Cognitive Neurology Unit, Hurvitz Brain Sciences Program, Sunnybrook Research Institute, University of Toronto, Toronto, ON, Canada

³McConnell Brain Imaging Centre, Montreal Neurological Institute and Hospital, McGill University, Montreal, QC, Canada

⁴Translational Neuroimaging laboratory, McGill Centre for Studies in Aging, Montreal, QC, Canada

⁵Department of Psychiatry and Neurochemistry, Institute of Neuroscience and Physiology, The Sahlgrenska Academy at the University of Gothenburg, Gothenburg, Sweden

⁶Department of Medicine (Division of Neurology), University of Toronto, Toronto, ON, Canada

⁷Clinical Neurochemistry Laboratory, Sahlgrenska University Hospital, Gothenburg, Sweden

⁸United Kingdom Dementia Research Institute at University College London, London, UK

⁹Department of Neurodegenerative Disease, University College London Institute of Neurology, London, UK

¹⁰Department of Medical Biophysics, University of Toronto, Toronto, ON, Canada

Background: The advent of plasma ptau species came with a surprising finding where various plasma ptau are more strongly associated with amyloid-beta (A β) than tau PET in Alzheimer's disease (AD). However, possible biological mechanisms associated with the pathways between ptau and A β /tau pathology are not yet elucidated.

Methods: 197 participants (A β -: 26 Young and 79 CN; A β +: 29 CN, 37 MCI and 26 AD) from TRIAD underwent [¹⁸F]AZD4694-PET and [¹⁸F]MK6240-PET. The brain was parcellated into 1631 uniformly divided DKT-based ROIs using a novel high-resolution atlas, and cerebellar grey was used as a reference region. Plasma ptau-181, 217 and 231 were quantified using the Simoa/Janssen R&D. Linear regression models were used to investigate regional associations between plasma ptau and A β -PET or tau-PET, adjusted for age, sex, education, and APOE ϵ 4. Partial least squares (PLS) analysis was employed to identify a set of transcriptomic profiles from Allen Human Brain Atlas associated with ptau-AD-PET relationships (t-statistics). Then, gene set enrichment analyses based on Gene Ontology database were conducted to highlight which molecular/biological processes and cellular components are associated with transcriptomic profiles.

Results: The relationships between plasma ptau and regional A β -PET or tau-PET were significantly associated with the spatial distribution of transcriptomic profiles explaining 91.1% (11441 genes) and 75.2% (11291 genes) in variance in 1st PLS component, respectively. Similar associations were observed in the 2nd component of ptau-pathology (A β : 7.8% variance (11305 genes); tau: 22.5% (8483 genes)). Gene enrichment analyses showed convergence towards synaptic processes in the 1st PLS component for both pathologies, but the 2nd component showed divergence – ptau-A β -PET associated with immune-related processes while ptau-tau-PET highlighted cell development/vascular remodelling pathways (Figure 1).

Conclusion: Imaging-transcriptomic analyses showed unique sets of transcriptomic profiles associated with plasma ptau-AD pathology with synaptic (both), immune (A β) and cell development/vascular remodelling (tau) processes as potential drivers of these relationships.

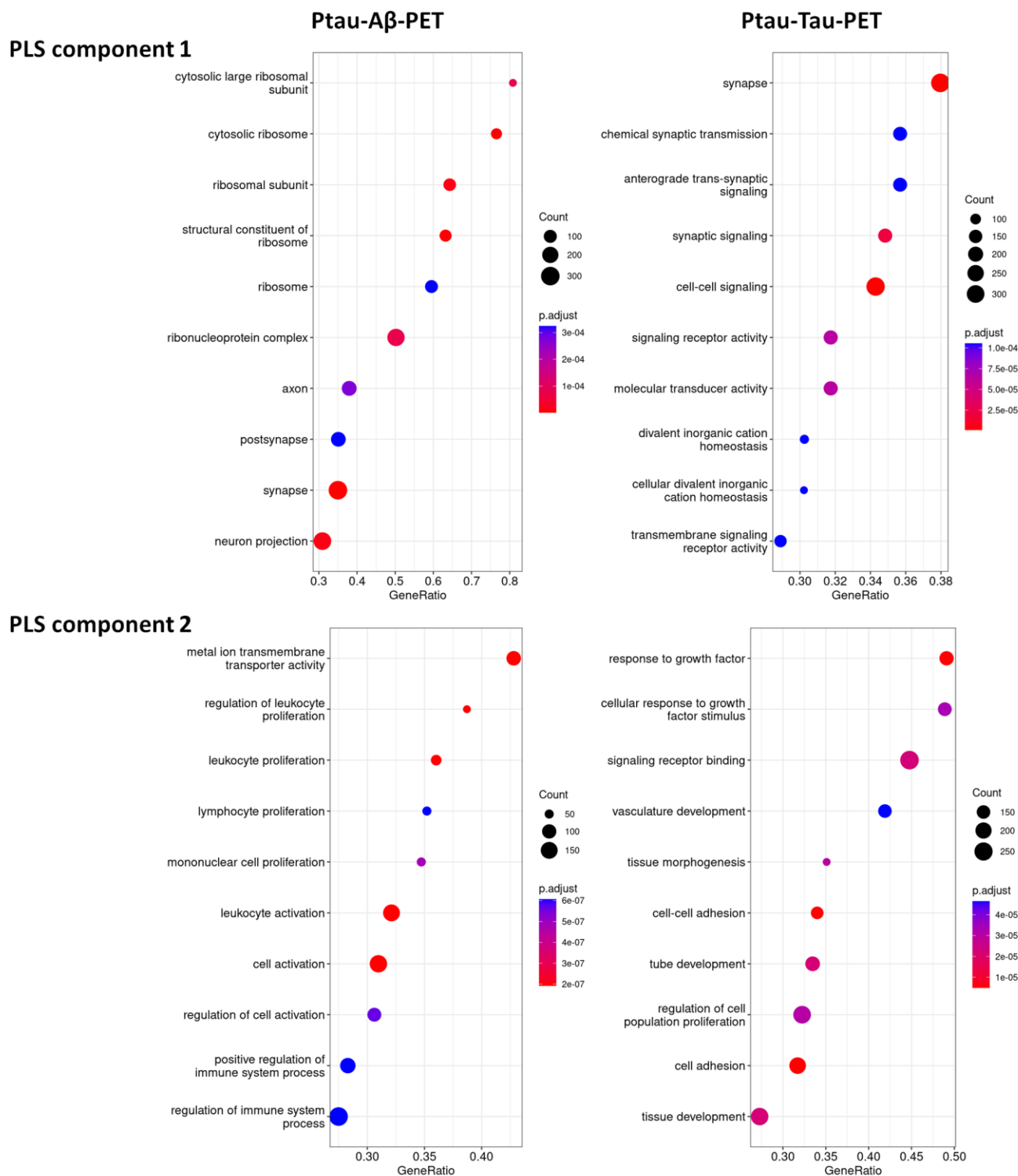


Figure 1. Gene set enrichment analyses based on the Gene Ontology (GO) database using a set of transcriptomic profiles identified from the PLS analyses between plasma tau-AD pathology. All gene enrichment analyses were corrected for multiple comparisons test using FDR $p < 0.05$. The size of the circle represents the number of genes included and the color represents FDR-adjusted p-values. The first row shows the gene enrichment analyses on the first PLS component from plasma tau-A β -PET (left) and plasma tau-tau-PET (right). Both results show biological pathways related to synapse and/or synaptic activity. The second row shows the gene enrichment analyses on the second PLS component from plasma tau-A β -PET (left) and plasma tau-tau-PET (right). The gene set enrichment shows immune-related mechanisms in the plasma tau-A β -PET PLS component but vasculature and cell development in the plasma tau-tau-PET PLS component.

Keywords: Amyloid-beta PET, tau PET, plasma tau, transcriptomics, gene enrichment

HAI2023 SUPPORT:



National Institute
on Aging

PLATINUM



GOLD/SCHOLARSHIPS



GOLD



SILVER



BRONZE

